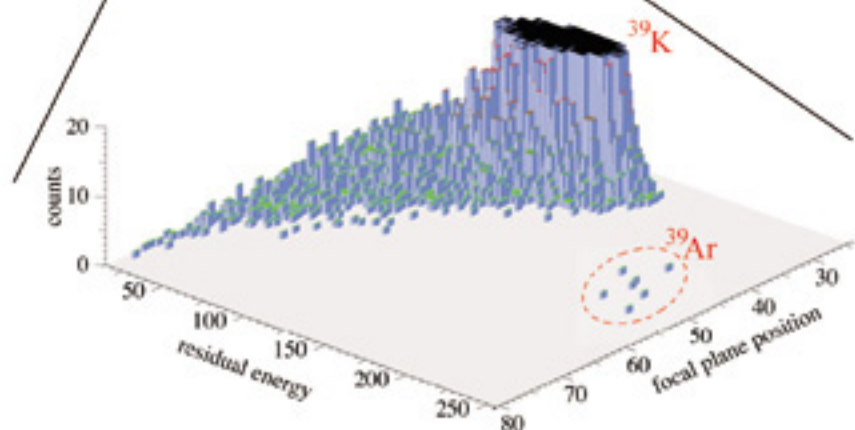
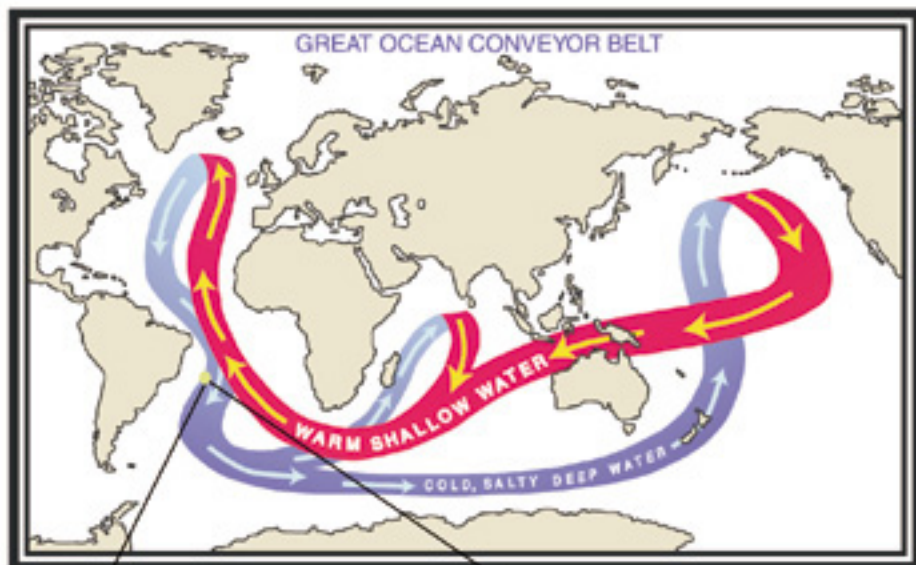


Physics Division Annual Report 2001



Argonne National Laboratory

operated by The University of Chicago
for the United States Department of Energy
under Contract W-31-109-Eng-38

Physics Division
Physics Division
Physics Division
Physics Division
Physics Division
Physics Division
Physics Division
Physics Division

Physics Division
Physics Division
Physics Division
Physics Division
Physics Division

Physics Division
Physics Division
Physics Division
Physics Division
Physics Division
Physics Division
Physics Division

Physics Division
Physics Division
Physics Division
Physics Division
Physics Division
Physics Division
Physics Division

Physics Division
Physics Division
Physics Division
Physics Division
Physics Division

Physics Division
Physics Division
Physics Division
Physics Division
Physics Division
Physics Division

Physics Division
Physics Division

Argonne National Laboratory, with facilities in the states of Illinois and Idaho, is owned by the United States Government and operated by The University of Chicago under the provisions of a contract with the Department of Energy.

DISCLAIMER

This report was prepared as an account of work sponsored by an agency of the United States Government. Neither the United States Government nor any agency thereof, nor The University of Chicago, nor any of their employees or officers, makes any warranty, express or implied, or assumes any legal liability or responsibility for the accuracy, completeness, or usefulness of any information, apparatus, product, or process disclosed, or represents that its use would not infringe privately owned rights. Reference herein to any specific commercial product, process, or service by trade name, trademark, manufacturer, or otherwise, does not necessarily constitute or imply its endorsement, recommendation, or favoring by the United States Government or any agency thereof. The views and opinions of document authors expressed herein do not necessarily state or reflect those of the United States Government or any agency thereof, Argonne National Laboratory, or The University of Chicago.

Available electronically at <http://www.doe.gov/bridge>

Available for processing fee to U. S. Department of Energy and its contractors, in paper, from:

U.S. Department of Energy
Office of Scientific and Technical Information
P.O. Box 62
Oak Ridge, TN 37831-0062
Phone: (865) 576-8401
Fax: (865) 576-5728
Email: reports@adonis.osti.gov

ABOUT THE COVER:

Schematic of the Global Ocean Circulation (“Great Conveyor Belt”), which plays a major role in the Earth’s climate through the transport of heat around the globe. The estimated circulation time is about 1000 years. The insert gives the result of a ^{39}Ar concentration measurement at ATLAS from a water sample taken at a depth of ~4700 m in the South Atlantic. From this measurement, a ‘ ^{39}Ar age’ of the sample of ~300 years is obtained.

ANL-02/15

ARGONNE NATIONAL LABORATORY
9700 S. Cass Avenue
Argonne, Illinois 60439-4801

**PHYSICS DIVISION ANNUAL REPORT
2001**

Donald F. Geesaman
Director

September 2002

Preceding Annual Reports

ANL-99/12 1998

ANL-00/20 1999

ANL-01/19 2000

Edited by Karen J. Thayer

FOREWORD

This report summarizes the research performed in 2001 in the Physics Division of Argonne National Laboratory. The Division's programs include operation of ATLAS as a national user facility, nuclear structure and reaction research, nuclear theory and medium energy physics research and accelerator research and development. The results reflect the talents and dedication of the Physics Division staff and the visitors, guests and students who bring so much to the research.

In 2001, the U.S. nuclear physics community continued its exemplary tradition of thoroughly examining the progress of our science and developing a long-term plan for the future. Several hundred scientists directly participated in the process to create the Nuclear Science Advisory Committee's Long Range Plan. I am very proud of the leadership provided by Argonne scientists in identifying and taking the pioneering steps in the science and in playing leading roles in the discussions and the formation of the NSAC plan. The final report, published in April 2002, names the Rare Isotope Accelerator as the highest priority of our field for major new construction. The essential concepts for RIA: a superconducting heavy-ion linac capable of accelerating all ions from H to U, the acceleration of multiple charge states to greatly enhance the available beam powers for the heaviest ions, the fast-gas-catcher to stop fast ions from fragmentation beams and rapidly extract them for reacceleration and trapping, and viable, innovative designs for high power targets were all developed and proven in the Physics Division. In the words of the Long Range Plan, "RIA will be the world leading facility for research in nuclear structure and nuclear astrophysics".

Research at ATLAS continues to define the frontiers of nuclear physics. New precision results on the beta decay spectrum of ${}^8\text{B}$ promise to have an impact on the understanding of neutrino oscillation results from solar neutrino detectors. Precise mass measurements with the Canadian Penning trap are helping to elucidate the rapid-neutron capture process while other direct and indirect measurements are playing a similar role in the rapid-proton capture process of nucleosynthesis. Nuclear structure measurements are defining the essential interplay of collective and single particle degrees of freedom in neutron-rich nuclei, proton rich nuclei and at high and low spin.

Unfortunately, budgetary constraints forced us to scale back ATLAS operations to ~ 5 days per week in mid 2001. In spite of this reduction, ATLAS provided over 5700 hours of beam for research with the remarkable operating reliability of 96%. Significant improvements were made to the accelerator. Most notably, a number of the original superconducting cavities were reconditioned with a high-pressure water rinse technique that resulted in operation at accelerating gradients that exceeded their original new-construction values. Accelerator Mass Spectroscopy was brought to a new level of sensitivity with the detection of Ar-39 at the 10^{-16} level, which permits investigation of the circulation of deep ocean currents for global climate studies.

In medium energy research, a remarkable, unexpected angular dependence was observed in the induced polarization in pion photoproduction from the proton. The HERMES

collaboration is making the first flavor decomposition of the polarized structure functions in deep inelastic positron scattering from the nucleon. Both HERMES and FNAL Drell-Yan results are constraining the poorly understood energy loss of fast quarks in nuclear material. Several new research proposals were approved at JLab and FNAL, promising exciting future courses of research.

The Division's role in theory ranges from the quark substructure of mesons to heavy nuclei and beyond to the fundamentals of quantum mechanics and quantum computing. Notable results were the application of Dyson-Schwinger equations to the structure of baryons. Comprehensive studies of meson photoproduction have guided much of the understanding obtained from recent Jefferson Lab data. With accurate ab-initio calculations of the spectra of all nuclei up to mass 10, there is a deeper understanding of which features of the nucleon-nucleon interaction are important for nuclear level structure: what makes it just so. Predictions of new regions of very extended shapes in nuclei are inspiring a new cycle of experiments.

While hiking in Chaco Canyon, New Mexico this summer, I came upon the Supernova Pictograph, an Anasazi eyewitness's rendering in stone of the 1054 supernova in the Crab nebula. Separated by almost a millennium in time, I could not help but feel a close kinship to this remarkable artist. We must share the passion for understanding why the world is just so. I see this passion in my colleagues in the Division daily and it shines through in the work reported here.



Donald F. Geesaman, Director, Physics Division

TABLE OF CONTENTS

	<u>Page</u>
I. HEAVY-ION NUCLEAR PHYSICS RESEARCH	i
A. REACTIONS OF ASTROPHYSICAL IMPORTANCE USING STABLE AND RADIOACTIVE BEAMS	1
a.1. Measurement of the ${}^8\text{B}$ Neutrino Spectrum with a New Technique.....	1
a.2. Study of the Branching Ratio of the 4.033 MeV $J^\pi = 3/2^+$ State in ${}^{19}\text{Ne}$	3
a.3. Study of the ${}^{12}\text{C}({}^{11}\text{C},\alpha){}^{19}\text{Ne}$ Reaction.....	4
a.4. Observation of γ -Ray Transitions in the rp Breakout Nucleus ${}^{20}\text{Na}$	5
a.5. Production of a ${}^{20}\text{Na}$ Beam Via the In-Flight Technique	7
a.6. Ne, Na and Al Burning in Astrophysically Important (p, γ) Reactions.....	7
a.7. Measurement of ${}^{44}\text{Ti}$ Half-Life	8
a.8. The ${}^{40}\text{Ca}(\alpha,\gamma){}^{44}\text{Ti}$ Reaction Measured by Counting of ${}^{44}\text{Ti}$ Residual Nuclei.....	9
B. STRUCTURE OF NUCLEI VERY FAR FROM THE VALLEY OF STABILITY	13
B.1. Proton-Rich Nuclear Spectroscopy	13
b.1.1. Low Level Density in Odd-Odd $N = Z$ Nuclei in the $A \sim 70$ Region	13
b.1.2. Alignment Effects in ${}^{72,73}\text{Kr}$	15
b.1.3. New Results in Proton Radioactivity.....	17
b.1.4. Population of the 168 keV First Excited State in ${}^{103}\text{Sn}$ in the Alpha Decay of ${}^{107}\text{Te}$	18
b.1.5. New Method to Study Sub- μs Proton and α Emitters	19
b.1.6. Identification of Excited States in ${}^{140}\text{Dy}$	21
b.1.7. Shape Coexistence Far from Stability.....	22
B.2. Neutron-Rich Nuclear Spectroscopy	25
b.2.1. A New Technique for Measuring g-Factor of Excited States in Fission Fragments Using Large Array of Ge Detectors	25
b.2.2. Medium-Spin Structure of ${}^{96,97}\text{Sr}$ and ${}^{98,99}\text{Zr}$ Nuclei and the Onset of Deformation in the $A \sim 100$ Region.....	25

b.2.3.	Selective Laser Ionization of $N \geq 82$ Isotopes: Use of the Two-Step Target Technique	26
b.2.4.	Magic Nucleus ^{132}Sn and its Odd-Neutron-Hole Neighbor ^{131}Sn	27
b.2.5.	Yrast Excitations in $N = 81$ Nuclei ^{132}Sb and ^{133}Te from ^{248}Cm Fission Studies	28
b.2.6.	Excitations of Two- and Three-Valence Proton Nuclei ^{134}Te and ^{135}I	29
b.2.7.	First Measurement of Yrast Excitations in ^{137}I and the Missing 12^+ Isomer in ^{136}Te	30
b.2.8.	First Observation of Excited States in ^{139}I	31
b.2.9.	Observation of Rotation Bands in Neutron-Rich ^{107}Ru Nucleus	32
b.2.10.	Mass Measurements of Short-Lived Neutron-Rich Isotopes at the Canadian Penning Trap Mass Spectrometer	32
C.	SPECTROSCOPY OF TRANS-LEAD NUCLEI	35
c.1.	Coulomb Excitation and Few Nucleon Transfer Reactions in $^{209}\text{Bi} + ^{248}\text{Cm}$ at 1450 MeV	35
c.2.	Coulomb Excitation and Few Nucleon Transfer Reactions with ^{209}Bi Beam on ^{237}Np and ^{241}Am Targets.....	36
c.3.	Estimation of the $N = 162$ Gap	38
c.4.	Spectroscopy of Transfermium Nuclei: ^{252}No	39
c.5.	Structure, Fission Barrier and Limits of Stability of ^{253}No	39
c.6.	Search for A High-K Isomer in ^{254}No by γ and Electron Spectroscopy	40
c.7.	Transition Intensities in ^{220}Th	41
c.8.	Production and Decay of ^{257}Rf	43
D.	OTHER TESTS OF NUCLEAR STRUCTURE UNDER EXTREME CONDITIONS	45
d.1.	Radiative Fusion of $^{12}\text{C} + ^{12}\text{C}$, $^{12}\text{C} + ^{16}\text{O}$ and $^{16}\text{O} + ^{16}\text{O}$	45
d.2.	Superdeformation in the Doubly Magic Nucleus ^{40}Ca	46
d.3.	Large Angle Alpha Scattering on ^{44}Ti	47
d.4.	Very Extended Shapes in the $A \sim 110$ Region	49
d.5.	Investigation of Anti-Magnetic Rotation in ^{100}Pd	49
d.6.	Direct Decay-Out from the Superdeformed Band to the Yrast Line in $^{152}\text{Dy}_{86}$	50
d.7.	Octupole Excitation in Superdeformed $^{152}\text{Dy}_{86}$	53
d.8.	Empirical Investigation of Extreme Single-Particle Behavior of Nuclear Quadrupole Moments in Highly Collective $A \sim 150$ Superdeformed Bands	56
d.9.	Competition Between Terminating and Collective Structures Above Spin 40 in ^{154}Dy	57
d.10.	First Evidence for Triaxial Superdeformation in ^{168}Hf	58
d.11.	Study of ^{169}Hf at High Rotational Frequency	58
d.12.	K-Hindered Decay of a 6-qp Isomer in ^{176}Hf	59

d.13.	Narrow Spreading Widths of Excited Bands in a Superdeformed Well	59
d.14.	Limits of the Energy-Spin Phase Space Beyond the Proton Drip Line: Entry Distributions of Pt and Au Isobars	61
d.15.	Investigation of the Decay Out of Superdeformed Bands in ^{194}Hg by Lifetime Measurements.....	62
d.16.	Effective Charge of the $\pi h_{11/2}$ Orbital and the Electric Field Gradient of Hg from the Yrast Structure of ^{206}Hg	63
d.17.	Unexpected Behavior of Heavy-Ion Fusion Cross Sections at Extreme Sub-Barrier Energies	63
d.18.	High Energy Photons from Very Symmetric Reactions: The Giant Dipole Resonance in the Highly Rotating ^{179}Au Nucleus	66
d.19.	Hot GDR in ^{118}Sn	67
d.20.	BaF ₂ GDR Measurement Collaboration	68
d.21.	Yield and Activity Calculations for Facilities for Short-Lived Nuclear Beams	69
E.	RELATIVISTIC HEAVY ION COLLISIONS	71
e.1.	The PHOBOS Experiment at RHIC	71
F.	ULTRA-HIGH SENSITIVITY MEASUREMENTS AND INVESTIGATION OF FUNDAMENTAL INTERACTIONS	79
f.1.	Developing an AMS Counting Technique for ^{39}Ar	79
f.2.	Measurement of the ^3He Component in Isotopically Purified ^4He by AMS	81
f.3.	Experimental Limit of Interstellar ^{244}Pu Abundance	82
f.4.	Search for the First Excited Level in the ^{229}Th Nucleus	84
f.5.	Search for X-Ray Induced Acceleration of the Decay of the 31-yr Isomer of ^{178}Hf Using Synchrotron Radiation	84
f.6.	Melting of Crystalline Confined Plasmas	87
f.7.	The Transition from Infinite to Finite Systems in Crystallized Coulombic Systems	89
f.8.	Precision Measurement of the ^{62}Ga Half-Life	90
f.9.	A Bragg Scattering Method to Search for the Neutron Electric Dipole	92
G.	EQUIPMENT DEVELOPMENT	93
g.1.	Data Acquisition Development.....	93
g.2.	New Double-Sided Si Strip Detector	93
g.3.	Delay-Line Shaping Amplifiers for a Double-Sided Silicon Strip Detector	94
g.4.	Split Anode for the First FMA Electric Dipole	94
g.5.	Design of a Recoil Separator for Superheavy Element Chemistry	95
g.6.	Test of Upgraded MWPC for High Count Rate Applications	96

g.7.	Development of Large Area Planar Germanium Detectors (HpGeDSSDs) for Future Tracking Arrays	97
g.8.	Design of the X-Array, an Efficient Gamma-Ray Detector for the Focal Plane of the FMA	98
g.9.	Participation in the GRETA Project	99
g.10.	The Science and Operation of Gammasphere at ATLAS: Phase 2	100
g.11.	Support for Gammasphere Operations.....	101
g.12.	High-Intensity Beam Tests at ATLAS.....	101
g.13.	A New Dedicated Chamber for Super-Heavy Element Research.....	102
g.14.	Design of a Large Area Window for the GSI Gas Cell	102
g.15.	Nuclear Target Development.....	103
g.16.	Developments at the Canadian Penning Trap Mass Spectrometer and Its Injection System	105
g.17.	Progress in the Construction of the Advanced Penning Trap System	107
H.	ATLAS USER PROGRAM	109
a.	Experiments Involving Outside Users	110
b.	Outside Users of ATLAS During the Period October 1, 2000 – September 30, 2001	114
c.	Upgrades to the ATLAS Web Page	117
II.	OPERATION AND DEVELOPMENT OF ATLAS.....	119
A.	OPERATION OF THE ACCELERATOR.....	120
a.1.	Operations Summary	120
B.	DEVELOPMENTS RELATED TO ATLAS	122
b.1.	Status of the ECR Ion Sources.....	122
b.2.	Two-Frequency Operation of ECR 2.....	124
b.3.	PII Transmission Line Traveling Wave Chopper	126
b.4.	ATLAS Control System.....	127
b.5.	ATLAS Cryogenic System	128
b.6.	New Solenoid for the In-Flight Production of Radioactive Beams at ATLAS.....	128
b.7.	Super-Conducting Resonator as Beam-Induced Signal Pickup	128
b.8.	Superconducting Surface Treatment.....	131

III.	R&D RELATED TO A FUTURE RARE ISOTOPE ACCELERATOR FACILITY.....	135
A.	HEAVY-ION LINAC TECHNOLOGY.....	137
a.1.	Superconducting RF: Prototype Superconducting Drift-Tube Cavities	137
a.2.	Superconducting RF: Test Facility Expansion	137
a.3.	Superconducting RF: Steering Effects in Quarter-Wave Cavities.....	139
a.4.	Superconducting RF: Upgraded Surface Processing and Single-Spoke Cavity Performance.....	139
a.5.	RIA Cryogenics	140
a.6.	Development of a Superconducting Solenoid for the RIA Facility	141
a.7.	57.5-MHz CW RFQ for the Driver Linac.....	143
a.8.	12.125-MHz Accelerating Structure: The Hybrid RFQ	144
B.	RIA BEAM DYNAMICS.....	146
b.1.	Update of the Driver Linac Benchmark Design	146
b.2.	Low-Charge State Heavy-Ion Beam Dynamics in the Hybrid RFQ.....	147
b.3.	Correction of Beam Steering Effects in Low-Velocity Superconducting Quarter-Wave Cavities	149
b.4.	Design of a RIA Driver Linac Switchyard	150
C.	RARE ISOTOPE PRODUCTION, SEPARATION, AND DIAGNOSTICS	152
c.1.	Bunch Shape Monitor for CW Heavy-ion Beams	152
c.2.	Assessment of the Radioactive Inventory Produced by the Current RIA Target Designs	153
c.3.	Implementation of Computer Codes for Use in the RIA Target Design Activities at the NERSC.....	155
c.4.	Implementation of Photonuclear and Low Energy D-Li Capabilities for Target Design.....	155
c.5.	Effusion/Diffusion Studies of ISOL Target/Ion Source Systems	157
c.6.	An Adjustable Thickness Li/Be Target for Fraagmentation of 4-Kw Heavy-Ion Beams	159
c.7.	Development and Operation of Gas Catchers to Thermalize Fusion-Evaporation and Fragmentation Products.....	163

IV. MEDIUM-ENERGY NUCLEAR PHYSICS RESEARCH	169
A. NUCLEON PROPERTIES	172
a.1. New Measurements of (G_E/G_M) for the Proton.....	172
a.2. Measurements of the Proton Elastic Electromagnetic Form Factor Ratio by Polarization Transfer	173
a.3. Polarization Measurements in the Neutral Pion Photoproduction.....	174
a.4. Charged Pion Photoproduction from the Nucleon.....	175
a.5. Search for QCD Oscillations in the $\gamma N \rightarrow \pi N$ Reactions	176
a.6. Separated and Unseparated Structure Functions in the Nucleon Resonance Region	176
B. SUBNUCLEONIC EFFECTS IN NUCLEI	178
b.1. High-Energy Angular Distribution Measurements of the Deuteron Photodisintegration Reaction	178
b.2. Measurement of Longitudinal and Transverse Cross Sections in the ${}^3\text{He}(e,e'\pi^+){}^3\text{H}$ Reaction at $W = 1.6$ GeV	179
b.3. Electroproduction of Kaons and Light Hypernuclei.....	180
b.4. Measurements of the Nuclear Dependence of $R = \sigma_L/\sigma_T$ at Low Q^2	181
b.5. Measurement of the EMC Effect in Very Light Nuclei.....	182
b.6. Measurement of High Momentum Nucleons in Nuclei and Short Range Correlations.....	183
b.7. Search for the Onset of Color Transparency (Letter of Intent LOI-02-004 to JLab-PAC21).....	184
b.8. Measurement of the Transparency Ratio for the $A(\gamma,\pi^+p)$ Reaction in Helium and Deuterium	185
b.9. New Optics and Acceptance Model for the Jefferson Lab High Resolution Spectrometers	186
C. QUARK STRUCTURE OF MATTER	187
c.1. Measurement of the Structure Function of the Pion	187
c.2. Measurements of Spin-Structure Functions and Semi-Inclusive Asymmetries for the Nucleon at HERA	187
c.3. Inclusive Measurements of the Deuteron Spin Structure Function.....	189
c.4. Flavor Decomposition of Polarized Structure Functions.....	190
c.5. Gluon Polarization	190
c.6. Azimuthal Asymmetries and Transversity.....	191

c.7.	Measurements with Unpolarized Targets: Hadron Formation Times.....	192
c.8.	A Dual Radiator Ring Imaging Cerenkov Counter for HERMES.....	193
c.9.	Nuclear Dependence of Lepton Pair Production: Parton Energy Loss, Shadowing and J/ψ and ψ' Suppression.....	195
c.10.	Production of Υ and J/ψ from 800 GeV Protons Incident on Hydrogen and Deuterium.....	195
c.11.	Polarization Measurement of Υ and ψ Production in Proton-Nucleus Collisions.....	196
c.12.	Measurement of the Antiquark Flavor Asymmetry of the Proton Sea Using Dress-Yan Scattering.....	197
c.13.	Drell-Yan Measurements with 120 GeV Protons, FNAL E906.....	198
D.	ATOMIC TRAP TRACE ANALYSIS.....	200
d.1.	Improvements on Detecting $^{81,85}\text{Kr}$ with ATTA.....	200
d.2.	Ultrasensitive Isotope Trace Analysis of ^{41}Ca	201
d.3.	Measuring the Charge Radius of ^6He	202
V.	THEORETICAL PHYSICS.....	203
A.	NUCLEAR DYNAMICS WITH SUBNUCLEONIC DEGREES OF FREEDOM.....	204
a.1.	Contemporary Applications of Dyson-Schwinger Equations.....	205
a.2.	Diquarks and Density.....	205
a.3.	Pair Creation and Plasma Oscillations.....	206
a.4.	Neutron Electric Dipole Moment: Constituent-Dressing and Compositeness.....	206
a.5.	Plasma Production and Thermalization in a Strong Field.....	207
a.6.	Meson Photoproduction.....	207
a.7.	Pair Creation and an X-ray Free Electron Laser.....	208
a.8.	X-ray Free Electron Laser: Vacuum Pair Creation, Back Reactions and Memory Effects.....	209
a.9.	Nucleon Mass and Pion Loops.....	210
a.10.	Bethe-Salpeter Equation and a Nonperturbative Quark-gluon Vertex.....	210
a.11.	Axial-Vector Diquarks in the Baryon.....	210
a.12.	Valence-Quark Distributions in the Nucleon.....	211
a.13.	J/ψ Suppression as a Signal of Quark Gluon Plasma Formation.....	211
a.14.	Schwinger-Dyson Approach to Nonequilibrium Classical Field Theory.....	211

a.15.	Numerical Approximations using Chebyshev Polynomial Expansions	212
a.16.	Dynamical Study of the Δ Excitation in $N(e,e'\pi)$ Reaction.....	212
a.17.	Nucleon Resonances in ω Photoproduction.....	214
a.18.	The Pion Contributions to the $\gamma N \rightarrow \Delta$ Transition.....	215
a.19.	Coupled-Channel Approach for $K^+\Lambda$ Photoproduction	215
a.20.	Meson-Exchange πN Models in Three-dimensional Bethe-Salpeter Formulation	216
a.21.	ϕ -N Bound State.....	216
a.22.	Compressed Nuclei with Δ s and Hyperons.....	216
a.23.	Dynamical Study of the ${}^2\text{H}(e,e'\pi^+)$ Reaction	217
a.24.	η Meson Production in NN Collisions.....	218
a.25.	Study of Nucleon Resonances with Double Polarization Observables in Pion Photoproduction.....	218
a.26.	From Light Nuclei to Nuclear Matter: The Role of Relativity	219
a.27.	Null-Plane Dynamics of Elastic Electron Deuteron Scattering	219
B.	NUCLEAR FORCES AND NUCLEAR SYSTEMS.....	220
b.1.	Quantum Monte Carlo Calculations of Light p-shell Nuclei.....	221
b.2.	Studies of Three-Nucleon Interactions in Nuclear Systems	222
b.3.	What Makes Nuclear Level Structure?.....	223
b.4.	Radiative Capture Reactions for Astrophysical Applications	224
b.5.	Microscopic Calculations of $A = 6-8$ Weak Decays.....	226
b.6.	Coupled Cluster Expansion Approach to Calculating Ground State Properties of Closed Shell Nuclei	226
b.7.	Neutron-Proton Density Differences in Nuclei.....	227
C.	NUCLEAR STRUCTURE AND HEAVY-ION REACTIONS	228
c.1.	Multipole Expansion for Relativistic Coulomb Excitation.....	229
c.2.	Vibrational Interpretation of Spherical and Near-Spherical Proton Emitters.....	230
c.3.	Accuracy of the Eikonal Model of Fragmentation Reactions.....	232
c.4.	Higher-order Effects in the Two-body Breakup of ${}^{17}\text{F}$	233
c.5.	Many Body Wave Functions	234
c.6.	Neutron-Proton Pairing.....	235
c.7.	Very Extended Shapes in Nuclei	236
c.8.	E1 Transition Probabilities Between Superdeformed States	236
c.9.	Single Particle States in the Heaviest Elements.....	237
c.10.	Studies of Nuclear Energy Surfaces	237
c.11.	Probing the Gateway to Superheavy Nuclei in Cranked Relativistic Hartree-Bogoliubov Theory.....	238

D.	ATOMIC THEORY AND FUNDAMENTAL QUANTUM MECHANICS	240
d.1.	Interactions of Photons with Matter.....	241
d.2.	Interactions of Charged Particles with Matter	241
d.3.	On the Connection Between Spin and Statistics in Quantum Mechanics	241
d.4.	A Virial Theorem for Nuclear Deformation.....	242
d.5.	The Representation of Numbers in Quantum Mechanics.....	242
d.6.	Efficient Implementation and the Product State Representation of Numbers.....	243
d.7.	Towards a Coherent Theory of Mathematics and Physics.....	243
d.8.	Cyclic Quantum Gate Networks	244
E.	OTHER ACTIVITIES	245
e.1.	Theory Workshop on Rare Isotope Physics.....	245
e.2.	14 th Annual Midwest Nuclear Theory Get-Together	245
	OTHER EDUCATIONAL ACTIVITIES IN THE PHYSICS DIVISION	247
a.	Enhancement of Minority Involvement in DOE Nuclear Physics Programs	247
b.	Nuclear Physics Award for Faculty in Undergraduate Institutions.....	247
c.	Scientific Support of SciTech Museum Exhibits and Outreach Programs.....	248
	Staff List.....	249
	Publications.....	259

I. HEAVY-ION NUCLEAR PHYSICS RESEARCH

OVERVIEW

This research involves investigating the structure, stability, reactions and decays of nuclei. This information is crucial for understanding the evolution of the universe, the workings of stars and the abundances of the elements that form the world around us. A forefront area of research is investigating the properties of nuclei which lie very far from stability, and which are critical in understanding nucleosynthesis. Most of our research is based at the Argonne Tandem-Linac Accelerator (ATLAS), a national heavy-ion user facility. Programs are also mounted at the Relativistic Heavy Ion Collider (RHIC), at the 88" cyclotron at Berkeley and at other forefront facilities. The major thrusts of the program are: a) deepening and generalizing our understanding of nuclear structure to allow a reliable description of all bound nuclear systems, b) studying the reactions which are important in the cataclysmic events in the cosmos which lead to the synthesis of the chemical elements, c) testing the limits of the Standard Model, the fundamental theory that currently best represents our understanding of the laws and fundamental symmetries of nature.

The specific research topics we are pursuing include the studies of transfermium nuclei ($Z > 100$) with a goal of studying the very heaviest nuclei, the study of the shapes, and stability of nuclei along the proton dripline, the effects of deformation on proton radioactivity, the production and acceleration of short-lived nuclei and their use in measurements of reactions which are important in astrophysics, and the high-precision measurement of nuclear masses. In addition, there are complimentary efforts in the use of Accelerator Mass Spectrometry (AMS) for environmental research; in the investigation of nuclear matter at relativistic energies; and in the dynamics of cooled ions confined in storage rings or traps. The ATLAS-based research exploits the unique capabilities of the accelerator, both in the stable beam program, and in production of accelerated beams of short-lived isotopes. The experiments employ state-of-the-art research equipment, including the Fragment Mass Analyzer (FMA), a large solid angle silicon array, "Ludwig", and the Canadian Penning Trap, (CPT) which is operating at ATLAS. Several new detector initiatives are being pursued including upgrading the FMA, refining the "In-Flight" radioactive beam facility, constructing the Advanced Penning Trap (APT) and developing next generation gamma ray detectors with "tracking" capability. Full participation in the Gammasphere program continues, in publication of results from the Argonne cycle of operation, in performing experiments at Berkeley, and in preparing the scientific case and planning a

return of Gammasphere to ATLAS in 2003. Intensive participation in the PHOBOS experiment at Brookhaven has continued, and has led to the first published results from this project.

Some of the specific goals of the program can be summarized as follows:

- Develop and utilize beams of short-lived nuclei, $^{17,18}\text{F}$, ^{21}Na , ^{25}Al , ^{44}Ti , ^{56}Ni , ^8B , ^{14}O and others, to improve the understanding of reactions of astrophysical importance. Particular emphasis has recently been focused on “in-flight” production of short-lived ion-species using kinematically inverse reactions on gaseous targets.
- Study the structure, stability, and modes of excitation and decay of the heaviest elements and study of the reaction mechanisms through which they can be synthesized. This research has many facets, including exploring the opportunities for producing the very heaviest nuclei ($Z > 106$), studies of isomeric decays, studies of “fine-structure” in the alpha decay of heavy elements, and “inbeam” spectroscopy and calorimetry.
- Study the shapes, stability and decay modes of nuclei along the proton dripline in order to improve understanding of partially bound nuclei. Studying proton tunneling through deformed barriers, in order to increase the spectroscopic information obtained through proton radioactive decay rates.
- Make high-precision measurements of nuclear masses with the CPT, particularly the masses of $N = Z$ nuclei which are of astrophysical interest and are important for testing CVC theory. Improve the efficiency for production, separation, cooling, transportation, and trap loading of ions to increase sensitivity.
- Developing position sensitive germanium detectors, for “tracking” gamma rays in order to allow the imaging of the source of radiation. The ANL focus has been on developing planar germanium wafer technologies, in parallel with involvement in national plans to construct a $4\text{-}\pi$ germanium shell, following the GRETA concept.
- Investigate the collisions and deconfinement of nucleons in nuclear matter at very high temperatures and densities that are achieved in relativistic heavy-ion collisions of gold nuclei at 200 GeV/u. Our participation is using the PHOBOS detector at the RHIC accelerator at Brookhaven National Laboratory.
- Perform detailed R&D studies for the Rare Isotope Accelerator (RIA) and participate in all efforts to refine the designs for the accelerators, target stations, post accelerator, and experimental equipment. Intense effort is being directed to development of the “gas catcher” technology for cooling primary beams.

A. REACTIONS OF ASTROPHYSICAL IMPORTANCE USING STABLE AND RADIOACTIVE BEAMS

In the last few years a variety of radioactive species were accelerated at ATLAS. Studying reactions involving these exotic nuclei has helped clarify and quantify some reaction processes like the “breakout” from the hot CNO cycle and the beginning of the more explosive rp-process. Their production was through the “two-accelerator” method [for longer-lived species like ^{18}F ($t_{1/2} = 110$ m), ^{56}Ni ($t_{1/2} = 61$ d) and ^{44}Ti ($t_{1/2} = 60$ y)] or using “in-flight” production through reactions with highly inverse kinematics [for example, ^{17}F ($t_{1/2} = 65$ s), ^{21}Na ($t_{1/2} = 22.5$ s), ^{25}Al ($t_{1/2} = 7.2$ s), ^8B ($t_{1/2} = 770$ ms), and ^{14}O ($t_{1/2} = 70.6$ s)]. The reconfigured radioactive ion production beam line, which now includes a large-bore solenoid, was tested and successfully used in experiments. In addition to the ATLAS projects with accelerated radioactive beams, several more conventional heavy-ion reaction studies produced data on nuclei critical to the rp-nucleosynthesis path. A significant opportunity lies in studying compound nuclear states near the (p,γ) reaction threshold, populated with near-barrier fusion of heavy ions, and spectroscopically investigated using Gammasphere. This technique seems to have many possibilities, as it is excellent for precisely determining the excitation energy of levels and their angular momentum properties

a.1. Measurement of the ^8B Neutrino Spectrum with a New Technique (K. E. Rehm, C. L. Jiang, I. Ahmad, J. Greene, A. Heinz, D. Henderson, R. V. F. Janssens, E. F. Moore, G. Mukherjee, R. C. Pardo, T. Pennington, G. Savard, J. P. Schiffer, D. Seweryniak, G. Zinkann, M. Paul,* W. Winter,† and S. J. Freedman†)

The neutrino spectrum from ^8B decay is a crucial ingredient in interpreting the data from solar neutrinos obtained in recent experiments by the SNO and Superkamiokande collaborations. Because of its high end point energy a direct measurement of the beta decay spectrum has so far been only performed once.¹ Since the beta decay populates a broad 2^+ state in ^8Be which subsequently decays into two α particles the shape of the neutrino spectrum can be more easily inferred from a measurement of the alpha-particle spectrum following the decay. Several measurements of the α -decay spectrum have been performed in the past.² These experiments disagree, however, in the critical low-energy region that influences the highest energy neutrinos.

A new technique has been developed at the ATLAS accelerator to accurately measure this spectrum. A beam of 28-MeV ^8B nuclei ($T_{1/2} = 0.77$ s) was produced by bombarding a ^3He filled gas cell with an intense ^6Li beam. ^8B nuclei with this energy were separated from the primary beam with a bending magnet and transported to the focal plane of the Enge split pole magnetic spectrograph where they were implanted into a 91- μm -thick Si detector cooled to -5°C . A measurement cycle consisted of a 1.5 s period of ^8B

implantation, followed by 1.5 s of decay counting during which the ^6Li beam was stopped near the accelerator.

The advantage of the implantation method, in comparison to the earlier experiments,^{2,3} is that both alpha particles are detected in the same detector and systematic effects due to energy loss in catcher foils and in dead layers of the detector are eliminated. Since the α decay of the 2^+ state in ^8Be is preceded by a β^+ decay from ^8B , the energy spectrum is shifted towards higher energies because of β - α summing in the Si detector. To minimize this effect a thin plastic scintillator was mounted directly behind the Si detector. A coincidence measurement restricted the β 's to be emitted within a $\sim 40^\circ$ cone which limits the energy shift to less than ~ 20 keV.

To calibrate the detector, α particles from the decay of ^{20}Na , produced and implanted with the same technique, were used. In this case about 1/5 of the decay energy is carried by the ^{16}O recoil, so a correction for the pulse height defect of oxygen (relative to α particles) had to be applied. This correction is believed to be accurate to ≤ 10 keV. Details of the production method of the ^{20}Na beam are described in section a.5. In addition, external

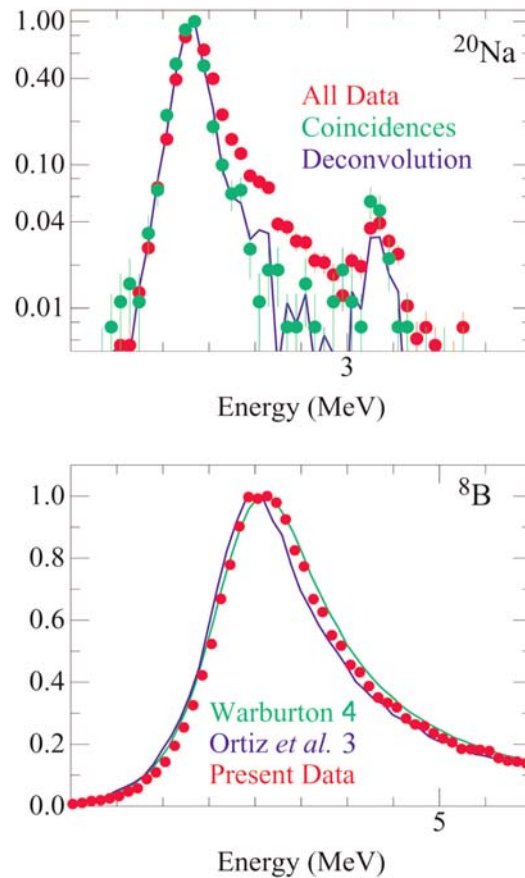


Fig. I-1. (a) Alpha calibration spectrum from the decay of ^{20}Na nuclei, implanted into a $91\ \mu\text{m}$ thick Si detector. The solid line corresponds to the deconvolution of the singles data. (b) Alpha spectrum measured from the decay of implanted ^8B nuclei, compared to previous measurements (3,4).

α -particle sources (^{228}Th , ^{148}Gd) were also used. For this part of the calibration the energy loss of the α particles in the source material and the dead layer of the detector was measured.

Figure I-1(a) shows part of the energy spectrum from ^{20}Na particles implanted into the Si detector, measured in singles (red) and in silicon-scintillator coincidences (green). The high energy tail which is much reduced in the coincidence spectrum is the result of the α - β^+ summing mentioned above. The blue line, which is the result of a deconvolution of the singles data using the electron energy deposition from a simulation of the

added pulse-height spectrum from electrons, is in excellent agreement with the experimental coincidence spectrum.

The α spectrum from the decay of ^8B , deconvoluted with the detector response is presented in Fig. I-1(b). It is found to be in reasonable agreement with the results obtained by Warburton⁴ (see green line) though somewhat narrower, but is shifted towards higher energies with respect to the spectrum by Ortiz *et al.*³ (blue line).

*Hebrew University, Jerusalem, Israel, †Lawrence Berkeley National Laboratory

¹J. Napolitano, S. J. Freedman and J. Camp, Phys. Rev. **C36**, 298 (1987).

²J. N. Bahcall, E. Lisi, D. E. Alburger, L. DeBraekeleer, S. J. Freedman and J. Napolitano, Phys. Rev. **C54**, 411 (1996).

³C. E. Ortiz, A. Garcia, R. A. Waltz, M. Bhattacharya and A. K. Komives, Phys. Rev. Lett. **85**, 2909 (2000).

⁴E. K. Warburton, Phys. Rev. **C33**, 303(1986).

a.2. Study of the Branching Ratio of the 4.033 MeV $J^\pi = 3/2^+$ State in ^{19}Ne (K. E. Rehm, A. Wuosmaa, C. L. Jiang, J. Greene, A. Heinz, D. Henderson, R. V. F. Janssens, G. Mukherjee, R. C. Pardo, T. Pennington, J. P. Schiffer, R. H. Siemssen, M. Paul,* L. Jisonna,[†] and R. E. Segel[†])

In the CNO cycle, which occurs in stars somewhat heavier than the sun, the rate of energy production is limited by the slow β -decays of $^{14,15}\text{O}$ ($T_{1/2} = 70.6$ and 123 s, respectively). These waiting points can be bypassed at higher temperatures by proton and α induced reactions on these nuclei, which results in a strong increase of the energy production as well as in a breakout from the hot CNO cycle into the rapid proton capture (rp) process -- a sequence of (p,γ) reactions and β decays producing nuclei above mass 20. The reaction Q-values in this mass region are such that once nuclei heavier than ^{19}Ne have been formed no reaction sequence can recycle the nuclei back into CNO material. Among the three possible breakout paths: $^{15}\text{O}(\alpha,\gamma)^{19}\text{Ne}$, $^{18}\text{F}(p,\gamma)^{19}\text{Ne}$ and $^{18}\text{Ne}(\alpha,p)^{21}\text{Na}$, the first reaction is thought to be the most important.

A direct measurement of the $^{15}\text{O}(\alpha,\gamma)^{19}\text{Ne}$ reaction which has an estimated cross section of ~ 100 pb is presently not possible because it requires a very intense ^{15}O beam. For this reason, only indirect measurements have been performed so far. The first levels in ^{19}Ne above the (α,γ) threshold at 3.534 MeV is a $3/2^+$ state at 4.033 MeV followed by $9/2^-$ and $7/2^-$ levels at 4.140 and 4.197 MeV, respectively. Because of the low angular momentum transfer ($\Delta l = 1$) and the low excitation energy, the $3/2^+$ level has the largest influence on the (α,γ) reaction at typical nova temperatures.

In indirect measurements of the $3/2^+$ state in ^{19}Ne the level is populated in a transfer reaction and the branching ratio of the subsequent decay of ^{19}Ne into an α -particle and ^{15}O is determined by detecting the decay products. While earlier attempts¹ used reactions in normal kinematics, e.g. bombarding a ^{19}F target with a ^3He beam, a large increase in detection efficiency can be achieved by using inverse kinematics i.e. bombarding a deuterium or ^3He target with a F or Ne beam. Under these conditions the high energy ^{19}Ne nuclei produced in the reaction are focused into a small forward cone which simplifies their detection and identification.

Because CD_2 is a readily available solid deuterium target we have studied the use of the $d(^{20}\text{Ne},t)^{19}\text{Ne}$ reaction to populate the 4.033-MeV state in ^{19}Ne . However, it was found that the spectroscopic factor for this state is small resulting in cross sections at forward

angles of only $\sim 20 - 30$ $\mu\text{b}/\text{sr}$. We have therefore investigated the use of other transfer reactions. The most promising among them is the $^3\text{He}(^{20}\text{Ne},\alpha)^{19}\text{Ne}$ reaction.

In a first test experiment we have used a 100-MeV ^{20}Ne beam from ATLAS to populate the 4.033-MeV state in ^{19}Ne . For this reaction, the α -particles associated with small center-of-mass angles have very low energies in the laboratory system (typically ≤ 1 MeV). Consequently, we have used α -particles from backward angles in the center-of-mass, which are emitted in the angular range $\theta_{\text{lab}} = 6 - 15^\circ$ with energies of about 50 MeV. The coincident ^{19}Ne reaction products have an energy of about 50 MeV and are emitted into the laboratory angular range $\theta_{\text{lab}} = 2.5 - 7^\circ$.

The ^3He target consisted of a 1.5-mm long gas cell with two 1.3-mg/cm² titanium windows, filled with 750 mbar of ^3He and cooled to LN₂ temperatures resulting in an areal density of about 50 $\mu\text{g}/\text{cm}^2$.

The α -particles from the $(^3\text{He},\alpha)$ reaction were detected in a 500 μ thick annular Si strip detector. The detector was segmented in the front into 16 1.5 mm wide rings covering the angle range $\theta_{\text{lab}} = 10 - 20^\circ$ and 16 wedges, each with an opening angle of 22.5° in the back.

The coincident ^{19}Ne and ^{15}O particles were separated from the incident ^{20}Ne beam with the Enge Split Pole magnetic spectrograph and identified in the focal plane in a hybrid position sensitive parallel-plate-avalanche-counter (PPAC) ionization chamber (IC) detector system. Two charge states of the outgoing particles ($q = 8,9$ for ^{19}Ne and $q = 7,8$ for ^{15}O) were detected simultaneously in the focal plane detector. With this setup very clean particle identification was achieved even for processes with very small cross sections.

The upper part of Fig. I-2 presents Q-value spectra measured in the Si detector for α particles which are in coincidence with ^{19}Ne (open circles) and ^{15}O particles (solid points) identified with respect to mass and Z in the split-pole spectrograph. The lower part of Fig. I-2 gives the ratio of the cross sections (corrected for detection efficiencies) which corresponds to the branching ratio $\Gamma_\alpha/\Gamma_\gamma$.

In this first test run the Q-value resolution was limited by the beam spot and the strip size of the Si detector to about 600 keV. With a higher granularity Si detector and improved geometry we should be able to improve

the resolution to less than 200 keV. This will allow us to measure branching ratios below 10^{-3} . The technique will also be useful for measurements of other branching ratios which are of interest to nuclear astrophysics.

*Hebrew University, Jerusalem, Israel, †Northwestern University

¹P. V. Magnus, M. S. Smith, A. J. Howard, P. D. Parker and A. E. Champagne, Nucl. Phys. **A506**, 332 (1990).

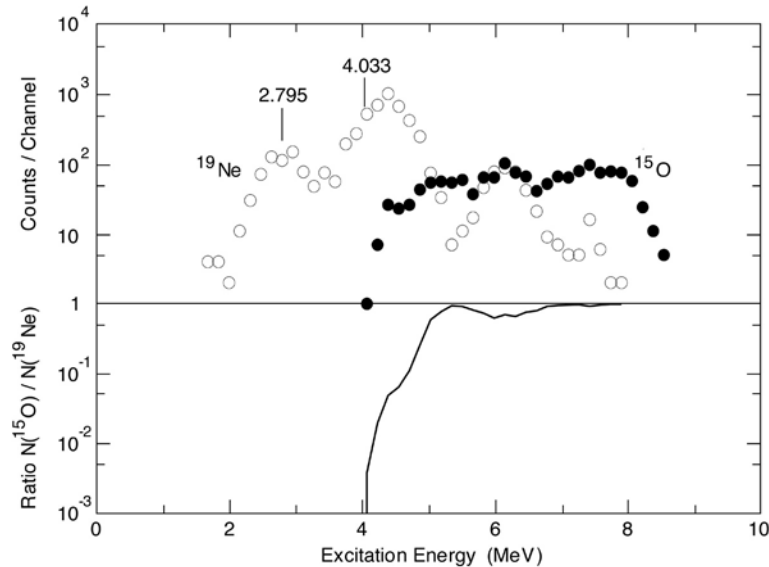


Fig. I-2. Top: Q-value spectra for α particles in coincidence with ^{19}Ne or ^{15}O identified with respect to mass and Z in the split-pole spectrograph. Bottom: Branching ratio $\Gamma_\alpha/\Gamma_\gamma$, obtained from the Q-value spectra which were corrected for detection efficiency.

a.3. Study of the $^{12}\text{C}(^{11}\text{C},\alpha)^{19}\text{Ne}$ Reaction (A. H. Wuosmaa, K. E. Rehm, J. Caggiano,* P. Collon, A. Heinz, D. Jenkins,† R. V. F. Janssens, C. L. Jiang, C. J. Lister, J. P. Schiffer, F. Guo,‡ P. McMahan,‡ J. Powell,‡ M. Rowe,‡ and I Wiedenhöver§)

The astrophysical importance of the $^{15}\text{O}(\alpha,\gamma)^{19}\text{Ne}$ reaction has encouraged us to try several alternative indirect approaches to measuring the breakup of the $J^\pi = 3/2^+$ 4.033-MeV state in ^{19}Ne . ^{19}Ne is of crucial importance in the production of elements heavier than C, N, and O through its role as a breakout path from the CNO cycle. Briefly, the CNO cycle, which produces energy through a series of proton-capture, β^+ decay, and (p, α) reactions, cycles through isotopes of carbon, nitrogen and oxygen, beginning and ending with ^{12}C . In the appropriate environment, however, it is possible to exit the CNO cycle via the alpha-capture reaction $^{15}\text{O}(\alpha,\gamma)^{19}\text{Ne}$. This alpha capture proceeds dominantly through a few near-threshold, low-spin levels in ^{19}Ne , the most important of which is the $3/2^+$ state at an excitation energy of 4.033 MeV. The fraction of nuclei leaving the CNO cycle is thus determined by the competition between alpha, and gamma decay of this

state; alpha decay leads back to the CNO cycle, whereas gamma-decay exits the cycle producing ^{19}Ne . The single most important piece of nuclear physics data relevant to this issue is the branching ratio for alpha decay of the 4.033-MeV $3/2^+$ state in ^{19}Ne , currently thought to be approximately $B(\alpha) \sim 10^{-3}$ to 10^{-4} .

A number of attempts have been made to isolate this quantity; none have yet been successful. Typically, ^{19}Ne has been produced by few nucleon transfer reactions, such as $^{20}\text{Ne}(d,t)^{19}\text{Ne}$, or the kinematic inverse $d(^{20}\text{Ne},t)^{19}\text{Ne}$, or $^{19}\text{F}(^3\text{He},t)^{19}\text{Ne}$. Such methods have the advantage that the state of interest may be populated with reasonable cross section (>10 s of $\mu\text{b}/\text{sr}$). Efforts to observe the subsequent alpha decay, in the inverse kinematic regime benefit from strong kinematic focusing of the reaction products but can be hampered by high beam-related backgrounds. All

efforts to study this alpha decay suffer from the complex level scheme of ^{19}Ne at low excitation energy, which contains a $9/2^-$ state just ~ 100 keV away at $E_x = 4.140$ MeV.

We have performed a test experiment to produce ^{19}Ne through an alternative method via the $^{12}\text{C}(^{11}\text{C},\alpha)^{19}\text{Ne}$ reaction using a 33 MeV ^{11}C beam from the BEARS facility at LBNL. Alpha particles from the $^{12}\text{C}(^{11}\text{C},\alpha)^{19}\text{Ne}$ reaction and elastically scattered ^{11}C ions were detected in two Position-Sensitive Strip Detectors (PSSDs) placed on either side of the beam. Two surface barrier detectors at small angles monitored the quality and intensity of the ^{11}C beam. The beam intensity on target was estimated to be between 1 and 2×10^8 particles per second. Figure I-3a shows a representative $^{11}\text{C} + ^{197}\text{Au}$ elastic scattering Q-value

spectrum, and Fig. I-3b displays the Q-value spectrum for the $^{12}\text{C}(^{11}\text{C},\alpha)^{19}\text{Ne}$ reaction. The lines in Fig. I-3b indicate the positions of various groups of states in ^{19}Ne . The estimated cross section for this reaction for the ground-state group is approximately $100 \mu\text{b}/\text{sr}$.

A number of improvements in terms of collimation, beam quality, and detection efficiency must be explored before it can be known whether this method can successfully compete with alternative methods of studying the very weak alpha-decay branch of the 4.033-MeV state in ^{19}Ne . It is clear from this test, however, that with the current beam intensities available from BEARS, light-heavy-ion reactions of this type are within reach of current experimental methods.

*Argonne National Laboratory and Yale University, †Argonne National Laboratory and University of Pennsylvania, ‡Lawrence Berkeley National Laboratory, §Florida State University

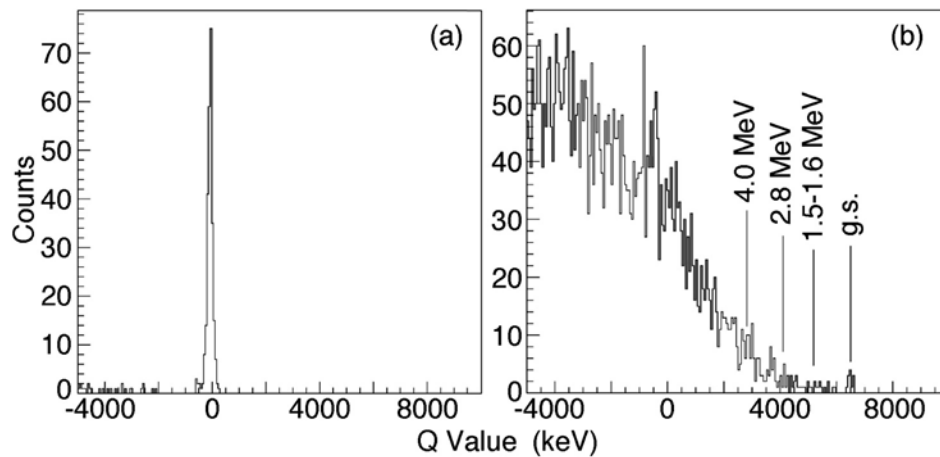


Fig. I-3. (a) Q-Value spectrum for $^{11}\text{C} + ^{197}\text{Au}$ elastic scattering. (b) Q-Value spectrum for the $^{12}\text{C}(^{11}\text{C},\alpha)^{19}\text{Ne}$ reaction. The vertical lines indicate the positions of various groups of excited states in ^{19}Ne .

a.4. Observation of γ -Ray Transitions in the rp Breakout Nucleus ^{20}Na (D. Seweryniak, A. Heinz, R. V. F. Janssens, T. L. Khoo, H. Mahmud, E. Rehm, P. J. Woods,* F. Sarazin,* J. Goerres,† A. Aprahamian,† M. Shawcross,† J. Shergur,‡ M. Wiescher,† and A. Woehr‡)

The reaction sequence $^{15}\text{O}(\alpha,\gamma)^{19}\text{Ne}(p,\gamma)^{20}\text{Na}$ is thought to be the dominated nucleosynthetic mechanism responsible for breakout from the hot CNO cycles into the rp-process. However, neither of these reaction rates have yet been determined. One of the key uncertainties in the $^{19}\text{Ne}(p,\gamma)^{20}\text{Na}$ reaction is the structure of the resonance states in ^{20}Na at an excitation energy of about

2.6 MeV near reaction threshold, which are thought to dominate the astrophysical reaction rate.

An in-beam γ -ray experiment was performed using the Argonne Fragment Mass Analyzer to study γ -decaying states in ^{20}Na . The $^{10}\text{B}(^{12}\text{C}, 2n)$ reaction was used to populate excited states in ^{20}Na . Gamma rays were detected using 2 Ge clover detectors and a 4π array of

BGO scintillators placed around the target. Recoiling reaction products were separated from the beam and dispersed according to their mass over charge state ratio in the FMA. Mass-20 residues, selected by the slits at the focal plane of the FMA, were stopped in an ionization chamber and their atomic number was deduced based on the energy loss and energy measurement. Several γ -ray transitions were assigned to ^{20}Na . Figure I-4 shows the spectrum of γ rays

detected in the Ge detectors and associated with ^{20}Na . The proposed preliminary partial ^{20}Na level scheme is shown in Fig. I-5. The energies of the first two excited states are in agreement with results of previous transfer reaction studies. The state deexcited by the 1029 keV γ -ray was seen for the first time. Evidence for other transitions feeding the 798-keV state, including a possible transition deexciting the 2650 keV state, is currently under evaluation.

*University of Edinburgh, United Kingdom, †University of Notre Dame, ‡University of Maryland

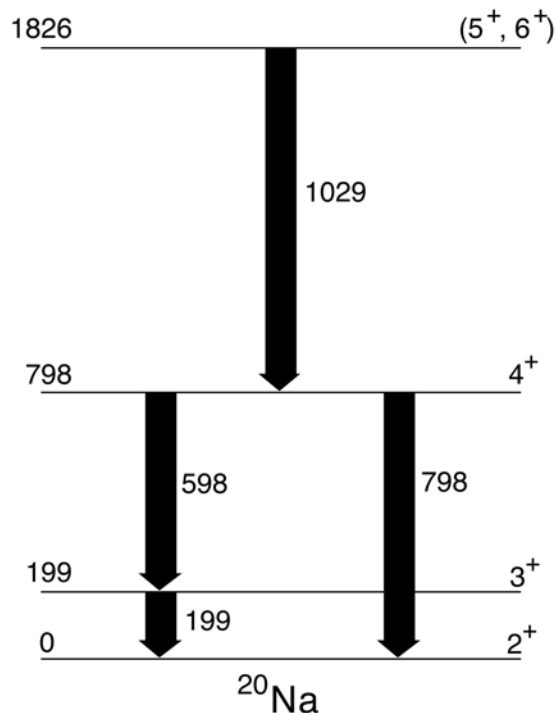


Fig. I-4. Preliminary partial ^{20}Na level scheme.

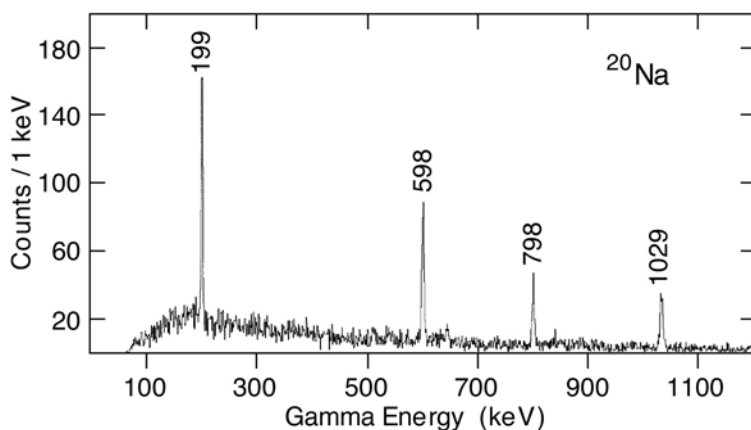


Fig. I-5. Ge γ -ray spectrum tagged by ^{20}Na residues selected in the FMA.

a.5. Production of a ^{20}Na Beam Via the In-Flight Technique (K. E. Rehm, J. Greene, A. Heinz, D. Henderson, R. V. F. Janssens, C. L. Jiang, E. F. Moore, R. C. Pardo, T. Pennington, J. P. Schiffer, G. Zinkann, M. Paul,* and W. Winter†)

For our study of the ^8B neutrino spectrum using the implantation technique (see contribution a.1) a calibration source with α -energies in the range of 2 - 5 MeV was required. In order to implant the nuclei sufficiently deep into a Si detector they needed to be available as a beam and should have a half-life of about 1 sec. The best candidate decays were found to be ^{20}Na which decays via β^+ -emission to high-lying states in ^{20}Ne which then subsequently decay into $\alpha + ^{16}\text{O}$.

The optimum reaction to produce ^{20}Na would be $^{20}\text{Ne}(p,n)^{20}\text{Na}$. However, because of its negative Q-value of $Q = -14.66$ MeV it requires a ^{20}Ne beam of at least 300 MeV in order to produce it with sufficient intensity via the inverse $p(^{20}\text{Ne}, ^{20}\text{Na})n$ reaction. This cannot be done with the present resonator configuration at ATLAS. Since for a calibration experiment even a low intensity beam is sufficient we have chosen the $^3\text{He}(^{19}\text{F}, ^{20}\text{Na})2n$ reaction, which has a Q-value of only -9.54 MeV.

A gas cell, filled with 700 mbar of ^3He at $T = 93$ K was bombarded with a 200-MeV ^{19}F beam from the ATLAS accelerator. After optimizing the beam transport system downstream of the production target a rate of $10^{20}\text{Na}/(\text{sec pnA of incident beam})$ was measured in the scattering chamber of the magnetic spectrograph. Although the intensity is considerably smaller than the one obtained for beams produced via (p,n) or (d,n) reactions, it was nevertheless sufficient to perform an in-situ calibration of the Si detector used in the ^8B experiment.

After treating all ATLAS resonators with the new high-pressure rinse technique it can be expected that ^{20}Ne beams with sufficient energy will be available to produce ^{20}Na via the more favorable (p,n) reaction which would lead to a 100 fold increase in beam intensity for producing this proton drip line nucleus.

*Hebrew University, Jerusalem, Israel, †University of California, Berkeley

a.6. Ne, Na and Al Burning in Astrophysically Important (p, γ) Reactions (C. J. Lister, M. P. Carpenter, G. Mukherjee, K. E. Rehm, A. H. Wuosmaa, D. G. Jenkins,* B. Truett,† B. R. Fulton,‡ J. Pearson,‡ R. A. Kaye,† M. Freer,§ A. O. Macchiavelli,¶ P. Fallon,¶ and A. Görgeň¶)

The breakout from the CNO burning cycle that is needed to produce heavier elements is through thermonuclear processes involving (p, γ) and (α , γ) capture reactions. The synthesis sites need to be hydrogen and helium rich, and are thought to occur in massive stars ($T \sim 10^8$ K) or in nova explosions ($T > 10^9$ K). The reactions rates are sufficiently high that many of the target nuclei are unstable, as they undergo new reactions faster than they can decay back to stability. The reaction rates are dominated by the properties of a few levels near the reaction threshold. Locating these key states and their quantum numbers is crucial in establishing the reaction rates, which, after suitable modeling, can tell us a great deal about both the synthesis sites and the final isotopic abundances. For stable nuclei, the (p, γ) and (α , γ) capture rates can be studied directly in the laboratory. The particle unbound states of interest are those with relatively large gamma branching ratios ($\Gamma_\gamma/\Gamma_{\text{tot}}$). For unstable nuclei, which are very important in this problem, the issue is more challenging and a variety of ingenious

experimental approaches have been used to infer reaction rates. These include fabrication of radioactive targets, using direct reactions like ($^3\text{He},d$), producing radioactive beams then studying kinematically inverse reactions, and invoking isospin symmetry to infer the positions and properties of the key states.

Big arrays, like Gammasphere, can shed new light on this interesting problem. Using near-barrier heavy-ion reactions, a broad range of states in the excitation region of interest can be populated. As only γ -rays are measured, the experiments are most sensitive to the key states of interest, those with relatively large γ -branches. The excitation energy of the states can be determined to a few keV, angular distributions can constrain spins, lifetimes can determine total widths, and γ - γ coincidences can resolve close-lying doublets. These data, when taken in conjunction with information from reaction studies (which can measure the far-stronger charged-particle breakup branches), can strongly constrain the problem. We have used the

$^{12}\text{C}(^{12}\text{C},n)^{23}\text{Mg}$, $^{12}\text{C}(^{12}\text{C},p)^{23}\text{Na}$ and $^{12}\text{C}(^{16}\text{O},n)^{27}\text{Si}$ reactions to investigate the $^{22}\text{Na}(p,\gamma)^{23}\text{Mg}$, $^{22}\text{Ne}(p,\gamma)^{23}\text{Na}$ and $^{26}\text{Al}(p,\gamma)^{27}\text{Si}$ sodium, neon, and aluminum burning processes. The experiments used intense (up to 150 pna) beams of low energy (20-30 MeV) carbon and oxygen from the ATLAS accelerator at ANL and the 88" cyclotron at LBNL, impinging on thin, (50-100 $\mu\text{g}/\text{cm}^2$) isotopically enriched carbon targets. Many results were obtained for the astrophysically critical states, and some new states found. The impact of these new measurements has been evaluated by recalculating the reaction rates as a

function of temperature. The predicted reaction rates have been redetermined. In some places they have changed by orders of magnitude and the uncertainties are greatly reduced. It appears that this technique is quite general and many similar problems might be addressed this way. The $A = 20$ case is discussed in section a.4. of this chapter. One example is shown in Fig. I-6, where the recalculated reaction rate for $^{22}\text{Na}(p,\gamma)^{23}\text{Mg}$ is shown as a function of T_9 , the temperature in billions of degrees. Both the reaction rate envelope and its uncertainty are now more tightly defined.

*University of Liverpool, United Kingdom, †Purdue University Calumet, ‡University of York, United Kingdom, §University of Birmingham, United Kingdom, ¶Lawrence Berkeley National Laboratory

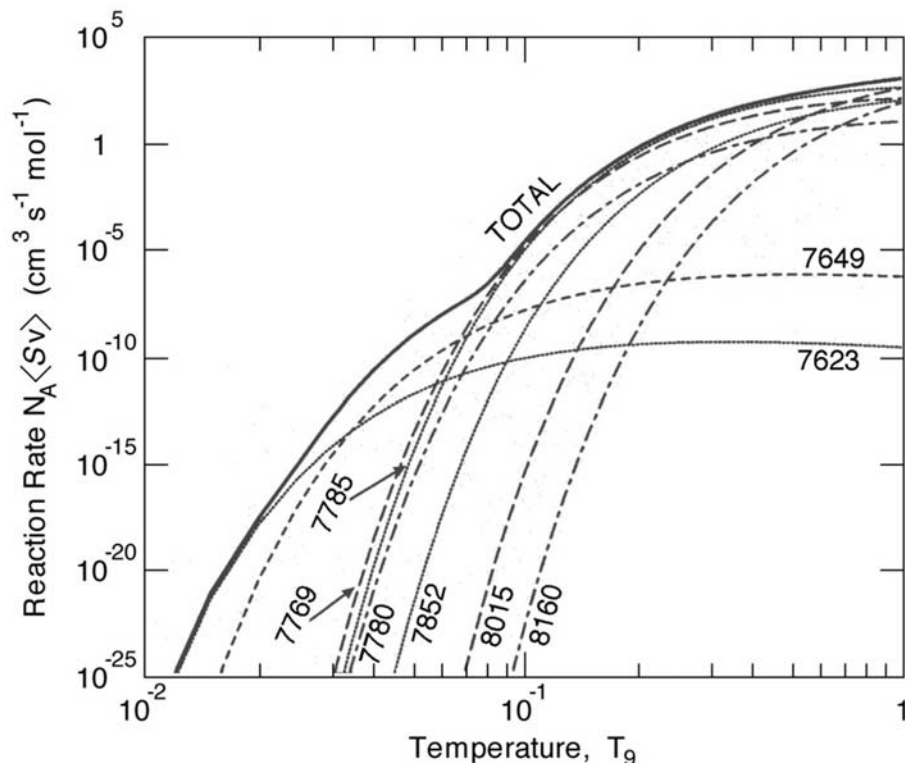


Fig. I-6. The $^{22}\text{Na}(p,\gamma)^{23}\text{Mg}$ reaction rate recalculated with the new spectroscopic information gathered from the present Gammasphere study. At some temperatures the new reaction rates are more than two orders of magnitude different from the current literature estimates.

a.7. Measurement of ^{44}Ti Half-Life (I. Ahmad, J. P. Greene, E. F. Moore, W. Kutschera,* and M. Paul†)

We have continued the measurement of ^{44}Ti half-life at Argonne and Jerusalem, which we started in March 1992, with the aim of improving the precision in the half-life value. The half-life determined from 5 years decay was published¹ in 1998. Now we have data for

about 10 years decay; the last set of spectra was measured in December 2001. The half-life is being measured by recording spectra of a mixed source of ^{44}Ti and ^{60}Co with a 25% germanium detector at regular intervals. At Argonne the spectra of the mixed source

are being measured at two source-to-detector distances of 5.2 cm and 10.2 cm. The half life values were obtained by analyzing the 1157/1173 and 1157/1333 ratios of the ^{44}Ti and ^{60}Co gamma rays. The preliminary analysis shows that the half-life of 59.2 ± 0.6 yr reported in our 1998 article is still correct within

the quoted uncertainty. The decay of the 1157/1173 ratio measured for a source-to-detector distance of 5.2 cm is displayed in Fig. I-7. We plan to measure one more set of spectra and then analyze and publish the result.

*University of Vienna, Austria, †Hebrew University, Jerusalem, Israel

¹Ahmad *et al.*, Phys. Rev. Lett. **80**, 2550 (1998).

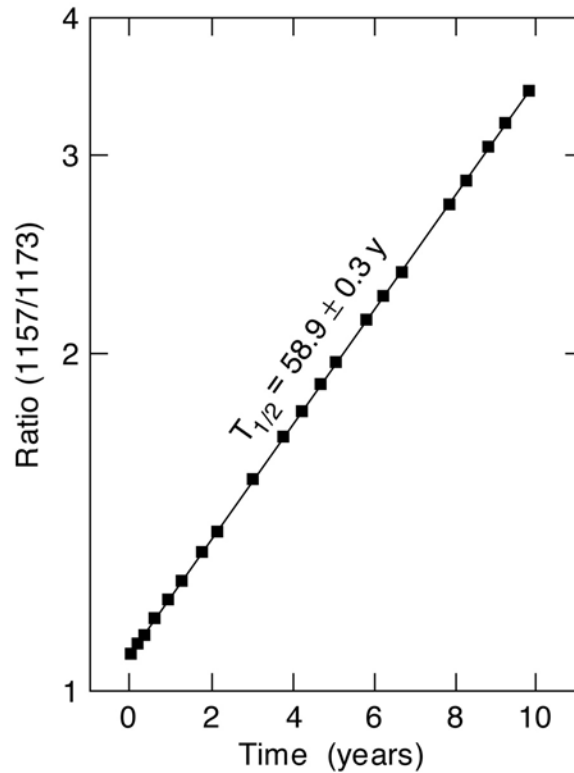


Fig. I-7. Semilogarithmic plot of the ratio of counts in the 1157-keV peak of ^{44}Ti and 1173-keV peak of ^{60}Co against decay time. The measurements were performed at ANL using a mixed source of ^{44}Ti and ^{60}Co .

a.8. The $^{40}\text{Ca}(\alpha,\gamma)^{44}\text{Ti}$ Reaction Measured by Counting of ^{44}Ti Residual Nuclei
 (I. Ahmad, J. Caggiano, J. Greene, A. Heinz, D. Henderson, R. V. F. Janssens, C. L. Jiang, R. C. Pardo, T. Pennington, K. E. Rehm, G. Savard, R. Vondrasek, I. Wiedenhöver, M. Paul,* C. Feldstein,* D. Berkovits,† C. Bordeanu,‡ J. Goerres,§ M. Hass,‡ S. K. Hui,* S. Jiang,* G. Verri,* and M. Wiescher§)

The importance of ^{44}Ti production in supernova nucleosynthesis was emphasized in the last years by the measurement of the 1.157 MeV light of supernova remnants by γ -ray astronomy.^{1,2,3} Produced in the decay of 59.2-yr ^{44}Ti ground state to ^{44}Sc and stable- ^{44}Ca isobars, it clearly indicates fresh nucleosynthesis of ^{44}Ti in these sites and confirmed the hypothesis of a type-II supernova in the case of the Cassiopea A remnant.^{4,5} Among the many production and

destruction nuclear reactions that bear on the net ^{44}Ti yield in the supernova environment,⁶ the α capture on ^{40}Ca stands out due to the importance of the α -rich freezeout phase conjectured by astrophysical models.

The $^{40}\text{Ca}(\alpha,\gamma)^{44}\text{Ti}$ reaction has been studied only by prompt γ -ray spectroscopy, yielding values for the resonance strengths and partial γ widths of excited levels in ^{44}Ti for $E_{\text{cm}} > 7.6$ MeV.^{7,8,9} We propose here

the counting of ^{44}Ti ground state nuclei produced in a laboratory activation experiment of ^{40}Ca on He. The recoiling ^{44}Ti ions are collected in a catcher, chemically separated using a $^{\text{nat}}\text{Ti}$ carrier and directly counted by accelerator mass spectrometry (AMS). Unlike the prompt γ -ray technique, this method yields values which are independent of the γ decay scheme and γ branching ratios in the ^{44}Ti compound nucleus. The AMS measurement of the $^{44}\text{Ti}/\text{Ti}$ ratio, together with the known amount of Ti carrier added, determine the number of ^{44}Ti nuclei produced in the activation, independent of any chemical yield or accelerator-transmission efficiency.

A ~ 1 μA beam of $^{40}\text{Ca}^{11+}$ ions from the ECR-ATLAS system bombarded a high-purity-He filled chamber (12 Torr); a 1.5-mg/cm² Ni rotating window was used to contain the gas and dissipate the beam power loss. The mean laboratory beam energy in the He gas was selected to populate a strong resonance at $E_{\text{cm}} = 1.13$ MeV/n. Recoiling ^{44}Ti nuclei were implanted in a water-cooled Cu catcher. A small Bragg chamber monitored continuously ions scattered off the entrance

Ni window. Correction was made for a 8.5% contamination of ^{40}Ar in the incident beam; these ions cannot produce ^{44}Ti in the He target. After irradiation (11 pmC) and radioactive cooling, a thickness of 10 mg/cm² was etched from the Cu catcher surface by an acid solution containing 3 mg $^{\text{nat}}\text{Ti}^{4+}$. After chemical separation of Ti and purification from Ca contamination, the ~ 4 mg sample of TiO_2 obtained was inserted in the cathode holder of the high-intensity Cs sputter source of our AMS system at the Weizmann Institute. A group of 20 ^{44}Ti counts was clearly identified and discriminated (Fig. I-7A) from the main background of ^{44}Ca (chemical impurity). An off-resonance activation, an activation made on Ar gas instead of He and the measurement of an unactivated Cu catcher lead to 0 or 1 ^{44}Ti count in the same conditions. The resonance strength measured by the on-resonance activation is 7.4 ± 2.5 eV in excellent agreement with previous prompt- γ measurements for two close-by levels in ^{44}Ti . We hope to extend now the technique to the lower energy range important for supernova nucleosynthesis.

*Hebrew University, Jerusalem, Israel, †Soreq NRC, Yavne, Israel, ‡Weizmann Institute, Rehovot, Israel,

§University of Notre Dame

¹A. F. Inyudin, *et al.*, A&A, **284**, L1 (1994).

²L.-S. The, *et al.*, A&A Suppl. Ser. **120**, 357 (1996).

³D. H. Hartmann, *et al.*, Nucl. Phys. A **621**, 83c (1997).

⁴I. Ahmad, *et al.*, Phys. Rev. Lett. **80**, 2550 (1998).

⁵J. Görres, *et al.*, Phys. Rev. Lett. **80**, 2554 (1998).

⁶L.-S. The, *et al.*, Ap. J. **504**, 500 (1998).

⁷E. L. Cooperman, M. H. Shaprio, and H. Winkler, Nucl. Phys. A **284**, 163 (1977).

⁸W. R. Dixon, *et al.*, Phys. Rev. C **15**, 1896 (1977).

⁹W. R. Dixon, *et al.*, Nucl. Phys. A **363**, 173 (1981).

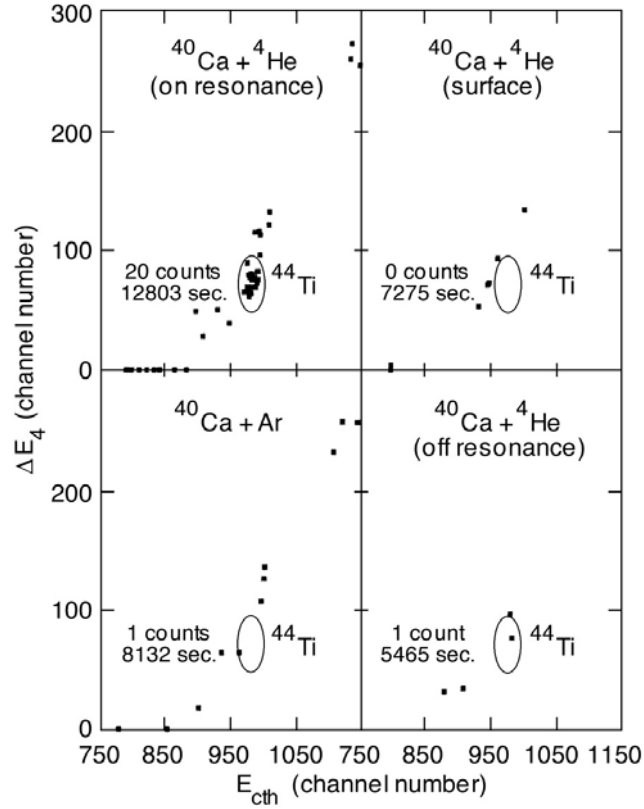


Fig. I-7A. Two-dimensional identification spectra of residual energy (ΔE_4) versus energy (E_{cth}); the events are first filtered through a software window on energy-loss parameters ΔE_1 and ΔE_2 to eliminate most of the ^{44}Ca background. The spectra are measured for Ti extracted from Cu catchers after He activation on resonance ($E_{cm} = 4.0 - 4.2 \text{ MeV}$; upper left) and off resonance ($E_{cm} = 3.8 - 4.0 \text{ MeV}$; lower right) and a background run (activation on Ar gas; lower left). The upper right spectrum was obtained from the etching of the surface of the on-resonance Cu catcher; the absence of ^{44}Ti atoms shows that ^{44}Ti was implanted in Cu at a depth $\geq 1 \text{ mg/cm}^2$.

B. STRUCTURE OF NUCLEI VERY FAR FROM THE VALLEY OF STABILITY

The program to explore the structure and stability of nuclei along the proton dripline continues to be a forefront theme in our nuclear structure research. It has many interesting facets, both for astrophysical processes and for extending our understanding of the structure and stability of nuclei. It provides a natural bridge that connects contemporary research with future projects which exploit radioactive beams. The successful Gammasphere campaign at ATLAS during 1998-2000 led to the acquisition of a vast amount of new data on far from stability nuclei. During the present LBNL Gammasphere cycle, we have been able to complete much of the analysis backlog, resulting in an unusually high level of publication. Plans for a higher sensitivity level of operation of Gammasphere are being developed, with the possibility of spectroscopy even further from stability during the next cycle starting in 2002. The techniques of proton decay spectroscopy also continue to be refined, allowing studies of shorter lived, and more weakly produced species further from stability. In both cases, upgrades to the FMA have increased sensitivity.

The possibility of studying the structure of very neutron-rich nuclei in the future seems very good, including some nuclei close to the predicted r-process nucleosynthesis trajectory. In this domain conventional heavy-ion fusion-evaporation is not useful, due to the curvature of the valley of stability, but by investigating the prompt gamma-ray spectroscopy of fission fragments, and by studying gamma-rays following multi-nucleon transfer reactions, very considerable progress is possible. Many of these studies provide a natural compliment to the data recently obtained from fast-fragmentation facilities. The fast fragmentation allows the identification of low-lying states in these nuclei, which can be developed in many cases with detailed spectroscopy using Gammasphere. Particular progress has been made in the region around ^{132}Sn . In addition to spectroscopic information, the precise determination of the masses of hundreds of very neutron-rich fission fragments now appears possible, using the gas-cooler and CPT.

B.1. Proton-Rich Nuclear Spectroscopy

b.1.1. Low Level Density in Odd-Odd $N = Z$ Nuclei in the $A \sim 70$ Region (C. J. Lister, D. G. Jenkins,^{a,*†} N. S. Kelsall,[‡] D. P. Balamuth,^{*} M. P. Carpenter, [†] T. A. Sienko, [†] S. M. Fischer,[§] R. M. Clark,[¶] P. Fallon,[¶] A. G6rgen,[¶] A. O. Macchiavelli,[¶] E. Svensson,[¶] R. Wadsworth,[‡] W. Reviol,^{||} D. G. Sarantites,^{||} G. C. Ball,^{**} J. Rikovska Stone,^{††} ^{‡‡} O. Juillet,^{§§} P. Van Isacker,^{§§} A. V. Afanasjev,^{†,¶¶,||} and S. Frauendorf^{¶¶,***})

Studying odd-odd $N = Z$ nuclei above nickel is topical for several reasons. The nuclei lie along the explosive rp-nucleosynthesis path, so their masses, shapes, decays and isomers need to be known for modeling x-ray bursts. The nuclei decay by "super allowed" Fermi β -decays, which, if precisely measured, can allow searches for physics beyond the standard model as long as small structure-dependent corrections can be made. Finally, the nuclei have near-degenerate low-lying configurations with $T = 0$ and $T = 1$ symmetries, so information on both long- and short-range np correlations may be sought. The experiments are technically challenging, as the production cross-sections are always low, and the decay patterns complicated. The key information lies in the low spin

states, but only heavy-ion reactions, either through fragmentation or fusion, can allow us access to these nuclei for spectroscopy. However, in the last few years heroic progress has been made in experiments on copper, gallium, arsenic, bromine, rubidium and yttrium nuclei which span this region. There have also been dozens of theoretical investigations into these matters. We have focused on a detailed study of $^{70}\text{Br}^1$, a nucleus which has a β -decaying high spin isomer, but otherwise no other levels were known. The experiments were aimed at as complete spectroscopy as is possible using current techniques, with the goals of investigating np-interactions and locating the (known) isomer. The experiments were quite successful in both regards.

A compilation of information so far gleaned from all the odd-odd nuclei in the region reveals a striking difference between the $N = Z$ nuclei and their neighbors. Several conclusions can be drawn from the data collected to date:

- (1) The number of states in the first MeV of excitation in the $N = Z$ nuclei is very low. This does not seem to be an experimental artifact. Figure I-8 illustrates the difference between $N = Z$ and $N > Z$ odd-odd nuclei in the region. This observation strongly constrains correlations between the uncoupled neutron and proton.
- (2) There is little evidence for low-lying $J^\pi = 1^+$ states, which would be a fingerprint of very strong $T = 0$ np-pairing correlations.
- (3) The low-lying shapes of the odd-odd nuclei seem to closely follow their neighboring even-even cores.
- (4) The location of analogs to the ground state bands in $(Z - 1, N + 1)$ isobars is difficult, as these states are quite non-yrast, so “mirror symmetry” tests are extremely challenging.
- (5) The known isomers arise from a wide variety of shapes and structure and do not have a single, common cause.

^aPresent address: Oliver Lodge Laboratory, University of Liverpool, UK, ^{*}University of Pennsylvania, [†]Argonne National Laboratory, [‡]University of York, UK., [§]DePaul University, [¶]Lawrence Berkeley National Laboratory, ^{||}Washington University, ^{**}TRIUMF, ^{††}University of Oxford, UK, ^{‡‡}University of Maryland, ^{§§}Grand Accelérateur National d'Ions Lourds, France, ^{¶¶}University of Notre Dame, ^{|||}University of Latvia, ^{***}IKH, Rossendorf Research Centre, Germany
¹D. G. Jenkins *et al.*, Phys. Rev. **C65**, 064307 (2002).

ANL-P-22,765

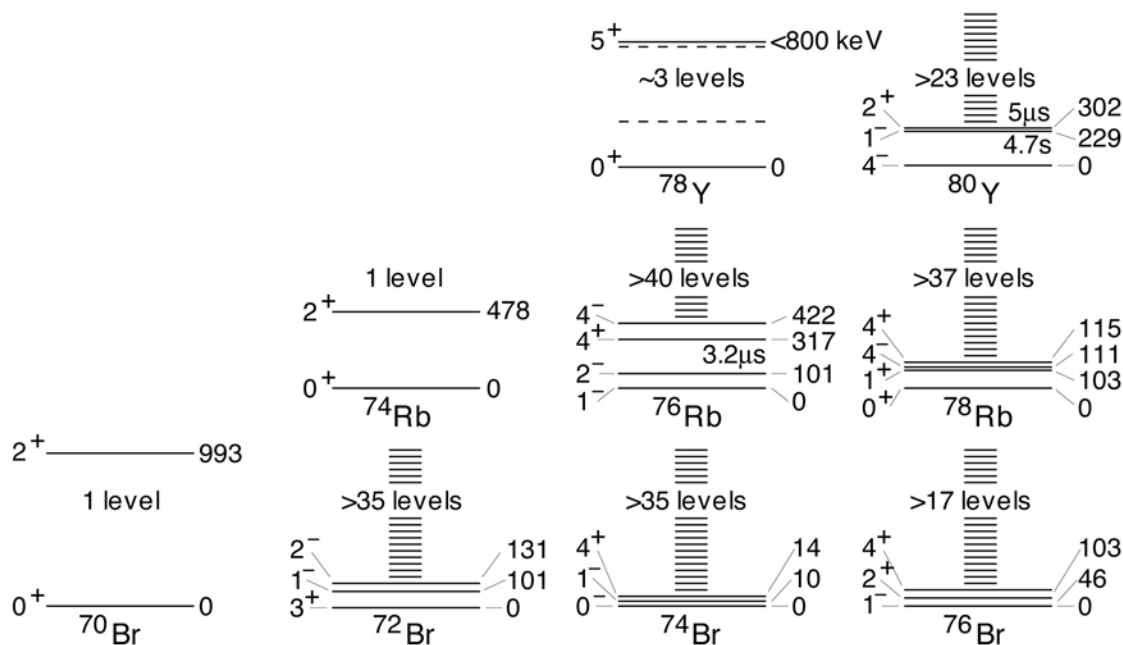


Fig. I-8. A compilation of known low-lying states in odd-odd nuclei in the mass $A \sim 70$ region. It is clear that the $N > Z$ nuclei have many more states than those with $N = Z$. Some of this difference can be attributed to collective rotational bands built on the intrinsic configurations, but even after accounting for this difference, there are still many less intrinsic states in the $N = Z$ nuclei.

b.1.2. Alignment Effects in $^{72,73}\text{Kr}$ (S. M. Fischer,* C. J. Lister, M. P. Carpenter, R. V. F. Janssens, D. Seweryniak, D. P. Balamuth,† N. S. Kelsall,‡ G. C. Ball,§ R. Bauer,¶ J. A. Becker,¶ L. A. Bernstein,¶ R. M. Clark,|| J. Durell,** P. Fallon,|| N. Fotiades,†† S. J. Freeman,** P. E. Garrett,¶ P. A. Hausladen,† D. G. Jenkins,† M. Leddy,** A. O. Macchiavelli,|| J. Ressler,‡‡ D. G. Sarantites,¶¶ D. C. Schmidt, ‡‡‡ J. Schwartz,§§ D. Svelnys, ‡‡‡ C. E. Svensson,|| B. J. Varley,** S. Vincent,|||| R. Wadsworth,‡ A. N. Wilson,‡ A.V. Afanasjev,|||| S. Frauendorf,|||| I. Ragnarsson,***

Theory predicts that neutron-proton (np) pairing effects are likely to be quite strong for $N = Z$ nuclei, and then diminish rapidly as one moves away from $N = Z$. It has proven to be both an experimental and theoretical challenge to observe and predict evidence for such effects. One possible effect may be a delay in the frequency at which np pairs break and their angular momentum aligns with the angular momentum of the rotating core. This was first suggested by de Angelis *et al.*,¹ in a study of high spin states in the $N = Z$ nucleus ^{72}Kr . We have recently extended this work on ^{72}Kr , and made additional studies of the $N = Z$ nuclei ^{76}Sr and ^{80}Zr .²

High spin states in ^{72}Kr were populated in the $^{40}\text{Ca}(^{40}\text{Ca},2\alpha)$ reaction at 160 MeV. Data were collected at the ATLAS facility with the Gammasphere and Microball detector arrays. The level scheme for ^{72}Kr was deduced by analyzing 2α -gated $\gamma\gamma$ coincidences and carefully subtracting backgrounds due to feedthrough from the $2\alpha p$ and $2\alpha 2p$ reaction channels. Particle-gated γ -ray angular distributions were used to determine the multipolarity of the transitions. The ground state band was extended to $J^\pi = (26^+)$. Figure I-9 shows the kinematic moments of inertia, $J^{(1)}$, versus frequency for ^{72}Kr (diamonds), ^{74}Kr (dashed) and ^{76}Kr (dotted). The data for $^{74,76}\text{Kr}$ show the sharp simultaneous alignment of neutron and proton pairs at similar frequencies of $\hbar\omega \sim 0.65$ MeV, while the data for ^{72}Kr indicate a delayed, gradual alignment as a function of frequency. This behavior is very different from that of the other $N = Z$ nuclei ^{76}Sr ² and ^{88}Ru ,³ where a much more modest delay in the alignment is observed.

We have performed two studies of ^{73}Kr ⁴ to determine whether a similar dramatic delay occurs for the neighboring odd-A isotope. In the first study, ^{73}Kr was created in the same $^{40}\text{Ca} + ^{40}\text{Ca}$ study that produced ^{72}Kr , but this time utilizing the $\alpha 2pn$ channel and an array of 20 liquid scintillator counters from the Universities of Manchester and Pennsylvania. The second study was also performed at ATLAS, and used the $^{40}\text{Ca}(^{36}\text{Ar},2pn)$ reaction at 145 MeV with the Gammasphere and Microball arrays plus a complement of 30 neutron detectors. The negative parity bands 1 and 2 of ^{73}Kr have been extended to spins $(63/2^-)$ and $(61/2^-)$, and the positive parity band 3 to spin $(57/2^+)$. In addition, the signature partner of the positive parity band was observed for the first time to $J^\pi = (31/2^+)$. Figure I-10 shows the Routhians, e' , as a function of the rotational frequency $\hbar\omega$ for bands 1-3. The solid and dashed curves show the results of Total Routhian Surface (TRS) calculations⁴ for two possible configurations. The observed alignment frequencies are systematically delayed relative to the theoretical predictions, although with a much smaller delay than in ^{72}Kr . Similar calculations are in excellent agreement with the experimental data for ^{75}Kr .

The alignment delay in ^{73}Kr is consistent with what might be expected for an odd-A nucleus based on the delays observed for ^{76}Sr and ^{88}Ru . However, whether these delays are indeed a consequence of np pairing remains in question. We know that alignment frequencies depend very sensitively on the shape of the nucleus, and that the nuclear shape can change with rotational frequency, as evident from a recent study of ^{74}Kr .⁵ Because of this, experimental measurements

*Argonne National Laboratory and DePaul University, †University of Pennsylvania, ‡University of York, United Kingdom, §TRIUMF Laboratory, Canada, ¶Lawrence Livermore National Laboratory, ||Lawrence Berkeley National Laboratory, **University of Manchester, United Kingdom, ††Rutgers University, ‡‡University of Maryland, §§Yale University, ¶¶Washington University, ||||University of Notre Dame, ***Lund Institute of Technology, Sweden, †††The Royal Institute of Technology, Sweden, ‡‡‡DePaul University

¹G. de Angelis, *et al.*, Phys. Lett. **B415**, 217 (1997).

²S. M. Fischer, *et al.*, Phys. Rev. Lett. **87**, 132501 (2001).

³N. Marginean, *et al.*, Phys. Rev. C **63**, 031303 (2001).

⁴N. Kelsall, *et al.*, Phys. Rev. C **65**, 044331 (2002).

⁵A. Algora, *et al.*, Phys. Rev. C **61**, 031303 (2000).

of the quadrupole deformation as a function of frequency are essential to our progress in understanding these nuclei, and should help to disentangle the shape and pairing degrees of freedom. The behavior of ^{72}Kr at high spin is clearly unusual and strikingly different from its odd-A neighbor, ^{73}Kr . We note that

an irregular sequence of γ rays was observed to feed into the main cascade above $J = 14$. We are currently working to understand this structure, its relationship to the main cascade which is clearly favored at very high spin, and its relationship to a similar positive parity band in ^{74}Kr .

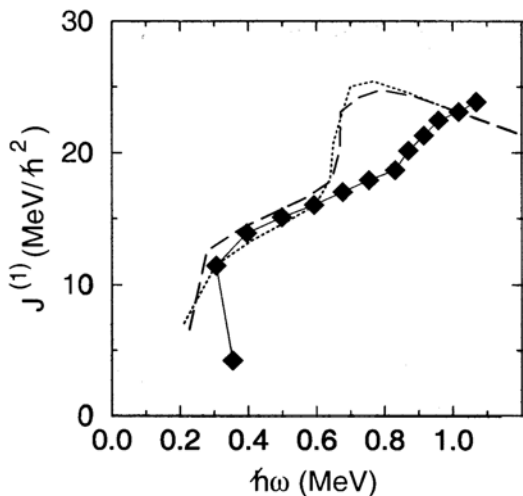


Fig. I-9. Kinematic moment of inertia versus rotational frequency for ^{72}Kr (diamonds), ^{74}Kr (dashed), and ^{76}Kr (dotted).

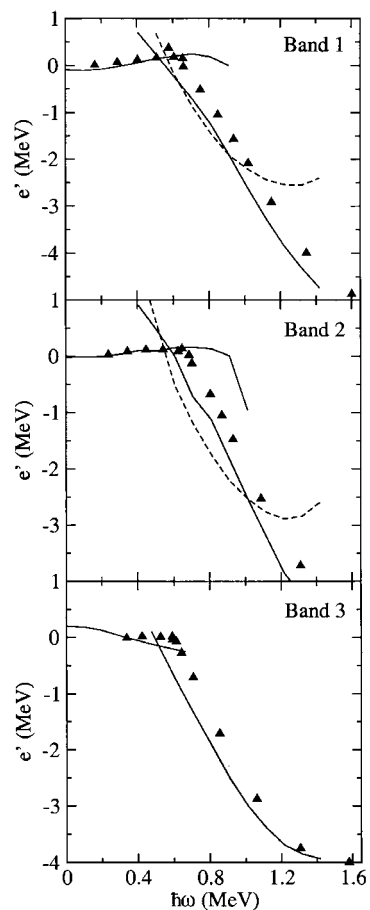


Fig. I-10. Routhians as a function of rotational frequency for the negative parity bands 1 and 2, and positive parity band 3 of ^{73}Kr . The dashed and full curves show the results of TRS calculations for two possible configurations.

b.1.3. New Results in Proton Radioactivity (C. N. Davids, D. Seweryniak, A. Heinz, P. J. Woods,* J. J. Ressler,† J. Shergur,† H. Mahmud,* P. Munro,* A. Robinson,* T. Davinson,* A. A. Sonzogni,‡ and W. B. Walters†)

The new proton emitter ^{135}Tb has been observed. It was produced with an estimated cross section of 2 nb via the $^{92}\text{Mo}(^{50}\text{Cr}, p6n)$ reaction, the first time that this extremely weak reaction channel has been used in proton radioactivity studies. The energy spectrum is shown in Fig. I-11. We observe a single proton peak around 1.18 MeV, with a half-life of <1 ms. This proton emitter is expected to be highly deformed. Data analysis is continuing.

A search for the heavy proton emitter ^{191}At ($Z = 85$) proved to be inconclusive. We used the $^{144}\text{Sm}(^{50}\text{Cr}, p2n)$ fusion-evaporation channel, but experienced

problems with target deterioration during bombardment, even though the targets were rotated and the beam was wobbled in the vertical plane to reduce heat deposition. We did observe $A = 191$ recoils, from ^{191}Po , and believe that the experiment to observe ^{191}At is still feasible under improved target conditions.

An experiment to search for the deformed proton emitter ^{125}Pm has been approved by the PAC. This experiment will be performed after installation and testing of the new split anode for the FMA is completed.

*University of Edinburgh, United Kingdom, †University of Maryland, ‡National Nuclear Data Center

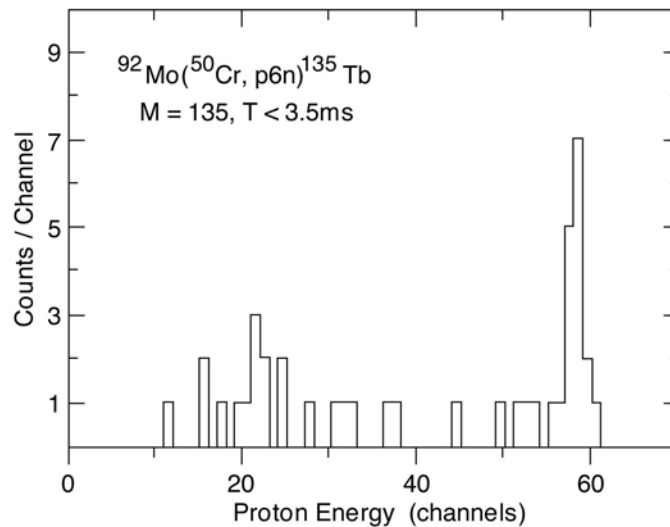


Fig. I-11. Energy spectrum of decay events correlated with $A=135$ and within 3.5 ms of implantation.

b.1.4. Population of the 168 keV First Excited State in ^{103}Sn in the Alpha Decay of ^{107}Te (D. Seweryniak, C. N. Davids, W. B. Walters,* A. Woehr,* M. Lipoglavsek,† J. Shergur,* and J. J. Ressler*)

There has been considerable interest in the structure of the light odd-mass Sn nuclides as the states observed there reflect the interactions between valence $d_{5/2}$ and $g_{7/2}$ neutrons in small numbers. Recently, Fahlander *et al.*¹ reported a new study of the excited states in ^{103}Sn that included a 168 keV energy for the $g_{7/2}$ first excited state. In previous extrapolations from the known structures in the heavier Sn nuclides, such as the one published by Sandulescu, Blomqvist and Liotta,² a smooth upward movement was expected for these $g_{7/2}$ states. In particular, as the $7/2^+$ level is found at 200 keV in ^{105}Sn , an energy as high as 350 keV was expected for this same state in ^{103}Sn . Therefore, the observation of the state at 168 keV was a surprise.

However, the low energy opened up the possibility of populating this state via alpha decay from 3 ms ^{107}Te . The Q-value for alpha decay is about 4.00 MeV, as established by the observation of an alpha energy of 3862(10) keV.³ Recoils with mass 107 from the $^{58}\text{Ni}(^{54}\text{Fe},2p3n)$ reaction were isolated with the Fragment Mass Analyzer and implanted into a double-

sided Si strip detector (DSSD). A gamma-ray detector was mounted behind the DSSD to permit alpha-gamma coincidence measurement. The resulting α spectrum is shown in Fig. I-12 where the small peak about 160 keV below the main peak can be readily seen. The area of this peak corresponds to 0.47(9)% of the area of the peak at 3860 keV. In the α - γ coincidence matrix (see Fig. I-13), there were three events where γ rays at 168 keV were in coincidence with the weak α line, and no γ -ray events in coincidence with the main α branch at 3860 keV. The unhindered $l = 2$ transition rate to the 168 keV level was calculated to be 6% relative to the main branch, yielding a hindrance of about 12. As this is the first well established “fine structure” in this mass region, comparisons with other hindrance factor are not possible.

In another short experiment the $^{58}\text{Ni}(^{58}\text{Ni},2p3n)$ reaction was used to study ^{111}Xe α -decay fine structure. The evidence for α - γ coincidences following the decay of ^{111}Xe is being analyzed.

*University of Maryland, †J. Stefan Institute, Ljubljana, Slovenia

¹C. Fahlander *et al.*, Phys. Rev. C 63, 021307R (2001).

²N. Sandulescu, J. Blomqvist, and R. J. Liotta, Nucl. Phys. A582, 257(1995).

³P. Heine *et al.*, Z. Phys. A34, 225(1991).

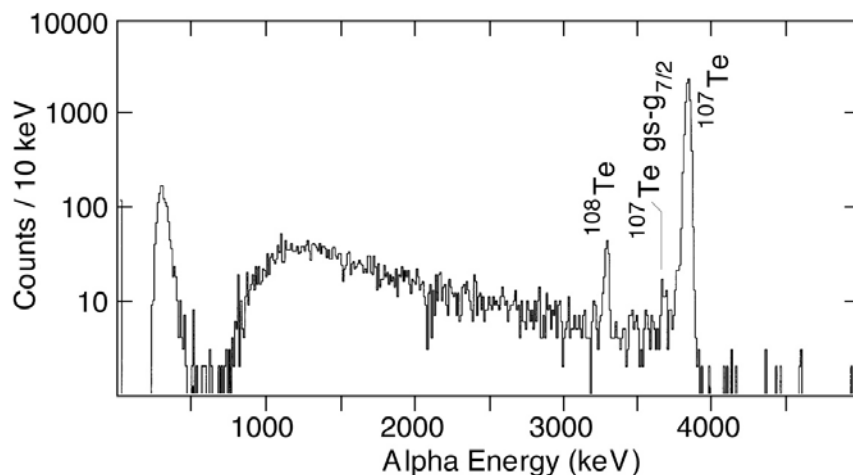


Fig. I-12. A portion of the α -decay spectrum measured using the $^{58}\text{Ni}(^{54}\text{Fe},2p3n)$ reaction.

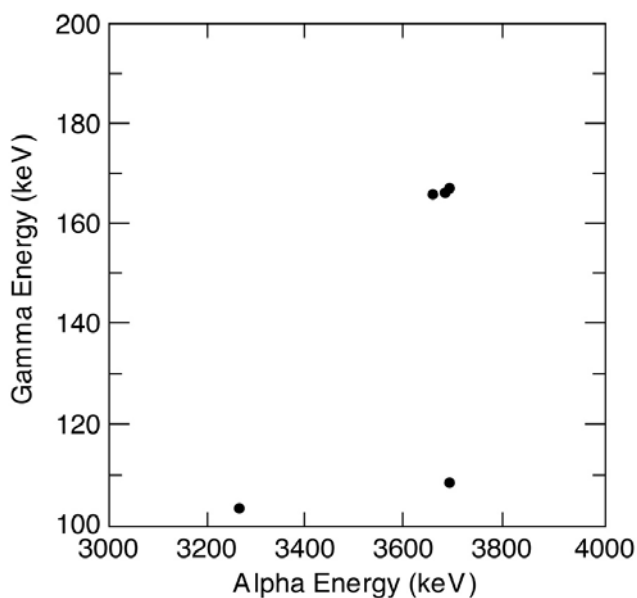


Fig. I-13. A portion of the α - γ matrix, clearly showing the correlation between the α -decay to the 168-keV state and its subsequent γ -decay.

b.1.5. New Method to Study Sub- μ s Proton and α Emitters (D. Seweryniak, A. Heinz, C. N. Davids, G. Mukherjee, J. J. Ressler,* J. Shergur,* and A. Woehr*)

The majority of methods for studying proton and α activities are based on the use of recoil mass separators. The time-of-flight of recoiling nuclei through a separator limits the observable half lives to 0.5 μ s and longer. The most exotic proton emitters have even shorter half lives.

A technique has been being developed to study proton and α activities down to half lives of about 1 ns. The experimental setup is shown in Fig. I-14. Products of heavy-ion fusion evaporation reactions are slowed

down in a Au degrader foil and are implanted on a surface of a thin catcher foil. Beam particles which do not undergo reaction in the target pass through the holes in the degrader and the catcher. The decay protons and α particles emitted by the implants are caught in 3 Si Δ E-E telescopes placed at backward angles with respect to the catcher.

This technique was tested using the $^{58}\text{Ni}(^{58}\text{Ni},p2n)^{113}\text{Cs}$ reaction. ^{113}Cs is a proton emitter which decays with the half life of about 15 μ s. In order to reduce

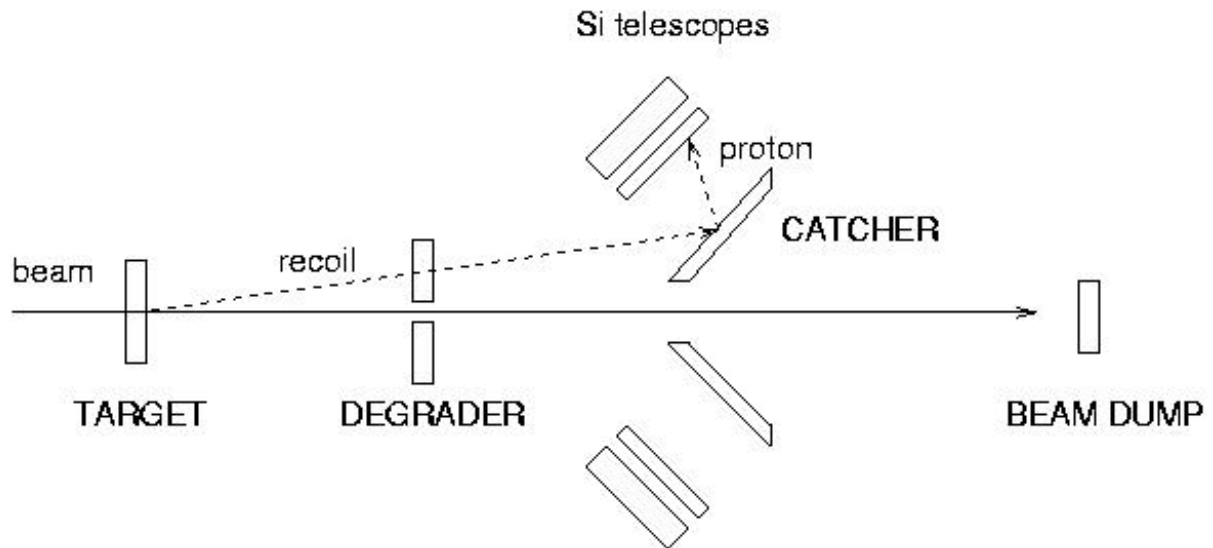


Fig. I-14. The experimental setup for studies of fast proton and α emitters.

background the target was irradiated for about 30 μ s and the beam was turned off for about 60 μ s to measure radioactivity. About 600 protons were observed in about 16 hours during the test. The measured proton spectrum is shown in Fig. I-15. The expected delayed proton peak near 900 keV is clear. Considerable effort is now being directed at understanding the underlying background which determines the sensitivity of this method at present.

In another experiment the $^{32}\text{S}(^{40}\text{Ca},p2n)$ reaction was used to produce the predicted proton emitter ^{69}Br . The upper limit of about 100 ns for its half life has been obtained from in-flight fragmentation experiments at GANIL and MSU. Due to much shorter half life in comparison to ^{113}Cs 3 beam pulses out of 4 were swept away. The background reduction achieved allowed us to study proton emitters produced with a cross section as low as 10 μ b, provided the lifetime were long enough for the residues to reach the catcher. Data analysis is in progress.

*University of Maryland

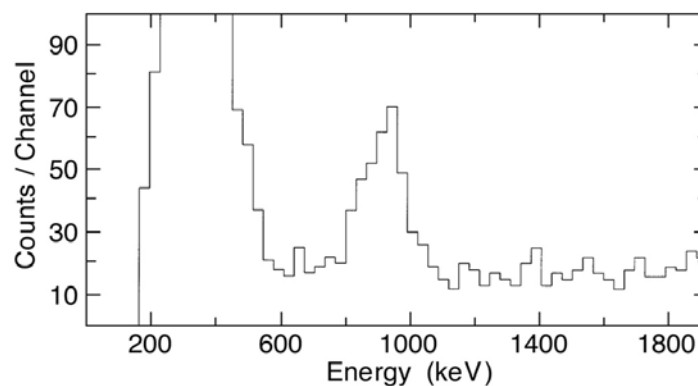


Fig. I-15. ^{113}Cs Proton spectrum measured using the $^{58}\text{Ni}(^{58}\text{Ni},p2n)$ reaction.

b.1.6. Identification of Excited States in ^{140}Dy (M. P. Carpenter, C. N. Davids, R. V. F. Janssens, C. J. Lister, D. Seweryniak, I. Ahmad, A. Heinz, T. L. Khoo, E. F. Moore, F. G. Kondev,* D. M. Cullen,† A. M. Fletcher,† S. J. Freeman,† L. K. Pattison,† J. F. Smith,† A. M. Bruce,‡ K. Abu Saleem,§ G. Mukherjee,¶ C. Wheldon,|| and A. Woehr**)

Recently, a new region of deformed proton emitters has been established ranging from La to Tm. The first cases found were in ^{131}Eu and ^{141}Ho .¹ Initially, the deformation and single-particle parentage of the proton-emitting states were deduced from calculations employing the multiparticle theory of Bugarov and Kadmsky.² In the case of ^{141}Ho , the deformation of the proton emitting states were confirmed by in-beam γ -ray spectroscopy utilizing the Recoil Decay Tagging (RDT) technique which established rotational bands on top of the these states.³ While the deformation of the ^{141}Ho rotational bands deduced from the in-beam work is consistent with those inferred from the proton decay measurements, critical information about the ^{140}Dy daughter nucleus was still missing. One of the important assumptions in the calculations of the decay rates from deformed proton emitters is that the parent and daughter have the same deformation. Proton emission to the 2^+ level in ^{140}Dy has not been observed, however, an upper limit for the branching ratio between the 2^+ and 0^+ feedings into ^{140}Dy has been placed at 1% for decays from the assigned $7/2^-$ ^{141}Ho , ground state.³ Due to the fact that ^{140}Dy decays by β emission, in-beam γ spectroscopy using the RDT technique is not possible.

Recently, Cullen *et al.*⁴ suggested that the yrast band of ^{140}Dy could be identified at least up to the 8^+ level by

measuring γ rays emitted following the decay of a predicted $K = 8^-$ isomer. Studies to identify this isomer in ^{140}Dy and its subsequent γ decay were performed recently at the ATLAS facility by looking for delayed γ rays after implantation of mass selected recoils at the focal plane of the Fragment Mass Analyzer. From an analysis of the data, the 8^- isomer in ^{140}Dy was established at 2.16 MeV, and its subsequent decay by γ emission was followed to the ground state. The half-life of the isomer was measured to be 7.3(15) μs , and the excitation energy of the 2^+ state is 202 keV. Figure I-16 shows both the time spectrum associated with the decay of the isomer and the proposed level structure deduced from the isomer's decay. Using the Grodzins formula, the deformation of the ground state in ^{140}Dy is deduced to be $\beta_2 = 0.24(3)$ which agrees well with the value of 0.25(3) deduced for the rotational bands in ^{141}Ho . The new information obtained here supports the role of deformation in proton emission and the previous assignments of single-particle configurations to the two proton emitting states in ^{141}Ho . In addition, the reduced hindrance factor measured for the isomer is consistent with the trend observed for 8^- isomers in the lighter even-even $N = 74$ isotones.

A paper reporting the results of this work was recently published in Physics Letters B.⁵

*Technology Division, Argonne National Laboratory, †University of Manchester, United Kingdom, ‡University of Brighton, United Kingdom, §Illinois Institute of Technology, ¶University of Massachusetts-Lowell, ||University of Surrey, Guildford, United Kingdom, **University of Maryland

¹C. N. Davids *et al.*, Phys. Rev. Lett. **80**, 1849 (1998).

²V. P. Bugrov and S. G. Kadmsky, Sov. J. Nucl. Phys. **49**, 967 (1989).

³D. Seweryniak *et al.*, Phys. Rev. Lett. **86**, 1458 (2001).

⁴D. M. Cullen *et al.*, Nucl. Phys. **A682**, 264c (2001).

⁵D. M. Cullen *et al.*, Phys. Lett. **B529**, 45 (2002).

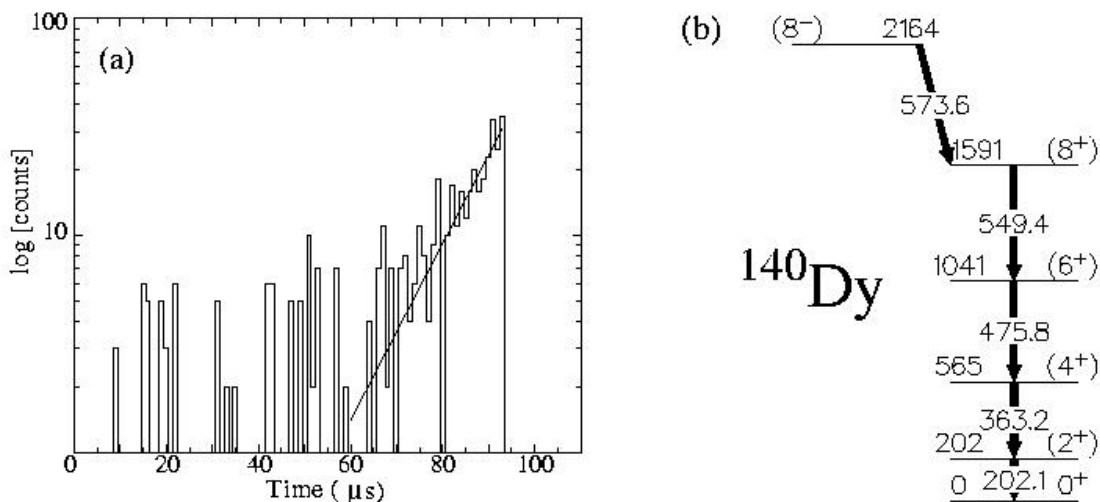


Fig. I-16. (a) Time delay between the implant of a residue and the detection in prompt coincidence of any two of the five γ transitions associated with the decay of the isomer. The solid line represents a fit to the data which yields a half-life of 7.3 μ sec. (b) Proposed level sequence following the decay of the 8⁻ isomer in ^{140}Dy .

b.1.7. Shape Coexistence Far from Stability (M. P. Carpenter, F. G. Kondev, R. V. F. Janssens, I. Ahmad, J. Caggiano, C. N. Davids, A. Heinz, T. L. Khoo, T. Lauritsen, C. J. Lister, G. L. Poli, P. Reiter, D. Seweryniak, A. A. Sonzogni, I. Wiedenhöver, K. Abu Saleem,* H. Amro,† J. A. Cizewski,‡ M. Danchev,§ D. J. Hartley,§ B. Herskind,¶ W. C. Ma,† J. Ressler,|| W. Reviol,** L. L. Riedinger,§ D. G. Sarantites,** S. Siem,†† M. B. Smith,‡ and P. G. Varnette†)

Above $N = 82$, the proton dripline follows closely the outer edges of the well deformed rare-earth region, and the ground states of nuclei which make up the dripline here are expected to have spherical or modestly deformed prolate shapes. Our recent experimental studies have concentrated in the upper portion of this region, namely the study of excited states in Os ($Z = 76$) through Pb ($Z = 82$) isotopes located in the vicinity of the proton dripline. One of our principle motivations has been to characterize the evolution of shape from the well studied deformed region to the near spherical ground states which constitute the dripline proton emitters.

In-beam γ -ray studies of such heavy systems far from stability are hampered by the large fission cross sections associated with the heavy-ion fusion reactions which are used to produce these proton-rich nuclides. However, the use of recoil separators allows one to easily distinguish fusion-evaporation residues from fission products. In addition, all nuclides in this region which lie at the dripline or beyond, decay via charge particle radioactivity. As a result, the recoil decay tagging (RDT) technique can be utilized allowing for in-beam γ -ray studies of nuclides produced with sub- μ b

cross-sections. By coupling the Fragment Mass Analyzer (FMA) with Gammasphere, the high-spin structure of a number of nuclides in this Os-Pb region have been investigated. In addition, complimentary decay studies of these same nuclides has allowed, in several instances, spin/parity and excitation energy assignments for all observed states.

Nearly all isotopes studied in this region exhibit evidence of shape-coexistence i.e. states at low-excitation energy built on two distinct shapes. For two isotopes, $^{175}\text{Au}^1$ and $^{179}\text{Hg}^2$, three shapes have been identified; moderately-deformed oblate, well-deformed prolate and near-spherical. Figure I-17 shows the new level schemes deduced for $^{173,175,177}\text{Au}$. Besides the three shapes identified in ^{175}Au , the new data on these three Au isotopes show a progression from a domination of deformed structures in ^{177}Au to no evidence of collectivity in ^{173}Au . Figure I-18 shows the level structure deduced for ^{179}Hg . In the heavier odd-A Hg isotopes, the ground state spin/parity is $1/2^-$ and associated with a deformed configuration. For ^{179}Hg , the ground state is established to be $7/2^-$ and is associated with a near-spherical shape.

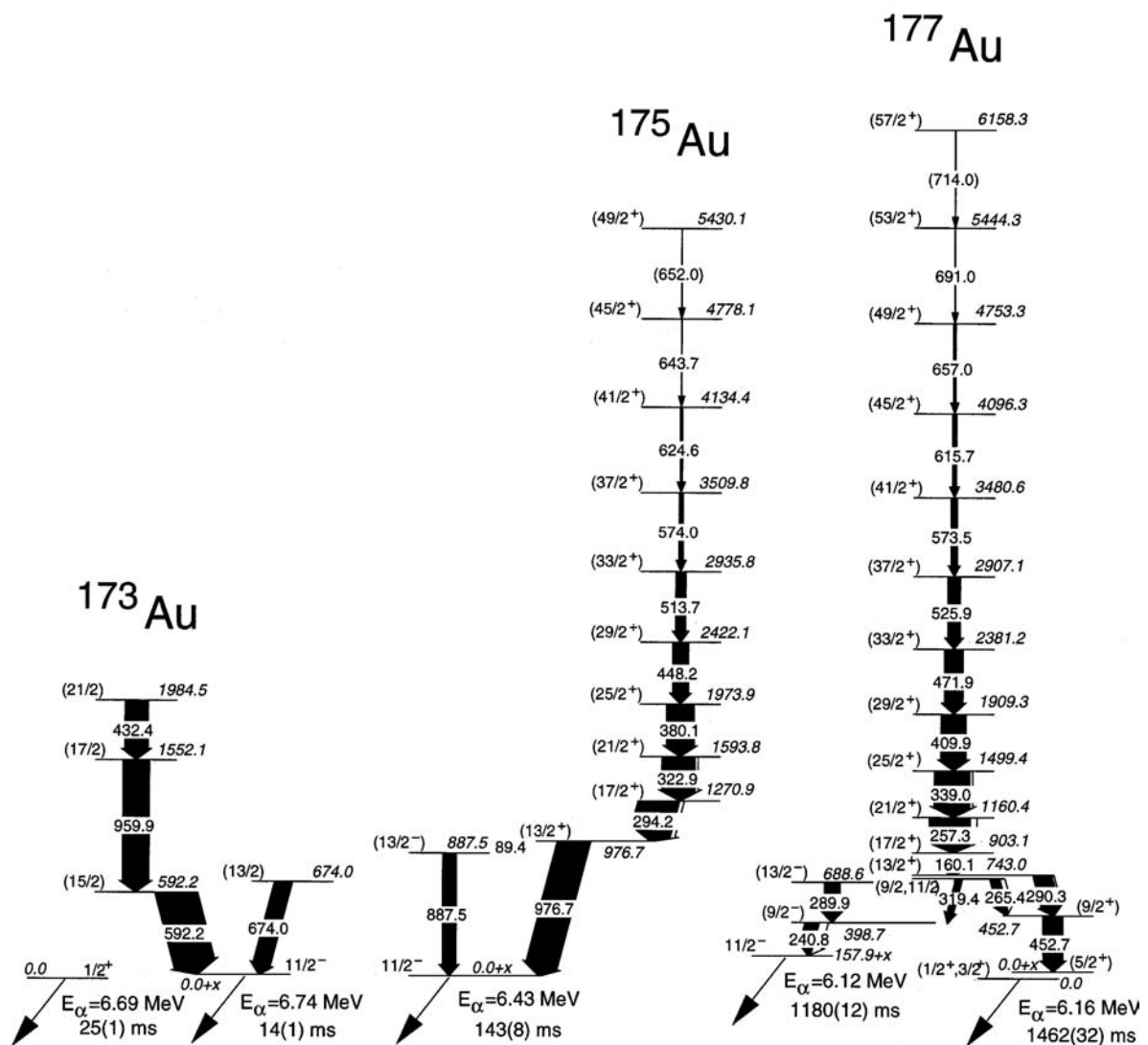


Fig. I-17. Level schemes for $^{173,175,177}\text{Au}$ deduced from γ -ray coincidence data measured with Gammasphere. High-spin states in these nuclei were populated via the $p2n$ evaporation channel from reactions using an ^{84}Sr beam on isotopically enriched targets of ^{92}Mo , ^{94}Mo and ^{96}Mo . The beam was supplied by the ATLAS accelerator at Argonne National Laboratory.

Three rotational bands are evident in the level scheme and have a deduced prolate deformation of $\beta_2 \sim 0.2$.

The oblate shape is associated with the $13/2^+$ isomer into which rotational band 3 decays into.

*Argonne National Laboratory and Illinois Institute of Technology, †Mississippi State University, ‡Rutgers University, §University of Tennessee, ¶Niels Bohr Institute, Copenhagen, Denmark, ||Argonne National Laboratory and University of Maryland, **Washington University, ††Argonne National Laboratory and University of Oslo, Norway

¹F. G. Kondev *et al.*, Phys. Lett. B **512**, 268 (2001).

²F. G. Kondev *et al.*, Phys. Lett. B **528**, 221 (2002)

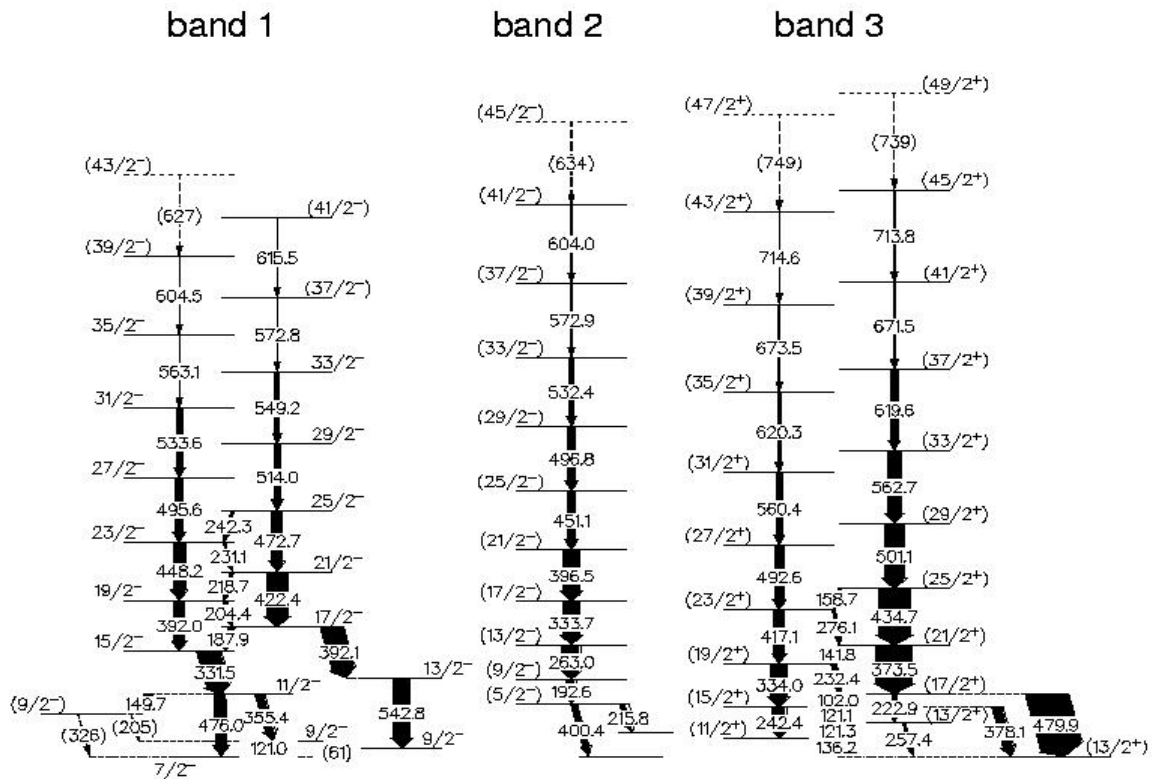


Fig. I-18. Level scheme for ^{179}Hg deduced from γ -ray coincidence data measured with Gammasphere. High-spin states in ^{179}Hg were populated in the $^{90}\text{Zr}(^{90}\text{Zr},n)$ reaction. The beam was supplied by the ATLAS accelerator at Argonne National Laboratory.

B.2. Neutron-Rich Nuclear Spectroscopy

b.2.1. A New Technique for Measuring g-Factor of Excited States in Fission

Fragments Using Gammasphere (I. Ahmad, J. P. Greene, C. J. Lister, R. V. F. Janssens, T. Lauritsen, D. Seweryniak, M. P. Carpenter, F. Kondev, D. Patel,* A. G. Smith,* G. S. Simpson,* R. M. Wall,* J. F. Smith,* O. J. Onakanmi,* B. J. P. Gall,† O. Dorveaux,‡ and B. Roux†)

A new technique has been developed to analyze multifold coincidence data on fission fragments and determine g factors. The g-factors determine the magnetic moments of states and are very sensitive to the underlying single-particle configurations. For neutron-rich nuclei, the successful measurement of g-factors following fission will provide a unique window on neutron-rich nuclear structure. The experiment was performed with the Gammasphere while at Argonne using a 100 μCi ^{252}Cf source. Special care was taken in the preparation of the source so that the fission fragments stop in iron reducing Doppler broadening of the gamma-ray peaks. The source was prepared by electroplating ^{252}Cf on a 15-mg/cm² iron foil and then placing another 15-mg/cm² Fe foil, on which In was evaporated, and pressing the sandwich

under a roller. The source was placed at the center of Gammasphere. A pair of small permanent magnets applying a field of 0.2 T were placed on either side of the source. The direction of the field was reversed every few hours by rotating the magnet assembly through 180 degree. The values of g factors for several nuclei were determined from the analysis of time-integral, perturbed angular correlation functions. The g-factor of the $I^\pi = 2^+$ state in ^{104}Mo was determined from the present data to be +0.248(22). This new measurement shows a factor of 5 improvements in the precision over the value attained in more conventional experiments. The theory behind this new technique and its application to our present data has just been published.¹

*University of Manchester, United Kingdom, †IREs, Strasbourg, France

¹D. Patel et al., J. Phys. G: Nucl. Part. Phys. **28**, 649 (2002).

b.2.2. Medium-Spin Structure of $^{96,97}\text{Sr}$ and $^{98,99}\text{Zr}$ Nuclei and the Onset of Deformation

in the $A \sim 100$ Region (I. Ahmad, W. Urban,* J. L. Durell,† A. G. Smith,† W. R. Phillips,† M. A. Jones,† B. J. Varley,† T. Rzaca-Urban,* L. R. Morss,§ M. Bentalab,‡ and N. Schulz‡)

The structures of $N = 58, 59$ nuclei $^{96,97}\text{Sr}$ and $^{98,99}\text{Zr}$ produced in the spontaneous fission of ^{248}Cm were studied with the Eurogam2 array. Level schemes were constructed from the coincidence relationship of gamma rays which are obtained from the detailed analysis of the $\gamma\gamma\gamma$ cubes. Spins and parities of levels were deduced from the angular correlations and directional-polarization correlations. Regular rotational bands were found in ^{97}Sr and ^{99}Sr , firmly establishing shape coexistence in both nuclei. Rotational bands were identified on 0_3^+ states in the $N = 58$ isotones ^{96}Sr and ^{98}Zr . Several negative-parity single-particle

excitations were observed in these nuclei which suggest the important role of $h_{11/2}$ shell in creating deformation. Quadrupole moments were determined for rotational bands in the $N = 58, 59, 60, 62$ and 64 Sr and Zr nuclei. Deformation parameters, which increase gradually from $\beta_2 \sim 0.1$ at $N = 56$, through $\beta_2 \sim 0.2$ at $N = 58$ to $\beta_2 \sim 0.4$ at $N = 64$, suggest that in Sr and Zr isotopes the shape change occurs gradually between $N = 56$ and $N = 62$, and is most likely due to occupancy of three or more deformation driving orbitals of $h_{11/2}$ parentage. These results have been published.¹

*Warsaw University, Poland, †University of Manchester, United Kingdom, ‡IREs, Strasbourg, France,

§Chemistry Division, ANL

¹W. Urban et al., Nucl. Phys. **A689**, 605 (2001).

b.2.3. Selective Laser Ionization of $N \geq 82$ Isotopes: Use of the Two Step Target

Technique (A. Woehr,* I. Dillmann,‡ U. Köster,§ V. N. Fedoseyev,¶ M. Hannawald,‡ B. Pfeiffer,‡ D. Fedorov,¶ J. Shergur,† L. Weissmann,‡ W. B. Walters,† and K.-L. Kratz‡)

The region around the neutron-rich, double-magic isotope ^{132}Sn has been the subject of intensive experimental investigations in recent years. One reason for this interest is the evolution of the single-particle structures over nearly 40 mass units between nuclides with $N/Z \cong 1.0$, near ^{100}Sn , and isotopes with $N/Z \geq 1.6$, near ^{132}Sn . Such measurements provide an opportunity to develop a unique approach to nuclear structure with predictive power towards nuclei at the particle drip-lines which are not currently accessible for experimental studies. In recent years, we have performed a number of beta-decay experiments of neutron-rich ($N \geq 82$) Ag, Cd, In and Sn isotopes. These studies have been performed at the CERN/ISOLDE facility using resonant laser ionization techniques prior to mass separation. Subsequently, beta-delayed neutron measurements to determine the half-life and beta-gamma spectroscopy to obtain nuclear structure properties have been used. In this report, we present the first results of a study of the decay of $^{132-135}\text{In}$ isotopes.

Neutron-rich medium mass nuclei are normally produced at ISOLDE by high-energy (1 or 1.4 GeV) proton induced fission of ^{238}U . Unfortunately, with this production mechanism neutron-deficient isobars are also formed in spallation and high-energy fission. The situation is particularly complicated in the mass region near $A \cong 80$ which is dominated by very high

backgrounds resulting from surface-ionized (therefore difficult to suppress) proton-rich isobars of rubidium and caesium, respectively. Fission induced by low to medium energy neutrons, however, does not create this problem. Such neutrons can be produced efficiently by heavy target materials, e.g. tantalum or tungsten. The use of a “mini-spallation-source” surrounded by a concentric ISOL fission target was proposed by Nolen *et al.*¹ While the realization of a concentric target requires sophisticated engineering, it is relatively simple to build a reduced version, by just installing a high-Z rod close to a standard ISOLDE fission target. In this experiment, a 10 mm diameter tantalum rod of 150 mm length was mounted parallel to the ^{238}U target at a distance of 21 mm axis to axis.² In this configuration, only part of the neutron flux produced in the “mini-spallation source” impinges on the ISOL target, but the primary beam and most of the secondary particles are located in a forward cone. In this experiment, a standard ISOLDE UC_x/graphite target³ with 50 g/cm² ^{238}U and about 10 g/cm² carbon was used. The target was kept at 2423 K and the niobium ionizer was kept at 2123 K. Pulses of 1.4 GeV Protons (5.3 μC each) hit the tantalum converter every 2.4 s. The Resonant Laser Ion Source (RILIS) was tuned for the ionization of indium. Details about the laser ionization scheme and the experimental setup can be seen in Ref. 2. The measured yields are shown in Table I.

Table I: Yields and half-lives of heavy indium isotopes from a 50 g/cm² UC_x/graphite target with the RILIS tuned for indium ionization. The yield Y is given in ions per μC of primary proton beam³ hitting the tantalum “converter” rod. Furthermore, the table contains the experimentally obtained β -decay half-lives ($T_{1/2}$) for $^{132-135}\text{In}$ from this work. For further discussion, see Ref. 2.

Isotope	^{130}In	^{132}In	^{133}In	^{134}In	^{135}In
Y [μC^{-1}]	$> 3.5 \cdot 10^5$	8000	900	≈ 95	≈ 2.4
$T_{1/2}$ [ms]		206(6)	165(3)	141(5)	92(10)

*Argonne National Laboratory and the University of Maryland, †University of Maryland, ‡Universität Mainz, Germany, §CERN, Geneva, Switzerland, ¶Petersburg Nuclear Physics Institute, Gatchina, Russia

¹J.A. Nolen *et al.*, AIP Conference Proceedings **473**, 477 (1998).

²I. Dillmann *et al.*, Europ. Phys. J. **A13**, in press.

³J. Lettry *et al.*, Nucl. Instrum. Methods **B126**, 130 (1977)

b.2.4. Magic Nucleus ^{132}Sn and its Odd-Neutron-Hole Neighbor ^{131}Sn (I. Ahmad, D. Seweryniak, I. Wiedenhöver, M. P. Carpenter, R. V. F. Janssens, T. L. Khoo, T. Lauritsen, C. J. Lister, P. Reiter, P. Bhattacharyya,* P. J. Daly,* C. T. Zhang,* Z. W. Grabowski,* B. Fornal,† R. Broda,‡ and J. Blomqvist‡)

In the exploration of nuclear structure in regions of nuclide chart far from N/Z stability valley, spectroscopic results for such magic nuclei as ^{48}Ni , ^{78}Ni , ^{100}Sn and ^{132}Sn (and their few valence particle neighbors) provide valuable benchmarks. The neutron-rich doubly closed shell nucleus ^{132}Sn has no excited state below 4 MeV and is thus marked as the most magic of all heavy nuclei. The spectroscopy of these nuclei is well worth studying since it should be a prime source of information about nucleon-nucleon residual interactions in an important sector of the nuclear chart.

The knowledge of the structure of ^{132}Sn and its neighbors comes from β -decay studies of fission products and prompt coincidence spectroscopy of fission products with large gamma-ray array. Our first results on the structure of these nuclei came from analysis of data on the fission products of ^{248}Cm measured with the Eurogam2 array. More recently we

performed an experiment with Gammasphere while it was located at Argonne where more rigorous timing conditions were imposed. A ^{248}Cm source was fabricated. A total of 1.8×10^9 fourfold and higher fold coincidence events were collected. The data was sorted offline into various cubes, both prompt and delayed, covering gamma-ray energies up to 5 MeV.

The analysis of the data determined new levels in ^{132}Sn and ^{131}Sn . In the case of ^{132}Sn , our data confirm all levels below 5 MeV reported in ref. 1. Only one new level, 9^+ member of the $\nu f_{7/2} h_{11/2}^{-1}$ multiplet was observed. In ^{131}Sn , several new levels were identified. Figure I-19 shows the level scheme of ^{132}Sn and ^{131}Sn . Interpretation of the observed states in ^{131}Sn and the comparison of the experimental energies with theoretical values are displayed in Fig. I-20. More details can be found in our publication.²

*Purdue University, †IFJ Krakow, Poland, ‡Royal Institute of Technology, Stockholm, Sweden

¹Fogelberg *et al.*, Phys. Scr. **T56**, 79 (1995).

²P. Bhattacharyya *et al.*, Phys. Rev. Lett. **87**, 062502 (2001).

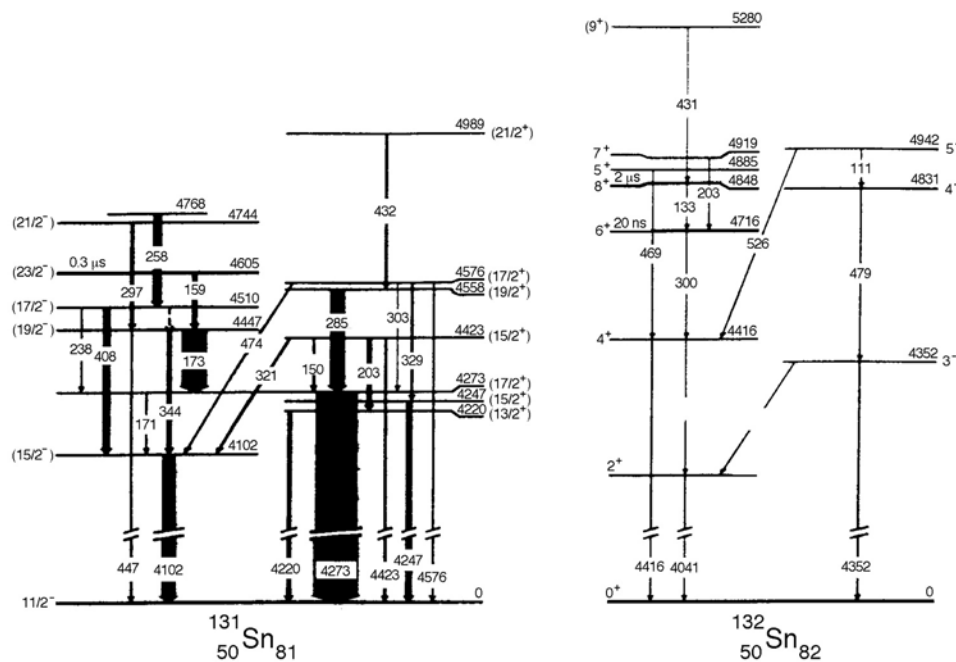


Fig. I-19. Level schemes of ^{131}Sn and ^{132}Sn deduced from analysis of coincidence gamma ray spectra measured with Gammasphere and a 5 mg ^{248}Cm source.

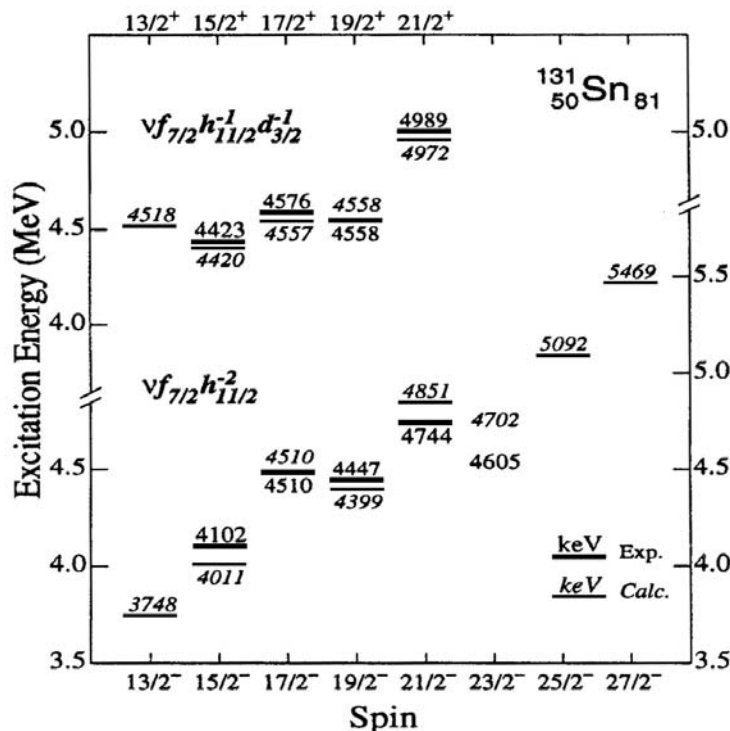


Fig. I-20. Comparison of observed level energies in ^{131}Sn with those calculated by shell model using empirical nucleon-nucleon interactions.

b.2.5. Yrast Excitations in $N = 81$ Nuclei ^{132}Sb and ^{133}Te from ^{248}Cm Fission Studies
 (I. Ahmad, D. Seweryniak, I. Wiedenhöver, M. P. Carpenter, R. V. F. Janssens, T. L. Khoo, T. Lauritsen, C. J. Lister, P. Reiter, P. Bhattacharyya,* P. J. Daly,* C. T. Zhang,* Z. W. Grabowski,* S. K. Saha,* B. Fornal,† R. Broda,† W. Urban,‡ and J. Blomqvist§)

Structures of $N = 81$ isotones ^{132}Sb and ^{133}Te were studied by measuring coincidence gamma rays in the deexcitation of ^{248}Cm fission fragments. The multifold coincidence gamma rays were measured with the Gammasphere and a 5 mg ^{248}Cm source. Previously unknown yrast cascades in ^{132}Sb and ^{133}Te were identified in cross coincidence with known gamma rays from the complementary Rh and Ru fission fragments.

The ^{132}Sb levels are explained as proton-neutron hole states as well as core excited states of $2p - 2h$ character. The level scheme of ^{133}Te , shown in Fig. I-21, was interpreted mainly on the basis of shell model calculations using empirical proton-proton interaction energies from ^{134}Te together with estimated proton-neutron hole interactions. The results of this investigation were published.¹

*Purdue University, †IFJ Krakow, Poland, ‡Warsaw University, Poland, §Royal Institute of Technology, Stockholm, Sweden

¹P. Bhattacharyya et al., Phys. Rev. C **64**, 054312 (2001).

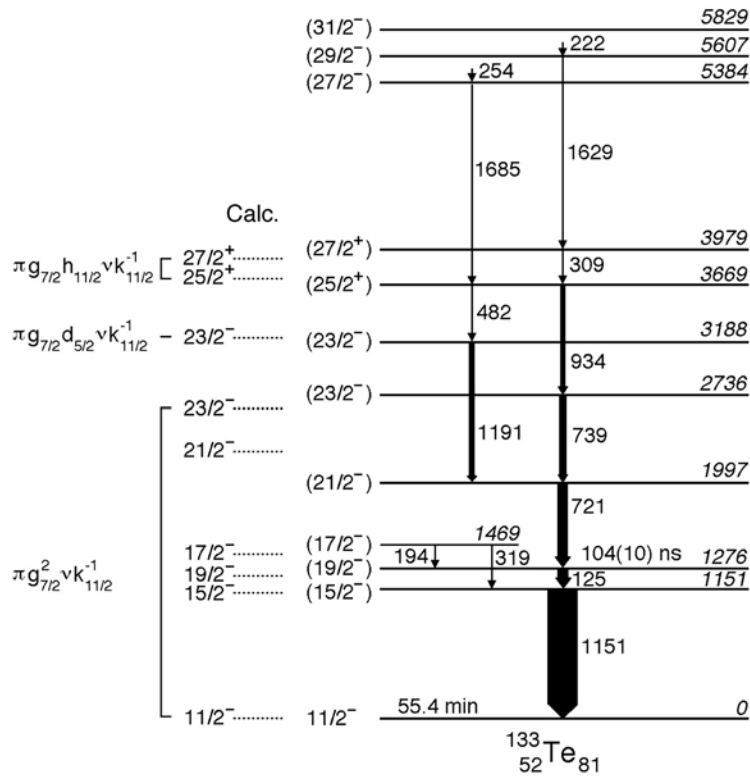


Fig. I-21. Level scheme of ^{133}Te showing the yrast gamma-ray cascade observed in the fission of ^{248}Cm . The dashed levels indicate calculated energies for $\pi^2 \nu^1$ states.

b.2.6. Excitations of Two- and Three-Valence Proton Nuclei ^{134}Te and ^{135}I

(I. Ahmad, D. Seweryniak, I. Wiedenhöver, M. P. Carpenter, R. V. F. Janssens, T. L. Khoo, T. Lauritsen, C. J. Lister, P. Reiter, S. K. Saha,* C. Constantinescu,* P. J. Daly,* P. Bhattacharyya,* C. T. Zhang,* Z. W. Grabowski,* B. Fornal,† and R. Broda†)

Prompt multifold coincidence gamma ray spectra were measured using a ^{248}Cm source and the Gammasphere when it was at Argonne. Analysis of the data set has provided structures of many neutron-rich nuclei. We have focused our analysis on structure of nuclei around the doubly magic ^{132}Sn . By studying nuclei with few

valence protons and/or valence neutrons we have been able to investigate neutron-proton interaction. The new analysis of the ^{248}Cm data has revealed new levels in ^{134}Te and ^{135}I . These levels are well explained by shell model calculations and thus provide further test of the interaction. The results of this study were published.¹

*Purdue University, †INP Krakow, Poland

¹S. K. Saha et al., Phys. Rev. C **65**, 017302 (2002).

b.2.7. First Measurement of Yrast Excitations in ^{137}I and the Missing 12^+ Isomer in ^{136}Te
 (I. Ahmad, L. R. Morss, ¶ A. Korgul,* W. Urban,* T. Rzaca-Urban,* M. Gorska, †
 J. L. Durell, ‡ M. J. Leddy, ‡ M. A. Jones, ‡ W. R. Phillips, ‡ A. G. Smith, ‡ B. J. Varley, ‡
 M. Bentaleb, § E. Lubkiewicz, § and N. Schulz, §)

The excited states in ^{137}I , populated in the spontaneous fission of ^{248}Cm , have been studied by means of prompt coincident gamma-ray spectroscopy using Eurogam2 germanium array. Medium-spin yrast excitations in ^{137}I were observed for the first time. The experimental level scheme was compared with calculations made

with shell model using Kuo-Herling interaction. The calculated values were found to differ significantly from the measured values. The two level schemes are displayed in Fig. I-22. The results of this study were published.¹

*Warsaw University, Poland, †Catholic University, Leuven, Belgium, ‡University of Manchester, United Kingdom, §IREs, Strasbourg, France, ¶Chemistry Division, ANL
¹A. Korgul et al., Eur. Phys. J. A **12**, 129 (2001).

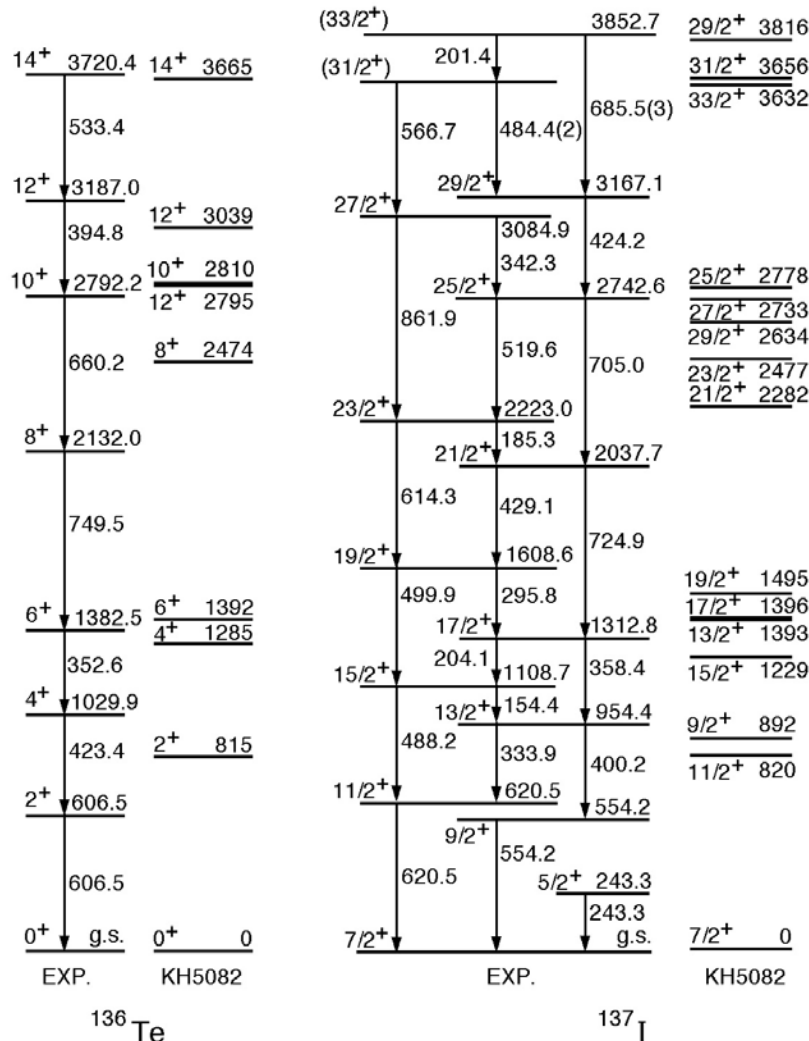


Fig. I-22. Partial level schemes of ^{137}I and ^{136}Te obtained in the present work. For both nuclei, shell model predictions are also included.

b.2.8. First Observation of Excited States in ^{139}I (I. Ahmad, L. R. Morss,§ W. Urban,* T. Rzaca-Urban,* A. Korgul,* J. L. Durell,† M. J. Leddy,† M. A. Jones,† W. R. Phillips,† A. G. Smith,† B. J. Varley,† and N. Schulz‡)

The structure of the nucleus ^{139}I has been determined for the first time. Levels in ^{139}I were studied by measuring coincidence gamma rays produced in the deexcitation of ^{248}Cm fission fragments. The experiment was performed with a 5 mg ^{248}Cm source and Eurogam2 gamma array. The assignment of the gamma rays to ^{139}I was based on the correlation between masses of iodine isotopes and the mean masses of complementary Tc isotopes. Multipolarities of transitions in ^{139}I were deduced from angular correlations and directional-polarization measurements.

Level scheme of ^{139}I deduced from the present work is shown in Fig. I-23. The level spins and parities are determined relative to $7/2^+$ ground state, which was deduced from the systematic trend of lowest yrast excitations in the odd-Z, N = 86 isotones. The excited states shown in Fig. I-23 indicate patterns characteristic of spherical vibrator. The level scheme of ^{139}I is similar to that of ^{137}I but it shows more collectivity as indicated by the lower transition energies. The results of this study were published.¹

*Warsaw University, Poland, †University of Manchester, United Kingdom, ‡IREs, Strasbourg, France, §Chemistry Division, ANL

¹W. Urban et al., Phys. Rev. C65, 024307 (2002).

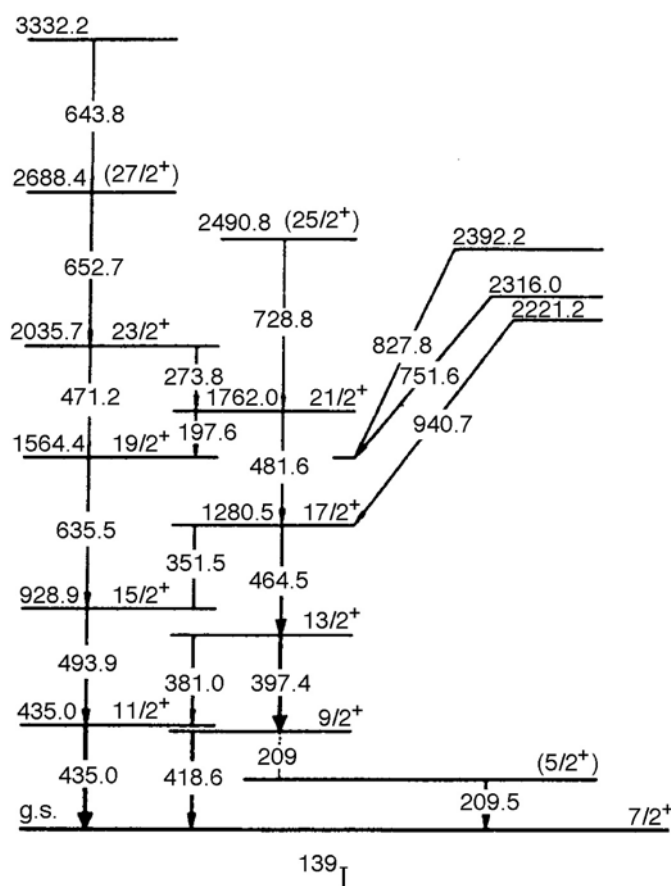


Fig. I-23. Partial level scheme of ^{139}I deduced from the analysis of ^{248}Cm fission data.

b.2.9. Observation of Rotation Bands in Neutron-Rich ^{107}Ru Nucleus (I. Ahmad, J. P. Greene, R. V. F. Janssens, S. J. Zhu,*†‡ J. H. Hamilton,† A. V. Ramayya,† J. K. Hwang,† C. Y. Gan,* X. Q. Zhang,† C. J. Beyer,† J. Kormicki,† M. Sakhee,* L. M. Yang,* L. Y. Zhu,* R. Q. Xu,* Z. Zhang,* Z. Jiang,* W. C. Ma,§ E. F. Jones,† P. M. Gore,† J. D. Cole,¶ M. W. Drigert,¶ I. Y. Lee,|| J. O. Rasmussen,|| T. N. Ginter,|| Y. X. Luo,†|| S. C. Wu,|| C. Folden,|| P. Fallon,|| P. Zielinski,|| K. E. Gregorich,|| A. O. Macchiavelli,|| S. J. Asztalos,‡ G. M. Ter-Akopian,** Yu. Ts. Ogenassian,** and M. A. Stoyer††)

Levels in the neutron-rich, odd-mass ^{107}Ru nucleus have been investigated with Gammasphere by measuring high-fold, prompt coincidence events following spontaneous fission of ^{252}Cf . A ~ 60 microCurie ^{252}Cf source sandwiched between two 15 mg/cm² iron foils was used for these measurements which were carried out with Gammasphere at Berkeley. On the basis of the results obtained in the present study, the ground state band of ^{107}Ru has been extended up to

27/2. The structure associated with $h_{11/2}$ excitation has been confirmed and extended to higher spin. The $h_{11/2}$ band head has been established at 301.8 keV. These results clarify the differences between our earlier work and results from other experiments published recently. A new collective band based on a $9/2^-$ level has been identified for the first time. The results of this investigation were published.¹

*Tsinghua University, Beijing, China, †Vanderbilt University, ‡Oak Ridge National Laboratory, §Mississippi State University, ¶INEEL, Idaho Falls, ||Lawrence Berkeley National Laboratory, **JINR Dubna, Russia, ††Lawrence Livermore National Laboratory

¹S. J. Zhu *et al.*, Phys. Rev. C **65**, 014307 (2001).

b.2.10. Mass Measurements of Short-Lived Neutron-Rich Isotopes at the Canadian Penning Trap Mass Spectrometer (G. Savard, J. P. Greene, A. Heinz, D. Seweryniak, J. A. Clark,* R. C. Barber,* C. Boudreau,† F. Buchinger,† J. E. Crawford,† S. Gulick,† J. C. Hardy,‡ J. K. P. Lee,† R. B. Moore,† K. S. Sharma,* G. Sprouse,§ J. Vaz,* and J. C. Wang*)

The Canadian Penning Trap (CPT) mass spectrometer is designed to make precise mass measurements on short-lived isotopes. Up until now, work had concentrated on short-lived neutron-deficient isotopes produced on-line at the ATLAS facility and stable isotopes. The recent overall efficiency gain in the injection system of the CPT now allows us to look at much more weakly produced isotopes. A region of great physical interest is that of the neutron rich-isotopes whose masses are critical to our understanding of the astrophysical r-process. These isotopes can be produced on-line but also, for a large fraction of them, they can be obtained more simply in small quantity from a fission source.

With the increased efficiency of the system, we have been able to perform a preliminary study of 6 heavy neutron-rich isotopes produced by the 6 μCi ^{252}Cf source that we have previously been using for efficiency calibration of the gas cell/gas cooler system.

^{252}Cf decays with 97% probability by alpha emission and only with 3% probability by fission. The yield of any specific isotope is further diluted by the fission fragment distribution shown in Fig. I-24. The fission distribution peaks at about 0.03 per fission, or 0.001 per ^{252}Cf decay. This yields for the source available a total production of about 200 ions per second emitted into 4π steradians. The fission source is installed outside the gas cell and about 8% of the heavy fission fragments are emitted in a solid angle such that they can go through the entrance HAVAR window and be stopped in the gas cell. About 45% of those are extracted as ions from the gas cell, with about 2/3 of them concentrated in one charge state. They are then cooled in the gas cooler (with about 80% efficiency) before being transferred every 50 ms to the CPT accumulation linear RFQ trap and then the precision Penning trap where the actual mass measurement takes place. These transfer processes have efficiencies of about 80% and

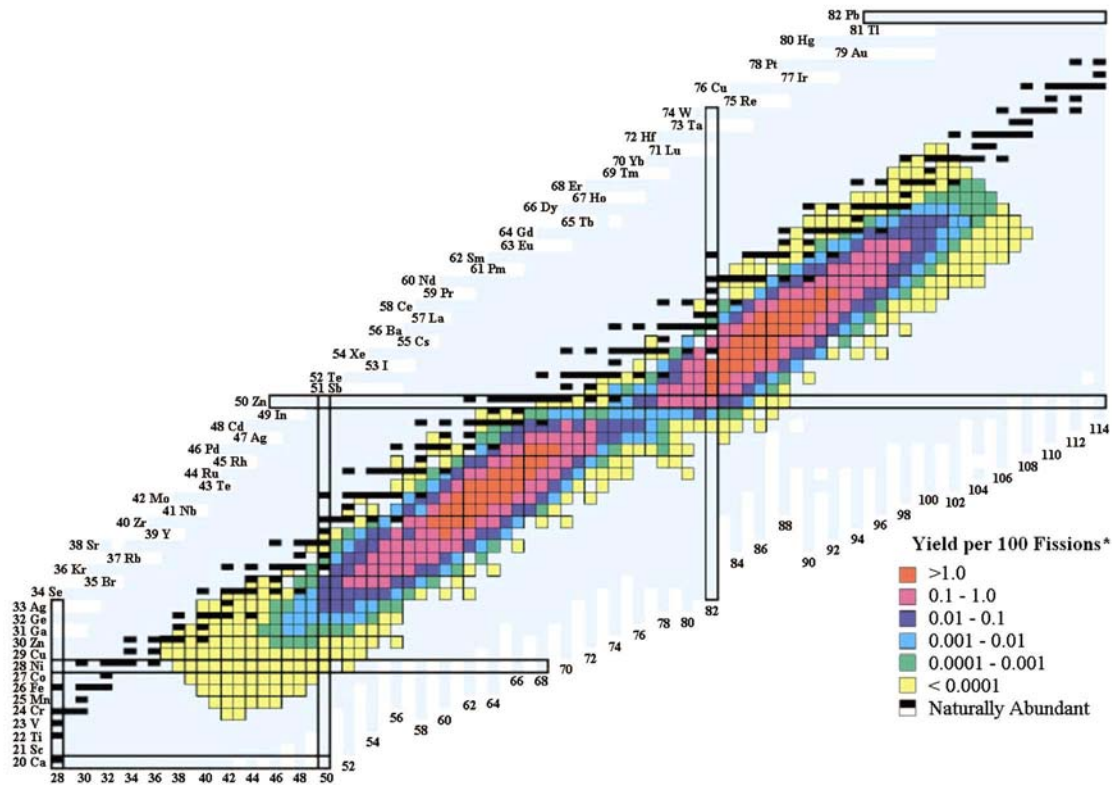


Fig. I-24. Fission yield distribution for ^{252}Cf .

60%. The cyclotron resonance used to determine the mass of the isotope of interest is measured with a time-of-flight technique where the ions are detected by a microchannel plate detector with a 40% efficiency. About 0.8 ion per second is detected at this final detector for an efficiency from the stopping in the gas cell to the detection of ions from one specific charge state after the precision Penning trap of about 5%. The total efficiency from production to detection, which also includes the low probability of stopping of the fission fragments inside the cell because of the emission in 4π solid angle, is about 0.4%.

Using this approach, we have measured with a resolution of about 1 part in 700000 and an accuracy of about 10^{-7} the mass of 6 neutron rich isotopes: ^{145}Ba (see Fig. I-25), ^{145}La , ^{147}La , ^{147}Ce , ^{149}Ce and ^{149}Pr . These isotopes have half-lives down to about 4 seconds and in all cases the new mass values will be a significant improvement over previously know masses. These measurements will be extended to more weakly produced nuclides in the coming year.

*University of Manitoba, Winnipeg, Manitoba†, McGill University, Montreal, Quebec, ‡Texas A&M University, §Argonne National Laboratory and State University of New York

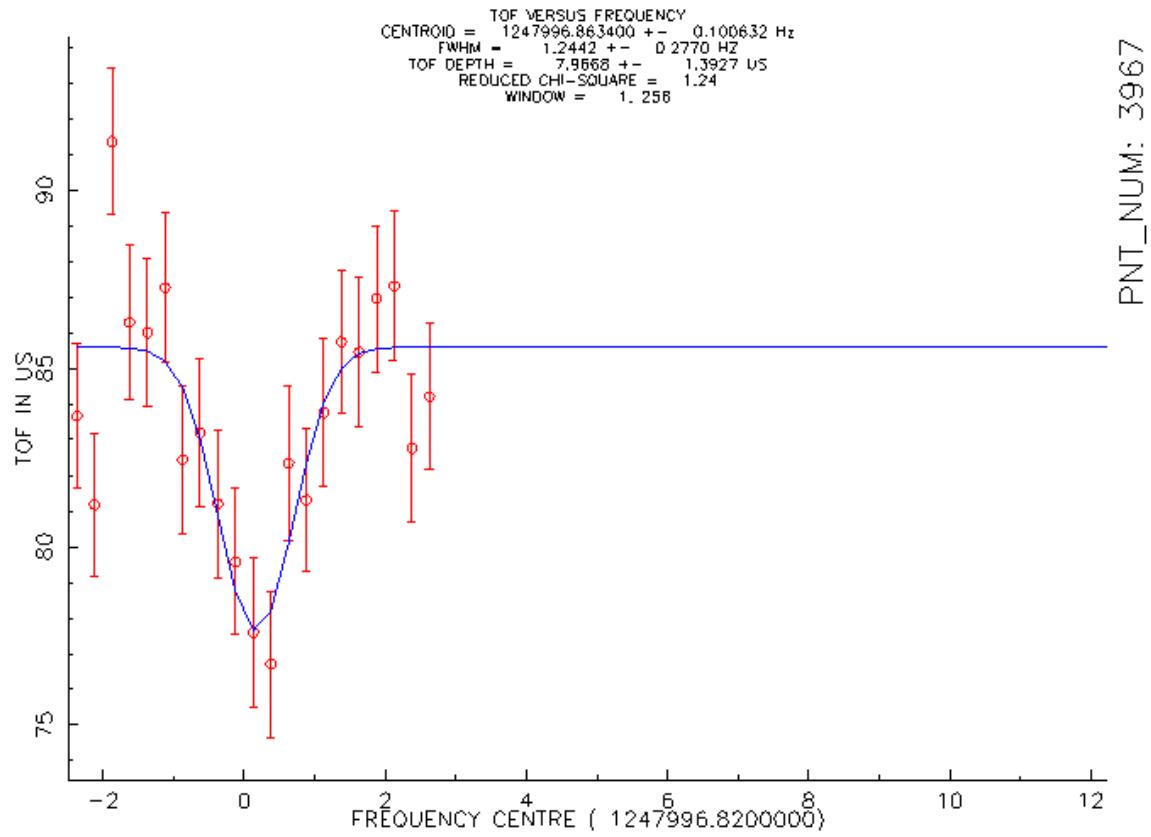


Fig. I-25. Typical resonance obtained in an afternoon of data taking for ^{145}Ba ($t_{1/2} = 4.0\text{s}$).

C. SPECTROSCOPY OF TRANS-LEAD NUCLEI

The structure and stability of the very heaviest elements continues as a forefront area of research, both theoretically and experimentally, as it provides one of the ultimate tests of our understanding of nuclear binding. Progress in understanding the shapes of nuclei and the sequence of quantum states near the Fermi surface of the very heaviest nuclei continues on many fronts. This progress will lead to an improved vision of the location and stability of possible “superheavy” elements. In addition, investigations of the spin and excitation dependence of the fission barrier in these very heavy systems may help guide future synthesis experiments. The development of a new FMA chamber with a large target wheel and with the possibility of gas cooling, combined with the production of very intense heavy-ion beams has opened the way for synthesizing nuclei beyond $Z = 104$, ^{257}Rf , the highest atomic number nucleus studied at ATLAS to date.

c.1. Coulomb Excitation and Few Nucleon Transfer Reactions in $^{209}\text{Bi} + ^{248}\text{Cm}$ at 1450 MeV (K. Abu Saleem,* R. V. F. Janssens, M. P. Carpenter, I. Ahmad, J. P. Greene, J. Caggiano, A. Heinz, T. L. Khoo, T. Lauritsen, C. J. Lister, D. Seweryniak, A. Sonzogni, F. G. Kondev,† I. Wiedenhöver,‡ G. Hackman,§ P. Chowdhury,¶ D. Cline,|| and A. O. Machiavelli**)

For the last few years, the behavior of the actinide nuclei at high spin has been investigated at ATLAS using the so-called "Unsafe" Coulex technique. In earlier reports we have described our work on the ^{232}Th nucleus studied by bombarding the target with a 1400 MeV ^{209}Bi beam from ATLAS. The Gammasphere array was used to detect the gamma rays of interest. In this pilot experiment 11 rotational bands were observed in the Coulomb excitation channel. In addition, several rotational bands associated with nucleon transfer/pick-up channels were identified as well.

The success of this experiment enticed us into continuing this project on other important actinide nuclei, and an experiment was performed using the $^{209}\text{Bi} + ^{248}\text{Cm}$ reaction at 1450 MeV (roughly 14%

above the Coulomb barrier). Again, the Gammasphere array was used to collect the data. The analysis has revealed four rotational bands in the target nucleus. The yrast sequence (see Fig. I-26) has now been traced up to 32^+ , considerably higher than reported earlier.¹ The spin assignments (tentatively proposed in Ref. 1) for the octupole band have been firmly established, and new out-of-band transitions have been placed in a coherent level scheme. Two additional positive parity bands have been assigned to this nucleus as well. In addition to rotational bands in the Coulomb excitation channel, the yrast band of ^{246}Cm , populated in the two-neutron pick-up channel, has also been observed. Several other rotational cascades are present in the data. They are still under investigation and have not yet been assigned to a specific nucleus.

*Argonne National Laboratory and Illinois Institute of Technology, †Technology Division, Argonne National Laboratory, ‡Florida State University, §University of Kansas, ¶University of Massachusetts at Lowell, ||University of Rochester, **Lawrence Berkeley National Laboratory
¹G. Hackman *et al.*, Phys. Rev. C **57**, R1506 (1998).

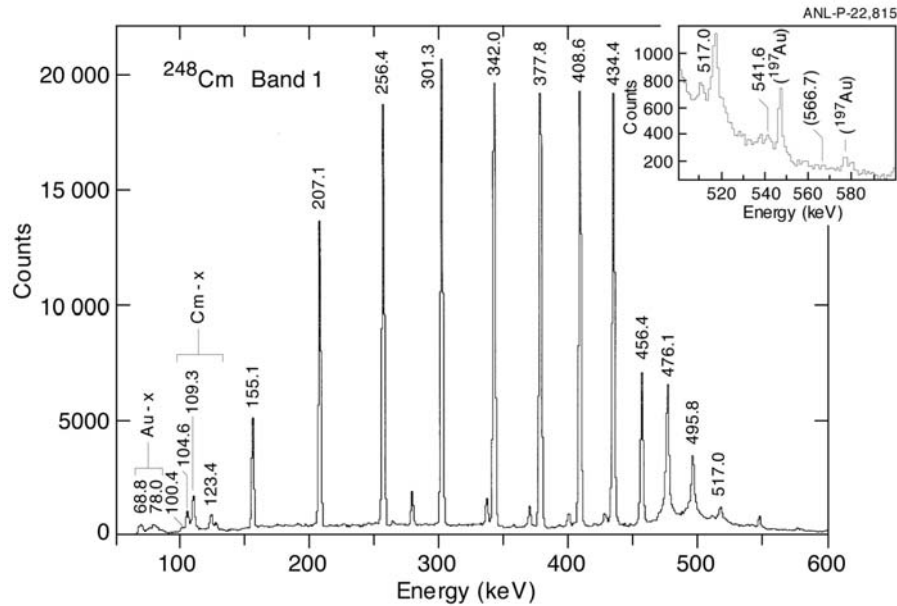


Fig. I-26. Coincidence spectrum produced from double gates on transitions in the yrast band of ^{248}Cm .

c.2. Coulomb Excitation and Few Nucleon Transfer Reactions with ^{209}Bi Beams on ^{237}Np and ^{241}Am Targets (K. Abu Saleem,* R. V. F. Janssens, M. P. Carpenter, I. Ahmad, J. P. Greene, J. Caggiano, A. Heinz, T. L. Khoo, T. Lauritsen, C. J. Lister, D. Seweryniak, A. Sonzogni, F. G. Kondev,† I. Wiedenhöver,‡ G. Hackman,§ P. Chowdhury,¶ D. Cline,|| and A. O. Machiavelli**)

In order to understand the evolution of the moment of inertia of even-even systems as a function of rotational frequency, and in particular, in order to understand the origin of the alignments observed in the various bands of these nuclei, it is often important to also investigate the properties of rotational sequences in the odd neighbors. In the actinide region, some information is available on a number of odd neutron nuclei, but odd proton systems are poorly known. Yet, alignments such as those of $i_{13/2}$ protons are thought to play an important role. In order to remedy this situation, we have extended our so-called "Unsafe" Coulex studies to the nuclei ^{237}Np and ^{241}Am .

A ^{209}Bi beam from ATLAS at 1450 MeV bombarded thin ^{237}Np and ^{241}Am radioactive targets evaporated on thick Au backings. The data from the two experiments were collected with the Gammasphere array. Four band structures have been delineated to high spin in ^{237}Np ; the representative level scheme is given in Fig. I-27.

The ground state band is constituted of two signature partners (bands 1 and 2) and is assigned to the $5/2[642]$ state, which originates from the $i_{13/2}$ orbital. The two other sequences, bands 3 and 4, are also signature partners. They are assigned to the $5/2[523]$ state, and originate from the $h_{9/2}$ orbital. The absence of a backbending or a significant upbending in the $i_{13/2}$ band structures and the presence of such a phenomenon in the $h_{9/2}$ excitations argue strongly in favor of an interpretation of the rise of the moments of inertia in the even-even U isotopes in terms of an $i_{13/2}$ proton alignment.

In addition to the bands measured in the Coulomb excitation channel, rotational cascades have also been observed corresponding to more complex reactions (the beam energy was $\sim 15\%$ above the Coulomb Barrier): rotational sequences belonging to ^{238}U and ^{236}Pu , for example, have been delineated.

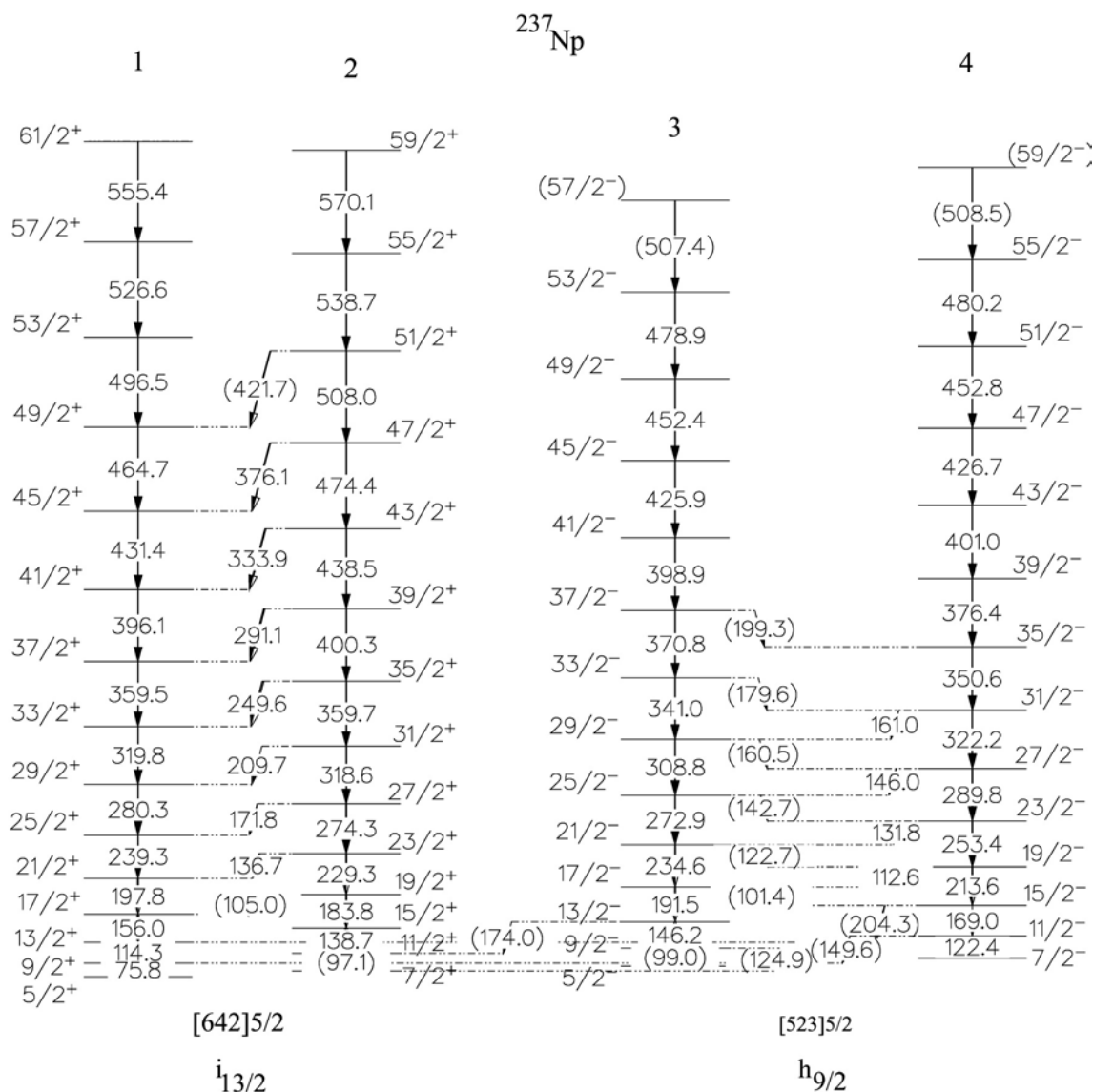


Fig. I-27. Level scheme of the nucleus ^{237}Np as obtained in the present experiment.

Six band structures have been established in ^{241}Am ; they can again be grouped in pairs of signature partners¹ based respectively on the $5/2[523]$ ($h_{9/2}$) configuration, the $5/2[642]$ ($i_{13/2}$) state, and the $3/2[521]$ ($2f_{7/2}$) level. As can be seen in Fig. I-28 where the experimental alignments of the various bands are presented as a function of the rotational frequency together with similar data for ^{242}Pu ,² a sharp upbending is seen in bands 1 and 2 at roughly the same frequency than in the yrast sequence of the even-even neighbor.

In contrast, the $i_{13/2}$ rotational bands show a decrease in alignment over the same frequency range. This observation unambiguously assigns the strong backbending in ^{242}Pu to the alignment of a pair of $i_{13/2}$ protons.

Cranked Shell Model calculations are underway in order to understand the band structures that are now known through out this actinide region.

*Argonne National Laboratory and the Illinois Institute of Technology, †Technology Division, Argonne National Laboratory, ‡Florida State University, §University of Kansas, ¶University of Massachusetts at Lowell, ||University of Rochester, **Lawrence Berkeley National Laboratory

¹R. B. Firestone *et al.*, Table of Isotopes, 8th edition, volume II, 1996.

²I. Wiendehöver *et al.*, Phys. Rev. Lett. **83**, 2143 (1999).

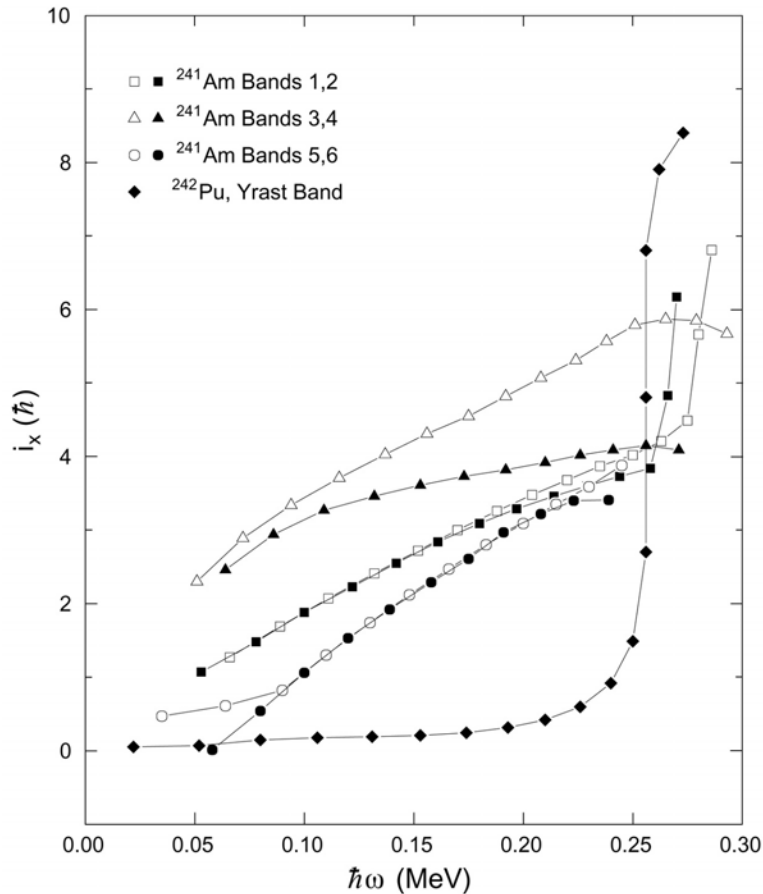


Fig. I-28. Experimental alignments as a function of rotational frequency for the six bands discovered in ^{241}Am . The data are being compared with those of ^{242}Pu from Ref. 2.

c.3. Estimation of the N = 162 Gap (I. Ahmad, R. R. Chasman, and H. Esbensen)

Alpha-decaying isomers were discovered¹ at GSI in 1996 in the nucleus $^{273}\text{110}$. Two favored alpha transitions were identified with energy differences of 1.35 MeV and a half-life ratio of 1545. We performed calculations of level energies in $^{273}\text{110}$ and the daughter ^{269}Hs using a Wood-Saxon potential and pairing force. On the basis of our calculations, we interpreted the lower energy transition of 9.73 MeV as a decay from the ground state of $^{273}\text{110}$ to the excited particle state in the daughter ^{269}Hs with the same configuration. The high-energy transition of 11.08 MeV was interpreted as a decay from the excited low-spin hole state to the ground state of ^{269}Hs , both states having the same single-particle configuration. Our calculations gave an energy difference of 1.69 MeV between the alpha

transitions of the two isomers which was in good agreement with the measured energy of 1.35 MeV. Figure I-29 shows our interpretation of the decay of the two isomers.

We submitted a paper for publication in Phys. Rev. C in August 2001. While the paper was being processed we received a preprint from GSI² in which the results of all heavy element data measured at GSI since 1994 were reanalyzed. These authors found that the 9.73 MeV decay was wrong; it did not have the correct decay chain. Since the existence of one of the isomers is no longer substantiated, we withdrew our paper. Even so, our calculations still predict an isomer in $^{273}\text{110}$ with half-life of several ms and α decay energy of ~ 10 MeV.

¹S. Hofmann, *et al.*, Z. Phys. **354**, 229 (1996).

²S. Hofmann, *et al.*, submitted to Eur. Phys. J.

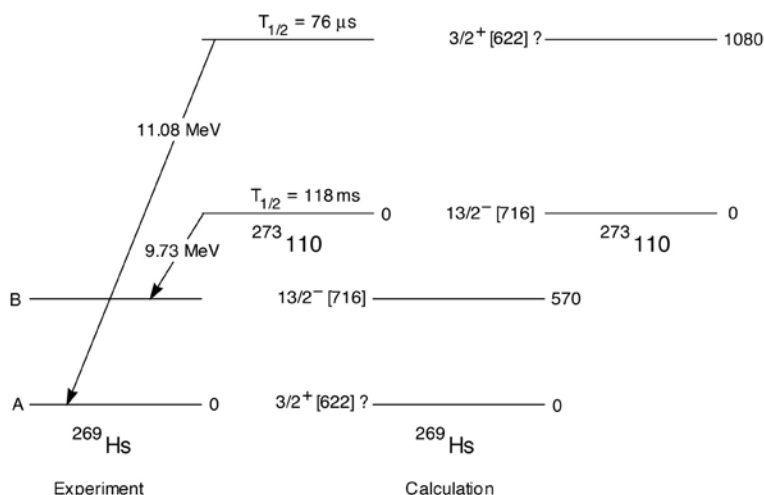


Fig. I-29. The original experimental¹ and the calculated quasiparticle energies in ²⁷³110 and ²⁶⁹Hs.

- c.4. Spectroscopy of Transfermium Nuclei:** ²⁵²No (T. L. Khoo, C. J. Lister, R.-D. Herzberg,* N. Amzal,* F. Becker,† P. A. Butler,* A. J. C. Chewter,* J. F. C. Cocks,‡ O. Dorvaux,‡ K. Eskola,§ J. Gerl,¶ P. T. Greenlees,‡ N. J. Hammond,* K. Hauschild,† K. Helariutta,‡,¶ F. Heßberger,¶ M. Houry,† G. D. Jones,* P. M. Jones,‡ R. Julin,‡ S. Juutinen,‡ H. Kankaanpää,‡ H. Kettunen,‡ W. Korten,† P. Kuusiniemi,‡ Y. Le Coz,† M. Leino,‡ R. Lucas,† M. Muikku,‡ P. Nieminen,‡ R. D. Page,* P. Rahkila,‡ P. Reiter,|| Ch. Schlegel,¶ C. Scholey,* O. Stezowski,* Ch. Theisen,† W. H. Trzaska,‡ J. Uusitalo,‡ and H. J. Wollersheim¶)

An in-beam study of excited states in the transfermium nucleus ²⁵²No has been performed using the recoil separator RITU together with the JUROSPHERE II array at the University of Jyväskylä. This is the second transfermium nucleus studied in an in-beam experiment. Levels up to spin 20 were populated and compared to levels in ²⁵⁴No. An upbend in the moment

of inertia is seen at a frequency of 200 keV, corresponding to spin 16. We also use an improved systematics to connect the energy of the lowest 2⁺ state with its half-life and find the deformation of ^{252,254}No, $\beta_2 = 0.28, 0.29$. This work has been published in Physical Review C.¹

*Oliver Lodge Laboratory, University of Liverpool, Liverpool, United Kingdom, †DAPNIA/SPHn CEA-Saclay, Gif-sur-Yvette Cedex, France, ‡University of Jyväskylä, Jyväskylä, Finland, §University of Helsinki, Helsinki, Finland, ¶Gesellschaft für Schwerionenforschung, Darmstadt, Germany, ||Ludwig Maximilians Universität, München, Germany

¹R.-D. Herzberg et al. Phys. Rev. C **65**, 014303 (2002).

- c.5. Structure, Fission Barrier and Limits of Stability of ²⁵³No** (T. L. Khoo, A. Heinz, T. Lauritsen, C. J. Lister, D. Seweryniak, I. Ahmad, M. P. Carpenter, C. N. Davids, W. F. Henning, F. Kondev, R. V. F. Janssens, A. A. Sonzogni, S. Siem, I. Wiedenhöver, P. Reiter,* N. Amzal,† P. A. Butler,† A. J. Chewter,† J. A. Cizewski,‡ P. T. Greenlees,¶ K. Helariutta,¶ R. D. Herzberg,† G. Jones,† R. Julin,¶ H. Kankaanpää,¶ H. Kettunen,¶ W. Korten,§ P. Kuusiniemi,¶ M. Leino,¶ J. Uusitalo,¶ and K. Vetter||)

The heaviest nuclei exist only because the shell-correction energy creates a fission barrier; otherwise they would fission instantaneously. An accurate calculation of the shell-correction energy of the heaviest nuclei depends on the single-particle energies,

which are also essential for interpreting the α decay of the superheavy elements. The most direct information on the single-particle energies comes from the quasiparticle energies of an odd nucleus. Direct information on the fission barrier for comparison with

theory may be obtained from the entry distribution, a method that we recently introduced.¹ With these motivations, we have studied the single-particle energies and fission barrier of ²⁵³No, by using the ²⁰⁷Pb(⁴⁸Ca,2n) reaction. The production cross section of ²⁵³No was measured as $\sim 0.5 \mu\text{b}$ in an experiment with the gas-filled separator RITU at Jyväskylä. This showed that a γ -ray experiment was feasible. In a subsequent experiment at Argonne, the γ rays were detected with Gammasphere, in coincidence with the FMA. The γ -ray spectrum for ²⁵³No is dominated by the K x-rays and the gamma transitions are much weaker due to huge conversion electron competition. Heavy odd nuclei, such as ²⁵³No, represent the limits of in-beam γ spectroscopy.

Fortunately, in ²⁵³No only one band, built on the $7/2^+[624]$ orbital, is expected to have sufficiently small M1 branching ratios to permit less converted E2 γ competition. All the other low-lying bands, which are expected² to have very small γ branching ratios due to overwhelming competition from M1 conversion electrons. The $7/2^+[624]$ band should have a correspondingly larger γ -ray multiplicity than the other bands and, indeed, it was enhanced by demanding that 4 or more Gammasphere modules fire. Coincidence spectra help to confirm the band assignments: despite the low statistics, with only a few coincidences are seen in individual gates (as expected from our model calculations), the sum spectrum from all the gates shows counts primarily at the expected energies. The enhancement by high multiplicity, the coincidence

spectra and a comparison with the calculated spectrum for the $7/2^+[624]$ band are all used to deduce the level scheme for the band. This combination of methods is necessary since conventional spectroscopic methods cannot be used due to the low cross sections (~ 50 nb) of the γ rays. The band head energy is assigned at 355 keV on the basis of an increased γ yield around this energy from E1 interband decays to the yrast band, which is expected² to be built on the $9/2^-[734]$ configuration. This energy is substantially lower than that calculated with the relativistic mean-field model (see Sec. c.11 in Chapter V. Theoretical Physics, of this document).

The moment of inertia $J^{(1)}$ of the $7/2^+[624]$ band in ²⁵³No is $\sim 13\%$ larger than that of ²⁵⁴No. A plot of $J^{(1)}$ as a function of transition energy shows that $J^{(1)}$ is almost constant at the lowest energies (up to 335 keV) and then monotonically increases thereafter. These are characteristic features of the moment of inertia of an odd nucleus. The smooth behavior of $J^{(1)}$ also provides support for the assignment of the transitions to the band.

We have also measured the two-dimension entry distribution as a function of spin vs. sum energy. It shows that the fission barriers in ²⁵³No are similar to that in ²⁵⁴No,¹ in both cases they are larger than 5 MeV at high angular momentum, thereby giving direct indication of significant fission barriers created by shell structure.

*University of Munich, Germany, †University of Liverpool, United Kingdom, ‡Rutgers University, §DAPNIA/SPhN CEA-Saclay, France, ¶University of Jyväskylä, Finland, ||Lawrence Berkeley National Laboratory
¹P. Reiter *et al.*, Phys. Rev. Lett. **84**, 3542 (2000).

²I. Ahmad *et al.*, Phys. Rev. C **14**, 218 (1976).

c.6. Search for A High-K Isomer in ²⁵⁴No by γ and Electron Spectroscopy

(G. Mukherjee,* T. L. Khoo, D. Seweryniak, I. Ahmad, M. P. Carpenter, C. N. Davids, A. Heinz, R. V. F. Janssens, F. G. Kondev, T. Lauritsen, C. J. Lister, A. Woehr, † A. Aprahamian, ‡ P. Boutachkov, ‡ P. A. Butler, § P. Chowdhury, ¶ J. A. Cizewski, || R. Herzberg, § G. Jones, § R. Julin, ** M. Leino, ** E. Ngijoi-yogo, ¶ P. Reiter, †† M. Shawcross, ‡ M. B. Smith, || A. Teymurazyan, ‡ and J. Uusitalo**)

The heaviest nuclei are stabilized against fission by shell effects. Hence the accuracy of theoretical predictions of superheavy elements depends on the correct proton and neutron shell structures. 2-quasiparticle states provide information on the single particle energies and on the pair gap. The primary aim

of the present work was to determine the properties of a reported¹ 2-qp isomer ($T_{1/2} = 0.28$ sec) in ²⁵⁴No.

The experimental study of nuclei with $Z \geq 102$ are difficult due to their low production cross sections. Even in the quiet environment at the focal plane of a recoil separator, such as the FMA at Argonne, the small

number of nuclei yield a decay rate much smaller than the background rate. Therefore, new techniques have to be developed to study the isomeric decays of these nuclei through delayed γ rays, alphas and electrons.

^{254}No was populated by the reaction $^{208}\text{Pb}(^{48}\text{Ca},2n)$ with 220 MeV, 50-pnA beam from ATLAS. Evaporation residues were identified by (M/Q) in the FMA and by gating on a ΔE -TF 2D matrix. ΔE is the energy loss in the focal plane PPAC and TOF the time of flight between the PPAC and a micro channel plate detector. After traversing these detectors, ~ 1000 ^{254}No residues

were implanted into a Si PIN diode, one of five detectors in a box array, which detected electrons and α 's and also served as an electron calorimeter. The γ rays were detected in two clover Ge detectors and two LEPS's, closely packed to maximize the solid angle.

Prompt γ - γ and e - γ coincidences, which occurred within 0.6 sec. of ^{254}No implantation, give tentative indication of an isomer, but further analysis is necessary. Data on e - e coincidences are also being analyzed for evidence of the isomer.

*Argonne National Laboratory and the University of Massachusetts, †Argonne National Laboratory and the University of Maryland, ‡University of Notre Dame, §University of Liverpool, United Kingdom, ¶University of Massachusetts, ||Rutgers University, **Univ. of Jyväskylä, Finland, ††Ludwig-Maximilians-Universität, Germany
¹A. Ghiorso et al., Phys. Rev. C 7 2032 (1973).
²P. Reiter et al., Phys. Rev. Lett. 82 509 (1999).

c.7. Transition Intensities in ^{220}Th (A. Heinz, T. L. Khoo, I. Ahmad, M. P. Carpenter, C. N. Davids, J. P. Greene, W. F. Henning, R. V. F. Janssens, F. G. Kondev, T. Lauritsen, C. J. Lister, D. Seweryniak, A. A. Sonzogni, I. Wiedenhöver, P. Reiter,* P. Bhattacharyya, † J. A. Cizewski, ‡ G. D. Jones, § R. Julin, ¶ J. Uusitalo, || and S. Siem**)

The nuclear fission barrier of unstable nuclei is difficult to determine. The measurement of the entry distribution - the total excitation energy of a compound nucleus after particle evaporation as function of the angular momentum¹ - provides a new method for determining the barrier. In this work, the fusion of ^{220}Th has been investigated using a ^{48}Ca beam at 206 MeV and 219.5 MeV impinging on a $810\text{-}\mu\text{g}/\text{cm}^2$ thick ^{176}Yb target. The recoils were identified using the mass-to charge information of the PPAC at the FMA focal plane. Gammasphere measured gamma radiation of the selected nucleus. In addition to the measured entry distributions we are able compare the transition intensities measured in this work with data from an experiment using the $^{208}\text{Pb}(^{16}\text{O},4n)^{220}\text{Th}$ reaction, as a complementary indicator of the angular momentum in the evaporation residues. The latter reaction is expected to introduce less angular momentum into the compound-nuclear system. Due to the level scheme of two alternating parity bands connected by E1 transitions, it was necessary to define the transition intensity T(I) as function of nuclear spin in the

following way: $T(I) = T(I^+) + T((I+1)^-)$. Figure I-30 shows the experimental result. Note that due to limits in the statistics, transitions beyond $11^- \rightarrow 10^+$ could not be observed for the higher beam energy.

This figure demonstrates clearly that neither the change of the reaction nor the increase in beam energy leads to a significant increase in angular momentum. A model calculation³ predicts that the initial compound nucleus will have on the average $20 \hbar$ more angular momentum at the higher beam energy. The experimental result indicates that fission is indeed limiting the maximum angular momentum that the compound nucleus can sustain. This finding is also consistent with the measured entry distributions⁴, which can be seen by comparing Fig. I-30 and Fig. I-31. For the entry distributions, as well as for the measured transition intensities, the maximum angular momentum is about $20 \hbar$.

Final analysis is in progress.

*University of München, Germany, †Purdue University, ‡Rutgers University, §University of Liverpool, United Kingdom, ¶University of Jyväskylä, Finland, ||University of Jyväskylä, Finland and Argonne National Laboratory, **University of Oslo, Norway and Argonne National Laboratory

¹P. Reiter *et al.*, Phys. Rev. Lett. **84**, 3542 (2000).

²B. Schwarz, Ph.D. thesis, University of Heidelberg, 1998.

³K. Hagino, private communication.

⁴A. Heinz *et al.*, Physics Division Annual Report 2000, ANL-01/19, p. 29 (2001).

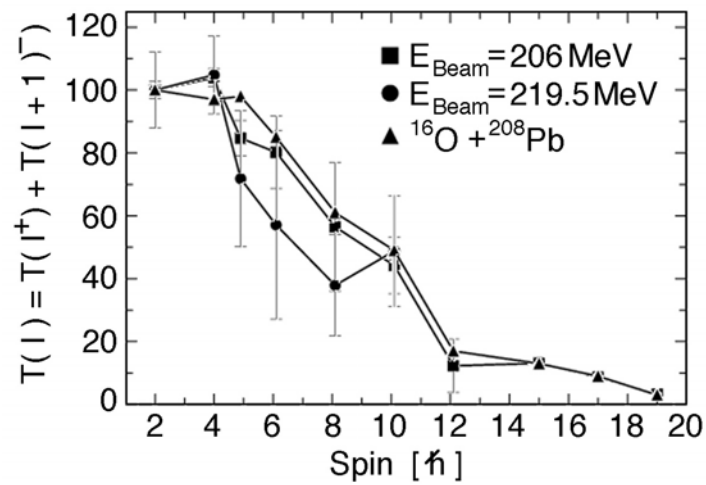


Fig. I-30. Intensities of gamma-ray transitions of ^{220}Th at beam energies of 206 MeV (squares) and 219.5 MeV (circles) in comparison with data from Schwarz (triangles).² Preliminary result.

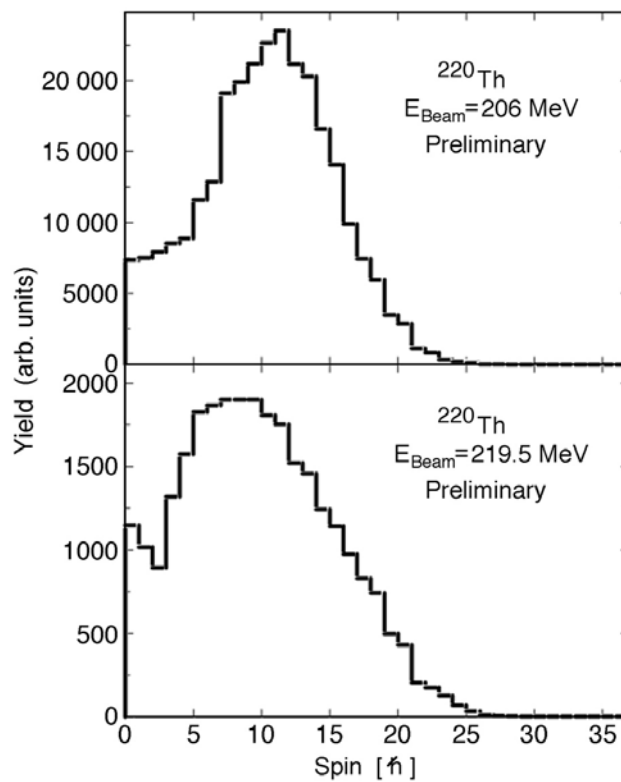


Fig. I-31. Projections of the entry distribution of ^{220}Th on the spin axis at beam energies of 206 MeV and 219.5 MeV (see Ref. 4).

c.8. Production and Decay of ^{257}Rf (A. Heinz, R. V. F. Janssens, D. Seweryniak, K. Abu Saleem, I. Ahmad, B. Back, M. P. Carpenter, C. N. Davids, J. P. Greene, D. J. Henderson, C.-L. Jiang, T. L. Khoo, F. G. Kondev, T. Lauritsen, C. J. Lister, E. F. Moore, R. C. Pardo, T. Pennington, G. Savard, J. P. Schiffer, R. H. Scott, R. C. Vondrasek, A. Woehr,* J. Shergur,* P. Collon,† and M. B. Smith‡)

As part of a program aiming at the study of the heaviest elements, the production and decay of ^{257}Rf ($Z = 104$) was investigated at ATLAS with the $^{50}\text{Ti} + ^{208}\text{Pb}$ reaction at 234 MeV. Beam intensities up to 73 pnA were obtained. The cross section for this reaction has been measured before to be about 5 nb.¹ Thus, this experiment presents a significant step towards lower cross sections in comparison with the experiments performed for the investigation of ^{254}No where the production cross section is $\approx 3 \mu\text{b}$.²

The ^{257}Rf residues were passed through the Fragment Mass Analyzer, which provides a direct measurement of the mass-to-charge ratio, and were implanted in a double-sided Si strip detector with 40×40 strips, allowing for recoil-decay and decay-decay correlations.

The mass information provides an additional tool in order to understand the rather complex decay spectrum.

In order to calibrate the measured alpha energies a ^{170}Er target was used at the same beam energy to produce alpha emitters around ^{215}Th .

First results confirm earlier measurements at GSI¹ which were made with higher beam intensities and show the feasibility of this kind of experiments with ATLAS.

A representative α energy spectrum and a position spectrum of the FMA focal plane are shown in Fig. I-32. Efficient α - γ spectroscopy will be needed to clarify the “fine structures” found in the α -spectrum.

*University of Maryland, †Columbia University, ‡Rutgers University

¹F. Heßberger *et al.*, *Z. Phys*, **A359**, (1997) 415.

²H. W. Gäggeler *et al.*, *Nuc. Phys.* **A502**, 641c (1989); P. Reiter *et al.*, *Phys. Rev. Lett.* **82**, 509 (1999)

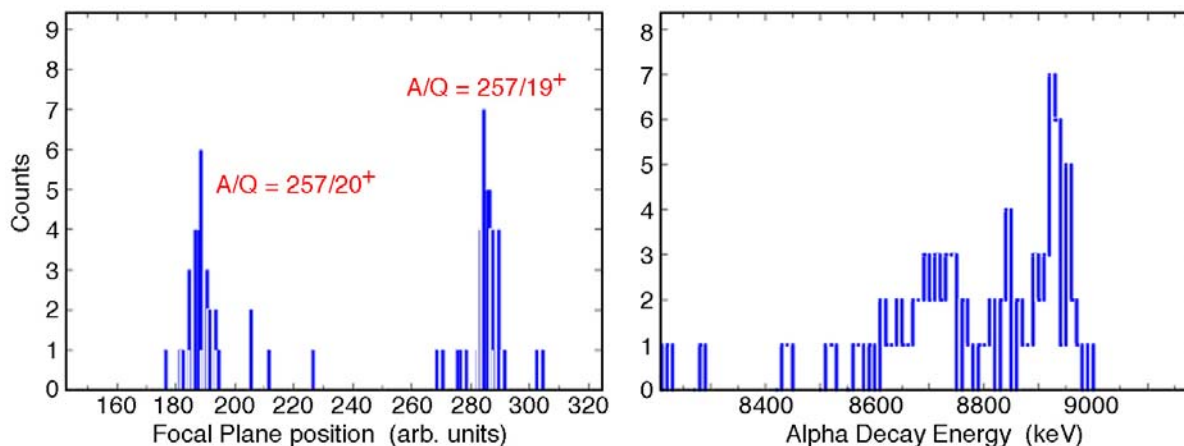


Fig. I-32. Left panel: Position spectrum of ^{257}Rf at the FMA focal plane. Right panel: Alpha energy spectrum of ^{257}Rf . Both spectra are preliminary.

D. OTHER TESTS OF NUCLEAR STRUCTURE UNDER EXTREME CONDITIONS

A broad-based program of nuclear structure studies continued during the last year. Radiative capture was one interesting theme with studies in both light ($^{12}\text{C}+^{12}\text{C}$) and heavy ($^{90}\text{Zr}+^{89}\text{Y}$) nuclei. The dynamics of the radiative capture process is interesting in itself, and these ultra-cold reactions seem to be rich in potential for populating unusual non-yrast structures. New high spin results continue, including observation of the long-predicted deformed multi-particle, multi-hole states in ^{40}Ca , the observation of extremely large deformation in cadmium nuclei, and finally, the observation of the direct decay between superdeformed bands in ^{152}Dy and lower-lying normally deformed configurations. This latter experiment was one of the prime motivations for building Gammasphere. The experiment which led to successful observation of this decay mode, and in addition, the decay of a more highly excited superdeformed band, arose from a close collaboration between groups from ANL and LBNL and data collected from Gammasphere at ATLAS and the 88" cyclotron.

d.1. Radiative Fusion of $^{12}\text{C} + ^{12}\text{C}$, $^{12}\text{C} + ^{16}\text{O}$ and $^{16}\text{O} + ^{16}\text{O}$ (C. J. Lister, M. P. Carpenter, R. V. F. Janssens, T. L. Khoo, A. Wuosmaa, D. Jenkins,* B. Truett,† B. R. Fulton,‡ J. Pearson,‡ M. Freer,§ P. Fallon,¶ A. Gorgen,¶ and A. O. Macchiavelli¶)

Radiative Capture of heavy ions, the process of complete fusion without particle evaporation, is never favored because the high Coulomb barrier in the entrance channel always leads to highly excited residues that dominantly decay by particle emission. However, studying the nuclei which do cool by gamma-emission can tell us a great deal about the fusion process, and appear to selectively populate states in the final nuclei which are very hard to reach by any other means.

The fusion of "light" heavy ions, like carbon and oxygen, is particularly interesting. The overall fusion-evaporation cross-section is known to vary rapidly in energy with resonance-like structures. The nature of these resonances has never been unambiguously determined. Clearly, radiative capture can help understand this puzzle, as gamma-spectroscopy might allow the widths and spins of the resonances to be determined. The seminal work of Sandorfi and Nathan^{1,2} showed that direct capture could be measured, and the resonant structure investigated. Their technique, using large NaI(Tl) detectors to measure high energy gamma rays, only allowed investigation of

"direct" single GQR gamma decays, although they did find tantalizing evidence for "multi-step" decay.

The development of large arrays, like Gammasphere, has opened the possibility of observing the entire decay flux and investigating the fusion and decay processes more directly, especially investigating higher spin resonances which do not decay to the groundstate in a single step. Our measurements show that multi-step pathways are the dominant decay mechanism. Gamma-gamma correlations can accurately allow reconstruction of the parent state and the intermediate steps which the decay proceeds through. With sufficient data, the widths of the reconstructed resonances can be measured, to a level which is not possible by other means.

We have performed a series of experiments at ANL and at LBNL to investigate radiative capture. Using Gammasphere as a total energy calorimeter, the radiative capture events can be clearly seen, as they have the highest "total sum energy". Selecting these events by total energy, one can then investigate them in more detail and look at the cooling paths. For the

*University of Liverpool, United Kingdom, †Purdue University, ‡University of York, United Kingdom, §University of Birmingham, United Kingdom, ¶Lawrence Berkeley National Laboratory

¹A. M. Sandorfi, *Treatise on Heavy Ion Science*, Vol. 2., Sec. 3, ed. D. Allan Bromley.

²A. Nathan, A. M. Sandorfi and T. J. Bowles, *Phys. Rev. C* **24**, 932 (1981).

$^{12}\text{C} + ^{12}\text{C}$ system we have conducted a thin target excitation function. The absolute yield of radiative capture can be seen to resonate, and the decay path changes character between “on” and “off” resonance. The “on resonance” pattern is confined to passing through rather few intermediate energy states. These states then preferentially seem to decay to the known low-lying $K = 2$ band, and not to yrast states, despite phase-space favoring the yrast decays. Recently, we also found multi-step radiative capture in $^{12}\text{C} + ^{16}\text{O}$ and $^{16}\text{O} + ^{16}\text{O}$ reactions.

The data analysis is still in progress. Qualitatively, it appears clear that the “one-step” decays observed by Sandorfi and Nathan constitutes only a small part of the total radiative capture cross-section. The key challenge is extract quantitative cross-sections. This is difficult,

as the calorimetric “event trigger” efficiency is very difficult to estimate, as it is a convoluted function of germanium and BGO responses, and is energy and multiplicity dependent. This needs careful simulation, and probably more detailed measurements. It is clear that the trigger efficiency falls rapidly with multiplicity, so the potential for investigating high spin ($J > 4$) resonances is very difficult through a calorimetric trigger. However, if the fused residues are independently detected and counted, and became the trigger, then much more efficient and quantitative studies should be possible. This approach was proven to be possible by Sandorfi¹ and appears appropriate for the “upgraded” FMA and Gammasphere when it returns to ATLAS. A proposal for a test experiment to detect the fused products is being developed.

d.2. Superdeformation in the Doubly Magic Nucleus ^{40}Ca (R. V. F. Janssens, M. P. Carpenter, T. Lauritsen, D. Seweryniak, C. J. Lister, E. Ideguchi,* D. G. Sarantites,* W. Reviol,* A. V. Afanasjev,† M. Devlin,* C. Baktash,‡ D. Rudolf,§ A. Axelsson,¶ A. Galindo-Uribarri,‡ D. R. LaFosse,|| F. Lerma,* M. Weiszflog,¶ and J. N. Wilson*)

The coexistence of spherical and highly deformed configurations in doubly magic ^{40}Ca has been predicted for many years, originally by Gerace and Green, and some candidates for the first members of the bands known since the 1970’s. Hartree Fock calculations by Zamick and Zheng have consistently indicated that a variety of multi-particle, multi-hole states should polarize the core and lead to deformation. It is an interesting issue to study the balance between the energy gained in deformation and the cost in promotion of particles into the $f_{7/2}$ shell. The predictions indicated that 8p-8h (i.e. two alpha particle) excitations would be energetically very favored and have a deformation close to $\beta = 0.6$, that is a “superdeformed” shape. However, only with the development of highly efficient 4π gamma arrays like Gammasphere, triggered by channel selection devices such as microball, has the experimental possibility of extending these highly deformed collective structures to high spin, and measuring their shapes, through lifetime determinations, became feasible. The experimental challenges are considerable, as it is difficult to create

light nuclei at very high spin, charged particle evaporation carries away much of the flux, the gamma-ray multiplicities are relatively low and the key gamma rays are of high energy so are difficult to detect.

In a recent experiment these challenges were overcome. The $^{28}\text{Si}(^{20}\text{Ne}, 2\alpha)^{40}\text{Ca}$ reaction was used with an 84-MeV neon beam from the ATLAS accelerator. Gammasphere and microball provided a sensitive and efficient setup. The known high spin level scheme of ^{40}Ca was greatly extended.¹ Several bands were developed, two of them to $J^\pi = 16^+$. The residual Doppler Shift Method was used to extract the mean quadrupole moments of the bands. The band based on the known third $J^\pi = 0^+$ has the properties expected from the 8p-8h band with a mean quadrupole moment of $Q = 1.80$ eb, consistent with a uniformly charged axial shape of $\beta = 0.59$. This observation confirms the predictions of highly deformed shapes co-existing with spherical configurations which were made more than 30 years ago.

*Washington University, †Argonne National Laboratory, University of Notre Dame, and University of Latvia, Latvia, ‡Oak Ridge National Laboratory, §Lund University, Sweden, ¶Uppsala University, Sweden, ||State University of New York

¹E. Ideguchi, D. G. Sarantites *et al.*, Phys. Rev. Letts. **87**, 222501 (2001).

d.3. Large Angle Alpha Scattering on ^{44}Ti (K. E. Rehm, C. L. Jiang, I. Ahmad, J. Caggiano, P. Collon, J. P. Greene, D. Henderson, A. Heinz, R. V. F. Janssens, R. C. Pardo, T. Pennington, J. P. Schiffer, R. H. Siemssen, A. Wuosmaa, M. Paul,* and P. Mohr†)

The analysis of large angle α scattering on ^{44}Ti , the first α -type $N = Z$ nucleus above ^{40}Ca , is complete. For lighter sd-shell nuclei enhanced cross sections for elastic α scattering were observed at angles beyond 90° .¹ Because this effect is especially pronounced for scattering on α -particle nuclei (e.g. ^{16}O , ^{20}Ne , ^{24}Mg , ^{28}Si , ^{32}S , ^{36}Ar , ^{40}Ca) it was argued² that α cluster and exchange effects in the target nucleus might also play a role. Since no stable $N = Z$ α -particle nuclei exist beyond ^{40}Ca the question whether anomalous large angle scattering ends at $A = 40$ could not be studied in the past.

Technical details for this experiment were presented in last year's annual report. We since performed optical model and Distorted Wave Born Approximation (DWBA) calculations to describe the measured angular distributions.

The angular distributions for elastic scattering of alphas from ^{40}Ca ($E_{\text{lab}} = 240$ MeV, $E_{\text{cm}} = 21.8$ MeV) and ^{44}Ti ($E_{\text{lab}} = 261.5$ MeV, $E_{\text{cm}} = 21.8$ MeV) obtained in this experiment are shown in Fig. I-33 by the open and solid points, respectively. While for ^{40}Ca at backward angles elastic cross sections in the vicinity of the Rutherford values are observed, the corresponding yields for ^{44}Ti are about a factor of 20 smaller and, thus, are comparable to the yields obtained for non-alpha-particle nuclei such as $^{42,44,48}\text{Ca}$ or heavier nuclei. The solid lines are the result of an optical model fits which follow closely the analysis³ which was successfully used for a description of elastic alpha scattering on a few nuclei

between ^{40}Ca and ^{208}Pb .³ The real part of the potential is calculated by the double folding model using the density of ^{44}Ti .⁴ For the imaginary part a pure Woods-Saxon parameterization was chosen, and the parameters were adjusted to the new experimental data. The smaller cross sections at backward angles for ^{44}Ti require a stronger absorptive potential roughly twice as strong as for ^{40}Ca , but comparable to the results obtained for heavier nuclei such as $^{58,60}\text{Ni}$.

The strong $B(E2)$ value of the first excited state in ^{44}Ti ($B(E2) = 0.061$ e²b²) allowed also for a measurement of the 2^+ $E_x = 1.083$ MeV angular distribution which is shown in Fig. I-34 together with the cross section of the elastic channel. The yields for inelastic scattering at backward angles are comparable to the elastic cross sections. The angular distribution from a DWBA calculation performed with the finite-range code PTOLEMY using the optical potential from Fig. I-33, a $B(E2) = 0.061$ e²b² and a nuclear deformation parameter $\beta = 0.2$ is shown by the solid line in Fig. I-34. Similar to the results observed for the 2^+ excitation in the system $\alpha + ^{44}\text{Ca}$ the ^{44}Ti data are found to be in good agreement with the calculations.

These first measurement of elastic and inelastic α scattering with an $N = Z$ nucleus heavier than ^{40}Ca showed that the anomalous large angle scattering (ALAS) seems to end at $^{40,41}\text{Ca}$. An optical-model analysis of the $\alpha + ^{44}\text{Ti}$ data gave parameters which are in good agreement for the scattering of α 's on heavier nuclei.

*Hebrew University, Jerusalem, Israel, †Technische Universität Darmstadt, Germany

¹R. Planeta, H. Dabrowski, L. Freindl and K. Grotowski, Nucl. Phys. **A326**, 97 (1979).

²D. Agassi and N. S. Wall, Phys. Rev. **C7**, 1368 (1973).

³U. Atzrott, P. Mohr, H. Abele, C. Hillenmayer and G. Staudt, Phys. Rev. **C53**, 1336 (1996).

⁴R. Ejnisman, D. Goldman, K. S. Krane, P. Mohr, Y. Nakazawa, E. B. Norman, T. Rauscher and J. Reel, Phys. Rev. **C 58**, 2531 (1998).

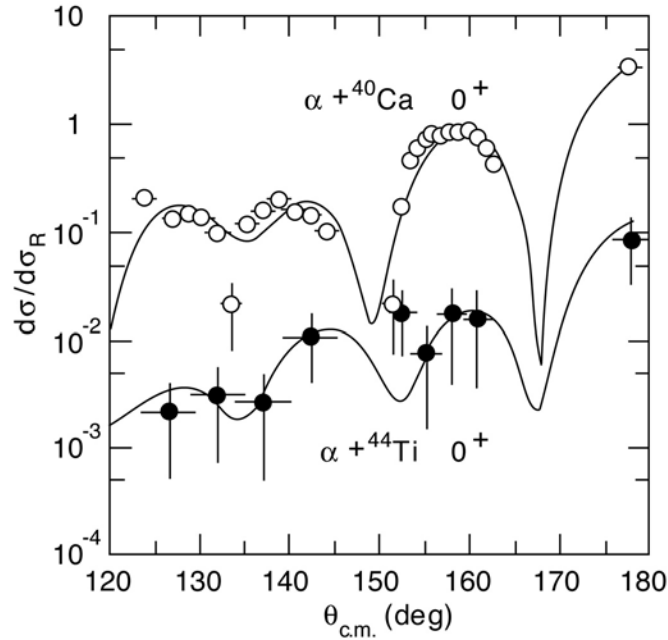


Fig. I-33. Ratio between the differential cross sections for elastic scattering and the corresponding Rutherford values measured for the systems $\alpha + {}^{40}\text{Ca}$ and ${}^{44}\text{Ti}$ at a center-of-mass energy of 21.8 MeV. The cross sections for the ${}^{44}\text{Ti}$ target are smaller than the ones for ${}^{40}\text{Ca}$ by 1 - 2 orders of magnitude. The solid lines are optical model calculations using a double-folding potential for the real part and a Woods-Saxon parameterization for the imaginary part. See text for details.

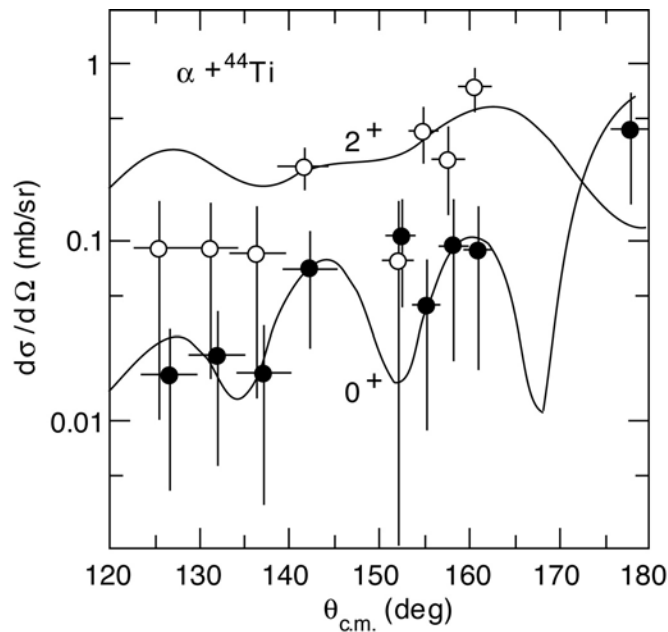


Fig. I-34. Differential cross sections for elastic scattering (solid points) and inelastic excitation of the first 2^+ state (open points) in ${}^{44}\text{Ti}$. The solid lines are the result of optical model (elastic) and DWBA (inelastic) calculations, described in the text.

d.4. Very Extended Shapes in the A ~ 110 Region (M. P. Carpenter, R. V. F. Janssens, R. M. Clark,* P. Fallon,* M. Cromaz,* M. A. Deleplanque,* R. M. Diamond,* A. Goergen,* G. J. Lane,* I. Y. Lee,* A. O. Macchiavelli,* R. G. Ramos,* F. S. Stephens,* C. E. Svensson,* K. Vetter,* D. Ward,* and R. Wadsworth†)

Over the last fifteen years, great strides were made in the study of superdeformed nuclei. Much of the initial effort was directed at identifying regions of superdeformation which were predicted by theoretical models using a standard parameterization of the nuclear shape. Until recently, in all regions for which superdeformed nuclei have been found, the major to minor axis ratios do not exceed 2:1. It was pointed out by Chasman that one must use a modified parameterization of the nuclear shape which explicitly treats necking degrees of freedom when the major to minor axis ratio exceeds 2:1.¹ Recently, calculations by Chasman,² using the cranked Strutinsky method with a four-dimensional shape representing quadrupole, octupole, hexadecapole, and necking degrees of freedom, predict that a region of "extended" shapes with axis ratios 2:1 and greater exist at high angular momentum in nuclei with A ~ 110.

In order to test these calculations, high-angular momentum states in ¹⁰⁸Cd were populated via the ⁶⁴Ni(⁴⁸Ca,4n) reaction at a beam energy of 207 MeV. The beam was provided by the ATLAS accelerator at Argonne National Laboratory. Gamma rays were detected with the Gammasphere spectrometer outfitted with 101 Compton-suppressed Ge detectors. From an analysis of the data, a rotational sequence of quadrupole transitions were identified in ¹⁰⁸Cd, and it is estimated that the states in the band lie between I = 40(2) - 60(2) \hbar . The moments of inertia and the deduced lower limit of the transition quadrupole moment suggest a very extended prolate shape for the nucleus, with a axis ratio >1.8:1. This is among the most deformed nuclear structures ever observed, and it is possible that the band may have an axis ratio greater than 2:1 as predicted by Chasman.²

A paper reporting the results of this work was recently published in Physical Review Letters.³

*Lawrence Berkeley National Laboratory, †University of York, United Kingdom

¹R. R. Chasman, Phys. Lett. **B302**, 134 (1993).

²R. R. Chasman, Phys. Rev. C **64**, 024311 (2001).

³R. M. Clark et al., Phys. Rev. Lett. **87**, 202502 (2001).

d.5. Investigation of Anti-Magnetic Rotation in ¹⁰⁰Pd (R. V. F. Janssens, M. P. Carpenter, F. G. Kondev, T. Lauritsen, A. V. Afanasjev,*† S. Zhu,† U. Garg,† S. Frauendorf,† B. Kharraja,† S. S. Ghugre,‡ and S. N. Chintalapudi‡)

"Magnetic rotation" is a topic of great interest and activity in nuclear structure over the past few years. Strong M1 bands were observed in the nuclei of the Pb and Sn regions. These bands, while as regularly spaced as the bands observed in well deformed and even superdeformed nuclei, show very weak E2 transitions, implying a small deformation. The interpretation of this apparent contradiction was given in terms of the "shears mechanism".¹ In case of the Pb nuclei, a pair of $h_{9/2}i_{13/2}$ protons and between one and three $i_{13/2}$ neutron holes generate the angular momentum. The particles are in stretched coupling and so are the holes. Their angular momenta form the two "blades" of a pair of shears, which gradually close when the total angular momentum increases along the band. The particles and holes move in circular orbitals in the planes perpendicular to their angular momenta. These loops of

nucleonic currents are crossed when the shears are open. This anisotropic arrangement breaks the rotational symmetry. "Magnetic rotation" alludes to these currents and the magnetic moment they create, generating the strong M1 radiation.

Associated with, and complementary to, magnetic rotation is the concept of "anti-magnetic rotation". In this scenario, the coupling for the A ~ 110 case is such that two pairs of stretched proton $g_{9/2}$ holes point in opposite directions and gradually align along the direction of the stretched $h_{11/2}$ neutrons creating a "fork", with the neutrons forming the middle prong and the proton holes forming two symmetric side prongs. Angular momentum, then, is generated mainly by "bending" the side prongs. In contrast to the M1 bands, this arrangement is symmetric with respect to a rotation

about the total angular momentum vector by an angle of π . Consequently, the signature, α , is a good quantum number and the resulting “fork bands” have a regular $\Delta I = 2$ structure, in contrast with the $\Delta I = 1$ sequences associated with the “shears bands”. The magnetic moment disappears in the symmetric arrangement of the current loops, which nevertheless specify the orientation. (The term “anti-magnetic” rotation alludes to the analogy with ferro and anti-ferromagnetism).

High spin states were studied in the nucleus ^{100}Pd with the aim of investigating this novel phenomenon of

“anti-magnetic rotation”. The reaction $^{72}\text{Ge}(^{35}\text{Cl}, \alpha p 2n)^{100}\text{Pd}$ was used at a bombarding energy of 135 MeV. The experiment was carried out at the ATLAS facility and the Gammasphere detector array was employed in its “stand alone” mode. A cascade of four “rotational-band-like” transitions is proposed as corresponding to anti-magnetic rotation, based on the observed spectroscopic properties and a comparison with calculations in the configuration-dependent cranking Nilsson-Strutinsky formalism.

A paper describing these results was recently published.²

*Argonne National Laboratory and the University of Notre Dame, †University of Notre Dame, ‡IUCDAEF-Calcutta Centre, Calcutta, India

¹S. Frauendorf, Nucl. Phys. A **557**, 259c (1993).

²S. Zhu *et al.*, Phys. Rec. C **64**, 041302(R) (2001).

d.6. Direct Decay-Out from the Superdeformed Band to the Yrast Line in $^{152}_{66}\text{Dy}_{86}$
(T. Lauritsen, M. P. Carpenter, R. V. F. Janssens, D. G. Jenkins, T. L. Khoo, K. S. Abu Saleem, I. Ahmad, J. P. Greene, A. M. Heinz, C. J. Lister, D. Seweryniak, S. Siem, R. C. Vondrasek, F. G. Kondev,* T. Døssing,† P. Fallon,‡ B. Herskind,† A. Lopez-Martens,§ A. O. Macchiavelli,‡ D. Ward,‡ R. Clark,‡ M. Cromaz,‡ F. Hannachi,§ A. Korichi,§ G. Lane,‡ P. Reiter,¶ and I. Wiedenhöver||)

The excitation energy, spin and parity of the yrast superdeformed band in $^{152}\text{Dy}^1$ have been firmly established. The evidence comes mainly from the measured properties of a 4011 keV single-step transition connecting the yrast superdeformed level fed by the 693 keV transition to the 27^- yrast state. Four additional, weaker, linking γ rays were placed as well. The excitation energy of the lowest superdeformed band member is 10,644 keV and its spin and parity was determined to be $J^\pi = 24^+$.

The first experimental evidence for a 4011 keV linking transition in ^{152}Dy , as well as hints of others, was found in a Gammasphere experiment performed at Argonne National Laboratory. Due to the low intensities of the observed linking transitions, another much longer experiment (12 days) was performed with Gammasphere at Lawrence Berkeley National Laboratory. The band was populated with the reaction $^{108}\text{Pd}(^{48}\text{Ca}, 4n)^{152}\text{Dy}$ with a 191 MeV (mid-target) ^{48}Ca beam.

Figure I-35a shows the spectrum obtained by placing pairwise coincidence gates on transitions in the yrast SD band in ^{152}Dy . At higher γ -ray energies, shown in

Fig. I-36a, several candidates for decay-out transitions are clearly seen. In particular, γ rays at 2713 and 4011 keV are prominent while a number of other, weaker, candidates are visible as well.

The coincidence spectrum obtained by placing pairwise gates on SD lines and on the 4011-keV transition is presented in Fig. I-35b. It is clearly seen that the 647 and 602 SD lines (see Fig. I-37) are not in coincidence with the 4011-keV γ -ray, whereas the 693 keV and higher SD lines are. This unambiguously establishes that the 4011 keV transition originates from the SD level fed by the 693 keV line. Of the normal yrast transitions in the spectrum, the 221 and 541 keV γ rays have the full intensity of the SD band (0.8(3) and 0.9(2), respectively), whereas there is no indication of the normal 967 keV transition (the intensity is 0.3(3)), which should be detectable despite the proximity of the 970 keV SD γ -ray. A comparison with the spectrum in Fig. I-35a shows no new peaks with an area larger than 3 standard deviations. This strongly suggests that the 4011-keV γ ray feeds directly into the 27^- yrast state in a single step. This establishes the excitation energy of the SD level fed by the 693 SD line as 11,893 keV -- as shown in the partial level scheme of Fig. I-37. To determine the spin of the 11,893-keV SD level an angular distribution analysis of the 4011-keV transition

was performed. The intensity of this γ ray, as a function of polar angle, is presented in Fig. I-36b. Using the functional form $\theta = A_0 (1 + A_2 P_2(\cos\theta) + A_4 P_4(\cos\theta))$, the angular distribution coefficients were determined to be: $A_2 = -0.35(12)$ and $A_4 = -0.02(16)$ – consistent only with a stretched or anti-stretched dipole character. Thus, based on the 4011-keV transition, the feeding SD level must have a spin of either 26 or 28 \hbar .

With the energy of the SD band determined by the 4011-keV line, four additional γ rays in the 3-MeV region of Fig. I-36 can be placed in the level scheme as direct links between the SD band and the normal states. They are included in Fig. I-37. All four of these additional links are very weak and, thus, it is difficult to place coincidence gates on them. However, in a spectrum of pairwise gates placed on the 693-keV line and on clean SD transitions above it, the 2895-, 3044-,

3364- and 3585-keV γ rays are clearly present, whereas a similar spectrum with a gate on the 647-keV line only shows the two transitions with the highest energy, i.e., the 2895- and 3044-keV γ rays are absent. Thus, the latter two transitions emanate from the 11893-keV SD level, and the two others are associated with the deexcitation of the SD state directly below it at 11,246-keV. These weaker one-step linking transitions also resolve any remaining ambiguity concerning the spins of the SD band members. Only when 28^+ is assigned to the 11893 SD level are the multiplicities of the 2895 and 3364 keV lines reasonable: M1 and E1, respectively. A 26^+ assignment would result in respective M3 and E3 multiplicities which are improbable, be it only because of the competition with the in-band, highly collective 602 keV γ ray.

These results were published.²

*Technology Division, Argonne National Laboratory, †Niels Bohr Institute, Copenhagen, Denmark, ‡Lawrence Berkeley National Laboratory, §C.S.N.S.M, Orsay, France, ¶Ludwig-Maximilians-Universität, Munich, Germany, ||Florida State University

¹P. J. Twin *et al.*, Phys. Rev. Lett. **57**, 811 (1986).

²T. Lauritsen *et al.*, Phys. Rev. Lett. **88**, 042501 (2002).

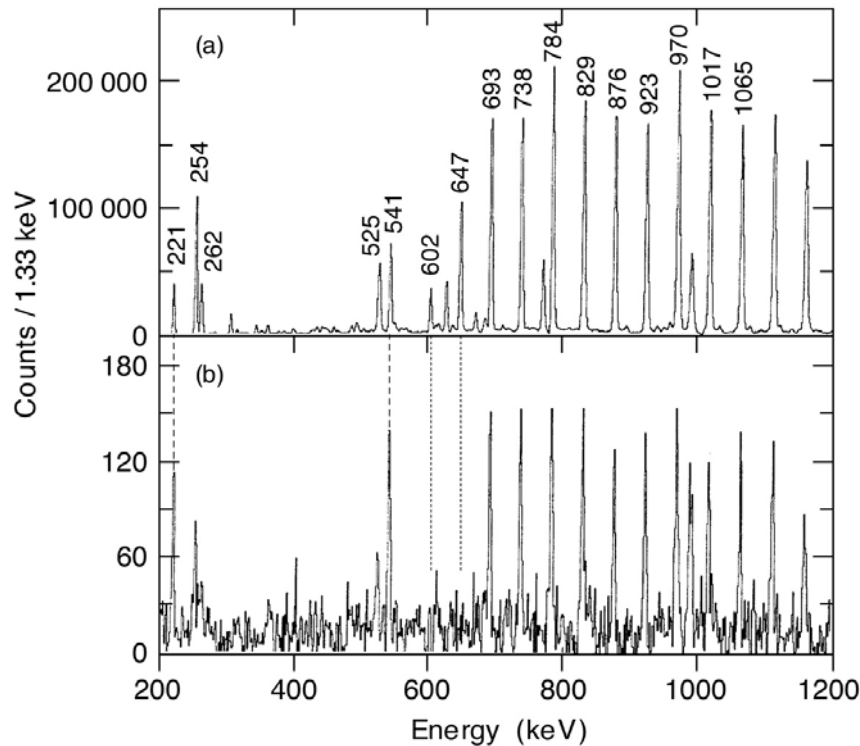


Fig. I-35. (a) Spectrum from pairwise coincidence gates in the yrast SD band of ^{152}Dy . The 94 cleanest combinations of the following SD transitions were used: 647, 693, 738, 784, 829, 876, 923, 1017, 1065, 1161, 1209, 1257, 1305, 1353, 1402 and 1449 keV. (b) Spectrum obtained from setting pairwise gates on a SD line and the 4011-keV transition. All SD transitions listed above (except that of 647 keV) were used as gates.

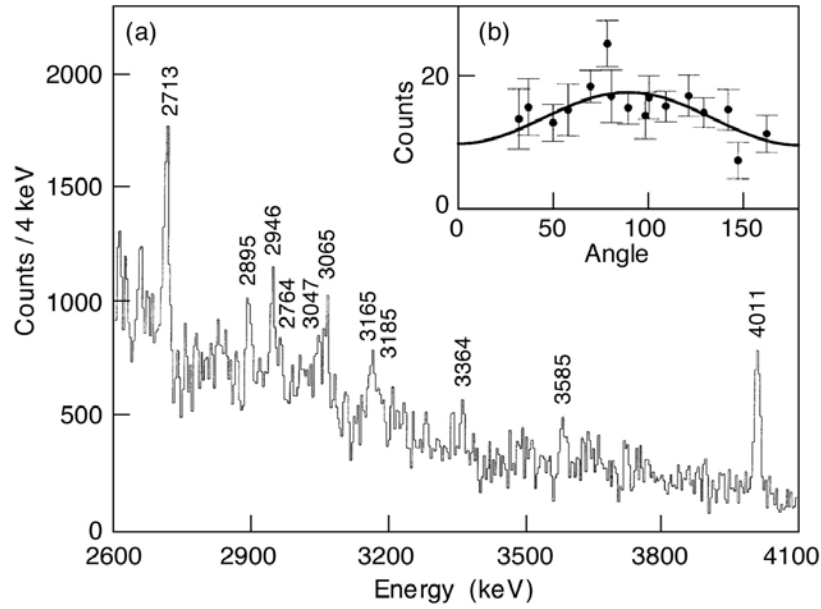


Fig. I-36. (a) High-energy portion of the spectrum in coincidence with ^{152}Dy SD transitions. (b) Angular distribution of the 4011 keV transition.

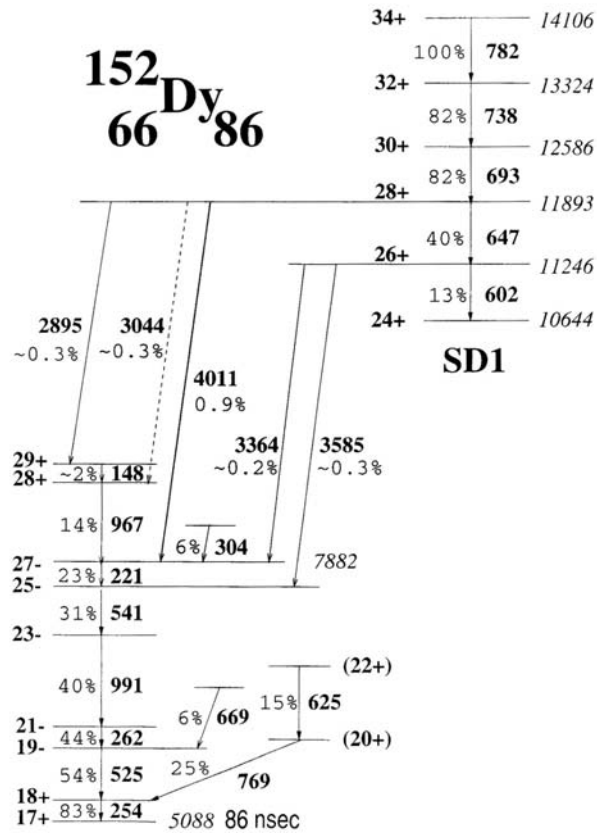


Fig. I-37. Partial level scheme of ^{152}Dy showing the lowest part of the yrast SD band and normal states to which the SD band mainly decays.

d.7. Octupole Excitation in Superdeformed $^{152}_{66}\text{Dy}_{86}$ (T. Lauritsen, R. V. F. Janssens, M. P. Carpenter, D. G. Jenkins, T. L. Khoo, K. S. Abu Saleem, I. Ahmad, J. P. Greene, A. M. Heinz, C. J. Lister, D. Seweryniak, S. Siem, R. C. Vondrasek, F. G. Kondev,* T. Døssing,† P. Fallon,‡ B. Herskind,† A. Lopez-Martens,§ A. O. Macchiavelli,‡ D. Ward,‡ R. Clark,‡ M. Cromaz,‡ F. Hannachi,§ A. Korichi,§ G. Lane,‡ P. Reiter,¶ and I. Wiedenhöver||)

Three transitions of dipole character were identified linking an excited superdeformed (SD) band in ^{152}Dy to the yrast SD band. As a result, the excitation energy of the lowest level in the excited SD band has been measured to be 14239 keV. The states in this band were determined to be of negative parity and odd spin. The measured properties are consistent with an interpretation in terms of a rotational band built on a collective octupole vibration.

In a number of nuclei, strong shell effects are responsible for an excited minimum associated with a large, prolate deformation (major to minor axis ratio of about 2:1). The physical properties of the excitations occurring in this superdeformed (SD) minimum continue to be the subject of much current interest.

The large data set that was used to link the ^{152}Dy yrast SD band to the normal deformed levels,¹ was also exploited to obtain the best possible spectrum of the very weakly populated ($\sim 5\%$ of the yrast SD band²) SD band 6. The band was populated with the reaction $^{108}_{64}\text{Pb} (^{48}\text{Ca}, 4n) ^{152}\text{Dy}$ with a 191 MeV (at mid-target) ^{48}Ca beam delivered by the 88-inch cyclotron facility at the Lawrence Berkeley National Laboratory. The target consisted of a stack of two 0.4-mg/cm^2 self-supporting ^{108}Pd foils. The Gammasphere array, with 100 Compton suppressed germanium detectors, was used to measure the γ rays of interest.

Band 6 has been proposed to decay into band 1² and Fig. I-38 clearly shows that, indeed, that is the case. A search was conducted for linking transitions between bands 6 and 1. Due to small differences in the moments of inertia of SD bands 1 and 6, any set of linking transitions between them will be characterized by specific energy spacings which depend on which levels are actually linked. Figure I-39a presents the high energy part of the coincidence spectrum of Fig. I-38a.

Three weak transitions can be seen at 1675, 1697 and 1716 keV separated by one of the possible energy spacings (~ 20 keV). Coincidence gates were placed on these transitions together with relevant lines in SD band 6, while also requiring the isomer tag: the resulting spectra are given in Fig. I-40. The spectrum with a gate on the 1697 keV line (panel B) clearly shows only transitions in SD band 6 with energies $E_\gamma \leq 849$ keV, i.e. the 804 keV and 760 keV γ rays of the sequence are clearly missing. Under the same coincidence conditions, only transitions of the yrast SD band with $E_\gamma \geq 783$ keV are observed. This unambiguously establishes the ordering in the level scheme proposed in Fig. I-41. The spectrum with a gate on the 1675-keV line (panel C), which connects the two SD bands just below the 1697-keV linking transition, exhibits the same expected coincidence relationships, i.e., only the band 6 SD lines with $E_\gamma \leq 804$ keV are seen together with band 1 SD transitions with $E_\gamma \geq 738$ keV. The appearance of a ~ 784 keV line in the latter gate is spurious since its intensity was found to change *dramatically* with the background subtraction when compared to the intensities of band 1 and 6 γ rays. Thus, the 784-keV line in this gate is an artifact of a difficult background subtraction. The coincidence spectrum gated on band 6 lines together with the 1716 keV linking transition (not shown) has less statistics, but corroborates the proposed level scheme. Thus, an excited SD band in the mass 150 region has for the first time been linked to an yrast SD band, which in turn is linked to the normal states it decays into.¹

An angular distribution analysis of the three linking transitions at 1675, 1697 and 1717 keV finds negative A_2 coefficients in every case ($-0.4(3)$, $-0.5(4)$ and $-0.9(5)$, respectively). If the areas of the three lines are added up and analyzed together, the combined A_2 coefficient is determined to be $-0.3(2)$, see Fig. I-39b. This value is consistent with those expected

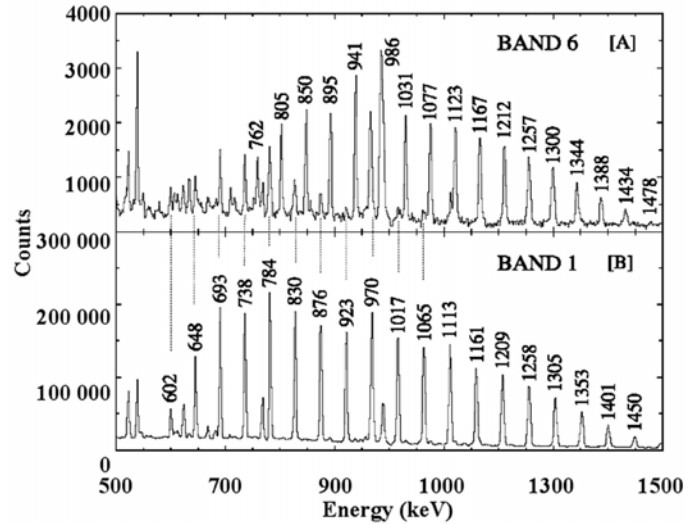


Fig. I-38. (a) Spectrum from triple coincidence gates on lines in SD band 6 of ^{152}Dy . Clean combinations of the following SD transitions were used in the analysis: 760, 804, 849, 894, 940, 1031, 1076, 1122, 1167, 1211, 1256, 1300, 1344 and 1389 keV. (b) Spectrum obtained from setting pairwise gates on clean SD lines in band 1 of ^{152}Dy .¹

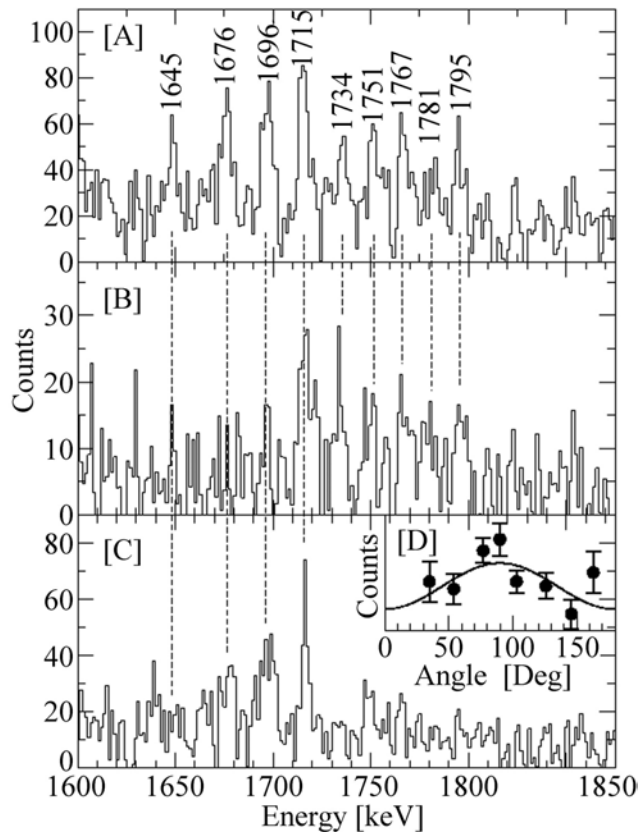


Fig. I-39. (a) Summed coincidence spectrum obtained by placing gates on clean SD-band 6 high-energy transitions and SD-band 1 low-energy transitions. The nine transitions linking SD band 6 to band 1 are marked with their energies. (b) As (a), but requiring the 830-keV transition in band 1. (c) As A, but requiring the 895-keV transition in band 6 and any SD-band 1 transitions below 876 keV. (d) Angular distribution of the sum of the intensities in the 1676-, 1696- and 1715-keV linking transitions vs. the polar angle of the Gammasphere detectors.)

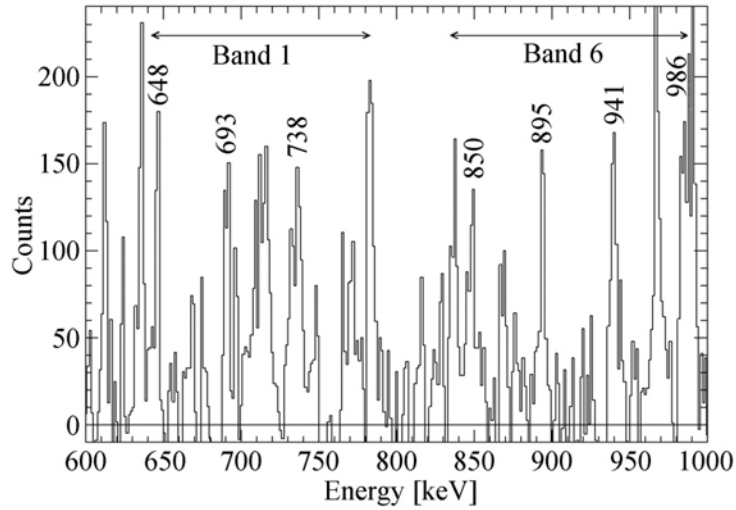


Fig. I-40. Summed coincidence spectrum obtained by placing gates on the 1696-keV linking transition and clean lines in SD band-6.

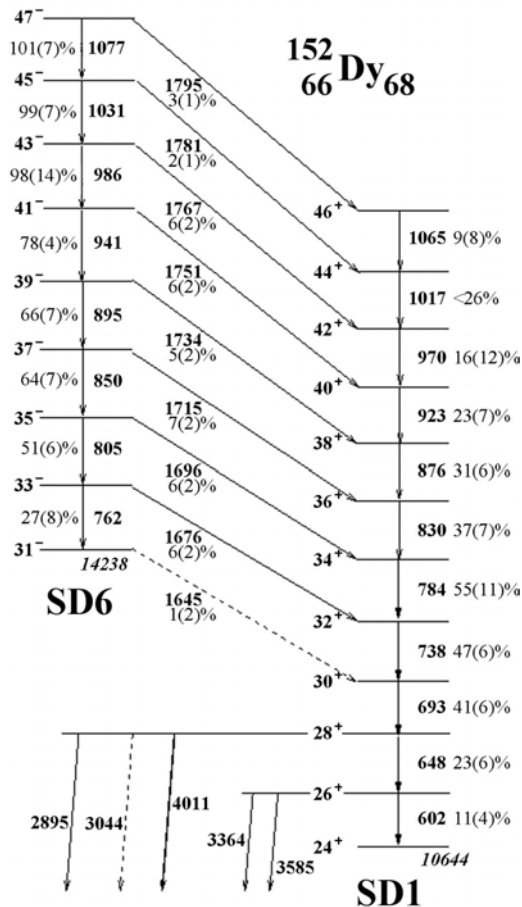


Fig. I-41. Partial level scheme of ^{152}Dy showing the lowest part of SD band 6, the lowest part of the yrast SD band 1 and the transitions that link the yrast SD band 1 to the normal states.¹ The transition intensities, given in %, reflect the requirement of the isomer tag and are with respect to the strongest lines in SD band 6.

for stretched or anti-stretched E1 or M1 transitions (-0.24 - -0.21), but inconsistent with transitions of E2 character or with E1 transitions involving no spin change (where large positive A_2 values of +0.34 and +0.45 are expected, respectively).

RPA calculations by Nakatsukasa *et al.*³ interpret SD band 6 as an octupole excitation with signature $\alpha = 1$. At zero frequency the band is characterized by $K = 0$, but K -mixing is significant at the frequencies of interest here because of the Coriolis force. Experiment and calculations are compared in Fig. I-42, where the Routhian of band 6 with respect to the yrast SD band is given as a function of the rotational frequency. The

figure presents the lowest octupole excitation (dashed line), and the first $1p - 1h$ configuration (solid line). The calculations reproduce the magnitude and evolution with frequency of the $J^{(2)}$ moment of inertia satisfactorily (see Fig. I-40 in Ref. 3), and the agreement is also reasonable for the energy of the octupole excitation: theory and experiment are only ~ 250 keV apart. Furthermore, the evolution of the Routhian with frequency is well reproduced when the interband transitions are considered to be of the $J + 1 \rightarrow J$ type. This agreement argues for the spin assignment given in Fig. I-41.

A publication of this result is in preparation..

*Technology Division, Argonne National Laboratory, †Niels Bohr Institute, Copenhagen, Denmark, ‡Lawrence Berkeley National Laboratory, §C.S.N.S.M, Orsay, France, ¶Ludwig-Maximilians-Universität, Munich, Germany, ||Florida State University

¹T. Lauritsen *et al.*, Phys. Rev. Lett. **88**, 042501 (2002).

²P. G. Dagnall *et al.*, Phys. Lett. **B335**, 313 (1994).

³T. Nakatsukasa *et al.*, Phys. Lett. **B343**, 19 (1995).

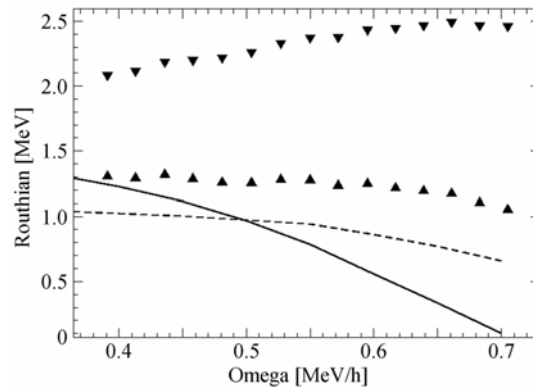


Fig. I-42. Routhians of band 6 with respect to band 1 as a function of rotational frequency. The up-triangles are the experimental data with the high spin assignment to band 6 and the down-triangles the experimental data with the low spin assignment. The dashed (solid) line is the result of the RPA calculation for negative-parity states with signature $\alpha = 1$.³ The dashed line characterizes the lowest excitation mode in the SD well associated with a collective octupole vibration. The solid line likewise shows the lowest $1p - 1h$ excitation. This excitation is associated with SD band 2.³

d.8. Empirical Investigation of Extreme Single-Particle Behavior of Nuclear Quadrupole Moments in Highly Collective $A \sim 150$ Superdeformed Bands (R. V. F. Janssens, S. T. Clark,* G. Hackman,* S. N. Floor,* J. Norris,* S. J. Sanders,* R. M. Clark,† P. Fallon,† G. J. Lane,† A. O. Macchiavelli,† and C. E. Svensson†)

The intrinsic quadrupole moment Q_0 of superdeformed rotational bands in $A \sim 150$ nuclei depends on the associated single-particle configuration. We derived an empirical formula based on the additivity of effective quadrupole moments of single-particle orbitals that

describes existing measurements from ^{142}Sm to ^{152}Dy . To further test the formula, the predicted Q_0 moments for two superdeformed bands in ^{146}Gd of 14.05 eb were confronted with a new measurement yielding 13.9 ± 0.4 eb and 13.9 ± 0.3 eb, respectively. The data were taken

with Gammasphere at the 88 Inch cyclotron facility at LBNL. This excellent agreement provides empirical evidence of extreme single-particle behavior in highly

deformed, collective systems. A paper reporting these results was recently published.¹

*University of Kansas, †Lawrence Berkeley National Laboratory
¹S. T. Clark *et al.*, Phys. Rev. Lett. 87, 172503 (2001).

d.9. Competition Between Terminating and Collective Structures Above Spin 40 in ¹⁵⁴Dy
 (R. V. F. Janssens, T. L. Khoo, M. P. Carpenter, I. Ahmad, S. M. Fischer, T. Lauritsen, D. T. Nisius, W. C. Ma,* I. Ragnarsson,† M. A. Riley,‡ J. R. Terry,* J. P. Zhang,* P. Bhattacharyya,§ P. J. Daly,§ J. H. Hamilton,¶ A. V. Ramayya,¶ R. K. Vadapalli, P. G. Varmette,* J. W. Watson,* C. T. Zhang,§ and S. J. Zhu*)

High-spin states in ¹⁵⁴Dy were studied with the Gammasphere spectrometer using the ³⁶S(¹²²Sn,4n) reaction. Band terminating states were identified in the spin range I = (36 - 48), and were found to compete with collective rotational cascades up to the highest observed spins. Several "sidebands" feeding the terminating structures were identified as well. A band dominated by M1 transitions was observed to terminate at I = 42⁻. The data are interpreted within the

framework of configuration-dependent cranked Nilsson-Strutinsky calculations without pairing. The calculations give good reproduction of the observed bands and terminating structures (see Fig. I-43). The results reveal the "anatomy" of a phase transition from collective to single-particle motion and show how terminating states descend below collective structures as the angular momentum increases. This work was published in Physical Review C.

*Mississippi State University, †Lund Institute of Technology, Lund, Sweden, ‡Florida State University, §Purdue University, ¶Vanderbilt University

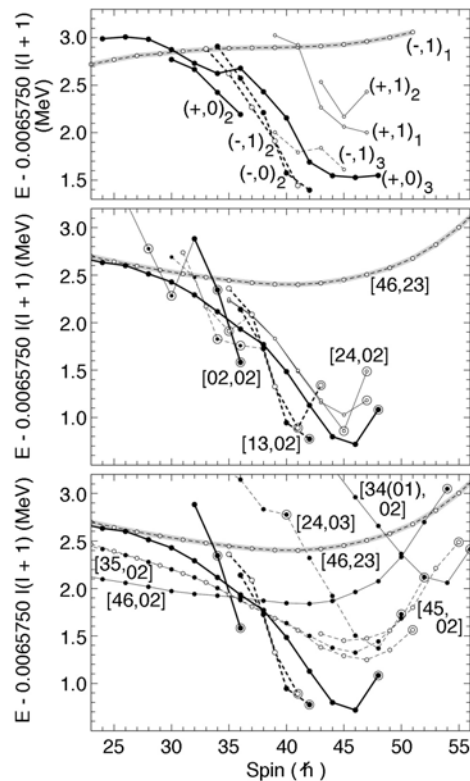


Fig. I-43. Observed terminating bands of ¹⁵⁴Dy in the upper panel with their calculated counterparts in the middle panel. Note that the [13,02] label refers to the two bands terminating at 41⁻ (43⁻) and 42⁻, and [24,02] refers to the three bands terminating at 47⁺ and 48⁺. In the lower panel, some configurations predicted to terminate in the I = (50 - 55) \hbar range are added. Collective configurations are indicated by thick shaded lines.

d.10. First Evidence for Triaxial Superdeformation in ^{168}Hf (R. V. F. Janssens, M. P. Carpenter, F. G. Kondev, T. L. Khoo, T. Lauritsen, C. J. Lister, S. Siem, I. Wiedenhöver, H. Amro,* P. G. Varmette,* W. C. Ma,* B. Herskind,† G. B. Hagemann,† G. Sletten,† A. Bracco,‡ M. Bergstrom,† J. Domscheit,§ S. Frattini,‡ D. Hartley,¶ H. Hubel,§ B. Million,‡ S. W. Odegard,* R. B. Piercey,* L. L. Riedinger,¶ K. A. Schimdt,† J. N. Wilson,† and J. A. Winger*)

Potential energy surface calculations predicted that nuclei with $Z \sim 72$ and $N \sim 94$ constitute a region of exotic shapes coexisting with the normally deformed prolate states. At high spins, these exotic shapes are predicted to lie lowest in energy and assume a stable triaxial superdeformed shape with a quadrupole deformation parameter $\beta_2 \sim 0.4$. Experimentally, rotational bands associated with this shape were reported in $^{163-165}\text{Lu}$. The association of these bands with the superdeformed triaxial minimum was inferred through a comparison of measured spectroscopic information with theoretical calculations. The most significant experimental observables include the quadrupole moments and the dynamic moments of inertia, which are strongly influenced by triaxiality.

In order to further extend this new region of superdeformation as well as test the predictive powers of model calculations, two separate measurements were undertaken to study high angular momentum states in ^{168}Hf . In both experiments, the $^{96}\text{Zr}(^{76}\text{Ge},4n)$ was used to populate high spin states in ^{168}Hf . The 310-MeV germanium beam was provided by the ATLAS accelerator at Argonne National Laboratory. Gamma rays were detected with the Gammasphere spectrometer

consisting of 101 Compton-suppressed Ge detectors. In the first experiment, a self-supporting thin foil (0.67 mg/cm^2) of ^{96}Zr was used as a target. From an analysis of the data, three rotational bands with characteristics consistent with those of the triaxial superdeformed structures identified in the Lu isotopes were identified and assigned to ^{168}Hf . Relative to the ground state transition in ^{168}Hf these bands are populated at 0.25, 0.15 and 0.12%. In the second experiment, the target consisted of a thin layer (0.67 mg/cm^2) of ^{96}Zr backed by 21 mg/cm^2 evaporated Au, which slowed down and stopped the recoiling nuclei. Due to the fact that the bands are weakly populated, an average quadrupole moment using the DSAM technique could only be established for band 1. The value of 11.4 eb established for the band provides a direct measure of the large deformation associated with the band and is consistent with theoretical calculations which predict a high-spin SD minima ($\beta_2 \sim 0.4$) with a stable triaxial deformation of $\gamma \sim 20^\circ$. This result constitutes the first evidence for triaxial superdeformation in an even proton system of this region.

A paper reporting the results of this work was recently published in Physics Letters B.¹

*Mississippi State University, †Niels Bohr Institute, Copenhagen, Denmark, ‡University of Milan, Italy, §University of Bonn, Germany, ¶University of Tennessee
¹H. Amro *et al.*, Phys. Lett. **B506**, 39 (2001).

d.11. Study of ^{169}Hf at High Rotational Frequency (M. P. Carpenter, R. V. F. Janssens, F. G. Kondev, T. L. Khoo, T. Lauritsen, C. J. Lister, S. Siem, I. Wiedenhöver, K. A. Schmidt,* M. Bergstrom,* G. B. Hagemann,* B. Herskind,* G. Sletten,* P. G. Varmette,* J. Domscheit,† H. Hubel,† S. W. Odegard,‡ S. Frattini,§ A. Bracco,§ B. Million,§ W. C. Ma,¶ R. Terry,¶ D. J. Hartley,|| L. L. Riedinger,|| and A. Maj**)

High-spin properties of the nucleus ^{169}Hf were studied through the fusion evaporation reaction $^{96}\text{Zr}(^{76}\text{Ge},3n)^{169}\text{Hf}$ at a beam energy of 310 MeV. The 310-MeV germanium beam was provided by the ATLAS accelerator at Argonne National Laboratory. Gamma rays were detected with the Gammasphere spectrometer consisting of 101 Compton-suppressed Ge detectors. The main focus of this investigation was to identify triaxial superdeformed bands in the Hf isotopes. Such structures were found in ^{168}Hf ,¹ but no evidence for these types of bands could be found in

^{169}Hf . Nevertheless, a thorough analysis of the data has yielded considerable new information on the level structure of ^{169}Hf . The previously known rotational bands were extended considerably, and 6 new bands were established. Quasiparticle assignments are suggested for the new band structures, and it appears that coupling to vibrational degrees of freedom play a role.

Of the six new bands, four form coupled pairs of strong M1 transitions. Both coupled pairs of bands are

believed to contain two quasiprotons in their three quasiparticle configuration. Four bands were extended to such high spin that a second clear upbend was observed. It has been suggested that these bands are associated with a five quasiparticle configuration at the highest spins and, furthermore, that the aligning orbitals are a proton pair. Based on a comparison of the data to

model predictions, the alignment of a mixture of $h_{9/2}$ and $h_{11/2}$ proton orbitals is the most likely explanation for the observed upbend.

A paper reporting the results of this work was recently published in the European Physical Journal A.²

*Niels Bohr Institute, Copenhagen, Denmark, †University of Bonn, Germany, ‡University of Oslo, Norway, §University of Milan, Italy, ¶Mississippi State University, ||University of Tennessee, **Niewodniczanski Institute of Physics, Krakow, Poland.

¹H. Amro *et al.*, Phys. Lett. **B506**, 39 (2001).

²K. A. Schmidt *et al.*, Eur. Phys. J. A **12**, 15 (2001).

d.12. K-Hindered Decay of a 6-qp Isomer in ¹⁷⁶Hf (G. Mukherjee,* F. Kondev, K. Abu Saleem, I. Ahmad, M. P. Carpenter, A. Heinz, R. V. F. Janssens, T. L. Khoo, T. Lauritsen, C. J. Lister, D. Seweryniak, I. Wiedenhöver, P. Chowdhury,† R. D'Alarcao,† I. Shestakova,† H. El-Masri,‡ P. M. Walker,‡ D. M. Cullen,§ C. Wheldon,‡¶ D. L. Balabanski,|| M. Danchev,|| T. M. Goon,|| D. J. Hartley,|| L. L. Riedinger,|| O. Zeidan,|| M. A. Riley,** R. Kaye,†† G. Sletten,‡‡ and G. D. Dracoulis§§)

High-K isomers in the Hf region provide an opportunity to test the conservation of the K quantum number at high spin. In this work, a known 6 quasiparticle isomer in ¹⁷⁶Hf was studied. The fusion evaporation reaction ¹³⁰Te(⁴⁸Ca, 2n)¹⁷⁶Hf with a pulsed 194 MeV beam from ATLAS was used to investigate the K-hindered decays from high-K states in ¹⁷⁶Hf using the Gammasphere array. The beam was pulsed in two different time windows: a 1 ns “ON” and 820 ns “OFF” and an “on-demand” beam switching in which the beam was switched off for 100 μs following a triple coincidence. Gamma-rays of the $K^\pi = 14^-$ band are observed in the

gated spectra from out-of-beam a γ - γ matrix and a γ - γ - γ cube with no extra line above 20⁻. This gives an indication that the $K^\pi = 14^-$ band is fed from the $K^\pi = 22^-$ six-quasiparticle isomeric ($t_{1/2} = 43 \mu\text{s}$) state. Since no γ -ray transition was observed to account for this, we propose a K-hindered decay of the $K^\pi = 22^-$ isomer to the 20⁻ state of $K^\pi = 14^-$ band through an unobserved, highly converted 37 keV E2 transition. The reduced hindrance factor for this $\Delta K = 8$ decay was estimated to be very low ($f_v = 2.5$) suggesting K-mixing and a mixed configuration of a nearby $K^\pi = 20^-$ state.

*Argonne National Laboratory and the University of Massachusetts, †University of Massachusetts, ‡University of Surrey, United Kingdom, §University of Manchester, United Kingdom, ¶University of Liverpool, United Kingdom, ||University of Tennessee, **Florida State University, ††Purdue University, Calumet, ‡‡Niels Bohr Institute, Denmark, §§Australian National University, Australia

d.13. Narrow Spreading Widths of Excited Bands in a Superdeformed Well (T. L. Khoo, T. Lauritsen, D. Ackermann, I. Ahmad, H. Amro, D. J. Blumenthal, I. Calderin, S. M. Fischer, G. Hackman, R. V. F. Janssens, D. Nisius, M. P. Carpenter, A. Lopez-Martens,* T. Døssing,† B. Herskind,† M. Matsuo,‡ K. Yoshida,§ S. Asztalos,¶ R. M. Clark,¶ M. A. Deleplanque,¶ R. M. Diamond,¶ P. Fallon,¶ F. Hannachi,* A. Korichi,* R. Krücken,¶ I. Y. Lee,¶ A. O. Macchiavelli,¶ R. W. MacLeod,¶ G. J. Schmid,¶ F. S. Stephens,¶ and K. Vetter¶)

Excited states within a superdeformed (SD) well provide opportunities to investigate: (i) the excited states of a false vacuum; (ii) a transition from ordered motion along the yrast line to chaotic motion above,

where quantum numbers and symmetries break down, perhaps through an ergodic regime; (iii) the robustness of collectivity with increasing excitation energy; (iv) the evolution with energy and spin of moments of

inertia, collective spreading widths, in-band probabilities, quadrupole moments; and (v) the largely-unexplored feeding mechanism of SD bands.

Data for the present work came from a Gammasphere experiment¹ conducted at LBNL with the $^{150}\text{Nd}(^{48}\text{Ca},4n)^{194}\text{Hg}$ reaction. $E_\gamma - E_\gamma$ matrices were constructed from pair wise gates on (a) SD and (b) normal-deformed (ND) transitions in ^{194}Hg ; (a) selects only transitions feeding SD band 1, while (b) includes other SD transitions, which do not necessarily feed into the SD yrast line, but continue to lower spin. In the SD-gated matrix (see Fig. I-44), 3 ridges (parallel to the diagonal) with $E_\gamma > 450$ keV could be seen and, in the other matrix, 5-6 ridges, which persist down to ~ 340 keV. The former matrix represents the first instance where ridges are detected with gates on SD transitions. The persistence of ridges to lower energy in the ND-gated matrix occurs because the γ cascades are not forced into the SD yrast line and implies small tunneling to ND states - even ~ 2 MeV above the SD minimum. The ridges reveal the following properties:

(1) narrow spreading widths ($\sim 5 - 10$ keV), which increase with spin; (2) ridge spacings and, hence, $J^{(2)}$ identical to that of SD band 1; (3) $N_{\text{path}} \sim 100 - 150$, from fluctuation properties; (4) in-band probability ~ 1 , for $E_\gamma > 790$ keV; and (5) ratio of ridge intensity/total E2 strength ~ 1 for $E_\gamma < 770$ keV. The large number of unresolved bands suggests that they are excited, probably from an interval 1.5 - 2 MeV above the SD yrast line. Yet, unexpectedly, the moments of inertia are nearly identical to that of the yrast SD band.

Features (1 - 3) were anticipated by theory;² further analyses indicate that there are 2 - 8 components in the wave functions, which are, hence, quite complex. Despite this large mixing among many bands, which should broaden the rotational strength, the ridge spreading widths are narrow. This implies surprisingly small changes in the amplitudes and phases of the wave function with repeated spin increments of $2 \hbar$, suggesting rotational coherence. Perhaps the excited unresolved SD bands in ^{194}Hg are candidates for ergodic bands.³

*C.S.N.S.M, IN2P3-CRNS, Orsay, France, †The Niels Bohr Institute, Denmark, ‡Graduate School of Science and Technology, Niigata University, Niigata, Japan, §Institute of Natural Science, Nara University, Nara, Japan, ¶Lawrence Berkeley National Laboratory

¹R. Krücken *et al.*, Phys. Rev. C 54, R2109 (1996).

²K. Yoshida and M. Matsuo, Nucl. Phys. A 636, 169 (1998).

³B. R. Mottelson, Nucl. Phys. A 557, 717c (1993).

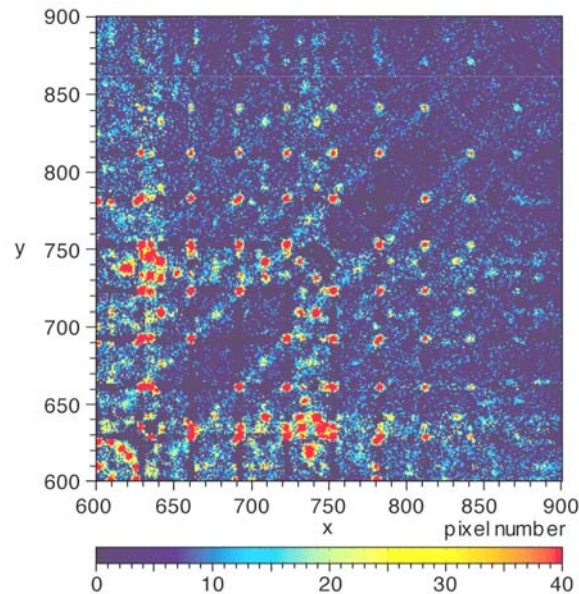


Fig. I-44. $E_\gamma - E_\gamma$ matrix obtained with pair wise gates on lines of the yrast superdeformed (SD) band 1 in ^{194}Hg . Note that the 3 ridges, which are parallel to the diagonal, are narrow and have the same spacings as the regular grid points from SD band 1.

d.14. Limits of the Energy-Spin Phase Space Beyond the Proton Drip Line: Entry Distributions of Pt and Au Isobars (M. P. Carpenter, F. G. Kondev, T. L. Khoo, T. Lauritsen, R. V. F. Janssens, K. Abu Saleem, I. Ahmad, C. N. Davids, A. Heinz, C. J. Lister, G. L. Poli, J. J. Ressler, D. Seweryniak, I. Wiedenhöver, M. B. Smith,* J. A. Cizewski,* H. Amro,† M. Danchev,‡ D. J. Hartley,‡ W. C. Ma,† W. Reviol,§ and L. L. Riedinger‡)

Nuclei lying beyond the proton drip line provide an ideal laboratory for the study of the amount of energy and angular momentum which a weakly-bound system can sustain. These limits of existence can be determined by measuring the entry distribution¹ populated in a fusion-evaporation reaction. The entry distribution is the initial population as a function of excitation energy E and spin I , after particle evaporation from the compound system, from which γ emission to the ground state originates. It was suggested² that the entry distribution should be limited beyond the drip line, since only a small region of the energy-spin phase space, just above the yrast line, does not decay by proton emission.

Entry distributions were measured for $^{173-177}\text{Au}$ nuclei, all of which lie beyond the drip line, and compared with those of the more stable Pt isobars. These systems were populated following the bombardment of $^{92,94,96}\text{Mo}$ targets by beams of ^{84}Sr , provided by the ATLAS accelerator. Fusion-evaporation products were selected

using the Argonne Fragment Mass Analyzer, and the recoil-decay tagging method was used to select the α -decaying states of interest. Prompt γ rays were detected using the 106-module Gammasphere array as a calorimeter. Total modular energy H and multiplicity K were measured. The response functions of the array enable the conversion of modular (H, K) to energy and multiplicity, which can be related to spin by realistic assumptions¹ of the angular momenta carried by the components of the γ -ray cascade. Comparisons have been made between the entry distributions associated with odd- A Au and Pt isobars. In ^{173}Au the entry distribution (Fig. I-45) is colder than that at ^{173}Pt , which provides the first evidence for the limits of excitation energy and angular momentum which a nucleus beyond the proton drip line can sustain. The observed results cannot be explained by simple calculations based on Q -values or by statistical model calculations, both of which predict similar distributions for isobars.

*Rutgers University, †Mississippi State University, ‡University of Tennessee, §Washington University

¹P. Reiter *et al.*, Phys. Rev. Lett. **84**, 3542 (2000).

²T. L. Khoo, in *Tunneling in Complex Systems*, Proceedings from the Institute for Nuclear Theory, v. 5, p. 229, ed. Steven Tomsovic (World Scientific 1998).

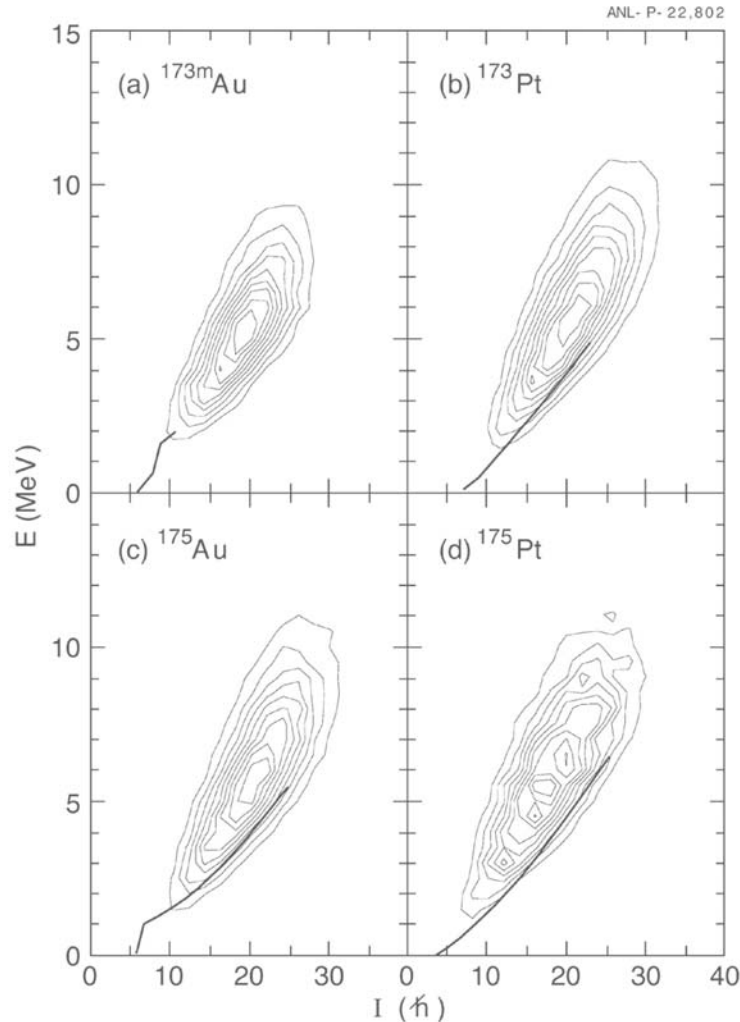


Fig. I-45. Two-dimensional (I, E) entry distributions for (a) ^{173m}Au , (b) ^{173}Pt , (c) ^{175}Au and (d) ^{175}Pt . Each contour line represents a change of 10% of the maximum value. The yrast line for each isotope is presented as a thick line.

d.15. Investigation of the Decay Out of Superdeformed Bands in ^{194}Hg by Lifetime Measurements (T. L. Khoo, P. Reiter, A. Dewald,* R. Kühn,* R. Peusquens,* P. von Brentano,* R. Krücken,† M. A. Deleplanque,† I. Y. Lee,† R. M. Clark,† P. Fallon,† A. O. Macchiavelli,† R. W. MacLeod, † and F. S. Stephens,† and K. Hauschild‡)

The lifetimes of low-lying states in the superdeformed (SD) bands of ^{194}Hg were measured by means of the recoil distance method using Gammasphere and the Cologne plunger device. The deduced transitional quadrupole moments in all three bands were found to be constant within the experimental uncertainties and equal those extracted from Doppler-shift attenuation

method measurements for the higher-lying states, confirming that the decay out does not strongly affect the structure of the SD bands. The experimental findings are used to discuss the different mechanisms proposed for the decay out of SD bands. This work was published in Physical Review C.¹

*Institut für Kernphysik, Universität Köln, Köln, Germany, †Lawrence Berkeley National Laboratory, ‡Lawrence Livermore National Laboratory

¹A. Dewald et al., Phys. Rev. C **64**, 054 309 (2001).

d.16. Effective Charge of the $\pi h_{11/2}$ Orbital and the Electric Field Gradient of Hg from the Yrast Structure of ^{206}Hg (R. V. F. Janssens, M. P. Carpenter, I. Wiedenhöver, B. Fornal,* R. Broda,* K. H. Maier,* J. Wrzesinski,* G. J. Lane,† M. Cromaz,† A. O. Macchiavelli,† R. M. Clark,† K. Vetter,† A. P. Byrne,‡ G. D. Dracoulis,‡ M. Rejmund,¶ and J. Blomqvist||)

The γ -ray decay of excited states of the two-proton hole nucleus, ^{206}Hg , was identified using Gammasphere and $^{208}\text{Pb} + ^{238}\text{U}$ collisions. The yrast states found include a $T_{1/2} = 92(8)$ ns 10^+ isomer located above the known 5^- isomer. The $B(E 2; 10^+ \rightarrow 8^+)$ strength is used to derive

the quadrupole polarization charge induced by the $h_{11/2}$ proton hole. Also, the implied quadrupole moment was used to provide an absolute scale for the electric field gradient of Hg in Hg metal. These results were published.¹

*Niewodniczański Institute of Nuclear Physics, PL-31342 Cracow, Poland, †Lawrence Berkeley National Laboratory, ‡Australian National University, Canberra ACT 0200, Australia, §Dapnia/SPhN, CEA Saclay, F91191 Gif-sur-Yvette Cedex, France, ¶Royal Institute of Technology, S-10405 Stockholm, Sweden

¹B. Fornal *et al.*, Phys. Rev. Lett. **87**, 212501 (2001).

d.17. Unexpected Behavior of Heavy-Ion Fusion Cross Sections at Extreme Sub-Barrier Energies (C. L. Jiang, H. Esbensen, K. E. Rehm, B. B. Back, R. V. F. Janssens, J. A. Caggiano, P. Collon, J. Greene, A. M. Heinz, D. J. Henderson, I. Nishinaka, T. O. Pennington, and D. Seweryniak)

In an earlier report it was found¹ that the behavior of excitation functions of some heavy-ion fusion reactions exhibits an abrupt decrease of the cross section at extreme sub-barrier energies. This behavior cannot be reproduced with present models, including those based on a coupled-channels approach. In order to study this phenomenon in more detail excitation functions for fusion-evaporation in the systems $^{58}\text{Ni} + ^{89}\text{Y}$ and $^{60}\text{Ni} + ^{89}\text{Y}$ were measured at low cross sections.

The excitation function for evaporation residue production in the system $^{60}\text{Ni} + ^{89}\text{Y}$, covering cross sections from about 100 mb to less than 100 nb, is presented in Fig. I-46a by open circles, while the results for $^{58}\text{Ni} + ^{89}\text{Y}$ are shown by solid circles. It should be noted that precise measurements of very small fusion cross sections are experimentally challenging.

Reactions on small amounts of heavier isotopic target contaminants can dominate the low-energy yields due to their higher center-of-mass energies. Since yttrium has only one stable isotope, it was chosen as the target. In addition, even low-intensity isobaric contaminants in the beam, e.g., a ^{58}Fe contamination in a ^{58}Ni beam can also affect the fusion cross sections at the lowest energies because of the strong dependence of these cross sections on the respective Coulomb barriers, as seen in our experimental results of $^{58}\text{Ni} + ^{89}\text{Y}$. The excitation function decreases first exponentially followed by a slower decrease caused by the contamination of a weak ^{58}Fe beam. Estimates show that a $^{58}\text{Fe}/^{58}\text{Ni}$ ratio of $10^{-5} - 10^{-4}$ can produce this result. In the following, only data for $^{60}\text{Ni} + ^{89}\text{Y}$ will be discussed.

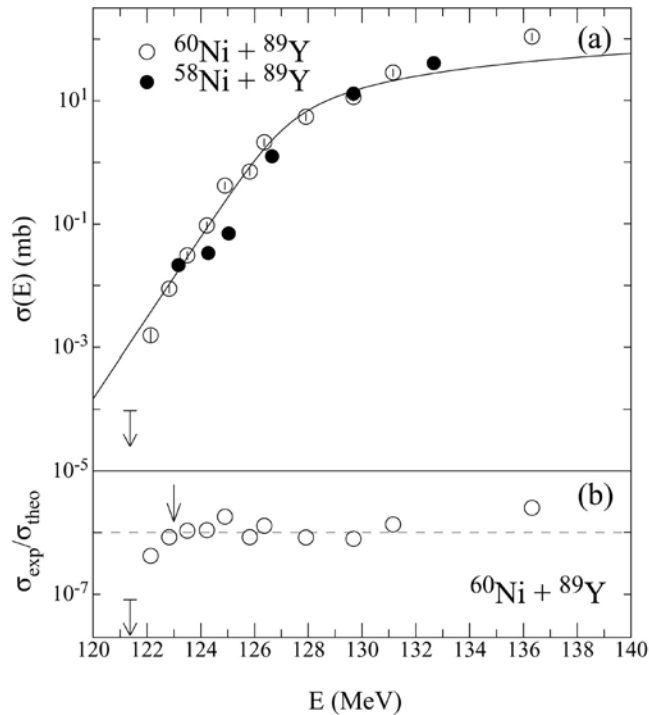


Fig. I-46. Experimental evaporation residue cross sections $\sigma(E)$, (a) and $\sigma_{\text{exp}}/\sigma_{\text{theo}}$, (b) (σ_{theo} calculated from the Wong formula), plotted as function of the center-of-mass energy for systems $^{60}\text{Ni} + ^{89}\text{Y}$ and $^{58}\text{Ni} + ^{89}\text{Y}$. The incident energies have been corrected for the finite target thickness (including the influence of drastic change in the cross section with energy).

The solid line in Fig. I-46a is the result of a calculation using the Wong parameterization² for $^{60}\text{Ni} + ^{89}\text{Y}$ with the parameters $\hbar\omega_0 = 4.16$ MeV and $V_W = 126.6$ MeV. At the lowest energies the experimental cross sections fall below the calculated values, as is best seen from the ratio $\sigma_{\text{exp}}/\sigma_{\text{theo}}$ given in Fig. I-46b. From these data an energy E_0 (defined as the energy at which the drop-off occurs, see arrow in Fig. I-46b) can be derived. Remarkably, the values E_0 for $^{60}\text{Ni} + ^{89}\text{Y}$ and four other systems ($^{58}\text{Ni} + ^{58}\text{Ni}$,⁴ and $^{90}\text{Zr} + ^{89}\text{Y}$, ^{90}Zr , ^{92}Zr)⁵ indicate that the onset of the steeper than expected decrease in the fusion cross section occurs at an energy $E_0 \sim 0.91 V_b$, where V_b is the Coulomb barrier calculated from the systematics of Ref. 3. This observation suggests that this reduction in cross section is an entrance channel effect. The systems mentioned above all involve closed-shell ("stiff") nuclei in the entrance channel. For

reactions involving open-shell ("soft") nuclei in the entrance channel, firm E_0 values are not yet available, and the upper limits obtained suggest that there is a nuclear structure dependence to this phenomenon. It is likely that larger channel-coupling effects for these softer participants are pushing the appearance of the phenomenon towards lower E_0/V_b values.

To better illustrate the steep fall-off in the product σE , the exponential slopes defined as $L(E) = d(\ln(\sigma E))/dE$ are plotted as a function of E/E_0 for three systems in Fig. I-47. In addition to the straightforward determinations from consecutive data points, slopes were also derived from least-squares fits to three data points in an attempt to avoid

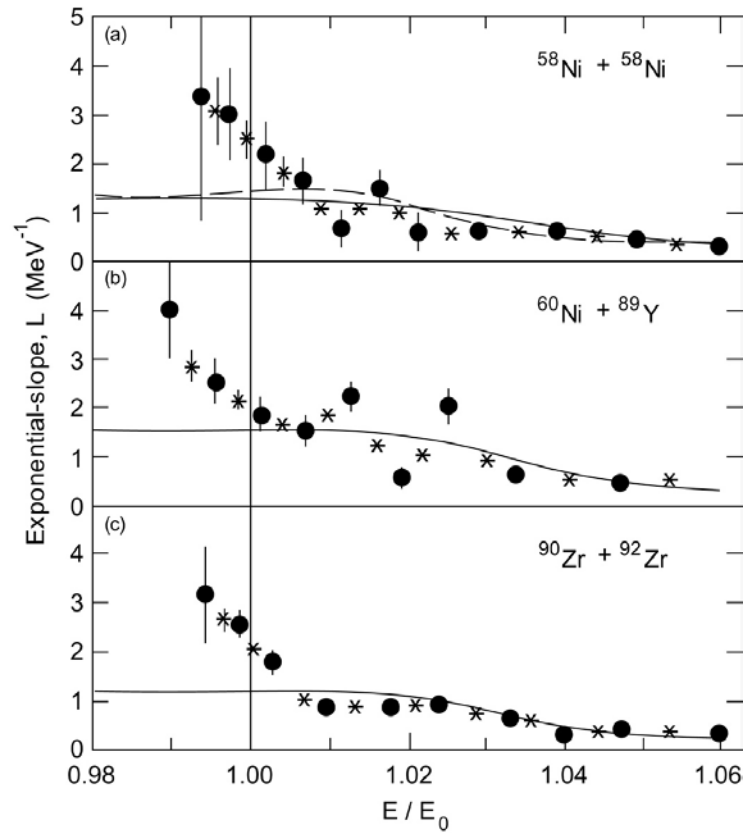


Fig. I-47. Exponential slopes $L(E)$, $d(\ln(\sigma E))/dE$, plotted as function of E/E_0 for the systems $^{58}\text{Ni} + ^{58}\text{Ni}$, $^{60}\text{Ni} + ^{89}\text{Y}$ and $^{90}\text{Zr} + ^{92}\text{Zr}$. Solid circles and stars correspond to slope determinations from consecutive data points and from least-squares fits to three data points, respectively. Solid and dashed lines are the results of theoretical calculations with the Wong formula and the coupled-channel formalism, respectively.

fluctuations, which may arise as a result of large errors for small cross sections or of uncertainties in the determination of the beam energy. In Fig. I-47, the slopes determined from two or three consecutive points are given as solid circles and stars, respectively, at the corresponding average energies. The dashed and solid lines in the figure represent the results of coupled-channels calculations and of the Wong formula, respectively. While all calculated slopes approach a constant value of $\sim 1.5 \text{ MeV}^{-1}$, the experimental data exhibit a continuous increase with decreasing energies. It would clearly be of great interest to investigate whether the behavior observed here persists at even lower energies for systems involving soft nuclei in the entrance channels.

Some aspects of the cross sections at low energies can be understood on the basis of the underlying Q -values, while others remain unexplained. In fusion reactions

between two heavy ions, the reaction Q -values are always negative. As a result, once the excitation energy in the compound system E_{ex} reaches zero, which occurs at a finite bombarding energy, the cross section must be zero, and thus the exponential slope of σE should approach infinity. Hence, for a heavy-ion system, the slope $L(E)$ should increase towards infinity with decreasing energy. Any theoretical model attempting to describe the fusion behavior at extreme sub-barrier energies should include the properties of the fused system as expressed through the Q -value. The Q -value alone is, however, not sufficient to explain the phenomenon explored in this study. Present fusion models assume that the fused system can be populated at an excitation energy and spin corresponding to the entrance channel kinetic energy and angular momentum. This assumption is valid only as long as the total width of the compound state remains larger than the level spacing. When this condition is not

satisfied a reduction of the fusion probability ensues, as is well known from capture reactions with thermal neutrons. For most of the systems under study here, however, the fall-off of the cross sections occurs at excitation energies $E_{ex} \sim 20 - 30$ MeV where the level densities are still very high. These observations argue for another physical reason for the reduced penetration

or another hindrance implied by the negative Q -value; the most likely being an entrance channel phenomenon. More low-energy cross section measurements for both fusion-evaporation and fusion-fission are needed to fully understand this interesting behavior, in particular for soft systems.

¹C. L. Jiang, H. Esbensen, K. E. Rehm, Physics Division Annual Report 2000, Argonne National Laboratory, page 72.

²C. Y. Wong, Phys. Rev. Lett. **31**, 766 (1973).

³L. C. Vaz and J. M. Alexander, Phy. Rep. **69**, 373 (1981).

⁴M. Beckerman *et al.*, Phy. Rev. C **25**, 837 (1982).

⁵J. G. Keller *et al.*, Nucl. Phys. **A452**, 173 (1987).

d.18. High Energy Photons from Very Symmetric Reactions: The Giant Dipole Resonance in the Highly Rotating ^{179}Au Nucleus (M. P. Carpenter, V. Nanal, B. B. Back, F. G. Kondev, T. L. Khoo, C. J. Lister, A. M. Heinz, R. V. F. Janssens, D. Jenkins, T. Lauritsen, E. F. Moore, D. Seweryniak, F. Camera,* A. Bracco,* F. Della Vedova,* S. Leoni,* S. Mantovani,* B. Million,* M. Pignanelli,* O. Wieland,* M. Thoenessen,† R. Varner,‡ I. Dioszegi,§ A. Lopez-Marten¶, and D. Hofman||)

The high energy gamma-rays emitted by the symmetric reaction $^{90}\text{Zr} + ^{89}\text{Y}$ at a beam energy of 352 MeV were measured with an experimental set up consisting of four clusters of $^{37}\text{BaF}_2$ detectors, the Fragment Mass Analyzer (FMA) and a BGO multiplicity filter. Such symmetric fusion of two nearly closed shell medium heavy nuclei has the special feature of leading to radiative fusion, where a warm compound nucleus can deexcite to its ground state without the evaporation of nucleons. There are two possible mechanisms leading to "radiative fusion: (a) a direct reaction in which the emission of a single γ -ray populates "directly" the states below the nucleon separation energy or (b) a two-step process, namely the formation of the compound nucleus ^{179}Au and the 0 nucleon channel is one of several decay modes in a statistical decay process.

The first attempt to measure γ -rays from the symmetric reactions of medium mass nuclei was performed at GSI over a decade ago. It was found that the relative population of the 0, 1 and 2 nucleon evaporation

channels strongly depends on the E1 strength (measured with reasonable statistics only up to 4-5 MeV) but it was not possible to draw conclusions on the properties of the giant dipole resonance and on nuclear shapes involved in the reaction. In the present experiment the high-energy γ -ray spectra associated with the evaporation of 0, 1 and 2 nucleons were measured up to 13 MeV with an increase of statistics of more of two orders of magnitude. Our analysis (see Fig. I-50) indicates that the radiative-fusion process is a statistical one, namely the zero particle emission channel can be described as statistical decay from the compound nucleus with a shape and deformation similar to that deduced from the yrast line. The GDR spectra for the 1n and 1p channels also imply similar deformations. This suggests that shell effects are also important when the nucleus is excited at a moderate temperature. This conclusion is supported by the fact that the width of the GDR has a value that is close to that predicted by a thermal fluctuation model including shell effects.

*Dipartimento di Fisica Università di Milano and INFN, Milano, Italy, †Michigan State University, ‡Oak Ridge National Laboratory, §SUNY, Stony Brook, ¶CSNSM, Orsay, France, ||University of Illinois, Chicago.

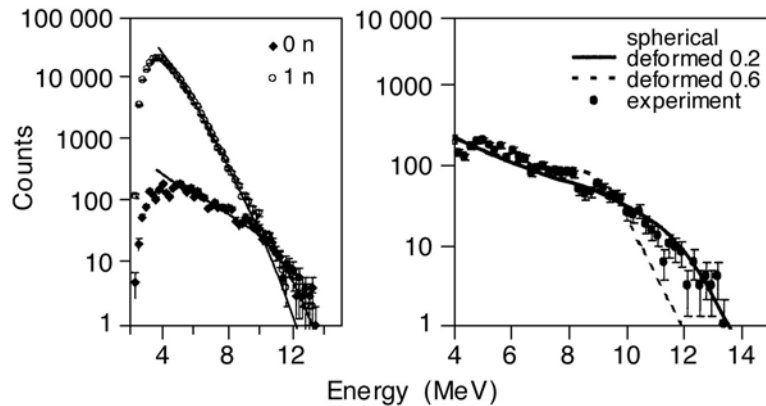


Fig. I-50. Left panel: The high-energy γ -ray spectra associated with the 0- and 1-nucleon emission channels are shown in comparison with statistical model calculations. Right panel: The high-energy γ -ray spectra associated with the 0-particle emission channel in comparison with different statistical model calculations corresponding to different nuclear deformations.

d.19. Hot GDR in ^{118}Sn (B. B. Back, M. Carpenter, T. L. Khoo, T. Pennington, P. Heckman,* J. P. Seitz,* E. Tryggestad,* T. Baumann,* M. Thoennessen,* R. L. Varner,† D. J. Hofman,‡ and V. Nanal§)

In December of 2000, an experiment was performed at Argonne National Laboratory (Exp. 889) to study the giant dipole resonance (GDR) in ^{118}Sn . The experiment employed two fusion-evaporation reactions, namely $^{18}\text{O} + ^{100}\text{Mo}$ and $^{17}\text{O} + ^{100}\text{Mo}$. The beams of ^{18}O and ^{17}O were accelerated to energies of 95 and 78.8 MeV, respectively.

The typical way to study the GDR is to excite the nucleus of interest, and measure the γ -decay spectrum. This spectrum is then compared to statistical model calculations to extract the parameters of the GDR. The spectrum contains information from the initial excited nucleus, as well as all daughter nuclei populated along its decay. Consequently, to extract the GDR parameters from the γ -ray spectrum, it is necessary to average over many decay steps.

In this experiment, the γ -decay spectrum for both ^{118}Sn and ^{117}Sn were measured. This was done with the intention of subtracting out all daughter contributions from the ^{118}Sn decay spectrum. By exciting ^{117}Sn to the energy of the ^{118}Sn nucleus after it evaporates one neutron, the contributions of daughter nuclei can be

measured and subtracted. The subtracted spectrum will only contain information from the initial excited nucleus. As a result, the parameters of the GDR can be extracted without having to average over many decay steps. This will allow for the first direct comparison of the GDR built on excited states with the ground state measurement. It will also be possible to investigate the effects of averaging over many decay steps on the extracted GDR parameters.

The γ rays were measured with the BaF_2 array, while the FMA detected evaporation residues. A coincidence condition between the two detector systems was required to ensure that detected γ rays originated from the initial compound nucleus. The array of BGO detectors was used as a multiplicity filter, and allowed for the initial spin of the excited nucleus to be determined.

Preliminary results are shown in Fig. I-51. In this figure, the γ -ray spectra are shown for the two reactions studied in this experiment. These spectra were extracted from data in the following way: first, gates were placed on Sn

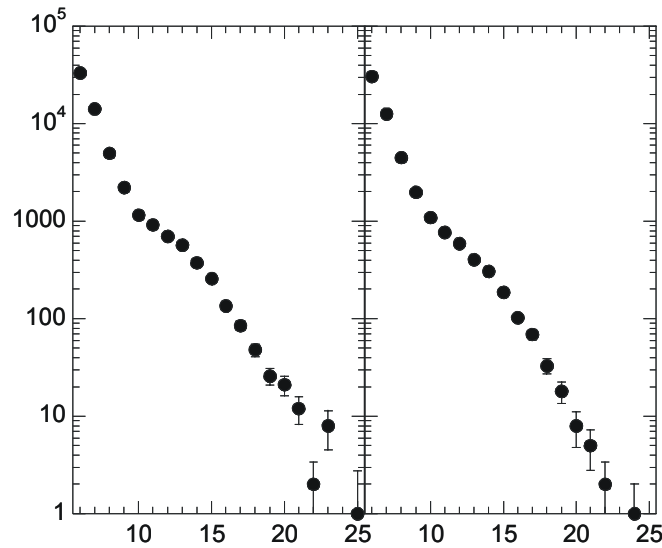


Fig. I-51. Gamma-ray spectra from experiment 889. The left panel shows the result from ^{118}Sn formed in the reaction $^{18}\text{O} + ^{100}\text{Mo}$, while the right panel shows the result from ^{117}Sn formed in the reaction $^{17}\text{O} + ^{100}\text{Mo}$.

evaporation residues. The residues were detected with a PPAC located in the focal plane of the FMA. Next, all events detected with the BaF_2 array in coincidence with the gated residues were analyzed. The γ rays were isolated using time of flight techniques. The final energy of a γ ray was determined by using a

reconstruction routine. This routine adds the energy of neighboring detectors together to reconstruct the true energy. Finally, if the multiplicity of the BGO array was between three and five, the energy of the γ ray was put into a histogram.

*Michigan State University, †Oak Ridge National Laboratory, ‡University of Illinois at Chicago, §Tata Institute of Fundamental Research, Mumbai, India

d.20. BaF_2 GDR Measurement Collaboration (B. B. Back, M. Carpenter, P. Collon, A. Heinz, D. Henderson, D. Jenkins, J. Joswick, M. Kelly, T. L. Khoo, F. Kondev, C. J. Lister, T. Pennington, J. Rohrer, R. Siemssen, D. Seweryniak, P. Wilt, V. Nanal,* D. J. Hofman,† S. Mitsuoka,‡ I. Dioszegi,§ A. Bracco,¶ F. Camera,¶ M. Halbert,|| R. Varner,|| K. Eisenman,** P. Heckman,** J. Seitz,** M. Thoennessen,** U. Garg,†† B. McClintock,‡‡ and R. J. van Swol‡‡)

A set of experiments to study the properties of hot nuclei with, for the first time, well-defined specification of spin and excitation energy has been completed. This work is a collaboration of Argonne, Oak Ridge, Michigan State University, Texas A&M University, Tata Institute for Fundamental Research, Stony Brook, Notre Dame University, and INFN Milano. The BaF_2 detectors were supplied by Oak Ridge, Michigan State and Texas A&M. A total of 148 BaF_2 were mounted in four packs of 37 crystals each centered at angles of ± 90 and ± 121 degrees with respect to the beam axis in front of the Fragment Mass Analyzer.

The advantage of this arrangement is that it is possible to uniquely identify the mass of the γ -emitting nuclei as they are detected in the focal plane of the FMA. In addition, a BGO array, consisting of 48 crystals from the Argonne-Notre Dame array and from Yale, was mounted at the target position to provide information on the total γ -ray energy and multiplicity of the final γ -ray cascade to further define the entry distribution in angular momentum and excitation energy of the fusion product. For a given decay channel at different bombarding energies, it is thus possible to map out a wide range of angular momentum while keeping the excitation energy above yrast line similar.

The physics topics were chosen to study the emission of high-energy γ -rays in different areas of the nuclear chart and of different ground state shapes. In one study, we chose three nuclei, namely Sn, Er and Dy to represent different mass regions likely to be sensitive to different mechanisms responsible for the broadening of GDR width. We selected spherical nuclei, stiff deformed nuclei and transitional nuclei. These efforts constitute the most comprehensive systematic

investigation of the GDR spectra from hot nuclei in exclusive measurements. Subsequently, nuclei ranging in mass from ^{118}Sn to ^{224}Th were studied. A pair of experiments focused on high-energy γ rays from radiative-capture reactions, which represents a unique case with emission of only γ rays and no particles. Data analysis is still in progress. It is almost complete in the radiative capture work led by the Milan group (see section d.18).

*Tata Institute of Fundamental Research, Mumbai, India, †University of Illinois at Chicago, ‡JAERI Advanced Science Research Center, Japan, §State University of New York, ¶University of Milan, Italy, ||Oak Ridge National Laboratory, **Michigan State University, ††University of Notre Dame, ‡‡ANL Summer Students

d.21. Yield and Activity Calculations for Facilities for Short-Lived Nuclear Beams

(C. L. Jiang, B. B. Back, I. Gomes, A. M. Heinz, J. Nolen, K. E. Rehm, G. Savard, and J. P. Schiffer)

As mentioned in the last annual report¹ detailed yield calculations were carried out in response to the recommendations of the ISOL Task Force Report to NSAC for a 100-kW, 400-MeV/u accelerator,² for beams re-accelerated to precise low energies as well as for fast fragmentation beams. These yield calculations were extended to rates of 10^4 particles/sec, which are adequate for certain experiments. The results were submitted for publication and are available on the web.³

For medical and material science applications, radioisotopes play an important role. Large intensities of relatively short lived isotopes, that are not easily

obtained at other facilities, can be produced at the coming advanced RIA. Very large activities could be produced in dedicated primary production targets, but the detailed extraction procedures of the isotopes depend on the chemistry of the element and have to be applied case by case. In the following we therefore used only the data from the yield calculations to estimate the activities for longer lived isotopes that can be readily collected in a stopping foil after the mass separator for reaccelerated beams. The collection time should depend on the half lives of the nuclei to be used. Some activity results are shown in Fig. I-48

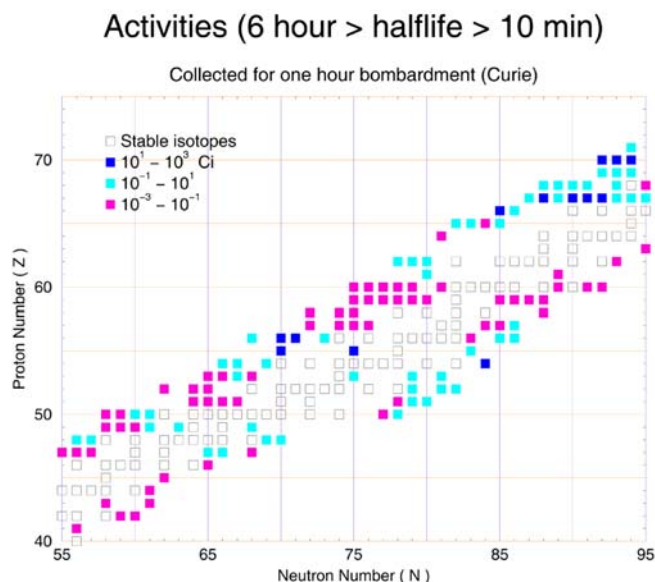


Fig. I-48. Contour map of calculated activities for isotopes collected with a 100-kW, 400-MeV/u RIA facility in a one-hour bombardment after the mass separator. The map includes only isotopes whose half lives are longer than 10 minutes and shorter than 6 hours.

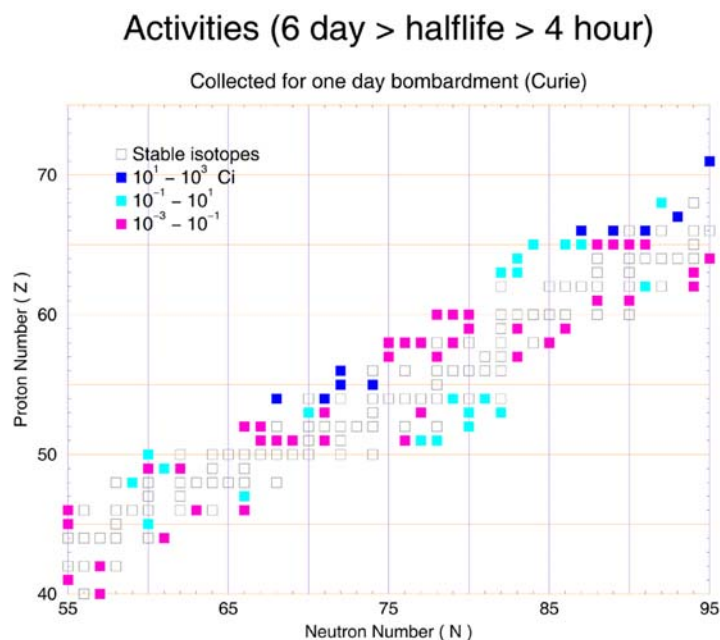


Fig. I-49. Same as in Fig. I-49 for a one-day bombardment and half lives are longer than 4 hours and shorter than 6 days.

and Fig. I-49 for nuclei in the mass range $A = 100 - 150$. The results for radioisotopes covering the whole mass range can be found at the same web address. The bombarding time was taken as one hour and activities produced for half lives between 10 minutes and 6 hours are shown in Fig. I-48, while in Fig. I-49 the bombarding time was taken as one day and half lives are between 4 hours and 6 days. This probably covers

the range of lifetimes that are most likely to be of interest in applications. There are many blanks in the figures, corresponding to nuclei whose lifetimes are out of their range of the specific calculations. For a number of elements and isotopes much higher (in some cases up to 4 - 5 orders of magnitude) intensities might be feasible with specially designed primary target and fast chemical processing.

¹C. L. Jiang, B. Back, I. Gomes, A. M. Heinz, J. Nolen, K. E. Rehm, G. Savard and J. P. Schiffer, Physics Division Annual Report 2000, Argonne National Laboratory, page 75.

²ISOL Task Force Report to NSAC, November 22, 1999. See <http://srfsrv.jlab.org/isol/>.

³See <http://www.phy.anl.gov/ria/index.html>.

E. RELATIVISTIC HEAVY ION COLLISIONS

The PHOBOS experiment made significant advances over the past year, with the publication of several new results, the completion of the analysis of much of the data from the 2000 running cycle, and successful operation during the 2001 running period. Adding to the data obtained at $\sqrt{s_{NN}} = 56$ and 130 GeV, PHOBOS obtained a number of new results for collisions at $\sqrt{s_{NN}} = 200$ GeV, as well as some data taken at a low energy of $\sqrt{s_{NN}} = 20$ GeV to establish a connection with the work done at the SPS at CERN. Finally, data were also obtained for polarized proton-proton collisions at $\sqrt{s_{NN}} = 200$ GeV. These results provided many insights into the physics of these ultra-relativistic collisions, including the systematic dependence of charged-particle production on bombarding energy and impact parameter, the dynamics of charged particle production, baryon stopping and the temperature and chemical potential of the system.

e.1. The PHOBOS Experiment at RHIC (B. B. Back, A. H. Wuosmaa, and the PHOBOS Collaboration - ANL, BNL, Krakow, MIT, NCU Taiwan, U. of Rochester, UIC, and U. of Maryland)

At RHIC, heavy ions collide at center of mass energies an order of magnitude higher than was previously available anywhere. At these energies, it is expected that a baryon-free region of extremely high energy density will remain in the central region after the two colliding nuclei have passed through each other. It is believed that this situation will be more than sufficient to create a system of deconfined quarks and gluons- the "Quark Gluon Plasma." After formation, the plasma should expand and cool before passing into the normal hadronic phase that, in turn, expands further until the hadrons cease to interact with each other ("freezeout"). The important questions that need to be answered are: what are the direct probes and signatures of the plasma phase, and what identifiable traces of the quark-gluon phase remain in the observed hadronic final state? The PHOBOS experiment seeks answers to these questions.

The PHOBOS experiment focuses on measurements of hadronic observables for a large sample of events. The PHOBOS apparatus consists of a 4π multiplicity detector and two multi-particle tracking spectrometers capable of measuring and identifying particles with very low transverse momenta. The multiplicity detector can provide event-by-event charged particle multiplicity distributions, which will be used to find interesting events for study in more detail using the spectrometers. The multiplicity distributions are interesting in their own right, and contain information on fluctuations and correlations, which relate to some of the proposed signatures of the plasma. The multiplicity distributions also contain information about the dynamic evolution of the collision.

An overall view of the PHOBOS apparatus as it was installed for the Year 2001 Physics run is shown in Fig. I-52; several different components are identified. The apparatus is now complete with the installation of the second of the two tracking-spectrometer arms, which was completed in early 2001. The fabrication and installation of the multiplicity and vertex detectors was the responsibility of the groups at Argonne and UIC. Together, these systems contain over 22000 channels of silicon pad detector.

The Multiplicity detector provides event-by-event information on the charged particle multiplicity distributions over ± 5.4 units of pseudo-rapidity (η), with complete azimuthal coverage. The multiplicity measurement (see results below) is made using a centrally located, 11000 channel "Octagon" array of silicon pads supplemented with six 512 channel "Ring" counters placed up and down the beam pipe. These detectors measure the energy deposited as a function of angle with respect to the collision vertex.

The Vertex detector is designed to locate the position of the interaction vertex on an event-by-event basis. It is composed of two pairs of planes of silicon pad detectors, each plane segmented into 2048 channels so that the occupancy is low. Particles emitted from the collision vertex can be tracked by combining pairs of hits on the inner and outer Vertex planes such that the position of the reconstructed interaction point can be determined to a precision

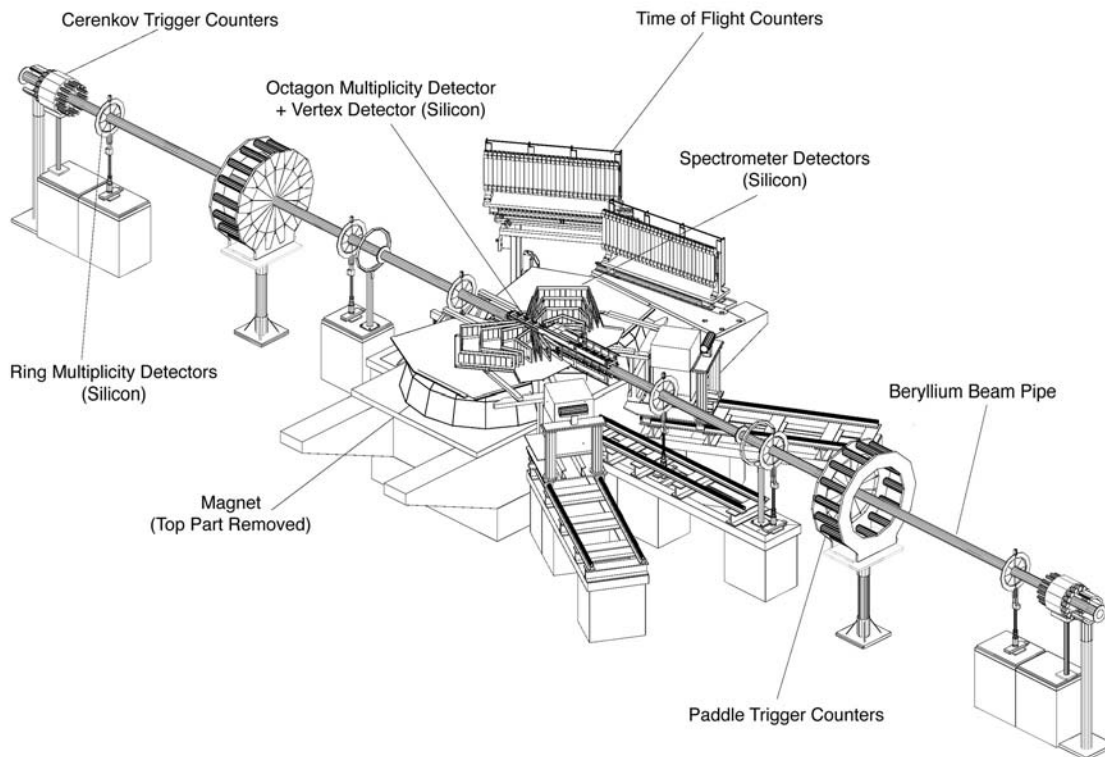


Fig. I-52. Overview of the PHOBOS experiment.

of better than 300 μm . Vertices are reconstructed over the entire range of the RHIC collision diamond, nominally corresponding to ± 20 cm about the center of the intersection region.

Installation, Performance and Operation during 2001

As mentioned above, in the spring of 2001 the second spectrometer arm was installed, doubling the efficiency for tracking and identification of charged particles emitted at mid-rapidity. Also, the performance of the data acquisition (DAQ) was improved, yielding better stability and functionality than in the previous year. The apparatus continues to function well.

Au + Au operations at RHIC at $\sqrt{s_{NN}} = 200$ GeV commenced in July 2001, and continued through November. Throughout this period, 56 of the possible 60 beam-bunches were filled, with an average intensity of many times 10^9 ions circulating per fill. The initial design luminosity goals for the accelerator were approached, and all of the RHIC experiments accumulated over an order of magnitude more data than in the previous years running.

Throughout the entire running period, frequent measurements of the noise and gain calibration of the entire PHOBOS system were taken to monitor the stability of the detectors. The noise, and hence the response of the detector were remarkably stable, with observed variations less than 2% throughout this period. The variations in the measured gain response for this period were similarly small. The total fraction of non-functioning channels was less than 3% out of the total 13700 channels installed.

Some difficulty was encountered during two incidents when control of the Au beams was lost, and large radiation fluxes were incident on the experiment. In these cases, the FEE protection circuits were overwhelmed and some degraded performance of some of the ASICS FEE chips was observed. Fortunately, by modifying the operating parameters of the affected chips, nominal operation of the detector was restored and the radiation incidents did not significantly affect the ultimate performance of the detector.

One additional improvement to the operation of the detector was the implementation of selective triggering. During most of the 2000 running period, data were taken with an effectively minimum-bias trigger, requiring only timing cuts on data from the plastic-

scintillator trigger detectors to signify a valid event. With the large increase in collision rates that accompanied the luminosity improvements from the accelerator, the minimum bias event rate increased from several 10 s of Hz in 2000, to as much as 1000 Hz. To enhance the fraction of the most interesting events from collisions in the central region of the detector, and from the most central collisions, a new triggering scheme was implemented. This scheme enhanced the fraction of good analyzable events by nearly an order of magnitude relative to the minimum bias trigger.

Physics results

Systematic behavior of charged particle production at mid-rapidity:

Energy Dependence

The most straightforward observable quantities from energetic heavy-ion collisions involve the number and distribution of the emitted charged particles. These quantities are of particular interest as they are sensitive to all processes contributing to particle production, and serve as measures of the energy, and entropy densities

achieved during the collision. The PHOBOS experiment has a number of elements designed to study the charged-particle multiplicity from such collisions. One of the earliest and most fundamental questions about charged-particle production in heavy-ion collisions concerns the energy dependence of $dN_{ch}/d\eta$ at mid-rapidity.

The first measurements of charged particle production from relativistic Au + Au collisions at RHIC were reported from the PHOBOS experiment,¹ from data obtained during the commissioning phase of RHIC running in June 2000. These first measurements were confined to the most central collisions, for particles emitted in the mid-rapidity region ($|\eta| < 1$). Additional data from $\sqrt{s_{NN}} = 200$ GeV were reported.² The pseudo-rapidity density was determined by counting “tracklets” – tracks measured in the partial spectrometer arm or vertex detector that connect either hits in two of the 6 spectrometer planes, or the two vertex detector planes, with the reconstructed vertex position. After corrections are applied for detector acceptance, and the effects of secondary particle production and combinatorial background, the pseudo-rapidity density $dN_{ch}/d\eta(|\eta| < 1)$ can be determined.

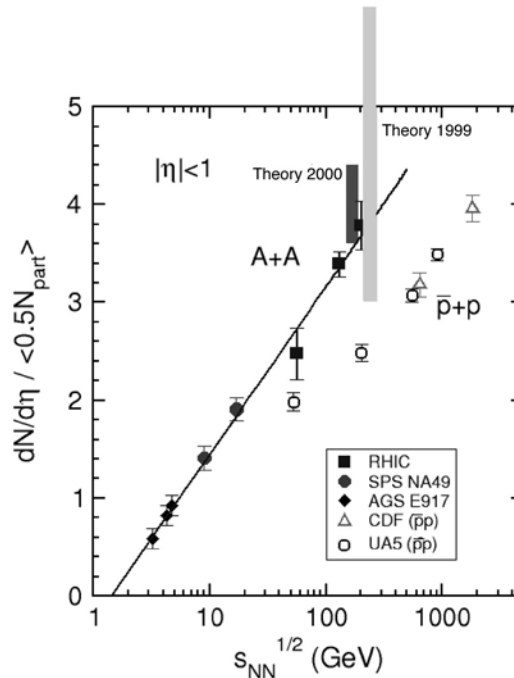


Fig. I-53. Bombarding energy dependence of charged particle production. The PHOBOS points are the solid squares.

Figure I-53 shows the measured bombarding energy dependence of the charged-particle pseudo-rapidity density at mid rapidity for the 6% of the most central collisions, divided by the number of nucleon pairs participating in the collision ($N_{pp} = 1/2 N_{part}$). For comparison, data at lower energies from the AGS³ and CERN SPS Pb + Pb program⁴ are also shown. The heavy-ion data show a logarithmic increase with bombarding energy. Compared to proton-antiproton scattering⁵ the charged particle density per participant nucleon-nucleon pair is as much as 70% higher for the heavy-ion system as compared to proton-antiproton collisions. This enhancement clearly indicates that charged-particle production at mid rapidity in the heavy-ion system reflects process beyond simple nucleon-nucleon scattering. These data also provide significant constraints on theoretical predictions for such collisions. The bar labeled “Theory 1999” shows the range of theoretical predictions for $dN_{ch}/d\eta$ at mid rapidity before Au + Au operations began at RHIC. This range was tightly restricted by our $\sqrt{s_{NN}} = 56$ and 130 GeV data (bar labeled “Theory 2000”). The $\sqrt{s_{NN}} = 200$ GeV data point lies at the lower edge of the range of the “Theory 2000” bar.

Centrality dependence of $dN_{ch}/d\eta$ at $\eta = 0$:

A measurement of the impact parameter, or centrality, dependence of $dN_{ch}/d\eta$ is sensitive to the relative

contributions of hard (parton-parton) and soft (nucleon-nucleon) scatterings. With increasing energy, the collisions probe shorter distances and hard collisions are expected to have a greater influence. Also, different theoretical pictures yield differing contributions of hard and soft scatterings. Generally, particle production from soft nucleon-nucleon is expected to depend linearly on the number of participating nucleon-nucleon pairs ($N_{part}/2$), while for hard collisions $dN_{ch}/d\eta$ is expected to depend approximately linearly on the number of nucleon-nucleon collisions, which approximately follows $N_{part}^{4/3}$. A measurement of $dN_{ch}/d\eta$ vs N_{part} can provide information about this division.

Figures I-54(a) and (b) show $(dN_{ch}/d\eta)/(N_{part}/2)$ plotted versus the number of participating nucleons N_{part} , for $\sqrt{s_{NN}} = 130^6$ and 200 GeV. The systematic uncertainty of approximately 6% was determined by comparing the results from different detector systems. Also plotted are the predictions from HIJING,⁷ saturation models,⁸ and from more empirical fits to the data assuming a combination of hard and soft scatterings.⁹ The data do not support either the HIJING or saturation pictures, and in fact fall somewhere in between the two. The hard/soft fits do a better job, with the contribution of hard scattering increasing from approximately 9% to 11% with increasing bombarding energy.

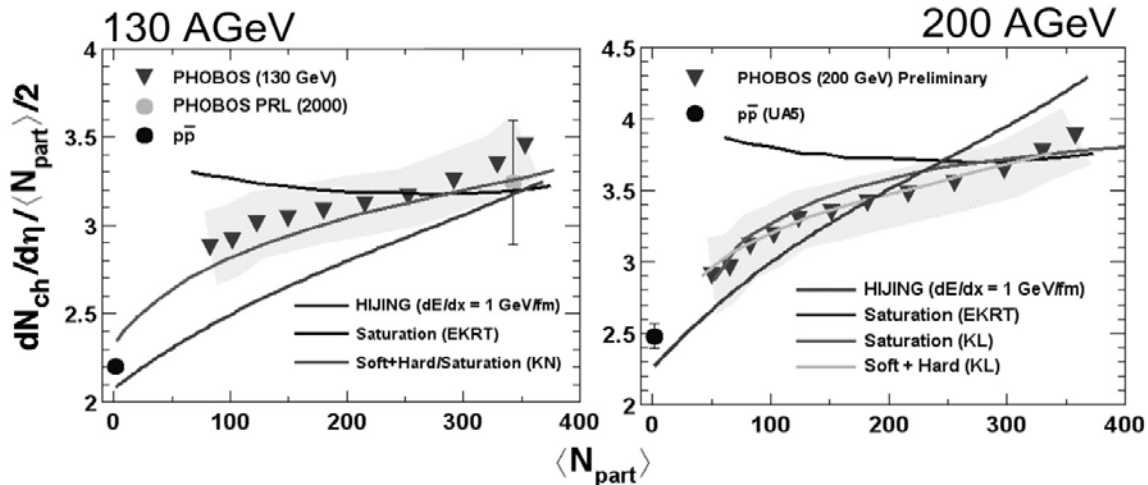


Fig. I-54. Centrality dependence of charged-particle production for central collisions at mid rapidity at $\sqrt{s_{NN}} = 130$ (a) and 200 (b) GeV.

$4\pi dN_{ch}/d\eta$:

Further information may be obtained by studying the pseudo-rapidity dependence of $dN_{ch}/d\eta$. This measurement was performed using the multiplicity detectors that were constructed by the Argonne-UIC group. This multiplicity measurement is completely independent of the tracklet analyses described above. Two methods were used to study $dN_{ch}/d\eta(\eta)$. One method relies on counting the hit pads in the multiplicity detector, as a function of pseudorapidity. The number of hit pads is corrected for the acceptance, as well as the effects of detector occupancy, secondary particle production, weak decays, and background. The background corrections were made using a comparison to a Monte Carlo simulation of the detector. The alternative method involves measuring the total energy deposited in the multiplicity detector $\Delta E(\eta)$ as a function of pseudorapidity. The measured deposited energy is then compared to the average energy

deposited by a charged particle vs pseudorapidity, and corrected for contributions of background, also carried out using a Monte Carlo simulation. The two methods provided results that were in excellent agreement with each other.

The measured distributions of $dN_{ch}/d\eta$ at $\sqrt{s_{NN}} = 130$ GeV for several centrality bins appear in Fig. I-55.¹⁰ The centrality dependence of these data appears in Fig. I-56, where the panels (b) - (f) represent data taken at various values of η . Figure I-56(a) shows the integrated charged-particle yield as a function of centrality. For the most central collisions, we measure a total of approximately 4200 charged particles produced within $|\eta| < 5.4$. In most cases the data are not well reproduced by the calculations with the HIJING code (solid lines). Other models^{11,12} which include hadronic rescattering are better able to reproduce the data for large values of $|\eta|$.

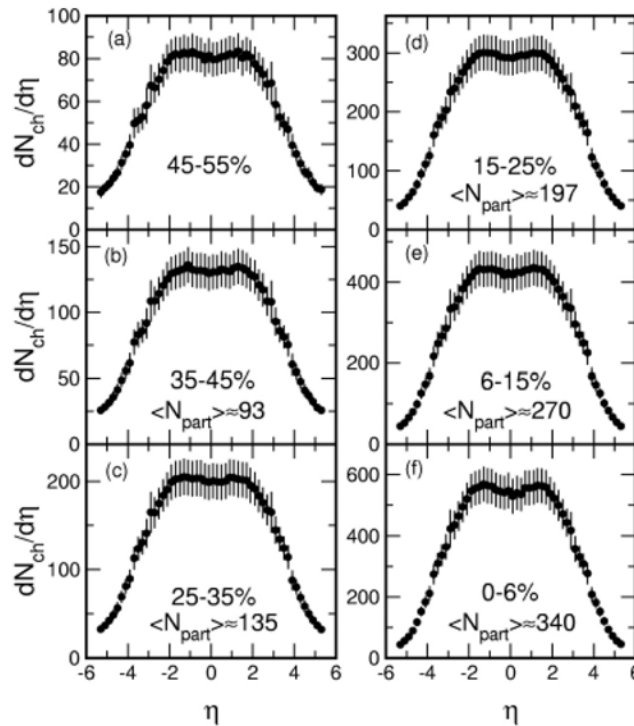


Fig. I-55. $dN_{ch}/d\eta$ vs. η for various collision centralities.

Figure I-57(a) shows a comparison between the distributions of $dN_{ch}/d\eta/(N_{part}/2)$ for the 6% most central collisions at $\sqrt{s_{NN}} = 130$ and 200 GeV. Figure I-57(b) compares the 200 GeV central Au + Au data with data from proton-antiproton scattering at that energy. The enhancement of charged-particle

production at mid rapidity is clear, however at larger values of $|\eta|$ the two data sets are closer to each other, perhaps suggesting that charged particle production for $|\eta| > \sim 3$ may be governed by simpler mechanisms following nucleon-nucleon scattering.

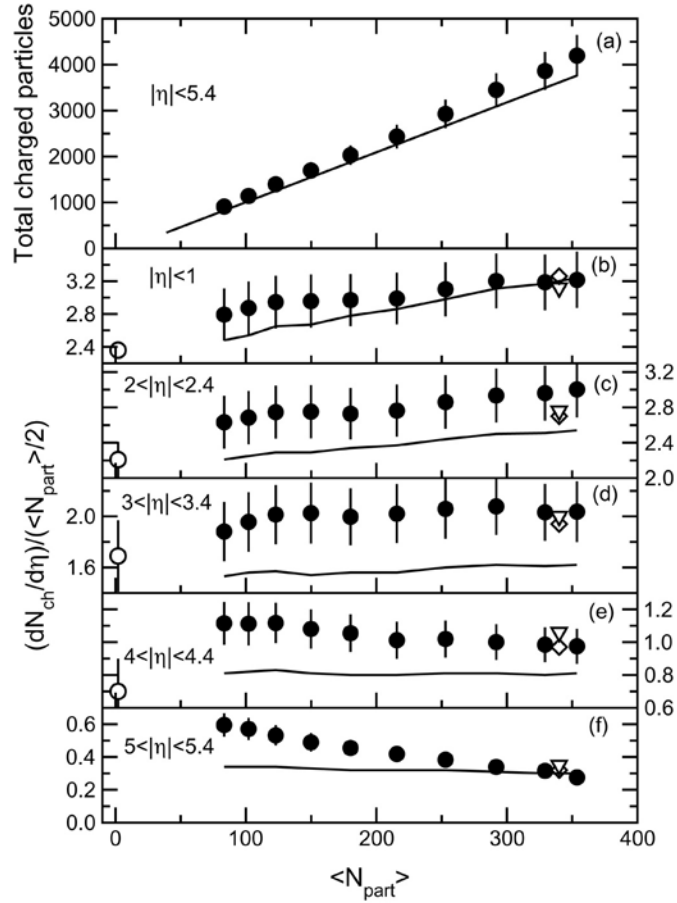


Fig. I-56. Centrality dependence of (a) total charged-particle production for $|\eta| < 5.4$ and (b - f) $dN_{ch}/d\eta$ at various values of η . The solid curves represent calculations using the HIJING model.

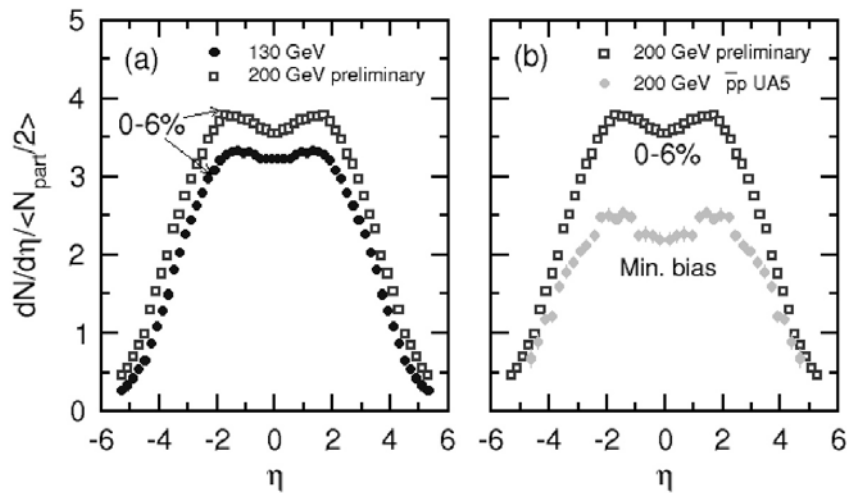


Fig. I-57. (a) $dN_{ch}/d\eta$ vs η for central collisions at $\sqrt{s_{NN}} = 130$ GeV (solid circles) and 200 GeV (open squares). (b) Central $dN_{ch}/d\eta$ for Au + Au (open squares) and $\bar{p}p$ (solid circles) collisions at $\sqrt{s_{NN}} = 200$ GeV.

Evidence in favor of this view may be supported by a comparison between, for example, the data for central collisions at $\sqrt{s_{NN}} = 130$ and 200 GeV, when viewed in the rest frame of one of the colliding nuclei. When plotted as a function of the so-called “shifted pseudorapidity” $\eta' = \eta - y_{BEAM}$, where y_{BEAM} is the

beam rapidity. Here, for values of $\eta' < 2$, the two sets of data lie virtually on top of each other. This behavior is reminiscent of the phenomenon called “limiting fragmentation” which is well known in proton-proton and proton-nucleus scattering (see, for example, Fig. I-58(a)).

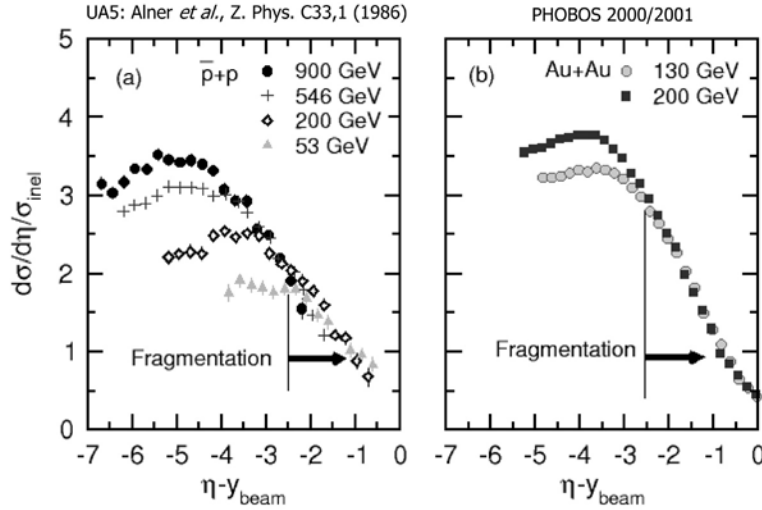


Fig. I-58. (a) Distributions of $dN_{ch}/d\eta$ vs $\eta' = \eta - y_{BEAM}$ from $\bar{p}p$ scattering at different energies. (b) $dN_{ch}/d\eta$ vs η' from Au + Au collisions at $\sqrt{s_{NN}} = 130$ (circles) and 200 GeV (squares).

Baryon density at mid rapidity:

One prediction of the situation achieved in heavy-ion collisions at highly relativistic energies is that the two nuclei pass through each other, leaving a very hot, but essentially baryon free, region between them from which particles and anti-particles are produced. In order to determine whether this central region is actually baryon-free, it is useful to study the ratio of anti-baryons to baryons at mid-rapidity. If the participant baryons carried within the colliding nucleons are indeed swept out of the hot central zone, then the ratio of the numbers of observed baryons, and anti-baryons at mid-rapidity should be approximately unity. Furthermore, this ratio may be related to the amount of kinetic energy transformed into energy available for particle production.

The ratio of anti-protons to protons at mid rapidity was measured in PHOBOS using data from the tracking spectrometer with the magnet energized to its full field value of 2T. Tracks were analyzed by first identifying straight tracks in the 6 spectrometer planes within the field-free region near the beam pipe. These tracks were followed into the magnetic field region and then

momentum analyzed by comparing hits in the remaining spectrometer planes with predetermined patterns in a look-up table. The particles were identified by a measurement of their differential energy loss in the spectrometer planes. In order to address systematic uncertainties, data obtained with the two magnet polarities were compared. The different acceptances for positively and negatively charged species obtained with the two polarities effectively cancel. The results for \bar{p}/p and K^-/K^+ are shown in Fig. I-59(a),¹³ with data from Au + Au collisions at lower energies from the AGS, and from Pb + Pb collisions at the SPS. The value of $\bar{p}/p = 0.6$ is somewhat less than one, implying that the mid-rapidity region is not yet entirely baryon free. The measured value is, however, approximately six times larger than that observed in Pb + Pb collisions at the SPS. The \bar{p}/p ratio is expected to more closely approach unity as the collision energy is increased to $\sqrt{s_{NN}} = 200$ GeV in the RHIC 2001 physics run.

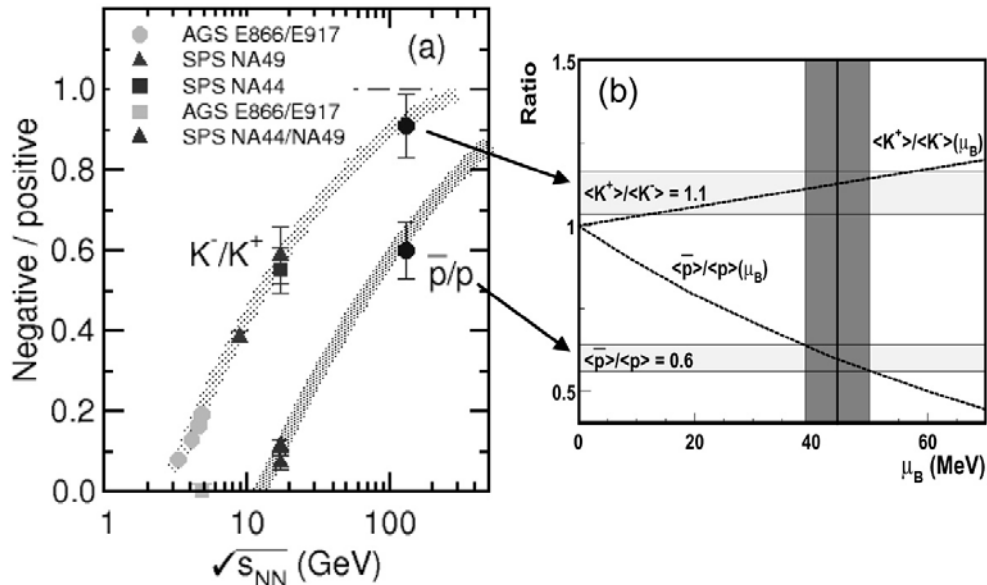


Fig. I-59. (a) Bombarding energy dependence of anti-particle/particle ratios. (b) Thermal model prediction of Redlich.¹⁴

The combined \bar{p}/p and K^-/K^+ ratios can be used to infer the temperature and baryon chemical potential of the system. Figure I-59(b) shows a calculation by Redlich¹⁴ performed in a thermal model. The horizontal bands represent the measured values of the anti-particle/particle ratios. Within the context of this

model, the data for $\sqrt{s_{NN}} = 130$ GeV are consistent with a baryon chemical potential $\mu_B = 45$ MeV, and a temperature of approximately 165 MeV. These values are within the range where quark and gluon degrees of freedom are expected to become important.

¹B. B. Back *et al.*, Phys. Rev. Lett. **85**, 3100 (2000).

²B. B. Back *et al.*, Phys. Rev. Lett. **88**, 022302 (2002).

³B. B. Back *et al.*, Nucl. Phys. **A661**, 690 (1999).

⁴J. Bachler *et al.*, Nucl. Phys. A **661**, 45 (1999).

⁵F. Abe *et al.*, Phys. Rev. D **41**, 2330 (1990).

⁶B. B. Back *et al.*, Phys. Rev. C, **88**, 031901(R) (2002).

⁷X. N. Wang and M. Gyulassy, Phys. Rev. D **44**, 3501 (1991).

⁸K. J. Eskola *et al.*, Nucl. Phys. B **570**, 379 (2000).

⁹D. Karzhev and M. Nardi, Preprint nucl-th/0012025.

¹⁰B. B. Back *et al.*, Phys. Rev. Lett. **87**, 102303 (2001).

¹¹Z. Lin *et al.*, Preprint nucl-th/0011059.

¹²D. E. Kahana and S. H. Kahana, Phys. Rev. C **59**, 1651 (1999).

¹³B. B. Back *et al.*, Phys. Rev. Lett. **87**, 102301 (2001).

¹⁴K. Redlich, Proceedings of the 15th International Conference on Ultra-relativistic Heavy Ion Collisions, (2001).

F. ULTRA-HIGH-SENSITIVITY MEASUREMENTS AND INVESTIGATION OF FUNDAMENTAL INTERACTIONS

The nucleus continues to be one of nature's classic laboratories for investigating both the strong and weak interactions. The equipment and techniques developed for investigating nuclei can be used to tackle many problems in nature. A range of ultra-sensitive investigations was pursued. Using ATLAS, the tradition of developing new and cutting edge Accelerator Mass Spectrometry (AMS) techniques continued with investigations of ^{39}Ar in sea water, ^3He in ^4He , and ^{244}Pu in the cosmos. Beyond these projects, synchrotron radiation from the Argonne Advanced Photon Source (APS) was used to determine the probability in enhancing the decay rate of the 31-year nuclear isomer in ^{178}Hf and refuting earlier claims of substantial enhancements. Investigations into the dynamics of confined plasmas also continued, focusing on the melting of confined cold plasmas. We continue to be interested in finding new avenues where our knowledge and equipment allow us to make significant contributions to important fundamental projects.

f.1. Developing an AMS Counting Technique for ^{39}Ar (I. Ahmad, J. Caggiano, C. L. Jiang, A. Heinz, D. Henderson, R. C. Pardo, K. E. Rehm, R. H. Scott, R. Vondrasek, Ph. Collon,* M. Bichler,† W. S. Broecker,* L. DeWayne Cecil,‡ Y. El Masri,§ R. Golser,§ W. Kutschera,¶ B. E. Lehmann,|| P. Leleux,§ H. H. Loosli,|| M. Paul,** P. Schlosser,* and W. M. Smethie, Jr.*)

Scientific Justification

It is generally accepted that more geochemical and geophysical data is needed for proper modeling of the climate on Earth. Ocean currents play a particularly important role in this respect, because they transport large amounts of heat around the globe. Obviously, any advance in collecting data about the ocean system in this respect is welcome. A measurement of the cosmogenic radionuclide ^{39}Ar in ocean water was considered for some time to make an impact in oceanography due to a number of useful properties. The half-life of 268 years fits well to the time scale of oceanic currents and mixing (100 to 1500 years), the atmosphere is the only major pool of ^{39}Ar , and the inertness of argon makes it relatively easy to understand the distribution of ^{39}Ar on a global scale. An ^{39}Ar dating method for argon extracted from large water samples (~1000 liter) was developed some time ago using a low level decay counting technique.¹ Based on the results of Loosli's group at the University of Bern, a recent comparison of ^{39}Ar and ^{14}C ages for waters in the deep ocean emphasized the need for more ^{39}Ar measurements.²

The AMS method for measuring other radionuclides of interest (e.g. ^{14}C , ^{129}I) requires only ~1 liter of ocean water, making low level decay counting of ^{39}Ar virtually obsolete, hence, our effort to develop an AMS

technique for ^{39}Ar . One liter of ocean water in equilibrium with the atmosphere contains about 9000 atoms of ^{39}Ar (about 6 cm³ STP argon are dissolved in one liter of water). If this sample is detached from contact to the atmosphere for 1000 years, only about 700 atoms of ^{39}Ar will be left. To achieve the ultimate goal of $^{39}\text{Ar}/^{40}\text{Ar}$ ratio measurements with a 3% precision for 1000-year-old ocean water, one would have to collect 20 liter of ocean water, and to measure ^{39}Ar atoms from it with an overall detection efficiency of 7% (^{39}Ar atom detected per ^{39}Ar atom in the sample). Although this is currently still out of reach for our AMS technique at ATLAS, we believe that one can ultimately meet this goal.

The Technical Challenge

Measuring ^{39}Ar with AMS at natural levels is arguably the biggest technical challenge for the AMS method, and ATLAS is probably the only facility where it can currently be achieved. The difficulties can best be envisioned by comparing $^{39}\text{Ar}/^{40}\text{Ar}$ ratio measurements with those of $^{14}\text{C}/^{12}\text{C}$. The latter is by far the most used radionuclide with AMS, partly because of the ease of performing the isotope ratio measurement. The natural (pre-bomb) $^{14}\text{C}/^{12}\text{C}$ ratio in atmospheric CO_2 is 1.2×10^{-12} , whereas the $^{39}\text{Ar}/^{40}\text{Ar}$ ratio in atmospheric argon

is only 8×10^{-16} . In addition, the stable isobaric background in ^{14}C measurements, ^{14}N , is virtually absent because nitrogen does not form negative ions. Therefore ^{14}C AMS measurements are performed exclusively with negative ions (mostly at tandem accelerators). In contrast to ^{14}C , ^{39}Ar measurements must be performed with positive ions because argon doesn't form stable negative ions. As a consequence, the stable isobar, ^{39}K , is also produced in the ECR ion source at ATLAS. Since potassium is a ubiquitous background at the trace element level in almost any material, one has to deal with a very strong isobaric interference.

In our last ATLAS run the $^{39}\text{K}^{8+}$ background ions arriving at the gas-filled spectrograph were 3 billion times more abundant in the beam than the $^{39}\text{Ar}^{8+}$ ions from a 1000-year-old water sample. Physical separation of ^{39}K from ^{39}Ar with the gas-filled spectrograph in the focal plane reduced ^{39}K by 4 orders of magnitude before the ions entered the focal plane detector. The remaining ^{39}K background was then separated from ^{39}Ar in the new large-acceptance focal plane ionization chamber (See Fig. I-60). This detector was developed by Michael Paul at the Racah Institute of Physics of the Hebrew University of Jerusalem, and was tested in an ATLAS run in July 2001.

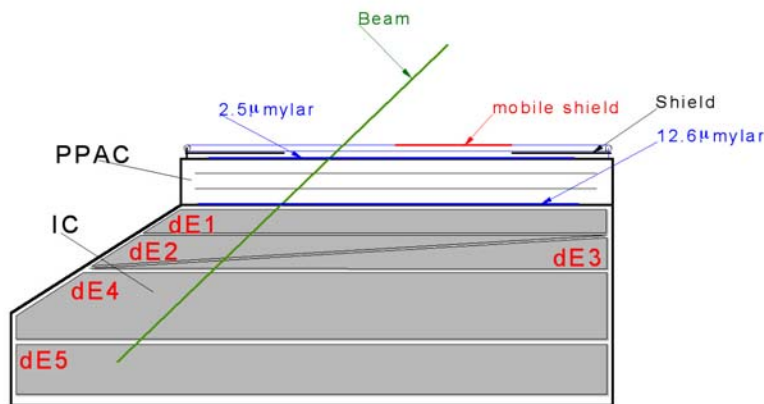
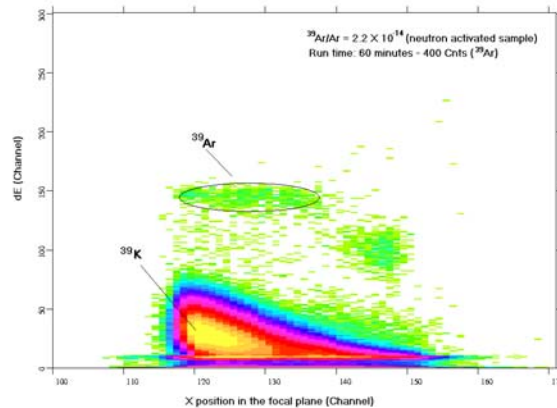


Fig. I-60. Typical focal plane position vs. ΔE signal obtained for a neutron activated argon sample using the ionization chamber (IC) coupled to the position sensitive PPAC detector. The clear separation of the ^{39}Ar from the ^{39}K background can clearly be seen.

Results from the Last ^{39}Ar Run

As compared to the run in February 2001, three major changes were implemented in order to reduce the ^{39}K

background and to increase the overall detection efficiency, respectively:

- 1) A quartz liner was installed in the ECR II ion source. The $^{40}\text{Ar}^{8+}$ current was about the same as previously (45 - 50 e μ A), but the ^{39}K background decreased by at least a factor of 10. During initial running with the quartz liner we noticed a defect of one bar of the permanent-magnet sextupole lens in ECR II, which resulted in burning a hole into the wall of the quartz cylinder. After replacing the faulty sextupole bar with a spare one, a second quartz liner was used, which was open ended on the front and the back, whereas the first liner had both ends of the cylinder closed by quartz plates. This latter configuration may have reduced the ^{39}K background further.
- 2) As mentioned above, we used the new focal plane detector from Israel, which accepts virtually all ^{39}Ar ions arriving at the split pole spectrograph. This resulted in a factor of about 2.5 in detection efficiency as compared to the standard focal plane detector.
- 3) A new gas-handling system for argon samples was developed during the past year and tested online for the first time during the august run. This system made it possible to measure up to 3 different samples/standards without having to gain access to the ECR source enclosure as all the pneumatic valves can be operated remotely. This new system coupled with the use of low neutron

activated argon standards greatly improved our normalization procedures.

Together with a reduction of sample consumption due to a reduced pumping in the ECR II source (because the cylinder of the quartz liner did not allow pumping through the side port), and due to an improvement of ion optical transmission from ECR II to the split pole spectrograph, the overall efficiency was about 2×10^{-3} . This is about a factor of 5 higher than the overall efficiency of the February 2001 run. Normalization of the samples was achieved by using neutron-activated samples with known $^{39}\text{Ar}/^{40}\text{Ar}$ ratios of 2×10^{-14} . We measured several samples of known $^{39}\text{Ar}/^{40}\text{Ar}$ ratio in the range from atmospheric ($^{39}\text{Ar}/\text{Ar} = 8.1 \times 10^{-16}$) to 10% atmospheric ($^{39}\text{Ar}/\text{Ar} = 9.7 \times 10^{-17}$) values.

Future Plans

Recent results encourage us to pursue this technique. We will concentrate our efforts on the ECR source in order to try and reduce the ^{39}K background by several orders of magnitude so that we may be able run with higher intensity Argon beams (in the present state, running with higher intensity beams would swamp the detector with ^{39}K ions). For this we must identify the sources of ^{39}K and start a systematic analysis of the factors influencing its intensity in the beam. This information will then be used in the next phase of this project: the development of a small ECR source dedicated to noble gas AMS.

*Lamont-Doherty Earth Observatory of Columbia University, †Atominstiut der Oesterreichischen Universitaeten, Wien, Austria, ‡U.S. Geological Survey, §Universite Catholique de Louvain, Belgium, ¶Universitaet Wien, Austria, ||Universitaet Bern, Switzerland, **Hebrew University of Jerusalem, Israel

¹H. H. Loosli, Earth Planet. Sci. Lett. **63**, 51-62 (1983).

²W. S. Broecker and T.-H. Peng, Nucl. Instrum. Methods **B172**, 473-478 (2000).

f.2. Measurement of the ^3He Component in Isotopically Purified ^4He by AMS

(R. C. Pardo, A. Heinz, R. V. F. Janssens, C. L. Jiang, K. E. Rehm, J. P. Schiffer, R. H. Scott, R. C. Vondrasek, J. M. Doyle, * P. Collon, † P. R. Huffman, ‡ and D. McKenzie*)

An experiment to determine the fractional concentration of ^3He remaining in isotopically purified ^4He was initiated. This measurement is in support of a program to improve the accuracy of the neutron beta decay lifetime.⁴ The lifetime measurement is achieved by trapping free neutrons in a superfluid helium bath and observing their subsequent decay. Any capture of free neutrons by ^3He in the bath will reduce the apparent lifetime in this measurement. To achieve the desired

neutron lifetime accuracy, the liquid helium trap material must be free of ^3He to a level of 1 part in 10^{14} .

The dominating problem in such a highly sensitive measurement of the $^3\text{He}/^4\text{He}$ ratio is the background ^3He present from past usage of natural helium ($\sim 2\text{-}10 \times 10^{-8}$ $^3\text{He}/^4\text{He}$). By operating the source at extremely high pressures, we hoped to "overpower" the background with the material of interest. In an initial

run, the standard ECR-I source was used except that a 1-mm diameter extraction aperture replaced the standard 8-mm diameter aperture. Measurements were made with and without the standard pumping available to the source. The results are shown in Fig. I-61 and show the generally expected trend, but indicate that the actual ^3He background in this source is higher than anticipated.

Therefore a "new" source was constructed consisting of a new extractor electrode with a quartz tube directly

attached forming a small isolated volume for creating the helium plasma. Off-line tests confirmed its ability to deliver sufficient beam with over 100 microamps of ^4He extracted. A two-day test in September determined that the background helium in this new "source" is at least two orders of magnitude lower than the original ECR-I source.

Our goal is to achieve a sensitivity of the order of 10^{-15} in the $^3\text{He}/^4\text{He}$ ratio.

*Harvard University, †Lamont-Doherty Earth Observatory of Columbia University, ‡National Institute of Standards and Technology

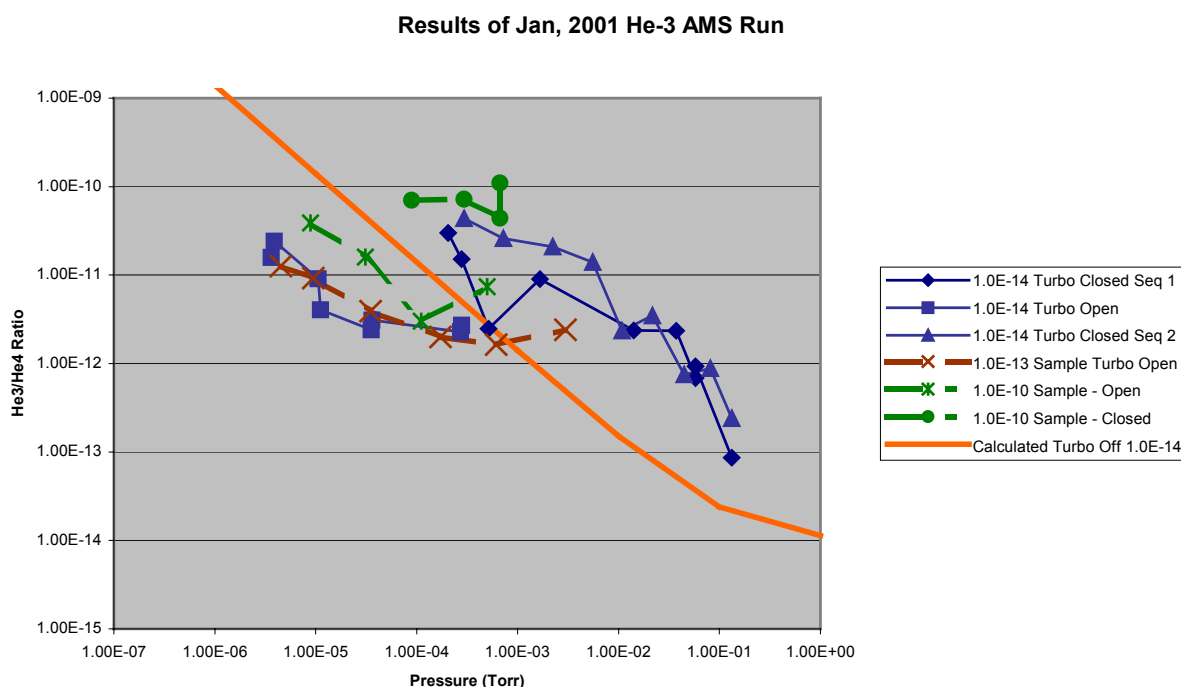


Fig. I-61. Summary of ^3He AMS Data from January 2001 run.

f.3. Experimental Limit of Interstellar ^{244}Pu Abundance (I. Ahmad, C. Feldstein,* A. Valenta,* S. Ghelberg,* S. Jiang,* Y. Bendov,† D. Berkovits,† C. Bordeanu,‡ Y. Hashimoto,§ T. Nakanishi,§ and K. Sakamoto§)

Recent data of the Ulysses and Galileo space missions and of the AMOR ground-based radar array point to the penetration of a population of interstellar medium (ISM) grains into the inner Solar System.¹ A steady-state deposition of such grains onto Earth would result in their accumulation in earth reservoirs such as deep-sea sediments and ferromanganese nodules. These two reservoirs are characterized by extremely low sedimentation rates (respectively of the order of 1 mm/kyr and 1 mm/Myr), resulting in a favorable ratio

between extraterrestrial and terrestrial matter.

Several short-lived nuclides ($T_{1/2} \leq 100$ Myr) are known to have been alive in Early-Solar material. These radioactivities, now extinct in the Solar System, are expected to be present in the ISM where it is estimated that nuclides with lifetimes ≥ 5 - 10 Myr attain approximate steady-state abundances.² An unmistakable signature of fresh ISM material deposited on Earth would be the presence of such short-lived

species. Among those, transuranium elements are favored since their natural production by other means, e.g. cosmic-ray interaction with matter, is unlikely.

We determined the ^{244}Pu content of the Pu fraction separated from 1 kg of North-Pacific deep-sea sediment.³ The chemical separation and alpha-counting of the Pu-fraction were performed at Kanazawa University. The accelerator-mass-spectrometry (AMS) analysis of the Pu isotopes shows a distribution expected for nuclear fallout (Fig. I-62) and sets a limit of < 0.2 ^{244}Pu atoms $\text{cm}^{-2} \text{yr}^{-1}$ (90% confidence level) for extraterrestrial deposition. Using

existing experimental data on the rate of accretion of ISM grains onto Earth and further assuming that the ISM has an Early-Solar uranium abundance, we derive a limit of $(^{244}\text{Pu}/\text{U})_{\text{ISM}} < 1 \times 10^{-3}$.

These results are compared with the recent measurements^{4,5} of the Munich group on ^{60}Fe and ^{244}Pu in deep-sea ferromanganese crusts. We are also pursuing our measurements with the separation of Pu, Cm and Hf from a deep-sea piston core (sediment depth from 3 cm to 230 cm), clean of material of fallout origin.

*Hebrew University, Jerusalem, Israel, †Soreq NRC, Yavne, Israel, ‡Weizmann Institute, Rehovot, Israel, §Kanazawa University, Japan

¹E. B. Grün *et al.*, Nature **362**, 428 (1993); M. Baguhl *et al.*, Science **268**, 1016 (1995); J. W. Baggaley, JGR **105**, 10353 (2000).

²B. S. Meyer and D. D. Clayton, Space Sci. Rev. **92**, 133 (2000).

³M. Paul, A. Valenta, I. Ahmad, D. Berkovits, C. Bordeanu, S. Ghelberg, Y. Hashimoto, A. Hershkowitz, S. Jiang, T. Nakanishi and K. Sakamoto Ap. J. **558**, L133 (2001).

⁴K. Knie, G. Korschinek, T. Faestermann, C. Wallner, J. Scholten, W. Hillebrandt, Phys. Rev. Lett., **83**, 18 (1999).

⁵C. Wallner, T. Faestermann, U. Gertsmann, W. Hillebrandt, K. Knie, G. Korschinek, C. Lierse, C. Pomar, G. Rugel, Nucl. Instr. and Methods **172**, 333 (2000).

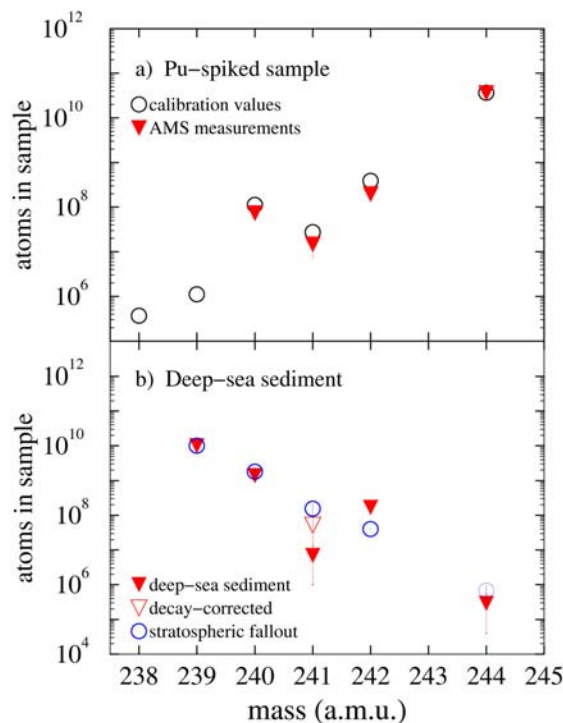


Fig. I-62. Isotopic distribution of plutonium (solid triangles) measured by AMS for: (a) a calibration sample containing 3.7×10^{10} ^{244}Pu atoms. The open circles show the distribution measured by alpha counting of a thin source. The AMS results were normalized to the number of ^{244}Pu atoms obtained from the alpha counting. (b) The plutonium fraction extracted from the 1.020-kg deep-sea dry sediment. The AMS results were normalized to the combined number of $^{239,240}\text{Pu}$ atoms measured by alpha spectrometry. The open circles represent the expected Pu isotopic distribution of nuclear-bomb stratospheric fallout.

f.4. Search for the First Excited Level in the ^{229}Th Nucleus (I. Ahmad, K. Bailey, Z.-T. Lu, C. Law, D. L. Bowers,* and D. G. Graczyk*)

The first excited level of the ^{229}Th nucleus was deduced to be 3.5 ± 1.0 eV above the ground-level.¹ Considering nuclear excitation energies are typically in the 10^4 - 10^6 eV range this would be by far the lowest known nuclear excitation energy, both extremely unique and unexpected – even lower than the atomic ionization energy. This state, if confirmed, could be used to study the interactions of the nucleus and its surrounding, as well as novel ways to achieve nuclear excitation (such as visible lasers).

This experiment was designed to test the validity and clarify discrepancies from a number of recent experiments.^{1,2,3,4} Rather than using ^{233}U samples for observation, isotopically and chemically pure ^{229}Th samples were used. The ^{229}Th samples were observed within hours of production (via ^{233}U alpha decay), which should leave a large number of ^{229}Th in the first excited state for our observation. Our experiment also includes very low detection thresholds due to cooled, low-background photo-multiplier tubes.

We extracted freshly produced ^{229}Th atoms from a 250 mg isotopically pure ^{233}U ($^{232}\text{U}/^{233}\text{U} < 10^{-9}$). We allowed the ^{229}Th to accumulate for approximately 15 hours in the ^{233}U solution before being chemically separated. The ^{229}Th sample had an alpha activity of 20 Bq (there were no other detectable radioisotopes in the sample), and was dissolved in HCl (12 M) and placed in a quartz cell for observation. The sample was placed in the photon detection system approximately one hour after the chemical separation.

*Chemical Technology Division, ANL

¹R. G. Helmer and C. W. Reich, Phys. Rev. C **49**, 1845 (1994).

²G. M. Irwin and K. H. Kim, Phys. Rev. Lett. **79**, 990 (1997).

³D. S. Richardson *et al.*, Phys. Rev. Lett. **80**, 3206-3208 (1998).

⁴R. W. Shaw, J. P. Young, S. P. Cooper and O. F. Webb, Phys. Rev. Lett. **82**, 1109-1111 (1999).

Our detection system consisted of two UV sensitive PMTs. The sample was placed between the two PMTs on a pneumatic sled. The system is sensitive to photons with wavelengths from 210 nm (determined by absorption in the HCl) to 800 nm (PMT window material), or 1.5 - 5.9 eV. The sled was operated with a period of 45 s, to allow for background counting with a sample in the system. The PMT's were cooled to approximately 0°C in order to reduce the dark counting rate.

Compared with the dark counting rate of 1000 cpm, we were able to detect significantly higher count rates with the ^{229}Th sample inserted (1500 cpm), however, this difference did not vary significantly with time and was several orders of magnitude below expectations. This would indicate that the photons being observed were not from a low-energy nuclear transition in ^{229}Th , but from α and high-energy γ decay of ^{229}Th and its daughter products.

There are several possible reasons for our inability to verify this low energy state. The photon energy could be outside of our detectable limit, or the lifetime of the state could be extremely long or short compared with our expectations.

In future we plan to use phototubes with lower dark currents and reduce the time between the chemical separation and the start of the measurement.

f.5. Search for X-Ray Induced Acceleration of the Decay of the 31-yr Isomer of ^{178}Hf Using Synchrotron Radiation (I. Ahmad, D. S. Gemmell, E. F. Moore, J. P. Schiffer, J. Banar,* J. A. Becker,† A. Kraemer,† A. Mashayekhi,‡ D. McNabb,† G. G. Miller,* L. N. Pangault,* S. Rundberg,* S. D. Shastri,‡ T. F. Wang,† and J. B. Wilhelmy*)

Releasing the energy stored in an isomeric nuclear state in a controlled way with an atomic or electromagnetic trigger is an attractive speculation: the energy gain is on the order of the ratio of nuclear/atomic energies $\sim \text{MeV/keV}$. Nuclear isomers, therefore, represent an

opportunity for stand-alone energy source if suitable schemes for trigger and control of energy release could be identified. Potential applications include space propulsion as well as very bright gamma-ray sources.¹

Recently, reports of triggered decay of a ^{178}Hf isomer induced by x rays delivered by a dental x-ray machine were made.^{2,3} Enhancements of 1-2% in the isomer decay rate were reported for several gamma-rays in the decay cascade (Fig. I-63). The reported integrated

cross section for the decay was $10^{-21} \text{ cm}^2\text{-keV}$, so large as to demand new physics. We sought to verify these claims using the intense photon flux available at the Advanced Photon Source facility.

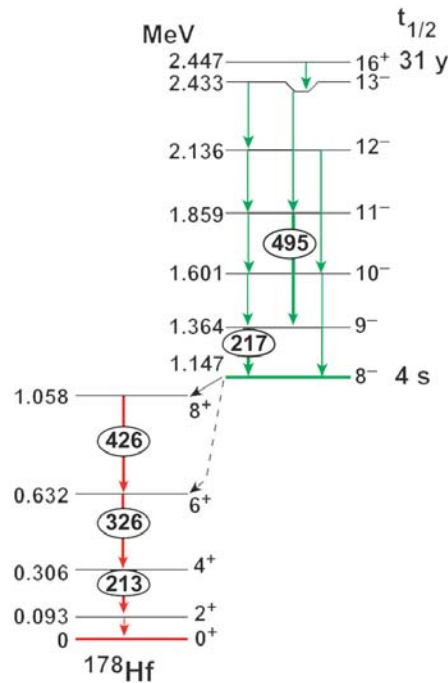


Fig. I-63. Energy level diagram showing the decay of 31-y ^{178}Hf isomer. Transition energies are given in keV.

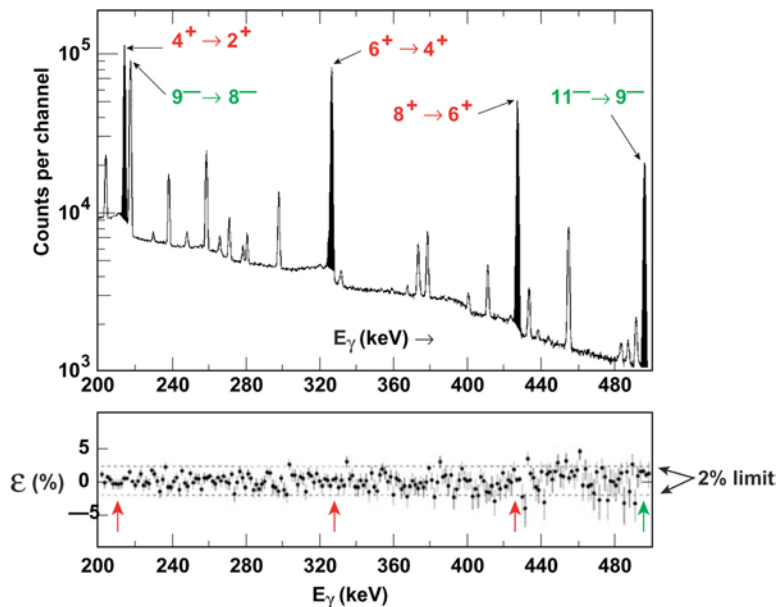


Fig. I-64. Gamma-ray spectrum showing transition in the 200 - 500 keV range in the decay of ^{178}Hf isomer. The lower part shows the difference in spectrum between the first half and second half of the 22-s beam-off data.

Samples of HfO_2 containing $\sim 10^{15}$ atoms of the 31-y ^{178}Hf were irradiated at the SRI CAT 1-ID in March 2001. Samples were fabricated at LANL using material chemically isolated from LANSCE/LAMPF target/beam stop. The undulator 1-ID was operated with maximum taper (5 mm) in the gap and two average settings: 15 mm and 20 mm. This arrangement generated a smooth "white" photonflux peaking at 2×10^{15} photons/keV-s at $E_{\text{ph}} = 16$ keV and extending up to 100 keV. The beam was mechanically chopped to form a pulse train of 11-s beam-on and 22-s beam-off during irradiation intervals of 8 h for each of the three samples. Two Low Energy Photon Spectrometers (LEPS) were used to measure the gamma-ray spectra of the $^{178\text{m}}\text{Hf}$ source. The Hf K x rays produced by fluorescence of Hf atoms by the beam were used to monitor the beam flux. The experimental signal of triggered isomer decay is an increase in the yields of ^{178}Hf gamma rays above the

background gamma rays of the sample.

The intensities of gamma rays were measured both during beam-on period and beam-off period for the gamma rays decaying through the 4-s isomer. For the latter analysis, the off-line spectra were divided into two 11-s spectra. The difference of the two spectra will show if there were any population of the 4-s isomer during irradiation. Figure I-64 shows the spectrum and the difference measured. The bottom part of the figure shows the difference between the two spectra. As can be seen, within the statistics, there is no enhancement.

By analyzing the spectra measured with beam-on and beam-off conditions, we obtained an upper limit for the integrated cross section. Our upper limit of the integrated cross section for 20-60-keV photons is 2×10^{-27} $\text{cm}^2\text{-keV}$ (Fig. I-65), which is five orders of magnitude lower than the published value. Results of this experiment were published.⁴

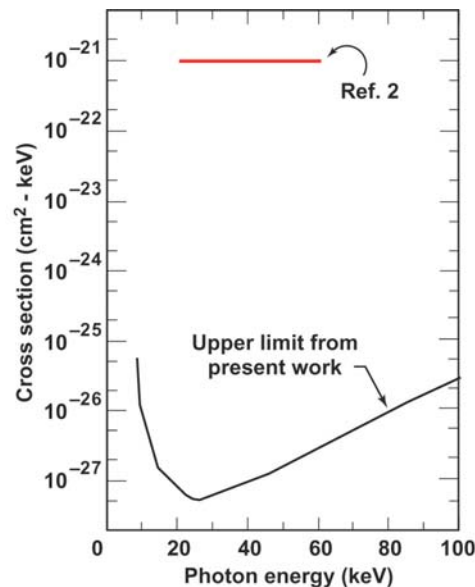


Fig. I-65. Upper limit of the cross section for the photon induced deexcitation of the 31-y ^{178}Hf isomer through the 4-s isomer. The upper horizontal line shows the value reported in Ref. 3.

*Los Alamos National Laboratory, †Lawrence Livermore National Laboratory, ‡Advanced Photon Source, ANL
¹Science **283**, 769 (1999).

²C. B. Collins *et al.*, Phys. Rev. Lett. **82**, 695 (1999).

³C. B. Collins *et al.*, Laser Physics **9**, 8 (1999).

⁴I. Ahmad *et al.*, Phys. Rev. Lett. **87**, 072503 (2001).

f.6. Melting of Crystalline Confined Plasmas (J. P. Schiffer)

The behavior of confined plasmas, such as occur in ion traps, was studied in simulations. For an infinite array of charges it was known for some time that a phase transition from liquid to solid behavior occurs at a well defined temperature, defined by the dimensionless parameter that scales the temperature with density

$$\Gamma \equiv (q^2/a_{ws})/kT$$

where $a_{ws} \equiv 1/\rho^{1/3}$ is the Wigner-Seitz radius. The phase transition for infinite Coulombic matter occurs at $\Gamma \approx 173$. For finite confined systems, the ordering is not the body-centered cubic form that is seen in infinite matter, instead they form an ordered state with concentric shells, with hexatic order of equilateral triangles within the shells.¹ In any case, finite systems do not have sharp phase transitions. Molecular Dynamics simulations were carried out by running

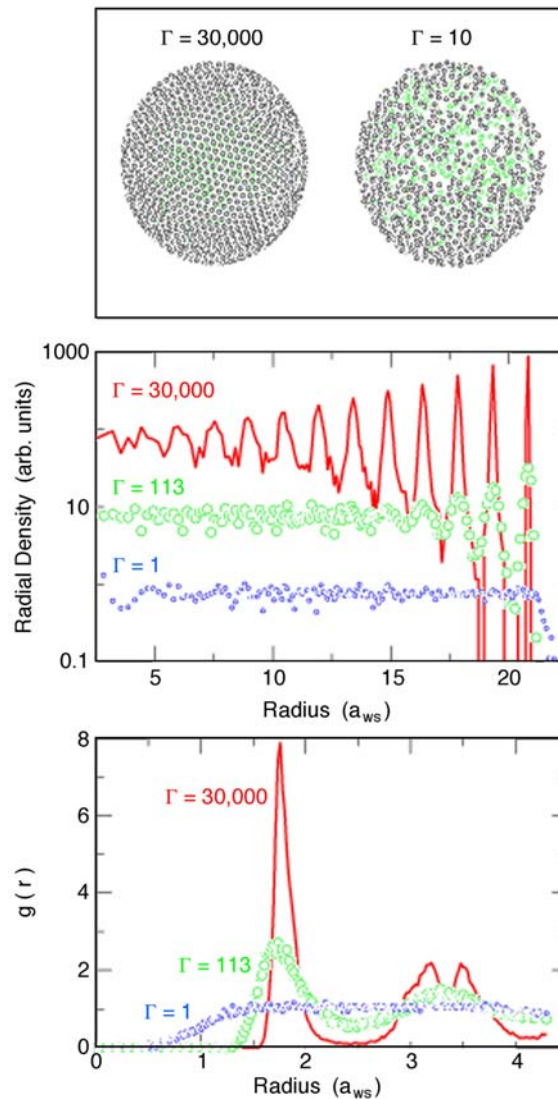


Fig. I-66. On top the outer two layers of ions are displayed for a 10,000 ion system. The ions in the outermost layer are shown in black, the next layer in grey. On the left, a cold ordered array is shown, while on the right a disordered one at high temperature, with the ions in different shades corresponding to similar radial intervals. The middle box shows the radial density within the ion cloud at three different temperatures with the vertical scaled displaced for visibility. On the bottom, the correlation function $g(r)$ is shown at three temperatures. For the lower two boxes the distance scale is in units of the Wigner-Seitz radius.

finite systems for long periods of time, to establish an equilibrium state for a given temperature. The total potential energy of the system was extracted, as were the near-neighbor correlation functions, and the diffusion rates. In Fig. I-66 the properties of 10,000 ions are displayed at several temperatures, from liquid to very cold.

The total energy of the system of 10,000 ions as a function of temperature, and the corresponding specific heat for an infinite system published previously² is displayed in Fig. I-67. It is clear that both systems display similar behavior, but the transition is less sharp

in the finite system and the temperature at which the transition takes place is slightly lower. The transition temperature coincides with the point where the rate of change in the correlation function and that in the diffusion rate are the steepest, as expected. The diffusion rates within a shell are higher than between shells, and the ratio seems to be largest near the melting point. The shift in the melting temperature seems to depend on the size of the system, as is displayed in Fig. I-68. The decrease in melting temperature seems to depend linearly on the fraction of ions that are in the surface layer. Qualitatively similar behavior was observed for the melting of finite atomic clusters,

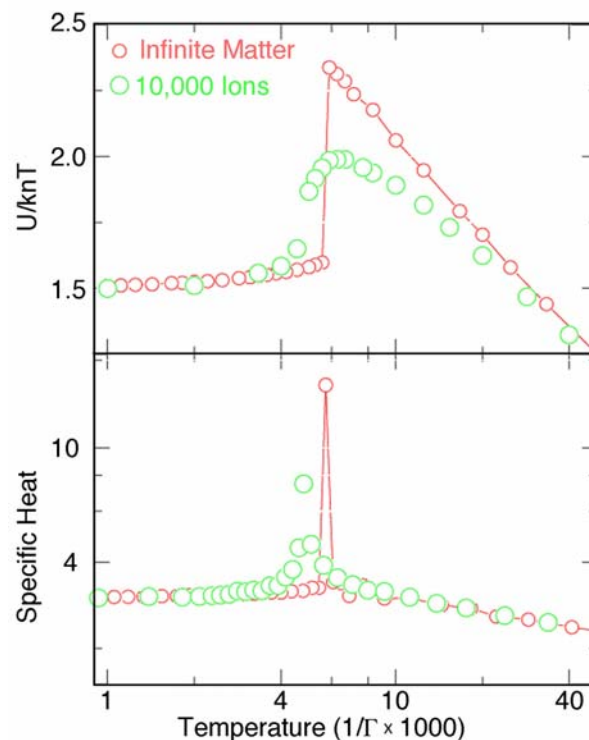


Fig. I-67. The total energy of a system of charges is shown on top for an infinite system of ions from Ref. 2 as open circles and for a 10,000 ion system as solid dots. The lower plot is the corresponding specific heat. Note that at low temperatures both approach the value of 3.0. The temperature scale is in units of $1/\Gamma$.

¹A. Rahman and J. P. Schiffer, Phys. Rev. Lett. **60**, 511 (1988).

²R. T. Farouki and S. Hamaguchi, Phys. Rev. E **47**, 4330 (1993).

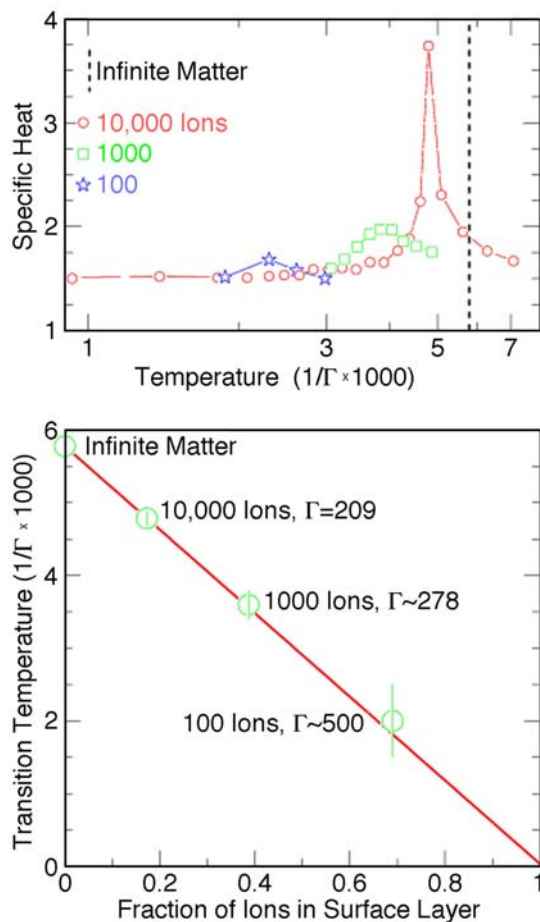


Fig. I-68. Specific heat plots of the type that was shown in Fig. I-67 for 10,000, 1000, and 100 ions. The lower plot shows the temperature at which the specific heat has its maximum value, as a function of the fraction of ions that are in the outermost shell.

f.7. The Transition from Infinite to Finite Systems in Crystallized Coulombic Systems (J. P. Schiffer)

Cold systems of charges in an infinite array show body-centered cubic (bcc) order in their lowest-energy configuration. However, finite arrays of charges confined in a harmonic potential, such as is provided by ion traps, show a different form of ordering with equally spaced concentric shells, with the surface density constant in each shell and the form of order within each shell forming equilateral triangles, as far as this is possible.¹ In very large clouds, with over 100,000 ions, bcc order was observed experimentally, but until recently simulations did not show this type of order.²

Recently Totsuji *et al.*³ reported simulations in which this transition regime was observed. They started with an array of bcc ions of the anticipated density and of the

shape (spherical) consistent with the confining potential, and then allowed this system to relax in Molecular Dynamics simulations. The present effort is to investigate this transition regime further, in order to better understand this transition regime. Simulations starting with bcc order were carried out for different numbers of ions and these were allowed to propagate forward in time until a minimum in potential energy was obtained. For a large number of ions (100,000) this process takes a long time, and the simulation is still running and improving (reaching lower total energy) after 3 months. In Fig. I-69 the state of the system is shown using angles between nearest neighbors to determine whether an ion was in a bcc or other

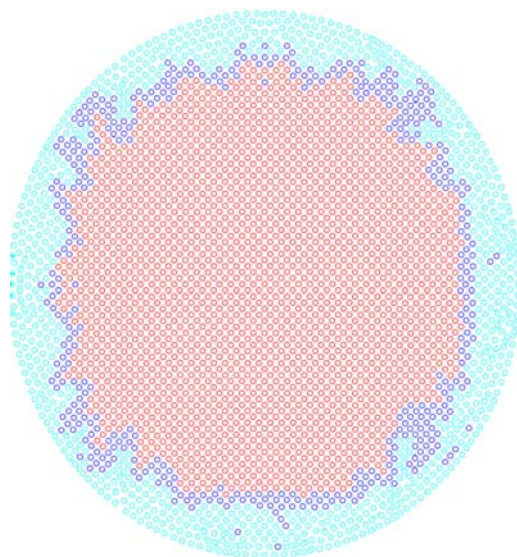


Fig. I-69. The configuration of about 100,000 (99,809) ions that were started from bcc order, progressing toward lower total energy in a molecular dynamics simulation. A central slice of ions is displayed, with all ions shown in light blue, the ions with all 24 angles to nearest neighbors having the bcc value to ± 1 degree of the bcc value shown in red, and those with 12 of the angles being correct shown in dark blue.

environment. In a bcc lattice one ion (taken as a center of its cube) is surrounded by 8 nearest neighbors forming the corners of the cube. Lines to adjacent corners from the center should form an angle of 70.529 degrees. There are 12 possible angles corresponding to the 12 edges of the cube. The next 6 nearest neighbors are the ions at the centers of adjacent cubes. Lines drawn to these form 90 degree angles. The 14 nearest

neighbors of each ion were identified, and then all possible angles were computed within the 8 nearest, and the 6 next-nearest ions. The figure displays the location of ions, with different colors designating those with all 24 angles within 1 degree of the bcc criterion, those with 12 ions satisfying it, and all ions. This simulation is still progressing to lower energies as the bcc order is gradually replaced in the outer regions.

¹A. Rahman and J. P. Schiffer, Phys. Rev. Lett. **57**, 1133 (1986); D. H. E. Dubin and T. M. O'Neil, Phys. Rev. Lett. **60**, 511 (1988).

²X. P. Huang *et al.*, Phys. Rev. Lett. **80**, 73 (1998).

³H. Totsuji *et al.*, Phys. Rev. Lett. **88**, 125002 (2002).

f.8. Precision Measurement of the ^{62}Ga Half-Life (G. Savard, D. J. Henderson, B. Blank,* A. Blazhev,† G. Cachel,* M. Chartier,‡ J. Doering,† Z. Janas,§ R. Kirchner,† I. Muhka,† E. Roeckl,† and K. Schmidt†)

As part of the program to extend the set of high-precision superallowed Fermi emitters to heavier systems, we remeasured the half-life of ^{62}Ga . An accuracy of about 0.05% is required for this particular application, about an order of magnitude better than previous results. This measurement will then complete the set of measurements required (branching ratio, half-life and Q-value) and presently underway to determine the ft-value and together with calculated corrections provide the heaviest point for which a full high-precision data set is available to improve the CVC and CKM unitarity test.

To obtain the required accuracy it was necessary to develop a dedicated detector and electronics system. A 4π gas counter was built for this application (Fig. I-70). The counter is made of 2 independent halves that close around a tape transport system bringing in the short-lived activity. The counter has thin aluminised mylar windows separating the chambers from the tape system. The counter is operated with P10 gas at just above atmospheric pressure. Both halves were characterized independently with sources and found to have similar plateaux. They were therefore biased together and the signals extracted together to behave as a single 4π

counter. The signals from the counter were sent through a preamplifier and a timing filter amplifier followed by a discriminator firing 2 independent gate generators which provide long fixed deadtime for each event. The overall efficiency of the counter and electronics for high-energy betas was in excess of 90%.

This system needed to be installed at a location where a high-intensity high-purity ^{62}Ga beam at low-energy is available. Within the framework of GSI Experiment U183 it was shown that a monoisotopic beam of ^{62}Ga can be delivered by the GSI on-line mass separator with

an intensity of 1200 atoms/s. A proposal was therefore put forth to the GSI PAC for beamtime to perform this measurement (and a branching ratio measurement). The proposal was accepted and the half-life measurement was run in December 2001. The activity was produced by a ^{40}Ca beam at about 4.8 MeV/u degraded by a 2.7 mg/cm² Nb degrader before impinging on a thick $^{\text{nat}}\text{Si}$ target. The recoils are stopped in the catcher of a high-temperature FEBIAD source and extracted as a singly charged ion beam. The beam is mass separated and then implanted on a tape transport system.

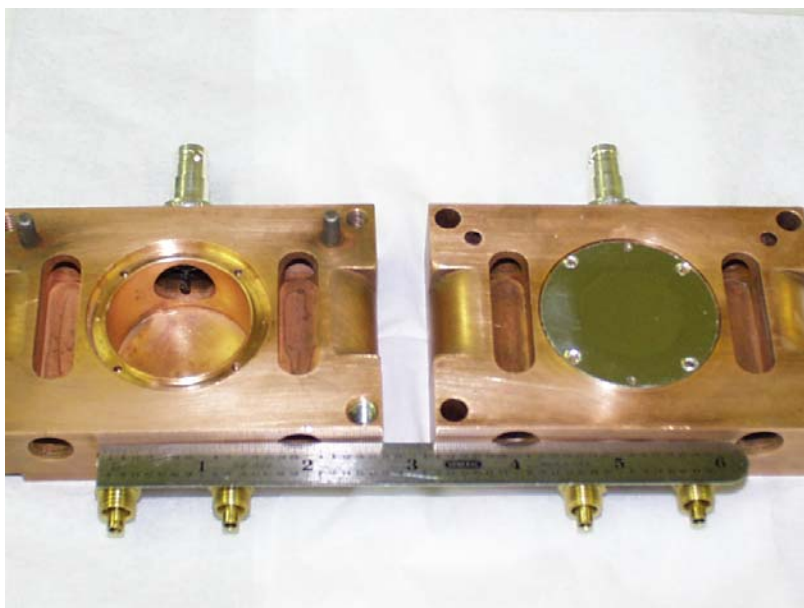


Fig. I-70. Picture of the 4π beta counter used for the experiment. The two halves shown here (one with window, the other with the window removed) surround the tape transport system carrying the activity.

The activity was accumulated on the tape for about 350 ms before being moved 20 cm (about 150 ms) to the center of the beta-counter where a long (10 to 14 half-lives) counting cycle begins where each beta event is multiscaled to create a decay curve per cycle. The mass separator beam is deflected away during the counting cycle. This cycle was repeated about every 2 seconds for about 4 days with brief interruptions for tape rewinding and accelerator tuning. In this fashion, a total of about 20 millions beta events were obtained in well over 10^5 independent decay curves. The average

collection held between 100 and 300 ^{62}Ga atoms by the time the counting started. A germanium detector was used to monitor contaminant activity and none were present at a level sufficient to affect the measurement.

The data sample accumulated is of extremely high-quality, taken under conditions selected to minimize systematic effects and with all important parameters well controlled. It is currently being analyzed and we expect a final error bar at the 0.03% level, well within the required 0.05%.

*University of Bordeaux, France, †GSI, Darmstadt, Germany, ‡University of Liverpool, United Kingdom, §Warsaw University, Poland

f.9 A Bragg Scattering Method to Search for the Neutron Electric Dipole Moment

(M. Peshkin, G. R. Ringo, T. W. Dombeck,* H. Kaiser,† D. Koetke,‡ and S. A. Werner¶)

Polarized neutrons will undergo several thousand Bragg reflections in a slot cut in a perfect silicon crystal and the rotation of their polarization by the interaction of the neutron electric dipole moment (EDM) with crystalline fields in the silicon will be measured.¹ We hope to achieve a sensitivity several times better than the best previous experiment, which finds that the EDM vanishes with an uncertainty limited by systematic errors to around 1×10^{-25} e-cm, and equally importantly to do that in an experiment with very different systematic errors. Progress includes the development of a suitable slotted silicon crystal and the experimental demonstration of reflectivity of 0.99998 for each Bragg reflection.

In a preliminary experiment, we are now attempting to measure the neutron magnetic dipole moment (MDM) in the same way, using the interaction of the moving neutron's effective EDM, equal to v/c times the MDM, with the crystalline electric field. The MDM measurement, which requires only a few hundred Bragg reflections because it looks for a much stronger effect, should test the principles of the EDM experiment in an easier case. We have now produced a suitable slotted silicon crystal for the MDM experiment and tested it successfully at the Missouri University Research Reactor. A solenoid to provide the necessary magnetic guide field is under construction and a proposal for the MDM experiment has been written.

*Fermi National Accelerator Laboratory, †University of Missouri, ‡Valparaiso University, ¶National Institute of Standards and Technology

¹Argonne National Laboratory Physics Division report PHY-9814-TH-2001, March 2001

G. EQUIPMENT DEVELOPMENT

One strength of the heavy-ion group program is continuing excellence in developing new equipment. During the last year, considerable progress was made in many areas. A new data-acquisition system was developed and is now almost ready to be deployed in experiments. The FMA is being upgraded and its focal plane detectors enhanced. The production, separation, capture and transport of ions to the CPT was greatly improved, and our development of large area planar detectors for gamma-ray tracking reached sufficient maturity to start a full program of measurements. Finally, intense planning for the return of Gammasphere to ATLAS is underway, including “two-beam line” operation, and numerous small modifications to the electronics designed to reduce deadtime and enhance the quality of the data collected.

g.1. Data-Acquisition Development (B. Nardi, K. Teh, and A. H. Wuosmaa)

A new data acquisition and analysis system is under development for experiments at ATLAS. The end goal of the project is to introduce both new hardware for data acquisition, and software tools for the analysis and visualization of data. These will become necessary with the phasing out of the existing DAPHNE system and the VMS/Alpha computers on which it runs. Hardware development includes work on a system based upon a commercially available CAMAC-PC interface built by Wiener Systems (the CC32), as well as a system designed and developed primarily within the Physics Division, called PICA (see below). The CC32 system was tested and used in an experimental environment in an experiment conducted at Lawrence Berkeley National Laboratory (see Secs. a.2 and a.3 in this chapter). The data acquisition and control software package (called SCARLET) was produced in the Physics Division, and can be used with either the CC32 or PICA systems.

For data analysis and visualization, there exists an interface between SCARLET and the ROOT system developed at CERN. ROOT possesses the advantages that it is readily available, widely used, well supported and continually upgraded. A ROOT-based analysis package provides easier portability for data, and runs on

a wide variety of platforms, freeing the user from the VMS operating system currently in use.

PICA

The PICA system is currently in the final prototype construction stage. PICA is built around an intelligent CAMAC crate controller module containing an embedded Intel x86 microprocessor running the RealTime Linux (RTLlinux) operating system. Within the CAMAC controller, a CAMAC logic sequencer communicates directly with the x86 processor via the embedded processor’s PCI bus. Data from the PICA controller in each CAMAC crate in an experiment are sent via a private Ethernet link to a separate event builder that consolidates the data for each event, fills them into event buffers, which are then sent via Ethernet to data-consumer processes. Proof-of-principal prototype versions of the CAMAC logic sequencer and PCI communication hardware were built and tested. Based upon the results of these tests the design was refined, and the first full prototypes were designed and are being constructed by the ANL Division of Electronics and Computing Technologies. It is planned to deploy the first production modules in mid-2002.

g.2. New Double-Sided Si Strip Detector (D. Seweryniak, C. N. Davids, A. Heinz, P. J. Woods,* T. Davinson,* H. Mahmud,* P. Munro,* J. Shergur,† A. Woehr,† and W. B. Walters†)

In order to improve the α and proton decay implantation station behind the focal plane of the FMA a new Double-sided Si Strip detector was installed and instrumented. The new detector is more versatile than its predecessors and offers both high granularity and large area. The front and the back face of the new detector is divided into 80 400- μm wide strips. The

picture of the detector mounted on the flange is shown in Figure I-71. The detector was used for the first time in a successful search for the new proton emitter ^{135}Tb . The estimated cross section for populating ^{135}Tb is about 2 nb, and is the weakest proton emitter ever observed. Presently, the new detector is routinely available for experiments.

*University of Edinburgh, United Kingdom, †University of Maryland

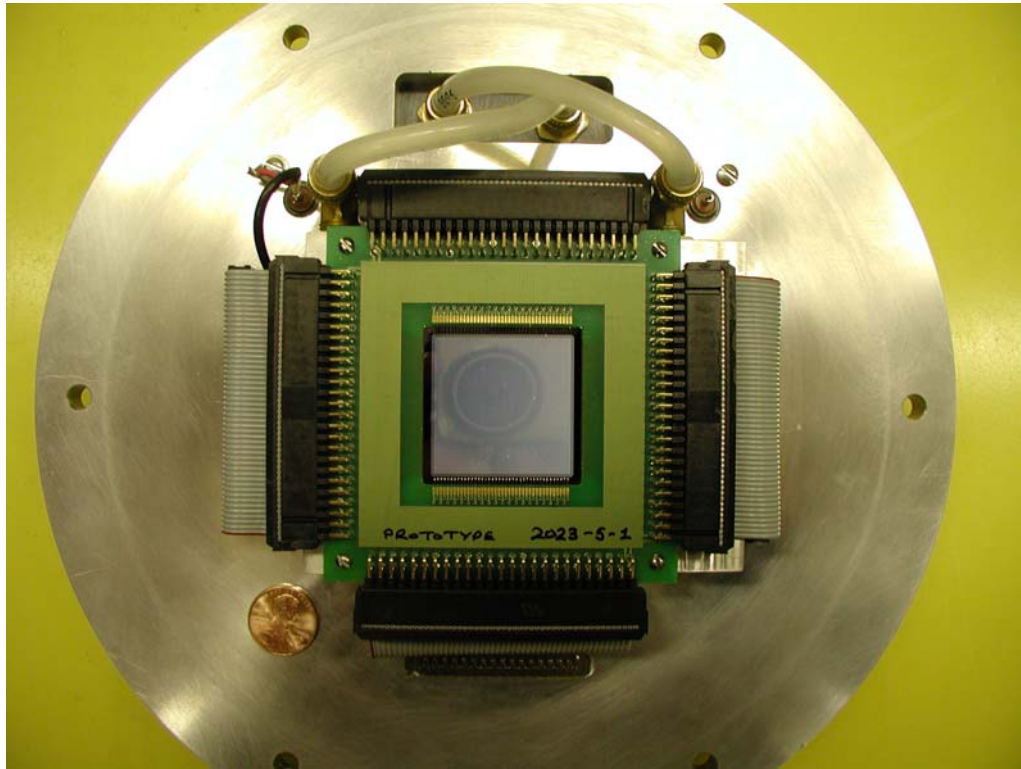


Fig. I-71. New 80×80 DSSD.

g.3. Delay-Line Shaping Amplifiers for a Double-Sided Silicon Strip Detector
(C. N. Davids, P. Wilt, and D. Seweryniak)

The prototype delay-line shaping amplifier mentioned in the previous report was tested in-beam with heavy recoils from a reaction, and found to perform as expected. It should be possible to observe decay protons with energies of only a few hundred keV, and starting ~ 1.5 microsecond after the beginning of the implant

pulse. The printed circuit boards for the amplifiers and the associated motherboards were obtained, and construction of the 160 amplifiers needed began. A test run of the system has been approved by the ATLAS PAC, and this should take place in the coming year.

g.4. Split Anode for the First FMA Electric Dipole (C. N. Davids and J. Falout)

A new anode was designed for the first electric dipole of the FMA. In the current situation, the unreacted primary beam is stopped on this anode. Some particles can scatter out of the anode and make their way to the focal plane, where they induce a background signal. The new anode is split vertically, leaving a 1-cm gap, and the unreacted primary beam particles enter the

anode structure and are stopped near the end on a tantalum plate. This should considerably reduce the flux of scattered beam that is detected at the focal plane.

The new anode was delivered, and has been installed and tested during the Spring of 2002.

g.5. Design of a Recoil Separator for Superheavy Element Chemistry (C. N. Davids)

A recoil separator to be used in studies of superheavy element chemistry was designed. The main goal was to obtain a high efficiency for transporting recoils from the $^{244}\text{Pu}(^{48}\text{Ca},4n)^{288}114$ reaction. Other design goals include small transmission efficiencies for the primary beam and transfer products ($<10^{-3}$), as well as providing as small an image size as possible.

The design evolved out of the ion-optical configuration of the Fragment Mass Analyzer. To achieve high transmission, the M/Q acceptance was broadened by increasing the interior sizes of all ion-optical elements. The resulting fields are all within the range of those achieved with the FMA. In addition, the target was placed closer to the input quadrupole, and the tuning of all elements was adjusted for zero mass dispersion at the focal plane. In order to better match the properties of the resulting beam inside the separator, the focusing of the last two quadrupoles in the horizontal direction was made converging-diverging instead of diverging-converging.

Preliminary transmission calculations for $^{288}114$ have been made, using rectangular distributions for angle, energy, and charge state. Using an angular range of ± 105 mr ($\pm 6^\circ$ both horizontal and vertical), an energy

range of $\pm 5\%$, and a charge state distribution range of $\pm 15\%$ (7 charge states around $Q = 20$), an overall transmission of 30% was obtained. The use of rectangular distributions means that this transmission figure represents a lower limit, since the actual distributions tend to be more peaked around their central values. The image size obtained was 1 (horiz.) \times 4 (vert.) cm^2 .

The presence of an electric dipole at the front of the separator means that transfer products and primary beam particles lie outside the energy/charge acceptance of the separator. Unwanted particles will be dumped in a shielded Faraday cup after passing through the split anode of the electric dipole. An additional feature of the separator is the fact that the ion-optical configuration of the FMA can be recovered by reversing the polarities of the last two quadrupoles. This means that the device can be used to obtain M/Q information if desired, with somewhat lower transmission.

Figure I-72 shows the horizontal (x) and vertical (y) optics for 38-MeV beams of $^{288}114$ having input angles between ± 80 mr (horiz.) and ± 50 mr (vert.), and charge states 19 -21 (charge state 20 not shown).

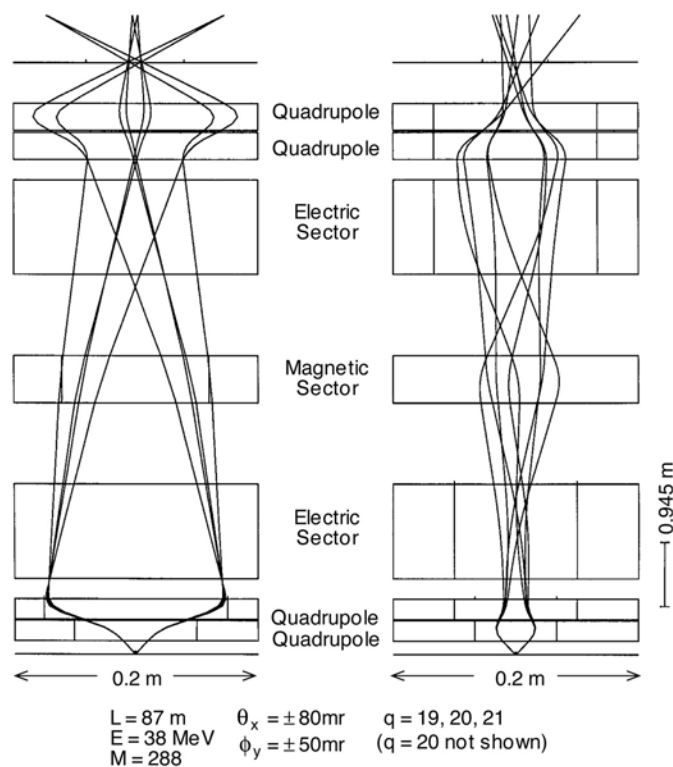


Fig. I-72. Vertical and horizontal optics for a recoil separator designed for use with superheavy elements chemistry.

g.6. Test of Upgraded MWPC for High Count Rate Applications (T. Pennington, D. J. Henderson, C. N. Davids, D. Seweryniak, J. P. Greene, C. J. Lister, A. M. Heinz, G. Mukherjee, A. Woehr,* and B. J. Truett†)

With ten years of exceptional service from the Fragment Mass Analyzer (FMA) using the Multi-Wire Proportional Counter (MWPC) as a focal plane detector, many experiments were completed successfully. The present design of the MWPC is limited in count rate to 5 kHz, for lengthy (five days or longer) experiments. This count rate restriction is a direct result of the cracking of the isobutane in the MWPC by both scattered beam and by the heavy ion recoils. The recombination of dissociated organic molecules results in the formation of solid or liquid polymers, which accumulate on the cathode and anode of the detector. Ions reaching the cathode and anode must then slowly diffuse through this polymer layer to be neutralized. This reduction in the diffusion rate of the ions in the detector causes a decrease in the efficiency, gain and resolution of the detector. This process occurs until a continuous discharge takes place in the detector, which continues even after the scattered beam and heavy ion recoils are removed. Only a complete cleaning of the wire planes can restore the detector. The MWPC can be cleaned with the use of ethanol and the physical rubbing of the wires with a cotton swab. This style of cleaning only works for a limited number of times. If the wires are too "dirty" the entire wire plane has to be replaced.

UPGRADE OF THE MWPC

We substituted the cathode and anode wire planes with three metallized mylar foils (two cathodes and one anode). The new anode and cathodes were constructed as follows; a 70 $\mu\text{g}/\text{cm}^2$ mylar foil was stretched and attached to an OFHC copper frame. Then a layer of gold 17 $\mu\text{g}/\text{cm}^2$ thick was evaporated onto both sides of the mylar foil. Figure I-73 is a cutaway view of the MWPC with the new anode and cathodes. The brown frames are the location of the anode and cathodes. The internal electrical connections are not shown in the figure for clarity. The gas pressure used in the upgrade was the same as the gas pressure used in the original arrangement 3 Torr of isobutane. The operating voltage used in the upgrade was -250 V for the cathodes and +250 V for the anode. This is different from the bias scheme used in the original MWPC, which was -200 V for the cathode and +350 for the anode. The spacing of the planes in the upgrade is the same as the original, 0.125 inches. Energy loss and multiple scattering

calculations show that this upgrade would not adversely affect the detector due to the extra material that has been introduced, except for very heavy, slow-moving ions. We believe that the shape of the electric field near a planar electrode will eliminate some of the problems produced by the $1/r$ dependence of the electric field near a wire. The upgrade was tested offline using a ^{240}Pu - ^{244}Cm alpha source at the rear of the FMA. The detector was then tested with heavy ion recoils under experimental conditions. In most there are usually one or two mass strong peaks in the MWPC. This means that there are one or two localized regions in the detector that receive most of the heavy ion flux. This localized flux also contributes to a lower maximum count rate for the detector, since the recombination of the dissociated organic molecules and the formation of the solid and liquid polymers occur at an increased rate in these localized regions.

HEAVY ION RECOIL TESTS

We tested the upgraded MWPC at high count rates (above 20 kHz) with heavy ions. The reaction that was used for the first test was a ^{92}Mo beam on a ^{58}Ni target. The use of this beam target combination produced the needed high count rate of both scattered beam and heavy ion recoils. Once the response to scattered beam was observed, the scattered beam component was removed by the use of slits at the FMA focal plane. Due to beam current limitations, the average limit rate during a two-day run did not exceed 13 kHz. In a second test, a ^{58}Ni beam was used to bombard a ^{56}Fe target. This average count rate achieved during this one-day run was 20 kHz, again using slits at its focal plane to remove the scattered beam component. No degradation of the MWPC was observed during these tests. At present the maximum count rate for the upgrade is unknown. Work continues on the analysis of the data from the two tests.

Work is continuing to improve the MWPC by reducing the added material from the metallized foil planes. One improvement will be to use aluminum instead of gold for the metallization and have metal on only one side of the cathodes. An other possible improvement is the used of thin freestanding aluminum foils instead of the metallized mylar.

*University of Maryland, †University of Purdue-Calumet

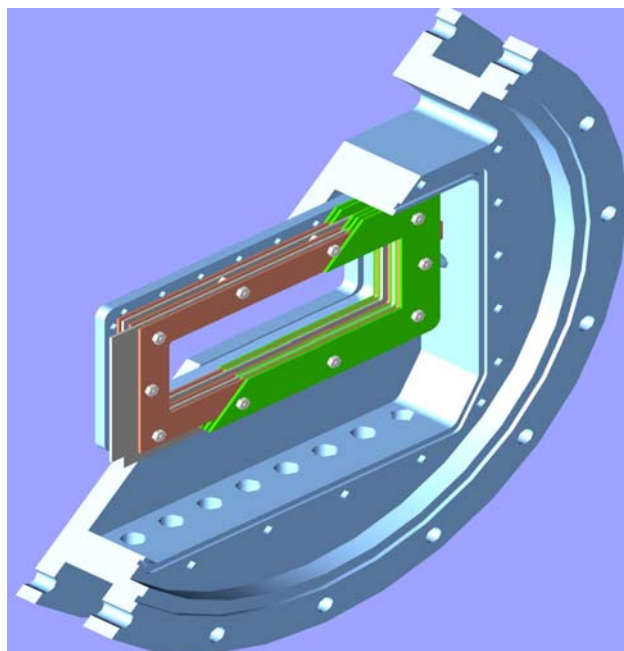
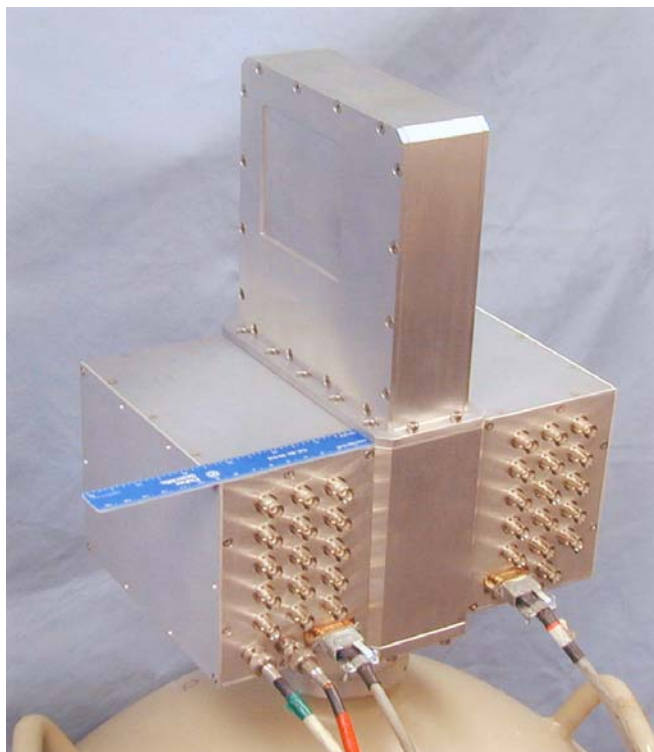


Fig. I-73. Cutaway view of the MWPC with the new anode and cathodes.

g.7. Development of Large Area Planar Germanium Detectors (HpGeDSSDs) for Future Tracking Arrays (C. J. Lister, M. P. Carpenter, R. V. F. Janssens, T. L. Khoo, G. Mukherjee, Š. M. Fischer, E. F. Moore, T. Lauritsen, D. Seweryniak, J. Ammann,* B. J. Truett,† P. Chowdhury,‡ P. Sangsingkeow,§ T. A. Underwood,§ R. Kroeger,¶ and B. Philips¶)



“Next Generation” gamma-ray detectors will combine excellent energy and time response normally associated with germanium counters with very high efficiency and the ability to “track” incident radiation and determine the “hit position” and direction of incoming photons. Considerable progress was made in developing and exploiting position sensitive planar germanium detectors. The “Mark 3” detector was delivered in February 2002, and shows considerably improved performance, compared to earlier prototypes. The germanium wafer is 90 mm × 90 mm × 20 mm, still the largest operating planar in the world. The big improvements appear to arise from the use of a “guardring” around the perimeter of the counter. All of the orthogonal 16 × 16 (85 mm × 5.3 mm strips) are functional, with a mean resolution of 2.8 keV for 122 keV photons. The detector package was tidied up, reducing noise. Figure I-74 shows the latest detector. The uniformity of efficiency is also improved.

Fig. I-74. The “Mark 3” planar germanium HpGeDSSD detector, now ready for physics applications.

We implemented a “fine positioning” system which enables a source to be moved by computer control and is reproducible at the few micron level. In addition, we built a slit collimator, which allows restricted regions of each strip of the detector to be illuminated. Collimation as tight as 25 microns was achieved. To exploit this, and make measurements of position sensitivity, “line” calibration sources of ^{57}Co and ^{137}Cs were fabricated.

Investigation of the pulse shapes started. Capturing digital pulses using a 1 GHz oscilloscope clearly reveals strong image charge pulses developing on strips adjacent to the ones which collect real charge created by the incoming photons. These signals clearly show that full position characterization of the first interaction (x, y, z, E, t) is possible in many cases. The lateral strip-to-strip interpolation appears straightforward, with a resolution which is a function of incident energy and depth, but can be as good as 0.5 mm and seldom is worse than 2.5 mm. Depth profiling seems straightforward at the <1 mm level.

*DePaul University, †Purdue University Calumet, ‡University of Massachusetts-Lowell, §Ortec, ¶Navel Research Laboratory

g.8. Design of the X-Array, an Efficient Gamma-Ray Detector for the Focal Plane of the FMA (C. J. Lister, E. F. Moore, R. V. F. Janssens, M. P. Carpenter, D. Seweryniak, and T. L. Khoo)

A very productive line of research in the last few years is the exploitation of charged particle groundstate radioactivities to infer spectroscopic information. At ATLAS these decays are usually studied after mass separation using the Fragment Mass Analyzer. The decays, proton emission in very neutron deficient nuclei, and alpha decay in heavy nuclei, can provide a wealth of data on relative binding energies, shapes and single particle states. Of particular interest, especially in heavy nuclei, are particle decays which proceed to excited states (so called “fine structure”). The states thus populated then usually decay by gamma emission. The correlations between particles and subsequent gammas can often provide extremely clean and unique information on the location of the single particle states, can strongly restrict spins and parities, and can remove ambiguities over level positions which can arise from particle (or gamma) spectroscopy alone. One recent example is rigorously establishing the location of the

The Mark 2 detector is to return to Ortec for an upgrade, developed in the light of progress with the present detector. A guardring will be implanted. It will be fitted with cold-FET preamps, which will further improve the resolution significantly. The two detectors will then be used for construction of a Compton Camera, in collaboration with the ANL Technology Division.

Test experiments are continuing. We are pursuing the precision and linearity of digital pulse processing. A full compliment of analog electronics is being installed, and parallel digital readout of interesting events is being planned. Full 2D uniformity can be then investigated, including the absolute efficiency of the wafer. An “in-beam” experiment is scheduled for May, in which precise Doppler reconstruction will be demonstrated. The detectors are being used for an SBIR project, with Bio-Imaging Company, a local business interested in imaging objects with x-rays and gamma rays. First publication of our results is being prepared.

first excited state in ^{103}Sn following the α -decay of ^{107}Te (see Sec. b.1.4 in this chapter).

In addition to charged-particle radioactivities, beta-decay continues to provide important information on nuclear structure across the nuclear landscape. The decay selection rules tend to favor low spin and often non-yrast states, so act as a natural compliment to “in-beam” spectroscopy. Technically, the continuous beta spectrum and the relatively long halflives make ultra-selective, low cross-section, beta decay experiments difficult, so many of the most interesting β -decays from near the proton dripline have yet to be studied. However, β -decay is frequently followed by γ -deexcitation, so efficient detection of gamma-rays, and correlation of their spatial position of emitter and γ -decay, can provide a means of achieving enhanced sensitivity.

The current generation of decay experiments can be made much more efficient by improving the γ -detection part of the experiments, which, using small single germanium detectors are, at present, only a few percent efficient. This increase in efficiency directly maps into a commensurate improvement in sensitivity. We

performed MCNP Monte Carlo calculations to examine how to build an efficient experiment for these decay studies. It would appear that an array can be built which has an efficiency about twice that of Gammasphere (~20%) for 1.332 MeV γ -rays and ~50% for low energy radiation.

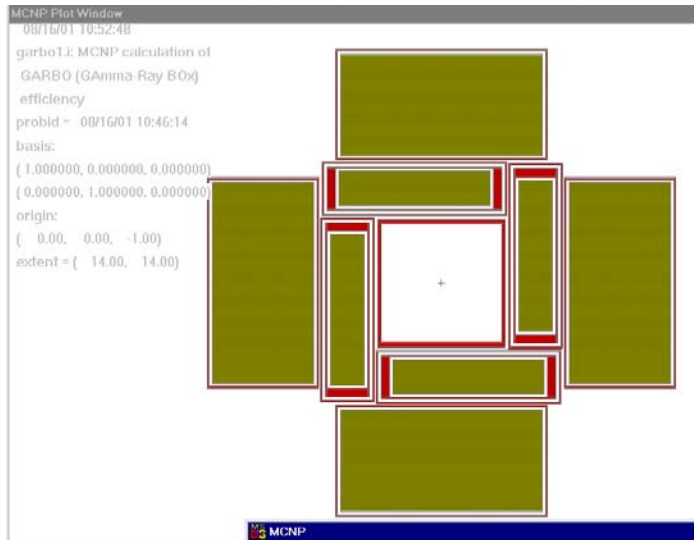


Fig. I-75. A possible schematic layout of the X-Array, a spectrometer for studying radioactive decays, viewed from the FMA. It consists of a five-sided box of gamma detectors.

The array is designed to surround our existing silicon detector system which is deployed inside the focal plane vacuum system and detects implanted ions, and their subsequent α - β -electron- or proton decays. It consists of a five-sided cubic box: the sixth side is open to admit recoil ions from the FMA. The gamma spectrometer is in two layers: a planar layer optimized for detecting low energy radiation, at high countrates, with excellent timing, good energy resolution, and excellent spatial information. The detectors are ultra-large germanium planar wafers. This array is backed by a second layer of large conventional “clover” detectors to enhance efficiency for higher energy radiation. The array appears to have many attractive features. In particular, for some events it will allow “gamma tracking” to ensure the detected radiation

originates from the implant site. The array will also be very efficient for x-rays, from which the atomic number (Z) of the decaying parent can be inferred. Z -tagging, when combined with the mass separation of the FMA, can provide unique isotopic identification. In addition, the high efficiency will be ideal for γ - γ and α - γ angular correlations which help constrain spin and parity both of the parent and daughter states.

The design of the array is being finalized and the specification of the detectors refined. The first two “clover” detectors will be used with our existing planars to conduct first experiments with a “two-wall” box in FY2003, and we project the entire array can be complete by 2005.

g.9. Participation in the GRETA Project (C. J. Lister, M. P. Carpenter, T. L. Khoo, and R. V. F. Janssens)

Considerable effort is being dedicated to planning a “next generation” gamma ray spectrometer to replace Gammasphere in the future. Ideally, the detector would consist of a contiguous $4\text{-}\pi$ shell of germanium, and would allow “tracking” of all interactions, that is the ability to infer the sites of all the interactions as the radiation is absorbed. This information should allow full event reconstruction, thus improving the “peak-to-total” ratio (through identifying “background” events

where radiation leaked from the detector), allowing excellent Doppler reconstruction even for the swiftest moving ions (through inferring the exact angle of the first interaction), and allowing polarization measurements (through measuring the asymmetry of scattering).

Much of the pioneering R&D into this concept, known as GRETA, was done at Lawrence Berkeley National

Laboratory. However, as the project gains momentum and the financial and manpower scope of the project becomes clearer, involvement of other national laboratories and universities is increasing. At ANL several directions are being pursued.

1) The development of “tracking” in planar detectors at ANL offers a complimentary challenge with a huge overlap in necessary R&D. All the downstream digitization, event building, reconstruction, storage and analysis are very similar. The technology of “tracking” is new and requires considerable effort, but may have great spin-off into other fields, especially where gamma-ray imaging is needed. These areas include space science, medical physics, environmental clean-up, and national security. In these applied areas, the planar germanium wafer technology will probably

have many applications. Parallel development of tracking in the large segmented detectors needed for GRETA, and in planar germanium wafers, will allow efficient utilization of the developing “tracking” technologies, to the benefit of all applications.

- 2 We are involved in the GRETA steering committee, and in the National Gamma Ray Tracking Co-Coordinating Committee.
- 3 We have been involved in specialized workshops to sharpen the GRETA concept: a digital electronics workshop held at ANL, and a GRETA workshop which was organized at U. Massachusetts, Lowell.

We anticipate these efforts will increase during the next few years as the project moves from a concept to a full design.

g.10. The Science and Operation of Gammasphere at ATLAS: Phase 2 (C. J. Lister, M. P. Carpenter, R. V. F. Janssens, T. L. Khoo, and D. Seweryniak)

The scientific case for moving Gammasphere from Berkeley to Argonne in 1996 was to re-direct the power of the device towards the spectroscopy of nuclei far from stability, especially along the proton drip line and in heavy nuclei (the original proposal can be found at <http://www.phy.anl.gov/gammasphere/science/index.html>). It allowed us to investigate a key issue in contemporary nuclear physics: the extent to which we can extrapolate the well known physics of near-stability out to the limits of nuclear binding. This campaign, which lasted from January 1998 until March 2000, 27 months, was successful in all respects. The device achieved unprecedented performance and reliability. The project broadened the base of gamma-ray spectroscopy in our community, especially exploring nuclei far from stability, a new direction that is a natural match to the physics goals of the NSAC Long Range Plan, the RIA project and to the program of the NSCL at MSU. In addition, the ATLAS accelerator reliably provided a very wide range of beams, with excellent emittance, energy reach and timing characteristics, which allowed the Gammasphere project to diversify in many other directions.

In February 2002 we proposed to return Gammasphere to ATLAS for a second campaign, with the move being initiated in October 2002 so that operations at ANL can start early in 2003. Two years of operation are anticipated, based on past experience showing this period of time to be optimal for maximal science output and efficient operation of the device. This proposal is

aimed at building the momentum of the overall national program to understand the physics of nuclei far from stability. The first campaign was an exploratory sortie into new territory. 100 different experiments were performed, involving over 300 users (of which more than 100 were students) from 71 institutions in 17 countries. The data are undergoing intensive analysis, and to date the research already produced more than 15 Physical Review Letters and 50 papers (a full bibliography can be found at <http://www.phy.anl.gov/gammasphere/pub/index.html>)

During the campaign, experiments of increasing complexity and sensitivity were achieved, until in some of the later studies technical obstacles were identified which hampered further progress. In the last two years we worked hard on improvements to ATLAS and our equipment to overcome many of these barriers and allow the projects to make major advances once more. In addition, we developed a cost-effective plan to allow Gammasphere to operate on two adjacent beam lines and to run either free-standing or coupled to the Argonne Fragment Mass Analyzer (FMA), a plan which will further enhance our flexibility. In the following pages we will review the progress in the first cycle of operation at ANL and discuss the exciting opportunities that lie ahead.

By now it is clear that re-siting Gammasphere on a two-year cycle has many advantages, for new physics ideas, for efficient manpower commitment, for analysis and

publication, and for equipment regeneration and upgrades. The present LBNL cycle will end in the summer of 2002. We feel it fits into the natural cycle of RIA buildup; as the RIA project grows it will

demand more and more effort from the ANL heavy-ion group, so a further move away from ANL after 2004 may then be optimal.

g.11. Support for Gammasphere Operations at LBNL (M. P. Carpenter, J. P. Greene, R. V. F. Janssens, T. Lauritsen, C. J. Lister, and P. Wilt)

The Gammasphere array is currently located at the 88-inch cyclotron facility of the Lawrence Berkeley National Laboratory. As part of the Physics Division's commitment to the successful operation of the device, several activities continue at Argonne on an "as needed" basis. These include: repairs of Germanium detectors, development and modifications of data-acquisition and analysis software, repair and modifications to electronics modules, fabrication of targets, and preparation of special calibration sources. It is worth noting that, during the past year, three

germanium detectors were shipped to Argonne for repair. In all cases, problems with electronics components located inside the cryostats were diagnosed. Thus, the repairs involved breaking the cryostat's vacuum and replacing components (mostly FET's). Following such operations, "pump and bake" annealing cycles took place. The three detectors were subsequently found to function satisfactorily with resolutions equal or even better than those reported at the time of original delivery from the manufacturer.

g.12. High-Intensity Beam Tests at ATLAS (A. Heinz, R. V. F. Janssens, D. Seweryniak, K. Abu Saleem, I. Ahmad, B. Back, J. Caggiano, M. P. Carpenter, C. N. Davids, J. P. Greene, D. J. Henderson, C.-L. Jiang, T. L. Khoo, F. G. Kondev, T. Lauritsen, C. J. Lister, E. F. Moore, R. C. Pardo, T. Pennington, G. Savard, J. P. Schiffer, R. H. Scott, R. C. Vondrasek, A. Woehr,* and J. Shergur*)

In preparation for a program to study heavy-elements at ATLAS, experiments with high-intensity ^{86}Kr beam impinging on $^{\text{nat}}\text{Pb}$ targets were performed. The goal of those experiments was to improve techniques to monitor targets exposed to high beam currents and to enhance the survival of low melting-point targets under such conditions. This program also allowed testing the accelerator reliability at high beam intensities. A test setup using the standard FMA scattering chamber and a target wheel with a radius of 8.8 cm was used in the general purpose area. The targets were made of $^{\text{nat}}\text{Pa}$ with a thickness of about $500 \mu\text{g}/\text{cm}^2$ with an upstream backing of $40\text{-}\mu\text{g}/\text{cm}^2$ carbon. To reduce sputtering, a $5\text{-}\mu\text{g}/\text{cm}^2$ layer of carbon covered the downstream side of the target. The wheel was operated at about 1000 RPM. In addition to the target rotation, the beam was

defocused. The maximum beam intensity on target was 190 pA according to a reading on the last Faraday cup in the beamline. The targets were able to stand this intensity without any problems after careful conditioning with lower beam intensities.

To monitor the targets, a silicon monitor detector was used. In addition the transmission through the target was monitored using a IR sensor and a light source. A second silicon detector and an alpha-source were employed to determine continuously the energy-loss inside the target.

The experience gained in this experiment will be used to improve future experiments at high beam intensities.

*University of Maryland

g.13. A New Dedicated Chamber for Super-Heavy Element Research (A. Heinz, R. V. F. Janssens, J. Falout, J. P. Greene, C. J. Lister, D. Seweryniak, B. Back, T. Pennington, D. Henderson, B. Nardi, and G. Savard)

The production cross sections for the heaviest known nuclei are in the order of pb^1 and are thus among the lowest cross sections measured in nuclear physics. In order to cope with such low cross sections, it is necessary to optimize the event rates as much as possible. One important factor is the beam intensity. But while the increase of the beam intensity requires optimizing the ion-source output and the transmission of the accelerator, the experimental setup has to be able to cope with large beam currents. Especially for targets with a low melting point this becomes a non-trivial problem. A dedicated target chamber for this kind of experiment has been designed and is nearing completion.

In this chamber three different mechanisms are used in order to prevent the target from melting: rotation, wobbling and gas-cooling. Mounting several targets on a wheel allows to spread the heat deposited by the beam over a larger area and allows the target material to cool until the beam hits the same target spot again.² It is possible to use the available target area further by implementing a periodic deflection of the beam in the vertical direction by using a steering magnet. This is referred to as wobbling. In vacuum, targets will cool by emission of radiation and by heat conduction of the target material. If the target is surrounded by a gas-filled volume the cooling will be enhanced.

In the new target chamber, a wheel with an active radius of 15.5 cm was installed. It is possible to spin

this target wheel with a design speed of 1000 rpm, even though higher rotational speeds are possible. The chamber itself is 30.5-cm long and has a diameter of 36.8 cm. At the entrance and the exit of that chamber rotating windows made of carbon will be installed. These windows will allow containing a gas (such as N_2 , for example) at pressures of 1-3 torr. The provision for rotation is intended to reduce the possibility of breaking the windows under high beam intensities.

Even with those techniques the lifetime of a target wheel might be shorter than the duration of an experiment. Thus, it becomes necessary to monitor the condition of the target continuously. The chamber provides several methods to achieve this. First, two types of monitor detectors can be used; a standard silicon monitor detector, which is mounted on a rotating arm, and an ionization chamber at a fixed angle of 44° . The latter detector might prove to be superior to the silicon detector due to the fact that it does not suffer from radiation damage. The target wheel supports frames for 16 targets. An infrared sensor/source will sweep the beam at the spoke positions. A second infrared sensor/source combination measures the target transmission. Also, a strong alpha source and a silicon detector are used to detect any change in energy-loss of the target material. The chamber provides also viewing ports for optical inspection of the target wheel and a faraday cup for beam tuning.

¹S. Hofmann, G. Münzenberg, *Rev. Mod. Phys.* **72**, 733 (2000).

²J. P. Greene, R. Gabor, and J. Neubauer, *Applications of Accelerators in Research and Industry*, CAARI 2000, AIP **576**, 1152 (2001)

g.14. Design of a Large Area Window for the GSI Gas Cell (T. Pennington, G. Savard, B. Zabransky, J. P. Greene, and J. Falout)

A large area Havar window ($\sim 77 \text{ cm}^2$) was designed for the GSI Gas Cell tests being conducted at ATLAS. The window is 2 mg/cm^2 ($\sim 2.4 \mu\text{m}$) thick and is supported by 28 - 250 μm diameter beryllium copper wires. The wires are laid out in a rectangular pattern with a spacing of 0.635 cm on center. The wires will be soldered into grooves cut into a 0.635-cm thick OFHC copper plate. The window will be mounted to this support structure. The completed window will then be mounted to a specially machined double-sided knife-edge flange with

an indium vacuum seal between the flange and the window support structure. The window is designed for a differential pressure of $\sim 103 \text{ kPa}$ (15 psia). At this differential pressure the stress on the Havar is approximately 8% of the tensile strength of Havar and the stress on the support wires is approximately 74% of the yield strength and 58% of the tensile strength of beryllium copper. At present the flange and window support structure is being machined and will be tested in the near future.

g.15. Nuclear Target Development (J. P. Greene and G. E. Thomas)

The Physics Division operates a target development laboratory that produces targets and foils of various thicknesses and substrates, depending on the requirements, for experiments performed at the ATLAS and Dynamitron accelerators. The targets are prepared from both naturally occurring materials and stable isotopes that are supplied either in pure, elemental form or as stable compounds. Although typically, the responsibilities of the target laboratory were constrained to providing targets for experiments at ATLAS, in reality it has become much more far ranging. In addition to ATLAS experiments, targets and foils are provided for all staff members whether working within the Physics Division or undertaking experiments at other facilities, for instance, the Advance Photon Source (APS). Also, wherever possible, support is provided to other ANL Divisions, and in particular to requests from researchers at the University of Chicago. Collaborations have grown out of efforts between the Physics Division and target laboratory staff with outside groups in order to provide targets. Many of these, unfortunately, cannot be accepted due to the limited resources of, and time constraints placed on the target laboratory staff.

In the past year, numerous targets were fabricated either as self-supporting foils, on various substrates or as "sandwich" targets. Targets produced included Al, Al₂O₃, Ag, Au, ¹⁰B, Be, ¹²C, ⁴⁰Ca, CaO, ^{106,116}Cd, CD₂, ⁵²Cr, Cu, ^{54,56}Fe, formvar, Havar, ¹⁸⁰Hf, ⁷LiH, ²⁴Mg, ^{92,94,96,97,98,100}Mo, mylar, ^{142,150}Nd, ^{58,61}Ni, ^{207,208}Pb, PbF₂, ¹¹⁰Pd, phosphor, polypropylene, ⁹⁶Ru, Si, ^{28,30}SiO₂, ^{144,149,154}Sm, Ta, ¹²⁶Te, Th, ^{46,48,50}Ti, Y, ¹⁷²Yb, and ^{90,92,96}Zr. Many of these target foils were fabricated via mechanical rolling using our small rolling mill. During the 2001 calendar year, approximately 700 targets were prepared for various experiments.

The Argonne/MSU/ORNL BaF₂ array concluded a successful research program with a great majority of the experiments requiring a rotating target wheel so as to increase target lifetimes and allow for higher beam currents. The Gammasphere style target wheel found routine use within the LEPPEX array target chamber. The target laboratory fabricated approximately 40 targets (mainly as target wheels) for the LEPPEX research effort during this time period. Gammasphere, although relocated to LBL, still demands many targets prepared by the target laboratory. For the year, 186 targets were prepared for experiments at Gammasphere.

Experiments were undertaken to explore and increase the production of the heaviest elements. Intense beams, by necessity, must be employed, requiring new demands upon target performance. Target wheels of isotopic lead on carbon backings were prepared for these initial experimental runs using the existing large FMA target wheel. The goal of this present work was the production of Rf, element 104 and look at detection limits and beam rejection using the FMA. Beam intensities up to 250 pA were put on target. An online target monitoring system was developed to anticipate target degradation. Calculations were performed in an effort to model the target behavior. The next step is to increase the target wheel diameter in a new chamber set-up at the FMA, which will also allow for gas cooling of the target. A larger wheel of similar design is already in use within a new target chamber at the front end of the CPT experiment using the SPS in Area II. By employing a target wheel station, increased beam currents will be available for the production of low cross-section reaction products for measurement.

Outside of target development, support is being provided for the production of thin plastic films and foils for use in various detector systems developed for experiments at ATLAS as well as energy degraders needed for astrophysics research using radioactive beams at SPS III. Several variations of metallized plastic foils were prepared for use in the gas counter and channel plate detectors used at the FMA.

As part of ATLAS support, the target lab routinely produces carbon stripper foils of 2 μg/cm² for use in the Tandem as well as other thickness for additional stripping throughout the accelerator. Over 800 carbon stripper and gold foils of various types were prepared for ATLAS during this past year. There continues to be an increase in the preparation of various dilutions of isotopic source material into a form and shape suitable for introduction into PIIIECR and SNICS sources for the production of enriched beams at ATLAS. These included ⁵⁴Fe, Li⁶F, Mn, ⁶¹Ni, and ⁵⁰Ti. The continuing procurement of stable and enriched material for ATLAS consumption and maintenance of isotope inventories for enriched beam production is being provided by the target laboratory staff.

The target development laboratory includes state-of-the-art equipment used for thin-film fabrication. The available techniques consist of multiple resistive heating, focused ion beam sputtering, glow-discharge plasma deposition, electron beam and electron

bombardment evaporation, electrodeposition and mechanical rolling. The evaporators are maintained under high vacuum and each vessel contains a quartz-crystal film-thickness monitor with deposition rate indicators. Also included are movable shutters, quartz-lamp substrate heaters and thermocouple temperature sensors, allowing for complete process monitoring during target deposition.

Other auxiliary equipment used for target development includes electrodeposition equipment, a small rolling mill, an alpha particle counting chamber, inert atmosphere glove box, laminar flow clean bench, pellet press, a reduction furnace, and a variety of precision balances. A turbo-pumped target storage facility is in operation for maintaining, under high vacuum, those targets that readily oxidize in air. This system utilizes computer-controlled circuitry to prevent targets from exposure to atmosphere during power interruptions. A second storage system employing a bank of vacuum desiccators and connected to a mechanically pumped manifold is available for use by individual experimenters. Similar systems are in operation at ATLAS just inside the entrance to Target Area II. A new additional set-up, consisting of two large glass desiccators evacuated using a small turbo-pump system, is in operation for long-term material storage. This allows a separation of material storage from target storage, hence eliminating repeated exposure when transferring and retrieving targets.

A low-level radioactive source and target preparation laboratory exists at a separate location within the division that is dedicated to the production of these sources and targets. Available preparation techniques include multiple resistive heating, employing a diffusion-pumped vacuum evaporator. A second, smaller evaporator system was constructed for close proximity evaporations of higher activity materials, to be used as targets as well as radioactive sources. The small size of this system allows for installation within a

hood. Preparation and handling of fission targets (mainly ^{252}Cf) by electrodeposition was done for experimental studies at ATLAS.

Another area of increased research effort is development of radioactive beams for the RIA proposal and involves neutron producing targets which in turn induce fission in uranium or a uranium compound production target. Toward this end, direct measurements of the thermal conductivity of uranium carbide were made using the method of heating by electron bombardment and measuring the surface temperature of thin UC_2 disks by optical pyrometry. The uranium carbide sample disks are first prepared by the reduction of uranium oxide using carbon in a resistively heated source in the Radioactive Target Laboratory. Next, the samples are heated by a 10-kV electron beam provided by a mortar source in a vacuum evaporator in the target lab and the temperature measured as a function of beam current using a two-color pyrometer. This work is still in progress.

Finally, the selection and procurement of a new, general purpose, high-vacuum deposition system is becoming necessary to insure the reliable and continued availability of high-purity targets. The recommended specifications for this system should include an automated, high-vacuum pumping station (cryopump) with a large volume chamber (box-coater) capable of handling large area foils or installation of a substrate planetary system for uniform coating capabilities. The state-of-the-art in coating technology points toward ion beam and plasma assisted deposition. Although not directly applicable to isotopic evaporations, there has always been a need for sputtered films of many kinds from the target laboratory. Any new deposition system procured should include the most advanced coating technology. If possible this equipment should be sought together as an integrated system, for ease of operation. Selection of a suitable system is being investigated and new funding sought.

g.16. Developments at the Canadian Penning Trap Mass Spectrometer and Its Injection System (G. Savard, J. A. Caggiano, J. P. Greene, A. Heinz, D. Seweryniak, J. A. Clark,* R. C. Barber,* C. Boudreau,† F. Buchinger,† J. E. Crawford,† S. Gulick,† J. C. Hardy,‡ J. K. P. Lee,† R. B. Moore,† K. S. Sharma,* G. Sprouse,§ J. Vaz,* and J. C. Wang*)

The Canadian Penning Trap (CPT) mass spectrometer is designed to make precise mass measurements on nuclides with half-lives longer than 50 ms. The radioactive nuclides are produced through fusion evaporation reactions using heavy-ion beams from the Argonne Tandem Linac Accelerator System (ATLAS). Once created, the nuclides of interest are separated from the beam in an Enge magnetic spectrometer operated in the gas-filled mode. They are then stopped in a gas catcher filled with 150 Torr of helium, extracted and subsequently guided to a radio-frequency quadrupole ion trap where they are accumulated before being transferred to a high-precision Penning trap. Activities at the CPT spectrometer have continued to improve the transfer efficiency of ions from the target to the Penning trap, decreasing the number of contaminants and performing mass measurements on short-lived isotopes. The most significant improvements in the last year involved the installation of a large diameter rotating target, a magnetic triplet situated after the target chamber to increase the acceptance of the Enge spectrometer, a velocity filter to

more effectively separate the beam from the reaction products and the replacement of the Paul trap with a linear trap resulting in more efficient capture and accumulation of ions from the ion cooler. These improvements will be described in details below.

The production target has been moved approximately 3 metres upstream to accommodate the insertion of a magnetic triplet and velocity filter in front of the Enge spectrograph. The single rotating target has been replaced by a rotating target wheel (see Fig. I-76) which can hold 16 individual targets at the edge of the wheel's 6" radius. The position of the wheel is continually monitored by a CAMAC module, which can be programmed to issue a signal to deflect the beam at prescribed positions of the wheel. This prevents the beam from hitting the 'spokes' between targets or specific targets themselves. On-line tests of this target wheel have shown that 1 mg/cm² ¹²C targets can easily withstand 100 pA of ⁵⁸Ni for the duration of a run, typically four days.



Fig. I-76. Picture of the large rotating target wheel installed at the Enge spectrograph. The beam hits the targets at 6 inch radius with the target rotating at about 1000 rpm.

Downstream immediately following the new target wheel lies a magnetic triplet to focus the recoil products into the Enge spectrometer. This combination of three magnetic quadrupoles has increased the number of recoil products entering the Enge by about a factor of three. Following the magnetic triplet (see Fig. I-77) is a velocity filter whose purpose is to separate the recoil product of interest from the primary beam. The electric field of the velocity filter is provided by two 70-cm long parallel plate electrodes separated by 5 cm. A potential difference of 100 kV can be applied across the

plates. The perpendicular magnetic field of the velocity filter is provided by a box type magnet with 40 turns of hollow copper tubing. Fields of up to 1500 Gauss can be obtained by applying up to 300 A through the water-cooled coils. The appropriate balance of electric, E , and magnetic, B , field strengths allows ions of a particular velocity, v , to traverse the 70-cm length of the filter unhindered as $v = E/B$. The rejection of ions of other velocities is determined by the dispersion which can be augmented by increasing the strengths of the two fields while maintaining the ratio.

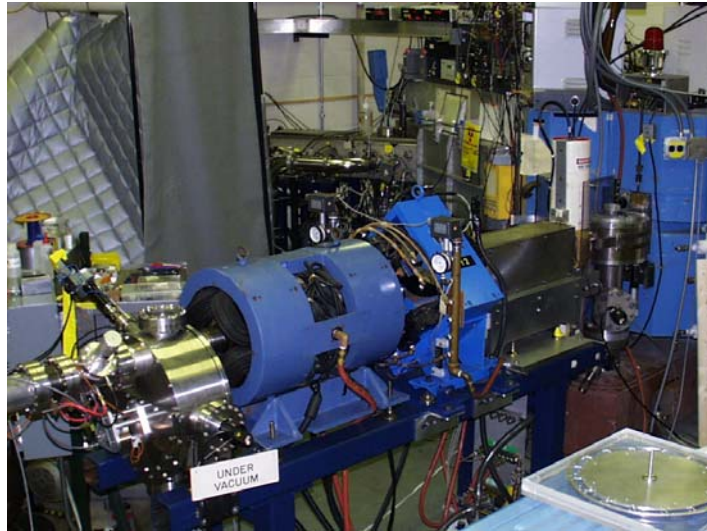


Fig. I-77. View of the new target chamber, magnetic triplet and velocity filter leading to the “old” target chamber and entrance to the Enge spectrograph.

For our purpose, a deflection of the primary beam by 1 cm over the 70-cm length of the filter is sufficient to prevent the beam from entering the Enge spectrometer. Through on-line tests of the velocity filter, we successfully suppressed the primary beam by five orders of magnitude while accepting the reaction products.

On the CPT side, the standard three-electrode structure of the Paul trap (two endcap electrodes with an intermediate ring electrode) was replaced by a linear Paul trap (see Fig. I-78). Essentially, the ring electrode of the Paul trap was replaced by two pairs of segmented parallel rods. The linear Paul trap has a greater phase-space acceptance and is much easier to operate. For

example, the RF applied to the ring electrode of the original Paul trap results in a time-varying force along the longitudinal axis, or the axis in which the ions are injected and subsequently ejected. Ions must then be injected carefully into the Paul trap by synchronizing the injection with the RF applied. However, the RF applied to the rods of the new linear trap creates no such time-varying force along the longitudinal axis, and therefore the RF-phase criterion is not as critical. Recall that the Paul trap is used to collect, accumulate, and cool the ions before transport to the Penning trap. The typical efficiency of this process with the original Paul trap was about 15%, whereas, we routinely get 80% or better with the new linear Paul trap.

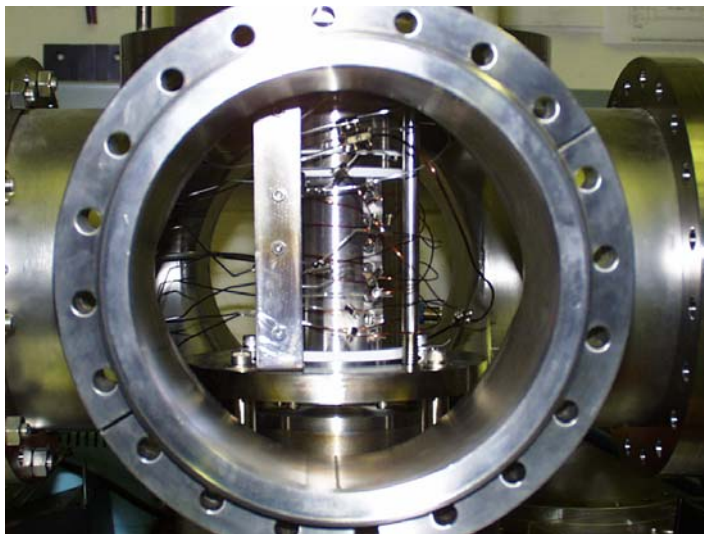


Fig. I-78. New linear Paul trap used for ion accumulation and cooling.

The CPT penning trap itself saw no changes this year except for a retuning of the magnetic field shims in the spring which yielded much improved resonance shape and better cleaning in the precision trap.

The overall efficiency of the injection system of the mass spectrometer improved by a factor of 5 after the gas cooler and a factor of 3 to 5 in the Enge spectrograph as seen on-line with detected yields of

^{68}Ge and ^{68}As . At the same time, the contaminant ions were reduced by a factor of about 3. This not only made new measurements of ^{68}Ge and ^{68}As much easier, but more importantly, more weakly-produced isotopes of importance to the astrophysical rp-process, such as ^{68}Se , are now within our reach. This efficiency improvement also allowed us to study neutron-rich radioactive ions produced by a fission source as reported in Sec. b.2.10. of this chapter.

*University of Manitoba, Winnipeg, Manitoba, †McGill University, Montreal, Quebec, ‡Texas A&M University, §State University of New York

g.17. Progress in the Construction of the Advanced Penning Trap System (G. Savard, A. Heinz, D. Seweryniak, J. A. Clark,* C. Boudreau,† F. Buchinger,† J. E. Crawford,† S. Gulick,† J. K. P. Lee,† R. B. Moore,† K. S. Sharma,* J. Vaz,* and J. C. Wang*)

The technical developments in ion trapping of radioactive isotopes demonstrated at the CPT mass spectrometer open new venues to probe fundamental aspects of the electroweak sector of the standard model of particle physics. This can be done through the observation of angular correlations in the beta-decay of specific radioactive isotopes stored selectively in an open geometry ion trap surrounded by a detector array. This approach could lead to significantly improved limits on the presence of interactions outside the standard V-A form in the charged weak interaction.

Stringent constraints on extension of the Standard Model come from high-precision measurements of angular correlations in the beta-decay of short-lived isotopes. These short-lived isotopes are available with

increasing intensity but the present measurement methods are limited by interaction of the particles emitted in the decay with the source holder. With the recent developments mentioned above, it is now possible for essentially all species of short-lived isotopes to be captured efficiently in ion traps where these radioactive ions are confined, floating at rest in vacuum. This effectively removes the need for a source holder and opens up the possibilities of experiments with much improved accuracy. We therefore started building a new ion trap system, the Advanced Penning Trap (APT) system, suited to angular correlation measurements in nuclear beta-decay.

The APT system will consist of two ion traps, an open geometry linear RFQ trap and a Penning trap sitting in a

large bore 7 Tesla magnet, which are injected by the gas cell/gas cooler system developed for the CPT. The APT will be located besides the CPT in the triangular room adjacent to experimental area II.

The isotopes that will be studied at the APT will, in general, be short-lived superallowed emitters. The extraction of such light ions from the gas cooler and transfer to the APT was simulated in details and minor modifications to the gas cooler implemented to avoid losses. Monte Carlo simulations for the first experiment to be performed at the APT, a prototypical experiment to look for possible scalar interactions, to be conducted with trapped radioactive isotopes of ^{14}O , are completed. The computer simulations determined the optimum ion trap and detector array geometry. This was completed with a simulation for the trap geometry and ion transport based on the SIMION software to which a

number of subroutines were added (and are being upgraded) over the years to take into account the effects of buffer gas collisions for cooling of the ions in the trap. The detector geometry was simulated using GEANT and the response of different beta detectors compared. The response of the full system was then simulated incorporating a proper Fermi distribution for the positrons and the recoil distribution calculated with the theoretical electron-neutrino correlation. The design of the injection system and first trap of the APT was optimized for this first experiment.

The second trap of the APT, a Penning trap, will be used for experiments that required polarization of the radioactive sample. The superconducting magnet (see Fig. I-79) was received in Dec. 2001. It will be installed on a non-magnetic frame to avoid perturbing the magnetic field.



Fig. I-79. Picture of the 5 inch warm bore, 7 Tesla, superconducting solenoid that will be used to host the Penning trap of the APT.

The additional services required in area II to host the APT were identified and are being installed. Most large components (vacuum, electronics, control system) are

either received or ordered. Assembly of the 2 traps is expected to proceed in FY2002.

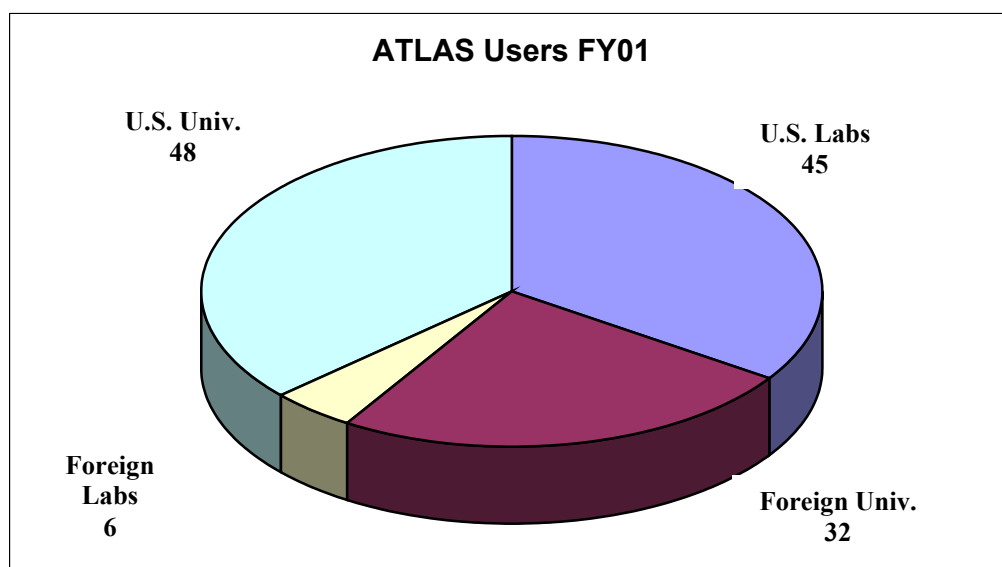
*University of Manitoba, Winnipeg, Manitoba, †McGill University, Montreal, Quebec

H. ATLAS USER PROGRAM

E. F. Moore

Following the departure of Gammasphere in March 2000, the research program at ATLAS resumed its traditional diversified nature. During the fiscal year 2001, ATLAS hosted strong “campaigns” involving radioactive beams, the BaF₂ array, the CPT, the super-heavy element program, as well as the resurgence of the AMS program. Some of these programs were driven by outside Users, and in all programs, there was considerable outside User involvement. Over 95% of all experiments performed in fiscal year 2001 included one or more outside Users and roughly 50% of the approved experiments had an outside User as the Principal Investigator. Frank Moore continued to be available in a user liaison capacity to handle the scheduling of ATLAS experiments, provide assistance in experiment proposal submission matters, and help facilitate the effective performance of research at ATLAS by outside scientists. In addition, a large portion of the Heavy-Ion in-house scientific staff and members of the technical support staff spent time in experiment setup, preparation and assistance for the many different experiments performed at ATLAS.

A total of 131 Users from 47 different institutions were present at ATLAS for experiments in FY 2001. The pie chart below shows the distribution of the institutions represented by ATLAS Users and the number of Users of each type. Of the 45 Users from U.S. National Laboratories, 39 are from Argonne (28 from the Physics Division, 11 from other divisions). There were 32 students at ATLAS for experiments this FY, of which 11 were based at Argonne long-term. The names and institutions of all outside Users who were present at ATLAS in FY 2001 are listed below in section (b).



The program advisory committee met once during the 2001 fiscal year, on March 2, 2001. However, much of the beam time scheduled in FY2001 was approved at the September 22, 2000 PAC meeting. The PAC also met again on October 5, 2001. In FY 2001 the Program Advisory Committee members were:

James Beene
 Jolie Cizewski
 Stuart Freedman
 David Morrissey
 Lee Riedinger (*chair*)
 Robert Tribble
 Alan Wuosmaa

Oak Ridge National Laboratory
 Rutgers University
 University of California
 Michigan State University
 University of Tennessee
 Texas A&M University
 Argonne National Laboratory

The PAC reviewed 25 proposals for 170 days of requested running time at the March meeting. There were also 29 proposals for 179 days of running time that were reviewed at the September, 2000 meeting. Of the submitted proposals for the two meetings, the program advisory committee recommended acceptance of 38 proposals for a total of 179 days of running time. The reduction in days approved from last FY partially reflects the reduction in ATLAS operations from seven to five days average per week that occurred in June, 2001 and continued through the end of the FY.

The fall meeting of the American Physical Society was held in Maui, Hawaii, from 17th to 20th Oct 2001. It was the first ever joint meeting between the American Physical Society and the Japanese Physical Society. The US national nuclear laboratories with low energy heavy ion facilities; ATLAS at Argonne, HHRF at Oak Ridge, and the 88" cyclotron at Lawrence Berkeley National Laboratory, held a joint User Meeting. The purpose was to present the capabilities and performance of current facilities to our Japanese colleagues, and then to have our normal users discussions. Dr. J Cizewski (U. Rutgers) introduced the ATLAS user program, and C. J. Lister presented an overview of the ATLAS facility and some elements of the current physics program. Unfortunately, due to the events of Sept 11th, the meeting was much less well attended than the normal annual gatherings. However, the joint-user-meeting format continues to be generally beneficial as many university groups use more than one of the accelerators, so often issues come up for discussion which need responses from all the national user facilities.

In FY 2001 the ATLAS Executive Committee consisted of Jolie Cizewski (Rutgers University) as Chairperson, Michael Wiescher (University of Notre Dame), Partha Chowdhury (U. Mass Lowell), and Gene Sprouse (SUNY Stony Brook).

a. Experiments Involving Outside Users

All experiments in which outside users directly participated during FY 2001 are listed below. The spokesperson for each experiment is given in square brackets after the title, and the collaborators who were present for the experiment are given with their home institution (as of the end of the FY) below each entry.

1. Proton Radioactivity of Deformed Tb and Pm Isotopes [Davids]
J. Ressler, J. Shergur, W. Walters, University of Maryland; J. Uusitalo, University of Jyväskylä; T. Davinson, A. Mahmud, K. Schmidt, P. Woods, University of Edinburgh; A. Sonzogni, Brookhaven National Laboratory; C. Davids, A. Heinz, D. Seweryniak, Argonne National Lab.
2. Patterning of Columnar Defects: Fabrication of Vortex Ratchet System for Manipulating Trapped Flux in High Temperature Superconductors [Kwok]
L. Paulius, Western Michigan University; R. Olsson, Michigan State University; W. Kwok, A. Mazilu, V. Tobos, Argonne National Lab.
3. K-Shell Excitation of He-Like Ni at Intermediate Energy-II [Dunford]
H. Berry, A. Livingston, University of Notre Dame; P. Mokler, T. Stöhlker, GSI, Darmstadt; R. Dunford, E. Kanter, Argonne National Lab.
4. Coulomb Excitation of Unstable Nuclei [Mueller]
D. Jenkins, University of Liverpool; J. Church, T. Glasmacher, Z. Hu, K. Miller, W. Mueller, H. Olliver, Michigan State University; I. Wiedenhoever, Florida State University; M. Carpenter, R. Janssens, F. Kondev, K. Lister, J. Schwartz, Argonne National Lab.
5. The Quest for a Detection Method of Natural ³⁹Ar [Collon]
W. Kutschera, Universität Wien; Y. El Masri, Universit, Catholique de Louvain; M. Paul, Hebrew University of Jerusalem; P. Collon, R. Scott, Columbia University; I. Ahmad, J. Caggiano, A. Heinz, R. Pardo, K. Rehm, R. Vondrasek, Argonne National Lab.

6. High-Energy Photons from Very Symmetric Reactions: The Giant Dipole Resonance in Highly Rotating Cold Nuclei [Bracco]
A. Bracco, F. Camera, F. Della Vedova, S. Leoni, B. Million, O. Wieland, University of Milano; D. Hofman, University of Illinois- Chicago; V. Nanal, Tata Institute of Fundamental Research; B. Back, M. Carpenter, R. Janssens, Argonne National Lab.
7. Test of a Method to Study Sub-ms Proton and α Emitters [Seweryniak]
W. Reviol, D. Sarantites, Washington University; J. Ressler, J. Shergur, A. Woehr, University of Maryland; M. Carpenter, A. Heinz, R. Janssens, D. Seweryniak, Argonne National Lab.
8. Low-Spin Levels in Light Odd-Mass Sn Nuclides Populated in the Decay of Sb Nuclides [Ressler]
J. Ressler, J. Shergur, W. Walters, University of Maryland; T. Sienko, Purdue University, Calumet; K. Abu Saleem, Illinois Institute of Technology; D. Brenner, Clark University; C. Davids, A. Heinz, D. Seweryniak, Argonne National Lab.
9. Highly Selective Studies of the GDR in Hot Nuclei [Hofman]
D. Jenkins, University of Liverpool; D. Hofman, University of Illinois- Chicago; R. Siemssen, University of Groningen; V. Nanal, Tata Institute of Fundamental Research; P. Heckman, M. Thoennessen, Michigan State University; B. Back, M. Carpenter, D. Henderson, M. Kelly, T. Khoo, F. Kondev, Argonne National Lab.
10. Study of the ^8B Neutrino Spectrum Through the $^8\text{B}(\beta^+)^8\text{Be}(2\alpha)$ Decay Chain-II [Freedman]
S. Freedman, University of California; W. Winter, Lawrence Berkeley National Lab.; J. Greene, D. Henderson, R. Janssens, C. Jiang, E. Moore, R. Pardo, T. Pennington, K. Rehm, G. Savard, J. Schiffer, G. Zinkann, Argonne National Lab.
11. Decay Properties of Particle-Unbound States in ^{19}Ne -III [Rehm]
L. Jisonna, R. Segel, Northwestern University; M. Paul, Hebrew University of Jerusalem; P. Collon, Columbia University; J. Caggiano, J. Greene, A. Heinz, R. Janssens, C. Jiang, R. Pardo, K. Rehm, J. Schiffer, A. Wuosmaa, Argonne National Lab.
12. Study of Unstable Osmium Nuclei by Coulomb Excitation [Mueller]
D. Jenkins, University of Liverpool; J. Church, J. Enders, T. Glasmacher, Z. Hu, Z. Hu, K. Miller, W. Mueller, H. Olliver, Michigan State University; I. Wiedenhoever, Florida State University; M. Carpenter, R. Janssens, F. Kondev, K. Lister, T. Pennington, D. Seweryniak, Argonne National Lab.
13. Drip-Line Decay Studies Around $A = 76$ [Davids]
J. Ressler, J. Shergur, W. Walters, A. Woehr, University of Maryland; A. Mahmud, P. Munro, P. Woods, University of Edinburgh; F. Sarazin, TRIUMF; C. Davids, A. Heinz, D. Seweryniak, Argonne National Lab.
14. Non-Equilibrium Neutron Emission in Ni + Mo Reactions [Charity]
R. Charity, L. Sobotka, Washington University; R. de Souza, A. Caraley, Indiana University Cyclotron Facility
15. Preparations Towards a Search for Super-Heavy Elements at ATLAS: Phase I [Heinz]
J. Shergur, A. Woehr, University of Maryland; K. Abu Saleem, Illinois Institute of Technology; J. Caggiano, M. Carpenter, J. Greene, A. Heinz, D. Henderson, R. Janssens, F. Kondev, R. Pardo, T. Pennington, G. Savard, D. Seweryniak, Argonne National Lab.

16. Radiative Capture and Fusion Dynamics in Cold Fusion $^{90}\text{Zr} + ^{92}\text{Mo}$ Reaction [Kondev]
A. Woehr, University of Maryland; D. Jenkins, University of Liverpool; I. Ahmad, M. Carpenter, C. Davids, A. Heinz, R. Janssens, T. Khoo, F. Kondev, T. Lauritsen, K. Lister, D. Seweryniak, Argonne National Lab.
17. Measurement of Helium-3 to Helium-4 Ratios in Isotopically Purified Helium [Doyle]
P. Huffman, Nat'l. Inst. of Standards & Tech.; D. McKinsey, Harvard University; P. Collon, R. Scott, Columbia University; J. Caggiano, A. Heinz, R. Janssens, C. Jiang, D. Moehs, R. Pardo, K. Rehm, J. Schiffer, R. Vondrasek, Argonne National Lab.
18. Coulomb Excitation of ^{124}Xe , ^{126}Xe , and ^{128}Xe [Wiedenhoever]
A. Gade, Universität zu Köln; T. Glasmacher, P. Lofy, K. Miller, W. Mueller, H. Olliver, Michigan State University; I. Wiedenhoever, Florida State University; M. Carpenter, R. Janssens, K. Lister, Argonne National Lab.
19. Controlling the Dynamics of Vortex and Domain Motion in Superconducting and Magnetic Materials Through Heavy-Ion Irradiation [Miller]
J. Hettinger, Rowan College of New Jersey; R. Olsson, Michigan State University; D. Kim, D. Miller, E. Moore, Argonne National Lab.
20. Test of the New Transport System for the In-Flight Secondary Beam Production Setup [Pardo]
R. Segel, Northwestern University; M. Paul, Hebrew University of Jerusalem; P. Collon, Columbia University; J. Caggiano, J. Greene, A. Heinz, D. Henderson, R. Janssens, C. Jiang, R. Pardo, T. Pennington, K. Rehm, J. Schiffer, G. Zinkann, Argonne National Lab.
21. Hot GDR in ^{118}Sn [Heckman]
D. Hofman, University of Illinois- Chicago; V. Nanal, Tata Institute of Fundamental Research; R. Varner, Oak Ridge National Laboratory; P. Heckman, M. Thoennessen, Michigan State University; B. Back, M. Carpenter, M. Kelly, T. Khoo, Argonne National Lab.
22. A New Technique for Producing ^{25}Al Beams at ATLAS [Caggiano]
P. Collon, Columbia University; J. Caggiano, J. Greene, A. Heinz, D. Henderson, C. Jiang, T. Pennington, K. Rehm, D. Seweryniak, Argonne National Lab.
23. Limits of Stability of ^{254}No in Spin and Excitation Energy [Reiter]
A. Woehr, University of Maryland; C. Bhattacharya, Université, Louis Pasteur; J. Cizewski, M. Smith, Rutgers University; P. Reiter, Ludwig Maximilians-Universität München; K. Vetter, Lawrence Livermore National Lab.; I. Ahmad, J. Caggiano, M. Carpenter, A. Heinz, R. Janssens, T. Khoo, F. Kondev, T. Lauritsen, K. Lister, D. Seweryniak, Argonne National Lab.
24. The $N = Z$ Waiting Point Nucleus ^{68}Se [Arahamian]
A. Aprahamian, J. Goerres, University of Notre Dame; A. Woehr, University of Maryland; S. Fischer, De Paul University; R. Janssens, D. Seweryniak, Argonne National Lab.
25. Measuring the Charge Radius of He-6 [Lu]
C. Law, Monmouth College; M. Paul, Hebrew University of Jerusalem; P. Collon, Columbia University; K. Bailey, J. Caggiano, A. Heinz, D. Henderson, R. Holt, R. Janssens, C. Jiang, Z. Lu, T. O'Connor, R. Pardo, T. Pennington, K. Rehm, J. Schiffer, Argonne National Lab.
26. Structure of Hot Dy Nuclei as a Function of Spin and Excitation Energy Probed Through the Giant Dipole Resonance [Nanal]
D. Jenkins, University of Liverpool; D. Hofman, University of Illinois- Chicago; V. Nanal, Tata Institute of Fundamental Research; P. Heckman, Michigan State University; B. Back, M. Carpenter, A. Heinz, T. Khoo, F. Kondev, Argonne National Lab.

27. Test of the RIA Gas Cell Prototype [Savard]
J. Clark, J. Vaz, University of Manitoba; C. Boudreau, McGill University; J. Caggiano, A. Heinz, G. Savard, J. Schwartz, D. Seweryniak, Argonne National Lab.
28. Mass Measurements Along the $N = Z$ Line With the CPT Mass Spectrometer [Savard]
J. Clark, K. Sharma, J. Vaz, University of Manitoba; G. Sprouse, S.U.N.Y. at Stony Brook; C. Boudreau, F. Buchinger, McGill University; M. Maier, GSI, Darmstadt; J. Caggiano, A. Heinz, G. Savard, D. Seweryniak, J. Wang, Argonne National Lab.
29. Studies of Sub-ms Proton and α Emitters [Seweryniak]
A. Woehr, University of Maryland; M. Carpenter, C. Davids, A. Heinz, D. Seweryniak, Argonne National Lab.
30. Spectroscopy of Proton-Unbound States in ^{26}Si - II [Caggiano]
P. Parker, Yale University; Y. Nagame, Japan Atomic Energy Res. Inst.; P. Collon, Columbia University; J. Caggiano, J. Greene, A. Heinz, R. Janssens, C. Jiang, K. Lister, K. Rehm, Argonne National Lab.
31. High Energy Photons From Very Symmetric Reactions: the Giant Dipole Resonance in Highly Rotating Cold Nuclei [Carpenter]
A. Bracco, F. Camera, O. Wieland, University of Milano; D. Jenkins, University of Liverpool; R. Varner, Oak Ridge National Laboratory; M. Carpenter, A. Heinz, R. Janssens, T. Khoo, F. Kondev, T. Lauritsen, K. Lister, E. Moore, D. Seweryniak, Argonne National Lab.
32. Preparations Towards a Search for Super-Heavy Elements at ATLAS: PHASE I [Heinz]
M. Smith, Rutgers University; A. Woehr, University of Maryland; P. Collon, Columbia University; I. Ahmad, B. Back, M. Carpenter, A. Heinz, R. Janssens, C. Jiang, T. Khoo, F. Kondev, T. Lauritsen, K. Lister, E. Moore, G. Savard, J. Schiffer, D. Seweryniak, Argonne National Lab.
33. Continuation of the Mass Measurement Program Along the $N = Z$ Line with the CPT Mass Spectrometer [Savard]
J. Clark, M. Froese, K. Sharma, J. Vaz, University of Manitoba; L. Frankland, University of Brighton; C. Boudreau, P. Coulombe-Pontbriant, J. Crawford, S. Gulick, McGill University; J. Caggiano, A. Heinz, G. Savard, D. Seweryniak, J. Wang, Argonne National Lab.
34. Proton Decay of ^{135}Tb [Davids]
J. Shergur, W. Walters, A. Woehr, University of Maryland; T. Davinson, A. Mahmud, P. Munro, P. Woods, University of Edinburgh; C. Davids, A. Heinz, D. Seweryniak, Argonne National Lab.
35. Identification of the Astrophysical Resonance in the $^{19}\text{Ne}(p,\gamma)^{20}\text{Na}$ Reaction [Woods]
J. Goerres, M. Shawcross, University of Notre Dame; J. Shergur, A. Woehr, University of Maryland; A. Mahmud, C. Ruiz, P. Woods, University of Edinburgh; F. Sarazin, TRIUMF; U. Greife, Colorado School of Mines; M. Carpenter, C. Davids, A. Heinz, R. Janssens, T. Khoo, K. Rehm, D. Seweryniak, Argonne National Lab.
36. Study of the Fusion Evaporation Cross Section at Very Low Energies [Jiang]
Y. Nagame, Japan Atomic Energy Res. Inst.; P. Collon, Columbia University; B. Back, J. Caggiano, A. Heinz, R. Janssens, C. Jiang, K. Rehm, D. Seweryniak, Argonne National Lab.
37. Upgrading of the Large-Acceptance Focal Plane Detector for Use in Gas-Filled Spectrograph Mode [Paul]
M. Paul, Hebrew University of Jerusalem; P. Collon, Columbia University; A. Heinz, D. Henderson, C. Jiang, K. Rehm, Argonne National Lab.

38. A Measurement of the Efficiency and Linear Polarization Sensitivity of a Planar Germanium Strip Detector (HPGe DSSD) [Jenkins]
D. Jenkins, University of Liverpool; T. Sienko, Purdue University, Calumet; A. Goergen, Lawrence Berkeley National Lab.; M. Carpenter, R. Janssens, T. Khoo, F. Kondev, E. Moore, Argonne National Lab.
39. Accelerator Mass Spectrometry of ^{39}Ar for Oceanographic Research [Collon]
W. Kutschera, Universität Wien; P. Collon, R. Scott, Columbia University; I. Ahmad, A. Heinz, C. Jiang, R. Pardo, K. Rehm, R. Vondrasek, G. Zinkann, Argonne National Lab.
40. Identification of the $g_{7/2}$ Neutron Single-Particle Level in ^{103}Sn and Search for ^{105}Te [Walters]
J. Ressler, J. Shergur, W. Walters, A. Woehr, University of Maryland; M. Lipoglavsek, Jozef Stefan Institute; C. Davids, D. Seweryniak, Argonne National Lab.
41. Test of the Recoil-Beta Tagging Method [Seweryniak]
M. Shawcross, University of Notre Dame; J. Ressler, J. Shergur, A. Woehr, University of Maryland; F. Sarazin, TRIUMF; A. Heinz, D. Seweryniak, Argonne National Lab.

b. Outside Users of ATLAS During the Period October 1, 2000 - September 30, 2001

This list includes all outside Users who were an experiment spokesperson (a), alternate spokesperson (b), student (*), or collaborator actually present at ATLAS for an experiment. An additional 21 Users listed as collaborators on the various experiment proposals were not at ATLAS in person, and thus are not represented in the list below.

- | | |
|---|---|
| 1. Brookhaven National Laboratory
A. Sonzogni | 10. Illinois Institute of Technology
* K. Abu Saleem |
| 2. Clark University
D. Brenner | 11. Indiana University Cyclotron Facility
A. Caraley
R. de Souza |
| 3. Colorado School of Mines
U. Greife | 12. Japan Atomic Energy Res. Inst.
Y. Nagame |
| 4. Columbia University
ab P. Collon
* R. Scott | 13. Jozef Stefan Institute
M. Lipoglavsek |
| 5. De Paul University
b S. Fischer | 14. Lawrence Berkeley National Lab.
b A. Goergen
* W. Winter |
| 6. Florida State University
a I. Wiedenhoever | 15. Lawrence Livermore National Lab.
K. Vetter |
| 7. GSI, Darmstadt
M. Maier
P. Mokler
T. Stöhlker | 16. Ludwig Maximilians-Universität München
a P. Reiter |
| 8. Harvard University
a J. Doyle
* D. McKinsey | 17. McGill University
* C. Boudreau
F. Buchinger
* P. Coulombe-Pontbrian
J. Crawford
S. Gulick |
| 9. Hebrew University of Jerusalem
a M. Paul | |

18. Michigan State University
 - * J. Church
 - J. Enders
 - b T. Glasmacher
 - a* P. Heckman
 - Z. Hu
 - * P. Lofy
 - * K. Miller
 - a W. Mueller
 - * H. Olliver
 - * R. Olsson
 - b M. Thoennessen
19. Monmouth College
 - * C. Law
20. Nat'l. Inst. of Standards & Tech.
 - P. Huffman
21. Northwestern University
 - * L. Jisonna
 - b R. Segel
22. Oak Ridge National Laboratory
 - R. Varner
23. Purdue University, Calumet
 - * T. Sienko
24. Rowan College of New Jersey
 - J. Hettinger
25. Rutgers University
 - J. Cizewski
 - M. Smith
26. S.U.N.Y. at Stony Brook
 - G. Sprouse
27. TRIUMF
 - F. Sarazin
28. Tata Institute of Fundamental Research
 - a V. Nanal
29. University of Brighton
 - * L. Frankland
30. University of California
 - a S. Freedman
31. University of Edinburgh
 - T. Davinson
 - * A. Mahmud
 - * P. Munro
 - * C. Ruiz
 - K. Schmidt
 - ab P. Woods
32. University of Groningen
 - R. Siemssen
33. University of Illinois- Chicago
 - a D. Hofman
34. University of Jyväskylä
 - J. Uusitalo
35. University of Liverpool
 - a D. Jenkins
36. University of Manitoba
 - * J. Clark
 - M. Froese
 - K. Sharma
 - * J. Vaz
37. University of Maryland
 - * J. Shergur
 - a W. Walters
 - A. Woehr
38. University of Milano
 - a A. Bracco
 - F. Camera
 - * F. Della Vedova
 - S. Leoni
 - B. Million
 - O. Wieland
39. University of Notre Dame
 - a A. Aprahamian
 - H. Berry
 - J. Goerres
 - A. Livingston
 - M. Shawcross
40. Université, Catholique de Louvain
 - Y. El Masri
41. Université, Louis Pasteur
 - * C. Bhattacharya

42. Universität Wien
b W. Kutschera

43. Universität zu Köln
* A. Gade

44. Washington University
a R. Charity
b L. Sobotka
D. Sarantites
W. Reviol

45. Western Michigan University
L. Paulius

46. Yale University
P. Parker

c. Upgrades to the ATLAS Web Page

Several improvements to the ATLAS web page (<http://www.phy.anl.gov/atlas/index.html>) were made during FY01. During the summer, a student from Richard J. Daley College in Chicago, Terri Haslinger, worked with Frank Moore on the web page upgrades as part of the Community College Institutes (CCI) program sponsored by the Department of Energy (<http://www.scied.science.doe.gov/scied/CCI/about.html>) and administered by the ANL Division of Educational Programs. While many of the improvements were related to formatting and appearance, there were several that had direct impact on the User program. In particular, a web-based proposal submission process was implemented using the forms/CGI interface. This allows Users to submit ATLAS proposals electronically through the web and by e-mail. A screen snapshot of part of the form is shown below. Over half of the proposals submitted for the October 5, 2001 meeting of the PAC were submitted electronically.

ATLAS Proposal Fact Sheet - Submission Form

Proposal Title:

Proposal Type: Previous Exp. Number (continuation and resubmissions):

Experimental Spokesperson: Telephone and e-mail:

Alternate Spokesperson: Alternate Telephone and e-mail:

****Please list all additional Participants and their home institute on the proposal itself.**

Targets:	Beams:	Energies (MeV):	Intensities (pnA):	Beam Stop Material:
			Indicate maximum needed	Required (e.g. Ta)
<input type="text"/>	<input type="text"/>	<input type="text"/>	<input type="text"/>	<input type="text"/>

Additional Beam Requirements:

Beam Sweeper Yes: No: Period:

Rebuncher/Debuncher Yes: No: Max Width: ps (FWHM)

II. OPERATION AND DEVELOPMENT OF ATLAS

OVERVIEW

Highlights of the operation of the Argonne Tandem Linear Accelerator System (ATLAS) as a national user facility and related accelerator physics R&D projects are described in this chapter. ATLAS is used for basic research in nuclear physics and occasionally for other areas of research and development, including atomic physics and material science. ATLAS is also used as an accelerator mass spectroscopy facility applied to a wide range of scientific interests. Over half of the beam time is allocated to experiments for which the spokesperson is an outside user. Recent ATLAS operating performance and related development projects are described in the next section. ATLAS personnel are also involved in developing technology in support of a future advanced facility, based on ATLAS technologies, for beams of short-lived nuclei. Projects related to the exotic beam facility are described in the third section below.

Due to budgetary constraints, the ATLAS operating schedule was reduced in June 2001 from a 7 day-per-week schedule to a running schedule averaging 5.33 days per week. Even with the reduced operating schedule ATLAS provided over 5700 hours of beam for research and provided thirty-four different isotopic beams. Statistics about beam hours and users are given in Table II-1.

ATLAS continued to provide a range of radioactive species with intensities generally in the range of 10^5 to 10^6 particles per second. This year 3% of all beam-time went to radioactive beams. Beams of long-lived ($T_{1/2} > 2$ hours) species produced at other facilities and placed in the ATLAS tandem ion source and beams of short-lived species produced in-flight by inverse-kinematics reactions have been developed at ATLAS. See the Heavy-Ion Research section for a summary of recent physics results from experiments using radioactive beams.

TABLE II-1. SUMMARY OF ATLAS EXPERIMENTS AND USER STATISTICS

	<u>FY2001</u> (Actual)	<u>FY2002*</u> (Extrap.)	<u>FY2003*</u> (Pred.)	<u>FY2004</u> (Pred.)
<u>Beam Use for Research (hr)</u>				
Nuclear Physics	4740	3360	5050	5260
Atomic Physics	90	50	100	70
Accelerator R & D	194	120	150	174
Accelerator Mass Spectroscopy	570	400	500	400
Other	<u>122</u>	<u>70</u>	<u>100</u>	<u>100</u>
Total	5716	4000	5900	6004
Number of Experiments Receiving Beam	42	35	53	53
Number of Scientists Participating in Research	123	120	200	200
<u>Institutions Represented</u>				
Universities (U.S.A.)	22	22	19	19
DOE National Laboratories	4	4	5	5
Other	22	22	27	27
<u>Usage of Beam Time (%)</u>				
In-House Staff	49	59	35	35
Universities (U.S.A.)	31	30	38	38
Other DOE National Laboratories	5	5	12	12
Other Institutions	15	15	<u>15</u>	<u>15</u>
Total	100	100	100	100

*Assumes 5-days/week operations, started June 1, 2001, continues through FY2002 and 7-day/week operation resumes in FY2003.

A. OPERATION OF THE ACCELERATOR

(R. C. Pardo, D. Barnett, J. Bogaty, B. E. Clifft, S. Daley, A. Deriy, G. Gribbon, R. Jenkins, A. Krupa, E. Lindert, S. McDonald, F. H. Munson, Jr., D. R. Phillips, D. Quock, A. Ruthenberg, R. H. Scott, S. Sharamentov, J. R. Specht, P. Strickhorn, R. C. Vondrasek, and G. P. Zinkann)

a.1. Operations Summary

ATLAS provided a total of 34 different isotopes for research in FY2001. The distribution of species is shown in Fig. II-1. This is a significant increase in the diversity of requested beam species over past years and is a new record for ATLAS. Even with this large array of beams provided, ^{58}Ni stood out in popularity, commanding over 22% of all beam time. Beams heavier than nickel were provided 27.6% of the time.

The tandem injector was used for beam delivery approximately 22% of the scheduled time. A new

SNICS-II ion source was procured over a year ago and has now become the most used source on the tandem. In addition, a new extraction optics system obtained when the new source was purchased was installed near the end of the year and has resulted in a significant improvement in analyzed beam from the source as well as a 15% improvement in transmission to the tandem from the source. The total improvement is difficult to quantify, but appears to be as much as a factor of 5 in total efficiency.

The tandem corona voltage grading system is now eight years old and has begun to show serious signs of deterioration. We are now unable to properly regulate current flow in the four separate sections of the system due to deterioration of the needle assemblies. This also impacts voltage stability and beam quality by increasing longitudinal emittance of the beams from the tandem.

The in-flight radioactive beam program was able to resume when a new 6-Tesla superconducting solenoid was received and installed in early 2001. This solenoid replaces an older solenoid that developed an open condition in the coil winding which could not be repaired. Acceptance tests of the new solenoid showed a factor of two improvement in beam transmission compared to the old solenoid, possibly due to better field uniformity.

The rebuilt ECR-I ion source has developed into an excellent performing source. The source has demonstrated over 200 eμA of Ar⁹⁺ and 17 eμA of Ni¹⁷⁺, excellent results for a 10 GHz source. The source operating modes have clearly demonstrated the need to go to increased solenoid field strength, presently limited by the existing power supplies. New supplies allowing a 20% increase in coil current will be purchased in the coming year to allow further improvements in source performance.

In support of a significant new research initiative to search for super-heavy elements at ATLAS, work to obtain higher beam currents from ECR-II has been undertaken. High intensity beams including ⁵⁸Fe, ⁵⁰Ti, and ⁸⁶Kr are needed for the super-heavy element search program. A new traveling-wave tube transmitter, tunable over a frequency range of 11-13 GHz, has been purchased for two-frequency operation on ECR-II. In two-frequency mode a beam current of over 210 eμA of ⁸⁶Kr¹⁴⁺ was obtained.

In another test, 7.5 pμA of ⁸⁶Kr¹⁵⁺ was accelerated through the PII linac and studies of the linac performance and stability were made. No accelerator instabilities were observed during these tests. In order to make use of these high intensity beams, a revision of the ATLAS Safety Assessment Document and associated Safety Envelope and Operations Envelope was initiated. The approval of a new SAD and Safety Envelope is expected to be granted during 2002. Upon approval of the new SAD and Safety Envelope, preparations for tests of acceleration of multi-particle microampere beams through the entire accelerator facility will commence. Automatic beam interruption systems will be developed to interrupt these high power beams when an accelerator failure is detected. Without such safety features in place, in the event of a beam-delivery failure equipment damage could result.

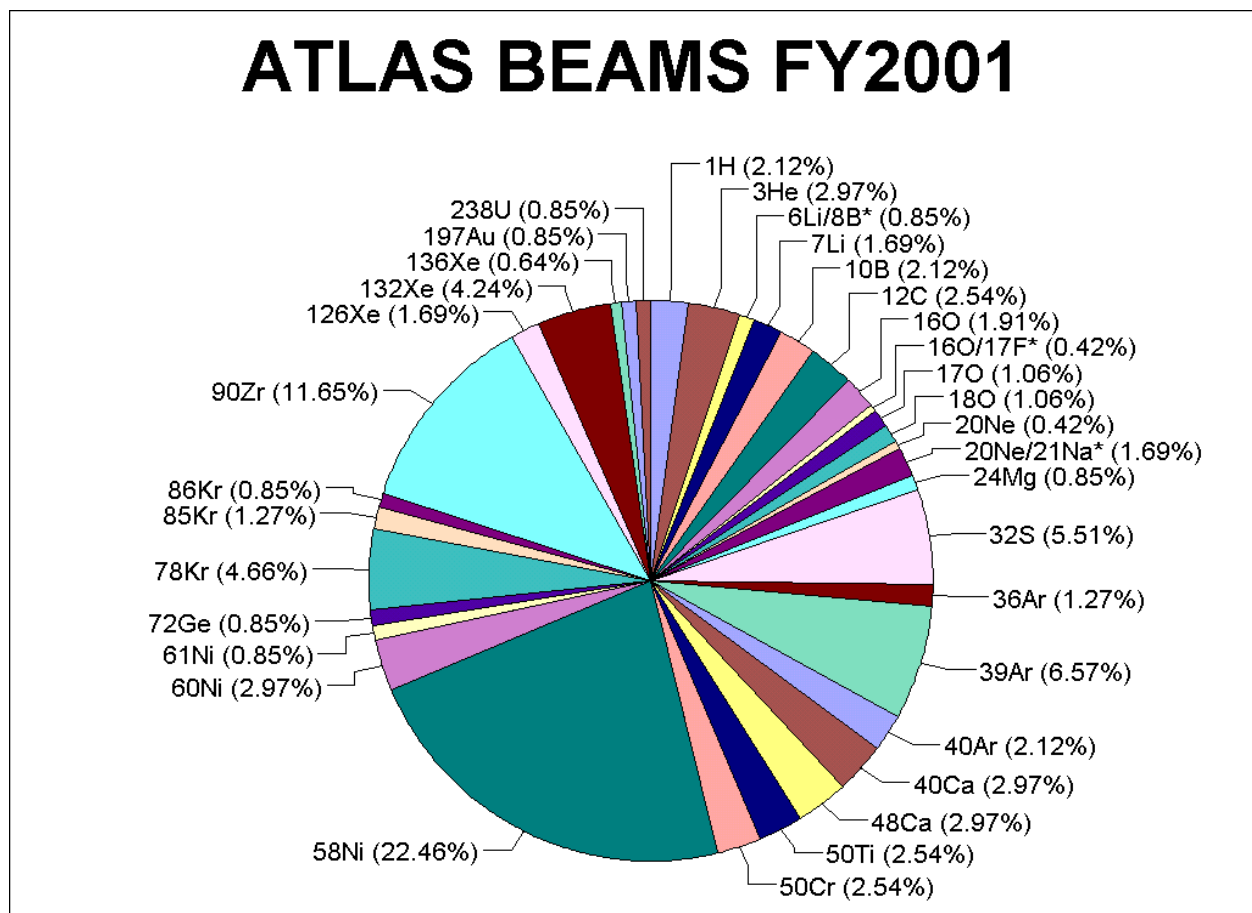


Fig. II-1. Distribution of beam time by isotope provided by ATLAS in FY2001. A total of 34 different isotopes were provided to the research program. Radioactive beams, indicated by an "*" in the chart, comprised 3% of all beam time in FY2001.

B. DEVELOPMENTS RELATED TO ATLAS

b.1. Status of the ECR Ion Sources (R. C. Vondrasek, R. H. Scott, and R. C. Pardo)

The ECR 1 rebuild, described in the previous status report, was completed in October 2000 and the source returned to full operation in 2001. The upgrade has produced a marked increase in the available beam currents for many ion species, as detailed in Table II-2, and has greatly simplified and stabilized source operation. The sputter performance of the source has been exceptional. The peak charge state of ^{58}Ni has increased from 13+ to 17+ with a corresponding factor of 25 increase in beam current. The speed of sputter sample changes has also been improved with the use of an air-lock system. The time from shutting off one

sample, changing to the next, restarting the source, and delivering beam to the linac is typically 30 minutes.

The source performance continues to improve as new operational modes are reached, and the behavior of the source indicates the need for higher magnetic fields. An increase in the axial magnetic field will be accomplished through an upgrade of the solenoid power supplies. The resulting improvement in the plasma confinement should lead to an increase in beam intensity and charge state distribution.

TABLE II-2. PRE AND POST UPGRADE PERFORMANCE OF ECR-I FOR VARIOUS ION SPECIES

BEAM SPECIES	PRE-UPGRADE INTENSITY (euA)	POST-UPGRADE INTENSITY (euA)	% INCREASE FROM OLD ECR-I
Oxygen 16/5+	31	225	625
Oxygen 16/6+	54	263	385
Oxygen 16/7+	4	52	1200
Nickel 58/15+	1.6	11	585
Nickel 58/16+	1.1	15	1260
Nickel 58/17+	0.6	16	2565
Krypton 86/13+	9.5	92	870
Krypton 86/15+	8.8	99	1025
Krypton 86/17+	3.8	61	1505
Krypton 86/18+	1.5	38.5	2465

Development work at ECR 2 has focused on improving beam currents for the super-heavy research program. A ^{50}Ti beam was delivered for an experiment designed to produce ^{257}Rf . The titanium was introduced into the source via a high temperature oven which operated at $\sim 1600^\circ\text{C}$. To achieve this high operating temperature the oven was shifted from a radial to an axial position, allowing additional heating from the plasma. A beam of $^{50}\text{Ti}^{11+}$ (70% enrichment) was delivered on target for a period of 7 days with a maximum intensity of 72 pA.

The high operating temperature of the oven was at the thermal limit of the alumina structural elements, and during the run the oven failed two times due to breakdown of the alumina body. New oven bodies, constructed of a higher purity alumina with a maximum operating temperature $\sim 250^\circ\text{C}$ higher than that of the previously used material, have been purchased and will soon be tested.

The production of an iron beam has been pursued using the MIVOC method (Metal Ions from Volatile Compounds). In this method volatile compounds having metal atoms in their molecular structure are introduced into the plasma. The compound used for the production of an iron beam is ferrocene – $\text{Fe}(\text{C}_5\text{H}_5)_2$ – which has a high vapor pressure at room temperature ($\sim 10^{-3}$ Torr). The material is placed in a chamber attached to the gas inlet valve of the ion source, the air in the chamber is evacuated, and the high vapor pressure of the material allows for the injection of the iron compound into the source as a gas. This has produced a peak charge state of $^{56}\text{Fe}^{15+}$ with an intensity of 25.0 euA. At present the efficiency and beam production of this method is superior to that of a high temperature oven. The ferrocene produced 56% more beam in the 15+ charge state with a decrease in material

consumption from 1.05 to 0.88 mg/hr and an increase in efficiency from 0.13 to 0.32% for beam into the 15+ charge state. Work continues with this method to reduce the consumption rate and improve the efficiency.

During an AMS experiment designed to detect ^{39}Ar in ocean water samples, a quartz liner was used in the source to reduce background contamination. The stable isobar for ^{39}Ar is ^{39}K and is naturally present in the ion source. In an effort to reduce the potassium contaminant, the aluminum plasma chamber wall was covered with a quartz liner to provide a clean and less porous surface to the plasma. This method was successful with a factor of 10 reduction in the potassium background with no effect on the ^{39}Ar output.

The use of the liner revealed a problem with the radial magnetic confinement of the plasma provided by a permanent magnet hexapole constructed of six NdFeB bars. During the experiment the source performance degraded and the decision was made to open the source in order to investigate the cause. A 1.0 cm hole in the quartz liner produced by a concentrated loss of plasma was discovered. The plasma loss was the result of a localized 45% drop in the magnetic field of a 1.0 cm section of the hexapole bar at the hole location. The bar was replaced with a spare and the experiment resumed within 7 hours. It was later determined that the bar was originally damaged in 1997 during a cooling water failure which allowed a section of the bar to reach its Curie temperature ($\sim 50^\circ\text{C}$) and induce a partial demagnetization. Over the next several years, the weakened state of the bar allowed the plasma to concentrate its loss at the damaged area and locally heat the bar, further lowering the field.

Work has been taking place in collaboration with Fartech, Inc. under an SBIR grant to model the charge state distribution in an ECR plasma. The model attempts to use ion source parameters such as RF power, magnetic field, and gas flux as input parameters to predict the core plasma properties. This could become a powerful predictive tool for the behavior and performance of an ion source before construction takes place.

As part of this effort, a technique for the discrete injection of a diagnostic impurity into the ECR plasma was developed in order to measure the transient extracted currents of the impurity. This technique

functioned as a core plasma diagnostic that allowed the accuracy of the Fartech steady-state ECRIS core plasma code to be determined. Previously only solid materials in conjunction with a pulsed laser were used to produce the required discrete material pulse. With this new technique the pulsed laser was replaced with a fast high voltage pulse applied to a gold sputter sample. The high voltage pulse had a rise time of 100 nsec and a variable pulse duration. The resulting rise times of the gold charge states are shown in Fig. II-2. The variation in the rise times was studied as a function of RF power, gas mixing, and magnetic fields. This information was then utilized by the Fartech group to optimize their plasma model.

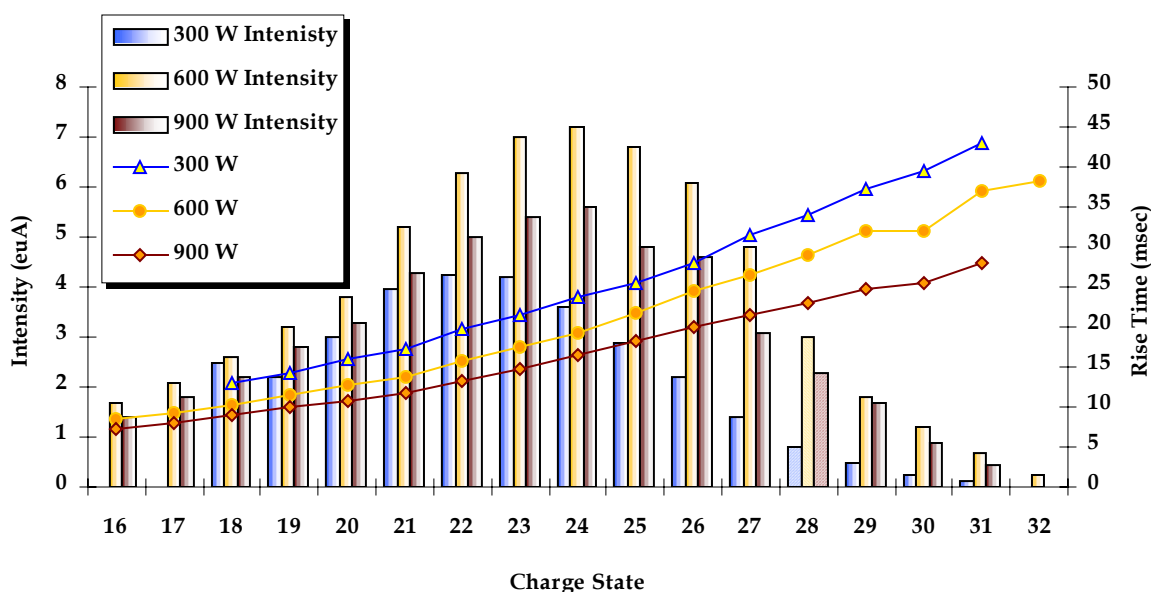


Fig. II-2. Rise times and beam intensities of ^{197}Au as a function of RF power.

b.2. Two-Frequency Operation of ECR 2 (R. C. Vondrasek, R. H. Scott, and R. C. Pardo)

The use of two frequencies is utilized to improve beam production as well as source stability. The two frequencies create two nested ECR zones leading to a higher density of energetic electrons. This increases the production of the high charge state ions and improves the overall plasma stability. ECR 2 originally took advantage of this condition through operation at 10.5 and 14.0 GHz, and ECR 1 has been designed to operate with two frequencies but has not yet run in this mode. The unit used to provide a second frequency for ECR 2, a 10.5 GHz magnetron, failed in 1998 and no replacement magnetron was available. To replace the

failed unit, a traveling wave tube amplifier (TWTA) with a tunable range of 11.0-13.0 GHz was recently purchased. The tunable aspect of the TWTA allows the transmitter to operate as either the primary or secondary frequency for either ion source.

The first test with two-frequency heating at ECR 2 was performed with ^{16}O and was intended to find the optimum operating frequency of the TWTA. The source output and stability was found to improve as the gap between the primary (a 14 GHz klystron) and the secondary frequencies was increased. A shift in

frequency from 11.67 GHz to 10.85 GHz produced an 11.5% increase in $^{16}\text{O}^{7+}$ beam production as well as improved stability. Further testing demonstrated that the increase in beam output was not a result of the higher overall RF power being launched into the source but rather was due to the two distinct ECR zones established by the two frequencies. This is demonstrated in Fig. II-3., which shows the performance of $^{16}\text{O}^{7+}$ at various TWTA frequencies as well as RF power levels. The source was optimized on O^{7+} using only 445 watts from the 14 GHz transmitter. The TWTA was then energized and its power output set to 60 watts, resulting in a 46.2% increase in beam current. The source was again optimized at these RF power settings with a further extension in improvement to 69.2%. De-energizing the TWTA reduced the beam current to the original output level, and the addition of

60 watts from the 14 GHz klystron could not duplicate the 66.0 euA achieved with the combined frequency operation.

Further tests were performed with ^{56}Fe from ferrocene material and 99% enriched ^{86}Kr with the results shown in Fig. II-4. The peak charge state for ^{56}Fe shifted from 13+ to 15+ with the addition of 150 W of RF power at 10.85 GHz accompanied by a factor of 2 increase in the beam intensity. The goal of the ^{86}Kr test was to produce 15 μA of $^{86}\text{Kr}^{14+}$. This beam would meet one of the requirements for the RIA driver linac. This goal was achieved with the production of 210 μA of $^{86}\text{Kr}^{14+}$ from the ion source with 974 W of 14 GHz RF power and 400 W from the TWTA at 10.81 GHz.

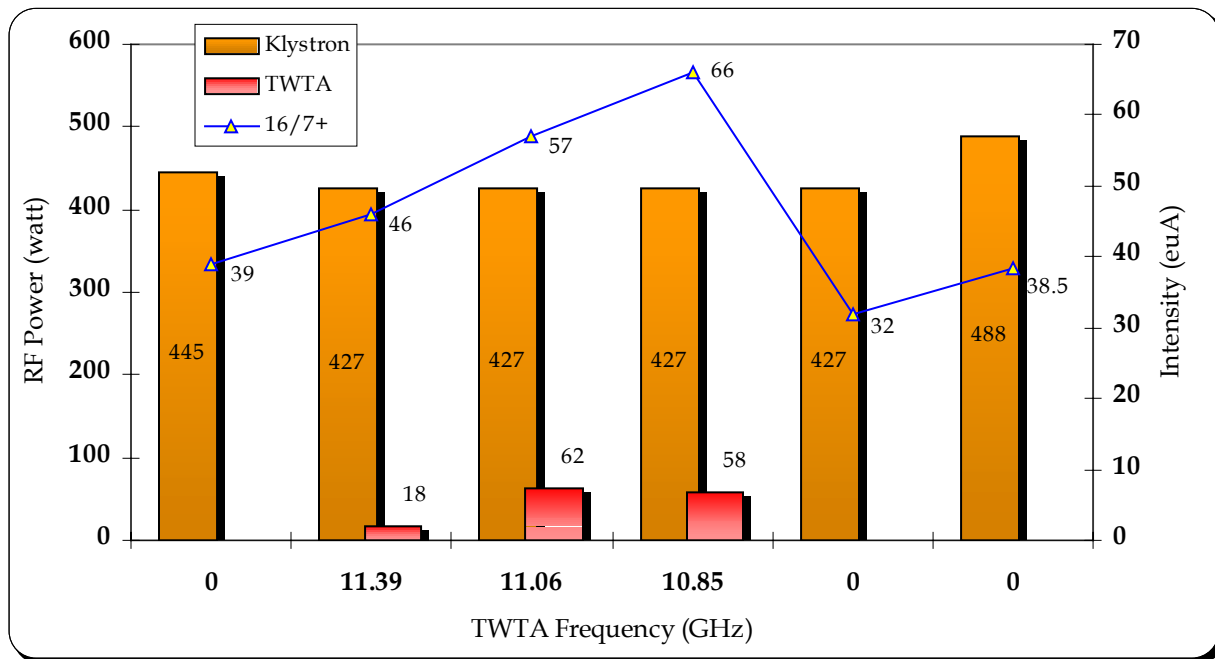


Fig. II-3. Oxygen 7+ performance from ECR 2 as a function of RF power from the 14 GHz klystron and the tunable TWTA.

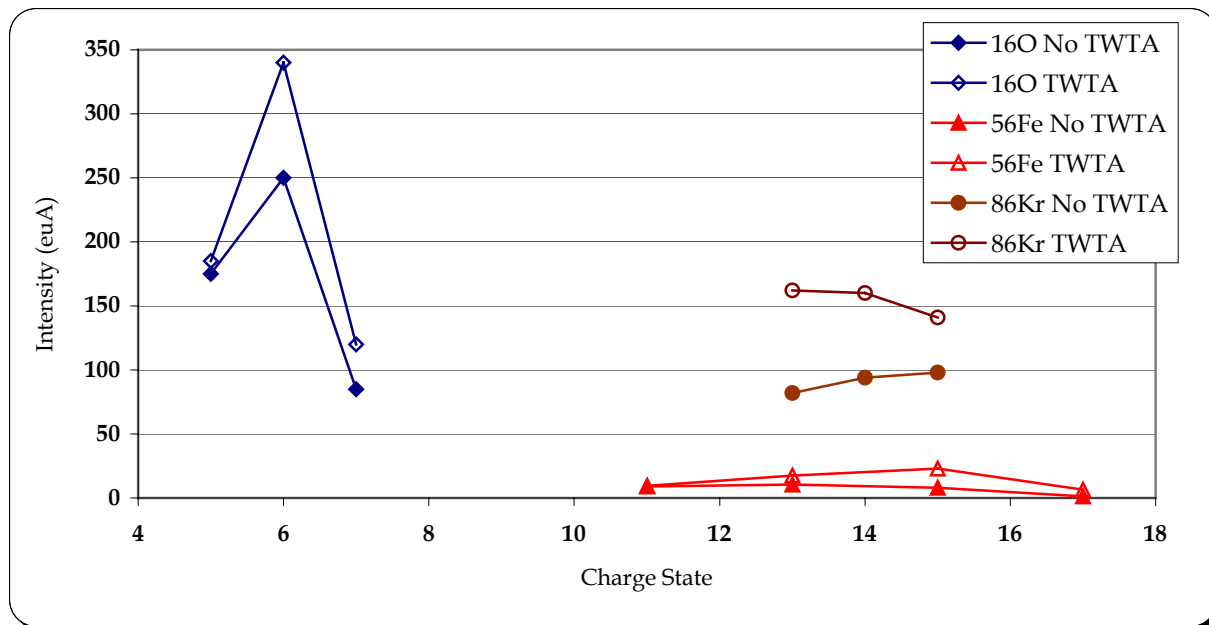


Fig. II-4. Increase in beam intensity of various ion species due to two-frequency heating.

b.3. PII Transmission Line Traveling Wave Chopper (J. M. Bogaty, S. Sharamentov, B. E. Clifft, and R. C. Pardo)

The Transmission Line Traveling Wave Chopper is now fully operational at 12.125 MHz. In routine use since early January 2002, the new chopper is reliable and easy to use. Three computer-controlled operating modes are available to make PII beam tuning easier. The high power vacuum tube RF output stage has all critical voltages and currents continuously monitored. Monitoring circuitry insures against accidental damage to sensitive components and allows automated change over from one operating mode to another. Modes are selected by computer menu, which makes beam tuning more efficient.

To date, we have chopped ions as light as neon and as heavy as nickel. Chopping voltages are within expected levels and the necessary voltages for heavy ions like lead and uranium are available. Operationally, beam transmission through PII has improved to as high as 75% with the implementation of the full bunching system. A photograph of chopper output voltage shows how wide beam bunches are at the choppers location. The thirty-nanosecond window of zero deflection voltage was determined by experimentation. This shows why a sine wave chopper is not an acceptable alternative for this bunching geometry, as beam quality would be severely degraded.

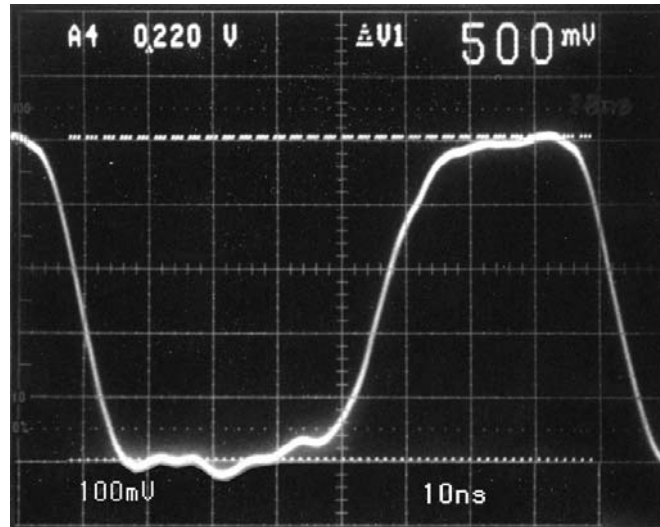


Fig. II-5. Transmission-Line Traveling-Wave Chopper voltage waveform shown is 550 V at a 12.125 MHz repetition rate.

b.4. ATLAS Control System (F. H. Munson, D. Quock, S. Dean, and K. Eder)

The foundation of the real-time aspects of the ATLAS control system is the commercial product known as Vsystem marketed by Vista Control Systems. Recently, on a prototype off-line system, it has been demonstrated that a port of Vsystem from the VMS operating system to PC-based operating systems provides a relatively low cost approach to distributed CAMAC I/O processing. The prototype system is capable of performing CAMAC I/O to a local crate, as well as accessing Vsystem databases on the main VMS server via Ethernet. This enables the PC to modify parameters of CAMAC modules located in CAMAC crates that are connected to the main CAMAC serial highway as well as module parameters in the crate connected directly to the PC. This is the first time Vsystem has been run on a platform other than VMS/Alpha since Vsystem was first introduced at ATLAS.

The control system's primary relational database system is Oracle Rdb, which runs on a VMS server. The method of access to this system, most often used by the operator, is a second relational database system called Paradox. This PC-based database system retrieves data from the Oracle Rdb database via

Ethernet and archives accelerator parameters for individual experiments. Paradox provides an inexpensive graphical view of these archived parameters and can be used to restore the accelerator to a previous configuration. Recently this system has been upgraded to Version 9.0 the current offering of this product.

The control system intranet and WEB site that was established last year now has expanded features. Using a standard WEB browser, links provide the user access to data stored in the control system's Oracle Rdb relational database, an on-line control system manual, and a "bulletin board" describing recent changes to the control system.

A sampling of new or upgraded processes include a new "Tandem Calculation" process that performs much like a calculator, a new process and interface that scales beam line devices with energy changes, a new process that enables the selection of one magnet for a "fast scan" mode of operation for gauss meter readouts, and a new process and interface to control a new solenoid located in the post SCM beam line that is used for the latest radioactive beam experiments.

b.5. ATLAS Cryogenic System (J. R. Specht, S. W. MacDonald, and R. C. Jenkins)

The cryogenics group has continued to provide support to both the ATLAS accelerator and the SRF groups. Our responsibility is to provide the required cooling to all the accelerator superconducting components as well as providing many cool-downs and operations for tests using the test cryostat.

The model 1630 liquid helium refrigerator was removed from the ATLAS cryogenic system. This allowed its internal adsorbers to be replaced and internal heat exchangers to be flushed and cleaned with solvents. The refrigerator was then reinstalled. A planned ATLAS shutdown, for the removal of Gammasphere, provided the time required for this maintenance activity. The refrigerator had been in continuous use for 15 years.

Because of the required maintenance to keep the model 1630 operating, a replacement refrigerator using turbine expanders instead of pistons is desired. A model 2800 and three compressors were located at Lawrence

Livermore National Laboratory. These units were about to be removed from their facility because of programmatic needs changes. We helped remove the equipment and shipped it to Argonne. Presently we have two similar model 2800 refrigerators operating. The model 2800 refrigerators use turbine expanders instead of pistons and provide additional cooling capacity. This would reduce maintenance and thus increases accelerator operation time. The planning for this installation will be done next year.

Partial installation of a computerized vacuum readout system was installed this year. When completed next year, the system will monitor all LHe and LN₂ distribution line vacuums. Individual, outdated, and expensive readouts are presently installed in a few locations, which have proven to be very useful. The new expanded readout system will also allow the readings to be consolidated into the existing ATLAS control system.

b.6. New Solenoid for the In-Flight Production of Radioactive Beams at ATLAS (R. C. Pardo, C. L. Jiang, K. E. Rehm, J. Specht, B. Zabransky, and A. Heinz)

In 2000 the 2.5T superconducting solenoid used in the in-flight radioactive beam program at ATLAS failed by developing an open state in the coil winding. Inspection of the device convinced us that it was not repairable and so a replacement solenoid, with a significantly higher field was procured. The new 6T maximum-field solenoid, made by American Magnetics, was received in February 2001.

Installation proceeded quickly and initial tests using a ¹⁷F beam made by the d(¹⁶O, ¹⁷F)n reaction were carried out in April 2001. Results confirmed the proper operation of the new solenoid. Total transmission appears to be slightly improved over the old solenoid. Most importantly is the increased focusing field available which allows improved performance for other RIBs at higher energies than could be adequately captured by the previous device.

b.7. Super-Conducting Resonator as Beam Induced Signal Pickup (S. Sharamentov, P. Ostroumov, B. Clift, R. Pardo, and G. Zinkann)

A new method which can be used for longitudinal tuning of super-conducting linac resonators has been experimentally tested both with the first few 48.5 MHz PII resonators and with a 97 MHz booster resonator. The new idea is to use a downstream super-conducting resonator as a beam-induced RF field detector. By changing accelerating conditions at an upstream resonator (varying the amplitude and phase

of the RF field) and measuring the amplitude and phase of the beam induced signal in a downstream resonator, one can get information which can be used to set the proper amplitude and phase in the upstream resonator.

An experimental implementation of this method for PII resonators is shown in Fig. II-6.

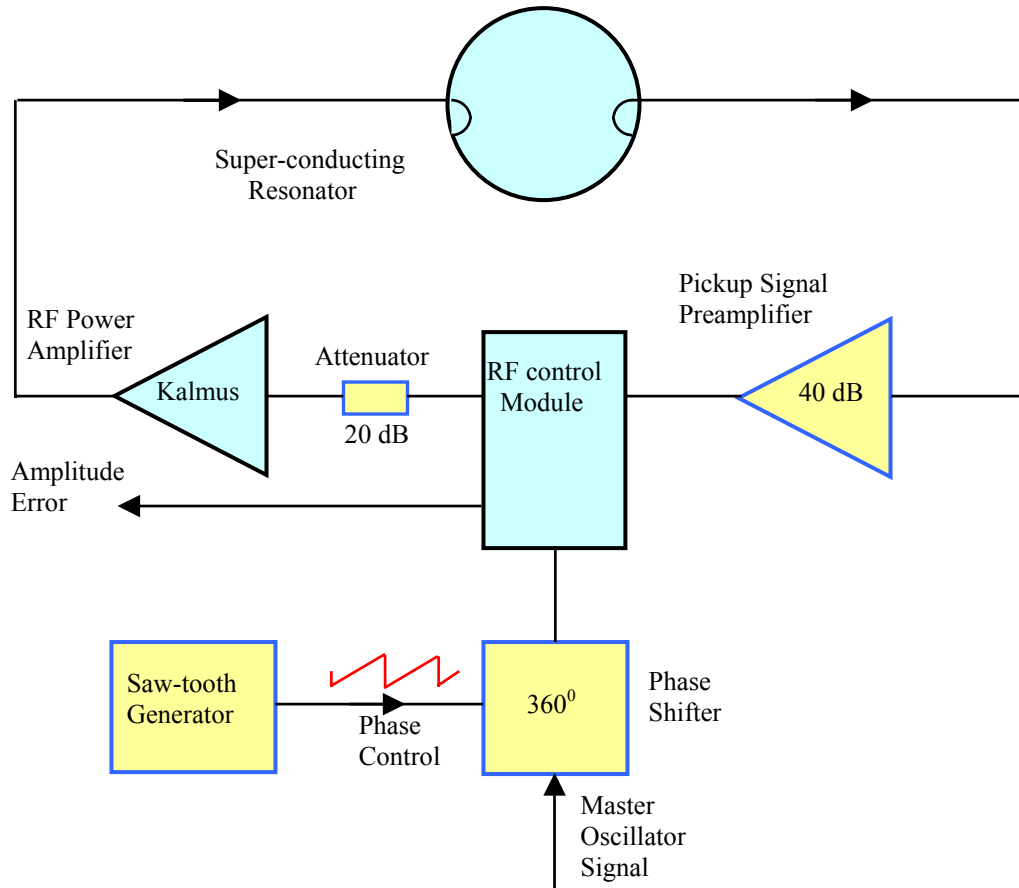


Fig. II-6. Experimental implementation of the new method. New elements designated in yellow color.

As in a normal accelerating configuration, the detector resonator works in a self-excited loop. An additional preamplifier with gain ~ 40 dB is added in the resonator pickup line that allows the amplitude, phase and slow tuner feedback loops to be locked at extremely low amplitude of the RF field. The low amplitude of RF field is necessary to prevent additional acceleration of the beam in the detector resonator. An external linear phase shifter, with 360° range, controlled by a saw-tooth shape signal is installed in the master oscillator

line. Parameters of the phase modulation are adjusted in such a way as to get continuous circular rotation of the RF field vector in the resonator, with 6-7 Hz rate. Because of the interaction between the rotating RF field vector and the beam-induced RF vector inside the resonator, an amplitude error signal in the amplitude feedback loop is also modulated. An example of this modulation is shown in Fig. II-7.

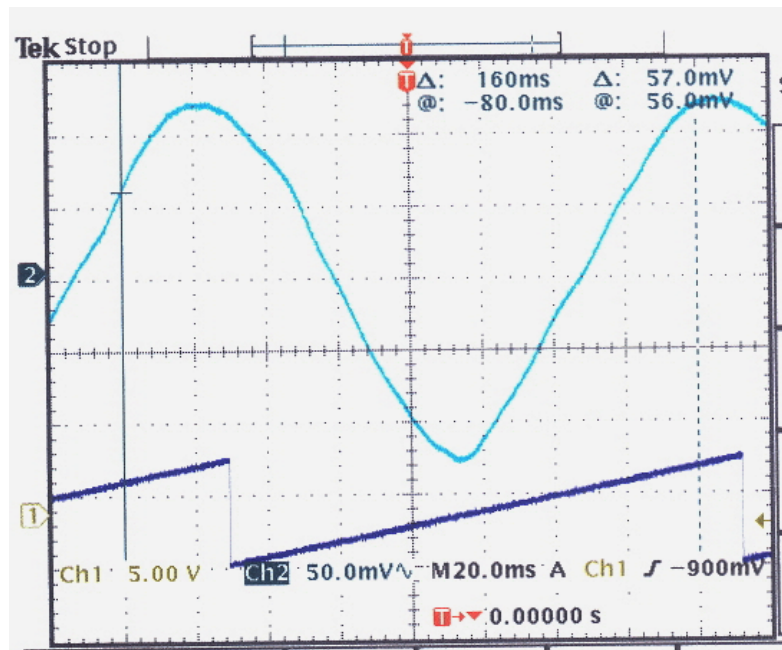


Fig. II-7. Amplitude error (top trace) and saw-tooth modulation (bottom trace) signals for R112 resonator.

Figure II-8. shows experimental results of the relative phase of the amplitude error signal for resonators R112, R113 and R114 as a function of resonator R111 RF field phase, for the $^{20}\text{Ne}^{8+}$ beam at energy of 1.99 MeV. An interpretation of the experimental curves is that the bunched beam gets maximum energy gain (maximum velocity) at R111 RF phase equals to $\sim 300^\circ$. In other words, the value of R111 RF phase 300° corresponds to a peak value of the sinusoidal RF field.

These first experimental results, using a downstream resonator as a detector of the beam induced signal, show that this method can be successfully used for tuning the first few PII resonators. The next steps will be to modify the electronic hardware and elaborate on the setup configuration to make the measurements a routine procedure.

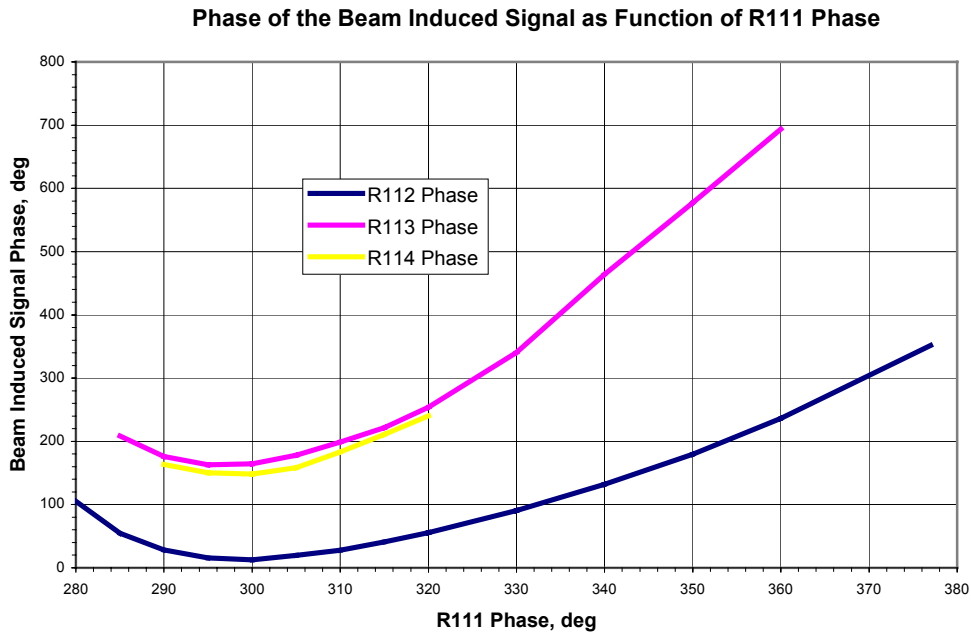


Fig. II-8. The dependence of the phase of the beam induced signal for R112, R113 and R114 PII resonator vs. R111 RF phase. R111 RF amplitude equals to 4.0 V.

b.8. Superconducting Surface Treatment (G. P. Zinkann, M. Kelley, M. Kedzie, and R. Jenkins)

A high-pressure rinse (HPR) using 1400 psi de-ionized water has been applied to 12 of the superconducting high-beta cavities in the ATLAS accelerator. The goal of this process is to restore past resonator accelerating field levels by removing accumulated particulates and water-soluble materials from the inner resonator surfaces.

The HPR application was performed in three stages. For the first stage, a high beta cavity (H29) was rinsed and tested in the Superconducting Research Facility's off-line test cryostat. The results of the HPR of cavity H29 are displayed in the Q curve in Fig. II-9. One sees a dramatic improvement in the maximum filed performance for this resonator.

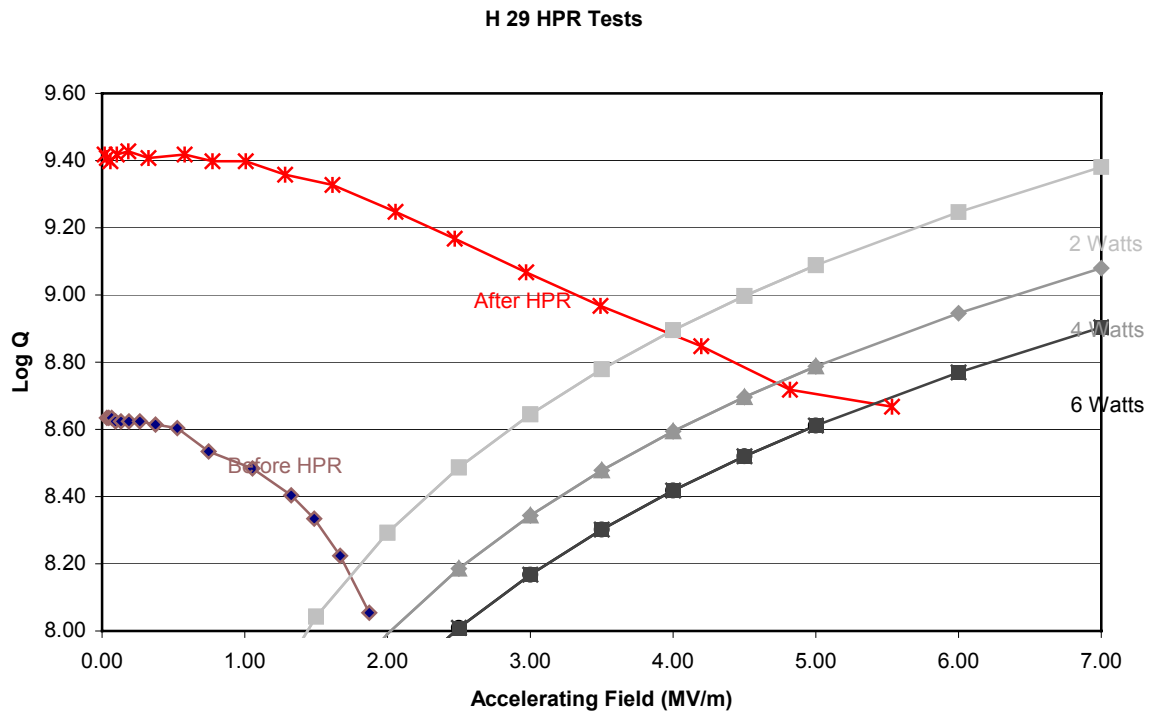


Fig. II-9. Resonator H-29 field performance before and after high-pressure water rinsing in off-lines tests before and after rinsing. The ATLAS cryogenic system is designed to have an average cooling capacity of 4 watts for each resonator.

Based on the successful results of this test rinse, all six high beta cavities in “C” Cryostat were removed and underwent the HPR process. After the HPR the total

accelerating field increased by 48.1%. The before and after results are listed in the bar chart in Fig. II-10.

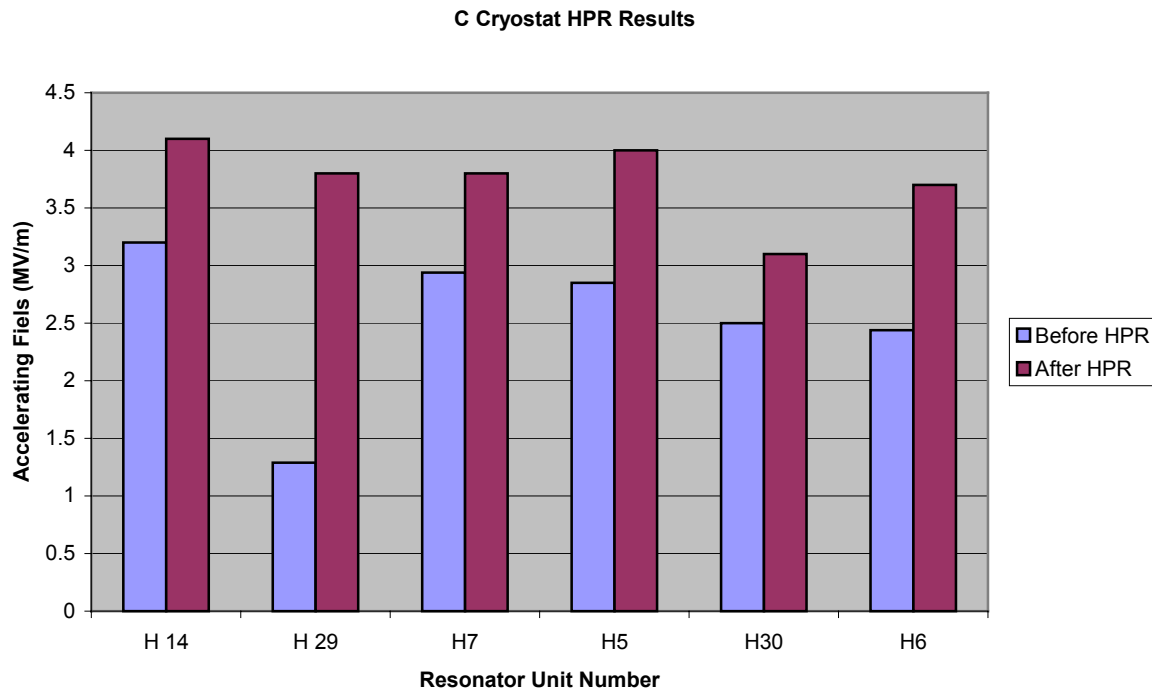


Fig. II-10. Maximum accelerating fields achieved by resonators in the Booster linac “C” cryostat before and after high-pressure water rinsing of the resonators.

The third stage of the rinse program has just been completed. Six resonators in “F” Cryostat have been removed from their cryostat and given the high-pressure rinse cycle. The evaluation of the accelerating field levels will be performed as the operating schedule

permits. At this time, only the first cavity has been conditioned and evaluated. The results for this cavity show an increase in operating field from 3.75 MV/m to 5.3 MV/m.

III. R & D RELATED TO A FUTURE RARE ISOTOPE ACCELERATOR FACILITY

OVERVIEW

The Rare Isotope Accelerator (RIA), a next-generation facility for basic research in nuclear physics, is a high priority for construction in the United States by the Department of Energy. The overall concept for RIA was developed during 1999 by the ISOL Task Force, a sub-committee of the Nuclear Science Advisory Committee (NSAC). A preliminary cost analysis of the RIA project was developed jointly by Argonne National Laboratory and the National Superconducting Cyclotron Laboratory of Michigan State University. The costs were reviewed by another subcommittee of NSAC in January, 2001. Based on this analysis and review the estimated construction cost (TEC) for RIA is \$644M in year 2001 dollars. It is possible that construction of RIA could begin in 2005 following various preliminary decisions and site selection. In the meantime, to prepare for construction on this time scale it is essential to continue a vigorous R&D program for RIA. This section is a progress report on the RIA R&D efforts at Argonne.

The RIA R&D topics addressed at Argonne during the year 2001 fall under four main categories: Heavy-ion Linac Technology, RIA Beam Dynamics, and Rare Isotope Production, Separation and Diagnostics, sections A-C below.

We have continued to develop and improve the baseline design for the RIA proposal. Highlights of developments during 2001 include:

- Successful operation of a prototype 345 MHz superconducting resonator continuously for 28 days at 7 MV/m accelerating gradient.
- Development of methods to refine drift-tube resonator designs to compensate for beam steering effects that are inherent in certain quarter-wave resonators.
- Extensive refinements of the beam dynamics simulations and improvements to the lattice of the RIA Driver Linac.
- Development of a novel new RFQ structure, called the hybrid-RFQ, to greatly improve the efficiency of the initial post-acceleration of radioactive species up to mass 240 from the 1+ charge state.

- Successful development of a bunch shape monitor with 20 psec resolution for heavy ions.
- Completion of the design of a novel adjustable-thickness, liquid-lithium target for use with heavy ion beams up to 4 kW for in-flight fragmentation at the NSCL A1900 fragment separator.



A. HEAVY-ION LINAC TECHNOLOGY

a.1. Superconducting RF: Prototype Superconducting Drift-Tube Cavities (K. W. Shepard, Joel Fuerst, Michael Kelly, and Mark Kedzie)

Three drift-tube cavities (Fig. III-1) covering a velocity range of $0.12 < v/c < 0.6$ are being developed for the RIA driver linac. Preliminary designs for a 115 MHz quarter-wave (QWR) cavity and a 172.5 MHz half-wave (HWR) cavity have been completed. The design

of a two-spoke 345 MHz cavity for RIA has been completed and construction of a niobium prototype has begun. Figure III-2 shows the niobium end-cap assembly for the two-spoke prototype cavity.

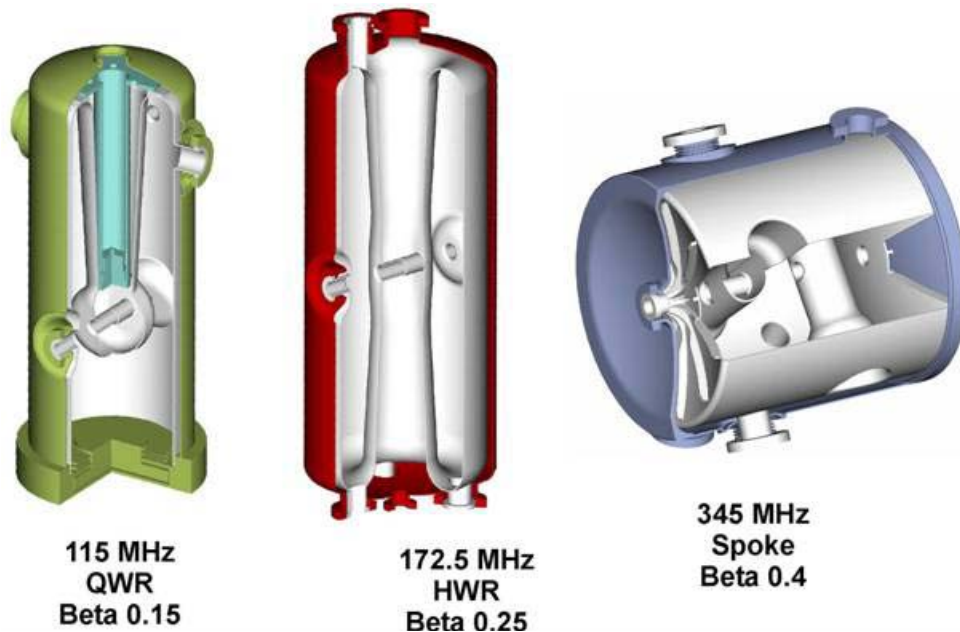


Fig. III-1. Cut-away section views of the niobium shell and stainless-steel housing of three drift-tube loaded cavities for the RIA driver linac



Fig. III-2. Niobium end-cap assembly for the prototype two-cell cavity after welding.

a.2. Superconducting RF: Test Facility Expansion (K. W. Shepard, Joel Fuerst, Michael Kelly, and Mark Kedzie)

The prototype 2-cell spoke cavity does not fit the vertical test cryostats located in the existing shielded

test area. A new cryostat has been designed to permit testing the 2-cell spoke cavity with separate cavity and

cryogenic vacuum systems. This will enable development of procedures to reduce particulate contamination of the cavity and increase operating field levels. The new cryostat (shown in Fig. III-3) can be extended to permit future installation of a

focusing/steering magnet adjacent to the resonator for possible tests with beam. Figure. III-4 shows the cryostat installed in a new resonator test cave constructed with a shield wall of high density concrete blocks.

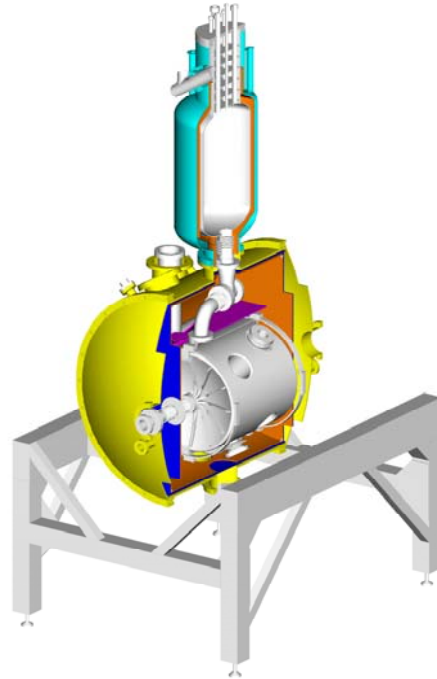


Fig. III-3. Horizontal cryostat assembly.

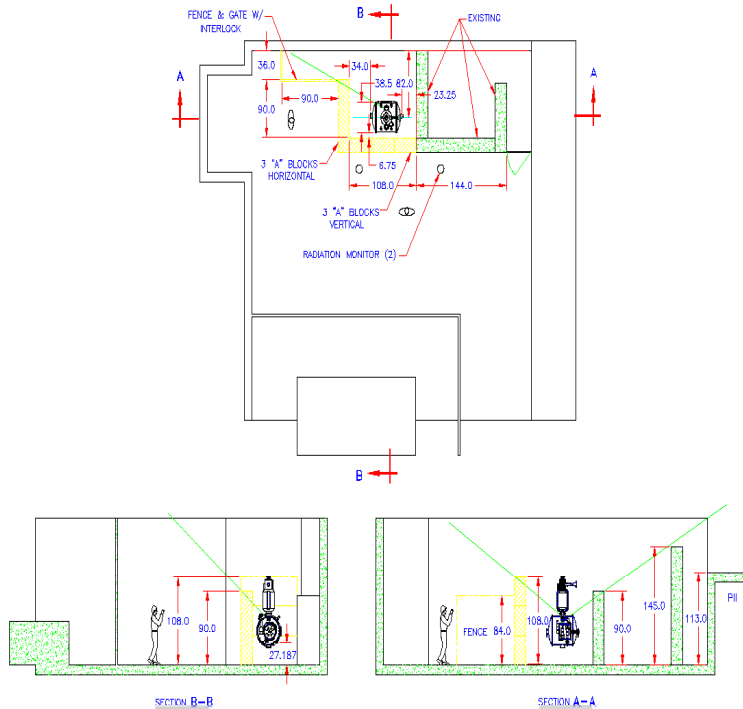


Fig. III- 4. Layout of new resonator test cave.

a.3. Superconducting RF: Steering Effects in Quarter-Wave Cavities (K. W. Shepard, Joel Fuerst, Michael Kelly, and Mark Kedzie)

Quarter-wave drift tube structures exhibit rf magnetic fields on the beam axis which steer the beam and can cause significant emittance growth. A method of

shaping the drift-tube to substantially reduce steering has been developed and will be tested in the prototype 115 MHz QWR cavity.

a.4. Superconducting RF: Upgraded Surface Processing and Single-Spoke Cavity Performance (K. W. Shepard, Joel Fuerst, Michael Kelly, and Mark Kedzie)

Figure III-5 shows the computer-controlled, automated high-pressure water rinse apparatus for cleaning and removing particulate contaminants from high-field niobium drift-tube cavities. The upgraded facility was used to process a $\beta=0.4$ 350 MHz niobium spoke cavity and obtain an accelerating gradient of 7 MV/m at T =

4.3 K and 10 W of input rf power as shown in Fig. III-6. The cavity was subsequently operated cw 24 hours/day for 28 days at 7 MV/m with no performance degradation, evidence that properly cleaned drift-tube cavities can operate at high fields for extended periods of time in a realistic accelerator environment.

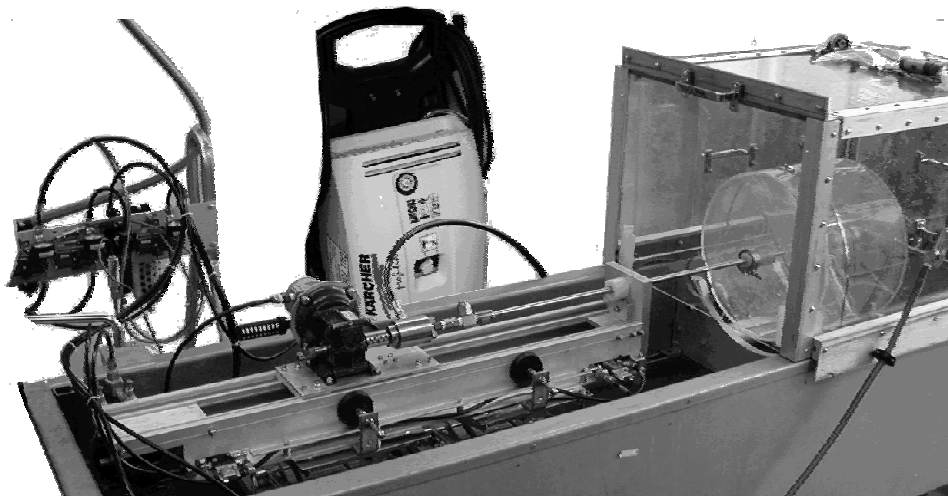


Fig. III-5. Automated, computer-controlled high-pressure water rinse apparatus.

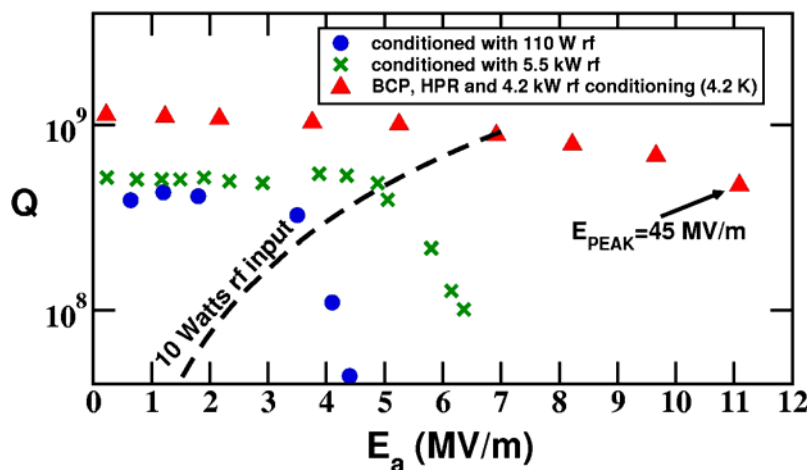


Fig. III-6. Performance of a 350 MHz single-cell spoke cavity after buffered chemical polish (BCP) and high-pressure water rinse using the upgraded facility.

a.5. RIA Cryogenics (J. R. Specht)

Major efforts this year were devoted to issues related to the liquid helium refrigerator, its loads and systems, and a distribution system. The cryogenic plant would be two times the size of the TJLab/CEBAF system and because of the variable load requirements, with an assortment of 2.0 K, 4.4 K, 35 K, and liquefaction loads, will require a complex and reliable cryogenic plant and distribution system.

Two separate vacuum insulated coaxial lines, a supply and return, will be used along all portions of the system. There are four types of lines used at RIA. These are tabulated below. All four types are similar in design, only the dimensions of the various parts change. Exact dimensions have yet to be determined for all the lines listed. Preliminary pressure drop calculations have been made using the mass flow for each line and the dimensions of the TJNAF/CEBAF lines. Some of the

lines will need to be made larger because of their length and the additional mass flow. Vacuum breaks will be installed at regular intervals along all of the distribution lines. This will provide isolation and allow for leak detection. The linac supply and return lines have the required bayonet ports, valves, and expansion/contraction built in at the appropriate spacing to match the various cryostat lengths. The LN2 distribution will use sub-cooled liquid to allow single phase liquid to be delivered to the various loads. The 2.0 K linac and 4.4 K linac return lines differ in the type and size u-tubes/bayonet used. Vacuum guarding is used in the 2.0 K sub-atmospheric returns along with larger u-tubes. The distribution system will accommodate cool-down, normal operation, and maintenance modes. Removable u-tubes will permit removal of cryostats for maintenance activities.

Line Type	Portion of coaxial line	Supply Line	Return Line	Length (m)
4 K linac	inner	4.4 K @ 3 bar He	4.4 K @ 1.5 bar He	259
	outer	80 K @ 3 bar LN ₂	80 K @ 1.5 bar N ₂	259
4 K CHR	inner	4.4 K @ 3 bar He	4.4 K @ 1.5 bar He	350
	outer	80 K @ 3 bar LN ₂	80 K @ 1.5 bar N ₂	350
2 K linac	inner	4.4 K @ 3 bar He	3.5 K @ 0.03bar He	316
	outer	35 K @ 5 bar He	50 K @ 5 bar He	316
2 K CHR	inner	4.4 K @ 3 bar He	3.5 K @ 0.03 bar He	28
	outer	35 K @ 5 bar He	50 K @ 5 bar He	28

The Central Helium Refrigerator (CHR) must be able to operate efficiently with different loads. Because the driver and post linac's ion and energy are variable, different loads will be presented to the refrigerator for

various accelerator requirements. In order to reduce the operating expenses, turndown capability will be required.

PLANT REQUIREMENTS	TEMPERATURE (K)	PRESSURE at LOAD (bar)	DESIGN	OFF-DESIGN
REFRIGERATION	4.6	1.50	5.0 kW	1.80 kW
REFRIGERATION	2.0	0.03	8.6 kW	0.60 kW
LIQUEFACTION	4.6	1.50	15 g/s	15 g/s
SHIELD COOLING	35	5	15.3 g/s	15.3 g/s

Tabulated here are the requirements for the refrigerator. Because of its large size, the cold box would be built in several sections. Cold box #1 would be an 80 K system while cold box #2 would contain the 4 K system. The cold compressors will be located in cold

box #3. This allows the 4.4 K portion of the cryogenic system to maintain liquid helium in the linacs if maintenance is required on the cold compressors. A system block diagram is shown in Fig. III-7. The cycle used for the refrigerator has yet to be chosen. There are

two major types to be considered to provide the sub-atmospheric 2.0 K portion: 1) cold-compressors only or 2) cold compressors along with room temperature compressors. Each of these methods has original hardware investment costs with an associated operating cost as well as operating advantages/disadvantages. An optimization of cost versus benefits will be necessary to determine which cycle is best suited to this project.

The total inventory of LHe in the RIA system is about 73,000 L. A 20,000 gallon dewar would provide an adequate storage capacity for the liquid, while eight 30,000 gallon warm storage tanks would provide a reasonable buffer for the gas management system.

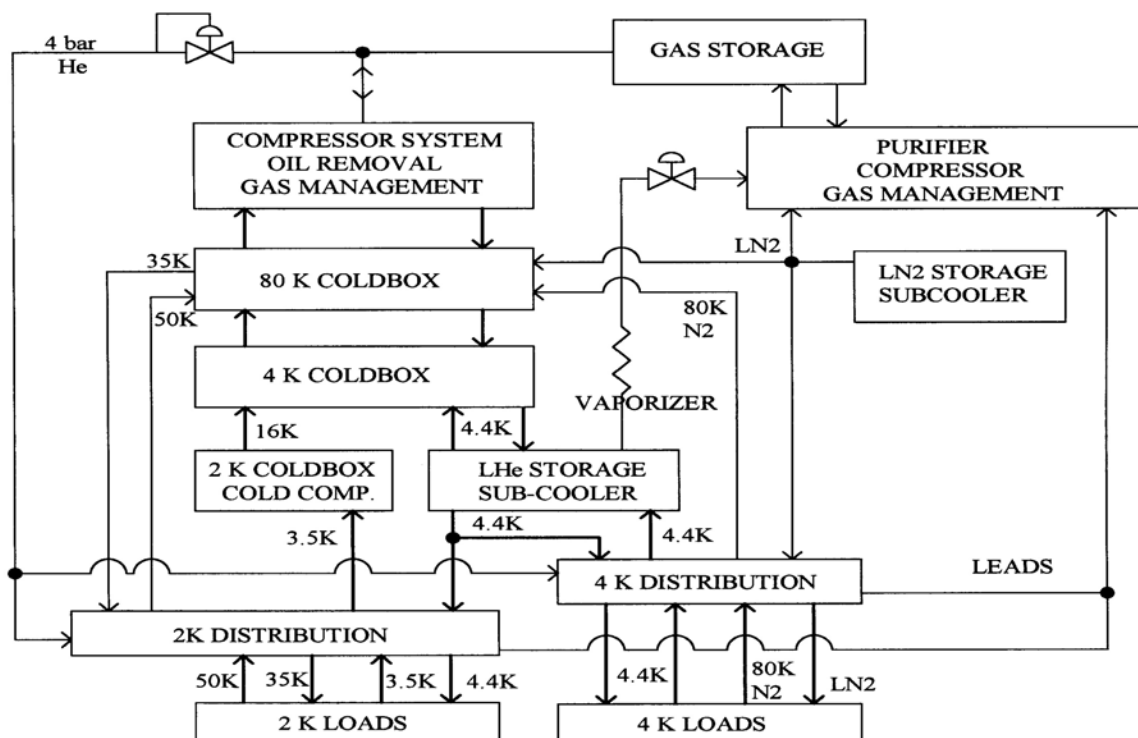


Fig. III-7. A block diagram of the RIA cryogenics system.

High reliability is a must for the RIA cryogenic plant. Because of the large capital cost for large refrigerators, a redundant or stand-by refrigerator may not be included in the initial construction. To improve the

reliability of the refrigeration system, several additional pieces of hardware will be required: 1) a reliable and flexible control system, 2) a warm gas purification system, and 3) a gas recovery system.

a.6. Development of a Superconducting Solenoid for the RIA Facility (P.N. Ostroumov, K.W. Shepard, and S.H. Kim*)

The beam dynamics of the drift tube section of the driver linac require a compact accelerating-focusing lattice. The use of SC solenoids together with SRF resonators within a common cryostat can solve this problem. The solenoids must have low fringing fields to avoid magnetic flux capture in the SRF resonators. Also, the compactness of the linac lattice can be increased by incorporating dipole steering coils together

with the SC solenoids in one magnet assembly. R&D work has been carried out to determine the feasibility of combining the three elements of high solenoid field, low fringe field, and integral dipole field into one compact package. A 9 Tesla magnet has been initially designed and prototyped, with the goal of eventually developing 14 Tesla solenoids of similar design. The most important design issues are 1) to minimize stray field in the RF cavity region using superconducting bucking coils and 2) to achieve adequate mechanical

*AOD Division, Argonne National Laboratory.

stability of the transverse dipole windings in the presence of forces produced by the solenoid/bucking coil assembly. The overall length of the prototype magnet assembly is 30 cm and includes a 9 Tesla solenoid formed from 4 coaxial sections, 2 coaxial bucking coils along the Z axis at each end of the solenoid, and a steering dipole producing 0.2 Tesla on the Y axis. An exploded view of the magnet assembly is shown in Fig. III-8. The bucking coils produce a low-field region, less than 0.1 Tesla, between 15 and 18 cm from the magnet center. Axial profile of the solenoidal magnetic field is shown in Fig. III-9. The racetrack coil is a constant current winding and located at 45 degree

with respect to X and Y axes. Dipole field distribution from the coil is uniform. Within 10-mm circle dB/B is less than 1% and within 12-mm less than 1.5%. The dipole field distribution in the XY plane is shown in Fig. III-10.

The assembly including terminals, switches and protection circuit are designed to fit inside a 25 cm diameter helium reservoir. The magnet assembly will be constructed in cooperation with TRIUMF (Vancouver, Canada) and tested at ANL.

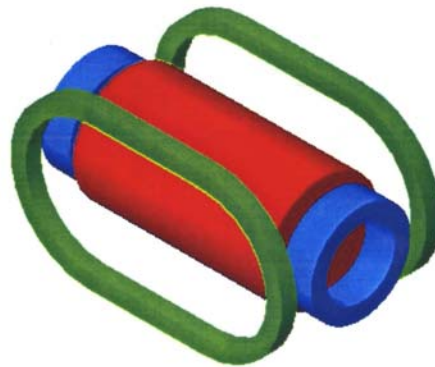


Fig. III-8. An exploded view of the superconducting magnet assembly containing solenoid, bucking coils and racetrack coils.

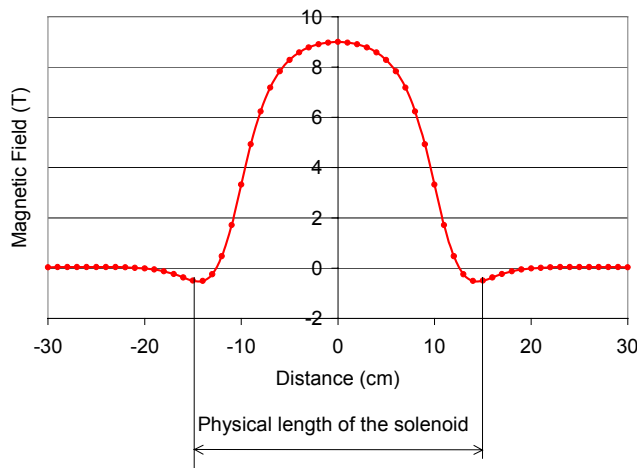


Fig. III-9. Profile of the magnetic field on the solenoid axis.

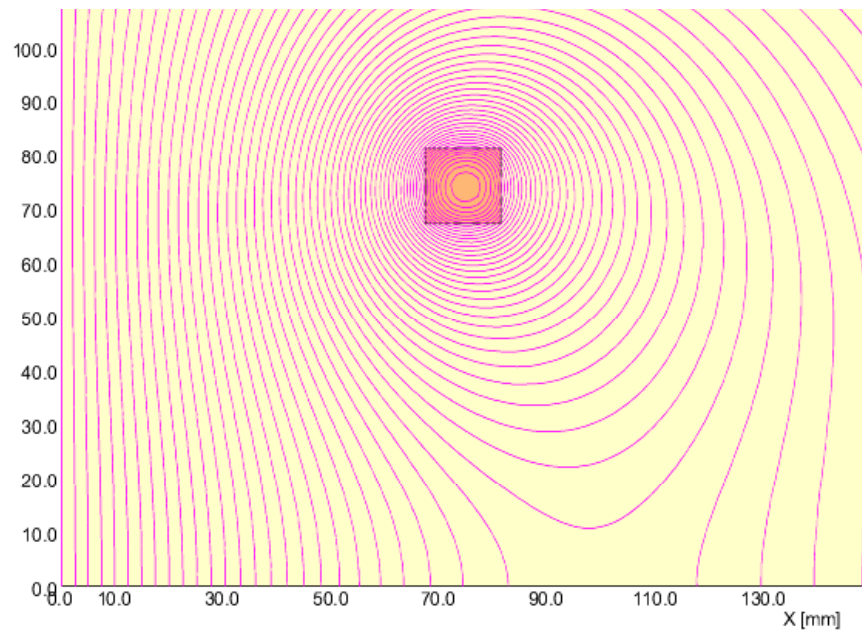


Fig. III-10. The magnetic flux lines of the racetrack coil are shown in the first quadrant. The coil-winding cross section is 14×14 with its center at $(x,y) = (74,74)$ in mm units. The magnetic field at the origin is 0.2 T @ 31.7 kA . The field uniformity within 10 mm from the origin is better than 1%

a.7. 57.5 MHz CW RFQ for the Driver Linac (P.N. Ostroumov and A.A. Kolomiets)

In the driver linac the initial acceleration of heavy-ions delivered from an ECR ion source can be effectively performed by a 57.5 MHz four-meter long room temperature RFQ. The principal specifications of the RFQ are: 1) formation of extremely low longitudinal emittance; 2) stable operation over a wide range of voltage for acceleration of various ion species needed for RIA operation; 3) simultaneous acceleration of two-charge states of uranium ions. CW operation of an accelerating structure leads to a number of requirements for the resonators such as high shunt impedance, efficient water cooling of all parts of the resonant cavity, mechanical stability together with precise

alignment, reliable rf contacts, a stable operating mode and fine tuning of the resonant frequency during operation. To satisfy these requirements a new resonant structure has been developed. This new RFQ structure provides 57.5 MHz resonant frequency within a tank of 0.56 meter diameter. Three-dimensional electromagnetic, thermal, and structural analysis of the structure have been completed, and a mechanical design based on a brazing technique is being developed. Figure III-11 shows 57.5 MHz RFQ resonant structure and engineering design of one section. The full RFQ will contain 6 such sections (see Fig. III-12).

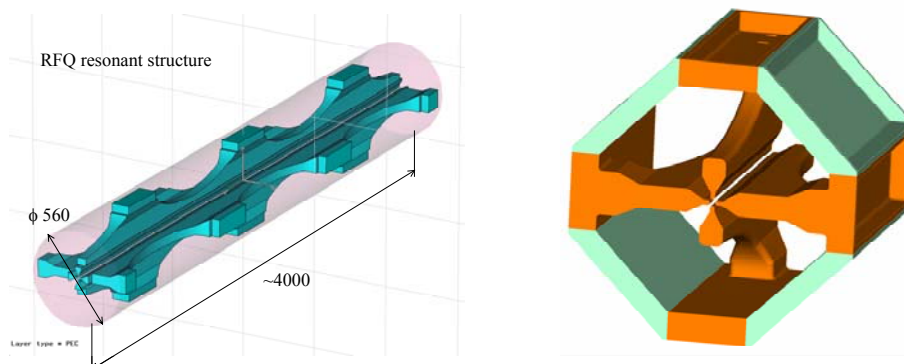


Fig. III-11. 57.5 MHz CW RFQ. On the left: computer model for electrodynamics simulations; On the right: engineering computer model of a RFQ section.

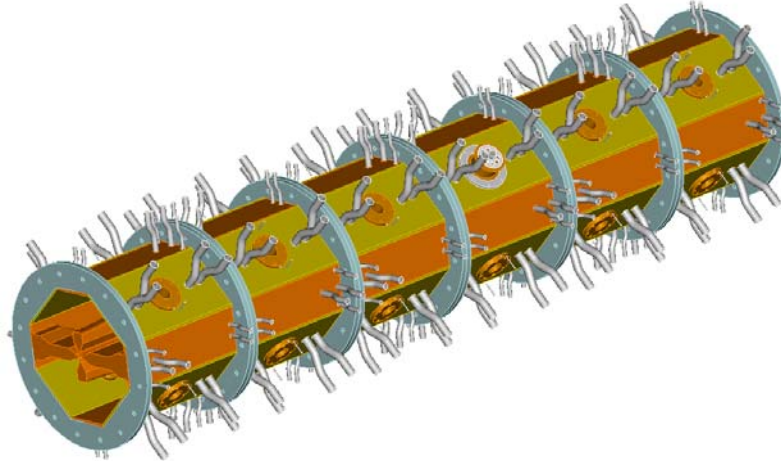


Figure III-12. Computer model of the RFQ final assembly, 6 sections.

a.8. 12.125 MHz Accelerating Structure: The Hybrid RFQ (P.N. Ostroumov, A.A. Kolomiets, J.A. Nolen, S. Sharma,* E. Rotela,* A. Barcikowski†)

Several resonant structures have been considered as candidates for the hybrid RFQ. The main specifications for our application are: 1) the structure length ~ 3.34 m is determined by the given input and output beam energies; 2) the structure should be mechanically stable; and 3) the shunt impedance should be high. Though split-coaxial structures have been used in several low frequency RFQs, the Wideroe-type structure better satisfies the abovementioned conditions. The side view of the accelerating structure used for the electro-dynamics simulation by the code Microwave Studio (MWS) is shown in Fig. III-13. An engineering model of the first section of the H-RFQ containing 13 drift tubes is shown in Fig. III-14. According to MWS the rf losses are 11.6 kW at 100 kV inter-vane voltage

in this copper resonator. The losses are lower than in split-coaxial RFQ of similar length because the total capacitive loading of the drift tubes is about half that of the four-vane structure. Due to the short length of the structure compared to the wavelength, a voltage distribution on all vanes and drift tubes is uniform which is confirmed by 3D simulations. For verification of electro-dynamics properties of the H-RFQ we decided to build a half-scale cold model. Figure III-15 shows general side view of the model during the assembly. Detailed study of the model with the goal of determination of final resonator dimensions, accelerating and focusing field distribution and coupling to the external power supply will be carried out in the near future.

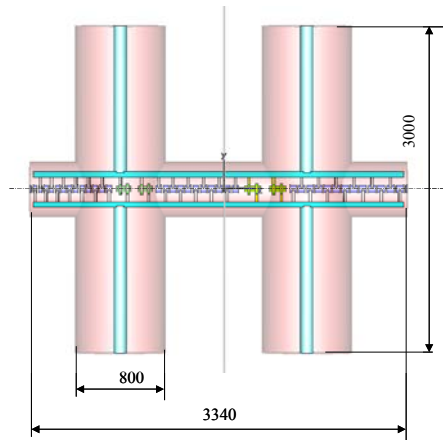


Fig. III-13. Side view of the hybrid RFQ accelerating structure. (Dimensions are in mm.)

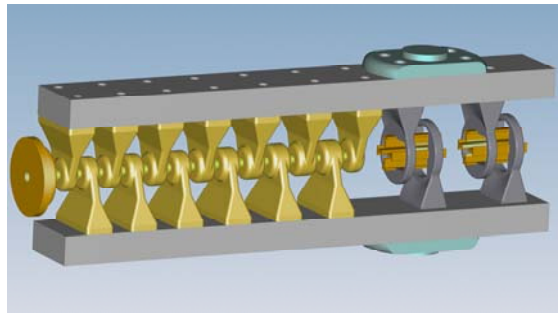


Fig. III-14. Computer drawing of the first section of the accelerating structure.

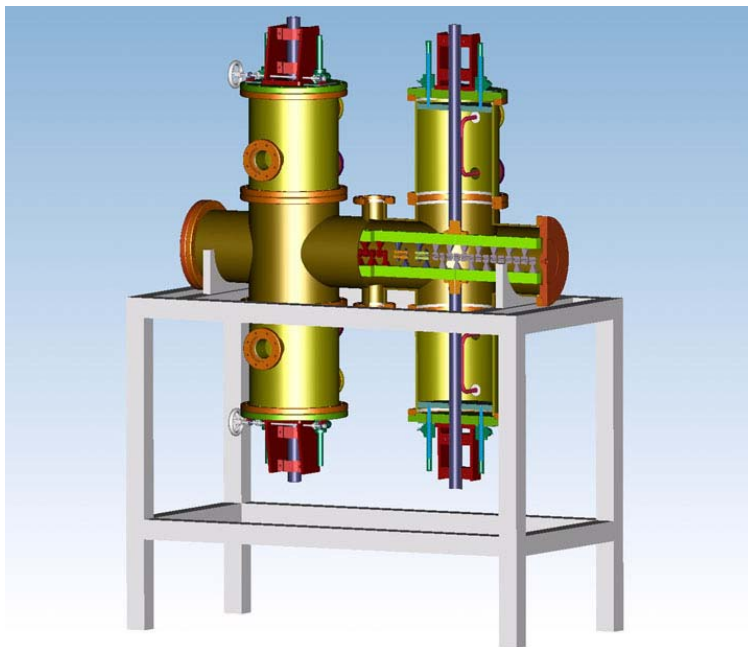


Fig. III-15. Computer drawing of the 12 MHz Hybrid RFQ half-scale cold model.

*AOD Division, Argonne National Laboratory.

†ASD Division, Argonne National Laboratory.

B. RIA BEAM DYNAMICS

b.1. Update of the Driver Linac Benchmark Design (P.N. Ostroumov, K.W. Shepard)

Significant progress has been made in beam dynamics design of the RIA driver linac. This linac will accelerate multiple-charge-states (multi-q) of the heaviest ion beams, for which the beam current is limited by ion-source performance. Beam dynamics studies have been performed with the goal of optimization of the linac structure in order to reduce a possible effective emittance growth of multi-q uranium beam. The location of two strippers naturally divides the linac into the three parts: low-, medium-, and high-beta sections. A detailed design has been developed for the focusing-accelerating lattice of the linac. The sources of the effective emittance growth have been identified. In longitudinal phase space main sources of the emittance growth are 1) multiplicity of charge states; 2) random errors of rf field; 3) passage of the stripper and 4) effect of higher-order terms in the field expansion in the multi-q beam transport systems. In the transverse phase space similar sources are 1) misalignments of SC resonators and focusing elements and their effect on multi-q beam emittance; 2) passage of the stripper and 3) effect of higher-order terms in the field expansion in the multi-q beam transport systems.

Long inter-cryostat spaces in the low- and medium- β sections will require the large stability area in the longitudinal phase space which can result in cavity setting at high value of synchronous phases. Therefore several important measures will be applied in order to minimize the length of the inter-cryostat spaces and to facilitate an impact of the drift spaces on the beam dynamics:

- The RFQ and multi-harmonic buncher are specially designed in order to provide very low longitudinal emittance of two charge-state uranium beam.
- Inter-cryostat space will contain only vacuum valves and a beam profile monitor. These devices will be designed for the lowest possible space occupation along the beamline.
- Beam steering coils will be combined with the SC focusing solenoids and will not require an additional space along the beamline.
- Standard accelerating SRF cavities can be switched to the mode of a beam phase monitor in order to set up phases and amplitudes of the accelerating fields in the upstream cavities. No space is required for beam phase monitors between the cryostats.
- Transverse matching between the cryostats is facilitated by the absence of the first SRF cavity in the very first focusing period of the cryostats. This focusing period incorporates inter-cryostat drift space instead of the SRF cavity.
- A special transition section is designed between the first two cryostats of low- β linac where beam energy is low and beam matching is extremely critical to the length of the drift space.

The effective longitudinal emittance of multi-q uranium beam oscillates along the linac sections as is shown in Fig. III-16 due to the slightly different synchronous phases of each charge state. The beam energy exiting low- and medium-beta sections should be selected in order to obtain the lowest effective emittance for the multi-q uranium beam.

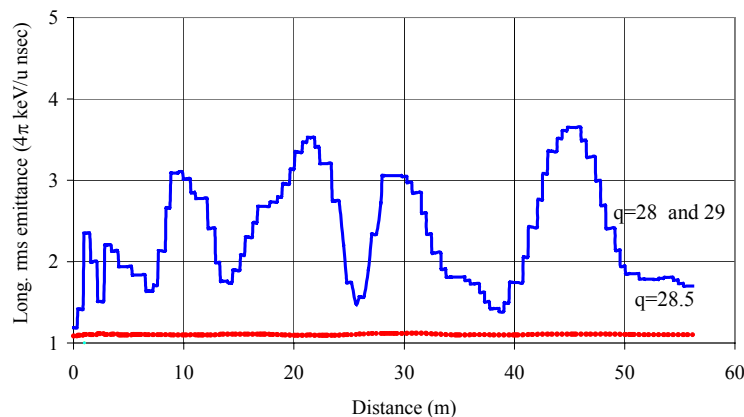


Fig. III-16. RMS longitudinal emittance variation of single- (the red curve) and two charge-state (the blue curve) beams along the low- β linac.

To insure all requirements can be met, we have numerically simulated the dynamics of multi-q uranium beams from the ion source, through the driver linac, all the way to the production targets. These simulations have been iterated repeatedly with the design for the overall linac architecture.

The code TRACK has been written in order to integrate charged particle motion in the presence of all components of the electromagnetic field. The electromagnetic fields in all types of SRF cavities were obtained from the code CST Microwave Studio (MWS). The TRACK code simulates multi-particle motion in six-dimensional phase space by an iterative solution of the equations of motion. The MWS code running on modern PCs can calculate all six components of electromagnetic field distributions within the beam-cavity interaction area with a mesh size less than 1 mm. The simulation of beam dynamics in the presence of all components of both electric and magnetic fields is essential in superconducting quarter-wave resonators (SC QWR). The driver linac will use more than 85 QWRs operating at 57.5 MHz and 115 MHz.

Beam dynamics simulation in each of the three sections of the driver linac included the following steps:

- Beam matching in transverse and longitudinal phase spaces for a trial beam with the mean value of charge-to-mass ratio. Simulation of the trial ion

beam to minimize beam sizes, to obtain smooth rms envelopes in transverse planes. The rms oscillations in longitudinal phase space due to the effect of inter-cavity drift spaces were minimized but not eliminated completely. In the parts of the linac the synchronous phase is equal to -30° , which produces a large linear region for the beam size oscillations. Therefore the longitudinal emittance of the trial beam does not grow.

- Simulation of a multi-q beam. Final determination of beam energies at stripping foil and total required number of the cavities.
- Beam dynamics simulation of the multi-q beam under the effect of random errors both in transverse and longitudinal phase space.

The simulations, which include misalignments of focusing and accelerating elements and random errors of the rf fields, show that beam emittances are well within the six-dimensional acceptance of the driver linac. The results of this simulation are summarized in Fig. III-17. The latter shows longitudinal phase space plot of 400 MeV/u multi-q uranium beam including all errors of rf field and amplitude along the whole linac. As is seen the multi-q uranium beam can be accelerated up to 400 MeV/u within $\pm 0.25\%$ of energy spread and remains within $\pm 10^\circ$ phase width. The longitudinal effective emittance $75.8 \pi \cdot \text{keV/u-nsec}$ contains all particles shown in Fig. III-17.

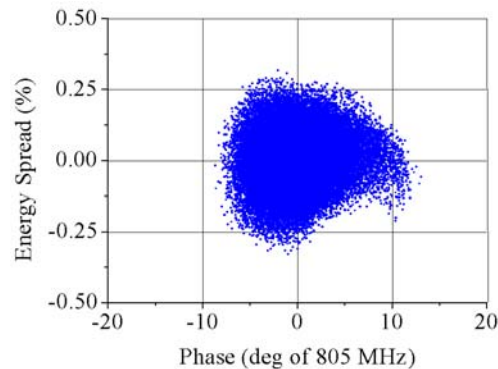


Fig. III-17. Longitudinal phase space plots of a four charge state uranium beam at the exit of the driver linac.

b.2. Low-Charge State Heavy-Ion Beam Dynamics in the Hybrid RFQ (P.N. Ostroumov, A.A. Kolomiets, N.E. Vinogradov)

A design has been developed for a low charge state injector for the RIB linac to provide for the post-acceleration of singly-charged beams as heavy as uranium. A RIB linac will accelerate heavy ions in the mass range 6 to 240, initially with charge state 1+. The acceleration of slow, low-charge-state heavy ion beams

is a difficult problem. A device that can be utilized is a conventional RFQ accelerator. The rf electric fields of such devices are very effective at focusing heavy ions, but the longitudinal electric field provided only by the vane modulations makes it an inefficient accelerating structure. For low velocity ions the structure must

operate at a low rf frequency leading to a very large and expensive structure. To overcome this drawback we proposed a hybrid accelerating structure that is formed by an alternating series of drift tubes (DTL) and RFQ sections. In such a structure the accelerating and focusing functions are decoupled. An unmodulated four-vane RFQ forms two sections each with length $\beta\lambda$ separated by a drift space $\beta\lambda/2$. The focusing strength of each RFQ lens with the length $\beta\lambda/2$ is adjusted and fixed by the aperture radius R_0 . A section of the RFQ with length $\beta\lambda$ acts as a “doublet”. The drift space between the “doublet” is necessary in order to ease the required electric field between the vanes. The whole focusing system works as a symmetric triplet. At higher q/m lower focusing gradients are required and it can be shown that in such cases the RFQ triplet can contain only three $\beta\lambda/2$ cells. A remarkable feature of the RFQ triplet is the lack of fringing field effects because the arrival time of beam bunches is synchronized to zero field at the edges of the RFQ vanes.

A hybrid RFQ (H-RFQ) operating at 12 MHz was designed for acceleration of heavy ion beams with $q/A=1/240$. The accelerating structure is ~ 3.4 m long and consists of three sections of DTL and two sections of RFQ. Each section of the DTL comprises 10 to 14

drift tubes. The RFQ sections comprise five $\beta\lambda/2$ cells and form a focusing triplet. The average accelerating gradient of the H-RFQ is about twice that of a conventional RFQ while the transverse acceptances are the same for both types of accelerator. Figure III-18 shows the accelerating efficiency of the hybrid RFQ compared to the conventional RFQ.

We have designed a cw H-RFQ for acceleration of singly-charged uranium in the front end of the RIB linac. For cw operation the peak surface field must be chosen very carefully. Our design is based on a 12 MHz accelerating structure with 100 kV between the drift tubes (DT) and RFQ vanes. The peak surface electric field occurs on the vanes of the first RFQ lens and it is 20% lower than in our previously tested 12-MHz split-coaxial RFQ structure. The surface field on the drift tubes is kept even lower by selecting long accelerating gaps.

The results of three-dimensional beam dynamics simulations in the H-RFQ performed with the DYNAMION code are shown in Fig. III-19. In these simulations 2D electric fields in the accelerating gaps are calculated with DYNAMION and 3D fields in the RFQs calculated with the SIMION code.

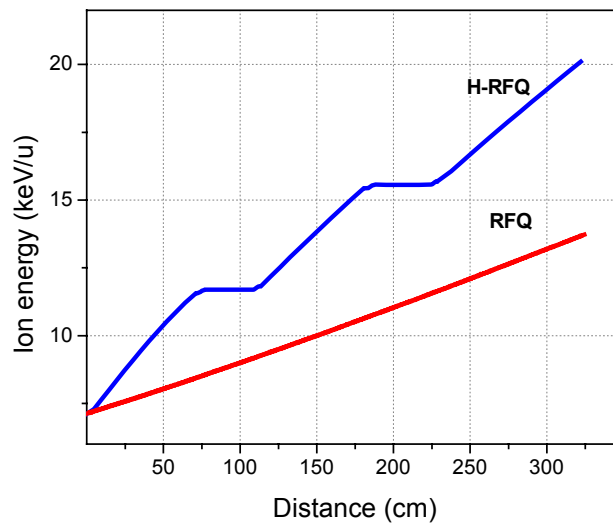


Fig. III-18. Beam energy gain in the hybrid and conventional RFQs. The structures have equal voltage between electrodes.

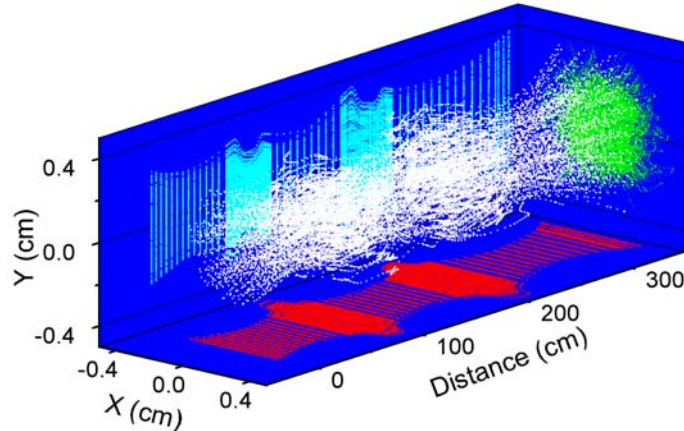


Fig. III-19. Particle trajectories along the H-RFQ shown in real space.

b.3. Correction of Beam Steering Effects in Low-Velocity Superconducting Quarter-Wave Cavities (P.N. Ostroumov and K.W. Shepard)

Superconducting cavities presently used for acceleration of ions in velocity range $\sim 0.01c$ to $0.3c$ are based on quarter-wave resonators (QWR). Currently there are several design proposals in nuclear physics laboratories for application of this type of cavity for acceleration of light and heavy ions. Particularly, the RIA project will use about 85 QWRs. The operating frequencies of the cavities range from ~ 50 MHz to 360 MHz to satisfy various specifications. Electrodynamics studies of the field distributions in the beam-cavity interaction area indicate appreciable steering components of both electric and magnetic fields, especially for higher-frequency cavities. The dipole fields induce beam steering, which is a strong function of rf phase and which couples the longitudinal and transverse motions. This can result in growth in the transverse emittance of the beam. Such steering effects are most pronounced for light ions. While simple steering, or displacement of the beam centroid, can be compensated by using standard, static corrective steering elements, the present case is complicated by the phase dependence of both the electric and magnetic fields. In a two-gap QWR the phase-dependence of steering for both the electric dipole field and the magnetic field is shifted 90 degrees from the accelerating field. This means that at typical operating RF phase angles, the steering is a strong function of RF phase and couples the longitudinal and transverse motion. As a result, the steering fields can, depending on the longitudinal emittance, induce appreciable transverse emittance growth. Such emittance growth can not be compensated by static fields and can be a particularly serious problem in applications for high-intensity light-ion beams.

We found that the steering can be largely compensated by two different methods. Simply offsetting the cavities by a few mm can often provide adequate compensation. In this method, available range of steering is limited by the reduction of useful aperture of the linac. This method does not require manufacture of new types of cavities and can be applied for heavy-ion accelerators dealing with $q/A < 1/3$ in the velocity range $\sim 0.01c$ - $0.15c$. More generally, steering can be largely eliminated over the entire useful velocity range by shaping the drift-tube and cavity-wall faces adjacent to the beam axis to provide appropriate corrective vertical electric field components.

The particular examples of two quarter-wave resonators operating at 57.5 and 115 MHz designed for the driver linac of the Rare Isotope Accelerator (RIA) facility were analyzed. We have numerically modeled the electrodynamic properties and field distributions using Microwave Studio (MWS). The distributions of E_z , E_y , and H_x on the axis of the 115 MHz QWR are shown in Fig. III-20. As is seen there is an appreciable magnetic field, ~ 60 G in the accelerating gaps. The TRACK code was used to simulate a section of the RIA driver linac containing forty-two 115 MHz cavities. Multi-particle simulation of uranium and proton beams was carried out in the linac with modified, steering-corrected QWRs. The results of proton beam simulations are shown in Fig. III-21. As is seen transverse emittance growth is almost completely eliminated.

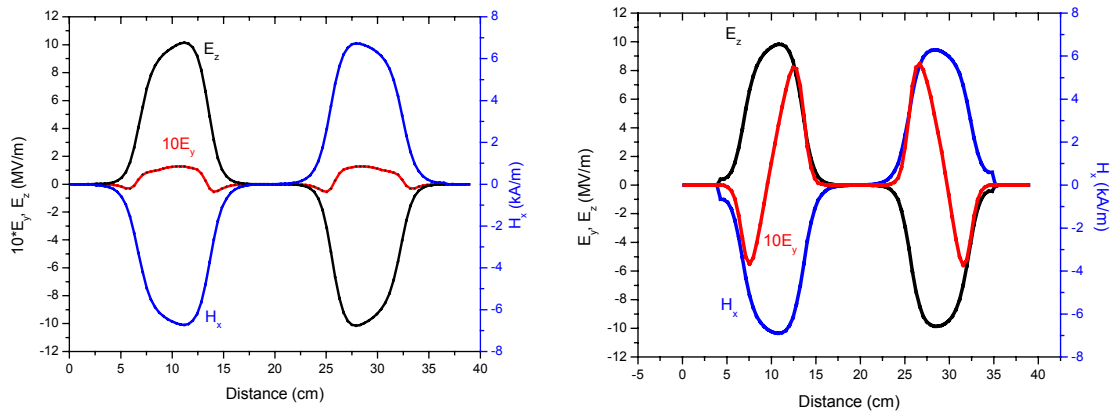


Fig. III-20. Field distribution along the axis of the 115 MHz QWR before (the left) and after (the right) the modifications to correct beam steering. For the clarity magnetic field is shown with opposite sign with respect to the electric field. The amplitude of E_y is multiplied by a factor of 10.

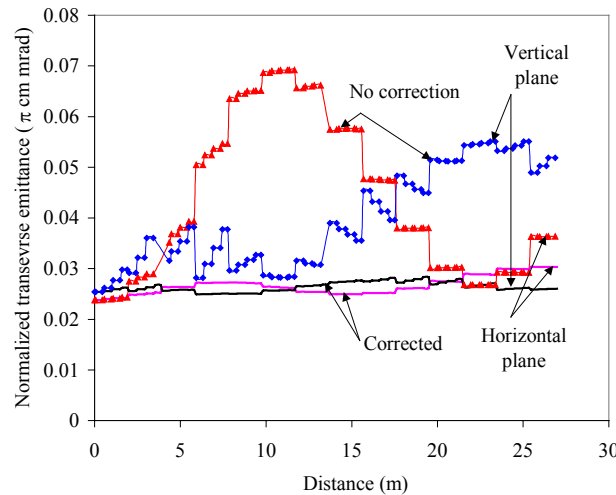


Fig. III-21. Transverse emittance growth in the section of driver linac containing 42 cavities of 115 MHz QWR with and without the compensation of beam steering effect.

b.4. Design of the RIA Driver Linac Switchyard (J.A. Nolen, V.N. Aseev, P. N. Ostroumov, and S. Kim*)

We have completed a preliminary design for a driver linac switchyard which can deliver beams to four production targets. Driver beam power of up to 400 kW will be available so that beam sharing between target stations is desirable. Design of the switchyard for the driver beams of RIA is a unique task due to the following features: 1) Distribution of various ion species accelerated to a wide range of energies to four target stations; 2) Delivery of beams to two target stations simultaneously; 3) Providing high quality beam optics with higher order corrections for multiple charge state beams to produce small beam spots at the entrance

of the fragment separators. A rf sweeper is used for beam delivery to two targets simultaneously. The rf-sweeper is followed by two DC septum magnets. A room temperature IH-type cavity operating at 115 MHz is proposed for the rf-sweeper and it provides four-milliradian beam deflection. Figure III-22 shows layout of the beam switchyard. Beam envelopes of a four-charge state uranium beam in the transport system from the linac exit to the fragmentation targets are shown in Fig. III-23. The multi-q uranium beam can be focused to a spot $X \times Y = 1.0 \times 3.0 \text{ mm}^2$.

*AOD Division, Argonne National Laboratory.

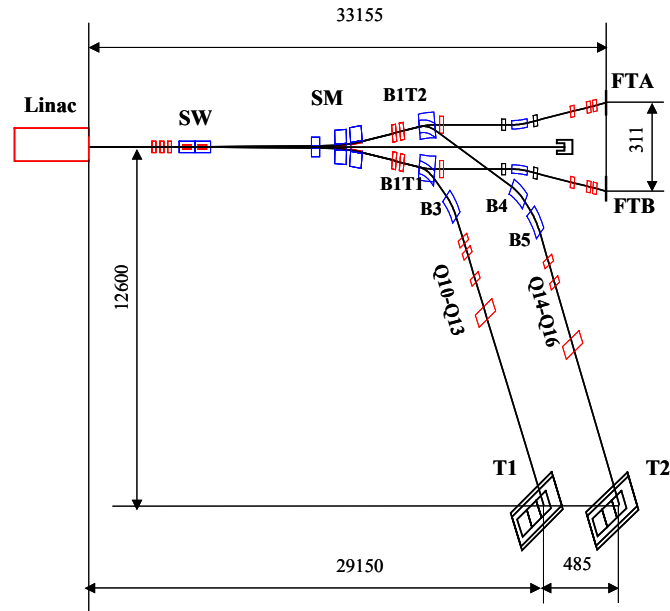


Fig. III-22. Layout of the driver linac switchyard. The distances are shown in mm. Legend: SW – rf sweeper; SM – septum magnets; BIT1, BIT2, B3, B4, B5 – bending magnets; Q10-Q13, Q14-Q16 – quadrupoles; FTA, FTB – fragmentation targets; T1, T2 – ISOL targets.

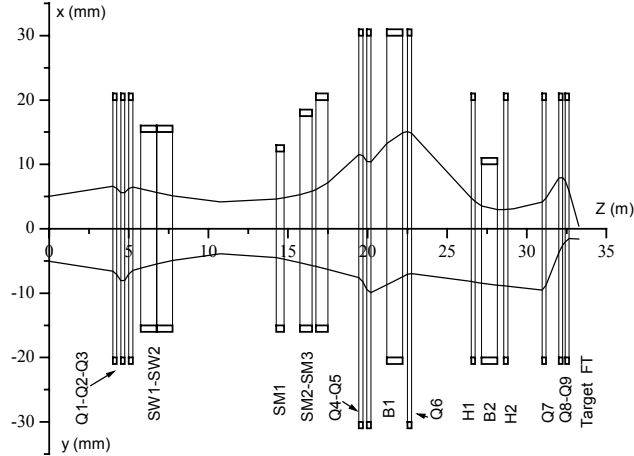


Fig. III-23. Multi-q uranium beam envelopes along the beamline from the linac to fragment separator targets FTA and FTB.

C. RARE ISOTOPE PRODUCTION, SEPARATION, AND DIAGNOSTICS

c.1. Bunch Shape Monitor for CW Heavy-Ion Beams (P.N. Ostroumov, P. Billquist, R.C. Pardo, M. Portillo, S. Sharamentov, N.E. Vinogradov, and G.P. Zinkann)

A new device for the measurement of CW heavy-ion beam time profiles with ~ 20 picosecond resolution has been constructed and successfully commissioned at ATLAS. Figure III-24 shows the general view of the BSM located ~ 3 m downstream of the Booster. The Bunch Shape Monitor (BSM) is based on the analysis of secondary electrons produced by a primary beam hitting a tungsten wire to which a potential of -10 kV is applied. In a BSM the longitudinal distribution of charge of the primary beam is coherently transformed into a spatial distribution of low energy secondary electrons through transverse rf modulation. This modulation is provided by a 97 MHz rf sweeper. The distribution of secondary electrons is detected by a chevron MCP coupled to a phosphor screen. The signal image on the screen is measured by using a CCD camera connected to the PC. Several test measurements have been done. First, a prebunched low energy (30

MeV) oxygen beam from tandem was transported to the BSM location. The FWHM of the bunch width was measured at the level of 2 nanoseconds. Recent measurements were done for an 80 MeV neon beam accelerated in the Booster. Typical beam currents in these measurements was from several pA to 100 pA. The longitudinal profile of the 80 MeV neon beam is shown in Fig. III-25. The resolution of the BSM depends from rf power in the sweeper. For this particular measurement the resolution was 30 picoseconds and the pulse width is 260 psec as shown. At this moment the time resolution is restricted by the background noise. It seems that this noise is caused by low energy secondary electrons produced by ions on beamline components and the residual gas. Additional measures to eliminate the background noise are being studied.

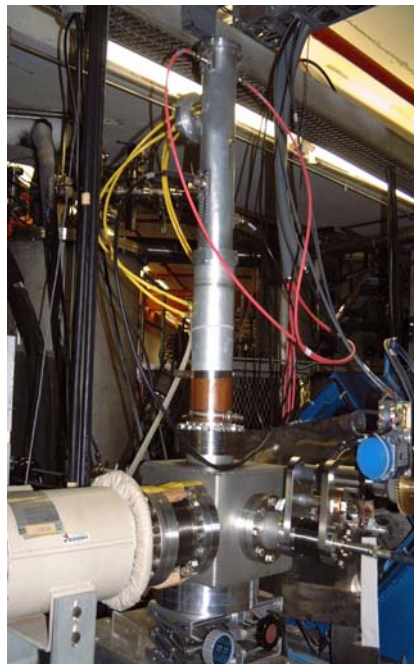


Fig. III-24. Bunch Shape Monitor installed at the exit of the Booster.

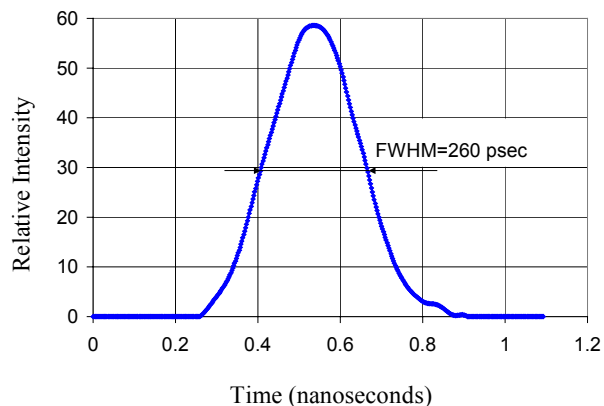


Fig. III-25. Longitudinal profile of 80 MeV $^{20}\text{Ne}^{8+}$ (the background noise is subtracted).

c.2. Assessment of the Radioactive Inventory Produced by the Current RIA Target Designs (I.C. Gomes and J.A. Nolen)

The Rare Isotope Accelerator (RIA) will produce besides the isotopes of interest by-products that will constitute a radioactive inventory in the facility. The large majority of these by-products will be produced in the target material during beam bombardment. The assessment of the radioactive inventory is important to classify the facility based on the Hazard Class Limits from DOE-STD-1027-92. During the assessment of the radioactive inventory a few assumptions were made, such as:

- a) All by-products produced during irradiation would stay in the target for the full length of the irradiation;
- b) That the target configuration is feasible meaning that the amount of target material would be compatible with a real target configuration;
- c) That there is no accumulation of inventory meaning that all radioactivity produced is carried to an outside repository when the irradiation ends; and
- d) That other materials inside the target cell would have negligible contribution to the radioactivity inventory.

The analysis was carried out for two-step, direct, and fragmentation targets. The two-step target was

composed of a primary 9-cm long, 1-cm diameter tungsten target and a secondary hollow cylinder 15-cm long with 2-cm internal diameter and 11-cm external diameter $2.5\text{g}/\text{cm}^3$ UC target. The direct target was $5\text{g}/\text{cm}^2$ UC target with a large copper beam-stop. Both the direct and two-step target were bombarded by 1.2-GeV deuteron beam. The fragmentation estimate was selected by considering the worst combination of a heavy ion beam with a lithium target. It was found that the two-step target produces the highest radioactive inventory among the configurations studied. Also, it was found that the fission product ^{131}I is the most offending isotope relative to the regulations. The calculations have shown that RIA is most likely to be classified as a Class 3 nuclear facility for the target cells and an accelerator facility otherwise.

Figure III-26 shows the ratio of the radioactive isotope accumulated for the two-step target during irradiation to the Class-3 inventory limit based on the DOE-STD-1027-92. It can be noticed that a large number of radioactive products are generated, however, just a few are produced in significant quantity. Table 1 shows the ratio to the Category-3 and Category-2 limits of those isotopes from the direct-target configuration with the largest ratios. Table 2 presents the same data as Table 1 for the two-step target. None of the isotopes is expected to have an inventory greater than the Category-2 limit.

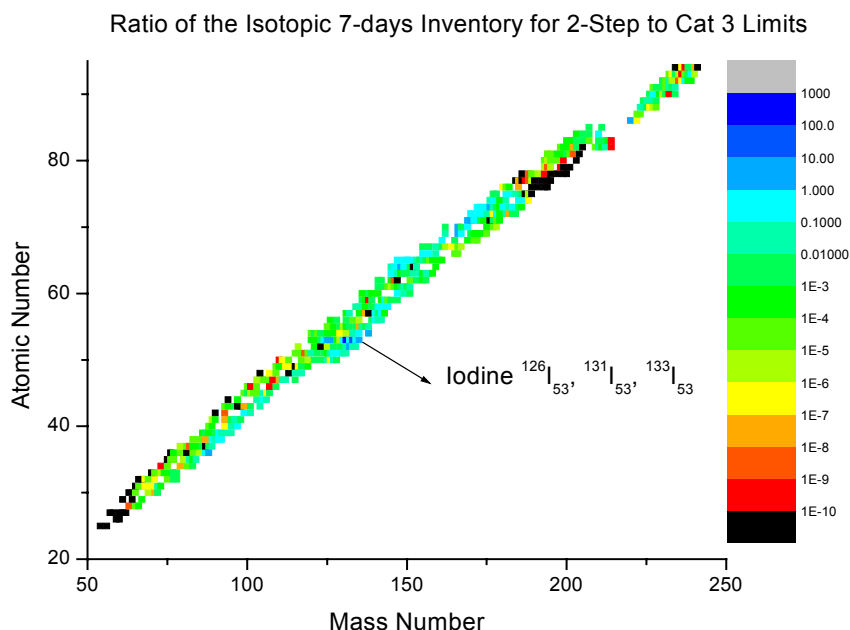


Fig. III-26. Ratio of the isotopic inventory accumulated after 7 (seven) days of continuous operation of a two-step target in RIA (1.2-GeV deuteron beam on tungsten with UC-2.5g/cm³ as secondary target) to the DOE Category-3 inventory limit.

Table 1. Ratio (of the products that have surpassed Category-3 limits) to the Category-2 and Category-3 limits. Isotopes indicated as “N/A” have no limit set by the DOE for Category 2 for that isotope, however all of them are barely over Category 3 limits and they should not be of any concern.

Isotope	Cat-2	Cat-3	Isotope	Cat-2	Cat-3
P-32	4.341e-03	1.602	I-125	3.152e-04	1.351
Mn-52	4.594e-04	5.404	I-126	N/A	3.423
Co-56	N/A	1.601	I-131	9.036e-03	17.68
Co-58	N/A	1.389	I-133	N/A	2.167
Cu-61	N/A	2.251	Po-210	2.435e-03	0.449
Cu-64	N/A	9.497	Rn-220	N/A	1.464

Table 2. Ratio of the isotopes that have concentration above Category-3 limit to the Category-2 limits for the Two-Step Configuration.

Isotope	Cat-2	Cat-3	Isotope	Cat-2	Cat-3	Isotope	Cat-2	Cat-3
Kr-88	N/A	1.038	I-126	N/A	4.185	I-135	N/A	2.537
Te-132	N/A	1.088	I-131	0.162	316.3	Tm-166	N/A	2.488
I-125	0.00029	1.234	I-133	N/A	55.2	Ta-176	N/A	2.297

c.3. Implementation of Computer Codes for Use in the RIA Target Design Activities at the NERSC (I. C. Gomes and J. A. Nolen)

The National Energy Research Super-Computer Center (NERSC) is a computer center supported by the DOE for the research community. NERSC currently has the most powerful non-classified and third most powerful computer on Earth, a 3,328-processor IBM supercomputer. The use of the computers at NERSC for RIA design activities has been on a trial basis because of the highly parallel computer environment structure used at NERSC. Computer codes such as MCNP, CINDER and TRAC (Transient Reactor Analysis Code) were successfully implemented at NERSC but only MCNP was used for production calculations in parallel mode. In the future it is expected to have MCNPX running in parallel mode at NERSC to take advantage of the savings in turnaround time that parallel processing can provide. Monte Carlo computer codes are highly suitable for parallel processing because of the intrinsic independence between histories. Parallel processing allows several Monte Carlo random walks to be performed at different processors and the relevant information stored in a common tally array. The RIA activities have received good support from NERSC

through availability of computer time and some technical support but there is not yet a heavy use of these computers because of the need for NERSC compatible parallel versions of the codes. Efforts have been devoted to obtain parallel versions of the codes but unfortunately, the operational system used at NERSC is not considered a high priority among code developers at the present time. However, it is expected that with modest support some codes can be implemented at NERSC, such as the MCNPX and others.

Currently there is a continuous effort to implement codes and data libraries that can support RIA target design activities. Due to the nature of RIA it will be necessary to adapt several codes to produce necessary engineering design parameters for target assessment. Quantities such as rare isotope production, spatial distribution of heat deposition, radioactive inventory, among others have to be correctly estimated to avoid failure or poor performance of the targets. This is an on-going activity that is expected to grow as the design activities of RIA evolve.

c.4. Implementation of Photonuclear and Low Energy D-Li Capabilities for Target Design (I. C. Gomes and J. A. Nolen)

The capability of performing photonuclear analysis in ISOL type targets was implemented and tested at the NERSC and Physics Division computers. A set of photonuclear cross section data and the compatible MCNPX code was implemented and tested. The remarkable forward peaked distribution of photons created by the interaction of an electron beam with a heavy element target presents some attractive features for ISOL type of applications. The photonuclear cross section library was obtained directly from Dr. MacFarlane (Los Alamos National Laboratory) and it is a revised version of all photonuclear libraries created by an IAEA workgroup that included many countries. The cross section library is compatible with the MCNPX photonuclear capability and contains data for photofission of a few isotopes. The applicability of a 45-MeV electron beam hitting a 2.5-g/cm³ uranium carbide target for rare isotopes production was analyzed. The advantage that this system provides is the highly concentrated fission distribution. However, while the compactness of the target is a highly desirable feature, problems derived from the heat deposition profile seem to impose a difficult hurdle for this

approach. Figure III-27 displays the fission distribution profile for a 500- μ A electron beam with 45 MeV of energy hitting directly a solid uranium carbide cylinder with 2.5-g/cm³ density. The fission rates were multiplied by the volume of the each ring to provide a more realistic picture of the importance of each target region on the total fission production.

Another implementation was to introduce in the MCNPX code a double-differential cross section set for the deuteron-lithium interaction. The cross section data was introduced into the source routine of the code in such a way that neutron production by the interaction of deuterons with energy up-to 40 MeV with a lithium target can be simulated. The advantage of using MCNPX is that the nuclear models included in the code allow a more realistic transport analysis of neutrons generated with energy above 20 MeV. Figure III-28 displays the fission distribution inside of a 2.5-g/cm³ uranium carbide target irradiated by neutrons produced from the interaction of a 5-mA beam of 40-MeV deuterons with a lithium jet. The fission rate was multiplied by the volume of the ring providing a better

picture of the importance of each radial position of the target regarding fission production. It can be noticed that the fission production spreads across the target much more than the photon fission of

Fig. III-27. However the total fission generation and the heat deposition profile are more favorable than the electron-beam case.

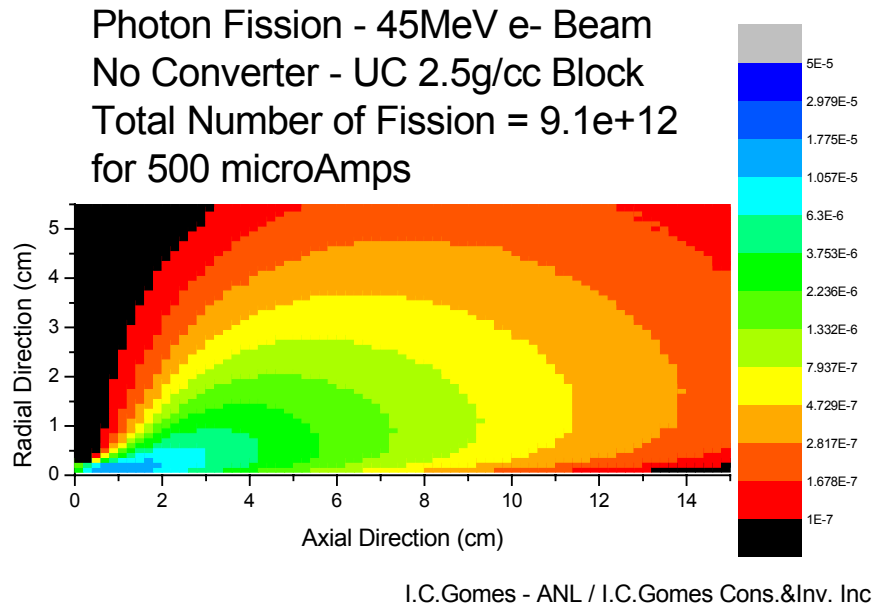


Fig. III-27. Fission Distribution profile for a 45MeV electron beam hitting a 2.5g/cm^3 UC target. The fission rates are multiplied by the volume of the ring segment represented by each cell of the geometric configuration.

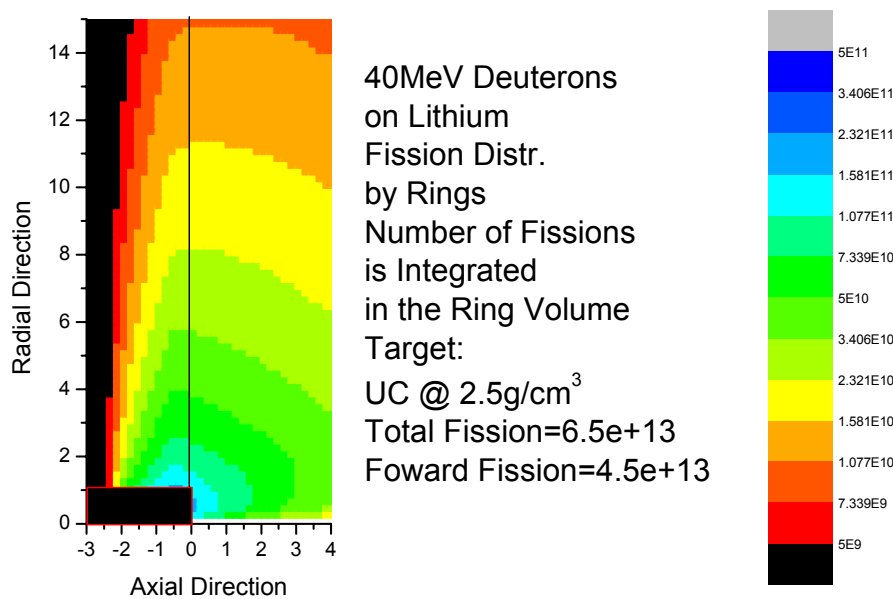


Fig. III-28. Fission Distribution profile for a 40-MeV, 5-mA deuteron beam hitting a lithium target. The produced neutrons induce fission in a 2.5g/cm^3 UC secondary target. The fission rates are multiplied by the volume of the ring segment represented by each cell of the geometric configuration.

c.5. Effusion/Diffusion Studies of ISOL Target/Ion Source Systems (B. Mustapha, J.A. Nolen, J.-C. Bilheux,* and G.D. Alton*)

In previous studies, we have shown that it is possible to characterize the release process and extract its important parameters by comparing simulated release curves to the experimental ones measured with a given target geometry for a given isotope. The extracted information can then be used to improve the efficiency

of existing targets and design new geometries more suitable to produce beams of rare isotopes. We report here on a more thorough study of the RIST target¹ and on the progress of the simulation of the ORNL target/ion source system used to measure effusion times of rare gases.²

RIST Target

A thorough study of the RIST target³ has shown that the diffusion coefficient (D) can not be determined when the decay of the considered isotope is faster than its diffusion through the target material, which is the case of most short lived isotopes. In this case data from the closest long-lived isotope can be used. For ⁸Li the best fit to the data was obtained for $D=10^{-8}$ cm²/s (measured for ⁷Li [Ref. 4] and a sticking time $t_s=0$ ns, but the data seems to be slightly faster than the simulation. In order to understand this discrepancy, two possible effects have been examined; first, a non uniform target

temperature and second, an electric field in the ionizer. The non-uniform temperature was simulated by adding a faster diffusion component and the electric field by shortening the ionizer length. A quite good fit was obtained by considering a 0.9 % contribution from a faster diffusion with $D=10^{-5}$ cm²/s, see Fig. III-29. A better fit was obtained, however, with a 2-cm ionizer length instead of the original 3.5-cm length, see Fig. III-30. To decide which effect is really acting (it could be both), dedicated measurements are needed.

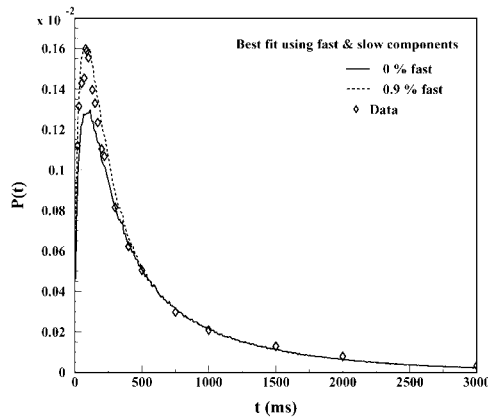


Fig. III-29. Best fit by considering a fast diffusion component.

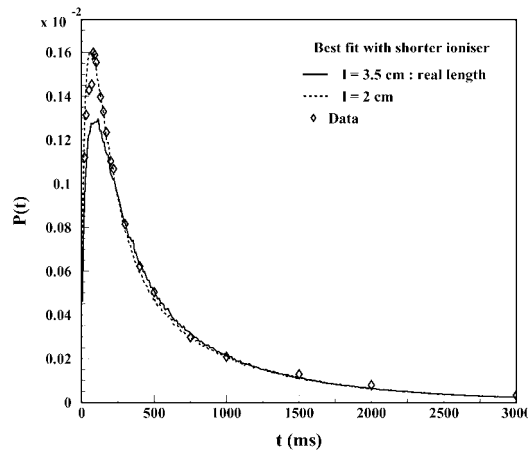


Fig. III-30. Best fit by shortening the ionizer.

ORNL Target/Ion Source systems

To better characterize the diffusion and effusion processes and avoid the uncertainty coming from the indetermination of D , we propose here to deconvolute the two processes and study them separately (the release process is the convolution of the diffusion and effusion processes). We report here on the progress of the simulation of Target/Ion Source systems used at Oak Ridge National Laboratory (ORNL)² to measure effusion times of some rare gases. Two different target geometries have been used at ORNL to measure effusion times of He, Ne, Ar, Xe and Kr at different temperatures. Data have been taken for both an empty target chamber and one filled with a Reticulated Vitreous Carbon Foam (RVCF) matrix.

We have implemented the geometry of their first system (serial coupling) for the empty target case and run the effusion part of the calculation. Figure III-31

shows the corresponding geometry and the track of one particle. The target tube is 19.3 cm long and 1.5 cm diameter. The connecting tube is about 10 cm long and 7.5 mm diameter coupling the target to an Electron Beam Plasma Ion Source (EBPIS). The output of the calculation is a number of collisions and a total path length for each event. We have found that on the average particles bounce 3000 times and travel about 24 m before exit the ion source. This output can be used to determine the effusion time for any isotope through the same system at any temperature.

The comparison of the simulation to the experimental data is in progress. This step is important to benchmark the effusion part of the calculation. Future studies of more reactive gases will permit the determination of sticking times for various gas and material combinations.

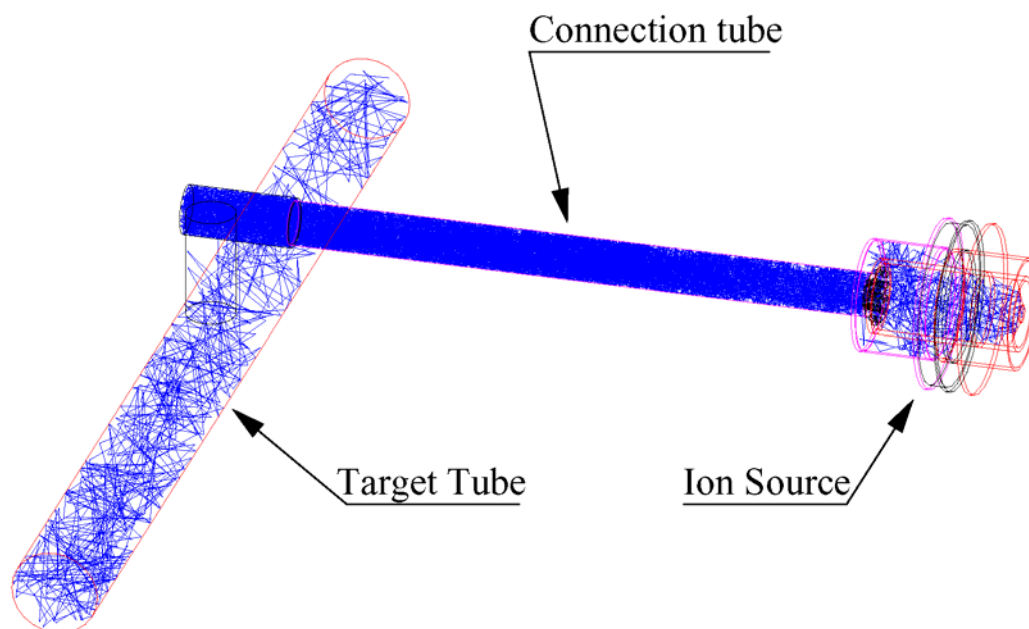


Figure III-31. Geometry of the first Target/Ion Source system (serial coupling) used at ORNL showing the track of one particle.

*Oak Ridge National Laboratory

¹J. R. J. Bennett et al, NIM B 126 (1997) 117.

²J. C. Bilheux and G. D. Alton et al, Proceedings of the 2001 Particle Accelerator Conference, Chicago.

³B. Mustapha and J. A. Nolen, EMIS-14 proceeding, to be published in Nuclear Instruments & Methods B.

⁴J. R. J. Bennett, private communication.

c.6. An Adjustable Thickness Li/Be Target for Fragmentation of 4-Kw Heavy-Ion Beams (J.A. Nolen, C.B. Reed,* A. Hassanein,† V. J. Novick,* P. Plotkin,* J.R. Specht, D.J. Morrissey,‡ J.H. Ottarson,‡ and B.M. Sherrill‡)

The need for a thick windowless liquid lithium target for use with high intensity uranium beams at next-generation radioactive beam facilities has been discussed.^{1,2} Lighter heavy ions at such high energy fragmentation facilities require thicker targets, in the 5-10 g/cm² range, which corresponds to 10-20 cm in thickness if pure lithium is used. Since the density of beryllium is about 4 times that of lithium, a hybrid

target using both lithium and beryllium was proposed.² A first-generation target of this type, for use with beam power of up to 4 kW, is currently under construction for use with beams from oxygen to calcium at the NSCL A1900 fragment separator.³ A schematic layout of this target concept is shown in Fig. III-32. The design of this target, which covers a thickness range from 0.7 to 3 g/cm², is described in this paper.

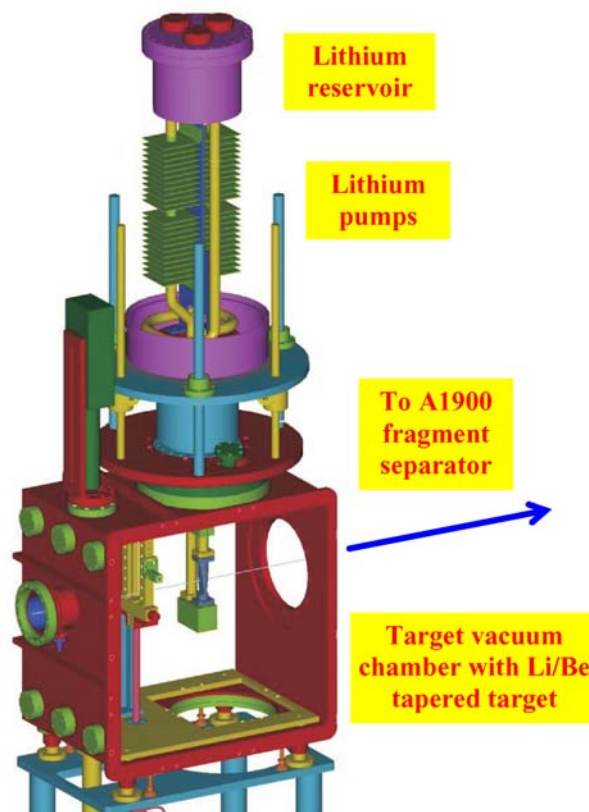


Fig. III-32. A schematic view of the target chamber at the NSCL A1900 fragment separator. The chamber is designed to accommodate the liquid lithium loop from above and a standard target ladder from below. The containment vessel is removed in this view.

At high energies there is relatively little influence of the target material on the distribution of produced fragments. In this case, low-Z target materials are preferred since the overall production rate is larger. Beryllium and graphite have been used extensively at existing fragmentation facilities. Lithium is also an appropriate choice for target material and, as discussed previously, is also an excellent cooling medium. A combination of beryllium and liquid lithium can be used to limit the total linear target thickness to

reasonable values. At the NSCL after the recently completed Coupled Cyclotron Upgrade,³ the most powerful beams are in the mass range between oxygen and calcium where beam power up to 4 kW is possible. For these beams a target thickness over the range from 0.7 to 3 g/cm² is a good match to the acceptance of the A1900. The hybrid-target spool piece designed to cover this thickness range is shown schematically in Fig. III-33.



Fig. III-33. A cutaway view of the beryllium target spool piece for the hybrid target. The beryllium entrance and exit windows vary from 1-mm thick at one end to 7-mm thick at the other. Lithium flows between the windows and is 5 mm thick. The overall target varies from 0.7 g/cm^2 to 3 g/cm^2 .

Three-dimensional thermal calculations of the temperature profiles in the entrance and exit regions of the target have been carried out using the HEIGHTS simulation program.⁴ The results of the simulations done for a ^{48}Ca beam at 160 MeV/u and 0.5 particle microampres at the thin end of the target (1-mm beryllium windows and 5-mm lithium thickness) are

shown in Fig. III-34. Corresponding results for an ^{16}O beam at 200 MeV/u and 1.0 particle microampers at the thick end (7-mm beryllium windows and 5-mm lithium) are shown in Fig. III-35. For these calculations a heat transfer coefficient of $20 \text{ W/cm}^2\text{-K}$ was used for the liquid lithium flowing at a velocity of 4 m/s.

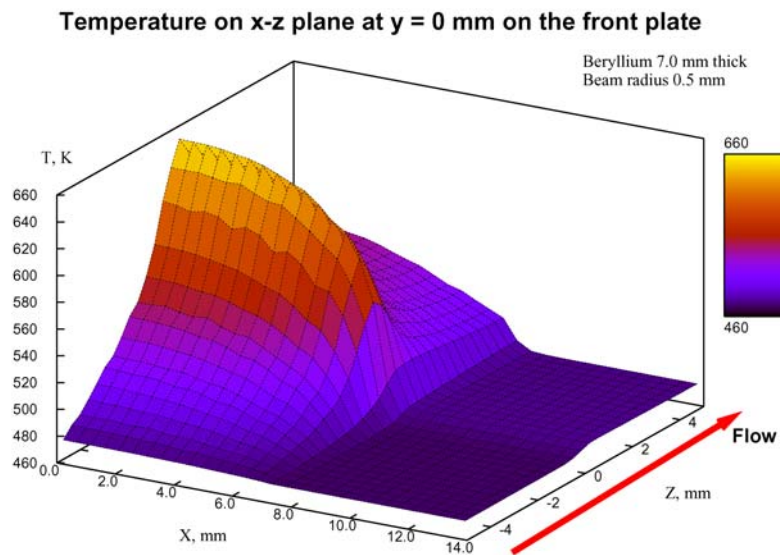


Fig. III-34. Three-dimensional thermal calculation of the temperature distribution in the beryllium window and flowing lithium for the case of a 200 MeV/u ^{16}O beam at an intensity of 1 particle microampere. The peak temperature is at the outside surface of the beryllium and is 660 K.

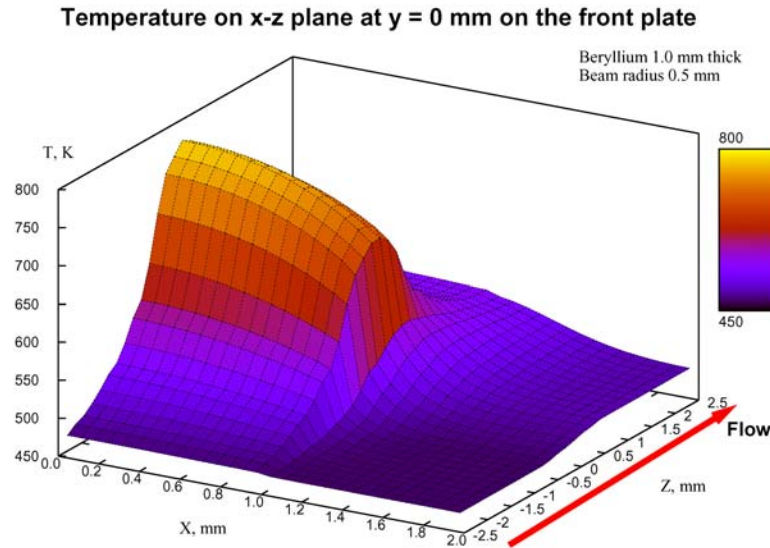


Fig. III-35. Three-dimensional thermal calculation of the temperature distribution in the beryllium window and flowing lithium for the case of a 160 MeV/u ^{48}Ca beam at an intensity of 0.5 particle microampere. The peak temperature is at the outside surface of the beryllium and is 800 K.

Pressure/flow requirements and pump design

The approximately 1-kW power dissipation in the target implies that only a relatively low volume flow rate, ~ 4 m/s, is required to keep the peak temperature rise in the lithium to about 100 °C. With a channel cross section of 5 mm by 10 mm in the target spool piece, the pressure drop across the target is only ~ 3000 Pascals. The liquid-lithium pump design and the pipe sizing of the lithium loop were chosen to be compatible with this target flow rate and pressure drop.

A DC, permanent magnet Lorenz-force type of pump was chosen for this application. This type and other

liquid metal pumps are reviewed in a NASA report.⁵ Because of the operating temperature of ~ 200 °C, $\text{Sm}_2\text{Co}_{17}$ permanent magnet material is being used for the pump. This material is also ~ 1000 times more radiation resistant than NdFeB permanent magnet materials.^{6,7} A prototype pump has been built and tested using a Ga/In alloy that is liquid at room temperature. A schematic of the present pump design is shown in Fig. III-36. It is a smaller and simpler version of a liquid gallium pump developed by Smither.⁸

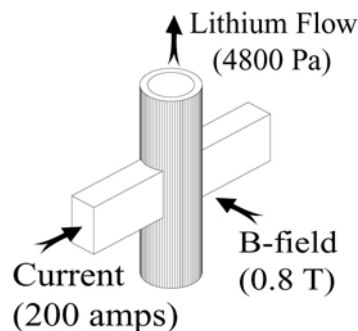


Fig. III-36. Schematic diagram of the permanent-magnet, liquid-lithium pump. The pump is designed to deliver a volume flow rate of $200 \text{ cm}^3/\text{s}$ at the pressure, current, and magnetic field indicated. With these parameters and the piping as designed, the flow velocity through the target spool piece is 4 m/s and the pump voltage is 24 mV. The no-flow voltage is 10 mV. The stainless steel tube through the pump is 12.7 mm outside diameter and the wall thickness is 1.6 mm.

Mechanical layout

The target assembly, liquid-lithium loop, lithium pump, and associated heaters and temperature monitors comprise an assembly that mounts on the top flange of the target vacuum chamber of the NSCL A1900 fragment separator and is compatible with the standard target ladder. The operating temperature of the liquid-

lithium loop is 200 °C so that the heater control system will have to adjust the heater power as required by the amount of beam power being dissipated in the target. A mechanical assembly drawing of the overall target system is shown in Fig. III-37. A detailed system design description is given in [Ref. 9].

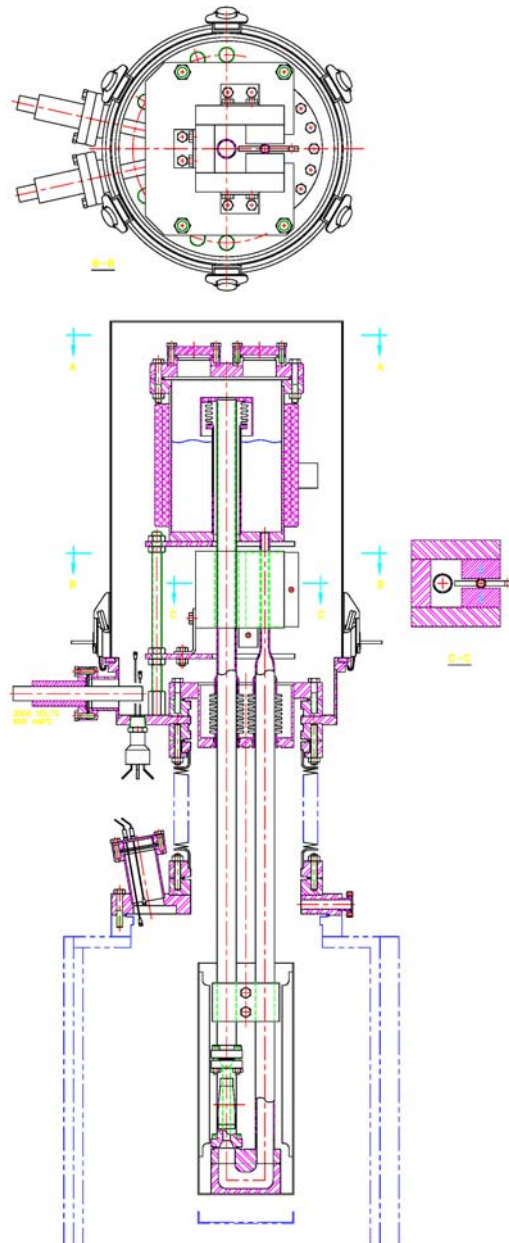


Fig. III-37. Drawing of the mechanical layout of the liquid-lithium loop. The mechanism can move vertically with respect to the beam in order to vary the target thickness or to withdraw the mechanism to make room for the standard target ladder. A section view of the permanent-magnet pump is shown to the right.

Safety issues and procedures

One of the goals of this project is to develop procedures for the safe operation of liquid-lithium target systems at a radioactive beam facility. The general safety issues associated with liquid alkalis were discussed at RNB-5.¹ Such procedures have been developed and used in fusion research programs and liquid-metal cooled reactors. The present target uses a closed lithium loop, which is an intermediate step towards the

operation of a windowless target at a nuclear physics accelerator facility. However, to provide an additional measure of isolation of the liquid lithium from the laboratory environment, the present design incorporates a secondary containment vessel as shown in Fig. III-37, as well as, a pressure relief valve for the inert cover gas above the lithium in the closed loop.

Construction and testing schedule

The design of this prototype target is complete and fabrication is in progress. The DC pump has been constructed and the beryllium spool piece has been procured. The present plan is to complete fabrication of

the target system at the NSCL in the fall of 2002, and to assemble and test it, without beam, at Argonne soon thereafter. It should be ready for commissioning at the NSCL A1900 in 2003.

*Technology Development Division, Argonne National Laboratory

†Energy Technology Division, Argonne National Laboratory

‡Michigan State University

¹J.A. Nolen, C.B. Reed, A. Hassanein, and I.C. Gomes, Nucl. Phys. **A701** (2002) 312c-322c.

²J.A. Nolen, et al., abstract #78, EMIS-14.

³D.J. Morrissey, abstract #70, EMIS-14.

⁴A. Hassanein and I. Konkashbaev, J. Nucl. Mater. **273** (1999) 326.

⁵J.P. Verkamp and R.G. Rhudy, "Electromagnetic Alkali Metal Pump Research Program," NASA Contractor Report CR-380, Feb. 1966.

⁶A.F. Zeller and J.A. Nolen, 9th Int. Workshop on Permanent Magnets, Bad Soden, FRG, (1987) 159.

⁷O.-P. Kähkönen, et al., Phys. Rev. **B49** (1994) 6052-6057.

⁸R.K. Smither, "Summary of the Operating Characteristics of the ANL Liquid Metal Pump after its Latest Modification, APS Technical Memo: AGP-III-M, September 20, 1995.

⁹"System Design Description for the ANL/MSU Li/Be Target Loop," ANL/TD document G0586-0003-SA, July 2002.

c.7. Development and Operation of Gas Catchers to Thermalize Fusion-Evaporation and Fragmentation Products (G. Savard,^{*} J. Clark,[†] C. Boudreau,[‡] F. Buchinger,[‡] J.E. Crawford,[‡] S. Gulick,[‡] A. Heinz,^{*} J.K.P. Lee,[†] A. Levand,^{*} D. Seweryniak,^{*} K.S. Sharma,[†] G. Sprouse,[§] J. Vaz,[†] J.C. Wang,[†] B.J. Zabransky,^{*} Z. Zhou^{*} and the S258 collaboration)

A new approach to the production of low energy radioactive beams involves the stopping of fast beams produced by fragmentation, in-flight fission or fusion-evaporation reactions into a large gas catcher where the reaction products are thermalized in high-purity helium and extracted as singly charged ions for post-acceleration. This removes the limitation present in standard ISOL technique for species that are difficult to extract from the target/ion source assembly. This approach has been implemented at Argonne since 1998 to inject fusion-evaporation products in an ion trap system. Via a series of improvements since then, we now reach efficiencies for these devices of close to 50%

with delay times below 10 ms. In preparation for the RIA project, a larger device for stopping fragmentation products has been designed and is currently under construction. Preparation for a test of this large gas cell at the full RIA energy at GSI is also in progress.

A large gas catcher system was first developed at Argonne in 1998 for the injection of radioactive ions into the CPT mass spectrometer.¹ It used a large high-purity helium gas volume where fast reaction products separated by a gas filled spectrograph were stopped and thermalized as 1+ ions before being extracted from the

catcher. For high-efficiency, the gas catchers must have a stopping volume large enough to contain the full range straggling of the reaction products in which case the gas flow alone (as in a typical IGISOL² system) cannot extract the ions quickly enough. The ion extraction is therefore assisted by electric DC and RF fields applied in the high-pressure catcher to pull out the ions faster than the gas itself is evacuated. We proposed at that time that this technique could be extended to the stopping of fragmentation products which led to an important new production mechanism for the proposed RIA³ facility.

In the years of operation of the fusion-evaporation gas catcher system at ATLAS, this technology have been developed and tested over a series of prototype, and extraction efficiencies of 45% with delay times below 10 ms are now reached, both of those with space-charge density inside the gas catcher typical of on-line operation. In particular, we have recently investigated the space-charge density that such devices can tolerate while maintaining high efficiency. This effect will ultimately limit the yield that can be extracted from such devices in large facilities like RIA. Finally, in preparation for the RIA project, we are now extending this work with the design and construction of a 1.25 meter long gas cell for stopping fragmentation product. This full scale RIA prototype will be characterized at Argonne before being installed on-line behind the FRS separator at GSI to demonstrate that this approach is valid even for very high-energy reaction products.

The gas catcher currently being used for stopping of fusion-evaporation products has an inner diameter of about 8 cm and a length of roughly 27 cm, and uses only UHV materials. It is installed at the focal plane of an Enge spectrograph. It is separated from the spectrograph vacuum chamber by an all metal 1.9 mg/cm² HAVAR window sealed by indium rings and supported by a gold coated tungsten wire grid. The cell is filled with ultra-high-purity helium gas fed by an all stainless steel gas system, with the gas purified by a Monotorr purifier (SAES getters Inc.) preceded by a standard cold trap. This catcher delivers the extracted ions into a 3 section RFQ gas cooler where the flowing helium gas is pumped away in the first section by clean booster pumps backed by a roots blower. Diagnostics for ions (counting and mass selectivity) and radioactivity is provided after the gas cooler. The gas catcher has DC fields guiding the positive ions towards the extraction region where an RF-focusing cone (Fig. III-38) focuses the ions on the 1.6-mm diameter extraction nozzle. The focusing force is essentially an RF wall which keeps the ions away from the cone. The repulsive force depends on the mobility of the ions in the gas and decreases with higher gas pressure. The RF cone used in the fusion-evaporation gas catcher has been operated successfully up to the maximum pressure the thin window to let the recoils enter the catcher can tolerate, which is about 250 mbar. The efficiencies and extraction times measured with the device are shown in Fig. III-39.

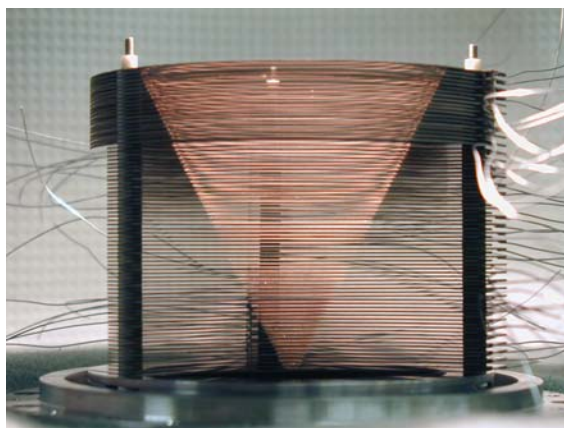


Fig. III-38. Conical RF structure used to focus the ions on the extraction nozzle of the gas catcher.

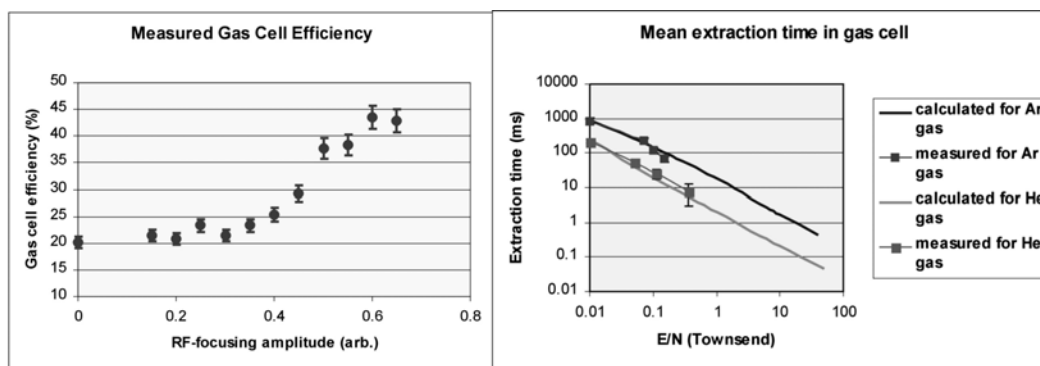


Figure III-39: Measured efficiency and mean extraction time as a function of RF and DC fields applied inside the gas catcher.

A number of systematic studies have been performed with the gas catcher system, looking at the effect of impurities in the gas, gas flow conditions, transmission through the cooler system, efficiency variation with DC and RF parameters inside the catcher, etc. While these studies are still ongoing, a few conclusions can already be drawn. The most important conclusion is that the effect of impurities in the gas reduces significantly as the field gradient inside the cell is increased. It appears that the long-range attraction of the ions and impurity molecules in the presence of the constant collisions which the molecule must undergo to “follow” the ion being dragged in the helium gas. Similarly, the adducts of ion plus helium which are weakly bound are not observed when the electric field becomes significant. Under optimal conditions we find no sign of activity at masses other than those of the radioactive ions being produced.

The device then underwent a series of tests to determine the dependence of the method on the chemical properties of the extracted ions. The basis of the argument for chemical independence is that all species have much lower ionization potential than helium so that they will remain ionized after the deceleration process. The presence of impurities in the gas might however still lead to losses for the most chemically active ions. We have produced a series of radioactive ions of different species and looked at their behavior as impurities are introduced in the ppb level purity gas available at the area II spectrograph. We have found that with sufficiently large accelerating fields inside the cell the system is quite insensitive to sub-ppm level contaminants and have even found a surprisingly large surviving fraction of 2+ ions extracted for some species.

In on-line studies, we have created radioactive species and brought them into the cell together with a fraction of the primary beam. This fraction can be varied by tuning the dispersion of a velocity filter⁴ that has been added at the entrance of the Enge spectrograph. While these studies are still coarse, we do observe saturation effects in the cell which occur at a rate consistent with that we predicted for the point where charge accumulation in the cell will shield the electric field applied. In these tests, the gas catcher has been operated with high efficiency at ionization densities in excess of 10^8 ion-electron pairs created per cm^3 per second, well above the maximum level predicted by a simple model in the literature.⁵ This number is therefore consistent, when scaled to a cell of the size required for RIA, with the roughly 10^9 ions per second limit we expect to be able to handle with this approach at RIA and which was used for the RIA yield calculations⁶ using this extraction system.

The next step in the gas cell evolution is a full scale RIA gas catcher prototype that will be tested with heavy beams at the full RIA energy which are available at GSI. The characteristics of the large gas cell system required for the high-energy test were developed from an analysis of the beam properties available at the FRS at GSI and of the recoil achromatization system that will be used. The $\pm 1\%$ momentum acceptance and 10 mrad angular acceptance of the FRS, together with the 7cm/% momentum dispersion that will be used for the achromatization of the beam and the angular straggling in the final degrader and the lateral straggling in the gas cell itself determine a stopping width of about 20 cm for the recoils. The longitudinal range straggling can be compressed by the achromatization by a factor of 10 or so as has been shown experimentally at the FRS.⁷ This yields the 0.5 atmosphere-meter of helium stopping length required. We have therefore designed the body of the cell that will mate to a large conical extraction

region to have a stopping volume with an inner diameter of 25 cm and a total length of about 1.2 meters. It is a scaled up version of the gas cell bodies developed for the CPT at Argonne. Because of the large surface area and the low pumping speed it is important to use only UHV techniques in the design and construction of the cell and the body and the inner rings and insulators are therefore constructed with only stainless steel, aluminum oxide, aluminum and indium seals (see Fig. III-40). The mechanical construction of the full scale RIA gas cell prototype has been ongoing since the end of FY2001. Final assembly of the full gas cell vacuum system with all its inner electrodes, about 7300 components with over 4000 components cleaned to UHV standards, is being completed (Fig. III-40). Construction of all tuned circuits for the different RF focusing electrodes and the DC gradient is ongoing, together with the connection to the gas cooler and basic diagnostics for slow ions. The full system will be surrounded by a high-voltage protection cage and will

form a movable unit that can easily be moved to different locations. This system will be first tested off-line with a fission source before on-going characterization on-line with low-energy radioactive species produced on-line at Argonne. Using the high-quality beams of ATLAS, thin production targets and a tunable degrader assembly, radioactive isotopes will be deposited at well-defined locations inside the cell. This will allow the efficiency to be determined as a function of position inside the cell. Pulsing the ATLAS beam on a slow time cycle (typically a half a second or so) will allow us to also determine the extraction delay times as a function of position inside the cell. Effect of space-charge saturation will also be investigated as a function of pressure inside the device. After these tests the device will be moved to GSI for operation behind the FRS where site preparation involving a large international collaboration (experiment S258: Argonne, GSI, Jyväskylä, Leuven, Giessen, Muenchen, Michigan State, Stony Brook and RIKEN) is ongoing.

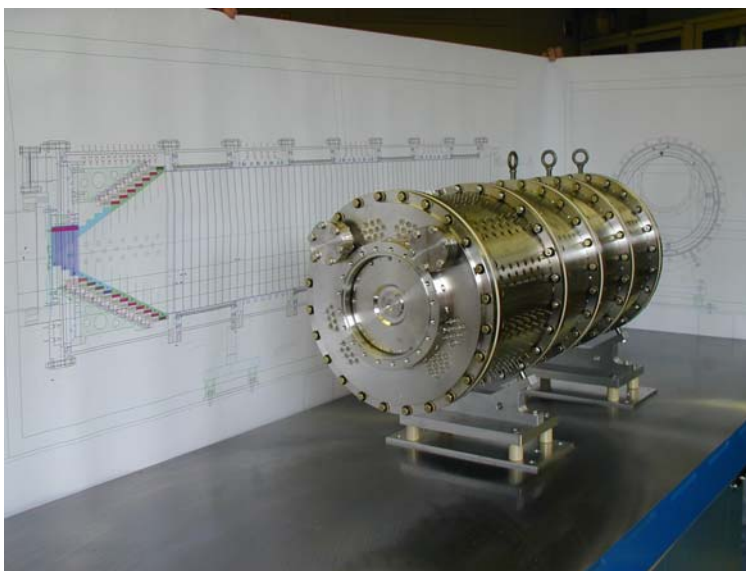


Figure III-40: View of the large gas catcher being developed for testing at the FRS.

*Physics Division, Argonne National Laboratory, Argonne, IL 60439

†Department of Physics and Astronomy, University of Manitoba, Winnipeg, MB R3T 2N2

‡Department of Physics, McGill University, Montreal, PQ H3A 2T8

§Physics Department, SUNY, Stony Brook University, Stony Brook, NY 11794

¹G. Savard, R.C. Barber, C. Boudreau, F. Buchinger, J. Caggiano, J. Clark, J.E. Crawford, H. Fukutani, S. Gulick, J.C. Hardy, A. Heinz, J.K.P. Lee, R.B. Moore, K.S. Sharma, J. Schwartz, D. Seweryniak, G.D. Sprouse, J.Vaz, *Hyperfine Interactions* 132 (2001) 223.

²P. Dendooven, *Nucl. Instr. Meth.* B126 (1997) 182.

³G. Savard, in *Proceedings of the 2001 Particle Accelerator Conference*, Chicago, Illinois, 2001, edited by P. Lucas and S. Webber (IEEE, Piscataway, NJ, 2001), p.561.

⁴J. Clark et al, "Improvements in the injection system of the Canadian Penning Trap mass spectrometer", EMIS-14

⁵M. Huyse et al, “Intensity limitations of a gas cell for stopping, storing and guiding of radioactive ions”, submitted to NIM B.

⁶C.-L. Jiang et al, “Yield calculations for a facility for short-lived nuclear beams”, submitted to NIM B, also available at <http://www.phy.anl.gov/RIA/>.

⁷C. Scheidenberger et al, “Energy and Range focusing of in-flight separated exotic nuclei – a study for the energy-buncher stage of the low-energy branch of the Super-FRS”, EMIS-14 proceedings.

IV. MEDIUM-ENERGY NUCLEAR PHYSICS RESEARCH

OVERVIEW

The overall goals of the Medium-Energy Physics research program in the Argonne Physics Division are to test our understanding of the structure of hadrons and the structure of nuclei, and to develop and exploit new technologies for high-impact applications in nuclear physics as well as other national priorities. In order to test our understanding of the structure of hadrons and the structure of nuclei within the framework of quantum chromodynamics, the medium-energy research program emphasizes the study of nucleons and nuclei on a relatively short distance scale. Because the electromagnetic interaction provides an accurate, well-understood probe of these phenomena, primary emphasis is placed on experiments involving electron scattering, real photons and Drell-Yan processes.

The electron beams of the Thomas Jefferson National Accelerator Facility (TJNAF) are ideally suited for studies of nuclei at hadronic scales and represent one center of the experimental program. Staff members led in the construction of experimental facilities, serve as spokespersons or co-spokespersons for 15 experiments and are actively involved in several others. The group constructed the broad-purpose Short Orbit Spectrometer which forms half of the coincidence spectrometer pair that is the base experimental equipment in Hall C. We continue to improve the understanding of the spectrometer optics and acceptance. Argonne led the first experiment to be carried out at TJNAF in FY1996 and has completed nine other experiments.

Recently, staff members have focused increasingly on studies of the nucleon. In FY1999 measurements were made on the ratio of the electromagnetic elastic form factors of the proton using the polarization transfer method. These results confirmed the reproducibility of the surprising result that this ratio decreases substantially at high values of momentum transfer. These polarization-transfer results disagree so markedly from data recorded previously with the Rosenbluth

method, that staff members are leading a new effort to test these methods with a newly developed modified Rosenbluth technique.

Also during FY1999, measurements were performed for polarization in exclusive neutral pion photoproduction from the proton. Surprisingly, the induced-polarization was observed to oscillate strongly as a function of the reaction angle, suggesting a relatively high spin state in the proton. In FY2000, the exclusive cross sections from charged photopion production on the neutron and proton were measured up to a photon energy of 5.6 GeV as a test of "transition region" models which describe the transition from hadronic degrees of freedom to quark-gluon degrees of freedom.

Although exclusive deuteron photodisintegration experiments established that this reaction obeys quark-counting rule scaling arguments at large transverse momenta, recent complete angular distribution data recorded in FY1999 for this reaction do not support simple transition region models. Measurements of kaon production on light nuclei provide important information on the basic strangeness production mechanisms and the poorly known low energy hyperon-nucleon interaction. Pion production measurements on hydrogen, deuterium and ^3He have determined the charge form factor of the pion and have found no indication of a change in the pion field in the nuclear medium. Since the pion contains valence antiquarks, these measurements complement our high-energy Drell-Yan measurements of the antiquark distributions in nucleons and nuclei. Results of new measurements of inclusive electron scattering in the resonance region provide evidence for the concept of semi-local duality in relating averaged resonance and deep inelastic scattering yields.


HERMES, a broadly based North American-European collaboration is studying the spin structure of the nucleon using internal polarized targets in the HERA storage ring at DESY. Deep inelastic scattering has been measured with polarized electrons on polarized hydrogen, deuterium and ^3He . Argonne has concentrated on the hadron particle identification of HERMES, a unique capability compared to other spin structure experiments. In 1999 and under Argonne leadership, the dual-radiator ring imaging Cerenkov counter (RICH) was brought into operation at the design specifications to provide complete hadron identification in the experiment. The RICH has been operating routinely since its installation. This has allowed HERMES to make decisive measurements of the flavor dependence of the spin distributions. HERMES can now perform a five-component decomposition of the proton's spin structure function and can produce the first measurement of the x-dependence of the strange sea polarization. In addition, HERMES provided the first direct indications of a positive gluon spin contribution to the nucleon.

Recently, single-spin asymmetries in the azimuthal distributions of π^+ and π^0 were observed from a longitudinally polarized proton target. This new result will render transversity measurements feasible at HERMES. Now, HERMES is

poised to make the first measurements of the chiral-odd transverse structure function of the proton over the next two years. In addition, HERMES was first to observe the spin-dependent deeply virtual Compton scattering process which is an important tool for investigating the structure of the proton. Also, HERMES measured the nuclear modifications of the fragmentation function for hadrons which constrain the parton energy loss in cold nuclear matter.

Measurements of high mass virtual photon production in high-energy proton-induced reactions have determined the flavor dependence of the sea of antiquarks in the nucleon. These measurements give insight into the origin of the nucleon sea. In the same experiment, the nuclear dependence of the Drell-Yan process and the nuclear dependence of the production of heavy quark resonances such as the J/ψ and Υ have been determined. The Drell-Yan results also provide constraints on the energy loss of quarks in the nuclear medium. The heavy vector meson results provide constraints on the gluon distributions of nucleons and nuclei and a significant baseline for attempts to use heavy vector meson production as a signal of the formation of the quark-gluon plasma in relativistic heavy-ion experiments. Recently, a new initiative was approved by the FNAL PAC to continue these measurements with much higher luminosity at the FNAL Main Injector.

The technology of laser atom traps provides a unique environment for the study of nuclear and atomic systems and represents a powerful new method that is opening up exciting new opportunities in a variety of fields, including nuclear physics. The group has developed a high-efficiency, high-sensitivity magneto-optical trap for rare, unstable isotopes of krypton. The group is poised to use this method for dating ancient ground water from the Nubian aquifer in Upper Egypt. In addition, the group has trapped calcium isotopes, which is a necessary step along the way to using ^{41}Ca for radiochronology or developing a new method for measuring rates of bone loss in humans. Presently, a trap is being constructed for the purpose of measuring the charge radius of ^6He at ATLAS.



A. NUCLEON PROPERTIES

a.1 New Measurement of (G_E/G_M) for the Proton (J. Arrington, D. F. Geesaman, K. Hafidi, R. J. Holt, H. E. Jackson, D. H. Potterveld, P. E. Reimer, E. C. Schulte, K. Wijesooriya, B. Zeidman, and E01-001 Collaboration)

The structure of the proton is a matter of universal interest in nuclear and particle physics. Charge and current distributions are obtained through measurements of the electric and magnetic form factors, $G_E(Q^2)$ and $G_M(Q^2)$. These form factors can be separated by measuring elastic electron-proton scattering at two or more values of the virtual photon polarization parameter ε (*i.e.* by performing a Rosenbluth separation). Several such measurements

have been made, and global fits to these measurements¹ indicated that the ratio of G_E to G_M was consistent with unity, indicating equal distributions of charge and magnetization within the proton. Recent measurements at Jefferson Laboratory² used a recoil polarization measurement to extract G_E/G_M at large values of Q^2 . They found that the ratio of G_E/G_M was unity at low Q^2 , but fell linearly with increasing Q^2 , reaching a value of 0.3 at $Q^2 = 5.5 \text{ GeV}^2$ (see Fig. IV-1).

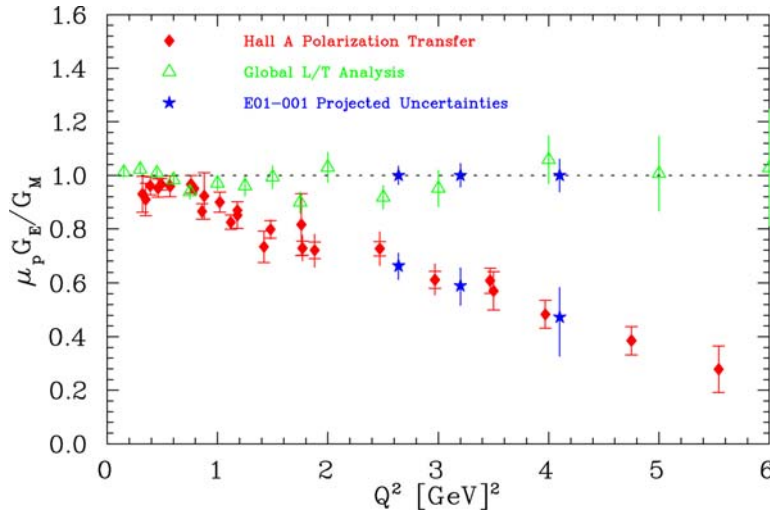


Fig. IV-1. Existing measurements of G_E/G_M , along with projected uncertainties for this experiment. There are two values shown for E01-001 at each Q^2 point. The top points show the projected uncertainty if the experiment indicates a ratio of unity, while the bottom points show the projected uncertainty if the experiment indicates the same falloff as seen by the recoil polarization measurements.

It has been suggested that the Rosenbluth data are unreliable at large Q^2 based on the fact that form factors extracted from different Rosenbluth measurements are inconsistent at large Q^2 values. We have reanalyzed the Rosenbluth measurements and find that the inconsistency between different extractions does not indicate a problem with the data or technique.³ Instead, it results from the incomplete treatment (or lack of treatment) of normalization uncertainties when data from different experiments are combined to extract the form factors. When the normalization uncertainties are properly included, or when the form factors are extracted from a single data set, the results are not inconsistent. In order to be confident in our knowledge of the proton form factors, we must determine not only

which result is correct, but also why these two techniques disagree. A systematic problem with either set of measurements would most likely affect other measurements which use the same techniques.

Experiment E01-001⁴ will perform a Rosenbluth separation to extract G_E/G_M in the range where the previous Rosenbluth data disagree with the recent measurements. The goal is to have a single data set that will provide a high-precision measurement of the ratio, with careful tests of the systematic uncertainties. In addition to careful monitoring of potential uncertainties, this measurement will use a different experimental technique which will significantly decrease our sensitivity to the systematics that have limited previous measurements.

The main difference in this measurement is that we will detect the struck proton, rather than the scattered electron. This significantly decreases almost all of the significant systematic uncertainties that have limited previous experiments. Taking data at two different ε values means detecting small-angle electron scattering with a high-energy beam and comparing this to large-angle electron scattering at lower energies. The result is that the measurements at large and small angles are detecting electrons with very different momenta, and are measuring cross sections that can vary by a 2-3 orders of magnitude. These measurements are therefore very sensitive to any momentum-dependent or rate-dependent effects. In addition, the cross section is very sensitive to knowledge of the scattering angle for the small angle electrons. When detecting protons, there are several advantages. There is no momentum-dependence because at fixed Q^2 , the proton momentum is constant. The cross section variation between small and large angle proton data is only a factor of 2-3, and the overall dependence of the cross section on scattering angle and beam energy is much smaller than

for the electron. Finally, the radiative corrections are smaller, and have less ε -dependence.

The other unusual feature of this measurement is that while we perform a Rosenbluth extraction at high- Q^2 in one spectrometer, we will make a simultaneous measurement at low Q^2 . Because the value of G_E/G_M at low Q^2 is relatively well known, and because the kinematics chosen make the low Q^2 measurement insensitive to the photon polarization ($\Delta\varepsilon$ is kept small), we can use the low Q^2 point as a pseudo-luminosity monitor to correct for any error in the beam charge and target thickness measurements.

The experiment was approved for 10 days of beam time in Hall A at Jefferson Lab, and is scheduled to run in May 2002. The uncertainty in the extraction of the ratio depends on the value of G_E/G_M . Figure IV-1 shows the existing Rosenbluth and recoil polarization results, along with projected uncertainties for E01-001 for two cases: $\mu_p G_E/G_M = 1$, and $\mu_p G_E/G_M$ consistent with the polarization measurements.

¹R. C. Walker *et al.*, Phys. Rev. D **49**, 5671 (1994); P. E. Bosted, Phys. Rev. C **51**, 409 (1994)

²M. K. Jones, *et al.*, Phys. Rev. Lett. **84**, 1398 (2000); O. Gayou, *et al.*, Phys. Rev. C **64**, 038292 (2001); O. Gayou, *et al.*, Phys. Rev. Lett. **88**, 092301 (2002)

³J. Arrington, in preparation

⁴Jefferson Lab Experiment E01-001, 'New Measurement of (G_E/G_M) for the Proton', J. Arrington and R. E. Segel, spokespersons

a.2 Measurements of the Proton Elastic Electromagnetic Form Factor Ratio by Polarization Transfer (R. J. Holt, E. C. Schulte, and K. Wijesooriya, and the JLab E89-019 Collaboration)

Measurements of the ratio of the proton elastic electromagnetic form factors, $\mu_p G_{Ep}/G_{Mp}$ were performed.¹ The Jefferson Lab Hall A focal plane polarimeter was employed to measure the transverse and longitudinal components of the recoil proton polarization in electron-proton elastic scattering. The ratio of these polarization components is proportional to the ratio of the two form factors:

$$\frac{G_{Ep}}{G_{Mp}} = -\frac{P_t}{P_\ell} \frac{(E + E')}{2M_p} \tan\left(\frac{\theta_e}{2}\right)$$

where the P_i are the transverse and longitudinal components of the polarization, the E and E' are the incident and scattered electron energies, and θ_e is the electron scattering angle. The data reproduce the observation of Jones *et al.* [Phys. Rev. Lett. **84**, 1398 (2000)] that the form factor ratio decreases significantly above $Q^2 = 1 \text{ GeV}^2$ as shown in Fig. IV-2.

¹O. Gayou *et al.*, Phys. Rev. C **64** 038202 (2001)

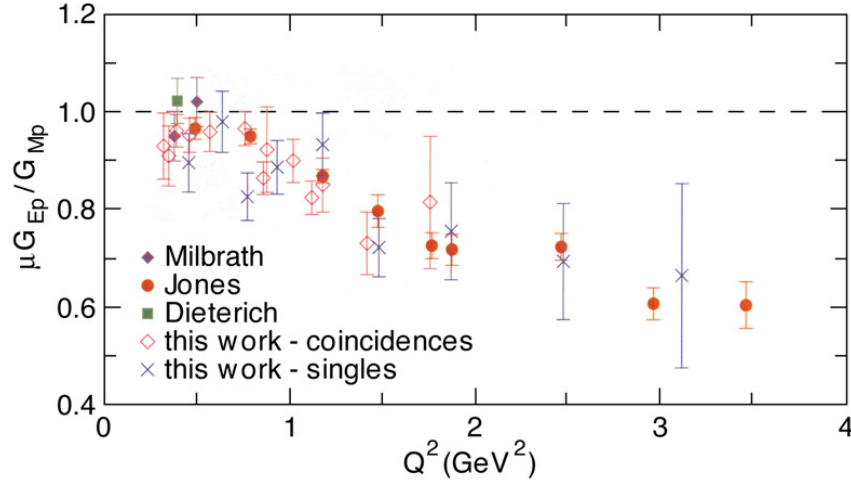


Fig. IV-2. Present results compared with the previous polarization transfer data.

a.3 Polarization Measurements in Neutral Pion Photoproduction (R. J. Holt, E. C. Schulte, and K. Wijesooriya, and JLab E94-012 Collaboration)

Measurements of the recoil polarization for the $p(\bar{\gamma}, \bar{p})\pi^0$ reaction were performed for a pion c.m. angular range of 60° to 135° and for photon energies from 0.8 to 4.0 GeV. These data represent the first polarization transfer results with circularly polarized photons measured for this reaction. The results for the induced polarization indicate much better agreement with the MAID model than the SAID model. Both models strongly disagree with the polarization transfer data.

A particularly surprising result is the observation of a strong oscillatory pattern in the angular distribution of the induced polarization at 2.5 and 3.1 GeV above the known resonance region. These results are given in Fig. IV-3. The induced polarization is related to the differential cross section $d\sigma/d\Omega$ and the differential polarization $dp/d\Omega$ by the expression

$$p_y = \frac{1}{j} \frac{dp/d\Omega}{d\sigma/d\Omega}$$

where j is the spin of the emitted proton in this case. The differential polarization can be written as

$$\frac{dp}{d\Omega} = \sum_{L=1} B_L P_L^1(\cos\theta)$$

where the B_L contain the reaction matrix elements, and assuming two amplitudes, L ranges from 1 to the sum of the angular momenta of the two amplitudes which interfere to give rise to the induced polarization. From the nature of the first associated Legendre polynomial in the equation above, the angular distribution will behave essentially like $\sin(L\theta)$. As an illustration of the strong oscillatory pattern, a $\sin(12\theta)$ curve is drawn in the figure at 2.5 GeV. The strong angular dependence noted in the data suggests an angular dependence up to $\sin(12\theta)$. This would mean that the background or a resonance contains relatively high partial waves. More finely binned data in angle and energy would be necessary to determine whether a high-spin resonance has been observed at this energy.

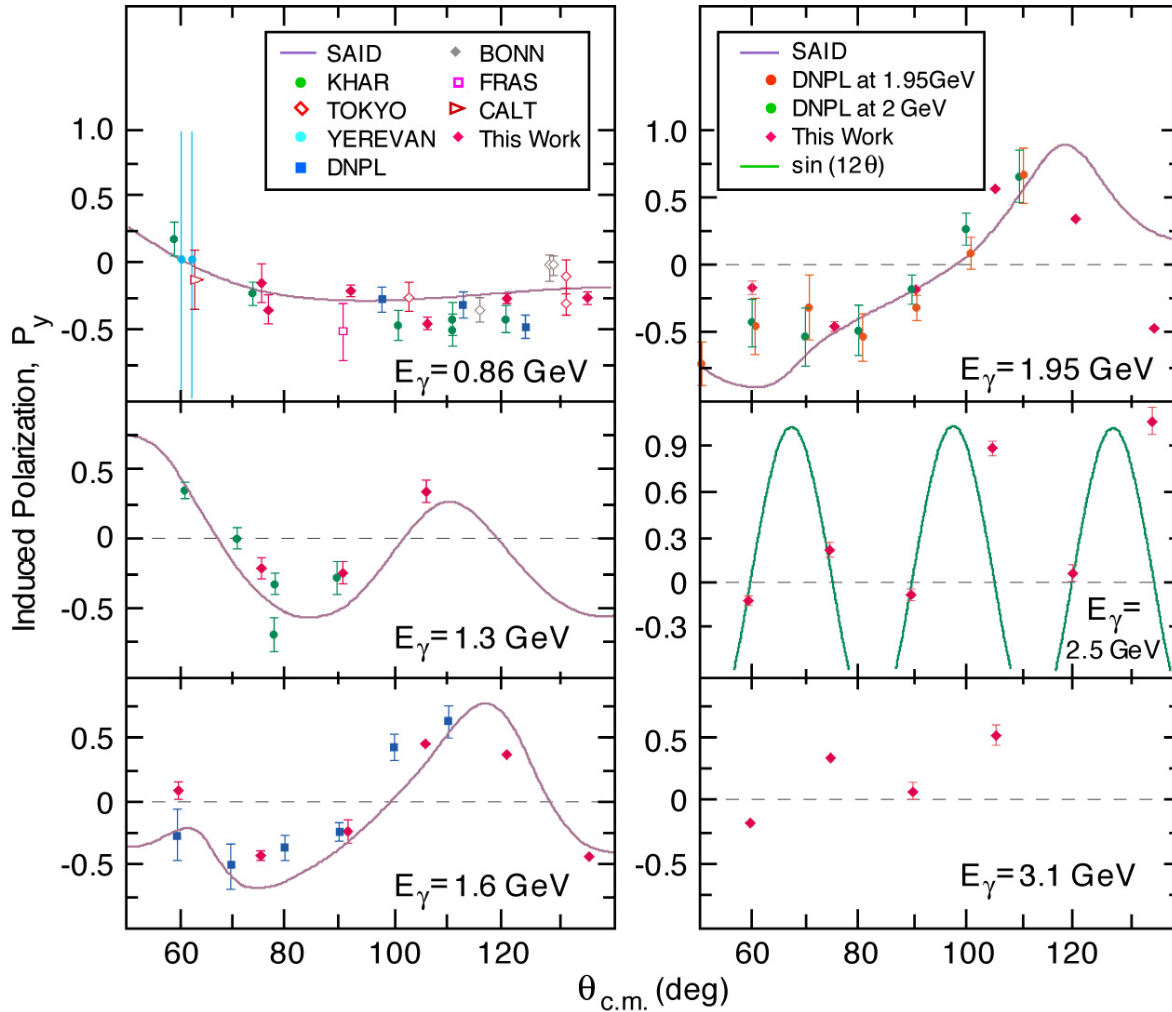


Fig. IV-3. Angular distributions of the induced polarization for neutral pion photoproduction. The $\sin(12\theta)$ curve at 2.5 GeV is drawn merely to illustrate the strong angular dependence.

a.4. Charged Pion Photoproduction from the Nucleon (R. J. Holt, J. Arrington, K. Bailey, P. E. Reimer, F. Dohrmann, K. Hafidi, T. O'Connor, E. C. Schulte, K. Wijesooriya, and JLab E94-104 Collaboration)

The goal of experiment E94-104 is to measure the cross sections for the $\gamma n \rightarrow \pi^- p$ and the $\gamma p \rightarrow \pi^+ n$ reactions for photon energies up to 5.5 GeV and at several reaction angles. The experiment was completed and the data are nearing the final analyses. From these data, the π^-/π^+ ratio can be formed and compared with existing models. One of the most celebrated models of the transition region from hadronic degrees of freedom to the quark-gluon degrees of freedom is represented by the “hand-bag” diagram. This model gives a definite prediction¹ for the ratio:

$$\frac{d\sigma(\gamma n \rightarrow \pi^- p)}{d\sigma(\gamma p \rightarrow \pi^+ n)} = \left(\frac{ue_d + se_u}{ue_u + se_d} \right)^2$$

Where the e_j are the charges of the quarks, and s and t are the usual Mandelstam variables. This model will be compared with the data over the relatively large s and t range measured in the experiment to determine whether the transition region is reached at presently available beam energies at Jefferson Lab. The data are presently undergoing analysis.

¹H. Huang and P. Kroll, Eur. Phys. J. C17, 423 (2000)

a.5. Search for QCD Oscillations in the $\gamma N \rightarrow \pi N$ Reactions (R. J. Holt, J. Arrington, D. F. Geesaman, H. E. Jackson, P. E. Reimer, K. Hafidi, E. C. Schulte, K. Wijesooriya, and JLab E02-010 Collaboration)

A proposal to search for QCD oscillations in exclusive charged photopion reactions was approved by the Jefferson Laboratory Program Advisory Committee. The goal of the experiment is to search in photopion reactions for the oscillatory effect observed in exclusive high-energy proton-proton elastic scattering. In p-p elastic scattering the cross section was found to oscillate about the $1/s^{10}$ dependence expected from the constituent counting rules. This oscillatory behavior has been ascribed¹ to a short distance (hard-scattering) amplitude which interferes with a long-distance

amplitude (Landshoff). This process is analogous to coulomb-nuclear interference observed in low energy charged particle scattering; however, the QCD oscillations arise from soft gluon radiation rather than from photon radiation as in the QED case. This interference also can give rise to polarizations observed in high energy exclusive hadron-hadron scattering processes. In the proposed experiment, the cross sections will be measured in a fine energy scan up to the highest energy available at Jefferson Lab.

¹S. J. Brodsky, C. E. Carlson, and H. Lipkin, Phys. Rev. D **20**, 2278 (1979); J. P. Ralston and B. Pire, Phys. Rev. Lett. **65**, 2343 (1990)

a.6. Separated and Unseparated Structure Functions in the Nucleon Resonance Region (J. Arrington, D. F. Geesaman, R. J. Holt, T. G. O'Neill, D. Potterveld, and E99-119, E00-002, and E00-116 Collaborations)

A great deal of our understanding of the quark structure of the nucleon comes from inclusive electron scattering. Reliable *global* descriptions of inclusive electroproduction data are necessary for electron-nucleon scattering model development, accurate radiative correction calculations, and the extraction of form factors, structure functions, and parton distribution functions from inclusive electron scattering experiments. However, most measurements have focused on the deep inelastic region. High precision cross section measurements in the resonance region, combined with a separation of the longitudinal (σ_L) and transverse (σ_T) components, will substantially improve the global description of electroproduction at moderate to high Q^2 and large Bjorken- x . While the ratio $R = \sigma_L/\sigma_T$ has been measured up to high Q^2 for elastic and deep inelastic scattering, there exist few measurements of R in the resonance region at moderate or high momentum transfers. The current uncertainty in R in the resonance region is greater than 100%. Experiment E94-110¹ ran in 1999 in Hall C at Jefferson Lab, and made a precision measurement of R in the resonance region, up to $Q^2 = 4.5 \text{ GeV}^2$. Figure IV-4

shows the preliminary results for the extraction of R as a function of W^2 for four Q^2 bins.

Previous JLab measurements of inclusive scattering in the resonance region, measuring just the F_2 structure function, have been analyzed in terms of Local Duality. It was observed that the resonance region data, when averaged over the Nachtmann variable, ξ , reproduced the structure function as measured in the deep inelastic region.² This duality of the DIS and resonance structure function held to better than 10%, down to $Q^2 = 0.5 \text{ GeV}/c^2$. It was also observed that at low ξ , the resonance region structure function deviated from the DIS value, and showed a valence-like behavior,³ going to zero as ξ decreased. While this duality has been observed for hydrogen, deuterium, and nuclear targets for F_2 , no such data existed for the F_1 structure function in the resonance region. In addition to extracting R , experiment E94-110 will also extract the separated structure functions F_1 and F_2 . These data will be used to perform tests of duality in F_1 in a similar Q^2 range to the previous F_2 measurements.

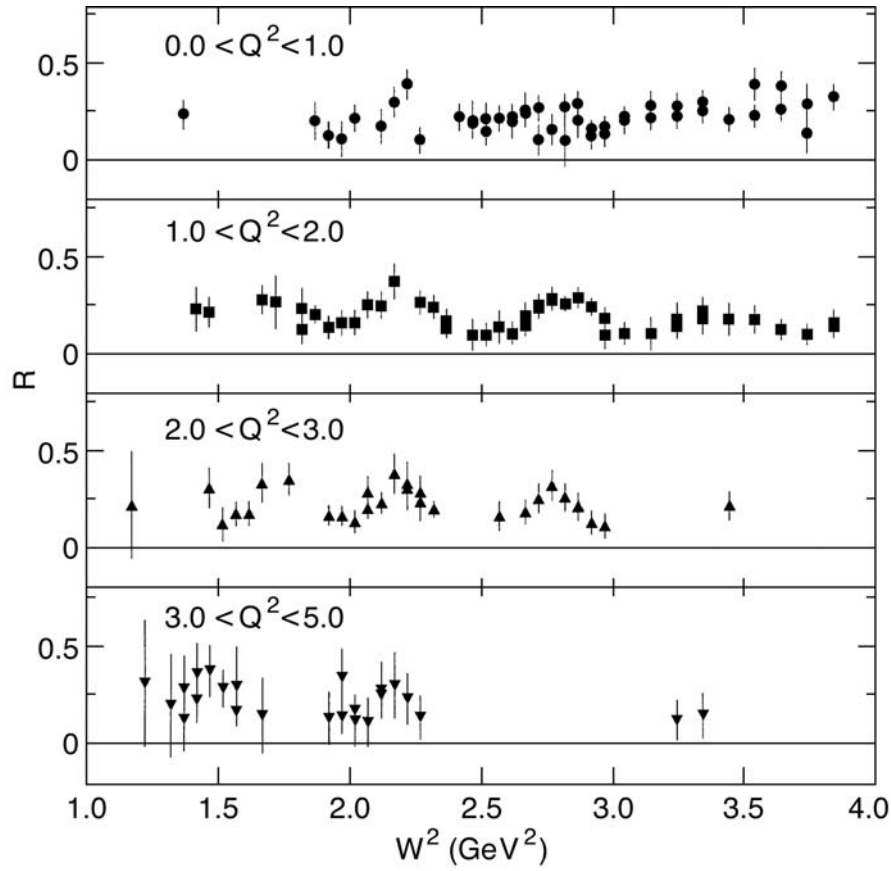


Fig. IV-4. The extracted value of $R = \sigma_L/\sigma_T$ as a function of W^2 for four Q^2 bins. These results are preliminary, and the uncertainties shown are statistical only.

Two future experiments will further extend these duality measurements. There is an approved experiment⁴ to extend duality studies on hydrogen and deuterium to $Q^2 = 7.5 \text{ GeV}^2$. Another experiment⁵ will

make additional resonance region measurements at low x and Q^2 to study the valence-like nature of the resonance region structure function.

¹JLab Experiment E94-110, "Measurement of $R = \sigma_L/\sigma_T$ in the Nucleon Resonance Region", C. E. Keppel, spokesperson

²I. Niculescu *et al.*, Phys. Rev. Lett. **85**, 1182 (2000)

³I. Niculescu *et al.*, Phys. Rev. Lett. **85**, 1186 (2000)

⁴JLab Experiment E00-002, " F_2^N at low Q^2 ", C. E. Keppel and I. Niculescu, spokespersons

⁵JLab Experiment E00-116, "Measurement of Hydrogen and Deuterium Inclusive Resonance Cross Sections at Intermediate Q^2 for Parton-Hadron Duality Studies", C. E. Keppel, spokesperson

B. SUBNUCLEONIC EFFECTS IN NUCLEI

b.1. High-Energy Angular Distribution Measurements of the Deuteron Photodisintegration Reaction (R. J. Holt, E. C. Schulte, and K. Wijesooriya, and JLab E99-008 Collaboration)

The overall goal of experiment E99-008 is to determine the mechanism which governs photoreactions in the GeV energy region. If the incoming photon couples to an interchange quark or an exchange meson, then one would expect¹ the angular distribution for the $d(\gamma,p)n$ reaction to be symmetric about 90° . If the photon couples to a nucleon or a constituent quark in the nucleon, however, one would expect^{2,3} that the differential cross section in the forward direction to be substantially larger than in the backward direction. Previous measurements⁴ extend only to a photon energy of 1.6 GeV. The previous data are consistent with the incident photon coupling to a nucleon in the deuteron. In E99-008 the angular distribution was measured from $\theta_{\text{cm}} = 30^\circ$ to 143° at photon energies between 1.6 and 2.4 GeV. The high-resolution spectrometer in Hall A was used to detect photoprotons which emerged from a

liquid deuterium target that was irradiated by bremsstrahlung photons.

Results at 1.6 and 2.4 GeV are presented in Figure IV-5. The data for E99-008 are the filled triangles presented along with the available data at the same energies from JLab experiment E89-012 (open triangles) and SLAC experiments NE8 (solid circles) and NE17 (open circles). Also presented are two angular distribution calculations for deuteron photodisintegration. The solid line is the prediction from the Asymptotic Meson Exchange (AMEC) model³ and the dashed line is the Reduced Nuclear Amplitude (RNA) prediction¹. Notice that the forward-backward asymmetry previously observed in the NE8 data (Freedman) persists up to the highest energies measured, consistent with the photon coupling to the nucleon in the deuteron.

¹S. J. Brodsky and J. R. Hiller, Phys. Rev. C **28**, 475 (1983)

²T.-S. H. Lee, Argonne National Laboratory Report No. PHY-5253-TH-88; T.-S. H. Lee, in Proceedings of the International Conference on Medium and High Energy Nuclear Physics, Taipei, Taiwan, 1988 (World Scientific, Singapore 1988), p. 563

³S. I. Nagorny, Yu. A. Kasatkin, and I. K. Kirichenkov, Sov. J. Nucl. Phys. **55**, 189 (1992)

⁴S. J. Freedman *et al.*, Phys. Rev. C **48**, 1964 (1993)

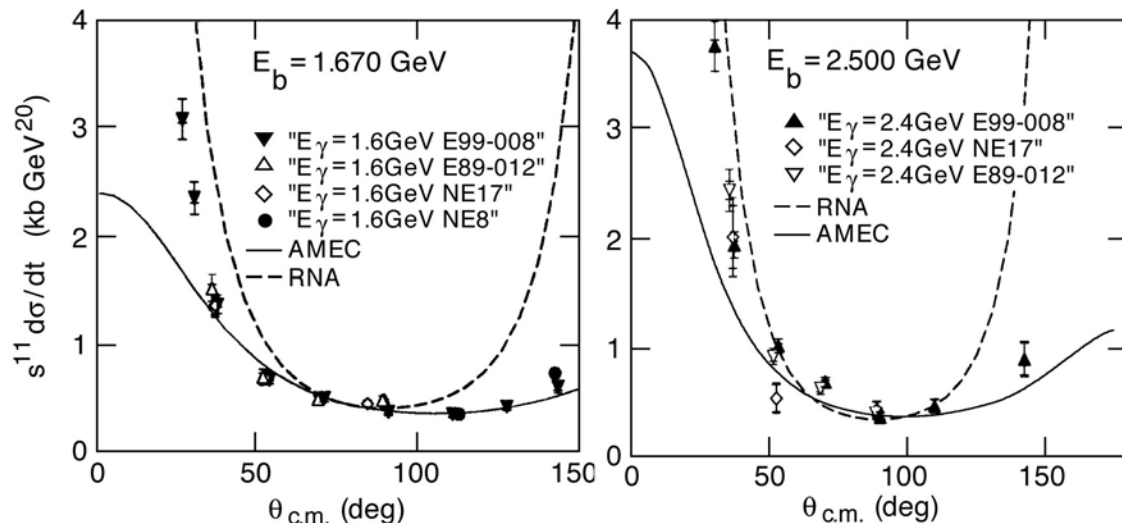


Fig. IV-5. The deuteron photodisintegration differential cross section at constant energy. Shown here are the data at 1.6 and 2.4 GeV incident photon energy, plotted as $s^{11} d\sigma/dt$, compared to previous data at forward angles. The JLab E99-008 data are the black triangles. The previous data shown are from JLab E89-012 (open triangles), SLAC NE17 (open diamonds), and SLAC NE8 (solid circles). The curves are the AMEC calculation (solid curve) and the RNA prediction (dashed curve).

b.2. Measurement of Longitudinal and Transverse Cross Sections in the ${}^3\text{He}(e,e'\pi^+){}^3\text{H}$ Reaction at $W = 1.6$ GeV (H. E. Jackson, J. Arrington, K. Bailey, D. De Schepper, D. Gaskell, D. F. Geesaman, B. Mueller, T. G. O'Neill, D. H. Potterveld, J. Reinhold, B. Zeidman, and JLab E91-003 Collaboration))

The ${}^3\text{He}(e,e'\pi^+){}^3\text{H}$ process holds much theoretical interest in that the mass-3 system is calculable using “exact” Faddeev type wave functions and hence serves as a good test of our understanding of nuclei. In addition, comparison to the fundamental $\text{H}(e,e'\pi^+)\text{n}$ process may shed some light on medium modifications to the pion electroproduction process. In general, one expects the ${}^3\text{He}(e,e'\pi^+){}^3\text{H}$ cross section to be suppressed by a factor roughly proportional to the square of the ${}^3\text{He}$ form-factor. Significant deviations from this behavior may signal changes to the pion electroproduction process in the nucleus. In experiment E91-003 at Jefferson Laboratory, the coherent ${}^3\text{He}(e,e'\pi^+){}^3\text{H}$ reaction was measured at $Q^2 = 0.4$ (GeV/c) 2 and $W = 1.6$ GeV for two values of the virtual photon polarization, ε , allowing the separation of longitudinal and transverse cross sections. The results from the coherent process on ${}^3\text{He}$ were compared to $\text{H}(e,e'\pi^+)\text{n}$ data taken at the same kinematics. This marks the first direct comparison of these processes. At these kinematics ($p_\pi = 1.1$ GeV/c), pion rescattering from the spectator nucleons in the ${}^3\text{He}(e,e'\pi^+){}^3\text{H}$ process is

expected to be small, simplifying the comparison to π^+ production from the free proton.

The unseparated and separated H and ${}^3\text{H}$ cross sections are given in Table IV-1. These cross sections are given in the laboratory frame at $Q^2 = 0.4$ (GeV/c) 2 and $\theta_{\text{pq}} = 1.72^\circ$. It is clear that both the separated and unseparated cross sections from the coherent process are, as expected, suppressed relative to the free nucleon cross section. This experiment improves upon previous ${}^3\text{H}$ experiments by measuring the cross section for a large final pion momentum such that rescattering effects should be small. Furthermore, this marks the first direct comparison of separated longitudinal and transverse ${}^3\text{He}(e,e'\pi^+){}^3\text{H}$ cross sections to those from the free proton. The results are consistent with the expectation that the suppression of the ${}^3\text{He}$ cross section relative to H is dominated by the ${}^3\text{He}$ form factor, indicating that the gross behavior of the reaction is understood and is an excellent candidate for more detailed theoretical calculation.

Table IV-1. Unseparated and separated laboratory cross sections for $\text{H}(e,e'\pi^+)\text{n}$ and ${}^3\text{He}(e,e'\pi^+){}^3\text{H}$ reactions at $W = 1.6$ GeV, $Q^2 = 0.4$ (GeV/c) 2 , and $\theta_{\text{pq}} = 1.72^\circ$. Uncertainties are statistical and systematic. A common value of the virtual photon flux Γ has been used in extracting the virtual photon cross sections to facilitate comparisons between the targets.

$d\sigma/d\Omega_\pi$ ($\mu\text{b}/\text{sr}$)		
	${}^3\text{H}$	H
Unseparated Cross Sections		
$\varepsilon = 0.490$	$14.89 \pm 0.36 \pm 1.00$	$44.23 \pm 0.36 \pm 2.52$
$\varepsilon = 0.894$	$21.80 \pm 0.40 \pm 1.50$	$58.18 \pm 0.44 \pm 3.42$
Separated Cross Sections		
σ_L	$17.12 \pm 1.36 \pm 2.38$	$34.57 \pm 1.41 \pm 4.38$
σ_T	$6.50 \pm 0.95 \pm 1.45$	$27.29 \pm 0.96 \pm 2.89$

b.3. Electroproduction of Kaons and Light Hypernuclei (J. Arrington, K. Bailey, F. Dohrmann, D. F. Geesaman, K. Hafidi, H. E. Jackson, B. Mueller, T. G. O'Neill, D. Potterveld, P. Reimer, B. Zeidman, and E91-016 Collaboration)

Jefferson Lab experiment E91-016, “Electroproduction of Kaons and Light Hypernuclei”, is a study of the production of Kaons on targets of H, D, ^3He , and ^4He at an incident electron energy of 3.245 GeV and $Q^2 \approx 0.37 \text{ GeV}^2$. For H and D targets, additional data were obtained at an energy of 2.445 GeV and $Q^2 \approx 0.5 \text{ GeV}^2$. The scattered electrons and emergent K^+ were detected in coincidence with the use of the HMS and SOS spectrometers in Hall C. Particle identification utilizing time-of-flight techniques together with Aerogel Cerenkov detectors provided clean missing-mass spectra and allowed subtraction of random backgrounds. In addition to obtaining spectra, angular distributions were measured at forward angles with respect to the virtual photons.

The fundamental interaction being studied is the $N(e,eK^+)Y$ where Y is either a Λ or Σ and N is a nucleon, either free or bound in a nucleus. For H, the final state can only be a Λ or Σ^0 , with a missing mass spectrum consisting of two distinct peaks. For heavier targets, however, not only can Σ^- be produced on the neutron, but the relative motion of the bound nucleons results in quasi-free broadening of the peaks, as is illustrated in Fig. IV-6. Since there is no known bound state in the mass 2 hyper-nuclear system, only quasi-free production is observed. For D, the Fermi broadening is less than the mass difference between hyperons so that separation of the Λ and Σ contributions utilizing Monte-Carlo simulations that include final-state-interactions, FSI, is relatively straightforward. Because of the small mass difference between Σ^0 and Σ , however, distinguishing between these contributions is not possible without assuming that the Λ/Σ^0 ratio is the same as that for the free proton. Subtraction of the normalized Σ^0 contribution yields a value for Σ^- production on the neutron. The ratio of cross sections for Σ^0/Σ^- suggests s-channel dominance for the $D(e,eK^+)$ reaction in the present kinematic regime.

For the heavier targets, $^3,^4\text{He}$, both Fermi broadening and a rapidly increasing number of final state configurations make it more difficult to separate the various contributions, as is evident in the figure. Indeed, there is no obvious indication of the Σ contributions for ^4He . As a result, the simulations are sensitive to detailed descriptions of the wave functions and final configurations for these nuclei. The simulations utilize various forms for the momentum distributions within the target nuclei, but there is

qualitative agreement for the shapes of the quasi-free distributions. The detailed fits require FSI and small variations in shape near the quasi-free threshold that make it difficult to extract precise cross sections for formation of bound states. Nevertheless, the analyses of the data for ^4He provide unambiguous evidence (Fig. IV-6) for the formation of the bound hypernucleus hyper- ^4H ; the first observation of electroproduction of a hyper-nuclear bound state. From other reactions, a 1^+ excited state bound by approximately 1 MeV is known to exist in this nucleus; the 0^+ ground state is bound by 2.04 MeV. The evidence for the electroproduction of the hypertriton, *i.e.*, the p-n- Λ bound state known to have a binding energy of approximately 130 keV, is less convincing. While barely discernible near zero degrees, the bound state becomes more evident away from 0 degrees, inasmuch as the quasifree peak moves to higher missing mass.

Extraction of cross sections for specific channels becomes more difficult with increasing mass because of the rapidly growing number of possible final configurations. As is seen in the figure, however, the various models that have been utilized for the Helium isotopes yield simulations that are in reasonable agreement with the shapes of the spectra. Since it is not possible to distinguish between Σ^0 and Σ^- production, the analyses assume the Λ/Σ^0 ratio data for H obtained at the same laboratory settings as input to extract the Σ^- yields. Further analyses of these results are in progress. There are suggestions of peaks in the missing mass regions near the Σ threshold. Inasmuch as there are issues related to detailed configurations, however, there is no plausible evidence for possible bound Σ states at this time.

E91-016 is a high-statistics study of Kaon electroproduction on light nuclei. During the course of the experiment, extensive data were obtained for the H target as well as additional calibration data for C and Al. These latter data have been analyzed in a relatively crude manner to ascertain the general mass dependence of the cross sections for Kaon electroproduction. Other aspects of the experiment, such as Omega production on the proton, will be reported later. E91-016 has provided all or a substantial fraction of the thesis data for students from Hampton University, University of Pennsylvania, and Temple University.

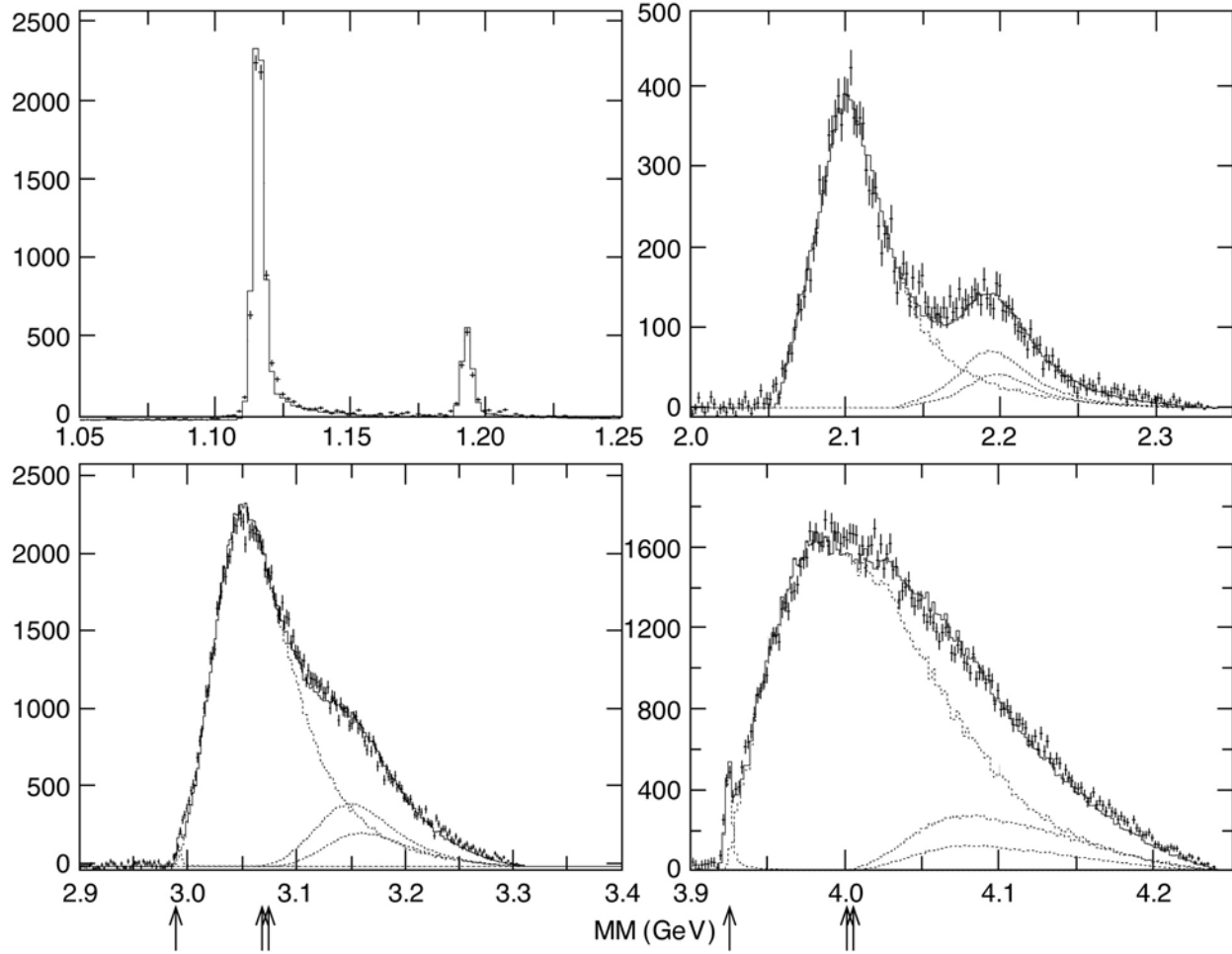


Fig. IV-6. Spectra obtained along the virtual photon direction for the $A(e, e'K^+)YX$ reaction where A is H , D , ${}^3\text{He}$, and ${}^4\text{He}$ (upper left, upper right, lower left, lower right, respectively) while X represents the residual system. The dotted curves indicate Monte-Carlo simulations for Λ , Σ^0 , and Σ^- production as well as possible bound-states; the solid curves are the sums of these individual contributions. The arrows indicate the thresholds for quasi-free Λ , Σ^0 , Σ^- production on ${}^3\text{He}$ and ${}^4\text{He}$.

b.4. Measurements of the Nuclear Dependence of $R = \sigma_L/\sigma_T$ at Low Q^2 (J. Arrington, D. F. Geesaman, T. G. O'Neill, D. Potterveld, and the JLab E99-118 Collaboration)

Inclusive electron scattering is a well-understood probe of the partonic structure of nucleons and nuclei. Deep inelastic scattering has been used to make precise measurements of nuclear structure functions over a wide range in x and Q^2 . The ratio $R = \sigma_L/\sigma_T$ has been measured reasonably well in deep inelastic scattering at moderate and high Q^2 using hydrogen and deuterium targets. However, R is still one of the most poorly understood quantities measured in deep inelastic scattering and few measurements exist at low Q^2 or for nuclear targets. Existing data at moderate to large values of Q^2 rule out significant nuclear effects in R .

Jefferson Lab Experiment E99-119 is a direct measurement of R at low x and low Q^2 . The experiment was performed in July of 2000 and recorded data on hydrogen, deuterium, and heavier nuclei. Because the data extend to very low x and Q^2 , the radiative corrections become extremely large and need to be modeled carefully. The analysis is still underway and is currently focused on testing the radiative corrections to determine how low in Q^2 the cross section can be reliably extracted. Final results are expected in the next year.

b.5. Measurement of the EMC Effect in Very Light Nuclei (J. Arrington, F. Dohrmann, D. Gaskell, D. F. Geesaman, K. Hafidi, R. J. Holt, H. E. Jackson, D. H. Potterveld, P. E. Reimer, B. Zeidman, and E00-101 Collaboration)

The EMC collaboration first measured the difference between the structure function of heavy nuclei and deuterium, indicating a modification of the quark distributions in the nuclear environment. They observed a suppression of the structure function in heavy nuclei at large values of x (corresponding to large quark momenta), and an enhancement at low x values. The EMC effect was subsequently measured by several other experiments for a variety of nuclei. The ratio of F_2 for the heavy nucleus to F_2 for the deuteron has the same shape for all nuclei, and only the magnitude of the enhancement and suppression depends on the nucleus. Many attempts have been made to explain the EMC effect, but none can fully reproduce the observed modifications, and there is still no consensus on which effect or combination (if any) explains the data.

The EMC effect for ${}^3\text{He}$ and ${}^4\text{He}$ experiment E00-101¹ will be measured. The current data cannot distinguish different models of the density dependence of the effect. By measuring the EMC effect for light nuclei (${}^3\text{He}$ and ${}^4\text{He}$) we will extend the range of nuclei for which precision data exists. Because ${}^4\text{He}$ has an anomalously large density for a light nucleus, it is the most sensitive test to determine if the EMC effect scales with A or with nuclear density. More importantly, we will take precision data that can be

compared to exact few body calculations. If the EMC effect is caused by few nucleon interactions, the universal shape in heavy nuclei may be a result of a saturation of the effect, and the shape may be different in few-body nuclei. Figure IV-7 shows the existing data on ${}^3\text{He}$, along with the projected uncertainties for the E00-101 measurement. The curves show calculations of the EMC effect for ${}^3\text{He}$ and ${}^4\text{He}$, along with the fit to the data from heavy nuclei. While the existing data on heavy nuclei all show the same x -dependence, these calculations predict significantly different dependences for very light nuclei. E00-101 will be able to measure these differences, and allow us to distinguish between different models of the EMC effect based on their predictions for few-body nuclei.

Finally, a measurement of $A \leq 4$ nuclei will provide a way to test models of nuclear effects in light nuclei. Models of the nuclear effects in deuterium and ${}^3\text{He}$ must be used to extract information on neutron structure, so we need to be able to test and evaluate these models. A high precision measurement including ${}^1\text{H}$, ${}^2\text{H}$, ${}^3\text{He}$, and ${}^4\text{He}$ will give a single set of data that can be used to evaluate these models in several light nuclei, and help quantify the model dependence of the neutron structure functions inferred from measurements on ${}^2\text{H}$ and ${}^3\text{He}$.

¹Jefferson Lab Experiment E00-101, "A Precise Measurement of the Nuclear Dependence of Structure Functions in Light Nuclei", J. Arrington, spokesperson

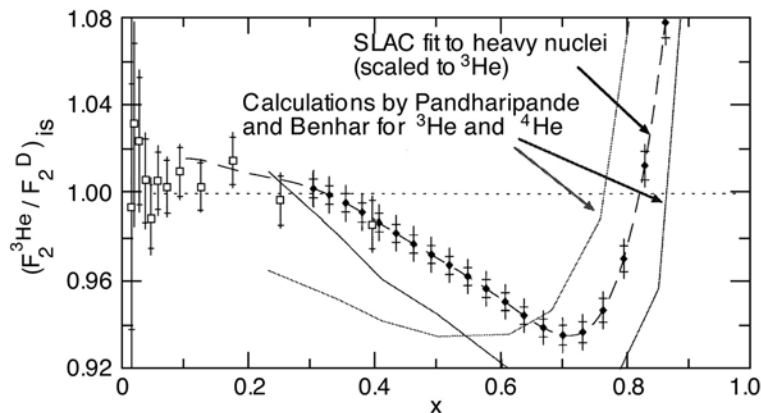


Fig.IV-7. Existing data for the EMC effect in ${}^3\text{He}$ from the HERMES experiment (hollow squares), along with projected uncertainties for the E00-101 measurement. The solid lines are calculations for ${}^3\text{He}$ and ${}^4\text{He}$, while the dashed line is the SLAC fit to the EMC effect in heavy nuclei.

b.6. Measurement of High Momentum Nucleons in Nuclei and Short Range Correlations
(J. Arrington, D. F. Geesaman, K. Hafidi, R. J. Holt, H. E. Jackson, P. E. Reimer,
E. C. Schulte and JLab E02-019 Collaboration)

Inclusive scattering from nuclei at low energy transfer (corresponding to $x > 1$) is dominated by quasielastic scattering from nucleons within the nucleus. As the energy transfer is decreased, the scattering probes nucleons of increasing momentum and we can map out the distribution of high momentum nucleons in nuclei. Experiment E89-008¹ measured inclusive scattering for deuterium, carbon, iron, and gold at $x > 1$ using 4 GeV electrons at Jefferson Lab. These data can be used to constrain the high momentum components of nuclear spectral functions. In addition, as the high momentum nucleons are dominantly generated by short-range correlations (SRCs), these data allow us to examine the strength of two-nucleon correlations in heavy nuclei.

Experiment E02-019² will extend these measurements to higher values of x and Q^2 using the 6 GeV electron beam at JLab. In addition to measuring scattering from deuterium and heavy nuclei, data will be taken on ^3He and ^4He . The higher Q^2 values in this experiment should simplify the extraction of the high momentum components, as effects such as final state interactions should be reduced as Q^2 is increased. Measurements with few-body nuclei (^2H , ^3He , and ^4He) allow contact with theoretical calculations *via* essentially “exact” calculations for few-body systems. This can be used to study in detail contributions to the interaction beyond the impulse approximation (*e.g.* final state interactions). Data on heavy nuclei can then be used to constrain the high momentum components of their spectral functions, as well as allowing an extrapolation nuclear matter.

The extension to higher energies will provide us with significantly greater sensitivity to the high momentum components of the nuclear wave function, probing nucleons with momenta in excess of 1000 MeV/c. This will improve our ability to study the structure of nucleon correlations in nuclei. Direct comparisons of heavy nuclei to deuterium at large x will allow us to map out the strength of two-nucleon correlations in both light and heavy nuclei. In addition, comparing heavy nuclei and ^3He at extremely large x values ($2.5 <$

$x < 3$) may provide the first experimental signature of multi-nucleon correlations. In this region, the contribution from two-nucleon short-range correlations (SRCs) should be small, and multi-nucleon correlations may dominate the momentum distribution. This would be a first step in the study of multi-nucleon correlations. These correlations are important because they are an integral part of the structure of nuclei, but also because they represent local configurations of extremely high density within the nucleus.

In addition to probing nucleon distributions and short range correlations, these data fill a significant void in our knowledge of the nuclear structure function. Little data exist for nuclei at large x , yet such data are important in the study of scaling and duality, higher twist effects, and nuclear dependence of the structure function. In addition, while the $x > 1$ structure function is often neglected, it must be included in studies of the energy-momentum sum rule or analysis of the QCD moments. While E02-019 will focus on the study of the high momentum nucleons in nuclei, it provides the data necessary for a variety of studies.

The experiment was approved by PAC21 for 28 days of beam time in Hall C with an A- scientific rating. Figure IV-8 shows the coverage of the proposed measurement compared to existing data from JLab E89-008 and SLAC-NE3. Over the entire x range, there is a significant increase in the Q^2 coverage compared to previous experiments. The data in the scaling region (above $Q^2 \sim 3 \text{ GeV}^2$) are especially important, as this is the region where final state interactions appear to be small. In the range of $1.5 < x < 2$ the sensitivity of the data to two-nucleon correlations is greatest, and we will increase not only the Q^2 range, but also add the helium isotopes to better study the A-dependence of the SRCs. For $2.5 < x < 3$, we will take the first high precision data in the scaling region, which will provide a much greater sensitivity to the presence of multi-nucleon correlations.

¹J. Arrington, *et al.*, Phys. Rev. Lett. **82**, 2056 (1999)

²Jefferson Lab Experiment E02-019, “Inclusive Scattering from Nuclei at $x > 1$ and High Q^2 with a 6 GeV Beam”, J. Arrington, D. B. Day, A. Lung, and B. W. Filippone spokespersons

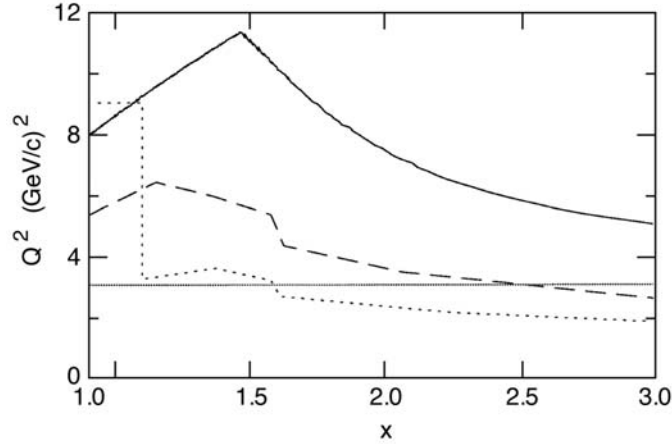


Fig. IV-8. Kinematic coverage in x and Q^2 for the proposed measurement (solid line) compared to the previous JLab (dashed) and SLAC (dotted) data. The horizontal line at $Q^2 = 3$ indicates the region where the current data show the onset of scaling.

b.7. Search for the Onset of Color Transparency (Letter of Intent LOI-02-004 to JLab-PAC21) (K. Hafidi, B. Mustapha, J. Arrington, F. Dohrmann, A. El Alaoui, D. F. Geesaman, R. J. Holt, H. E. Jackson, D. Potterveld, P. Reimer, E. C. Schulte and Hall B Collaboration)

According to QCD, pointlike colorless systems, such as those produced in exclusive process at high Q^2 have a vanishingly small transverse size. Therefore, they are expected to travel through nuclear matter experiencing very little attenuation. This effect, referred to as color transparency (CT), cannot be explained in the hadronic picture of nuclear matter (Glauber theory) and calls upon the quark's degrees of freedom. Earlier measurements were mainly focused on quasi-elastic hadronic (p , $2p$) and leptonic ($e,e'p$) scattering off nuclear targets. Although high energy experiments (Fermilab E791)¹ observed a clear signal of CT, none of the intermediate energy experiments (SLAC² and JLab³) produced an evidence for CT up to a $Q^2 \sim 8 \text{ GeV}^2$

In this experiment, we propose to look for CT in the incoherent diffractive ρ^0 electroproduction on hydrogen (or deuterium), carbon and copper. In this process, the virtual photon fluctuating into a $q\bar{q}$ pair could produce a vector meson by interacting with a nucleon inside the target, see Fig. IV-9. This fluctuation can propagate over a distance ℓ_c called "coherence length".

The observable carrying the signature of CT is the transparency ratio:

$$T_A = \frac{\rho_A}{A\rho_N}$$

where ρ_A is the ρ^0 production cross section on the nuclear target (A) and ρ^0 is measured on the nucleon. The possible manifestation of CT is a significant increase of T_A as a function of Q^2 . Recent theoretical calculations by Kopeliovich *et al.*⁴ predicted an increase of more than 40% at $Q^2 \sim 4 \text{ GeV}^2$, see Fig. IV-9.

Recent measurements by HERMES⁵ have shown that T_A increases when ℓ_c varies from long to short compared to the size of the nucleus. This so-called coherence length effect can mock the signal of CT and should be under control. Therefore, we propose to measure the Q^2 dependence of the transparency T_A at fixed coherence length ℓ_c . Figure IV-10 shows the proposed measurements at complementary ℓ_c values to map the whole Q^2 region up to 4 GeV^2 .

¹E. M. Aitala *et al.*, Phys. Rev. Lett. **86**, 4773 (2001)

²N. C. R. Makins *et al.*, Phys. Rev. Lett. **72**, 1986 (1994); T. G. O'Neill *et al.*, Phys. Lett B **351**, 87 (1995)

³D. Abbott *et al.*, Phys. Rev. Lett. **80**, 5072 (1998); M. Battaglieri *et al.*, Phys. Rev. Lett. **87**, 172002 (2001)

⁴B. Kopeliovich *et al.*, Phys. Rev. C **65**, 035201 (2002)

⁵K. Ackerstaff *et al.*, Phys. Rev. Lett. **82**, 3025 (1999)

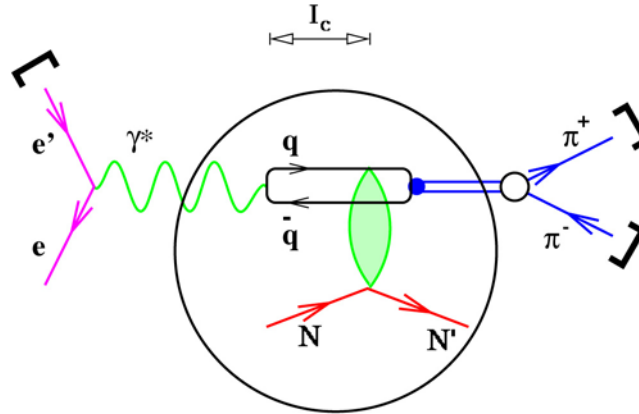


Fig. IV-9. Exclusive electroproduction of the ρ^0 meson.

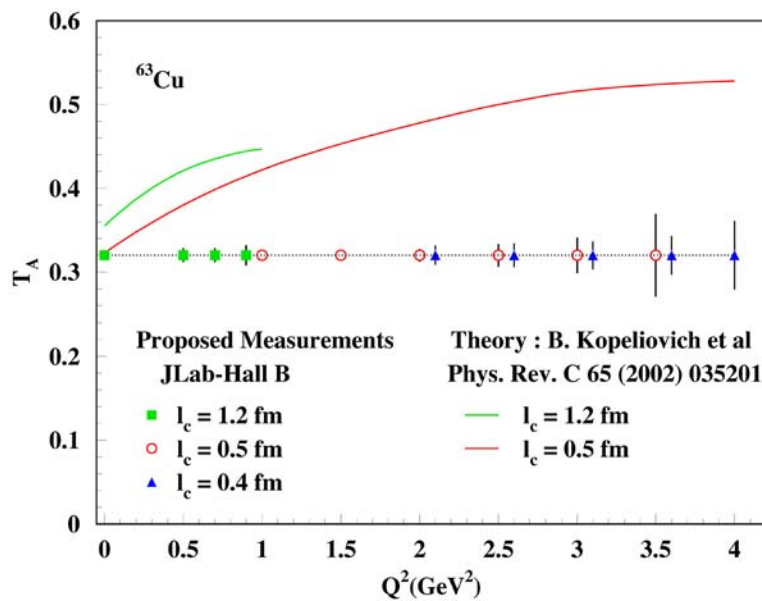


Fig. IV-10. Theoretical predictions and simulated results

b.8. Measurement of the Transparency Ratio for the $A(\gamma, \pi^- p)$ Reaction in Helium and Deuterium (R. J. Holt, J. Arrington, K. Bailey, P. E. Reimer, F. Dohrmann, K. Hafidi, T. O'Connor, E. C. Schulte, and K. Wijesooriya, and JLab E94-104 Collaboration)

The transparency for the ${}^4\text{He}(\gamma, \pi^- p)$ reaction compared with the $\text{D}(\gamma, \pi^- p)$ reaction was measured as a function of photon energy in Hall A at Jefferson Laboratory. The fundamental process $\gamma n \rightarrow \pi^- p$ exhibits a scaling behavior consistent with the constituent counting rules above a photon energy of 2.5 GeV. Thus, one can use

this reaction in the nuclear medium to determine whether the onset of color transparency has been observed. The pion is expected¹ to exhibit the phenomenon of color transparency more readily than the proton since the pion has only two constituent partons. The data are presently being analyzed.

¹B. Blättel *et al*, Phys. Rev. Lett. **70**, 896 (1993)

b.9. New Optics and Acceptance Model for the Jefferson Lab High Resolution Spectrometers (J. Arrington, O. Okafor, D. H. Potterveld and E. C. Schulte, M. Boswell,* R. Ent,* and D. Meekins*)

The standard equipment for Hall A at Jefferson Lab consists of a pair of nearly identical high resolution spectrometers (HRS). While these spectrometers provide a very good measurement of the momentum of detected particles, the optics models that have been used in the past did not accurately reproduce the acceptance of the spectrometer. Experiments that needed to extract a cross section have thus been forced to adjust the apertures in the model to reproduce the data (replacing physical apertures with effective ones), or apply cuts to the data to the region of uniform acceptance.

Experiment E99-008, a measurement of the angular distribution of deuteron photodisintegration, was performed in Hall A using the HRS spectrometers. To avoid applying cuts that would have significantly reduced the statistics of the measurements, a new optics and acceptance model was generated for this and future experiments. The new model uses COSY generated

transformations to model the magnetic elements, and applies cuts for the collimator, apertures within each of the magnets, and the active region of the detectors. The spectrometer model was incorporated into SIMC, the physics simulation code used by several experiments in Hall C. The new spectrometer model did a better job of reproducing the data, improving the acceptance of the spectrometer. The new HRS model is currently being incorporated into the standard Hall A physics simulation code, MCEEP, so that the new model can be evaluated more carefully and be used in the analysis of other experiments. While this new model fixes the obvious discrepancies between the old model and the data, there are still small differences in the distribution of events at the detector plane. We are currently working to optimize the optics model by including small position offsets and rotations of the magnets to reproduce the distortions observed in the event distributions at the detectors.

*Jefferson Laboratory

C. QUARK STRUCTURE OF MATTER

c.1. Measurement of the Structure Function of the Pion (R. J. Holt, P. E. Reimer, and K. Wijesooriya)

The light mesons have a central role in nucleon and in nuclear structure. The masses of the lightest hadrons, the mesons, are believed to arise from chiral symmetry breaking. The pion, being the lightest meson, is particularly interesting not only because of its importance in effective theories, but also because of its importance in explaining the quark sea in the nucleon and the nuclear force in nuclei.

Until recently, the pion structure function was only studied *via* πp Drell-Yan scattering. The analysis of the Drell-Yan data was questioned¹ recently, and now studies of this analysis are underway. New measurements² at a very low momentum fraction, x , have been made with semi-inclusive deep inelastic

scattering through the process $ep \rightarrow e'NX$. In this reaction, the virtual photon scatters off of the pion in the $|\pi^+n\rangle$ or $|\pi^0p\rangle$ or Fock components of the proton and the intact nucleon is detected.

Studies are underway of the feasibility of making such measurements at Jefferson Lab using an 11-GeV incident electron beam using a modified RAPGAP³ Monte Carlo program. Early results show that the relatively high luminosity which can be achieved at an upgraded Jefferson Lab will enable the pion structure to be measured, over a limited range in x . Additional investigations are being made of this reaction using a future electron-ion collider.⁴

¹M. B. Hecht *et al.*, Phys. Rev. C **63**, 025213 (2001)

²C. Adloff *et al.* (H1 Collaboration, Eur. Phys. J. C **6**, 587 (1999)

³H. Jung, Comp. Phys. Commun. **86**, 147 (1995)

⁴R. J. Holt and P. E. Reimer, Proc. of the Second Workshop on the Polarized Electron Ion Collider, MIT (2000)

c.2. Measurements of Spin-Structure Functions and Semi-Inclusive Asymmetries for the Nucleon at HERA (H. E. Jackson, A. El Alaoui, K. G. Bailey, T. P. O'Connor, K. Hafidi, D. H. Potterveld, P. Reimer, Y. Sanjiev, and the HERMES Collaboration)

HERMES, HERA Measurement of Spin, is a second-generation experiment to study the spin structure of the nucleon by using polarized internal gas targets in the HERA 30 GeV electron storage ring. Since 1995, the experiment has provided fundamental new insights into the structure of the nucleon and how it is affected by the nuclear medium. The unique capabilities of the experiment have produced data that were not possible with previous measurements at SLAC, CERN, and Fermilab. The collaboration has collected and analyzed millions of deep-inelastic scattering events using longitudinally polarized electrons and positrons incident on longitudinally polarized internal gas targets of ^1H , ^2H , and ^3He , as well as thicker unpolarized gas targets. These data together with large sets of photo-production events have yielded several results that were unexpected and are provoking new work, both theoretical and experimental.

The primary goal of HERMES is the study of the spin structure of the nucleon. Spin asymmetries have been measured using polarized targets of hydrogen, deuterium, and ^3He . Analysis of the inclusive and

semi-inclusive deep-inelastic scattering data from these unique undiluted targets has resulted in the world's most precise determination to date of the separate contributions of the up, down and sea quarks to the nucleon spin.¹ Further dramatic improvements are expected from the data under analysis. One of the surprises yielded by the experiment was a negative polarization asymmetry (though with large statistical uncertainty) in the cross section for photo-production of pairs of hadrons with high transverse momenta, providing the first direct indication of a positive gluon spin contribution to the nucleon. Again, recent and future data will much improve the statistical precision. Another exciting result is the observation of a single-spin asymmetry in the azimuthal distribution of positive pions detected in coincidence with the deep-inelastic scattering of positrons from a *longitudinally* polarized proton target. While the theoretical interpretation of this result is under vigorous discussion, it seems clear that the effect can be explained only by a particular chiral-odd fragmentation function that promises to make feasible at HERMES the first measurement of transversity, the only remaining unmeasured and one of

the three most fundamental (leading twist) flavor-sets of parton distribution functions. Finally, a result from HERMES of great interest has been the first measurement of a lepton-beam spin asymmetry in the azimuthal distribution of detected photons in Deeply Virtual Compton Scattering (DVCS). Interference with the indistinguishable but well-understood Bethe-Heitler process fortuitously gives rise to a rich variety of such asymmetries, which will continue to emerge from HERMES data. DVCS is considered to be the most reliable of the various hard exclusive processes that constrain the generalized or 'skewed' parton distributions, which are now the subject of intense theoretical development as, *e.g.*, they embody information about *orbital* angular momenta of partons. Most recently, this type of measurement has been extended to the study of exclusive electroproduction of pions, where substantial single-spin azimuthal asymmetries have been observed for the first time.

The HERMES physics reach extends well beyond nucleon spin structure. The large momentum and solid angle acceptance of the HERMES spectrometer have opened a much broader range of physics topics to exploration, and have resulted in a tool for the general study of photon-hadron interactions. Focusing its unique capabilities on specific applications of deep-inelastic scattering (DIS), HERMES has performed a measurement of the flavor asymmetry between up and down quarks in the nucleon sea,² several studies of fragmentation of up and down quarks to pions, measurement of the DIS and resonance contributions to the generalized Gerasimov-Drell-Hearn integral for both the proton and neutron,^{3,4} a measurement of the spin transfer from virtual photons to Λ^0 hyperons,⁵ and measurements of the effect of the nuclear environment. A broad program of measurements involving diffractive vector meson production is also underway with basic studies in ρ^0 , ϕ^0 , ω^0 , and J/ψ production,⁶ as well as the determination of photon \rightarrow vector-meson spin density matrix elements through the analysis of the angular distribution of the decay products.⁷ The ρ^0 semi-exclusive cross section has been found to have a large and unexpected spin dependence.⁸ The study of diffractive ρ^0 production in nuclei has led to the

observation of a lifetime (coherence length) effect on the initial-state nuclear interactions of the virtual quark pair that represent the hadronic structure of the photon, and will lead to new limits on the magnitude of color transparency effect.⁹ Recent developments and new results pertaining to these physics topics are discussed in more detail below, and references may be found at the end of this report. It is evident that HERMES has a broad physics program and has had scientific impact on an impressive number of fundamental questions about the strong interaction. HERMES is playing an important role in the worldwide experimental investigation of QCD.

The experiment is technically sound. The means to produce and measure high beam polarization and high target polarization are well understood. The spectrometer and its instrumentation have been carefully modeled and operate reliably and in an understandable fashion. Data analysis software and computational power are now at an advanced stage, allowing the collaboration to produce results in a timely fashion. Furthermore, a vigorous upgrade program has continued to enhance the capabilities of the spectrometer. The gas threshold Cerenkov detector was replaced by a dual-radiator ring-imaging Cerenkov (RICH) detector to identify pions, kaons, and protons over nearly the entire momentum acceptance, and both a new iron wall and the iron of the spectrometer magnet were instrumented to improve the acceptance and identification of high energy muons from charm decay. Finally, preparations are being made for the installation in the first months of 2002 of two new rings of silicon strip detectors just downstream of the target, primarily to enhance the detection of Λ^0 decay products. As will be discussed below, the combination of all these new detectors opens the door to new exciting measurements. This extraordinary and unique facility represents the investment of nearly a thousand person-years and 40 MDM, from over 33 institutes from 10 countries in Europe, Asia and North America. Nevertheless, in comparison with other experiments and laboratories, it is highly cost-effective with respect to its productivity and potential.

¹K. Ackerstaff *et al.*, Phys. Lett. B **464**, 123 (1999)

²K. Ackerstaff *et al.*, Phys. Rev. Lett. **81**, 5519 (1998)

³K. Ackerstaff *et al.*, Phys. Lett. B **444**, 531 (1998)

⁴A. Airapetian *et al.*, DESY 00-097, hep-ex/0008037

⁵A. Airapetian *et al.*, DESY 99-151, hep-ex/9911017

⁶A. Airapetian *et al.*, accepted by Eur. Phys. J.C

⁷K. Ackerstaff *et al.*, DESY 99-199, hep-ex/0002016

⁸F. Meissner, Proceedings of the 7th International Workshop on Deep Inelastic Scattering and QCD, Zeuthen, Germany, April 1999

⁹K. Ackerstaff *et al.*, Phys. Rev. Lett. **82**, 3025 (1999)

c.3. Inclusive Measurements of the Deuteron Spin structure Function (H. E. Jackson, A. El Alaoui, K. G. Bailey, T. P. O'Connor, K. Hafidi, D. H. Potterveld, P. Reimer, Y. Sanjiev, and the HERMES Collaboration)

Inclusive measurements of the spin structure functions for the proton and neutron continue to be an important element in the HERMES program. Measurements of $g_1^d(x)$ provide the basic data for the neutron structure function. The inclusive deuteron spin asymmetries are also an essential component of the global analysis of spin asymmetries used in the flavor decomposition of the polarized quark structure functions of the nucleon. HERMES has precisely determined the spin structure functions of both the proton and neutron, $g_1^p(x)$ and $g_1^n(x)$, over a range in Bjorken x from approximately ~ 0.001 to ~ 0.8 , using various beams, targets and spectrometers.

Results of the measurement of the inclusive spin dependent asymmetry from HERMES, and CERN/SMC are shown in Fig. IV-11, where the ratio g_1^d/F_1 of the deuteron is plotted. The data sets are in remarkable agreement, thus demonstrating that the experimental uncertainties are well understood. As the SMC data have an average Q^2 that is about a factor of 3 to 10 larger than those of the SLAC and the HERMES measurements, the Q^2 dependence of the asymmetry g_1/F_1 is revealed to be small. Such data have strongly confirmed the earlier EMC result and extended the range and precision of the knowledge of g_1 , which provides a strong constraint for all models and parameterizations of the polarized quark distributions.

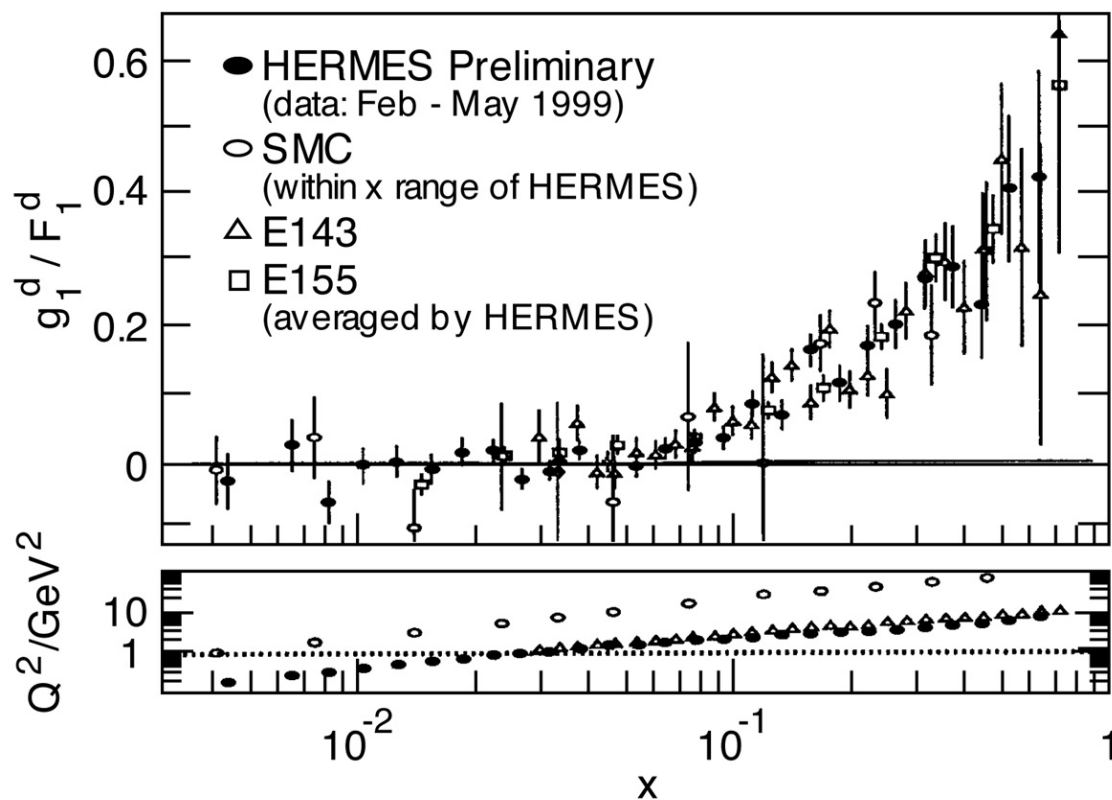


Fig. IV-11. The HERMES measurement of g_1^d compared to SLAC-143 and CERN/SMC. All data are given at their quoted mean Q^2 .

c.4. Flavor Decomposition of Polarized Structure Functions (H. E. Jackson, A. El Alaoui, K. G. Bailey, T. P. O'Connor, K. Hafidi, D. H. Potterveld, P. Reimer, Y. Sanjiev, and the HERMES Collaboration)

Information from inclusive scattering is inherently limited by the domination of scattering from up quarks, since the cross sections scale as the square of the electric charge, which is twice as large for up quarks as for down or strange quarks. Also, quarks and antiquarks of the same flavor obviously produce identical effects. To distinguish the contributions of the quark flavors and in particular of the sea quarks, it is necessary to use other types of experimental information. In semi-inclusive scattering, a leading hadron is detected in coincidence with the deep-inelastic scattering of a lepton. The essential principle behind this method is the likelihood of the leading hadron to 'contain' the quark originally struck by the virtual photon from the lepton. Scattering asymmetries with various leading hadrons in the final state can be analyzed to determine the fractional contributions of the various quark flavors to the nucleon spin.

The HERMES collaboration is in the process of determining the flavor dependence of quark polarizations in the nucleon in a global analysis of inclusive and semi-inclusive spin asymmetries for positive and negative pions and kaons which assumes a five component decomposition of quark spin, *i.e.* u, \bar{u}, d, \bar{d} , and $s + \bar{s}$. Data are included for both proton and deuteron targets. Factorization into parton distributions and fragmentation functions is assumed in the relation between the measured asymmetries and quark polarizations. The resulting coefficients or "purities" include effects of experimental acceptance, and are determined with a Monte Carlo generator and CTEQ low Q^2 parton distributions. An independent two-component purity analysis using only the deuteron inclusive and total kaon semi-inclusive asymmetries provides an independent check on the results for the polarization of the strange sea. The first complete analysis is in its final stages, and results will be released in the spring of 2002.

c.5. Gluon Polarization (H. E. Jackson, A. El Alaoui, K. G. Bailey, T. P. O'Connor, K. Hafidi, D. H. Potterveld, P. Reimer, Y. Sanjiev, and the HERMES Collaboration)

A measurement of the polarization of the gluons in the nucleon is of central importance to understanding the origin of the spin of the nucleon. A promising prospect is a direct measurement of $\Delta G(x)$ using scattering processes in which the gluon enters in leading order. Such a lepto-production process is photon-gluon fusion (PGF). Experimental signatures of this process are charm production and the production of jets on hadrons with high transverse momentum. Both of these signals have been successfully exploited at higher energy in measurements of the unpolarized gluon structure function. Such measurements are central goals of the COMPASS experiment¹ at CERN and of the RHIC-SPIN groups in the experiments STAR and PHENIX.² At HERMES the spin asymmetry in the polarized photo-production of pairs of hadrons with opposite charge and high transverse momentum has been studied.³ Under certain kinematical conditions, this signal is dominated by PGF, which has a strong negative polarization analyzing power.

A published HERMES result for the highest transverse momenta accessible suggested that gluons have a significant positive polarization. For h^+h^- pairs with $p_T^{h_1} > 1.5$ GeV/c and $p_T^{h_2} > 1.0$ GeV/c, the spin asymmetry is found to be $A_{||} = -0.28 \pm 0.12$ (stat) ± 0.02 (sys). This negative value is in contrast to the positive asymmetries typically measured in deep-inelastic scattering from protons. When these data are interpreted in a LO QCD model implemented in the PYTHIA Monte Carlo generator, a value for $\Delta G(x)/G(x)$ of $0.41 \pm 0.18 \pm 0.03$ has been determined at $\langle x_G \rangle = 0.17$. The sensitivity of the HERMES measurement can be increased by using high- p_T kaon pairs. The production of strange hadrons in fragmentation is suppressed compared to non-strange hadrons, with the result that background from DIS will be suppressed, and the sample of kaon pairs will be cleaner than the corresponding pion sample. For this reason, in the HERMES analysis, a lower cut on $p_T^{h_1}$ could be used to improve statistics. Fig. IV-12 shows preliminary results for high- p_T kaon pairs from proton and deuteron targets. The data are still under study, and

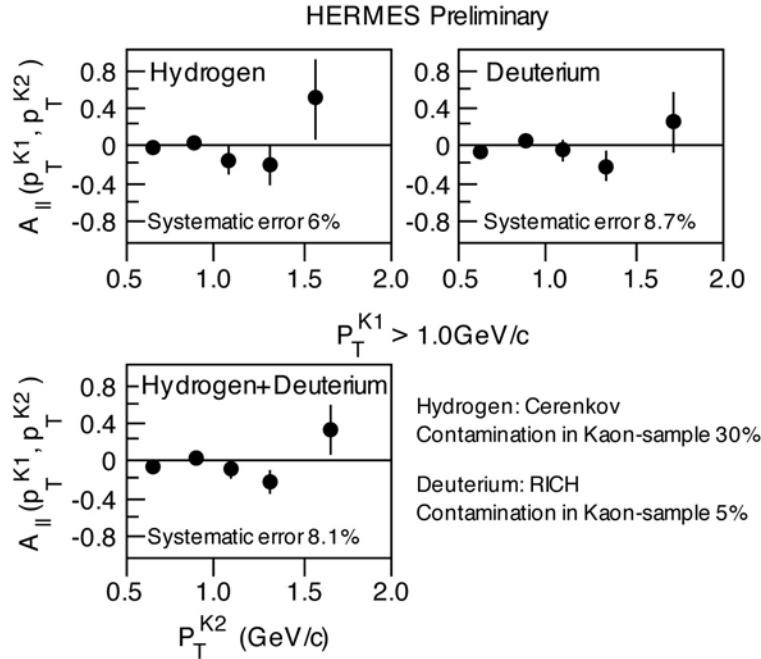


Fig. IV-12. The HERMES measurement of the double-spin asymmetry $A_{||}(p_T^{k+}, p_T^{k-})$ for polarized proton and deuterium targets. The error bars represent statistical errors.

the Monte Carlo treatment of the analyzing powers using the PYTHIA event generator is being refined. Nevertheless, the asymmetries observed for kaons

appear to be consistent with earlier conclusions of a positive gluon polarization.

¹The COMPASS Collaboration, CERN/SPSLC 96-14 (1996)

²PHENIX, BNL-PROPOSAL-R5, Aug. 1992; STAR, S. E. Vigdor *et al.*, hep-ex/9905034

³A. Airapetian *et al.*, Phys. Rev. Lett. **84**, 2584 (2000)

c.6. Azimuthal Asymmetries and Transversity (H. E. Jackson, A. El Alaoui, K. G. Bailey, T. P. O'Connor, K. Hafidi, D. H. Potterveld, P. Reimer, Y. Sanjiev, and the HERMES Collaboration)

Using a longitudinally polarized target, HERMES has recently reported the first observation of a single-spin asymmetry in the azimuthal distribution of hadrons detected in coincidence with deep-inelastic lepton scattering. The sinusoidal target-related spin asymmetry corresponds to an analyzing power of 0.022 ± 0.005 (stat) ± 0.003 (sys) for positive pions, and is consistent with zero for negative pions. It has been found¹ that these data are consistent with models for the relevant distribution functions together with a model for the Collins fragmentation function that is also consistent with a preliminary value for this function from $Z^0 \rightarrow 2\text{-jet}$ decay.² Hence it appears that the Collins fragmentation function is responsible for the

effect and has a substantial value, thus opening the way to future measurements of transversity using transversely polarized targets. Transversity h_1 is the third of three structure functions required to describe the structure of the nucleon in leading order. It is of fundamental interest because it is an all valence object which does not couple to gluons, and consequently, is expected to have unique scaling properties.

Recently these results have been extended³ to neutral pions. As with charged pions, a distinct $\sin\phi$ dependence is observed in the pion production asymmetry $A_{UL}(\phi)$ with respect to longitudinal target polarization. Here ϕ is the azimuthal angle of the pions

relative to the lepton scattering plane, around the virtual photon direction. In Fig. IV-13 the $\sin(\phi)$ moment of the asymmetry ($A_{UL}^{\sin\phi}$) is shown as a function of the pion fractional energy z , the Bjorken scaling variable x and the pion transverse momentum P_{\perp} . The π^0 and π^+ asymmetries exhibit a similar behavior in all kinematic variables, while the π^- asymmetry is consistent with zero. This is consistent with the expected dominance of scattering from u-quarks in the first two cases. The increase of the asymmetries with x suggests that they are associated with valence quark contributions. The

dependence on P_T may be related to the dominant kinematic role of intrinsic quark transverse momentum in the region where P_{\perp} remains below the typical hadronic mass scale of ≈ 1 GeV. The results have been successfully interpreted in terms of the unknown transversity function $h_1(x)$ together with the chiral-odd Collins fragmentation function $H_1^{\perp}(z)$. New data will be forthcoming from future HERMES measurements on a transversely polarized target, which will give direct access to transversity.

¹A. M. Kotzinian *et al.*, hep-ph/9908466

²A. V. Efremov, O. G. Smirnova, and L. G. Tkachev, Nucl. Phys. Proc. Suppl. **74**, 49 (1999)

³A. Airapetian *et al.*, Phys. Rev. Lett. **84**, 4047 (2000)

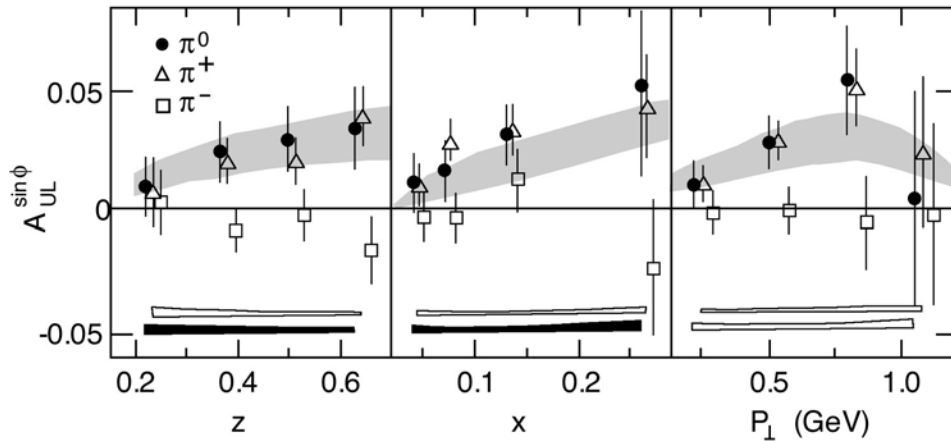


Fig. IV-13. The $\sin\phi$ moment of the asymmetry A_{UL} for π^0 production compared to previous HERMES results for π^+ and π^- . The open and filled bands represent the systematic uncertainties for neutral and charged pions respectively. The data for charged pions are shifted slightly for clarity.

c.7. Measurements With Unpolarized Targets: Hadron Formation Times (H. E. Jackson, A. El Alaoui, K. G. Bailey, T. P. O'Connor, K. Hafidi, D. H. Potterveld, P. Reimer, Y. Sanjiev, and the HERMES Collaboration)

HERMES has an active program of measurements with unpolarized targets which addresses a range of topics in photon-hadron interactions. As an example, HERMES has measured the charged pion fragmentation functions for up and down quarks from the nucleon, and their attenuation in a nuclear environment. By embedding the fragmentation process in the nuclear medium, one can study the time propagation of the hadron formation process. The attenuation of hadrons, which is measured as a function of the energy transfer ν and the hadron energy fraction $z = E_h/\nu$, can be related to the formation length (or time) of the hadron, or can be compared directly to model calculations. In fact, such data can also be used to derive empirical values for the hadron formation time and the energy loss of a quark

propagating in the medium. These quantities are of considerable theoretical and experimental interest, as it is possible to apply the same concepts in the description of the Drell-Yan process and heavy-ion collisions.

HERMES has recently released data on the attenuation ratios for nitrogen and krypton which have provoked widespread interest. The experimental results are developed as a multiplicity ratio which represents the ratio of the number of hadrons produced per DIS event for a nuclear target to that from a deuterium target. These data have been interpreted¹ in terms of final state interactions which soften the quark fragmentation functions. This medium modification of the fragmentation of the propagating parton results from

induced gluon radiation due to multiple parton scattering, and gives rise to additional terms in the QCD evolution equations that soften the fragmentation functions. As shown in Fig. IV-14, this treatment provides an excellent description of the HERMES

results. From these data, this treatment gives a quark energy loss of $dE/dx \approx 0.5$ GeV/fm in cold nuclear matter.

¹E. Wang, X.-N. Wang, LBNL-4956 (Feb 2002), hep-ph/0202105

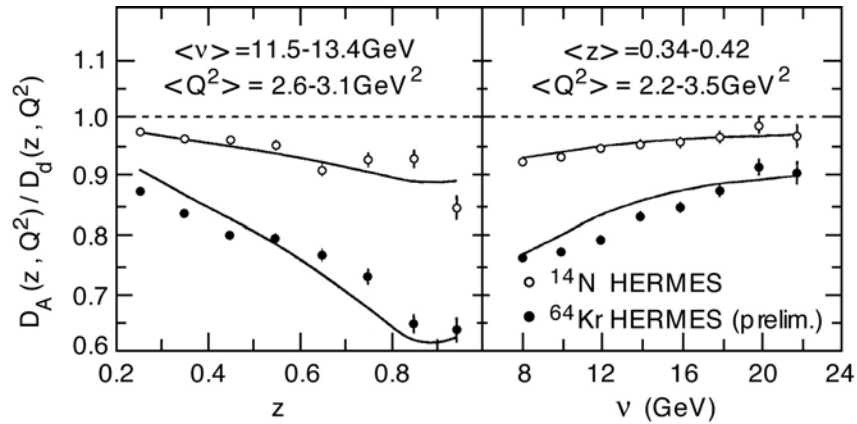


Fig. IV-14. At left, predicted nuclear modification of jet fragmentation functions (curves) compared to HERMES data on the ratios of hadron distributions between A and D targets in DIS. At right, the energy dependence of this predicted nuclear modification (curves) compared to the HERMES data.

c.8. A Dual Radiator Ring Imaging Cerenkov Counter for HERMES (H. E. Jackson, A. El Alaoui, K. G. Bailey, T. P. O'Connor, K. Hafidi, D. H. Potterveld, P. Reimer and the HERMES Collaboration)

A dual radiator Ring Imaging Cerenkov (RICH) detector for the identification of hadrons¹ has been in operation as part of the HERMES spectrometer since 1998. The HERMES experiment emphasizes measurements of semi-inclusive deep-inelastic scattering. However, most of the hadrons produced lie between 2 and 10 GeV, a region in which it had not previously been feasible to separate pions, kaons, and protons with standard particle identification (PID) techniques. The recent development of new clear, large, homogeneous and hydrophobic silica aerogel material with a low index of refraction offered the means to apply RICH PID techniques to this difficult momentum region for the first time. The HERMES instrument uses two radiators, C₄F₁₀, a heavy fluorocarbon gas, and a wall of silica aerogel tiles. A lightweight spherical mirror constructed using a newly perfected technique to make resin-coated carbon-fiber surfaces of optical quality provides optical focusing on a photon detector consisting of 1934 photomultiplier tubes (PMT) for each detector half. The PMT array is held in a soft steel matrix to provide shielding against the residual field of the main spectrometer magnet.

Ring reconstruction is accomplished with pattern recognition techniques based on a combination of inverse and direct ray tracing.

The Argonne group led the design and construction of the HERMES RICH, an effort which involved 8 collaborating institutions. With the successful commissioning of the system, attention turned to debugging, testing, and implementing the software required for data analysis. The identification of the different hadrons in the HERMES RICH detector is based on two different methods: the indirect ray tracing method (IRT) and the direct ray tracing method (DRT). Both methods are combined in a likelihood analysis which selects the most probable particle type. The IRT and DRT method exist in parallel; a decision network chooses the optimal method depending on the event topology. To date, as shown in Fig. IV-15, the IRT method has been demonstrated to give reliable results. Work continues on testing and tuning the DRT method. With the demonstration of reliable operation of the DRT method, a final training of the decision network will be performed, in order to implement its use in

providing the highest efficiency for reliable particle identification (PID). The efficiencies for particle identification are measured experimentally by using decaying ϕ , K_s , and Λ particles. Because of the limited topologies of this class of events, it is necessary to use a

Monte Carlo simulation to extend these efficiencies to a more extensive range of topologies. Work in this area continues. A careful analysis of error propagation in PID efficiencies remains to be done.

¹N. Akopov *et al.*, Nucl. Instr. Meth. A **479**, 511 (2002)

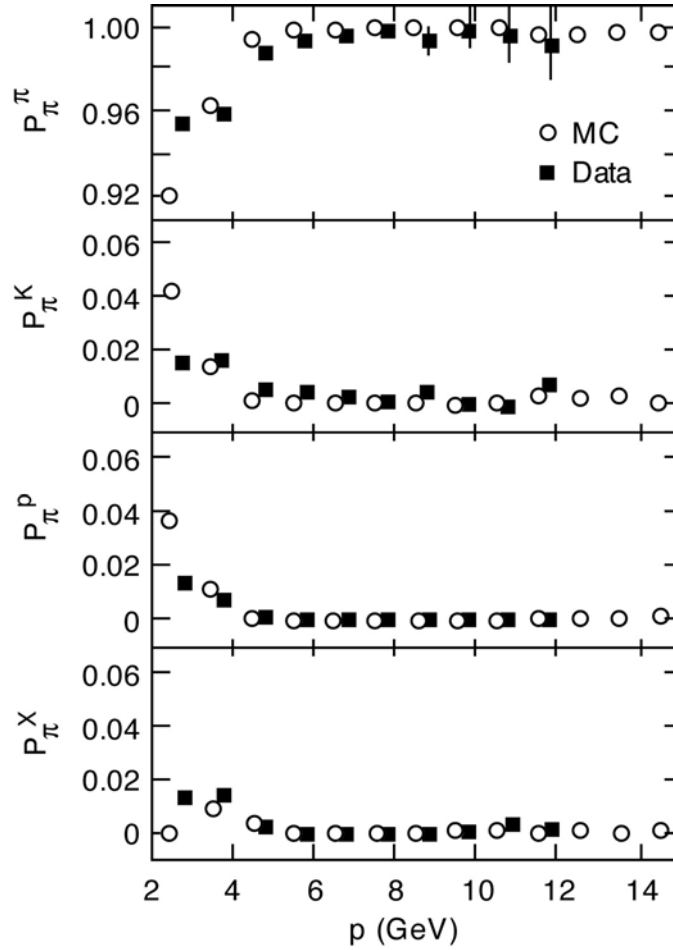


Fig. IV-15. Identification probabilities P_{π}^i that a pion is identified as pion, kaon, proton, or not identified (X) for single tracks per detector half. MC simulations (circles) in comparison with experimental data from ρ_0 - decays (solid squares); both results are based on the IRT likelihood analysis.

c.9. Nuclear Dependence of Lepton Pair Production: Parton Energy Loss, Shadowing and J/ψ and ψ' Suppression (D. F. Geesaman, S. B. Kaufman, N. C. R. Makins, B. A. Mueller, P. E. Reimer and the FNAL E866/NuSea Collaboration)

Through comparisons of production cross sections from different nuclear targets, we can deduce information about the behavior of quarks in a strongly interacting environment and learn how nuclear size affects the interaction processes. FNAL E866/NuSea collected Drell-Yan, J/ψ , and ψ' production data using Beryllium, Iron and Tungsten targets.

In the Drell-Yan process, the colored initial-state quarks (and antiquarks) from the beam interact strongly as they pass through the target nucleus before annihilating into a virtual photon. After the annihilation, the final state muons do not have significant interactions with the nuclear medium. In these strong initial state interactions, the quarks should lose some of their energy. Using the ratios of Drell-Yan cross sections from a variety of nuclear targets, and comparing with different models for the energy, tight limits were placed on the energy loss of a parton traveling through cold nuclear matter.

Before making these comparisons, it was necessary to account for a phenomenon known as shadowing, which manifests itself as a depletion in quark density at low x_{target} (the fractional momentum of carried by the struck

quark in the target) in heavy nuclei relative to light nuclei. Although not completely understood, it is well parameterized from Deep Inelastic Scattering (DIS) data. By comparing the Drell-Yan yields from nuclear targets we were able to confirm that shadowing in Drell-Yan quantitatively matches predictions based on shadowing in DIS. Since the observed Drell-Yan shadowing agrees with the DIS parameterizations, it was possible to remove this nuclear dependence from the quark energy loss analysis, described above.

Another nuclear effect, known as “suppression” causes the rate of production of J/ψ , and ψ' mesons in proton nucleus collisions to be diminished relative to the same process with a proton target. While the above-mentioned shadowing certainly plays an important role in this suppression, it is not the entire explanation. Using nuclear targets, E866/NuSea studied suppression as a function of the kinematic variables, Feynman- x (x_F) and transverse momentum (p_t). At low values of x_F , the surprising observation was made that the ψ' is more suppressed than the J/ψ , an effect that may be attributable to the absorption of the $c\bar{c}$ pair in the nucleus before hadronization.

c.10. Production of Υ and J/ψ from 800 GeV Protons Incident on Hydrogen and Deuterium (D. F. Geesaman, S. B. Kaufman, N. C. R. Makins, B. A. Mueller, P. E. Reimer and the FNAL E866/NuSea Collaboration)

Υ and J/ψ mesons are produced when partons from the beam and target annihilate and form a virtual gluon, which then hadronizes into a heavy meson resonance. The virtual gluon that produced the resonance can be generated by the annihilation of either a quark-antiquark pair or a pair of gluons (also called gluon-gluon fusion). Hence resonance production is sensitive to both the quark and gluon distributions with the target and beam. The J/ψ is believed to be produced primarily through gluon-gluon fusion, while Υ production is thought to proceed via both gluon-gluon fusion and quark-antiquark annihilation. Because the gluon distribution for the proton and neutron are similar, the per nucleon J/ψ cross section should be the same for both hydrogen and deuterium. For the Υ , on the other hand, the ratio of deuterium to hydrogen cross sections is expected to be larger than unity for the values of fractional momenta, x , probed by FNAL E866/NuSea,

since $\bar{u}_n > \bar{u}_p$, in this region, which allows for more $u_{\text{beam}} - \bar{u}_{\text{target}}$ annihilations with deuterium.

The FNAL E866/NuSea hydrogen and deuterium data contain 30 thousand Υ and one million J/ψ events. The production cross sections for these mesons have been extracted and can be compared to predictions based on models and parton distributions available in the literature. Color evaporation model calculations have been performed for both Υ and J/ψ production from hydrogen and deuterium. Although it is an extremely simple model and cannot predict the absolute value of the cross section, the color evaporation model does reproduce the observed x -Feynman shape of the cross section. In addition, when looking at the ratio of deuterium to hydrogen per nucleon cross sections, the unknown scale factor drops out. The measured cross

section ratios for both the J/ψ and the Υ are near unity as shown in Fig. IV-16. In the case of the J/ψ , this is not surprising, since J/ψ production is expected to proceed through gluon fusion. In the case of the Υ , however, the value near unity is in disagreement with color evaporation model calculations. The color

evaporation model also fails to explain the large transverse polarization seen in Υ production as discussed in the next section. This deviation may indicate that the parton distribution functions underestimate the hard gluon ($x \approx 0.25$) distribution in the proton.

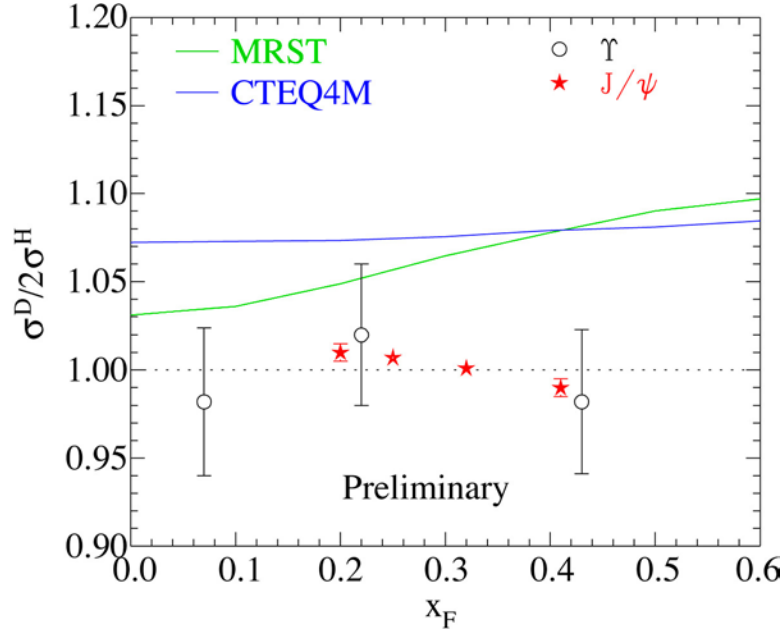


Fig. IV-16. The data points show the ratio of cross section for J/ψ and Υ production from deuterium to hydrogen. The curves represent color evaporation model calculations for this ratio for Υ production using two different parameterizations of the nucleon parton distributions. (J/ψ production is expected to have a ratio near unity.)

c.11. Polarization Measurement of Υ and ψ Production in Proton-Nucleus Collisions (D. F. Geesaman, S. B. Kaufman, N. C. R. Makins, B. A. Mueller, P. E. Reimer, and FNAL E866/NuSea Collaboration)

Despite Quantum Chromodynamics' (QCD) overwhelming success in describing many aspects of the strong interaction, an adequate description of quarkonia production is still lacking, due, in part, to its non-perturbative nature. Various models of quarkonia production have been proposed, including Color Octet and Color Singlet models. These models make definite predictions for the polarization of the produced quarkonia. Due to the clean experimental signature provided by their di-lepton decay mode, the Υ and ψ meson families provide important systems in which to study this. FNAL E866/NuSea has measured the polarization of the Υ and ψ mesons produced in proton-nucleus collisions.

In data from FNAL E866/NuSea, the $\Upsilon(1S)$ is seen to exhibit only slight polarization, and that only at large x -

Feynman (x_F) or large transverse momenta (p_T). Unfortunately, the $\Upsilon(1S)$ resonance is not the ideal place in which to study hadronization, since the observed $\Upsilon(1S)$ signal contains not only directly produced Υ 's but also Υ 's produced indirectly through the decay of higher mass $b\bar{b}$ states. Thus, the signal is less sensitive to the $b\bar{b}$ production mechanism. Due to their higher mass, the $\Upsilon(2S)$ and $\Upsilon(3S)$ have fewer states which can feed their production and the observed polarization better reflects the inherent production mechanism. FNAL E866/NuSea observes nearly complete transverse polarization in these two states (unresolved) as shown in Fig IV-17. Color octet production, but not color evaporation models are consistent with the present results.

In the ψ family, the J/ψ is observed to have only a slight polarization which changes from transverse to longitudinal as a function of x_F . Once again, however, the polarization signal from direct production is diluted

by feed down from other $c\bar{c}$ states. Data on the polarization of the ψ' is currently under analysis. While statistics are limited, this state has the advantage that the entire signal is from direct production.

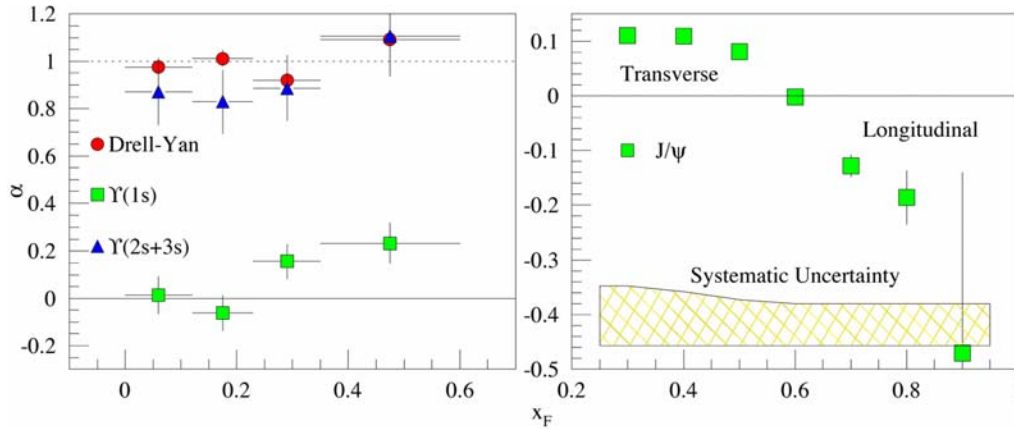


Fig. IV-17. The observed polarization of the $Y(1S)$ and the unresolved $Y(2S,3S)$ (left) as a function of Feynman- x , x_F . The observed polarization of the J/ψ (right) as a function of x_F .

c.12. Measurement of the Antiquark Flavor Asymmetry of the Proton Sea Using Drell-Yan Scattering (D. F. Geesaman, S. B. Kaufman, N. C. R. Makins, B. A. Mueller, P. E. Reimer, and FNAL E866/NuSea Collaboration)

While it is not required by any fundamental symmetry, it has—until recently—been widely assumed that the distributions of anti-down, \bar{d} , and anti-up, \bar{u} , quarks in the proton were identical. This was based on the assumption that the proton's sea arose perturbatively from gluons splitting into quark-antiquark pairs. Since the mass difference between the up and down quarks is small, equal numbers of up and down pairs would result. A ratio of \bar{d}/\bar{u} which is not unity is a clear sign of nonperturbative origins to the quark-antiquark sea of the proton, and recent evidence from deep inelastic scattering has shown an integral difference between the anti-up and anti-down distributions.

To further explore this difference, Fermilab E866/NuSea measured the ratio \bar{d}/\bar{u} as a function of the momentum carried by the struck quark, x . This was accomplished using the Drell-Yan mechanism, in which, a quark (or antiquark) in the proton beam annihilates with an antiquark (or quark) in the target. The resulting annihilation produces a virtual photon that decays into a pair of leptons, which are seen in the detector. Data were collected in 1996-1997 with the Meson East Spectrometer at Fermilab using an 800 GeV/c proton beam on hydrogen and deuterium targets.

From the ratio of hydrogen to deuterium Drell-Yan cross sections, the ratio \bar{d}/\bar{u} and difference $\bar{d}-\bar{u}$ have been extracted, and unexpected x -dependent flavor asymmetry in the proton's sea was revealed. The flavor difference in pure flavor non-singlet: Its integral is Q^2 independent and its Q^2 evolution, at leading order, does not depend on the gluon distributions in the proton. The large differences seen in Fig. IV-18 must be non-perturbative in nature. Several approaches have been suggested which could produce this difference. They include meson cloud models of the nucleon,¹ chiral quark models in which the mesons couple directly to the constituent quarks² chiral soliton and instanton models.³ These models are illustrated by the curves in Fig. IV-18.

The Drell-Yan absolute cross sections are also being extracted from the hydrogen and deuterium data. While the ratio of Drell-Yan cross sections is sensitive to the relative strength of the different flavors of anti-quarks, the absolute cross sections are sensitive to the total strength of the anti-quark sea, \bar{d}/\bar{u} . The Drell-Yan cross section is easily calculable next-to-leading order in α_s and can be compared directly with the measured

cross sections. Measurements were also made of the nuclear dependence of J/ψ , ψ' and Drell-Yan

production using Be, Fe, and W targets and of the polarization of the J/ψ , ψ' and Υ states.

¹J. C. Peng *et al.* (FNAL E866/NuSea Collaboration, Phys. Rev. D **58**, 092004 (1998); N. Nikoleav *et al.* Phys. Rev. D **60**, 014004 (1999)

²A. Szczurek *et al.* J. Phys. G **22**, 1741 (1996); P. V. Pobylitsa *et al.* Phys. Rev. D **59**, 034024 (1999)

³A. E. Dorokhov and N. I. Kochelev, Phys. Lett. B, 335 (1991); Phys. Lett. B **304** 167 (1993)

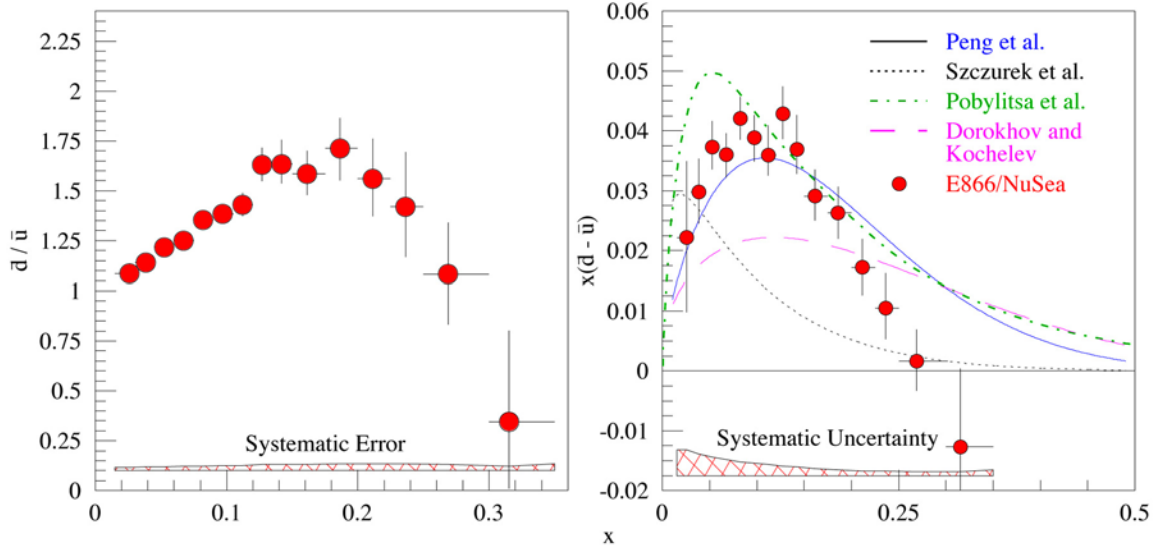


Fig. IV-18. The ratio of \bar{d}/\bar{u} (left) and $x(\bar{d}/\bar{u})$ (right) as a function of x , the fraction of the proton's momenta carried by the struck quark. The curves in the right graph represent different model calculations as described in the text.

c.13. Drell-Yan Measurements with 120 GeV Protons, FNAL E906 (D. F. Geesaman, K. Hafidi, R. J. Holt, D. H. Potterveld, P. E. Reimer, and the FNAL E906 Collaboration)

The Drell-Yan measurements of Fermilab E866/NuSea have provided new insight into the antiquark sea in the proton and nuclear dependence phenomena. FNAL E906 has been approved by Fermilab to extend Drell-Yan measurements to larger values of x (the fraction of the proton's momenta carried by the struck quark) using the new 120 GeV Main Injector at Fermilab.

FNAL E866/NuSea's measurements of ratio of anti-down, \bar{d} , to anti-up, \bar{u} , quarks in the proton, \bar{d}/\bar{u} , revealed an unexpected x -dependence. At small x this ratio increases from unity to a maximum asymmetry of over well 50%, as expected. For $x \geq 0.19$, however, the ratio of \bar{d}/\bar{u} decreases and becomes symmetric again at the highest values of x accessible to the experiment.¹ Unfortunately, in this region, the statistical uncertainty of the data also becomes large. E906 will be able to significantly reduce the statistical uncertainty of the data and extend these measurements to even larger

values of x . The expected sensitivity of E906 to the \bar{d}/\bar{u} ratio is shown in Fig. IV-19. In this higher- x region, E906 will be sensitive to the interplay between the nonperturbative and the perturbatively generated sea.

In addition to hydrogen and deuterium targets, the experiment will collect data with a number of heavy nuclear targets. These data will allow a systematic study of nuclear effects in the Drell-Yan process. Since the Drell-Yan process is sensitive to antiquark distributions, any enhancement in the sea due to nuclear effects (virtual pion contributions to nuclear structure functions) should be apparent in the ratio of Drell-Yan cross sections from nuclear targets. Previous data² from FNAL E772, however, did not show these enhancements. FNAL E906 will significantly reduce this statistical uncertainty and extend these measurements to larger x , where the effect is expected

to be greater. Additionally, the absolute magnitude of the proton's sea high- x distributions are derived from neutrino-nucleus deep inelastic scattering (DIS) data and may have unknown nuclear effects. By comparing light and heavy target Drell-Yan data, the experiment will be making a measurement of these effects. A comparison with muon-induced DIS will provide the ability to differentiate between valence and sea-based nuclear effects. The expected statistical uncertainty of E906 nuclear data and existing Drell-Yan and muon DIS are shown in Fig. IV-19.

Using the same nuclear target data, the energy loss of colored partons traveling through a strongly interacting media will be studied. E906's predecessor, FNAL E866/NuSea was able to extract upper limits on this energy loss within the context of several models.³ At the lower energy of the Main Injector, the energy loss is expected to be much greater, and the new data will be able to distinguish between these and other models.⁴ These measurements are important for RHIC where jet

quenching is expected to be an important signal for the formation of a Quark-Gluon Plasma.

FNAL E906 is able to make these improvements over previous measurements because of the lower beam energy available at the Fermilab Main Injector. For fixed x_1 and x_2 the cross section scales as the inverse of the beam energy. Thus a factor of seven more events for the same integrated luminosity can be achieved. At the same time, the primary background to the measurement, muons from J/ψ decays, decreases with increasing beam energy, allowing for an increase in instantaneous luminosity by another factor of seven. These two factors combine to provide roughly 50 times more events for the same beam time.

FNAL E906 has been approved by the Fermilab PAC and will most likely begin collecting data in late 2007. In the mean time, a number of new detector elements must be constructed, the most significant of which is a new large dipole magnet to focus the Drell-Yan muons.

¹E. A. Hawker *et al.* (FNAL E866/NuSea collaboration), Phys. Rev. Lett. **80**, 3715 (1998); R. S. Towell *et al.* (FNAL E866/NuSea Collaboration), Phys. Rev. D **64**, 052002 (2001)

²D. M. Alde *et al.* (FNAL E772 Collaboration), Phys. Rev. Lett. **64**, 2479 (1990)

³M. A. Vasiliev *et al.* (FNAL E866/NuSea Collaboration), Phys. Rev. Lett. **83**, 2304 (1999)

⁴M. B. Johnson *et al.* Phys. Rev. C **65**, 025203 (2002); M. B. Johnson *et al.* (FNAL E772 Collaboration) Phys. Rev. Lett. **86**, 4483 (2001)

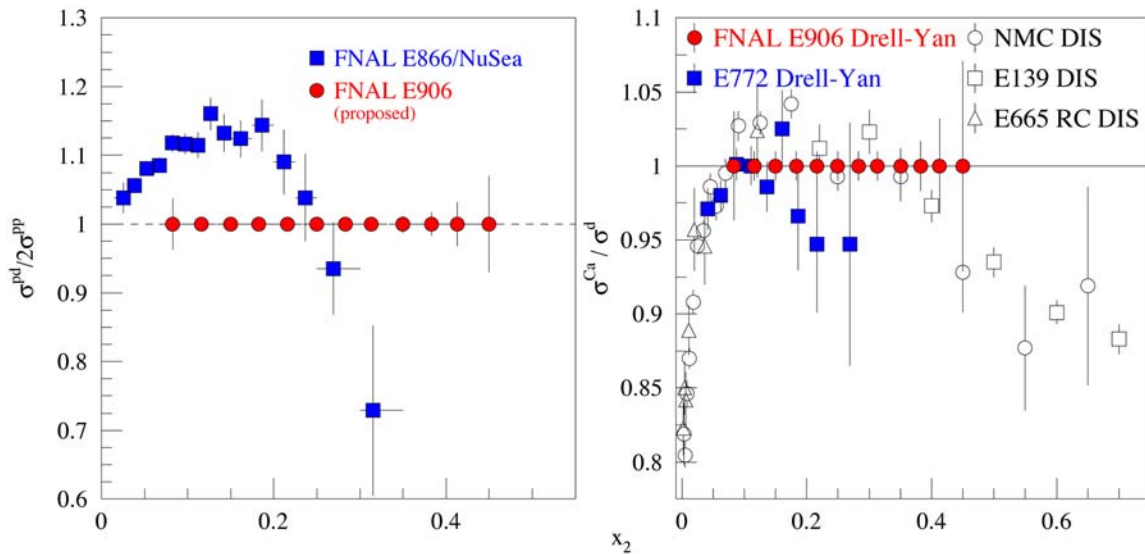


Fig. IV-19. The statistical uncertainty of E906's measurement of the ratio of hydrogen to deuterium cross sections (arbitrarily plotted at 1) compared with the E866 measurements of the same quantity (left). The statistical uncertainty of E906's measurement of the ratio of deuterium to Calcium cross sections (arbitrarily plotted at 1) compared with previous Drell-Yan and deep inelastic scattering (DIS) measurements (right).

D. ATOMIC TRAP TRACE ANALYSIS

d.1. Improvements on Detecting $^{81,85}\text{Kr}$ with ATTA (K. Bailey, X. Du, Z.-T. Lu, P. Mueller, T. P. O'Connor, and L. Young*)

We report on the refinements of the Atom Trap Trace Analysis (ATTA) setup, developed by our group for the detection of the two long-lived isotopes ^{81}Kr ($t_{1/2} = 2.3 \times 10^5$ years) and ^{85}Kr ($t_{1/2} = 10.8$ years). The ATTA method is based on selectively trapping the desired Kr isotope in a Magneto Optical Trap (MOT) and detecting it by observing its fluorescence. The principle of this method has been demonstrated by measuring the isotopic abundance of ^{81}Kr and ^{85}Kr in samples of atmospheric Kr, which is readily available in large amounts, with an overall counting efficiency of 2×10^{-7} . However, in order to allow measurements of samples extracted from ancient water or ice, where obtaining just 1 cc of Kr at STP means processing tons of material, the gas consumption rate had to be reduced substantially, i.e. the overall counting efficiency had to be increased by several orders of magnitude.

Since noble gas atoms do not permanently stick to walls, the efficiency can be increased significantly by recirculating the Kr within the vacuum chambers of the

trap system (Fig. IV-20). In 2001, we conducted tests of the Kr recirculation system. With the implementation of a two-stage recirculation system, the overall efficiency was increased by a factor of 350. We have also tested a completely sealed system by closing off the path between the Chopper and Trap chambers. The pressure of Kr gas gradually decayed in such a sealed system with a half-life of 6 hours. This decay of pressure only happened when the discharge source was on, which led us to postulate that the Kr atoms were ionized and implanted into the walls of the discharge source. By completing the recirculation path from the Trap to the Cooling chamber and performing the measurement for 6 hours, the efficiency is expected to increase by another order of magnitude. With a final overall efficiency in the range of 10^{-4} to 10^{-3} , the system will be ready for dating groundwater samples due to arrive later this year.

*Chemistry Division, ANL

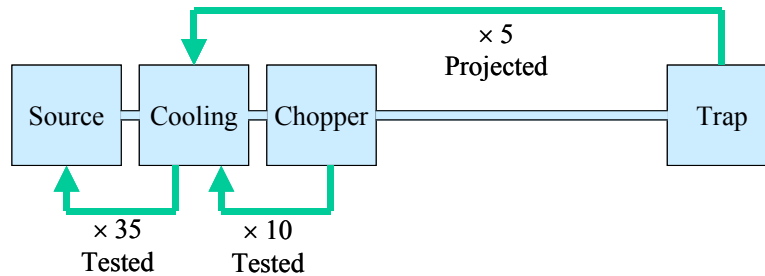


Fig. IV-20. Krypton sample recirculation system. The trap system consists of four vacuum chambers: Source, Cooling, Chopper, and Trap. Three turbopumps, attached to the downstream three chambers, are used to pump the sample gas back to the Source.

d.2. Ultrasensitive Isotope Trace Analysis of ^{41}Ca (K. Bailey, Z.-T. Lu, I. D. Moore, P. Mueller, T. P. O'Connor, and L. Young*)

An Atom Trap Trace Analysis (ATTA) system based on the technique of laser manipulation of neutral atoms is being developed to measure the isotopic abundance of ^{41}Ca in natural samples. ^{41}Ca has a half-life of 1.03×10^5 years and a natural isotopic abundance of $\sim 10^{-15}$. Trace analysis of ^{41}Ca has promising applications in archaeological dating of ancient bones and in the biomedical research of osteoporosis.

Trapping of all stable calcium isotopes has been demonstrated. For the most abundant isotope, ^{40}Ca (97% isotopic abundance), a MOT loading rate of 3×10^{10} atoms/s has been reached at the overall capture efficiency of 1×10^{-4} . An order of magnitude increase in this efficiency is realistically expected with the implementation of two-dimensional transverse cooling to reduce the atomic beam divergence and amplify the atom flux in the forward direction.

In order to analyze the rare isotope ^{41}Ca , the system must be able to detect single atoms. In 2001, we have achieved the single-atom-detection capability (Fig. IV-21) with this setup. The observed photon count rate from a single ^{40}Ca atom is 4 kHz, while the background rate is 5 kHz. With the addition of a 671 nm diode laser that pumps the trapped Ca atoms from the metastable $3d\ ^1D_2$ level back to the ground level, the average lifetime of the atoms in the trap is increased from 20 ms to 100 ms, and the time-integrated signal-to-noise ratio of a single trapped atom has reached 18.

We have also installed a new PC-based control system to monitor and control the laser frequencies, which will enable us to quickly address different Ca isotopes and measure the ratios of their abundances. This system uses a frequency-stabilized He-Ne laser to provide a reference that is transferred to the Ti:Sapphire and diode laser using a scanning Fabry-Perot cavity.

*Chemistry Division, ANL

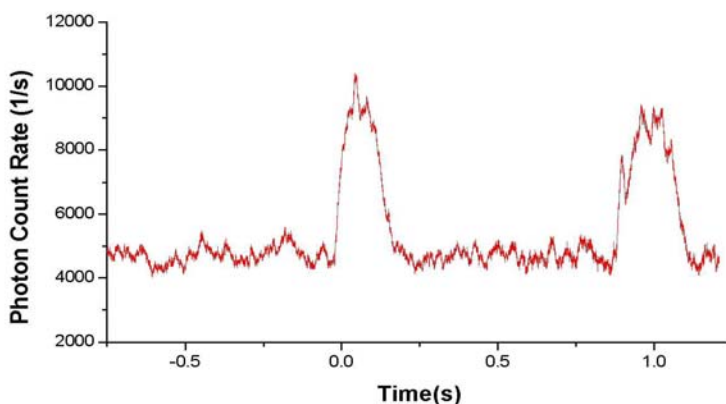


Fig. IV-21. Fluorescence signal of individual ^{40}Ca atoms in the trap.

d.3. Measuring the Charge Radius of ${}^6\text{He}$ (K. Bailey, X. Du, J. Greene, A. M. Heinz, R. J. Holt, D. Henderson, R. V. F. Janssen, C.-L. Jiang, Z.-T. Lu, I. D. Moore, P. Mueller, T. P. O'Connor, R. C. Pardo, T. Pennington, K. E. Rehm, J. P. Schiffer, G. Drake,* C. Law,† M. Paul,‡ and L.-B. Wang§)

The neutron-rich ${}^6\text{He}$ ($t_{1/2} = 807$ ms) nucleus is believed to consist of a ${}^4\text{He}$ -like core and two halo neutrons bound by less than 1 MeV. The charge radius of ${}^6\text{He}$ was predicted with the Quantum-Monte-Carlo calculations based on the Argonne v_{18} Two-Nucleon and the Illinois Three-Nucleon Potential model. This collaboration aims to determine the charge radius of ${}^6\text{He}$ by measuring the atomic isotope shift of the 2^3S_1 - 3^3P_2 transition between ${}^4\text{He}$ and ${}^6\text{He}$. Since ${}^6\text{He}$ atoms are short-lived and are available only in small numbers, we plan to produce the ${}^6\text{He}$ atoms at the ATLAS accelerator facility, capture individual ${}^6\text{He}$ atoms with a laser trap, and perform precision laser spectroscopy on the trapped atoms.

We will take advantage of the properties of Atomic Trap Trace Analysis (ATTA), which was developed by our group for the trace detection of ${}^{81,85}\text{Kr}$. This method is based on selectively trapping the atoms of the desired isotope in a magneto-optical trap (MOT) and detecting the trapped atom by observing its fluorescence. It was demonstrated that ATTA is virtually background free and is capable of detecting single atoms. The complete experimental setup will include a target chamber for on-line production of the isotopes with subsequent neutral extraction and transfer to a discharge source to produce metastable He atoms, a

Zeeman slower to decelerate the thermal beam of metastable He, a MOT with single atom detection capability and a laser system to produce the light for trapping and high resolution spectroscopy.

In 2001, we carried out two experimental runs at ATLAS. Here we report on the successful production, extraction, and detection of thermal neutral ${}^6\text{He}$ atoms. In this experiment (see Fig. IV-22), ${}^6\text{He}$ was produced via the ${}^{12}\text{C}({}^7\text{Li}, {}^6\text{He}){}^{13}\text{N}$ reaction and stopped in a porous graphite target, from which the atoms diffused out. The atoms were then compressed by a turbo-pump system, with an approximately 50% efficiency, into a small vacuum chamber where approximately 5% of the β particles from the decays of ${}^6\text{He}$ were detected by a plastic scintillation detector. We verified that the observed β particles were indeed emitted by ${}^6\text{He}$ based on the measured energy spectrum and the half-life of the β emission. From these measurements, we derived that, with a ${}^7\text{Li}$ beam current of 20 pA, ${}^6\text{He}$ atoms were extracted from the target chamber at a rate of $3 \times 10^5/\text{s}$. A factor of 10 increase in the extraction rate can be achieved at ATLAS by increasing the ${}^7\text{Li}$ beam current. The construction of the trapping setup including the laser system is currently under way.

*University of Windsor, Canada, †Monmouth College, Illinois, ‡Hebrew University, Israel, §ANL and University of Illinois-Urbana

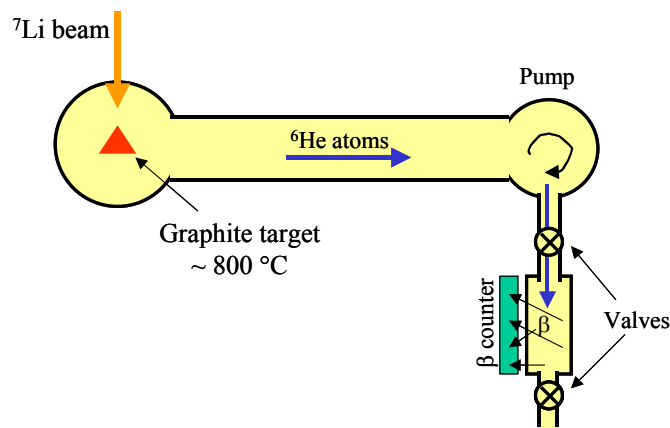


Fig. IV-22. The production, extraction, detection of neutral ${}^6\text{He}$ atoms.

V. THEORETICAL PHYSICS

OVERVIEW

Research in the Physics Division's Theory Group addresses a broad range of important problems involving the structure and dynamics of hadrons and nuclei. There is a strong emphasis on comparison with data from Argonne's ATLAS facility, from TJNAF, and from other laboratories around the world. Our work includes the modeling and application of quantum chromodynamics (QCD) to light- and heavy-hadron structure at zero temperature and density, and at the extremes of temperature and density appropriate to the early universe, neutron stars, and RHIC experiments. We develop reaction theories to use in exploring hadron structure using the data from meson and nucleon-resonance production experiments at TJNAF, MIT-Bates and Mainz. We construct realistic two- and three-nucleon potentials that give accurate fits to nucleon-nucleon elastic scattering data and trinucleon properties, and use them in detailed many-body calculations of light and near closed-shell nuclei, nuclear matter and neutron stars, and in a variety of astrophysically important electroweak reactions. Our nuclear structure and reaction studies include coupled-channels calculations of heavy-ion reactions near the Coulomb barrier and calculations of observables in breakup reactions of nuclei far from stability. We also study high-spin superdeformation, spectroscopy of the heaviest elements ($A \geq 250$), and nuclear structure near the proton-drip line. Additional research is pursued in atomic physics, neutron physics, quantum computing, and fundamental quantum mechanics. Several of our projects involve major numerical simulations using the massively parallel computer systems at Argonne and NERSC.

A. NUCLEAR DYNAMICS WITH SUBNUCLEONIC DEGREES OF FREEDOM

The objective of this research program is to investigate the role of: quark-gluon degrees of freedom in hadron structure and interactions, and in nuclear dynamics; the development and application of reaction theories for use in exploring hadron structure using the data from meson and nucleon-resonance production experiments at modern experimental facilities; and to investigate relations of Poincaré covariant dynamics specified by mass operators to complementary dynamics specified by Green functions.

At the level of quark-gluon degrees of freedom, the Dyson-Schwinger equations (DSEs) provide a Poincaré covariant, nonperturbative method for studying QCD in the continuum. The existence of symmetry preserving truncations enables the simultaneous exploration of phenomena such as: confinement, dynamical chiral symmetry breaking, and bound state structure and interactions. In addition the DSEs provide a generating tool for perturbation theory and hence yield model-independent results for the ultraviolet behavior of strong interaction observables. This means that model studies facilitate the use of physical processes to constrain the long-range behavior of the quark-quark interaction in QCD, which is poorly understood and whose elucidation is a key goal of modern experimental programs. The last year has seen many successful applications. For example, we solved a Faddeev equation for the nucleon and Delta and showed that a description in terms of confined-quark and nonpoint-like confined-diquark-correlations can readily be obtained. We found in addition that the self-energy contribution from the πN loop can reduce the nucleon's mass by up to several hundred MeV. We saw, however, that this effect does not qualitatively alter the picture that baryons are quark-diquark composites. And, using a Vlasov equation coupled to Maxwell's equation, we showed that focused laser beams at proposed X-ray free electron laser facilities can generate electric field strengths large enough to cause spontaneous electron-positron pair production from the QED vacuum. Our study predicts the production of a few hundred particle pairs per laser period and hence that an experimental verification of vacuum decay is within reach.

At the level of meson and baryon degrees of freedom, we have developed a dynamical model for interpreting γN reactions in terms of the quark-gluon substructure of nucleon resonances (N^*) as predicted by various QCD-based hadron models. In the past year the model has been instrumental in quantifying the pion cloud contribution to the Q^2 -dependence of the $\gamma N \rightarrow \Delta$ transition factors, extracted from the recent data obtained at TJNAF, Mainz, MIT-Bates and NIKHEF. We have also used the model to make predictions for the $d(e, e' \pi)$ reaction and η production in NN collisions, with an aim of using the new data from TJNAF and COSY to investigate the medium effects on meson and N^* propagation. Our investigation of vector meson photoproduction has been extended to consider coupled-channel effects and include the sub-threshold N^* excitations. Finally, we have provided theoretical guidance for designing experiments to use various spin observables in π photoproduction to resolve the “missing” resonance problem.

Relativistic quantum dynamics requires a unitary representation of space-time symmetries (Poincaré group) and localization of states, such that states localized in relatively space-like regions are causally independent. For finite systems Poincaré generators obtain as functions of mass and spin operators. With realistic restrictions of the mass operator the dynamics is “almost

local” as defined precisely in the context of algebraic quantum field theory. The fundamental limitation to finite systems may be overcome by the relation to relativistic dynamics specified by Green operators with the required spectral properties.

a.1. Contemporary Applications of Dyson-Schwinger Equations (M. B. Hecht, C. D. Roberts and S. M. Schmidt)

The contemporary application of DSEs is well illustrated by the calculation of pseudoscalar meson masses and the study of nucleon observables. For the former, we showed that a direct solution of the appropriate Bethe-Salpeter equations, combined with the knowledge provided by a DSE-derived model-independent mass-formula, predicts the current-quark-mass-dependence of pseudoscalar meson masses recently measured in lattice-QCD simulations. Importantly our analysis also provides an intuitive

understanding, relating the evolution to a large value of the vacuum and in-hadron quark condensates. For the latter, we showed that a Poincaré covariant Faddeev equation, which describes a baryon as a composite of a dressed quark and nonpoint-like, dressed scalar and axial-vector diquarks, provides an internally consistent picture of the nucleon and Δ . An article describing these results was published.¹

¹M.B. Hecht, C.D. Roberts and S.M. Schmidt, *Contemporary Applications of Dyson-Schwinger Equations*, in "Quark Confinement and the Hadron Spectrum IV," edited by W. Lucha and Kh. Maung-Maung (World Scientific, Singapore, 2002) pp. 27-39

a.2. Diquarks and Density (M. B. Hecht, C. D. Roberts, and S. M. Schmidt)

A diquark is a bosonic quark-quark correlation, which is necessarily colored in all but 2-color QCD (QC₂D). Therefore, in the presence of color-confinement, diquarks cannot be directly observed in a 3-color gauge theory's spectrum. Nevertheless, evidence is accumulating; *e.g.*, via Faddeev equation studies, which suggests that confined diquark correlations play an important role in hadronic spectroscopy and interactions. The significance of diquarks in those applications motivates a study of the possibility that dense hadronic matter may exhibit diquark condensation; *i.e.*, quark-quark pairing promoted by a quark chemical potential. To explore this we introduced a Gorkov-Nambu-like gap equation for QCD and applied it to QC₂D and, in two

qualitatively different truncations, to QCD itself. Among other interesting features, we demonstrated that QC₂D with massive fermions undergoes a second-order transition to a superfluid phase when the chemical potential exceeds $m_\pi/2$. In the QCD application we illustrated that the $\sigma := -\langle \bar{q}q \rangle^{1/3} \neq 0$ phase, which determines the properties of the strong-interaction's mass spectrum at zero temperature and chemical potential, is unstable with respect to the superfluid phase when the chemical potential exceeds $\sim 2\sigma$, and that at this point the diquark gap is large, $\sim \sigma/2$. This superfluid phase survives to temperatures greater than that expected in the core of compact stars. An article describing this work was published.¹

¹M.B. Hecht, C. D. Roberts and S. M. Schmidt, *Diquarks and Density*, in "Physics of Neutron Star Interiors," edited by D. Blaschke, N. K. Glendenning and A. Sedrakian (Springer Publishing, Berlin Heidelberg, 2001) pp. 218-234

a.3. Pair Creation and Plasma Oscillations (S. M. Schmidt, M. B. Hecht, C. D. Roberts, A. V. Prozorkevich,* and D. V. Vinnik*)

Ultra-relativistic heavy-ion collisions (URHICs) are complicated processes and their understanding requires a microscopic modeling of all stages: the formation, evolution and hadronization of a strongly coupled plasma. With RHIC now operating it is imperative to develop a microscopic understanding of URHICs, including their non-equilibrium aspects. In response to this challenge we studied particle creation in strong fields in the presence of thermalizing collisions. Our quantum kinetic equation involved a non-Markovian source term and a relaxation time approximation to the collision term, and the strong electric background field

was determined by coupling-in Maxwell's equation and solving the whole system self-consistently. Plasma oscillations are an almost inevitable outcome of this treatment. We found that the plasma frequency depends on at least three quantities: the field strength, the relaxation time and the mass distribution of the produced particles. In addition, we observed that incorporating a strongly momentum-dependent dressed-parton mass, which is an essential feature of QCD, can have a significant impact on the evolution of the plasma. In particular it promotes plasma oscillations. An article describing this work was published.¹

*Saratov State University, Armenia

¹A. V. Prozorkevich, D. V. Vinnik, S. M. Schmidt, M. B. Hecht, and C. D. Roberts, *Pair Creation and Plasma Oscillations*, in "Quark Matter in Astro- and Particle-physics," edited by G. R. G. Burau, D. B. Blaschke and S. M. Schmidt (Rostock University Press, Rostock, 2001) pp. 79-88

a.4. Neutron Electric Dipole Moment: Constituent-Dressing and Compositeness (M. B. Hecht, C. D. Roberts, and S. M. Schmidt*)

The action for any local quantum field theory is invariant under the transformation generated by the antiunitary operator CPT, which is the product of the inversions: C - charge conjugation; P - parity transformation; and T - time reversal. The decay of the CP-odd eigenstate K_0^L into a CP-even 2π final state demonstrates that the product of only C and P is not a good symmetry of the standard model. This entails that time reversal invariance must also be violated and that, too, has been observed in detailed studies of the neutral kaon system. It has long been known that the possession of an electric dipole moment (EDM) by a spin-1/2 particle would signal the violation of time-reversal invariance. (The existence of a dipole moment signals a spherically asymmetric distribution of charge.) Any such effect is likely small, given the observed magnitude of CP and T violation in the neutral kaon system, and this makes neutral particles the obvious subject for experiments: the existence of an electric monopole charge would overwhelm most signals of the dipole strength. It is therefore natural to focus on the neutron, which is the simplest spin-1/2 neutral composite system in nature. Attempts to measure the

neutron's EDM, d_n , have a long history and currently yield the upper bound:

$$d_n < 6.3 \times 10^{-26} \text{ e cm (90\% CL)} .$$

This has proven to be an effective constraint on attempts to extend the standard model and to assist in this we have calculated d_n using a well-constrained Ansatz for the nucleon's Poincaré covariant Faddeev amplitude. We found that the momentum-dependent quark dressing amplifies the contribution from the current-quarks' EDMs; and that dressed-quark confinement and binding make distinguishable the effect of the two CP and T violating interactions: $i\gamma_5\sigma_{\mu\nu}(p_1-p_2)_\nu$ and $\gamma_5(p_1+p_2)_\mu$, where $p_{1,2}$ are the current-quarks' momenta. In addition, our calculation showed that the value of $|d_n|$ obtained using the current-quark EDMs generated by a minimal three Higgs doublet model of spontaneous CP violation is perilously close to the experimental upper bound; *i.e.*, that the so-called Weinberg model is almost excluded by this bound. An article describing our work was published.¹

*University of Tuebingen, Germany

¹M. B. Hecht, C. D. Roberts, and S. M. Schmidt, Phys. Rev. C **64**, 025204 (2001)

a.5. Plasma Production and Thermalization in a Strong Field (M. B. Hecht, C. D. Roberts, S. M. Schmidt,* D. V. Vinnik,* A. V. Prozorkevich,† S. A. Smolyansky,† and V. Toneev‡)

We have extended and improved the collision term in our quantum Vlasov equation, and reanalyzed aspects of the formation and equilibration of a quark-gluon plasma. In addition, since leptons do not participate in the strong interactions that equilibrate the QGP, we calculated the thermal dilepton spectrum produced by the evolving plasma. We again found that field-current feedback generates plasma oscillations in all thermodynamic observables. The oscillations were also evident in the production rate of thermal dileptons.

While the time evolution of that rate may not be measurable, the plasma oscillations also acted to significantly enhance the time-integrated rate, which is easily accessible. This effect was marked by a sharp increase in the dilepton yield once the energy-density-per-parton became large enough to generate a high frequency and large amplitude plasma oscillation, which could survive the effect of damping for a significant time after the moment of impact. An article describing this work was published.

*University of Tuebingen, Germany, †Saratov State University, Armenia, ‡BLTP, JINR, Dubna
¹D. V. Vinnik, A. V. Prozorkevich, S. A. Smolyansky, V. D. Toneev, M. B. Hecht, C. D. Roberts, and S. M. Schmidt, Eur. Phys. J. C **22**, 341 (2001)

a.6. Meson Photoproduction (M. B. Hecht, C. D. Roberts, and S. M. Schmidt*)

The dichotomy of the pion as QCD's Goldstone mode and a bound state of massive constituents is easily understood using the Dyson-Schwinger equations. That provides the foundation for an efficacious phenomenology, which correlates the pion's charge radius and electromagnetic form factor with its valence quark distribution function; and simultaneously provides a Poincaré covariant description of the nucleon, its form factors and, more recently, meson photoproduction processes. The latter processes are important for developing an understanding of the structure of nucleon resonances and in searching for "missing" resonances; *i.e.*, those states predicted by constituent quark models that are hitherto unobserved. Preliminary parameter-free calculations of the t-channel pion-exchange contribution to the ω -photoproduction cross-section

reproduce the forward angle cross-section exactly, as illustrated in Fig. V-1. A comparison between the results in this approach and experiment at large-angles is meaningless until the contribution of the s- and u-channel processes are also included, a calculation that is underway. The analogous t-channel contribution to pion photoproduction has also been calculated and the results justify, a posteriori, the meson-exchange model expedient of neglecting quark-gluon substructure in the photon-pion vertex. The role of substructure in the meson-nucleon vertices is more important and such parameter-free calculations will facilitate the qualitative improvement of meson exchange models by making possible the explicit representation of these effects. Articles describing this work have been or will be published.^{1,2}

*University of Tuebingen, Germany

¹M. B. Hecht, C. D. Roberts and S. M. Schmidt, *The Character of Goldstone Bosons*, in "Lepton-Scattering, Hadrons and QCD," edited by W. Melnitchouk, A. W. Schreiber, A. W. Thomas and P. C. Tandy (World Scientific, Singapore, 2001) pp. 219-227

²M. B. Hecht and C. D. Roberts, *Modern Dyson-Schwinger Equation Studies*, to appear in the "πN Newsletter"

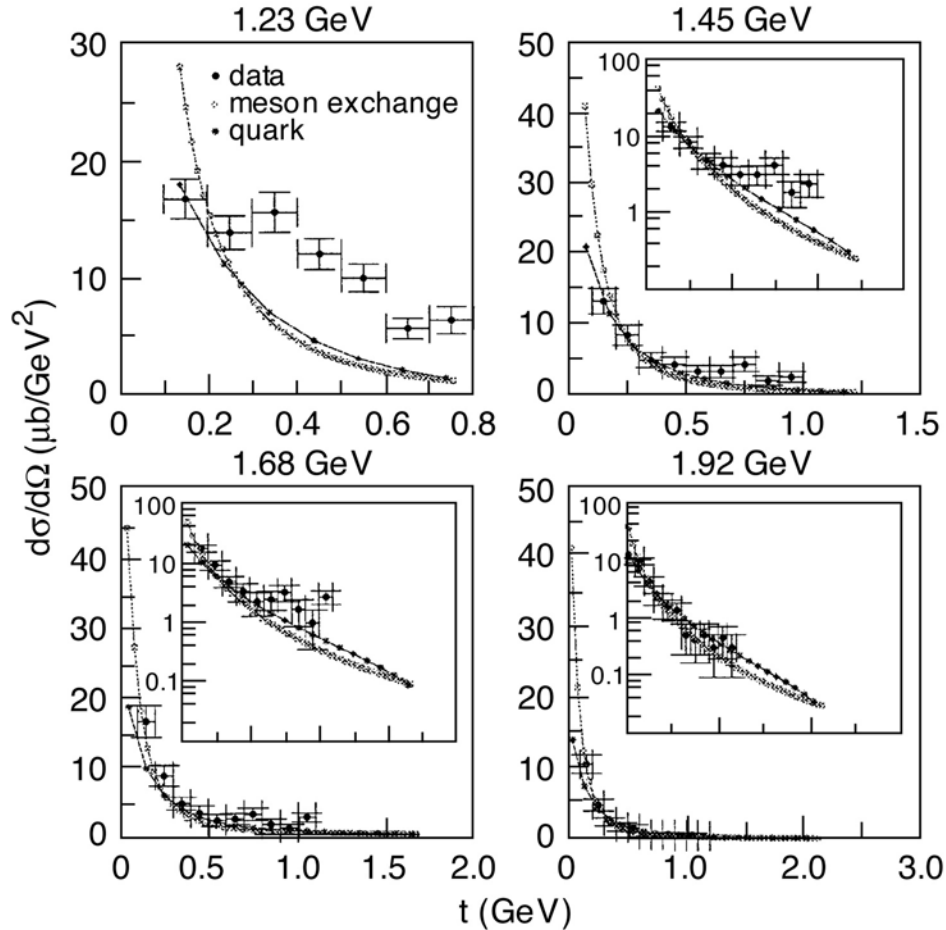


Fig.V-1. π -exchange contribution to the $\gamma N \rightarrow \omega N$ cross section obtained using the model of Hecht, Roberts, and Schmidt [Phys. Rev. C **64**, 025204 (2001)]. (Panels are labeled by the incident photon energy.) *, long-dashed line, our calculation (no parameters were varied to obtain this result); \square , short-dashed line, the meson-exchange model calculation of Oh, Tito, and Lee [Phys. Rev. C **63**, 025201 (2001)] (only the t -channel π -exchange contribution is shown); data from Klein et al. [Saphir Collaboration, πN Newsletter **14**, 141 (1998).]

a.7. Pair Creation and an X-ray Free Electron Laser (M. B. Hecht, C. D. Roberts, R. Alkofer,* S. M. Schmidt,* and D. V. Vinnik*)

Using a quantum kinetic equation coupled to Maxwell's equation we studied the possibility that focused beams at proposed X-ray free electron laser facilities can generate electric field strengths large enough to cause spontaneous electron-positron pair production from the QED vacuum; *i.e.*, to cause the "decay of the vacuum." We calculated the time and momentum dependence of the single particle distribution function, and established that field-current feedback and quantum statistical effects are small and can be neglected in this

application of non-equilibrium quantum mean field theory. We found that, under conditions reckoned achievable at planned facilities, repeated cycles of particle creation and annihilation take place in tune with the laser frequency. However, the peak particle number density is insensitive to this frequency, as evident in Fig. V-2, and hence we predict the production of a few hundred particle pairs per laser period. This means that an experimental verification of vacuum decay is within reach. An article describing this work was published.¹

*University of Tuebingen, Germany

¹R. Alkofer, M. B. Hecht, C. D. Roberts, S. M. Schmidt, and D. V. Vinnik, Phys. Rev. Lett. **87**, 193902 (2001)

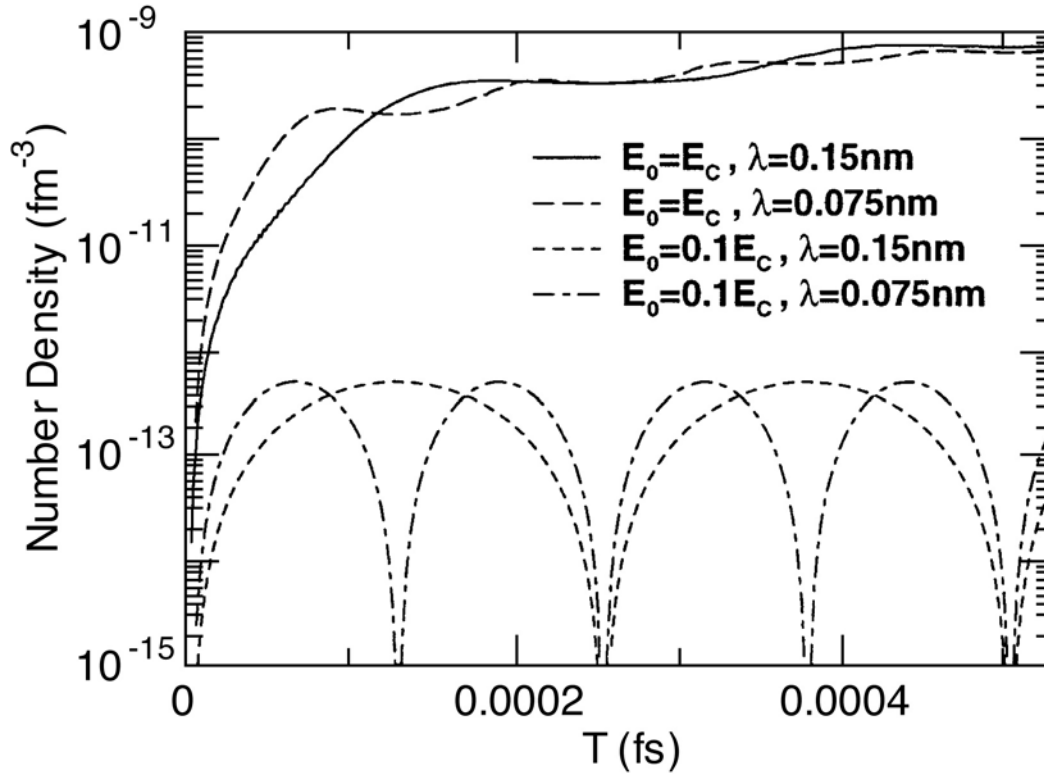


Fig.V-2. Time evolution of the particle number density for the XFEL design-goal field strength: $E = 0.1 E_{cr}$, and for strong fields: $E = E_{cr}$ [$E_{cr} = m_e^2/e = 1.3 \times 10^{18}$ V/m.]. In strong fields, particles accumulate, leading to the almost complete occupation of available momentum states. In weak fields, repeated cycles of particle creation and annihilation occur in tune with the laser frequency. We estimate that hundreds of particles will be produced in each cycle.

a.8. X-ray Free Electron Laser: Vacuum Pair Creation, Back Reactions and Memory Effects (C. D. Roberts, S. M. Schmidt,* and D. V. Vinnik*)

Spontaneous electron-positron pair production out of the QED vacuum is possible in the presence of homogeneous electric fields with a strength characterized by $e E_{cr} = m_e^2$. X-ray free electron laser (XFEL) facilities planned at DESY and SLAC will achieve fields $E \sim 0.1 E_{cr}$ and make vacuum decay observable but will not lead to an accumulation of particles (see Fig.V-2). We have applied our quantum kinetic approach and found that particle accumulation is likely to occur at fields $E \sim 0.25 E_{cr}$. We found, too, that with accumulation non-Markovian features in the particle source term become observable; i.e., the time between production events becomes commensurate

with the produced parton's Compton frequency and hence interference effects become apparent that expose the negative energy elements in the particle wave packets. This is a core quantum field theoretical feature. At larger field strengths: $E \sim 0.5 E_{cr}$, the accumulating system of partons will exhibit plasma oscillations. This study suggests that a greater body of fundamental phenomena will be accessible at XFEL facilities if the design goals can be modestly exceeded. It was possible only because we have developed and directly applied a quantum Vlasov equation. We are preparing an article that describes this research.

*University of Tuebingen, Germany

a.9. Nucleon Mass and Pion Loops (M. B. Hecht, C. D. Roberts, A. W. Thomas,*
M. Oettel,* S. M. Schmidt,† and P. C. Tandy‡)

We solved Poincaré covariant Faddeev equations for the nucleon and Δ to illustrate that an internally consistent description in terms of confined-quark and nonpoint-like confined-diquark-correlations can readily be obtained. Subsequently, we calculated the π N-loop induced self-energy corrections to the nucleon's mass and showed them to be independent of whether a pseudoscalar or pseudovector coupling is used. Applying phenomenological constraints, we argued that

this self-energy correction reduces the nucleon's mass by up to several hundred MeV. However, we demonstrated that this effect does not qualitatively alter the picture, suggested by the Faddeev equation, that baryons are quark-diquark composites, although neglecting the π -loops leads to a quantitative overestimate of the nucleon's axial-vector diquark component. An article describing this work was accepted for publication.

*CSSM, University of Adelaide, Australia, †University of Tuebingen, Germany, ‡Kent State University

a.10. Bethe-Salpeter Equation and a Nonperturbative Quark-gluon Vertex
(C. D. Roberts, A. Bender,* W. Detmold,* and A.W. Thomas*)

A Ward-Takahashi identity preserving Bethe-Salpeter kernel can always be calculated explicitly from a dressed-quark-gluon vertex whose diagrammatic content is enumerable. We illustrated that fact using a vertex obtained via the complete resummation of dressed-gluon ladders. While this vertex is planar, the vertex-consistent kernel is nonplanar and that is true for any dressed vertex. In an exemplifying model, the rainbow-ladder truncation of the gap and Bethe-Salpeter equations yielded many results; *e.g.*, π - and ρ -

meson masses, that are changed little by including higher-order corrections. However, repulsion generated by nonplanar diagrams in the vertex-consistent Bethe-Salpeter kernel for quark-quark scattering is sufficient to guarantee that diquark bound states do not exist. This analysis confirms the importance of preserving symmetries in studies of QCD's bound states. An article describing this work was submitted for publication.

*CSSM, University of Adelaide, Australia

a.11. Axial-Vector Diquarks in the Baryon (C. D. Roberts)

It has been shown that a product Ansatz for the nucleon's Faddeev amplitude using only a scalar-diquark can provide a good description of leptonic and nonleptonic couplings and form factors, with some notable exceptions; *e.g.*, the neutron's charge radius and axial vector coupling. Properly incorporating the lower component of the nucleon's spinor helps somewhat in addressing these exceptions. However, discrepancies

remain and I anticipate that their amelioration requires the inclusion of axial-vector diquark correlations and a pion cloud. With these features included, I will be able to calculate observables such as the $N \rightarrow \Delta$ transition form factor, in which the resonant quadrupole strength can be interpreted as a signal of nucleon deformation.

a.12. Valence-Quark Distributions in the Nucleon (C. D. Roberts)

The pion provides the simplest theoretical subject for a calculation of the valence quark distribution function. However, pion targets are not readily available for experiment and the most reliable measurements of quark distribution functions have been performed on nucleon targets. I intend to extend the approach developed for the pion so as to employ it in a calculation of the nucleon's valence quark distribution. In the first studies, the target nucleon will be represented by a quark-plus-scalar-diquark product Ansatz for its Faddeev amplitude. This promises to provide the first Poincaré covariant calculation of the

nucleon's valence quark distribution function. Improving the nucleon model via the inclusion of axial-vector diquark correlations and a pion cloud will enable the drawing of a connection between deep inelastic scattering measurements and the "soft physics" wrapped up in nucleon structure. For example, it will provide a means of testing the validity and importance of diquark clustering in the nucleon, and the relation between the d/u-ratio at large-x and confinement, as it is exhibited in the momentum-space extent of the Faddeev amplitude.

a.13 J/ψ Suppression as a Signal of Quark Gluon Plasma Formation (C. D. Roberts, D. B. Blaschke,* and Yu. L. Kalinovsky†)

We have developed a successful approach to describing heavy-meson observables at zero temperature. That enables a reliable extrapolation into the domain of nonzero temperature, which is relevant to the RHIC program. The suppression of the J/ψ production cross section is touted as a unique signal of quark gluon plasma formation, and such a suppression has been observed at CERN. We propose to study J/ψ production in the expectation that additional insight will follow from the Dyson-Schwinger equations' capacity to unify nonperturbative aspects of light- and heavy-meson observables via a microscopic description using QCD's elementary excitations. Our initial focus is the

T-dependence of J/ψ break-up by hadronic comovers; i.e., the substructure induced T-dependence of those interactions with other mesons in the medium that dissociates the J/ψ . These processes are likely to be affected by the dramatic T-dependence of the dressed-light-quark mass function in the neighborhood of the QGP phase boundary and a possible T-dependent reduction in the mass of the open-charm final states. Our goal is to elucidate the mechanisms involved and the fidelity of J/ψ suppression as a signal of quark gluon plasma formation.

*University of Rostock, Germany, †LCTA, JINR, Dubna, Russia

a.14. Schwinger-Dyson Approach to Nonequilibrium Classical Field Theory (B. Mihaila, F. Cooper*, J. Dawson†)

We discuss a Schwinger-Dyson [SD] approach¹ for determining the time evolution of the unequal time correlation functions of a non-equilibrium classical field theory, where the classical system is described by an initial density matrix at time $t = 0$. We focus on $\lambda\phi^4$ field theory in 1+1 space-time dimensions where we can perform exact numerical simulations by sampling an ensemble of initial conditions specified by the initial density matrix. We discuss two approaches. The first, the bare vertex approximation [BVA], is based on ignoring vertex corrections to the SD equations in the auxiliary field formalism relevant for $1/N$ expansions. The second approximation is a related approximation made to the SD equations of the original formulation in

terms of ϕ alone. We compare these SD approximations as well as a Hartree approximation with exact numerical simulations. We find that both approximations based on the SD equations yield good agreement with exact numerical simulations and cure the late time oscillation problem of the Hartree approximation. We also discuss the relationship between the quantum and classical SD equations.

Our results give us confidence that this approximation will be useful in future studies of quantum phase transitions in the $O(4)$ model. The fact that in homogeneous situations this approximation leads to thermalization will allow us to study the rate of

equilibration versus expansion rate for an expanding plasma undergoing a phase transition. We will then be able to see whether some of the interesting phenomena

occurring during the early stages of a chiral phase transition will survive the hard scatterings present in the BVA approximation.

*Los Alamos National Laboratory, †University of New Hampshire

¹B. Mihaila, F. Cooper, and J. Dawson, Phys. Rev. D **64**, 125003 (2001)

a.15. Numerical Approximations using Chebyshev Polynomial Expansions (B. Mihaila and I. Mihaila*)

We present numerical solutions¹ for differential equations by expanding the unknown function in terms of Chebyshev polynomials and solving a system of linear equations directly for the values of the function at the extrema (or zeros) of the Chebyshev polynomial of order N (El-gendi's method). The solutions are exact at these points, apart from round-off computer errors and

the convergence of other numerical methods used in connection with solving the linear system of equations. Applications to initial value problems in time-dependent quantum field theory and second order boundary value problems in fluid dynamics are presented.

*Coastal Carolina University

¹B. Mihaila and I. Mihaila, J. Phys. A: Math. Gen. **35**, 731 (2002)

a.16. Dynamical Study of the Δ Excitation in $N(e,e'\pi)$ Reactions (T.-S. H. Lee and T. Sato*)

We have completed our investigation of the Δ excitation in pion electroproduction on the nucleon. It is found that the model can describe, to a very large extent, the recent data on $p(e,e'\pi^0)$ and $p(e,e'\pi^+)$ reactions from Jefferson Lab, as shown in Fig. V-3. The magnetic dipole (M1), electric dipole (E2), and Coulomb (C2) strengths of the $\gamma N \rightarrow \Delta$ transition have been extracted. It is found that the C2/M1 ratio drops significantly with Q^2 and reaches about -14% at $Q^2 = 4$

(GeV/c)², while the E2/M1 ratio remains close to the value $\sim -3\%$ at the $Q^2 = 0$ photon point. The extracted M1 transition form factor drops faster than the usual dipole form factor of the proton. We also find that the nonresonant interactions can dress the $\gamma N \rightarrow \Delta$ vertex to significantly enhance its strength at low Q^2 , but much less at high Q^2 , as shown in Fig. V-4, for the Coulomb C2 form factor. A paper describing our results has been published.¹

*Osaka University, Japan

¹T. Sato and T.-S. H. Lee, Phys. Rev. C **63**, 055201 (2001)

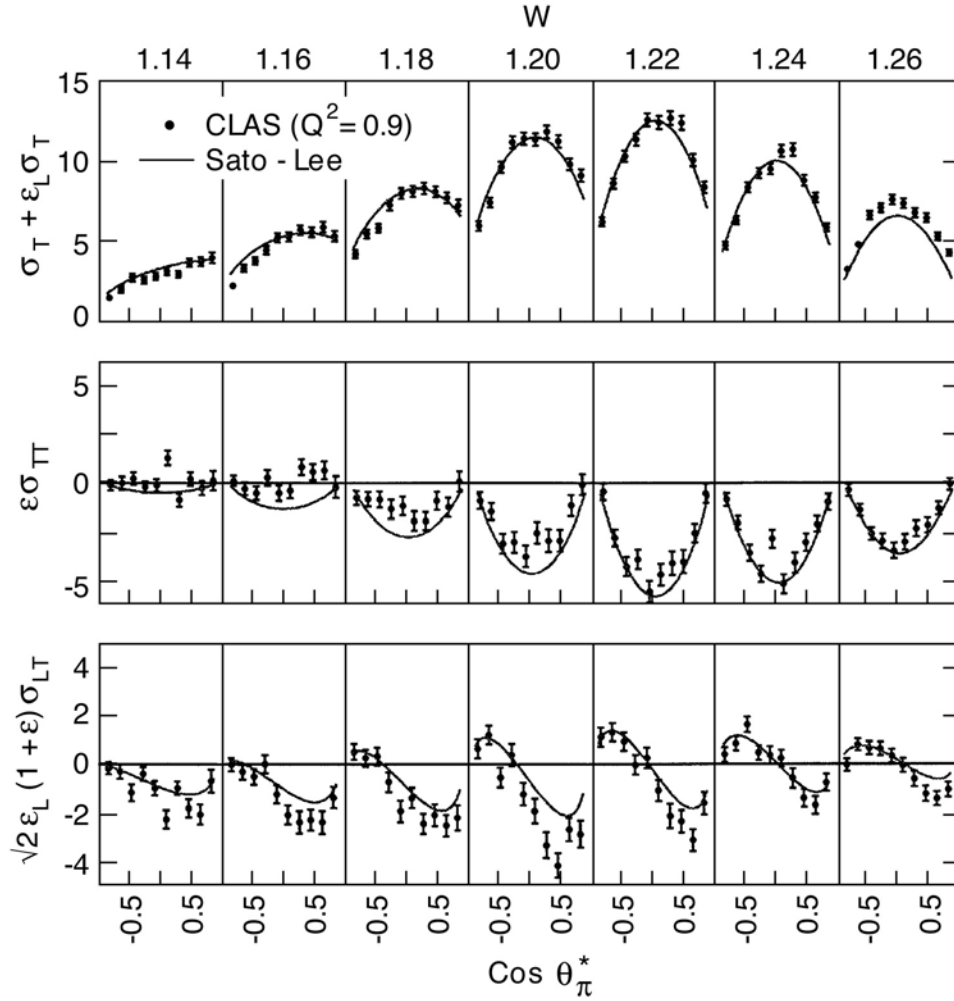


Fig. V-3. The predicted differential cross sections of $p(e, e' \pi^0)$ reaction at $Q^2 = 0.9 \text{ (GeV/c)}^2$ are compared with the 2001 data from Jefferson Lab.

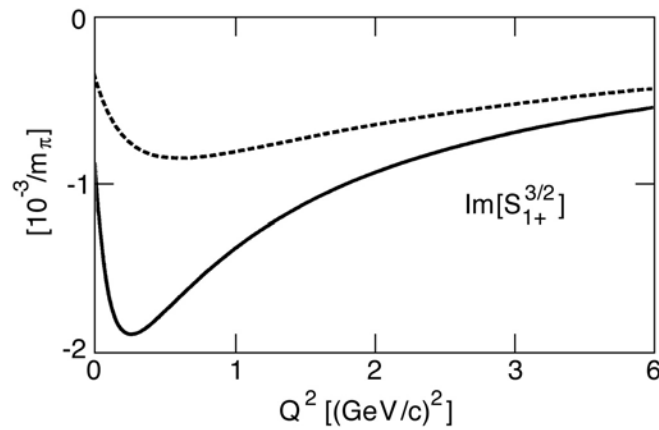


Fig. V-4. The predicted Coulomb C_2 form factor of $\gamma N \rightarrow \Delta$ is $\propto \text{Im}[S_{1+}^{3/2}]$. The dashed curve is obtained when the pion cloud effects are neglected.

a.17. Nucleon Resonances in ω Photoproduction (T.-S. H. Lee, Yongseok Oh,^{*} and Alexander I. Titov[†])

We have investigated the role of the nucleon resonances (N^*) in ω photo-production. In contrast with the previous investigations based on the $SU(6) \times O(3)$ limit of the constituent quark model, the employed $N^* \rightarrow \gamma N$ and $N^* \rightarrow \omega N$ amplitudes include the configuration mixing effects due to the residual quark-quark interactions. The contributions from the nucleon resonances are found to be significant relative to the nonresonant amplitudes in changing the differential cross sections at large scattering angles. We suggest that a crucial test of our predictions can be made by measuring the parity asymmetry and beam-target double asymmetry at forward scattering angles. The

dominant contributions are found to be from $N1/2^+(1910)$, a missing resonance, and $N3/2^-(1960)$ which is identified as the $D_{13}(2080)$ of the Particle Data Group. A paper describing our results has been published.¹ We have extended our investigation to address the questions concerning the sub-threshold N^* excitation and the coupled-channel effects due to πN and ρN channels. Both effects are found to be important and must be included in examining the N^* effects in energies near production threshold. Our results are shown in Fig. V-5. Two papers on this work are being prepared for publication.

^{*}Academia Sinica, Taiwan, [†]JINR, Dubna, Russia

¹Y. Oh, A. I. Titov, and T.-S. H. Lee, Phys. Rev. C **63**, 025201 (2001)

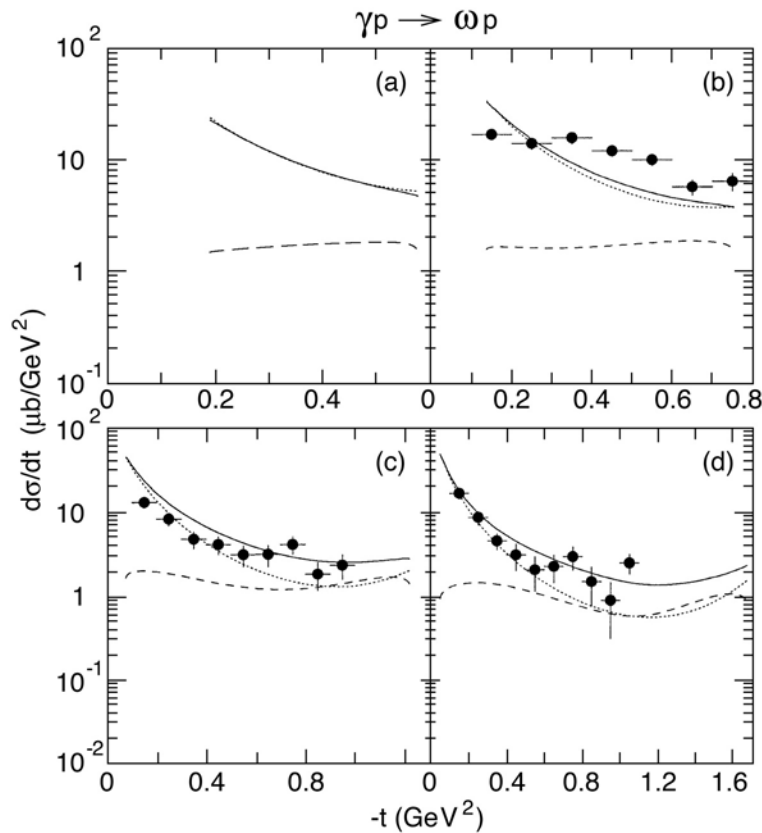


Fig. V-5. Coupled-channel effects on ω photoproduction. The dotted curves are from the tree-diagram, and the dashed curves are from the effects due to the intermediate πN channel. The solid curves are from the coherent sum of these two mechanisms. The energies for the incoming photon are 1.16 (upper-left), 1.23 (upper-right), 1.45 (lower-left), and 1.68 (lower-right) GeV.

a.18. The Pion Contributions to the $\gamma N \rightarrow \Delta$ Transition (T.-S. H. Lee, T. Nakamura,* and T. Sato*)

The $\gamma N \rightarrow \Delta$ parameters extracted from the dynamical model developed in [Phys. Rev. C **54**, 2660 (1996), Phys. Rev. C **63**, 055201 (2001)] are analyzed within the chiral constituent quark model. By using the unitary transformation to separate the baryon bound state properties from the scattering dynamics, we show how the extracted bare $\gamma N \rightarrow \Delta$ parameters can be related to the contributions from constituent quarks and virtual pion loops. It is found that the one-loop pion

contributions account for about 10% of the bare magnetic dipole (M1) transition. For the bare electric quadrupole (E2) and Coulomb (C2) strengths, the one-loop contributions are found to be in opposite sign of the values extracted from the data. This suggests that either the constituent quark configurations in Δ and/or N have d-state components, or there exists non-pionic exchange-current contributions. A paper describing our results is being prepared for publication.

*Osaka University, Japan

a.19. Coupled-Channel Approach for $K^+\Lambda$ Photoproduction (T.-S. H. Lee, Wen-Tai Chiang,* F. Tabakin,* , and B. Saghai†)

Kaon photoproduction on the nucleon is studied using a coupled-channel (CC) approach. A general method to include multi-step final-state interactions of electromagnetic strangeness production is developed, and then applied numerically to investigate the $\gamma p \rightarrow K^+\Lambda$ process. In addition to direct $K^+\Lambda$ production, we incorporate both $\pi^0 p$ and $\pi^+ n$ pion-nucleon channels in our CC approach. Cross sections are calculated and compared to recent data from SAPHIR, with emphasis

on the CC effects. We show that the CC effects due to the πN channels are significant at the level of inducing 20% changes in total cross sections; thereby demonstrating the need to include πN coupled-channels to correctly describe electromagnetic strangeness production. Our results on total cross sections are shown in Fig. V-6. A paper describing our results has been published.¹

*University of Pittsburgh, †CEA-Saclay, France

¹W.-T. Chiang, F. Tabakin, T.-S. H. Lee, and B. Saghai, Phys. Lett. B **514**, 101 (2001)

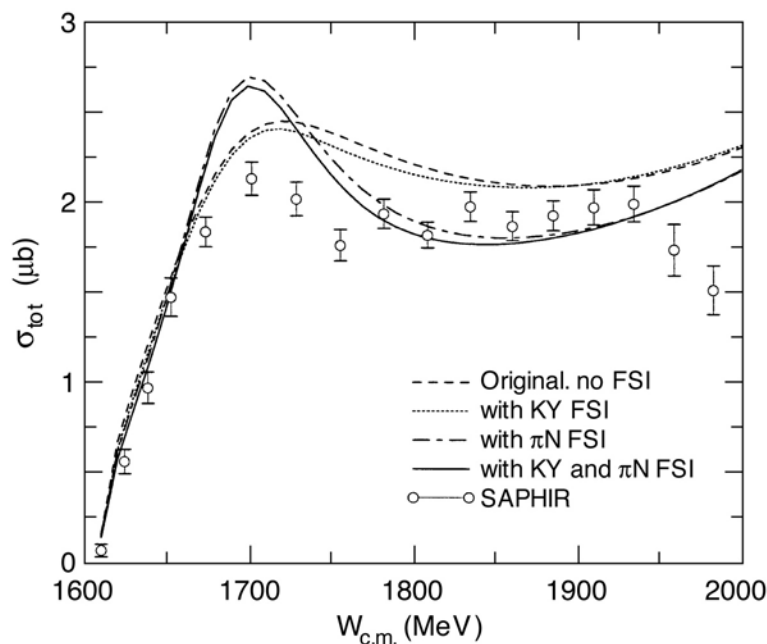


Fig. V-6. Coupled-channel effects of $\gamma p \rightarrow K^+\Lambda$ reaction.

a.20. Meson-Exchange π N Models in Three-dimensional Bethe-Salpeter Formulation (T.-S. H. Lee, Cheng-Tsung Hung,* and Shin Nan Yang†)

We have investigated pion-nucleon scattering by using several three-dimensional reduction schemes to the Bethe-Salpeter equation for a model Lagrangian involving π , N, Δ , ρ , and σ fields. It is found that all of the resulting meson-exchange models give similar good descriptions of the π N scattering data up to 400 MeV. However, they have significant differences in describing the π NN and π N Δ form factors and the π N

off-shell t-matrix elements. We show that these differences can best be distinguished by investigating the near-threshold pion production from nucleon-nucleon collisions and pion photoproduction on the nucleon. The consequences of using these models to investigate various pion-nucleus reactions are also discussed. A paper describing our results has been published.¹

*Chung-Hua Institute of Technology, Taiwan, †National Taiwan University

¹C.-T. Hung, S. N. Yang, and T.-S. H. Lee, Phys. Rev. C **64**, 034309 (2001)

a.21. ϕ -N Bound State (T.-S. H. Lee, H. Gao,* and V. Marinov*)

It has been suggested that the QCD van der Waals' interaction, mediated by multi-gluon exchange, is dominant when the interacting two-color singlet hadrons have no common quarks. We have found that such a QCD van der Waals' force is strong enough to bind a ϕ meson onto a nucleon inside a nucleus to form

a bound state. The direct experimental signature for such an exotic state is proposed in the case of sub-threshold ϕ meson photoproduction from a nuclear target. The predicted rates indicate the feasibility of such an experiment at JLab. A paper describing our results has been published.¹

*MIT

¹H. Gao, T.-S. H. Lee, and V. Marinov, Phys. Rev. C **63**, 022201 (2001)

a.22. Compressed Nuclei with Δ s and Hyperons (T.-S. H. Lee, Mahmoud A. Hasan,* and James P. Vary†)

To interpret the data from relativistic heavy-ion collisions, we are continuing our effort to investigate compressed nuclei with Δ 's and hyperons. The ground state properties of ^{90}Zr , ^{100}Sn , and ^{132}Sn at equilibrium and at large amplitude-compression have been investigated within the framework of the constrained spherical Hartree-Fock (CSHF) approximation. We use a realistic effective baryon-baryon Hamiltonian that includes the N-N, the N- Δ , and the Δ - Δ interactions. We specifically investigate the sensitivity to the sizes of the nucleon and Δ model spaces. At equilibrium, we find no case of mixing between nucleons and Δ 's in our largest model space of eight major nucleon shells plus sixteen Δ orbitals. On the contrary, there is mixing in ^{90}Zr and ^{132}Sn in the smaller model space of seven major nucleon shells plus eight Δ orbitals. Expanding the nucleon model space has a larger effect on reducing the static compression modulus and softening the nuclear equation-of-state than increasing the number of Δ states. Most of the excitation energy delivered to the

system during compression is employed by the two nuclei with a neutron excess (*i.e.*, ^{90}Zr , ^{132}Sn) to create the massive Δ resonances. On the other hand, in the ^{100}Sn nucleus most of the excitation energy goes to a simple reduction in the binding, suggesting a suppressed role for the Δ states. Under extreme compression at a density 2-3 times normal nuclear density, the excitation of nucleons to Δ 's increases sharply up to 10% of the total number of constituents. At finite excitation energy under compression, the number of Δ excitations is not dependent on the number of Δ -states over the range studied. The Δ -excitation results are consistent with heavy-ion collision data, and suggest an important mean-field mechanism for sub-threshold pion production in particle-nucleus and nucleus-nucleus collisions. A paper describing our results has been published.¹ We are currently extending the approach to include hyperons in the calculation of compressed nuclei.

*Applied Science University, Jordan, †Iowa State University, Ames

¹Mahmoud A. Hasan, J. P. Vary, and T.-S. H. Lee, Phys. Rev. C **64**, 024306 (2001)

a.23. Dynamical Study of the ${}^2\text{H}(e,e'\pi^+)$ Reaction (T.-S. H. Lee and K. Hafidi)

The ${}^2\text{H}(e,e'\pi^+)$ reaction in parallel kinematics has been investigated using a dynamical model of pion electroproduction on the nucleon. A unitary πNN model has been used in order to examine the effects due to the final two-nucleon interactions, pion rescattering from the second nucleon, and intermediate NN and $\text{N}\Delta$ interactions. Our results are compared with the data in Fig. V-7. It has been found that these πNN mechanisms are small, but they can have significant contributions to the ${}^2\text{H}(e,e'\pi^+)$ cross sections through

their interference with the dominant impulse term. For the longitudinal cross sections, the effects due to the interference between the pion pole term and other production mechanisms are also found to be very large. Our findings clearly indicate that these interference effects must be accounted for in any attempt to determine from the ${}^2\text{H}(e,e'\pi^+)$ data whether the pion form factor and/or πNN vertex of the pion pole term are modified in the nuclear medium. This work has been published.¹

¹K. Hafidi and T.-S. H. Lee, Phys. Rev. C **64**, 064607 (2001)

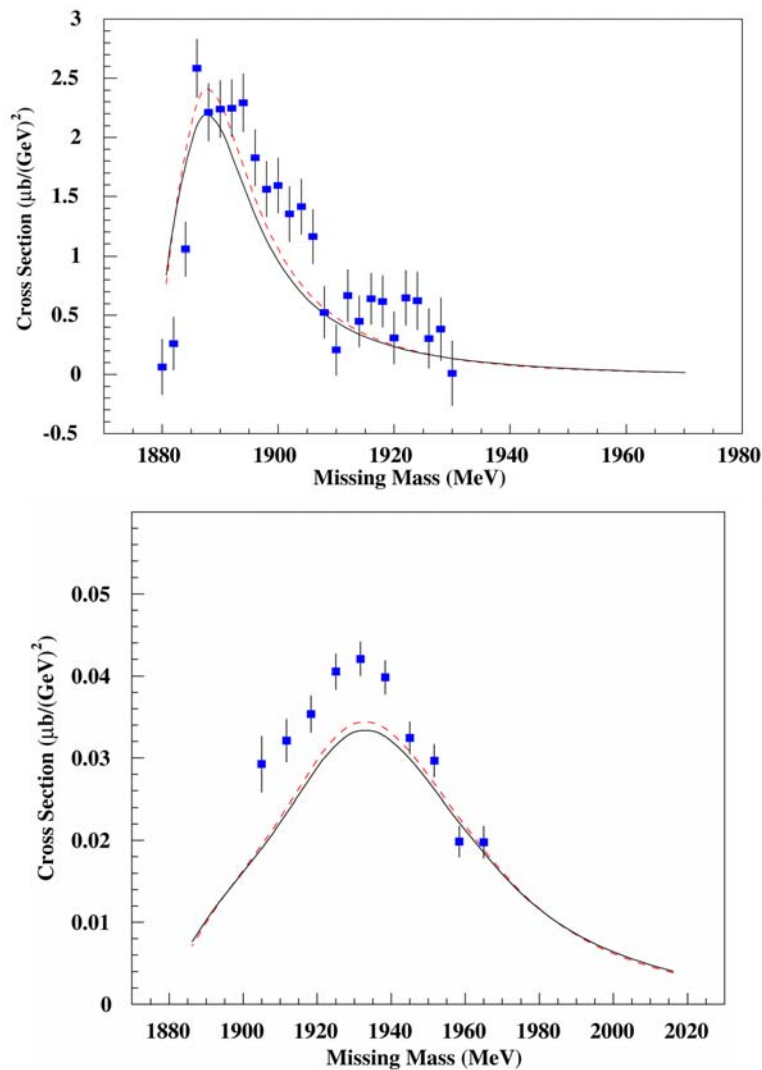


Fig. V-7. The calculated ${}^2\text{H}(e,e'\pi^+)$ cross sections in the parallel kinematics are compared with the data from Saclay, 1992 (top), and Jefferson Laboratory, 2001 (bottom). The dashed curves are obtained from neglecting the final NN interactions.

a.24. η Meson Production in NN Collisions (T.-S. H. Lee, K. Nakayama,* and J. Speth†)

η meson production in both proton-proton and proton-neutron collisions is investigated within a relativistic meson exchange model of hadronic interactions. It is found that the available cross section data can be described equally well by either the vector or pseudoscalar meson exchange mechanism for exciting

the $S_{11}(1535)$ resonance. Our results are compared with the data in Fig. V-8. It is shown that the analyzing power data can potentially be very useful in distinguishing these two scenarios for the excitation of the $S_{11}(1535)$ resonance. A paper describing our results has been submitted for publication.

*University of Georgia, †Forschungszentrum-Jülich, Germany

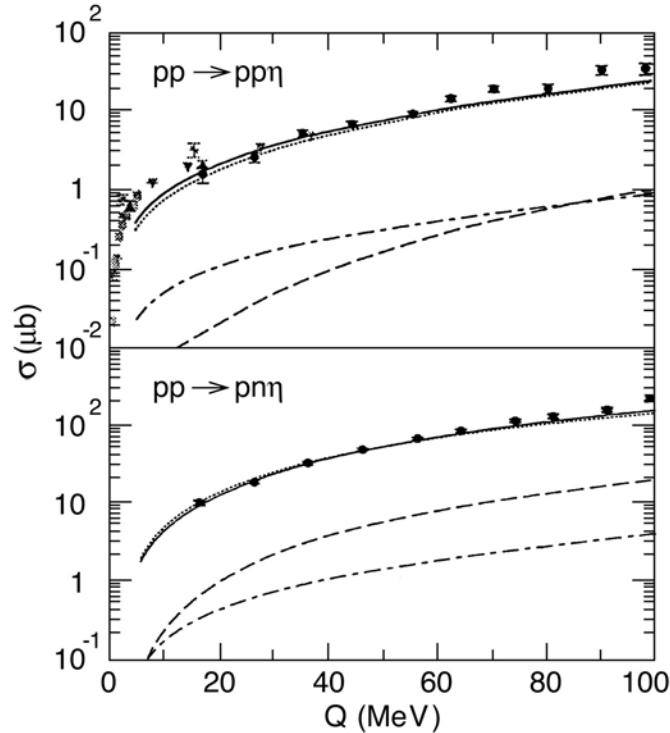


Fig. V-8 Total cross sections for $pp \rightarrow pp\eta$ (upper panel) and $pn \rightarrow pn\eta$ (lower panel). The dashed curves correspond to nucleonic current contribution while dot-dashed curves correspond to mesonic current contribution; the dotted curves represent the resonance current contribution. The solid curves are the total contributions.

a.25. Study of Nucleon Resonances with Double Polarization Observables in Pion Photoproduction (T.-S. H. Lee, D. Dutta,* and H. Gao*)

Motivated by new experimental opportunities at Jefferson Lab, the role of nucleon resonances in the double polarization observables of pion photoproduction is investigated. As an example, we show that the not-well-determined two-star resonance

$N_{3/2}(1660)$ can be examined by performing experiments on beam-recoil polarization at large angles. A paper describing our results has been submitted for publication.

*MIT

a.26. From Light Nuclei to Nuclear Matter: The Role of Relativity (F. Coester)

The success of non-relativistic quantum dynamics in accounting for the binding energies and spectra of light nuclei¹ with masses up to $A = 10$ raises the question whether the same dynamics, applied to infinite nuclear matter, agrees with the empirical saturation properties of large nuclei. Nuclear matter results of comparable accuracy for realistic Hamiltonians should become available. The simple unambiguous relation between few-nucleon and many-nucleon Hamiltonians is directly related to the Galilean covariance of nonrelativistic dynamics. Relations between the irreducible unitary representations of the Galilei and Poincaré groups indicate that the “nonrelativistic” nuclear Hamiltonians may provide sufficiently accurate approximations to Poincaré invariant mass operators.

There is, however, no firm theoretical basis for a prediction that there are “realistic” Hamiltonians which fit the empirical nuclear matter properties without additional many-body forces.

The essential feature of “relativistic” nuclear dynamics² is that the intrinsic nucleon parity is an explicit, dynamically relevant degree of freedom. The success of this approach to nuclear matter and large nuclei suggests the question how it might account for the spectral properties of light nuclei. Can hypothetical “realistic” Hamiltonians acting on tensor products of spinor functions account for both light nuclei and nuclear matter without a need for many-body forces?

¹Steven C. Pieper and R. B. Wiringa, *Ann. Rev. Nucl. Sci.* **51**, 53 (2001)

²Brian D. Serot and John Dirk Walecka, *Int. J. of Mod. Phys.* **E6**, 515 (1997)

a.27. Null-Plane Dynamics of Elastic Electron Deuteron Scattering (F. Coester and W. N. Polyzou*)

It is an inescapable feature of relativistic Hamiltonian dynamics that single-particle current density operators are covariant only under the kinematic subgroup. Null-plane dynamics has the unique feature that, like Galilei covariant dynamics, it allows a consistent impulse approximation, provided the momentum transfer is in the null plane. Model-independent interaction currents are introduced by the requirements of rotational covariance. They depend on the angle between the null vector and the transverse polarization vector used in the

computation of form factors. We find that the null-plane impulse approximation, with the null vector in the direction of the transverse canonical polarization vector together with a recent parameterization of the nucleon form factors,¹ provides a good representation of the deuteron structure functions A and B as shown in Fig. V-9. Covariant meson-exchange currents² can be added consistently in this framework. A quantitative investigation of meson-exchange currents is in progress.

*University of Iowa

¹E. L. Lomon, *Phys. Rev. C* **64** 035204 (2001)

²F. Coester and D. O. Riska, *Ann. Phys.* **234**, 141 (1994)

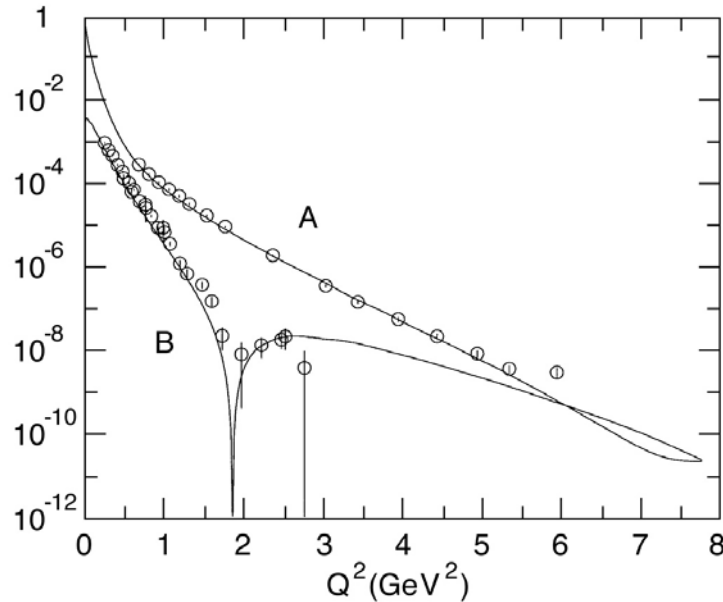


Fig. V-9. Null-plane impulse approximation of the deuteron structure functions *A* and *B*.

B. NUCLEAR FORCES AND NUCLEAR SYSTEMS

The goal of this program is to achieve a description of nuclear systems ranging in size from the deuteron and triton to nuclear matter and neutron stars using a single parameterization of the nuclear forces. Aspects of our program include both the construction of two- and three-nucleon potentials and the development of many-body techniques for computing nuclear properties with these interactions. Detailed quantitative, computationally-intensive studies are essential parts of this program.

Quantum Monte Carlo (QMC) calculations of light ($A \leq 10$) nuclei with realistic interactions have been the main focus of our recent efforts. Our nonrelativistic Hamiltonian contains the accurate Argonne v_{18} two-nucleon (NN) potential, which includes charge-independence breaking terms, and either the venerable Urbana IX three-nucleon (NNN) potential, or one of several new Illinois NNN models. The QMC calculations include both variational (VMC) and Green's function (GFMC) methods. We begin with the construction of variational trial functions based on sums of single-particle determinants with the correct total quantum numbers, and then act on them with products of two- and three-body correlation operators. Energy expectation values are evaluated with Metropolis Monte Carlo integration and parameters in the trial functions are varied to minimize the energy. These optimized variational wave functions can then be used to study other nuclear properties. They also serve as a starting point for the GFMC calculations, which systematically remove higher excited-state components from the trial wave functions by a propagation in imaginary time.

We are currently studying all $A \leq 10$ nuclei with experimentally known bound state or resonance energies, including some 55(30) excited states in VMC (GFMC). These are the first calculations treating $A \geq 6$ nuclei directly with realistic NN and NNN interactions. In GFMC calculations,

with the new Illinois NNN models, we can reproduce most of the experimental ground- and excited-state energies within 0.5 MeV. The VMC calculations, including two-body charge and current operators, are being used to study weak decays of $A = 6-8$ nuclei and for various $(e, e'p)$ and $(e, e'n)$ reactions. They are also being used to obtain astrophysically interesting cross sections, such as ${}^2\text{H}(\alpha, \gamma){}^6\text{Li}$ and ${}^3\text{He}(\alpha, \gamma){}^7\text{Be}$. Finally, we are also studying the properties of neutron drops with the goal of providing additional constraints for the construction of Skyrme interactions that are used in the modeling of neutron-rich nuclei in neutron star crusts.

In addition, a new effort using the coupled cluster $[\text{exp}(S)]$ method was initiated last year. The coupled cluster method is being used to study nuclei in the ${}^{12}\text{C}$ - ${}^{16}\text{O}$ range, using the same realistic Hamiltonian as the quantum Monte Carlo calculations. Comparisons of GFMC and $\text{exp}(S)$ results are being made for ${}^4\text{He}$ and neutron drops. We are also able to compare both methods with results of traditional shell model calculations. Finally, studies of hypernuclei are also continuing, particularly the charge-symmetry-breaking of ΛN interactions.

b.1. Quantum Monte Carlo Calculations of Light p-shell Nuclei (S. C. Pieper, R. B. Wiringa, J. Carlson,* V. R. Pandharipande,† and K. Varga‡)

Since the early 1990s, we have been studying the ground and low-lying excited states of light p-shell nuclei as A -body problems with realistic nucleon-nucleon (NN) and three-nucleon (NNN) interactions using advanced quantum Monte Carlo (QMC) methods. Our preferred Hamiltonians contain the Argonne v_{18} NN potential, which gives an excellent fit to elastic NN scattering data and the deuteron energy and Illinois NNN potentials, which were fit to binding energies of $A \leq 8$ nuclei, as described in the next section. The QMC methods include both variational Monte Carlo (VMC), which gives an initial approximate solution to the many-body Schrödinger equation, and the Green's function Monte Carlo (GFMC), which systematically improves on the VMC starting point and produces binding energies that are accurate to within 2%. This year we have concentrated on $A = 9, 10$ nuclei, and have made our first variational unnatural-parity-state calculations.

The VMC calculations begin with the construction of an antisymmetric Jastrow trial wave function that includes single-particle orbits coupled to the desired JM values of the state of interest as well as pair and triplet spatial correlations. It is then acted on by a symmetrized product of two-body spin, isospin, tensor, and spin-orbit correlation operators, induced by the NN potential, and three-body correlation operators for the NNN potential. The wave functions are diagonalized in the small basis of different Jastrow spatial symmetry components to project out higher excited states with the same quantum numbers.

In the GFMC calculations, we operate on a version of the VMC trial function with the imaginary time propagator, $\text{exp}[-(H'-E_0)\tau]$, where H' is a simplified Hamiltonian, E_0 is an estimate of the eigenvalue, and τ is the imaginary time. The excited-state components of the trial function will then be damped out for large τ , leaving the exact lowest eigenfunction with the quantum numbers of the input variational wave function. The expectation value of H is computed for a sequence of increasing values of τ to determine the convergence. Our H' contains the reprojected v_8 part of the NN potential and the full NNN potential. The small correction, $H-H'$, is computed perturbatively. The many-body propagator is written as a symmetrized product of exact two-body propagators, with the NNN potential treated in lowest order.

In previous years we have made significant improvements in the GFMC algorithms, especially in solving the fermion sign problem for nuclear systems. The method and program now seems stable and we have concentrated on extending the calculations to larger nuclei and on developing new models of the NNN potential. The computer resources (both CPU time and memory) required for these calculations increase exponentially with the number of nucleons. Therefore, progress to bigger nuclei usually requires a new generation of computers.

Phase-II of the IBM SP at NERSC was installed this year and we obtained a large amount of friendly-user time on it. As a demonstration of the scalability of our

GFMC program, we ran a more than 6-hour calculation of the 1^- state of ^{10}Be using 2048 processors. The sustained speed was 0.55 TFLOPS with a 92% speedup efficiency (that is the program ran 1886 times faster than it would have on just one processor). Due to scheduling considerations we routinely use only 256 to 512 processors. In addition to using the NERSC SP, we

continue to make extensive use of the Argonne Mathematics and Computer Science Linux cluster.

An Annual Reviews of Nuclear and Particle Science article describing our calculations of $A \leq 8$ nuclei was published this year.¹

*Los Alamos National Laboratory, †University of Illinois, Urbana, ‡Oak Ridge National Laboratory

¹S. C. Pieper and R. B. Wiringa, *Ann. Rev. Nucl. Part. Sci.* **51**, 53-90 (2001)

b.2. Studies of Three-Nucleon Interactions in Nuclear Systems (S. C. Pieper, R. B. Wiringa, V. R. Pandharipande,* D. G. Ravenhall,* and J. Carlson†)

Our GFMC calculations of nuclei with $3 \leq A \leq 8$ using the Hamiltonian consisting of the Argonne v_{18} two-nucleon (NN) and Urbana IX three-nucleon (NNN) potentials have shown that this Hamiltonian underbinds p-shell nuclei by 0.8 MeV in ^6Li to 5 MeV in ^8He . The error increases with both A and $|N-Z|$. This year we finished constructing improved “Illinois” models for the NNN potential.

Our approach is to use theoretical guidance to suggest the structure of new terms, but to consider the coupling constants and short-range shapes of the potential to be adjustable. This is in the same spirit as the development of realistic NN potentials. We have considered a number of new terms. We find that new potential terms are often not perturbative, *i.e.*, an expectation value of the new term using the GFMC wave function from just Argonne v_{18} and Urbana IX may be misleading. Thus each new term must be added to the GFMC propagator and a new GFMC calculation made. Furthermore, as the strength of the new term is adjusted, the propagations must be repeated.

The dominant term of the Urbana potential is the Fujita-Miyazawa (FM) two-pion term with intermediate excitation of one nucleon to a Δ . We have now studied three-pion ring terms containing one and two Δ excitations. These are repulsive in s-shell nuclei and attractive in p-shell nuclei and correct the overall loss of binding energy with respect to both A and $|N-Z|$. The Tucson-Melbourne potential contains the FM term and a two-pion term arising from s-wave πN scattering; we have also considered a corrected s-wave term.

The FM terms in the Urbana NNN potentials and the new models that we first constructed have coupling constants that are about $\frac{1}{2}$ the value suggested by soft-pion physics. We have also made a model that has the

stronger coupling constant; this required a significantly softer cutoff parameter (normally we use the same cutoff as is used in the NN potential). Most of the models have the two-pion s-wave term with the strength preferred by chiral perturbation theory, but one of the models omits this term. In all, five Illinois models have been developed with various strengths for the four potential terms. All of them give excellent fits to the $3 \leq A \leq 8$ binding energies – the rms errors are ≤ 10 keV. These results have been published.¹

This year we have made an extensive set of $A = 9, 10$ calculations with these new potentials. The reproduction of the nuclear levels continues to be satisfactory, although there is more dispersion than for $A \leq 8$. Preliminary calculations of nuclear matter with these potentials also show significant differences between the models. Figure V-10 compares GFMC values of ground and excited state energies for Argonne v_{18} with no NNN potential and one of the new Illinois models to experimental values. One sees the very important contributions made by the NNN potential to the p-shell binding energies, and the generally very good resulting agreement with the data.

A very interesting result can be seen in the ^{10}B spectra. Experimentally the ground state of ^{10}B is a 3^+ state. However the calculation with just AV18 very strongly predicts that the ground state is 1^+ . Petr Navratil (Livermore) first found this result using the no-core shell model and has shown that it is also true if the CD Bonn NN potential is used. Figure V-10 shows that including the Illinois-2 NNN potential results in the correct ground state. This is also true for the other Illinois potentials, but the older Urbana-IX potential also gives a 1^+ ground state.

*University of Illinois, Urbana, †Los Alamos National Laboratory

¹S. C. Pieper, V. R. Pandharipande, R. B. Wiringa, and J. Carlson, *Phys. Rev. C* **64**, 014001,1-21 (2001)

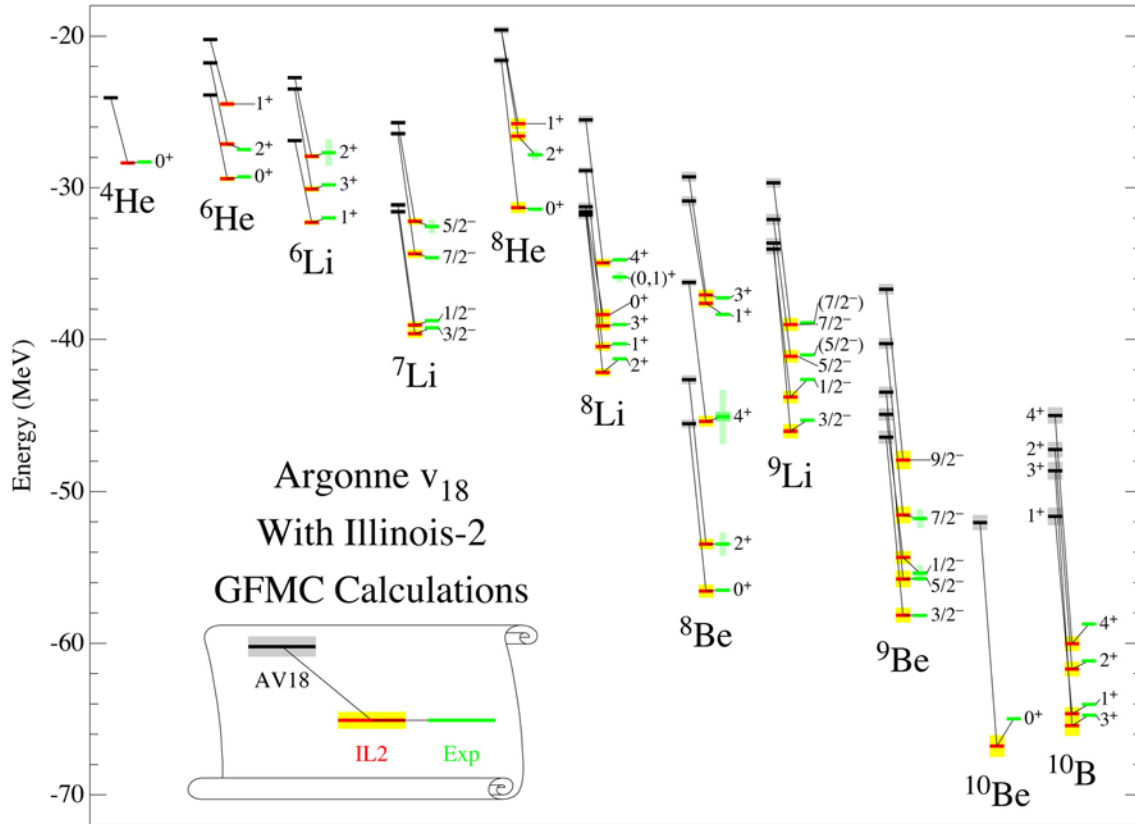


Fig. V-10. GFMC energies for $A = 4-10$ nuclei using the Argonne v_{18} NN potential by itself and with one of the new Illinois NNN potentials, compared to experiment.

b.3. What Makes Nuclear Level Structure? (S.C. Pieper and R.B. Wiringa)

As shown in the previous section, a Hamiltonian consisting of realistic, and hence complicated, NN and NNN potentials can accurately reproduce the level structure of light p-shell nuclei. We have investigated the effects of attempting to simplify the Hamiltonian. The previous section shows that the NNN potential is necessary to get the correct overall binding of all $A \geq 3$ nuclei and further that something like the sophisticated new Illinois potentials seems necessary to get the correct 3^+ ground state of ^{10}B .

In this study we made a series of calculations using no NNN potential and increasingly simpler versions of the Argonne v_{18} . In these NN potentials we kept a subset of the operators (for example AV8' contains central, spin-spin, tensor and spin-orbit terms with and without isospin exchange) and refit the radial forms to reproduce as many of the NN phase shifts as possible. Thus AV8' reproduces the $^1\text{S}_0$, $^3\text{S}_1$ - $^3\text{D}_1$, $^1\text{P}_1$, and $^3\text{P}_{0,1,2}$ phase shifts. Next AV6' has no spin-orbit operators and hence has very poor, almost degenerate, $^3\text{P}_{0,1,2}$ phase

shifts. The AV4' has no tensor operators and so no $^3\text{S}_1$ - $^3\text{D}_1$ mixing; the deuteron still has the correct binding energy, but has no D-wave. The AV2' has no spin-spin operator and hence reproduces only the $^1\text{S}_0$ and $^3\text{S}_1$ phases; the P-wave phases are attractive. Finally AV1' is an average of the two terms in AV2' and binds the deuteron with only 0.43 MeV.

These potentials give increasingly poor representations of nuclear structure as is shown in Fig. V-11. The AV8' (not shown) is generally close to full results with some spin-orbit splittings being too small and the same inversion of levels in ^{10}B as shown above. However the AV6' results in degenerate spin-orbit pairs. The AV4' does not mix different spatial symmetry states so the symmetry becomes a good quantum number. Also it results in too much binding as A increases. The AV2', with no repulsion in P waves, has lost all nuclear saturation; for example ^5He is much more bound than ^4He . Also, because of the repulsive core in the potential, the lowest spatial symmetry states become the

ground states of the nuclei instead of the highest spatial symmetry states. With AV1' the overbinding with increasing A is even worse and, since the only thing distinguishing neutrons from protons is the Coulomb potential, the valley of stability becomes severely

distorted; the helium isotopes are the most bound A = 4 to 10 nuclei. Thus one really needs the full complication of the NN and NNN potentials to get a realistic picture of nuclear level structure.

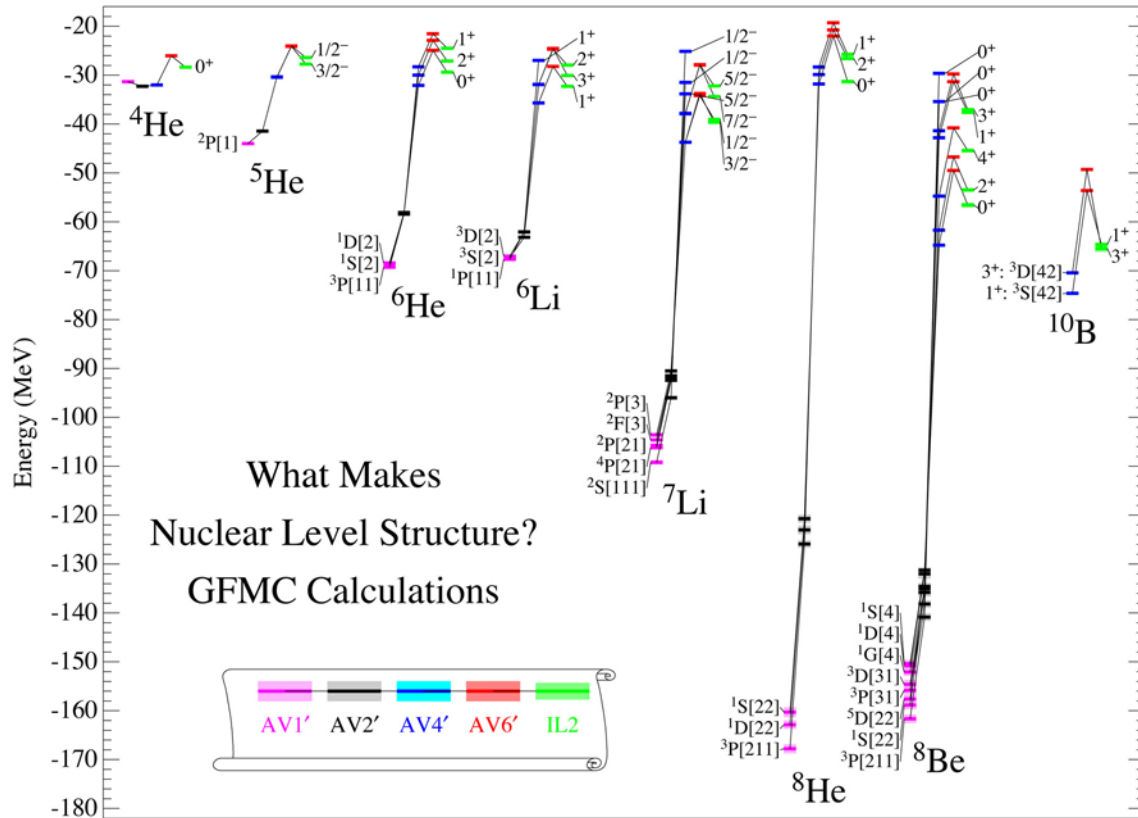


Fig. V-11. Energies of nuclear states using simplified Hamiltonians compared to results using a very complete Hamiltonian (AV18 + IL2).

b.4. Radiative Capture Reactions for Astrophysical Applications (R. B. Wiringa, K. M. Nollett,* and R. Schiavilla†)

Radiative capture reactions play a major role in many astrophysical processes, including primordial nucleosynthesis and stellar evolution, yet they are frequently very difficult to measure accurately in the laboratory because of their small cross sections. We have used the many-body variational Monte Carlo (VMC) wave functions for the Argonne v_{18} two-nucleon and Urbana IX three-nucleon potentials discussed above to study three capture reactions involving light p-shell nuclei: ${}^2\text{H}(\alpha,\gamma){}^6\text{Li}$, ${}^3\text{H}(\alpha,\gamma){}^7\text{Li}$, and ${}^3\text{He}(\alpha,\gamma){}^7\text{Be}$. These reactions are responsible for the primordial lithium abundance, and the last one is also important in solar neutrino production.

We evaluated the appropriate matrix elements (primarily E1 and E2) between initial 4+2- or 4+3-body clusters, and the final 6- or 7-body ground state. The VMC wave functions were used for all clusters, supplemented by a suitable optical potential found in the literature for the initial cluster-cluster scattering state. The problem factorizes into a one-dimensional energy-dependent integral and a multi-dimensional energy-independent kernel. The latter is over the coordinates of all particles and requires significant computation; it is evaluated by standard Metropolis Monte Carlo techniques. The outer integral, over the cluster-cluster separation, is evaluated for a large number of energies, and also with different choices for the folding optical potential, at little additional cost.

Results for the ${}^2\text{H}(\alpha,\gamma){}^6\text{Li}$ reaction¹ were presented in last year's annual report; here we show in Fig.V-12 the final results for the ${}^3\text{H}(\alpha,\gamma){}^7\text{Li}$ and ${}^3\text{He}(\alpha,\gamma){}^7\text{Be}$ reactions, which served as the University of Chicago Ph.D. thesis work of Ken Nollett.² The ${}^3\text{H}(\alpha,\gamma){}^7\text{Li}$ reaction was measured very accurately by Brune *et al.* in 1999, and for one choice of the optical potential our calculation agrees extremely well with the data. However, the measurements of the ${}^3\text{He}(\alpha,\gamma){}^7\text{Be}$ reaction show a very large dispersion, and our calculations only touch the bottom edge of the data. From our viewpoint, the data sets for the two reactions are not compatible.

The theoretical calculations can be improved in the future by: 1) using the more accurate GFMC wave functions, particularly for the p-shell final states; 2) using the better Illinois three-nucleon potentials discussed above, which give improved binding in the p-shell nuclei, to generate the cluster wave functions; and 3) using Monte Carlo techniques to develop consistent cluster-cluster scattering wave functions instead of depending on an external optical potential. It should also be possible to extend these calculations to additional reactions of astrophysical interest such as ${}^7\text{Be}(p,\gamma){}^8\text{B}$.

*Present address: California Institute of Technology, †TJNAF and Old Dominion University

¹K. M. Nollett, R. B. Wiringa, and R. Schiavilla, Phys. Rev. C **63**, 024003 (2001)

²K.M. Nollett, Phys. Rev. C **63**, 054002 (2001)

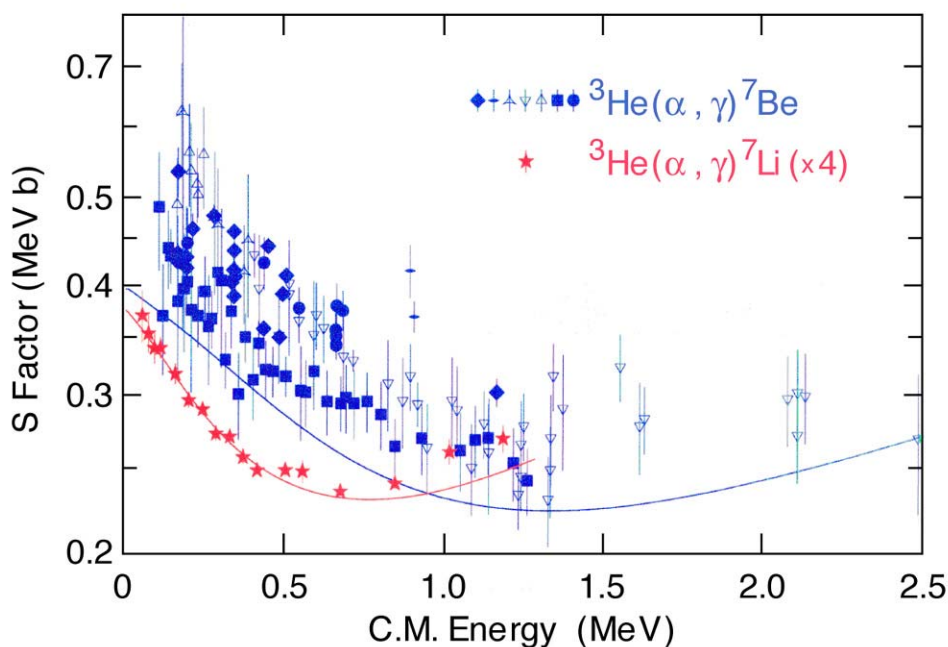


Fig. V-12. The total s -factor for $\alpha+{}^3\text{H}$ and $\alpha+{}^3\text{He}$ radiative capture compared to experimental data.

b.5. Microscopic Calculations of A = 6-8 Weak Decays (R. B. Wiringa, S. C. Pieper, and R. Schiavilla*)

We have studied the ${}^6\text{He}$ beta decay and ${}^7\text{Be}$ electron capture processes using variational Monte Carlo (VMC) wave functions, derived from a realistic Hamiltonian containing the Argonne v_{18} two-nucleon and Urbana IX three-nucleon interactions. The model for the nuclear weak axial current includes one- and two-body operators with the strength of the leading two-body term, associated with Δ -isobar excitation of the nucleon, adjusted to reproduce the Gamow-Teller matrix element in tritium β -decay. The measured half-life of ${}^6\text{He}$ is under-predicted by $\cong 8\%$, while that of ${}^7\text{Be}$ for decay into the ground and first excited states of ${}^7\text{Li}$ is over-predicted by $\cong 9\%$. However, the experimentally known branching ratio for these latter processes is in good agreement with the calculated value. Two-body axial current contributions lead to a $\cong 1.7\%$ (4.4%) increase in the value of the Gamow-Teller matrix element of ${}^6\text{He}$ (${}^7\text{Be}$), obtained with one-body currents only, and slightly worsen (appreciably improve) the agreement between the calculated and measured half-life. Corrections due to retardation effects associated with the finite lepton momentum transfers involved in the decays, as well as contributions of suppressed transitions induced by the

weak vector charge and axial current operators, have also been calculated and found to be negligible. A paper describing this work has been accepted for publication.¹

Several improvements in these calculations are being prepared, including the use of the improved Illinois three-body potentials in the Hamiltonian, and the use of Green's function Monte Carlo wave functions instead of the VMC trial functions. We have also made initial VMC calculations of the more complicated A = 8 weak decays. While the A = 6 and 7 decays are between states of predominantly the same spatial symmetry, the decays of ${}^8\text{He}$, ${}^8\text{Li}$, and ${}^8\text{B}$ involve transitions where the spatial symmetry of the initial state is only a small component in the final state. An additional complication is that the ${}^8\text{Li}$ and ${}^8\text{B}$ ground states both decay to the wide 2^+ first excited state of ${}^8\text{Be}$, which at present we approximate as a bound state. Initial calculations in impulse approximation give less than half of the experimental Gamow-Teller matrix element, indicating these will be much tougher transitions to explain.

*TJNAF

¹R. Schiavilla and R. B. Wiringa, to be published in Phys. Rev. C

b.6. Coupled Cluster Expansion Approach to Calculating Ground State Properties of Closed Shell Nuclei (B. Mihaila and J. Heisenberg*)

We continue our project regarding the quest for a realistic description of the ground state of closed-shell nuclei in the p-shell (${}^{12}\text{C}$, ${}^{16}\text{O}$). These calculations use the coupled cluster method [CCM] in configuration space, together with a realistic nuclear interaction and currents, which are purposely consistent with the work done by the GFMC collaboration. Just as the GFMC method, the CCM formalism is an exact approach to solving the many-body problem. In the past year we have put a lot of effort into obtaining a good description

for the ground-state of ${}^4\text{He}$. The difficulty of this task resides in the fact that higher order corrections in the CCM hierarchy are $1/A$ -type corrections, which are clearly increasingly important in lighter nuclei. When completed, this project will provide an accurate description of nuclear structure properties in the CCM framework, for a mass domain between A = 4 and 16, and effectively open the possibility of treating nuclei as heavy as ${}^{40}\text{Ca}$ on an equal footing.

*University of New Hampshire

b.7. Neutron-Proton Density Differences in Nuclei (A. R. Bodmer and Q. N. Usmani*)

We have studied the neutron/proton distributions in nuclei in a local density approach. We show explicitly, as was originally pointed out by one of the authors (A.R.B.), that the density dependence of the symmetry-energy density $F(\rho)$ drives the difference of distributions in the absence of coulomb and density-gradient contributions. In this limit we obtain an explicit solution λ_m , in terms of $F(\rho)$, for $\lambda = (\rho_n - \rho_p)/\rho$. For $F \equiv 1$: $\lambda_m = \lambda_0 \equiv (N-Z)/A$ and the difference between the neutron and proton rms radii is $\delta r = 0$. Additional contributions $\delta\lambda$ to λ_m are treated variationally. The gradient term makes only a small contribution to $\delta\lambda$, and λ is thus effectively determined only by the nuclear-matter quantity $F(\rho)$. The coulomb energy pushes ρ_p out relative to ρ_n , thus reducing δr . Decreasing the coulomb energy is equivalent to increasing u_τ (the coefficient of the asymmetry term in

the semi-empirical mass formula); $e = 0$ corresponds to $u_\tau = \infty$ and gives the maximum δr for a given $F(\rho)$. Our numerical results are for ^{208}Pb , see Fig. V-13. For a large range of $F(\rho)$ we find that δr and $u_{S\tau}/u_\tau$ ($u_{S\tau}$ is the calculated coefficient of the surface-symmetry energy) are approximately universal functions of a normalization integral N involving $F^{-1}(\rho)$, in particular for $\delta r \leq 0.5$ fm ($N-1 \leq 1.5$) when the dependence on $N-1$ is one-valued and approximately linear for small δr ($\delta r \approx 0$ for $N = 1$). Then N is effectively determined by δr . For such N there is also a strong correlation between δr and $u_{S\tau}/u_\tau$, allowing an approximate determination of the latter from δr . At larger N , δr has a maximum; absolutely of ≈ 0.75 fm (for $e = 0$) and of ≈ 0.65 fm for realistic $u_\tau \approx 25 - 35$ MeV.

*Universiti Putra Malaysia, Malaysia

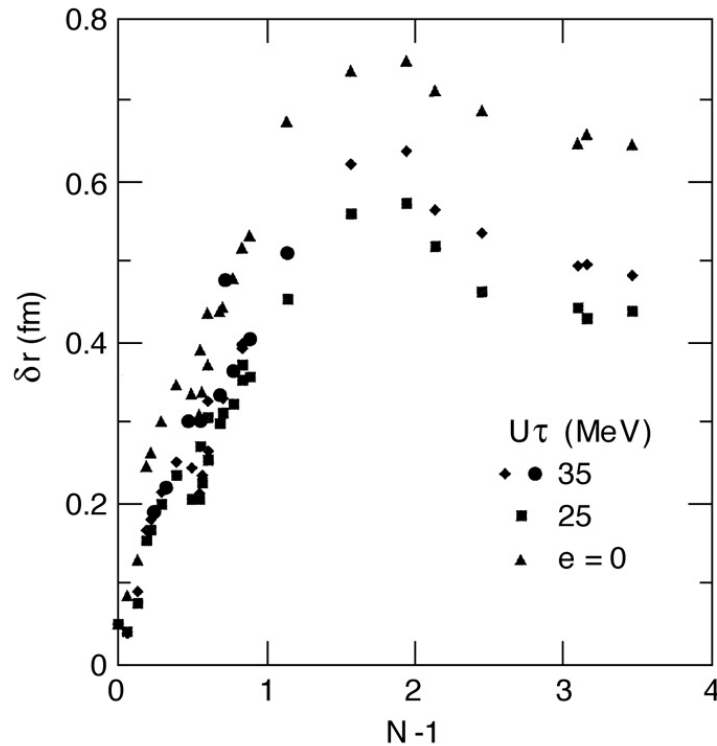


Fig. V-13. Difference δr between the neutron and proton rms radii. N is the norm of $F_{(\rho\rho)}^{-1}$, where F determines the density dependence of the symmetry-energy density.

C. NUCLEAR STRUCTURE AND HEAVY-ION REACTIONS

This research focuses on nuclear structure in unusual regimes: nuclei far from stability, and superdeformed nuclei at high spin. We also study heavy-ion reactions near the Coulomb barrier. Much of this work is closely tied to experiments performed at ATLAS and at radioactive beam facilities.

Our studies of drip-line nuclei focus on breakup reactions, induced by the Coulomb and nuclear fields from a target nucleus. A critical issue is to develop a realistic description of the breakup mechanisms as a necessary tool for extracting nuclear structure properties of drip-line nuclei. We have applied our numerical technique of calculating the time-evolution of the two-body wave function for the relative motion of a halo nucleon and a core nucleus, in the time-dependent fields from a target nucleus, in order to test the validity of simpler reaction models, such as the eikonal approximation for the nuclear induced breakup, and first-order perturbation theory for Coulomb dissociation.

Our numerical studies of the nuclear induced breakup of ^{11}Be on a light target show that the eikonal approximation becomes unrealistic at beam energies below 20 MeV/u. The breakup probabilities are reduced compared to the more realistic dynamical calculations. Our numerical studies of the Coulomb dissociation of ^{17}F on high-Z targets show that first-order perturbation theory is also a poor approximation at lower energies. The leading order correction is a dynamical polarization effect of order Z^3 in the target charge. We have also investigated other corrections, such as the Coulomb-nuclear interference and the effect of close collisions, where projectile and target have a non-zero overlap during the collision.

Our studies of the proton decay from nuclei beyond the proton drip-line are based on a coupled-channels technique. We have applied a particle-vibration model to analyze the decay from near-spherical proton emitters. The model explains very well the observed fine structure in the decay of ^{145}Tm . Moreover, the spectroscopic factors predicted in a low-seniority shell model are reproduced much better when we include particle-vibration coupling.

Some nuclear structure problems of interest are superdeformation, heavy and superheavy elements, proton radioactivity, the neutron deficient Pb region and neutron-proton pairing near the $N = Z$ line. To study these problems we make use of (1) the Strutinsky method as well as (2) self-consistent mean field (SCMF) calculations using the Gogny interaction, and (3) many-body (MB) wavefunctions.

In nuclides with roughly equal number of protons and neutrons, $T = 1$ and $T = 0$ n-p pairing will play an important role, in addition to the usual like-nucleon $T=1$ pairing. To adequately treat and understand these effects, it is necessary to go beyond the quasiparticle approximation and to study not only those nuclei that are exactly on the $N = Z$ line. The rare isotope accelerator (RIA) will provide considerable spectroscopic information on nuclides near the $N = Z$ line. We have extended our many-body code to include neutron-proton pairing interactions. We have found that there is a new quantum number for characterizing collective states; *i.e.*, the number parity of the $T = 0$ and $T = 1$ n-p pairs.

Our studies of superdeformation at both low and high spins address the issue of possible new regions of superdeformation and hyperdeformation. Special emphasis is being put on the study of fission barriers at high spin as this is crucial for the possible production of very extended nuclei. We have studied nuclei with masses ranging from $A \sim 80$ to $A \sim 200$, as a function of angular momentum, in a four-dimensional shape space using the Strutinsky method. We find several nuclides that are promising candidates for finding superdeformed and hyperdeformed shapes.

Our MB and SCMF calculations of nuclides in the neutron deficient Pb isotopes, in conjunction with J. L. Egido and L. M. Robledo, suggest the existence of many low-lying 0^+ excited states in this region. Experimental searches for these states are being carried out.

c.1. Multipole Expansion for Relativistic Coulomb Excitation (H. Esbensen and C. A. Bertulani*)

A theoretical description of relativistic Coulomb excitation has previously only been developed for distant collisions,¹ where projectile and target do not overlap. This description is often sufficient for reactions of stable nuclei but in reactions of proton-rich nuclei, where the density of the valence protons extends to large distances, one would also have to consider close collisions, where projectile and target penetrate each other. We have therefore studied² a general multipole expansion of the relativistic electromagnetic interaction between colliding nuclei, based on the Liénard-Wiechert potential and the associated current interaction. The Lorentz contraction introduces a deformation of this potential, and the multipole expansion will therefore contain diagonal as well as off-diagonal multipole components.

We have focused on monopole, dipole, and quadrupole single-particle excitations. For close collisions ($r > r'$, where r is the single-particle distance from the core, and r' is the projectile-target distance), the sum over off-diagonal components is finite but it is in principle infinite for distant collisions ($r < r'$). We have made a simple truncation in the sum over the off-diagonal

components, including just the monopole and quadrupole terms associated with the deformation of the Liénard-Wiechard potential. We have tested this approximation in first-order perturbation theory for distant collisions (including the contributions from the current interaction) against the exact answer of Ref. [1]. We find that the approximation is quite accurate at least up to $v/c = 0.6$. This is illustrated in Fig. V-14, where the approximate longitudinal ($m = 0$) and transverse ($m = 1$) dipole excitation amplitudes are shown (in reduced units) by open symbols. The solid curves are the exact results,¹ whereas the dashed curves are the non-relativistic results. It is seen that the approximate results are essentially identical to the exact answer.

The multipole form factors we have derived can be used in higher-order dynamical calculations of the relativistic Coulomb dissociation of halo nuclei. Finite size effects can be implemented numerically in a straightforward manner. The truncated expansion discussed above should be reliable up to a few hundred MeV per nucleon, which is sufficient for experiments performed at most fragmentation facilities. This work has been published.²

*Brookhaven National Laboratory

¹A. Winther and K. Alder, Nucl. Phys. A319, 518 (1979)

²H. Esbensen and C. A. Bertulani, Phys. Rev. C 65, 024605 (2002)

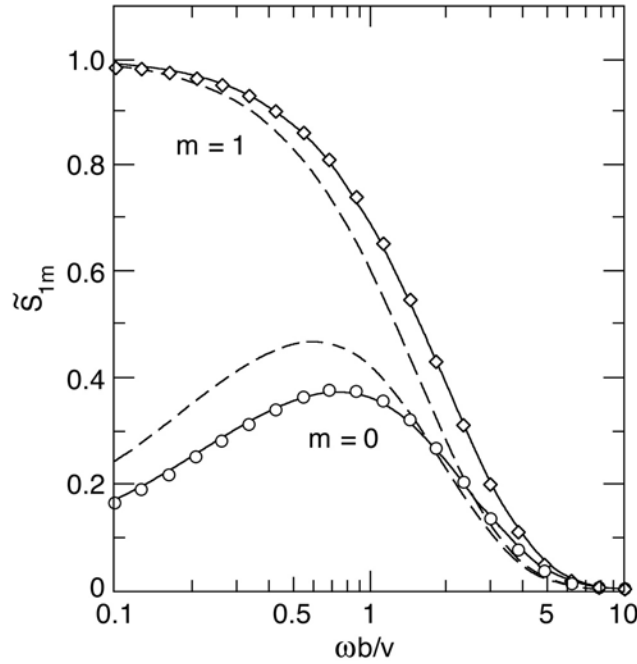


Fig. V-14. Excitation amplitudes (in reduced units) for longitudinal ($m = 0$) and transverse ($m = 1$) dipole excitations at distant collisions are shown as functions of the adiabaticity parameter $\omega b/v$, for $v/c = 0.6$. Approximate results (open symbols) are compared to exact results (solid curves) and to the non-relativistic results (dashed curves).

c.2. Vibrational Interpretation of Spherical and Near-Spherical Proton Emitters (C. N. Davids and H. Esbensen)

There has been a recent observation of fine structure in the proton decay of ^{145}Tm .¹ The ground-state and fine structure groups have energies of 1.728 MeV and 1.404 MeV, respectively, yielding an excitation energy of 0.326 MeV for the first 2^+ state in the daughter nucleus ^{144}Er . The 2^+ branching ratio is 9.9%. If this were a deformed nucleus, it would imply a deformation of $\beta_2 \approx 0.18$, but calculations in the adiabatic limit for these conditions cannot reproduce either the half-life or the branching ratio, for states near the Fermi surface.

This suggests that another approach be tried, namely, to consider the daughter nucleus to be vibrational in nature, rather than permanently deformed. We have modified our coupled-channels formalism² to include particle-vibration couplings in the single-particle Hamiltonian, along with the spherical Coulomb, nuclear and spin-orbit terms. The strength α_0 of the coupling to the 2^+ state of the daughter nucleus can be related empirically to the excitation energy $E_x(2^+)$ by the

relation $\alpha_2^{(0)} = 218/[A\sqrt{E_x(2^+)}]$. We have used the same nuclear potential parameters that were determined in Ref. [2]. Assuming a total spin of $11/2^-$ we obtain remarkable agreement with both the total and the partial proton decay widths of ^{145}Tm .

We have also applied the particle-vibration model to calculate the decay widths Γ_{th} of other near-spherical proton emitters, with a vibrational coupling strength determined from the 2^+ excitation energy when known, or from systematics. The spectroscopic factors, defined as the ratio $S_{\text{exp}} = \Gamma_{\text{exp}}/\Gamma_{\text{th}}$ of measured and calculated decay widths, are shown by symbols in Fig. V-15 (a) for a number of (odd-Z, odd-A) nuclei. The spectroscopic factors one obtains when the decay widths Γ_{th} are calculated in a spherical calculation (without any couplings) are shown in (b). Comparing (a) and (b), it is seen that particle-vibration coupling has a significant effect and improves the agreement with the

low-seniority shell model calculations of Ref. [3], which are shown by the solid curves. The results shown in (c) are for a number of (odd-Z, odd-N) nuclei. They were also obtained in the particle-vibration model,

treating the odd neutron as a spectator. Here, too, the agreement with the low-seniority calculation is quite good. This work has been published.⁴

¹K. Rykaczewski *et al.*, Nucl. Phys. A **682**, 270c (2001)

²H. Esbensen and C. N. Davids, Phys. Rev. C **63**, 014315 (2001)

³Cary N. Davids *et al.*, Phys. Rev. C **55**, 2255 (1997)

⁴Cary N. Davids and H. Esbensen, Phys. Rev. C **64**, 034317 (2001)

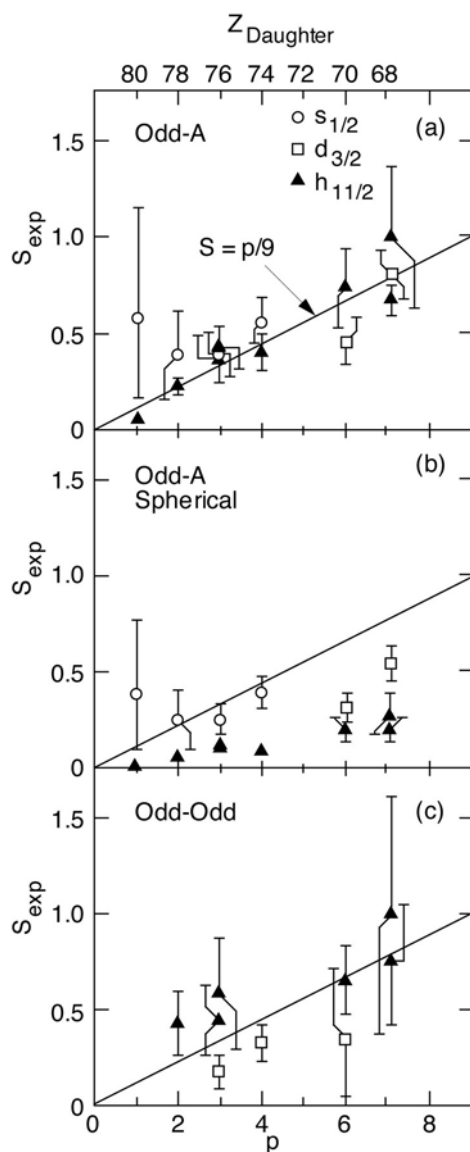


Fig. V-15. Spectroscopic factors of near-spherical proton emitters, as function of the number p of proton holes below $Z = 82$. The solid curves are the predictions of a low-seniority shell model calculation.³ The symbols in (a) are the values obtained for (odd-Z, odd-A) nuclei and include the effect of particle-vibration coupling. The symbols in (b) are the results for the same set of nuclei obtained without any particle-vibration coupling. The results in (c) are for odd-odd nuclei. They include the effect of particle-vibration coupling and treat the odd neutron as a spectator.

c.3. Accuracy of the Eikonal Model of Fragmentation Reactions (H. Esbensen and G. F. Bertsch*)

A convenient model of the nuclear induced breakup of halo nuclei is the eikonal approximation which is well justified at high energies. Since many fragmentation experiments have been performed in the energy range of 20-60 MeV/u, it is of interest to see how accurate the eikonal approximation is in this energy range and at which energy it becomes unreliable. We have tested the eikonal approximation by comparing it to solutions of the time-dependent Schrödinger equation, where we numerically follow the time evolution of the wave function for the relative motion of a halo nucleon and a core nucleus, under the influence of the nuclear field from a target nucleus. We take ^{11}Be as a typical example and use standard optical potentials to describe the interaction with the target. We have compared the one-neutron removal probabilities that we obtain from the two methods, and also the two separate components from stripping and diffraction dissociation.

We have calculated the breakup probabilities on a ^{12}C target as function of the beam energy, at a typical impact parameter of 8 fm. We found that the eikonal approximation becomes unreliable below 20 MeV/u. At higher energies, the eikonal breakup probability is

reduced compared to the dynamical calculation by roughly the factor $1 - E_x/E_{\text{beam}}$, where E_{beam} is the beam energy in MeV/u and $E_x \approx 4.5$ MeV. The reduction implies that an absolute spectroscopic factor extracted in the eikonal approximation from measurements at 60 MeV/u should be reduced by about 7%.

We have also investigated the longitudinal momentum distribution of neutrons emitted in the breakup. At 10 MeV/u we obtain an asymmetric distribution in the dynamical calculation, whereas the eikonal is symmetric. By decomposing the asymmetric distribution (shown by the solid curve in Fig. V-16) into contributions from low and high final state angular momenta l_f in the rest frame of ^{11}Be , we obtained a fairly narrow and symmetric distribution from $l_f \leq 5$ (long dashed curve). From $l_f > 5$, we obtained a very broad distribution centered around the target motion (short dashed curve). The latter component was interpreted as a towing mode, where some of the emitted neutrons are attracted to the target nucleus and follow its motion. This work has been published.¹

*Institute for Nuclear Theory, Univ. of Washington

¹H. Esbensen and G. F. Bertsch, Phys. Rev. C **64**, 014608 (2001)

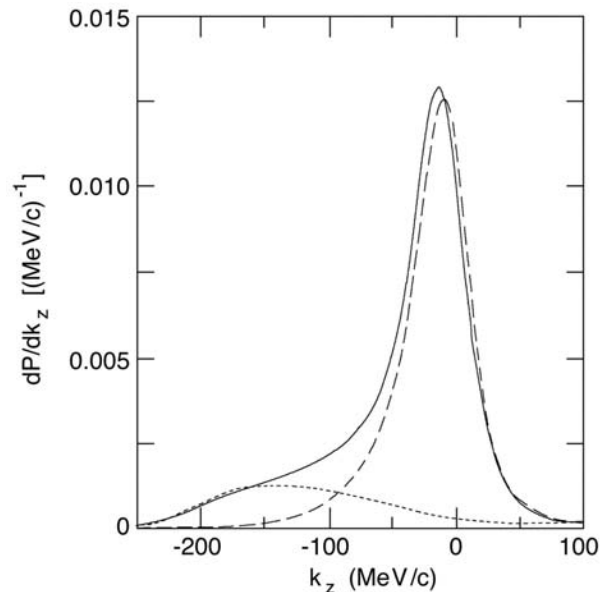


Fig. V-16. Longitudinal momentum distribution of neutrons emitted in the rest frame of ^{11}Be in reactions with a ^{12}C target at 10 MeV/u and an impact parameter of 8 fm. The full distribution (solid curve) has been decomposed into two components: from low-angular momenta (≤ 5 , long-dashed curve) and high-angular momenta (> 5 , short dashed curve).

c.4. Higher-order Effects in the Two-body Breakup of ^{17}F (H. Esbensen and G. F. Bertsch*)

Measurements of the Coulomb dissociation of weakly bound proton-rich nuclei (*e.g.*, ^8B) are commonly analyzed on the basis of first-order perturbation theory for distant collisions. We have investigated the validity of this approximation by calculating the diffraction dissociation of ^{17}F to all orders in the Coulomb and nuclear fields from a target nucleus. This is done by assuming a classical Coulomb trajectory for the relative motion of projectile and target and by numerically solving the time-dependent Schrödinger equation for the two-body wave function of the valence proton and the ^{16}O core, in the time-dependent fields from the target.

We find that the most dominant correction to the first-order Coulomb dissociation is a dynamic polarization effect which to lowest order is proportional to Z^3 of the target charge. This effect is known in atomic stopping theory as the Barkas effect.¹ It causes a reduction in the stopping power of negative charged particles and an enhanced stopping of positive charged particles, compared to first-order perturbation theory (Bethe's formula). The Coulomb dissociation of ^{17}F has some analogy with the stopping of negative charged particles because the Coulomb fields that are involved in the excitation of the proton state and the electrons in a solid, respectively, are repulsive in both cases. Thus we find a reduction in the Coulomb dissociation probabilities compared to the first-order calculation.

We have extracted the Barkas effect from our dynamical calculations by repeating them for a negative charged target. Denoting the two sets of Coulomb dissociation probabilities by $P_{\text{CD}}^{(\pm)}$, with positive and negative target charge, respectively, we define the Barkas factor: $B = [P^{(+)} - P^{(-)}]/[P^{(+)} + P^{(-)}]$, and also the ratio of the average compared to first-order perturbation theory (P_{pth}): $A = [P^{(+)} + P^{(-)}]/[2P_{\text{pth}}]$. The two factors

we obtain for a ^{58}Ni target are shown in Fig. V-17 as functions of the impact parameter b , at beam energies $E_{\text{beam}} = 10$ (solid points), 20 (squares), and 40 MeV/u (diamonds).

The A-factors, shown in the left panel, approach one at large impact parameters and higher beam energies. At small impact parameters, the A-factors are strongly reduced compared to one. The main reason is that the first-order calculation was performed under the assumption that the projectile and target densities do not overlap during the collision. The reduction is even more dramatic in the Coulomb dissociation of the $1/2^+$ excited state in ^{17}F , where it persists out to $b = 30$ fm.

The solid curves for the B-factors (right panel) show the parameterization

$$B = \frac{CZe^2}{E_{\text{beam}} \sqrt{b^2 + a^2}},$$

where $C = -1.68$ and $a = 20$ fm have been adjusted to fit the extracted values. The Z-dependence of this parameterization is consistent with the lowest-order Barkas effect. It was tested by repeating the dynamical calculations for a Pb target and good agreement was found at 40 MeV/u. However, the fit became poor at 10 MeV/u due to the onset of corrections of even higher order than Z^3 .

We also investigated the influence of Coulomb-nuclear interference. It appears from our results that the transition from Coulomb- to nuclear-dominated breakup occurs quite abruptly, with a surprisingly small effect of the Coulomb-nuclear interference at larger impact parameters. This work has been accepted for publication.²

*Institute for Nuclear Theory, Univ. of Washington

¹W. H. Barkas, N. J. Dyer, and H. H. Heckman, Phys. Rev. Lett. **11**, 26 (1963)

²H. Esbensen and G. F. Bertsch, Nucl. Phys. A (in press)

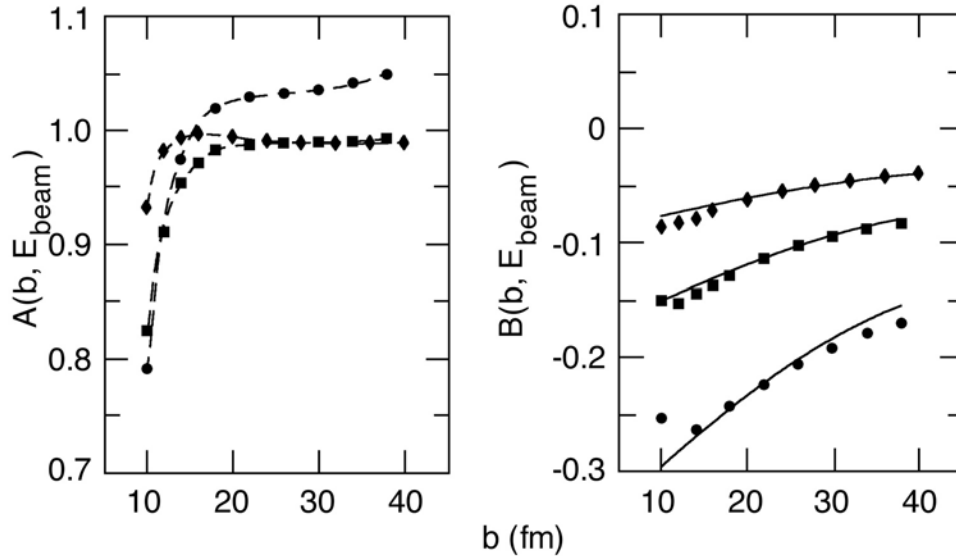


Fig. V-17. The A - and B -factors defined in the text have been extracted from dynamical Coulomb dissociation of ^{17}F on a ^{58}Ni target at 10 MeV/u (solid points), 20 (squares), and 40 MeV/u (diamonds). They are shown as functions of the impact parameter b . The solid curves show the simple parameterization of the B -factor suggested in the text. The dashed curves connect the A -values at fixed beam energy.

c.5. Many Body Wave Functions (R. R. Chasman)

We are continuing the development of a program for calculating many-body variational wave functions that puts pairing and particle-hole two-body interactions on an equal footing. The variational parameters are calculated with an iteration procedure. The complexity of the wave functions depends only on the number of levels included in the valence space, but does not depend on the number of nucleons in the system. In these wave functions, we conserve particle number and parity strictly; projecting states of good particle number and parity before carrying out the variational calculations. We have added a cranking term to the many-body Hamiltonian and modified the projection procedure to get states of good signature before variation. This allows us to study pairing collapse as a function of angular momentum. We have also extended the program to calculate the spectroscopic factors involved in proton decay. This is useful for studies of nuclides near the proton drip line.

By using residual interaction strengths (*e.g.*, the quadrupole interaction strength or pairing interaction strength) as generator coordinates, one gets many different wave functions; each having a different expectation value for the relevant interaction mode. Such wave functions are particularly useful when one is dealing with a situation in which a configuration interaction treatment is needed. This is particularly true for an adequate treatment of pairing at high spin as well

as for instances in which the single-particle level density is low. Because the same basis states are used in the construction of all of the many-body wave functions, it is possible to easily calculate overlaps and interaction matrix elements for the many-body wave functions obtained from different values of the generator coordinates (which are not in general orthogonal). The valence space can contain a very large number of single-particle basis states, when there are constants of motion that can be used to break the levels up into sub-groups.

Wave functions of this sort become more realistic as the size of each of the sub-groups is increased. To increase this size, we have parallelized our code to run on the SP computer system. We have also modified our codes to handle arbitrary two-body matrix elements. This latter feature allows us to include Coulomb matrix elements easily. Together with J. L. Egido and L. M. Robledo, we have developed subroutines for calculating Gogny interaction matrix elements and Coulomb matrix elements for this many-body code.

In the past year, our major effort has been to extend our many-body code to include neutron-proton pairing interactions, in both the $T = 0$ and $T = 1$ modes. Such pairing is expected to be important for nuclides near the $N = Z$ line.

c.6. Neutron-Proton Pairing (R. R. Chasman)

In most nuclides, the fermi levels of protons and neutrons are sufficiently different that $T = 1$ n-n and p-p pairing are the dominant particle-particle residual interaction modes. In nuclides with roughly equal numbers of protons and neutrons, one expects that the $T = 1$ n-p interaction will also play an important role, as well as the $T = 0$ n-p interaction. In order to get a good handle on these effects, it is necessary to go beyond the quasi-particle approximation. To get a clear signal of n-p pairing, it is necessary to study not only nuclei along the $N = Z$ line, but also the nuclides in the vicinity of the $N = Z$ line. With the advent of a rare isotope accelerator, we anticipate that considerable spectroscopic information will become available on nuclides near the $N = Z$ line.

We have extended¹ our many-body method to include n-p pairing, with full projection of neutron and proton particle number before doing a variational calculation. We have also found that there is a new quantum number that holds exactly for collective states; *i.e.* those states in which no levels are blocked. This new

quantum number (Q) is the number parity of the $T = 0$ and $T = 1$ n-p pairs. Fixing the number parity of one n-p mode fixes the other, when the number of neutrons and protons is fixed. This number parity is closely related to the isospin quantum number. The collective states are the ground states for $N = Z$ nuclides. We project Q - before doing a variational calculation. By doing calculations that conserve Q , we find a remarkable multiplicity of degenerate levels in odd-odd nuclides, with $N = Z \pm 2m$. Such multiplets are at or near ground for $m = 1$ or 2 . The form of our variational wave function includes an explicit amplitude for 'alpha like' correlations in each level as well as the usual amplitudes for n-n, p-p and n-p pairs. In Fig. V-18, we compare the amplitude for one of the two particle modes [$U(1,k)$] in a given level and four particles in that level [$U(5,k)$] as a function of the level number, in a model $N = Z$ even-even nucleus (^{60}EE). Level 15 is the fermi level. The insert in the figure shows the level degeneracies in odd-odd nuclides (^{62}OO , ^{64}OO , ^{66}OO) near the $N = Z$ line.

¹R. R. Chasman, Phys. Lett. B **524**, 81 (2002)

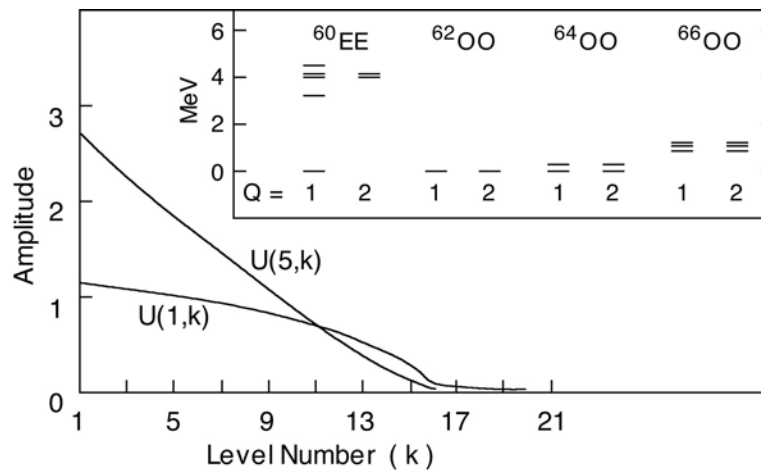


Fig. V-18. Ground state amplitudes in ^{60}EE . Low lying states in ^{60}EE , ^{62}OO , ^{64}OO and ^{66}OO are shown in the insert, illustrating the extra degeneracies arising from multiple pairing modes.

c.7. Very Extended Shapes in Nuclei (R.R. Chasman)

In the past few years, large computer resources have become available on the massively parallel processor IBM SP system at Argonne, in addition to the resources provided by NERSC. We have parallelized the code used to calculate single-particle spectra to exploit the SP system and have devoted a large part of our efforts to calculating energy surfaces in a four dimensional shape space that includes reflection asymmetric shapes. We study the nuclear energy surfaces as a function of mass, charge, shape and angular momentum, using the Strutinsky method. In this approach, one makes quantum corrections to a smooth liquid drop behavior using the calculated single particle energy levels. In earlier studies we found that it is often not sufficient to use only quadrupole and hexadecapole deformations to describe very extended reflection symmetric nuclear shapes. When we added a necking degree of freedom we found previously unknown minima. These minima are characterized by very extended capsule shaped nuclei with axis ratios of 2.2:1 in the $A = 180$ mass region. We have now added octupole deformation to this shape space. The inclusion of these two degrees of freedom to our shape space substantially increases our ability to describe nuclear shapes compared to a typical shape space consisting only of quadrupole and hexadecapole deformations. As parity is no longer a good quantum number when octupole deformation is included, the size of the matrices that we diagonalize is doubled. In a typical calculation, we diagonalize matrices that are 600×600 . Several thousand such diagonalizations are needed to determine energy surfaces.

There remains a need to test calculated fission barriers and to generally understand nuclear properties at the

¹R. R. Chasman, Workshop on the Science for an Advanced ISOL Facility, Columbus, OH, Jul. 31-Aug. 1, 1997, p. 69

²R. R. Chasman, Phys. Rev. C **64**, 024311 (2001)

c.8. E1 Transition Probabilities Between Superdeformed States (R. R. Chasman)

Recent experimental studies have found E1 transition probabilities between superdeformed states on the order of 1 milli-Weiskopf unit (mWu), and this observation has given rise to speculation that such transitions are evidence for octupole vibrational states in superdeformed minima. It was assumed that E1 transition probabilities of this magnitude are too large to be due to single-particle transitions.

highest spins. Using the four-dimensional deformation space described above, we have analyzed the high spin energy surfaces of the $N = 86$ isotones going from Sn ($Z=50$) to Dy ($Z=66$). There is a high spin superdeformed minimum in all of these nuclides ($\sim 1.85:1$ axis ratio) that becomes yrast at high spin. These shapes are well known experimentally in the Dy region.

We find that as the proton number decreases from $Z = 66$ to $Z = 50$, the fission barrier increases by roughly 10 MeV at a given angular momentum. The superdeformed minimum associated with $N = 86$ is present for both Sn and Dy. This result suggests that we can extend the study of nuclear properties at extreme deformations to a new regime of angular momenta, with the availability of radioactive nuclear beam facilities. A preliminary version of this work has been published.¹

We have extended our high spin Strutinsky calculations² to nuclei in the $A = 100$ mass region. Many of the very extended minima that we find will be accessible with projectiles produced at an exotic beam facility. However, our calculations show very extended minima in nuclides in the vicinity of ^{108}Cd that are accessible using existing facilities. Recent experiments, inspired by these calculations, show a superdeformed rotational band in ^{108}Cd . Our results for the $A = 100$ mass region have recently been published.

We are analyzing nuclides in the region $70 < A < 100$, searching for nuclides with well-deformed shapes.

We have calculated single-particle E1 transition rates for low-lying orbitals in the $A = 190$ and $A = 150$ regions of superdeformation. We find that there are indeed single-particle E1 transition matrix elements, for neutron orbitals near $N = 110$, that are sufficiently large to account for the observed transitions. Additionally, we have found other cases ($Z < 80$) in which equally large E1 transition probabilities between superdeformed levels might be found.

c.9. Single Particle States in the Heaviest Elements (I. Ahmad and R. R. Chasman)

The search for superheavy elements has been a major theme of nuclear structure research for the past forty years. Theoretical predictions of the stability of superheavy elements depend crucially on the single-particle energy level spacings in the vicinity of 114 protons and 184 neutrons. Our approach^{1,2,3,4} is to learn as much as possible about these levels from spectroscopic studies of nuclides in the $A = 250$ region. This is possible because there are members of the relevant spherical multiplets that drop rapidly in energy with increasing deformation, and are fairly close to the ground state in the strongly deformed nuclides near $A =$

250. Our analysis⁴ of excited states in ^{251}Cf populated in the alpha decay of ^{255}Fm allows us to characterize several single-particle and vibrational states beyond the $N = 162$ deformed gap. Another effect of the $N = 162$ gap would be on alpha decay properties of nuclides having 163 neutrons. Using the potential parameters derived from our studies, we find that there are two favored alpha decays that might be observed in $^{273}\text{110}$, having an energy difference of 1.7 MeV. The lower energy transition is the favored alpha decay from the ground state of $^{273}\text{110}$ and the higher energy one is the favored transition to the ground state of ^{269}Hs .

¹I. Ahmad *et al.*, Nucl. Phys. **646**, 175 (1999)

²R. R. Chasman and I. Ahmad, Phys. Lett. **B392**, 255 (1997)

³I. Ahmad, R. R. Chasman, and P.R. Fields, Phys. Rev. C **61**, 044301 (2000)

⁴I. Ahmad *et al.*, Phys. Rev. C **62**, 064302 (2000)

c.10. Studies of Nuclear Energy Surfaces (R. R. Chasman, J. L. Egido,* and L. M. Robledo*)

This collaborative research program^{1,2,3} is focused on the study of nuclear energy surfaces, with an emphasis on very deformed shapes using several complementary methods: 1) the Strutinsky method, 2) Hartree-Fock-Bogoliubov (HFB) calculations using the Gogny interaction, and 3) many-body variational wave functions that we have described above. Our strategy is to identify phenomena and nuclides of interest using the Strutinsky method and to study the most interesting cases with the HFB and many-body (MB) approaches. The two latter approaches include many-body effects and describe these features more accurately.

The great advantage of the Strutinsky method is that one can study the energy surfaces of many nuclides (~ 300) with a single set of calculations. Although the HFB and many-body calculations MB calculations are quite time consuming relative to the Strutinsky calculations, they have many advantages. For the studies of the Pb isotopes described below, they have the advantage that configuration interaction effects can easily be incorporated into the calculations. In this way, we deal directly with the issue of insuring the orthogonality of states that have the same spins and parities.

The neutron deficient nuclides ($N < 110$) in the Pb region have states that are characterized by three distinct shapes; spherical, prolate and oblate. In the oblate and prolate minima, there are low-lying single particle states derived from spherical states on both sides of the $Z = 82$ single particle gap. Although this gap is roughly 4 MeV, there are states within a few hundred keV of ground in the neutron deficient Tl($Z=81$) and Bi($Z=83$) isotopes that would be at ~ 4 MeV excitation, in the simplest single particle picture. Our approach is to determine the nuclear wave function as a function of quadrupole moment, letting other deformation modes (*e.g.* P4 and P6) vary freely. Using both the HFB and MB methods, we find³ three low-lying states in the isotopes $^{190,188,186,184}\text{Pb}$. There is remarkably good agreement between the HFB and MB results. In both the HFB and MB calculations, the three separate low-energy 0^+ states persist after the configuration interaction is taken into account. These are the first calculations that give a 0^+ oblate state in ^{186}Pb , in agreement with the experimental observation of two 0^+ excited states in this nuclide. Both calculations also predict an as yet unobserved 0^+ state in ^{184}Pb . Investigations are under way to search for this state.

*Universidad Autonoma de Madrid

¹R. R. Chasman and L. M. Robledo, Phys. Lett. **B351**, 18 (1995)

²J. L. Egido, L. M. Robledo, and R. R. Chasman, Phys. Lett. **B393**, 13 (1997)

³R. R. Chasman, J. L. Egido and L. M. Robledo, Phys. Lett. **B513**, 513 (2001)

c.11. Probing the Gateway to Superheavy Nuclei in Cranked Relativistic Hartree-Bogoliubov Theory (A. V. Afanasjev, T. L. Khoo, I. Ahmad, S. Frauendorf,* and G. A. Lalazissis†)

The cranked relativistic Hartree-Bogoliubov theory¹ (CRHB), including approximate particle number projection through the Lipkin-Nogami method and the Gogny force in the particle-particle pairing channel, has been applied for a systematic study of the nuclei around ²⁵⁴No.² These are the heaviest elements with a large body of spectroscopic data for testing the reliability of mean-field theory predictions for superheavy nuclei. The deformation, rotational response, pair correlations, quasiparticle spectra, nucleon separation energies and shell structure of these nuclei have been extensively studied with different RMF forces.

While the deformation properties are well reproduced, the calculations reveal that an accurate description of other observables requires better effective forces both in the particle-hole and particle-particle channels. The calculated moments of inertia show only small sensitivity to the RMF force and thus to the details of the single-particle structure. In contrast to previous studies, where the moments of inertia in lighter systems^{1,3} are well reproduced, good agreement in the heaviest nuclei can be obtained only with a decrease ($\approx 12\%$) of the strength of the D1S Gogny force in the pairing channel.

The CRHB theory has been extended for a detailed description of quasi-particle states in odd and odd-odd nuclei. For the first time, the blocking procedure in such nuclei has been performed fully self-consistently, with effects of the breaking of time-reversal symmetry (nuclear magnetism) taken into account. Analysis of quasi-particle spectra in odd ^{249,251}Cf and ²⁴⁹Bk nuclei with the NL1 and NL3 forces (see Fig. V-19 for an example) suggests that the energies of most of the spherical orbitals, from which active deformed states of

these nuclei emerge, are described with an accuracy better than 0.5 MeV. However, for a few subshells the discrepancies reach 1.0 MeV. Considering that the RMF forces were fitted only to bulk properties of spherical nuclei without considering single-particle energies, this level of agreement is impressive. However, in very heavy systems, where the level density is high, the accuracy is not sufficient for reliable predictions of the location of deformed shell gaps, which are small (≈ 1 MeV).

The results of the present investigation have a number of implications for the study of superheavy nuclei. The NL-SH and NL-RA1 forces do not provide satisfactory descriptions of the single-particle energies: the deviation between experiment and theory in the $A \sim 250$ mass region reach 2 MeV for some spherical subshells. Thus their application to superheavy nuclei is not recommended. The extrapolation of the results for quasiparticle states obtained in the $A \sim 250$ mass region suggest that the NL1, NL3 and NL-Z forces provide reasonable descriptions of most of the states in the vicinity of the $Z = 120$ and $N = 172$ spherical shell gaps. These are magic gaps in most parameterizations of the RMF theory. However, it is not possible to estimate the accuracy of the description of some low- j states, such as $\nu 3d_{3/2}$, $\nu 4s_{1/2}$ and $\pi 3p_{3/2}$, $\pi 3p_{1/2}$, which are located near these gaps by studying lighter deformed nuclei. Thus the particle numbers corresponding to magic gaps in superheavy nuclei still remain an open question. In addition, the study of a number of effects in superheavy nuclei, such as pairing and the importance of self-consistency, is in progress. A paper on this work is being prepared.

*University of Notre Dame, †Aristotle University, Thessaloniki, Greece

¹A. V. Afanasjev, P. Ring and J. König, Nucl. Phys. A **676**, 196 (2000)

²P. Reiter *et al.*, Phys. Rev. Lett. **82**, 509 (1999)

³A. V. Afanasjev *et al.*, Phys. Rev. C **62**, 054306 (2000)

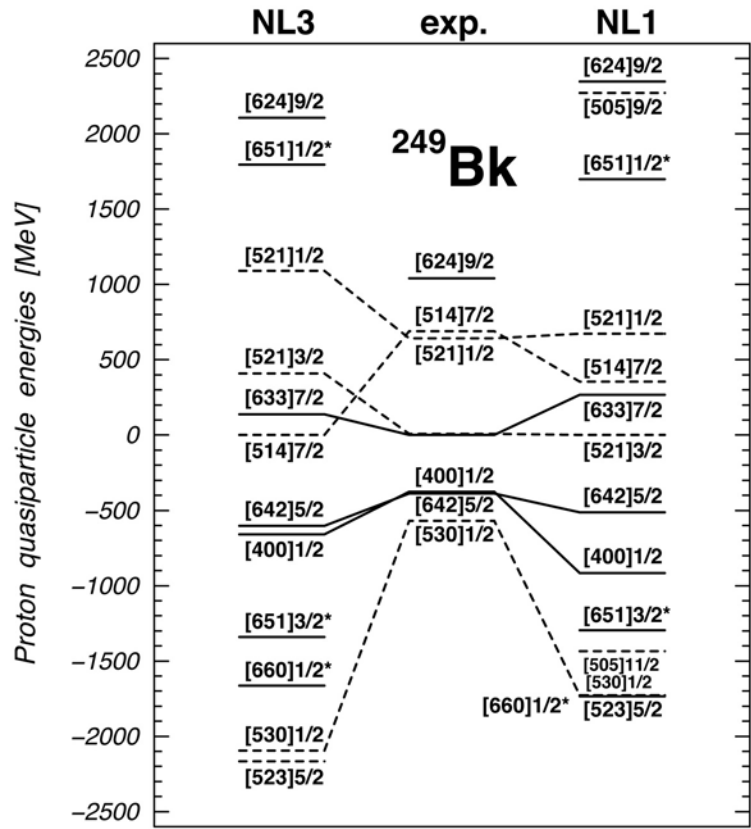


Fig. V-19. Experimental and theoretical quasiparticle energies of neutron states in ^{249}Bk . Positive and negative energies are used for particle and hole states, respectively. Solid and dashed lines are used for positive and negative parity states, respectively. The symbols 'NL3' and 'NL1' indicate the RMF force used in calculations.

D. ATOMIC THEORY AND FUNDAMENTAL QUANTUM MECHANICS

In addition to research on hadronic and nuclear physics, we also conduct research in atomic physics, neutron physics, and quantum computing.

Recent work in atomic physics includes the studies of interactions of high-energy photons with matter, in support of experiments performed at Argonne's Advanced Photon Source (APS). Theoretical studies are being conducted on the physics of the Photoeffect and Compton scattering by bound electrons, focusing on topics selected in view of basic importance, timeliness, and potential in applications. We also produced a review on "Electron collision cross sections of atoms" for inclusion in a volume on "Atomic Collisions" in the Landolt-Börnstein Numerical Data and Functional Relationships series.

Recent theoretical work in support of a new experiment to measure the neutron electric-dipole moment has been focusing on experimental challenges resulting from the time spent by the neutron inside a silicon crystal in the Bragg reflection process. Additionally, a new investigation of the basis of the spin-statistics theorem in nonrelativistic quantum mechanics, following the geometrical approach of Berry and Robbins, has shown that spin-zero particles must obey boson statistics without the usual assumptions of relativistic local field theory.

Work in areas related to quantum computing continued by extending, to integers and rational numbers, earlier work on the conditions that states of physical systems must satisfy in order to represent natural numbers. Emphasis was placed on the condition of efficient physical implementation of the basic arithmetic operations on the states whose properties are given by the appropriate axioms for the different types of numbers. The relation between efficient implementation and the product state representation of numbers was also studied.

Work was also begun on a framework for developing a coherent theory of mathematics and physics together. This work is partly based on the universal applicability of quantum mechanics, or a suitable generalization, and earlier work on an example of the use of mathematical logical concepts in quantum mechanics. In essence the idea is to integrate mathematical logical concepts with quantum mechanics. A basic and possibly defining requirement for a coherent theory was described and discussed, along with other aspects.

d.1. Interactions of Photons with Matter (M. Inokuti and D. Y. Smith*)

In support of experiments in atomic and condensed-matter physics with the use of synchrotron radiation, theoretical studies are being conducted on the physics of photo-absorption and Compton scattering, focusing on topics selected in view of basic importance, timeliness, and potential applications.

One theme of long-term studies has been the use of dispersion relations and sum rules for indices of response of matter over the entire range of photon

energies. A comprehensive analysis of optical data on silicon¹ is in progress, and a new expression for the refractive index in a region of near transparency² is applied to graphite, silicon, and germanium.

A sum rule for the absorption strength originally due to Vinti³ is applied to color centers in alkali halides to derive the spatial extent of the electronic structure of the color centers.⁴

*University of Vermont

¹D. Y. Smith, M. Inokuti, and W. Karsten, *Physics Essays* **13**, 465 (2000)

²D. Y. Smith and M. Inokuti, *J. Phys. C: Condensed Matter* **13**, 3883 (2001)

³J. P. Vinti, *Phys. Rev.* **41**, 432 (1932)

⁴D. Y. Smith and M. Inokuti, *Radiat. Effects Defects Solids* **155**, 43 (2001)

d.2. Interactions of Charged Particles with Matter (M. Inokuti)

Stopping power, the total yield of ionization, and its statistical fluctuations are examples of quantities describing the penetration of charged particles through matter and are important to applications such as the detection of particles and the analysis of their charges and kinetic energies. The understanding of those quantities in terms of individual collisions and associated cross sections remains a major challenge and is the goal of our continuing effort. A review¹ of cross sections for electron collision with atoms has been published.

Unpublished materials left by R. L. Platzman (1918-

73), a pioneer of radiation physics and chemistry and a former Argonne staff member (1958-65), are studied² and being prepared for an archive in the Joseph Regenstein Library of the University of Chicago.

An essay³ on the role of physics in radiation sciences was written in commemoration of the 50th anniversary of the Radiation Research Society. Extensive work for the International Commission on Radiation Units and Measurements (ICRU) continues on the editing of its reports and on physical data such as stopping powers and various interaction cross sections.

¹M. Inokuti, in *Landolt-Börnstein Numerical Data and Functional Relationships in Science and Technology*, Vol. 1/17, ed. Y. Itikawa (Springer-Verlag, Berlin 2000), pp. 2.1-2.34

²M. Inokuti, *Radiat. Phys. Chem.* **60**, 283 (2000)

³M. Inokuti and S. M. Seltzer, *Radiat. Res.*, in press

d.3. On the Connection Between Spin and Statistics in Quantum Mechanics (Murray Peshkin)

The connection between spin and statistics has traditionally been thought to depend upon the assumptions of local relativistic quantum field theory or at least upon the existence of antiparticles. However, Michael Berry and Jonathan Robbins recently identified it as a geometrical feature of nonrelativistic quantum mechanics. The key physical feature of their geometrical approach is taking seriously the indistinguishability of identical particles. Thus for two spinless particles, the dynamical variables are unordered coordinate pairs $\{\mathbf{r}_1, \mathbf{r}_2\}$, and similarly for the momenta. For particles with spin, the spin variables

must also be included. That $\{\mathbf{r}_1, \mathbf{r}_2\}$ is the same point in the configuration space as $\{\mathbf{r}_2, \mathbf{r}_1\}$ changes the topology from that in the case of distinguishable particles, and that has consequences for quantum mechanics. Berry and Robbins showed under reasonable mathematical assumptions that this leads to integer-spin particles having symmetric statistics and half-integer-spin particles having antisymmetric statistics. They also found other mathematical assumptions that could violate that result, but they are in some way weird and possibly do not apply to real physics.

I have implemented the Berry-Robbins approach in a somewhat different way in the simplest case, that of two spinless particles, and found that I can unambiguously exclude antisymmetric statistics in that case. I follow Berry and Robbins in assuming that $\{\mathbf{r}_1, \mathbf{r}_2\} = \{\mathbf{r}_2, \mathbf{r}_1\}$ and in requiring that the wave function must be continuous in the particles' coordinates because of the second derivative in the Schrödinger equation. Those conditions are sufficient to eliminate odd values of the angular momentum of the relative

motion of the two particles. The present approach has, in addition to its apparently stronger conclusion, the advantage that it illuminates directly the connection between the topology and orbital angular momentum in a very elementary way. In contrast to the Berry-Robbins work, it has the disadvantage that it does not directly demonstrate the relation between the statistics and the geometrical Berry phase. Whether my approach adds anything to Berry and Robbins in the case of spinning particles is not yet clear.

d.4. A Virial Theorem for Nuclear Deformation (Murray Peshkin)

Calculations of nuclear deformation frequently start by minimizing the ground-state energy of the nucleus with respect to a "volume preserving" deformation of some collective potential V . Specifically, one introduces a deformed potential $V_{abc}(x,y,z) = V(ax,by,cz)$ with the constraint that $abc = 1$ and minimizes the ground-state energy to determine the deformation parameters a,b,c . That long-used prescription has always been mysterious because no variation principle supports it and no reasonable nuclear structure model suggests it in any direct way. The nearest thing to a physical justification was given many years ago by Bohr and Mottelson, who observed that for a shell model with harmonic oscillator potential and no inter-particle or spin-orbit interactions, the minimum-energy assumption leads to a state whose kinetic energy tensor in the rotating system has spherical symmetry, *i.e.* $\langle \sum_n p_i^n p_j^n \rangle = T\delta_{ij}$, where n

labels the particles and i,j label the three axes. That condition suggests something akin to irrotational flow in the rotating system, which seems not unreasonable for the ground state.

I have shown that a simple virial theorem relates the minimum-energy condition to the spherical kinetic energy tensor for any shell-model potential, not just for the harmonic oscillator. Moreover, that relation remains valid in the presence of residual interactions $V_{ij}(\mathbf{r}_i, \mathbf{r}_j)$ between the nucleons, but only if the residual interactions are deformed in the same way as the collective potential. It is also valid in the presence of momentum-dependent potentials such as the spin-orbit interaction, but only if the spatial variables are scaled as in the collective potential and the momenta are scaled inversely so that $p_x \rightarrow p_x/a$, and similarly for p_y and p_z .

d.5. The Representation of Numbers in Quantum Mechanics (P. Benioff)

Earlier work on modular arithmetic of k -ary representations of length L of the natural numbers in quantum mechanics was extended to k -ary representations of all natural numbers, and to integers and rational numbers¹. Since the length L is indeterminate, representations of states and operators using creation and annihilation operators for bosons and fermions are defined. Emphasis is on definitions and properties of operators corresponding to the basic operations whose properties are given by the axioms for each type of number. The importance of the requirement of efficient implementability for physical models of the axioms is emphasized. This condition

requires the use of successor operations for each value of j , corresponding to addition of k^{j-1} if $j > 0$ and (for rational numbers) k^j if $j < 0$. It follows from the efficient implementability of these successors, which are used in all computers, that implementation of the addition and multiplication operators, which are defined in terms of iterations of the successors, should be efficient. Implementation of definitions of the addition and multiplication operators based on the successor for $j = 1$ only, which is the only successor defined in the usual axioms of arithmetic, are not efficient.

¹Paul Benioff, to appear in special issue of the journal *Algorithmica*

d.6. Efficient Implementation and the Product State Representation of Numbers (P. Benioff)

Work on the relation between the requirement of efficient implementability and the product state representation of numbers was carried out and completed¹. In this work numbers are defined to be any collection of objects with associated operations and properties that satisfy the axioms of number theory or arithmetic. Product state representations are representations by strings of k digits or k dimensional qubits in quantum mechanics for any $k \geq 2$. Efficient implementability (EI), which is a basic requirement on any physical model of the numbers, means that the basic arithmetic operations, which are those described by the axioms of arithmetic (successor, plus, and times), are physically implementable and the space-time and thermodynamic resources needed to

carry out the implementations are polynomial in the logarithm of the range of numbers considered (*i.e.*, polynomial in $\log N$ if the numbers 0 to N are represented.). Different models of numbers are described, including extremely entangled representations, to show that both EI and the product state representation are not required by the axioms. Nor do they imply the properties stated by the axioms. The relation between EI and the product state representation is examined. It is seen that the condition of a product state representation does not imply EI. The converse implication, EI does not imply a product state representation, seems reasonable, but it is an open question.

¹Paul Benioff, Phys. Rev. A **64**, 052310 (2001)

d.7. Towards a Coherent Theory of Mathematics and Physics (P. Benioff)

Work was begun on describing a framework for developing a coherent theory of mathematics and physics together¹. This work is partly motivated by the observation that in spite of a close connection, physics and mathematics as presently developed do not take account of any close connection at a foundational level. Also any universally applicable physical theory, by including in its domain observers using mathematics to validate the theory, must describe in some sense its own validation. The main and possibly defining characteristic of such a theory is discussed: the theory must be valid and sufficiently complete and it must describe its own validity and sufficient completeness to the maximum extent possible. Definitions of validity and completeness are based on those used in mathematical logic. The requirement of universal applicability for the theory at least means that it must include the description of intelligent systems and their

dynamics in validating a theory. The close connection between such a theory and the universe is supported by the observation that the reality status of very small or very large cosmological physical systems is more indirect in that it depends on more intervening layers of theory and experiment than for moderate sized systems. This suggests that the basic properties of the physical universe are entwined with and emerge from such a theory. In this case the basic properties may not have an *a priori* status independent of a theoretical description of them. Other aspects of a coherent theory include the observation that language is physical. All symbols and words of any language necessarily have physical representations as states of physical systems that are in the domain of a coherent theory. This is an important property not enjoyed by any purely mathematical theory and may have some important consequences.

¹Presented at 1st Brazilian Symposium on the Philosophy of Nature, Rio de Janeiro, Aug. 24-27, 2001, to appear in symposium proceedings

d.8. Cyclic Quantum Gate Networks (Paul Benioff and Peter Cabauy*)

We are also studying properties of very simple examples of cyclic networks of quantum gates. This work is based on the fact that studies so far have been limited to noncyclic networks of quantum gates as these have been shown sufficient to describe quantum computation. Cyclic networks would be quite useful in studies of quantum control and would be an essential component of any mobile quantum system such as a quantum robot.¹

We are theoretically exploring the properties of the simplest nontrivial example, and some extensions thereof, of a cyclic network of two qubits interacting through quantum gates. Quantum gates are two qubit interactions with one qubit functioning as the control system. The states of this qubit determine whether a unitary operation on the other qubit is active or is inactive.

This work will provide the bulk of a Ph.D. thesis that is expected to be completed in the spring of 2002.²

*ANL and University of Michigan

¹Paul Benioff, Phys. Rev. A **58**, 893-904, (1998)

²Peter Cabauy, Ph.D. Thesis, University of Michigan, in preparation

E. OTHER ACTIVITIES

e.1. Theory Workshop on Rare Isotope Physics (R. Chasman and H. Esbensen)

We organized a Theory Institute, which was held June 25-29, 2001, in the Physics Division. The emphasis of the workshop was the development of numerical techniques and new theoretical approaches that can be used in nuclear structure studies of relevance to RIA. Among the subjects discussed were proton emission

from nuclei beyond the proton drip-line, the structure of quasi-bound states, halo nuclei, pairing near the neutron drip-line, and proton-neutron pairing in $N=Z$ nuclei. The workshop was attended by some 20 theorists from outside the division, as well as by theorists and experimentalists from within the division.

e.2. 14th Annual Midwest Nuclear Theory Get-Together (C. D. Roberts)

The Theory Group hosted the Fourteenth Annual Midwest Nuclear Theory Get-Together on October 5th and 6th, 2001. Nuclear theorists from a number of Midwest universities get together every fall to find out what different people and groups in the region are working on. The organizational duties rotate among the participants, but Argonne has become the regular meeting place by virtue of its facilities and central location. The organizer for 2001 was Pawel Danielewicz of Michigan State University. The meeting provides a good chance for students to broaden their horizons and get some practical speaking experience in a friendly atmosphere. The format is very

informal, with an agenda of talks being volunteered at the beginning of the meeting. This year we set a record for the largest attendance ever: 37 faculty, postdocs and students from thirteen different universities and colleges in Illinois, Indiana, Iowa, Michigan, Missouri, and Ohio, along with the Argonne staff. Some 30 presentations were made over Friday afternoon and Saturday morning. Topics included relativistic quantum mechanics, gauge and effective field theories, QCD, quantum Monte Carlo methods, nuclear pairing, no-core shell model, relativistic heavy-ion collisions, and neutron matter. A good time was had by all.

OTHER EDUCATIONAL ACTIVITIES IN THE PHYSICS DIVISION

a. Enhancement of Minority Involvement in DOE Nuclear Physics Programs (B. Zeidman)

The ANL Physics Division, through its Minority Program, continues to attract highly qualified students who apply for participation in the programs of the Physics Division and other ANL divisions. The program is directed toward identification of physics departments with relatively strong programs and faculty interested in stimulating their students to pursue research, particularly in summer programs. Several returning, as well as new, minority physics majors participated in the ANL Summer Program during 2001. More than a dozen former participants are currently enrolled in programs leading to doctorates in physics. A Michigan State University student who spent several summers at ATLAS as an undergraduate received a Ph.D. in accelerator physics under J. Nolen's direction. Another former undergraduate student is currently performing his thesis research in the Physics Division and is

expected to receive a Ph.D. from Michigan this semester.

The program is an ongoing effort based upon personal interactions with a substantial number of qualified minority students and faculty. During visits to the Physics Departments of HBCU colleges (Historically Black Colleges and Universities) and other institutions with large minority populations, lectures are presented and there are discussions of activities in physics at ANL and other laboratories, graduate programs, etc. Other activities include attendance at meetings of minority organizations, appointment as Adjunct Professor at Hampton University including supervision of graduate thesis research, and serving on the Advisory Boards of the Centers of Excellence at both Hampton University and Morehouse College.

b. Nuclear Physics Award for Faculty in Undergraduate Institutions (B. Zeidman)

The goal of the 'Faculty Program', is to enhance undergraduate science education through faculty awards for minority and HBCU faculty that will allow them to directly participate in the ANL Physics Division research program and increase the number of undergraduates involved in research. A participant has obtained independent funding for continuing research collaboration with ANL that involves several undergraduate students. Several

minority faculty members and students have been involved in research collaboration with the Physics Division for the past few years and will return this year. In order to maximize the scope of the program, existing educational programs are being utilized to supplement support for some of the participants and more formal collaborative arrangements are being discussed.

c. Scientific Support of SciTech Museum Exhibits and Outreach Programs
(D. Henderson)

SciTech (Science and Technology Interactive Center) is a hands-on science museum located in Aurora, Illinois, near Argonne. With the help of volunteers and institutional support from Argonne, Fermilab, and several technological companies, SciTech has become an acknowledged leader in developing exhibits to teach modern science in a museum context.

D. Henderson of the Physics Division serves voluntarily as an exhibit developer on a regular basis. Several other staff members volunteer from time to time. The Physics Division collaborates with SciTech in developing exhibits for the museum and for use in Argonne's public educational activities. These efforts involve no significant programmatic costs.

STAFF MEMBERS OF THE PHYSICS DIVISION

Listed below are the staff of the Physics Division for the year ending December 31, 2001.
The program headings indicate only the individual's current primary activity.

SCIENTIFIC STAFF

EXPERIMENTAL NUCLEAR PHYSICS STAFF

Regular Staff

- Irshad Ahmad, Ph.D., University of California, 1966
 John Arrington Ph.D., California Institute of Technology, 1998
 Birger B. Back, Ph.D., University of Copenhagen, 1974
 Michael P. Carpenter, Ph.D., University of Tennessee, 1987
 * Cary N. Davids, Ph.D., California Institute of Technology, 1967
 † Stuart J. Freedman, Ph.D., University of California, 1972
 ‡ Donald F. Geesaman, Ph.D., State University of N.Y., Stony Brook, 1976
 § Walter F. Henning, Ph.D., Technical University of Munich, 1968
 Roy J. Holt, Ph.D., Yale University, 1972
 ¶ Harold E. Jackson, Jr., Ph.D., Cornell University, 1959
 || Robert V.F. Janssens, Ph.D. Univ. Catholique de Louvain, Belgium, 1978
 Cheng-lie Jiang, Ph.D. China Institute of Atomic Energy, 1960
 Teng Lek Khoo, Ph.D., McMaster University, 1972
 **Walter Kutschera, Ph.D., University of Graz, Austria, 1965
 Torben Lauritsen, Ph.D., State University of New York, 1990
 †† Christopher J. Lister, Ph.D., University of Liverpool, 1977
 Zheng-tian Lu, Ph.D., University of California, Berkeley, 1994
 Eugene Moore, Ph.D., Florida State University, 1988
 ‡‡ Jerry A. Nolen, Jr., Ph.D., Princeton University, 1965
 Peter N. Ostroumov, Ph.D. Moscow Engineering and Physical Institute, 1982
 Richard C. Pardo, Ph.D., University of Texas, 1976
 David H. Potterveld, Ph.D., Caltech, 1988
 Karl Ernst Rehm, Ph.D., Technical University, Munich, 1973
 Paul Reimer, Ph.D. University of Illinois, 1996
 §§ Guy Savard, Ph.D., McGill University, 1988
 §§ John P. Schiffer, Ph.D., Yale University, 1954
 Dariusz Seweryniak, Ph.D., Uppsala University, 1994
 Kenneth W. Shepard, Ph.D., Stanford University, 1970
 Kenneth Teh, Ph.D., Vanderbilt University, 1988
 Alan H. Wuosmaa, Ph.D., University of Pennsylvania, 1989

-
- * Adjunct Professor, Vanderbilt University.
 † On leave of absence at the University of California, Berkeley.
 ‡ Director of the Physics Division.
 § On leave of absence at GSI, Darmstadt.
 ¶ Associate Director of the Physics Division. Joint appointment with the University of Chicago.
 || Associate Director of the Physics Division. Adjunct Professor, Michigan State University and Adjoint Professor, Vanderbilt University.
 ** On leave of absence at the University of Vienna.
 †† Associate Director of the Physics Division.
 ‡‡ Director of the ATLAS Facility. Adjunct Professor, Michigan State University.
 §§ Joint appointment with the University of Chicago.

Special Appointments

- * R. Russell Betts, Ph.D., University of Pennsylvania, 1972
- Lowell M. Bollinger, Ph.D., Cornell University, 1951
- William J. Childs, Ph.D., University of Michigan, 1956
- Donald S. Gemmell, Ph.D., Australian National University, 1960
- F. Paul Mooring, Ph.D., University of Wisconsin, 1951
- † Michael Paul, Ph.D., Hebrew University of Jerusalem, 1973
- Gilbert J. Perlow, Ph.D., University of Chicago, 1940
- G. Roy Ringo, Ph.D., University of Chicago, 1940
- Ralph E. Segel, Ph.D., Johns Hopkins University, 1955
- George E. Thomas, B.A., Illinois Wesleyan, 1943
- § Ben Zeidman, Ph.D. Washington University, 1957

THEORETICAL NUCLEAR PHYSICS STAFF

Regular Staff

- Richard R. Chasman, Ph.D., University of California, 1959
- Henning Esbensen, Ph.D., University of Aarhus, 1977
- ¶ Tsung-Shung Harry Lee, Ph.D., University of Pittsburgh, 1973
- Steven C. Pieper, Ph.D., University of Illinois, 1970
- Craig D. Roberts, Ph.D., Flinders University of South Australia, 1989
- Robert B. Wiringa, Ph.D., University of Illinois, 1978

Special Appointments

- Paul Benioff, Ph.D., University of California, 1959
- Arnold R. Bodmer, Ph.D., Manchester University, 1953
- Fritz Coester, Ph.D., University of Zurich, 1944
- Mitio Inokuti, Ph.D., University of Tokyo, 1962
- Dieter Kurath, Ph.D., University of Chicago, 1951
- Robert D. Lawson, Ph.D. Stanford University, 1953
- Harry J. Lipkin, Ph.D., Princeton University, 1950
- || Vijay Pandharipande, Ph.D., University of Bombay, 1969
- Murray Peshkin, Ph.D., Cornell University, 1951

-
- * Special Term Appointee from the University of Illinois-Chicago.
 - † Special Term Appointee from the Hebrew University of Jerusalem.
 - § Special Term Appointee. Adjunct Professor, Hampton University.
 - ¶ Adjunct Professor, University of Pittsburgh.
 - || Special Term Appointee from the University of Illinois, Urbana.

TEMPORARY APPOINTMENTS

Postdoctoral Appointees

- * John Arrington (from California Institute of Technology, Pasadena, CA):
Medium-energy physics.
(June 1998--December 2000)
- Joseph A. Caggiano (from Michigan State University, E. Lansing, MI):
Heavy-ion research at ATLAS.
(March 1999--June 2001)
- Philippe Collon (from University of Vienna, Austria):
Heavy-ion research at ATLAS.
(November 1999—June 2001)
- Frank Dohrmann (from Hamburg University, Germany):
Medium-energy physics.
(January 2000—December 2001)
- Nigel George (from Brookhaven National Laboratory, Upton, NY):
Medium-energy physics.
(May 1999—September 2001)
- Kawtar Hafidi (from CEN, Saclay, France):
Medium-energy physics.
(November 1999-)
- Martin Hecht (from University of Melbourne, Australia):
Theoretical studies.
(January 2000—December 2001)
- † Andreas Heinz (from GSI, Darmstadt, Germany):
Heavy-ion research at ATLAS.
(February 1999-)
- David Jenkins (University of York, UK):
Heavy-ion research at ATLAS.
(January 2000--)
- Michael Kelly (from University of Washington, Seattle, WA):
Heavy-ion research at ATLAS.
(June 1999-)
- Filipe G. Kondev (from Australian National University, Canberra, Australia):
Heavy-ion research at ATLAS.
(February 1999—February 2001)

* Joined regular staff in January 2001

† Enrico Fermi Scholar

Yimin Li (from Peking University, China):
Medium-energy physics.
(February 1999--)

Bogdan Mihaila (from University of New Hampshire, Durham, NH):
Theoretical studies.
(October 2000--)

Douglas Moehs (from Texas A&M University, College Station, TX):
ATLAS operations and development.
(August 1998—May 2001)

Ian Moore (Shuster Laboratory, UK):
Medium-energy physics.
(November 2001--)

Gopal Mukherjee (from University of Massachusetts, Lowell, MA):
Heavy-ion research at ATLAS.
(October 2001--)

Brahim Mustapha (from University of Paris, France):
ATLAS operations and development.
(May 2000--)

Nikolai Vinogradov (from Moscow Engineering Physical Institute, Russia):
ATLAS operation and development.
(November 2001--)

Krishni Wijesooria (from Jefferson Laboratory, Newport News, VA):
Medium-energy physics.
(October 2000--)

TECHNICAL AND ENGINEERING STAFF
(and areas of activity)

Kevin G. Bailey (B.S. University of Nebraska, 1989).
Technical assistance, medium-energy physics.

* Peter J. Billquist
ECR heavy-ion source, ATLAS operation.

John M. Bogaty (A.A.S. DeVry, 1961).
Electrical systems, ATLAS operation and development.

Benny E. Clift (A.S.E.E., DeVry, 1959).
Electrical systems, ATLAS operation and development.

† Joseph Falout (B.S.M.E. University of Illinois, 1970).
Experimental equipment design.

Joel Fuerst (MSME, Northwestern University, 1990).
Cryogenic development at ATLAS.

John P. Greene (M.S. DePaul University, 1982).
Target preparation.

† Ray E. Harden (A.A.S. Milwaukee School of Engineering, 1957).
ATLAS operator

† Dale J. Henderson (B.S. Elmhurst College, 1951).
Detector development, technical assistance, heavy-ion physics.

James M. Joswick (A.A.S. Milwaukee School of Engineering, 1964).
ATLAS experimental equipment maintenance, technical assistance, heavy-ion physics.

Mark Kedzie
ATLAS experimental equipment development.

† Raymond B. Kickert
ATLAS experimental equipment maintenance, technical assistance, heavy-ion physics.

† Paul Markovich (B.S. Purdue University, 1972).
Surface chemistry, ATLAS development and operation.

Thomas P. Mullen (B.S. Marquette University, 1966).
Division ESH/QA engineer.

Floyd Munson, Jr. (A.A.S. DeVry, 1966, B.S. Lewis University, 1993).
Control system for ATLAS.

Bruce G. Nardi (A.A.S. Morton Jr. College, 1967; A.A.S. DeVry, 1969).
Electronics design and maintenance.

Tom O'Connor (M.S. DePaul University, 1995).
Technical assistance, medium-energy physics.

* In charge of Dynamitron operations.

† Special Term Appointee.

Tad Pennington (M.S. University of Missouri, 1989; M.S. University of Alabama, 1998)

Detector development, technical assistance, heavy-ion physics.

Deborah Quock (M.S. Rice University, 1985)

Technical assistance, ATLAS control system.

Sergey Sharamentov (MS, Moscow Engineering Physical Institute, 1976).

Electrical systems, ATLAS operation and development.

James R. Specht (A.A.S. DeVry, 1964).

Cryogenics engineer. ATLAS development and operation.

Philip Strickhorn (B.S. DeVry, 1990).

Electrical and technical assistance with ATLAS operations.

Richard Vondrasek (B.S. University of Chicago, 1990).

ATLAS operator.

Philip R. Wilt (Johnstown Technical School 1973).

Electronics design and maintenance.

Bruce J. Zabransky (M.S. University of Illinois, Chicago, 1973).

Mechanical Engineer.

Gary P. Zinkann (B.S. DeVry, 1975).

ATLAS operations supervisor.

ADMINISTRATIVE STAFF

- * Allan Bernstein, M.B.A., Rosary College, 1986
- * James E. Nelson, B.A., University of Illinois, 1975
- † Karen J. Thayer

VISITORS AND STUDENTS

Long-Term Visitors (at Argonne more than 4 months)

Anatolijs Afanasjevs (from University of Notre Dame, IN):

Theoretical physics studies.

(July 2001--)

Vladislav Asseev (from Institute for Nuclear Research of Russian Academy of Sciences, Russia)

Accelerator development.

(January-July 2000; May-August 2001)

Jason Clark (from University of Manitoba, Canada):

Heavy-ion research at ATLAS.

(May 1999-)

Moulay Ahmed El Alaoui (from Laboratory for Theoretical Physics, Morocco):

Medium-energy physics.

(February 2001--)

* Assistant Director of the Physics Division.

† Special Term Appointee.

Itacil Gomes (from Technology Division, Argonne National Laboratory)
 Linac development.
 (September 2000--)

Burt Holzmann (from University of Chicago, Chicago, IL):
 Heavy-ion research at ATLAS.
 (October 2001--)

Ioana Mihaila (from Coastal Carolina University, Conway, SC):
 Theoretical physics studies.
 (November 2001--)

Peter Mueller (from Johannes Gutenberg University, Mainz, Germany):
 Medium-energy physics.
 (November 2001--)

Ichiro Nishinaka (from Tokyo Metropolitan University, Japan):
 Heavy-ion research at ATLAS.
 (March—September 2001)

Iouri Sanjiev (from St. Petersburg Nucl. Phys. Institute, Gatchina, Leningrad, Russia):
 Medium energy studies.
 (November 2000)

Stefan W. Schramm (from University of Frankfurt, Germany):
 Theoretical physics studies.
 (November 2001--)

* Sergey Sharamentov (from Institute for Nucl. Phys. Of the Russian Acad. of Sci., Moscow, Russia):
 Linac development.
 (October 2000 – October 2001)

Joseph V. Vaz (from University of Manitoba, Canada):
 Heavy-ion research at ATLAS.
 (November 1999—November 2001)

Jicheng Wang (from University of Manitoba, Canada):
 Heavy-ion research at ATLAS.
 (January 2001--)

Andreas Woehr (from University of Maryland, College Park, MD):
 Heavy-ion research at ATLAS.
 (January 2001--)

Short-Term Visitors (at ANL for less than 4 months at a time)

† Nour-eddi Berrah (from Western Michigan University, Kalamazoo, MI):
 Atomic physics research.
 (October 1991--)

Chantal Boudreau (from McGill University, Montreal, Quebec):
 Heavy-ion research at ATLAS.
 (May 2000—April 2001; September 2001--)

* Joined regular staff October 2001

† Guest Faculty Research Participant

William Detmold (from University of Adelaide, Australia):
Theoretical physics studies.
(July—September 2001)

Thomas Dombeck (from University of Chicago, Chicago, IL):
Heavy-ion research.
(January 2000--)

* Christopher Fasano (from Monmouth College, Monmouth, IL):
Theoretical studies.
(February 1999-)

Susan Fischer (from DePaul University, Chicago, IL):
Heavy-ion research at ATLAS.
(October 1998--)

Michael Froese (from University of Manitoba, Canada):
Heavy-ion research at ATLAS.
(May 2001--)

Clive Halliwell (from University of Illinois, Chicago, IL):
Heavy-ion research at ATLAS.
(June 1998—June 2001)

Jeffrey Hangst (from University of Aarhus, Denmark):
Heavy-ion research at ATLAS.
(April 1995—September 2001)

David J. Hofman (from University of Illinois, Chicago, IL):
Heavy-ion research at ATLAS.
(September 2000--)

David Jenkins (from University of York, UK):
Heavy-ion research at ATLAS.
(February 2000)

Bruno Julia Diaz (from University of Salamanca):
Theoretical physics studies.
(October—December 2001)

Leonard Kalinine (from Russian Institute of High Power Radio Equipment, Russia):
Accelerator development.
(July--August 2000; August—October 2001)

* Judith Katzy (from University of Illinois, Chicago, IL):
Heavy-ion research at ATLAS.
(February 1998--)

Andre Kolomiets (from ITEP, Russia):
Accelerator development.
(July-October 2000; November 2000--)

* Donald McLeod (from University of Illinois, Chicago, IL):
Heavy-ion research at ATLAS.
(June 1994--)

* Guest Faculty Research Participant.

Sekazi Mtingwa (from North Carolina A&T State University, Greensboro, NC):
Heavy-ion research at ATLAS.
(July—August 2001)

Rachid Nouicer (from University of Chicago, Chicago, IL):
Heavy-ion research at ATLAS.
(April 1998--)

* David Smith (from University of Vermont, Storrs, VT):
Theoretical physics studies.
(February 2000--)

Qamar Usmani (from University of Putra, Malaysia):
Theoretical physics studies.
(April-May 2001)

Resident Graduate Students

Peter Cabauy (from University of Michigan, Ann Arbor, MI):
Theoretical studies.
(February-September 2000; January 2001—)

David Gaskell (from Oregon State University, Corvallis, OR):
Medium-energy physics.
(September 1998—May 2001)

Mauricio Portillo (from Michigan State University, E. Lansing, MI):
Accelerator development.
(September 1995--)

Issam Qattan (from Northwestern University, Evanston, IL):
Medium-energy physics.
(August 2001--)

Jennifer Ressler (from University of Maryland, College Park, MD):
Heavy-ion research at ATLAS.
(January 1999--July 2001)

Elaine Schulte (from University of Illinois, Urbana, IL):
Medium-energy studies.
(August 2000--)

Guest Graduate Students

Khalefeh Abu Saleem (from Illinois Institute of Technology, Chicago, IL):
Heavy-ion research at ATLAS.
(June 1999-)

Philippe Coulombe-Pontbriand (from McGill University, Montreal, Quebec, Canada):
Heavy-ion research at ATLAS.
(May—August 2001)

Xu Du (from Northwestern University, Evanston, IL):
Medium-energy physics.
(June 1999-)

* Guest Faculty Research Participant.

Andrew Geraci (from University of Chicago, Chicago, IL):
Accelerator development.
(December 1999-)

Louis Jisonna (from Northwestern University, Evanston, IL):
Heavy-ion research at ATLAS.
(June 2000--)

Masaharu Nakagawa (from Kyoto University, Japan):
Linac accelerator development.
(September—December 2001)

Iouri Sanjiev (from DESY Laboratory, Hamburg, Germany):
Medium-energy studies.
(November 2000--)

Christian Trempe (from McGill University, Montreal, QC):
Heavy-ion research at ATLAS.
(May-August 2000)

Li-Bang Wang (from University of Illinois, Urbana, IL):
Medium-energy studies.
(September 2001--)

Undergraduate Students

Martin Alcorta (University of Chicago)
John Amann (DePaul University)
David Bopp (North Central College)
Ivo Calderin (University of Miami, Coral Gables)
Stacy Dean (Saint Xavier College)
Kara Eder (St. Xavier College)
Javier Figueroa (Benedictine University)
Adam Frankel (Cornell University)
Rachel Gabor (Harvey Mudd College)
William Grimes (Monmouth College)
Teresa Haslinger (Richard J. Daley College)
Andy Hernandez (Harry S. Truman College)
Nikola Kunovski (North Central College)
Clint Law (Monmouth College)
Jeffrey Montgomery (New Mexico State University)
Chad Muir (North Central College)
Janelle Neubauer (North Central College)
Okechukwa Okafor (Southern University)
Gabriel Possin (North Central College)
Matthew Sunnott (North Central College)
Barbara Truett (Purdue University, Calumet)

PUBLICATIONS DURING 2001

HEAVY-ION NUCLEAR PHYSICS RESEARCH

Rotational Bands in the Proton Emitter ^{141}Ho

D. Seweryniak, P. J. Woods, J. J. Ressler, C. N. Davids, A. Heinz, A. A. Sonzogni, J. Uusitalo, W. B. Walters, J. A. Caggiano, M. P. Carpenter, J. A. Cizewski, T. Davinson, K. Y. Ding, N. Fotiades, U. Garg, R. V. F. Janssens, T. L. Khoo, F. G. Kondev, T. Lauritsen, C. J. Lister, P. Reiter, J. Shergur, and I. Wiedenhöver
Phys. Rev. Lett. **86**, 1458-1461 (2001)

Baryon Rapidity Loss in Relativistic Au + Au Collisions

B. B. Back, R. R. Betts, J. Chang, W. C. Chang, C. Y. Chi, Y. Y. Chu, J. B. Cumming, J. C. Dunlop, W. Eldredge, S. Y. Fung, R. Ganz, E. Garcia, A. Gillitzer, G. Heintzelman, W. F. Henning, D. J. Hofman, B. Holzman, J. H. Kang, E. J. Kim, S. Y. Kim, Y. Kwon, D. McLeod, A. C. Mignerey, M. Moulson, V. Nanal, C. A. Ogilvie, R. Pak, A. Ruangma, D. E. Russ, R. K. Seto, P. J. Stankas, G. S. F. Stephans, H. Q. Wang, F. L. H. Wolfs, A. H. Wuosmaa, H. Xiang, G. H. Xu, H. B. Yao, and C. M. Zou
Phys. Rev. Lett. **86**, 1970-1973 (2001)

Linear Polarization Measurement of Interband Transitions in Superdeformed ^{190}Hg : Model-Independent Evidence for Octupole Vibrational Structures

A. Korichi, A. N. Wilson, F. Hannachi, A. Lopez-Martens, M. Rejmund, C. Schück, Ch. Vieu, G. Chmel, A. Görge, H. Hübel, D. Rossbach, S. Schönwasser, M. Bergström, B. M. Nyakó, J. Timár, D. Bazzacco, S. Lunardi, C. Rossi-Alvarez, P. Bednarczyk, N. Kintz, S. Naguleswaran, A. Astier, D. M. Cullen, J. F. Sharpey-Schafer, T. Lauritsen, and R. Wadsworth
Phys. Rev. Lett. **86**, 2746-2749 (2001)

$S_{17}(0)$ Determined from the Coulomb Breakup of 83 MeV/Nucleon ^8B

B. Davids, D. W. Anthony, T. Aumann, Sam M. Austin, T. Baumann, D. Bazin, R. R. C. Clement, C. N. Davids, H. Esbensen, P. A. Lofy, T. Nakamura, B. M. Sherrill, and J. Yurkon
Phys. Rev. Lett. **86**, 2750-2753 (2001)

Magic Nucleus ^{132}Sn and Its One-Neutron-Hole Neighbor ^{131}Sn

P. Bhattacharyya, P. J. Daly, C. T. Zhang, Z. W. Grabowski, S. K. Saha, R. Broda, B. Fornal, I. Ahmad, D. Seweryniak, I. Wiedenhöver, M. P. Carpenter, R. V. F. Janssens, T. L. Khoo, T. Lauritsen, C. J. Lister, P. Reiter, and J. Blomqvist
Phys. Rev. Lett. **87**, 062502/1-4 (2001)

Search for X-Ray Induced Acceleration of the Decay of the 31-Yr Isomer ^{178}Hf Using Synchrotron Radiation

I. Ahmad, J. C. Banar, J. A. Becker, D. S. Gemmell, A. Kraemer, A. Mashayekhi, D. P. McNabb, G. G. Miller, E. F. Moore, L. N. Pangault, R. S. Rundberg, J. P. Schiffer, S. D. Shastri, T. F. Wang, and J. B. Wilhelmy
Phys. Rev. Lett. **87**, 072503/1-4 (2001)

Ratios of Charged Antiparticles-to-Particles Near Mid-Rapidity in Au + Au Collisions at $\sqrt{s_{NN}} = 130$ GeV

B. B. Back *et al.* (PHOBOS Collaboration)
Phys. Rev. Lett. **87**, 102301/1-4 (2001)

Charged-Particle Pseudorapidity Density Distributions from Au + Au Collisions at $\sqrt{s_{NN}} = 130$ GeV

B. B. Back, M. D. Baker, D. S. Barton, R. R. Betts, R. Bindel, A. Budzanowski, W. Busza, A. Carroll, M. P. Decowski, E. Garcia, N. George, K. Gulbrandsen, S. Gushue, C. Halliwell, G. A. Heintzelman, C. Henderson, D. J. Hofman, R. Holynski, B. Holzmann, E. Johnson, J. L. Kane, J. Katzy, N. Khan, W. Kucewicz, P. Kulinich, W. T. Lin, S. Manly, D. McLeod, J. Michalowski, A. C. Mignerey, J. Mlmenstdt, R. Nouicer, A. Olszewski, R. Pak, I. C. Park, H. Pernegger, C. Reed, L. P. Remsberg, M. Reuter, C. Roland, G. Roland, L. Rosenberg, P. Sarin, P. Sawicki, W. Skulski, S. G. Steadman, P. Steinberg, G. S. F. Stephans, M. Stodulski, A. Sukhanov, J.-L. Tang, R. Teng, A. Trzupek, C. Vale, G. J. van Nieuwenhuizen, R. Verdier, B. Wadsworth, F. L. H. Wolfs, B. Wosiek, K. Wozniak, A. H. Wuosmaa, and B. Wyslouch
Phys. Rev. Lett. **87**, 102303/1-4 (2001)

Alignment Delays in the $N = Z$ Nuclei ^{72}Kr , ^{76}Sr and ^{80}Zr

S. M. Fischer, C. J. Lister, D. P. Balamuth, R. Bauer, J. A. Becker, L. A. Bernstein, M. P. Carpenter, J. Durell, N. Fotiades, S. J. Freeman, P. E. Garrett, P. A. Hausladen, R. V. F. Janssens, D. Jenkins, M. Leddy, J. Ressler, J. Schwartz, D. Svelnys, D. G. Sarantites, D. OmSeweryniak, B. J. Varley, and R. Wyss
Phys. Rev. Lett. **87**, 132501/1-4 (2001)

Observation of ^{46}Cr and Testing the Isobaric Multiplet Mass Equation at High Spin

P. E. Garrett, W. E. Ormand, D. Appelbe, R. W. Bauer, J. A. Becker, L. A. Bernstein, J. A. Cameron, M. P. Carpenter, R. V. F. Janssens, C. J. Lister, D. Seweryniak, E. Tavukcu, and D. D. Warner
Phys. Rev. Lett. **87**, 132502/1-4 (2001)

Crossing of Shears Bands in ^{197}Pb : $B(M1)$ Values and Semiclassical Description

J. R. Cooper, R. Krücken, C. W. Beausang, J. R. Novak, A. Dewald, T. Klug, G. Kemper, P. von Brentano, M. P. Carpenter, R. V. F. Janssens, C. J. Lister, and I. Wiedenhöver
Phys. Rev. Lett. **87**, 132503/1-4 (2001)

Identification of the $I^\pi = 10^+$ Yrast Rotational State in ^{24}Mg

I. Wiedenhöver, A. H. Wuosmaa, R. V. F. Janssens, C. J. Lister, M. P. Carpenter, H. Amro, P. Bhattacharyya, B. A. Brown, J. Caggiano, M. Devlin, A. Heinz, F. G. Kondev, T. Lauritsen, D. G. Sarantites, S. Siem, L. G. Sobotka, and A. Sonzogni
Phys. Rev. Lett. **87**, 142502/1-4 (2001)

Empirical Investigation of Extreme Single-Particle Behavior of Nuclear Quadrupole Moments in Highly Collective $A \sim 150$ Superdeformed Bands

S. T. Clark, G. Hackman, R. V. F. Janssens, R. M. Clark, P. Fallon, S. N. Floor, G. J. Lane, A. O. Macchiavelli, J. Norris, S. J. Sanders, and C. E. Svensson
Phys. Rev. Lett. **87**, 172503/1-4 (2001)

Very Extended Shapes in the $A \sim 110$ Region

R. M. Clark, P. Fallon, A. Gorgen, M. Cromaz, M. A. Deleplanque, R. M. Diamond, G. J. Lane, I. Y. Lee, A. O. Macchiavelli, R. G. Ramos, F. S. Stephens, C. E. Svensson, K. Vetter, D. Ward, M. P. Carpenter, R. V. F. Janssens, and R. Wadsworth
Phys. Rev. Lett. **87**, 202502/1-4 (2001)

Effective Charge of the $\pi h_{11/2}$ Orbital and the Electric Field Gradient of Hg from the Yrast Structure of ^{206}Hg

B. Fornal, R. Broda, K. H. Maier, J. Wrzesniński, G. J. Lane, M. Cromaz, A. O. Macchiavelli, R. M. Clark, K. Vetter, A. P. Byrne, G. D. Dracoulis, M. P. Carpenter, R. V. F. Janssens, I. Wiedenhöver, M. Rejmund, and J. Blomqvist
Phys. Rev. Lett. **87**, 212501/1-4 (2001)

Superdeformation in the Doubly Magic Nucleus $^{40}_{20}\text{Ca}_{20}$

E. Ideguchi, D. G. Sarantites, W. Reviol, A. V. Afanasjev, M. Devlin, C. Baktash, R. V. F. Janssens, D. Rudolph, A. Axelsson, M. P. Carpenter, A. Galindo-Uribarri, D. R. LaFosse, T. Lauritsen, F. Lerma, C. J. Lister, P. Reiter, D. Seweryniak, M. Weiszflog, and J. N. Wilson
Phys. Rev. Lett. **87**, 222501/1-4 (2001)

Antilambda Production in Au + Au Collisions at 11.7 AGeV/c

B. B. Back *et al.* (The E917 Collaboration)
Phys. Rev. Lett. **87**, 242301/1-4 (2001)

Magnetic Dipole Bands in ^{190}Hg : First Evidence of Excitations Across the $Z = 82$ Sub-Shell in Hg Nuclei

A. N. Wilson, J. Timár, I. Ahmad, A. Astier, F. Azaiez, M. H. Bergström, D. J. Blumenthal, B. Crowell, M. P. Carpenter, L. Ducroux, B. J. P. Gall, F. Hannachi, H. Hübel, T. L. Khoo, R. V. F. Janssens, A. Korichi, T. Lauritsen, A. Lopez-Martens, M. Meyer, D. Nisius, E. S. Paul, M. G. Porquet, N. Redon, J. F. Sharpey-Schafer, R. Wadsworth, J. N. Wilson, and I. Ragnarsson
Phys. Lett. **B505**, 6-14 (2001)

First Evidence for Triaxial Superdeformation in ^{168}Hf

H. Amro, P. G. Varmette, W. C. Ma, B. Herskind, G. B. Hagemann, G. Sletten, R. V. F. Janssens, M. Bergström, A. Bracco, M. Carpenter, J. Domscheit, S. Frattini, D. J. Hartley, H. Hübel, T. L. Khoo, F. Kondev, T. Lauritsen, C. J. Lister, B. Million, S. W. Ødegård, R. B. Piercey, L. L. Riedinger, K. A. Schmidt, S. Siem, I. Wiedenhöver, J. N. Wilson, and J. A. Winger
Phys. Lett. **B506**, 39-44 (2001)

Identification of Excited Structures in Proton Unbound Nuclei $^{173,175,177}\text{Au}$: Shape Co-Existence and Intruder Bands

F. G. Kondev, M. P. Carpenter, R. V. F. Janssens, K. Abu Saleem, I. Ahmad, H. Amro, J. A. Cizewski, M. Danchev, C. N. Davids, D. J. Hartley, A. Heinz, T. L. Khoo, T. Lauritsen, C. J. Lister, W. C. Ma, G. L. Poli, J. Ressler, W. Reviol, L. L. Riedinger, D. Seweryniak, M. B. Smith, and I. Wiedenhöver
 Phys. Lett. **B512**, 268-276 (2001)

Band Structure of ^{68}Ge

D. Ward, C. E. Svensson, I. Ragnarsson, C. Baktash, M. A. Bentley, J. A. Cameron, M. P. Carpenter, R. M. Clark, M. Cromaz, M. A. Deleplanque, M. Devlin, R. M. Diamond, P. Fallon, S. Flibotte, A. Galindo-Uribarri, D. S. Haslip, R. V. F. Janssens, T. Lampman, G. J. Lane, I. Y. Lee, F. Lerma, A. O. Macchiavelli, S. D. Paul, D. Radford, D. Rudolph, D. G. Sarantites, B. Schaly, D. Seweryniak, F. S. Stephens, O. Thelen, K. Vetter, J. C. Waddington, J. N. Wilson, and C.-H. Yu
 Phys. Rev. C **63**, 014301/1-11 (2001)

Excited States in ^{103}Sn : Neutron Single-Particle Energies with Respect to ^{100}Sn

C. Fahlander, M. Palacz, D. Rudolph, D. Sohler, J. Blomqvist, J. Kownacki, K. Lagergren, L. O. Norlin, J. Nyberg, A. Algora, C. Andreoiu, G. de Angelis, A. Ataç, D. Bazzacco, L. Berglund, T. Bäck, J. Cederkäll, B. Cederwall, Zs. Dombradi, B. Fant, E. Farnea, A. Gadea, M. Górska, H. Grawe, N. Hashimoto-Saitoh, A. Johnson, A. Kerek, W. Klamra, S. M. Lenzi, A. Likar, M. Lipoglavšek, M. Moszyński, D. R. Napoli, C. Rossi-Alvarez, H. A. Roth, T. Saitoh, D. Seweryniak, Ö. Skeppstedt, M. Weiszflog, and M. Wolińska
 Phys. Rev. C **63**, 021307(R)/1-4 (2001)

Identification of Excited States in ^{117}Cs : Systematics of the $\nu(h_{11/2})^2$ Alignment

J. F. Smith, V. Medina-Chico, C. J. Chiara, D. B. Fossan, G. J. Lane, J. M. Sears, I. Thorslund, H. Amro, C. N. Davids, R. V. F. Janssens, D. Seweryniak, I. M. Hibbert, R. Wadsworth, I. Y. Lee, and A. O. Macchiavelli
 Phys. Rev. C **63**, 024319/1-11 (2001)

Few Particle Excitations of $N = 83$ Isotones ^{134}Sb and ^{135}Te from ^{248}Cm Fission

B. Fornal, R. Broda, P. J. Daly, P. Bhattacharyya, C. T. Zhang, Z. W. Grabowski, I. Ahmad, D. Seweryniak, I. Wiedenhöver, M. P. Carpenter, R. V. F. Janssens, T. L. Khoo, T. Lauritsen, C. J. Lister, P. Reiter, and J. Blomqvist
 Phys. Rev. C **63**, 024322/1-6 (2001)

$^{12}\text{C} + ^{12}\text{C}$ and $^{16}\text{O} + ^8\text{Be}$ Decay of ^{24}Mg States Populated in the $^{12}\text{C}(^{20}\text{Ne}, ^{24}\text{Mg}^*)^8\text{Be}$ Reaction

M. Freer, J. T. Murgatroyd, S. M. Singer, N. Curtis, D. J. Henderson, D. J. Hofman, and A. H. Wuosmaa
 Phys. Rev. C **63**, 034317/1-8 (2001)

First Evidence of Excited States in the Near-Drip-Line Nucleus ^{126}Pr and Signature Inversion in $A \sim 130$ Nuclei

D. J. Hartley, A. Galindo-Uribarri, C. Baktash, M. P. Carpenter, M. Danchev, M. Devlin, C. J. Gross, R. V. F. Janssens, M. Lipoglavsek, E. Padilla, S. D. Paul, D. C. Radford, W. Reviol, L. L. Riedinger, D. G. Sarantites, D. Seweryniak, C.-H. Yu, and O. Zeidan
Phys. Rev. C **63**, 041301(R)/1-5 (2001)

Proton and α Radioactivity of ^{185}Bi

G. L. Poli, C. N. Davids, P. J. Woods, D. Seweryniak, M. P. Carpenter, J. A. Cizewski, T. Davinson, A. Heinz, R. V. F. Janssens, C. J. Lister, J. J. Ressler, A. A. Sonzogni, J. Uusitalo, and W. B. Walters
Phys. Rev. C **63**, 044304/1-3 (2001)

High-Spin Structures and Alignment Properties in ^{126}Ce

A. N. Wilson, R. Wadsworth, J. F. Smith, S. J. Freeman, M. J. Leddy, C. J. Chiara, D. B. Fossan, D. R. LaFosse, K. Starosta, M. Devlin, D. G. Sarantites, J. N. Wilson, M. P. Carpenter, C. N. Davids, R. V. F. Janssens, D. Seweryniak, and R. Wyss
Phys. Rev. C **63**, 054307/1-11 (2001)

Lifetimes of Superdeformed Rotational States in ^{36}Ar

C. E. Svensson, A. O. Macchiavelli, A. Juodagalvis, A. Poves, I. Ragnarsson, S. Åberg, D. E. Appelbe, R. A. E. Austin, G. C. Ball, M. P. Carpenter, E. Caurier, R. M. Clark, M. Cromaz, M. A. Deleplanque, R. M. Diamond, P. Fallon, R. V. F. Janssens, G. J. Lane, I. Y. Lee, F. Nowacki, D. G. Sarantites, F. S. Stephens, K. Vetter, and D. Ward
Phys. Rev. C **63**, 061301(R)/1-5 (2001)

Evidence for a Strongly Deformed Band in ^{80}Y Using Isomer Decay Tagging

J. J. Ressler, W. B. Walters, R. Gryzwacz, J. C. Batchelder, C. R. Bingham, C. J. Gross, Z. Janas, M. Lipoglavsek, J. McConnell, S. D. Paul, A. Piechaczek, K. Rykaczewski, D. Radford, and J. Shergur
Phys. Rev. C **63**, 067303/1-4 (2001)

Consequences of Neutron-Proton Pairing Correlations for the Rotational Motion of the $N = Z$ Nucleus ^{72}Kr

N. S. Kelsall, R. Wadsworth, A. N. Wilson, P. Fallon, A. O. Macchiavelli, R. M. Clark, D. G. Sarantites, D. Seweryniak, C. E. Svensson, S. M. Vincent, S. Frauendorf, J. A. Sheikh, and G. C. Ball
Phys. Rev. C **64**, 024309/1-7 (2001)

Spectroscopy of ^{23}Al and ^{27}P Using the (^7Li , ^8He) Reaction and the Implications for ^{22}Na and ^{26}Al Nucleosynthesis in Explosive Hydrogen Burning

J. A. Caggiano, D. Bazin, W. Benenson, B. Davids, R. Ibbotson, H. Scheit, B. M. Sherrill, M. Steiner, J. Yurkon, A. F. Zeller, B. Blank, M. Chartier, J. Greene, J. A. Nolen, Jr., A. Wuosmaa, M. Bhattacharya, A. Garcia, and M. Wiescher
Phys. Rev. C **64**, 025802/1-9 (2001)

Proton Radioactivity of ^{117}La

H. Mahmud, C. N. Davids, P. J. Woods, T. Davinson, A. Heinz, G. L. Poli, J. J. Ressler, K. Schmidt, D. Seweryniak, M. B. Smith, A. A. Sonzogni, J. Uusitalo, and W. B. Walters
Phys. Rev. C **64**, 031303(R)/1-3 (2001)

Excited States in ^{155}Yb and $^{155,156,157}\text{Lu}$ from Recoil-Decay Tagging

K. Y. Ding, J. A. Cizewski, D. Seweryniak, H. Amro, M. P. Carpenter, C. N. Davids, N. Fotiades, R. V. F. Janssens, T. Lauritsen, C. J. Lister, D. Nisius, P. Reiter, J. Uusitalo, I. Wiedenhöver, and A. O. Macchiavelli
Phys. Rev. C **64**, 034315/1-13 (2001)

Particle-Vibration Coupling in Proton Decay of Near-Spherical Nuclei

Cary N. Davids and Henning Esbensen
Phys. Rev. C **64**, 034317/1-7 (2001)

Investigation of Antimagnetic Rotation in ^{100}Pd

S. Zhu, U. Garg, A. V. Afanasjev, S. Frauendorf, B. Kharraja, S. S. Ghugre, S. N. Chintalapudi, R. V. F. Janssens, M. P. Carpenter, F. G. Kondev, and T. Lauritsen
Phys. Rev. C **64**, 041302(R)/1-5 (2001)

Yrast Three-Quasiparticle *K*-Isomers in Neutron-Rich ^{181}Hf

I. Shestakova, G. Mukherjee, P. Chowdhury, R. D'Alarcao, C. J. Pearson, Zs. Podolyak, P. M. Walker, C. Wheldon, D. M. Cullen, I. Ahmad, M. P. Carpenter, R. V. F. Janssens, T. L. Khoo, F. G. Kondev, C. J. Lister, D. Seweryniak, and I. Wiedenhoever
Phys. Rev. C **64**, 054307/1-6 (2001)

Investigation of the Decay Out of Superdeformed Bands in ^{194}Hg by Lifetime Measurements

A. Dewald, R. Kühn, R. Peusquens, P. von Brentano, R. Krücken, M. A. Deleplanque, I. Y. Lee, R. M. Clark, P. Fallon, A. O. Macchiavelli, R. W. MacLeod, F. S. Stephens, T. L. Khoo, P. Reiter, and K. Hauschild
Phys. Rev. C **64**, 054309/1-6 (2001)

Yrast Excitations in $N = 81$ Nuclei ^{132}Sb and ^{133}Te from ^{248}Cm Fission

P. Bhattacharyya, P. J. Daly, C. T. Zhang, Z. W. Grabowski, S. K. Saha, B. Fornal, R. Broda, W. Urban, I. Ahmad, D. Seweryniak, I. Wiedenhöver, M. P. Carpenter, R. V. F. Janssens, T. L. Khoo, T. Lauritsen, C. J. Lister, P. Reiter, and J. Blomqvist
Phys. Rev. C **64**, 054312/1-4 (2001)

Stability of Oblate Shapes in the Vicinity of $N = Z = 34$ ^{68}Se : Bands in ^{69}Se and ^{67}As

D. G. Jenkins, D. P. Balamuth, M. P. Carpenter, C. J. Lister, S. M. Fischer, R. M. Clark, A. O. Macchiavelli, P. Fallon, C. E. Svensson, N. S. Kelsall, and R. Wadsworth
Phys. Rev. C **64**, 064311/1-8 (2001)

Thermal Excitation-Energy Deposition in 5-15 GeV/c Hadron-Induced Reactions with ^{197}Au . II.
Relation Between Excitation Energy and Reaction Variables

L. Beaulieu, T. Lefort, K. Kwiatkowski, W.-C. Hsi, G. Wang, D. S. Bracken, E. Cornell, D. S. Ginger, K. B. Morley, V. E. Viola, F. Gimeno-Nogues, R. Laforest, E. Martin, E. Ramakrishnan, D. Rowland, A. Ruangma, E. Winchester, S. J. Yennello, R. G. Korteling, L. Pienkowski, H. Breuer, B. Back, S. Gushue, L. P. Remsberg, M. J. Huang, W. G. Lynch, M. B. Tsang, and H. Xi
Phys. Rev. C **64**, 064604/1-11 (2001)

Lifetime of the 21.8-keV State in ^{98}Tc

J. F. Smith, J. S. Lilley, W. R. Phillips, I. Ahmad, K. E. Rehm, and A. Garcia
Phys. Rev. C **64**, 067301/1-4 (2001)

Studies of Light Charged Particle Emission from Fission and ER Reactions in the System 344 MeV $^{28}\text{Si} + ^{121}\text{Sb} \rightarrow ^{149}\text{Tb}$ ($E^* = 240$ MeV)

Morton Kaplan, Craig J. Copi, Paul A. DeYoung, Gerard J. Gilfoyle, Paul J. Karol, David J. Moses, Winifred E. Parker, K. Ernst Rehm, John Sarafa, and Emanuele Vardaci
Nucl. Phys. **A686**, 109-128 (2001)

Medium-Spin Structure of $^{96,97}\text{Sr}$ and $^{98,99}\text{Zr}$ Nuclei and the Onset of Deformation in the $A \sim 100$ Region

W. Urban, J. L. Durell, A. G. Smith, W. R. Phillips, M. A. Jones, B. J. Varley, T. Rzaca-Urban, I. Ahmad, L. R. Morss, M. Bentaleb, and N. Schulz
Nucl. Phys. **A689**, 605-630 (2001)

Core-Excited States and Core-Polarization Effects in ^{210}At and ^{211}At

S. Bayer, A. P. Byrne, G. D. Dracoulis, A. M. Baxter, T. Kibédi, and F. G. Kondev
Nucl. Phys. **A694**, 3-62 (2001)

Preparation of Thin Plastic Conductive Foils for Use in a Position-Sensitive Micro-Channel Plate Detector System

John P. Greene, Christopher J. Lister, Peter Reiter, George E. Thomas, and Keri L. Unterzuber
Nucl. Instrum. Methods **A459**, 334-338 (2001)

Silicon Pad Detectors for the PHOBOS Experiment at RHIC

R. Nouicer, B. B. Back, R. R. Betts, K. H. Gulbrandsen, B. Holzman, W. Kucewicz, W. T. Lin, J. Mülmenstädt, G. J. van Nieuwenhuizen, H. Pernegger, M. Reuter, P. Sarin, G. S. F. Stephans, V. Tsay, C. M. Vale, B. Wadsworth, A. H. Wuosmaa, and B. Wyslouch
Nucl. Instrum. Methods **A461**, 143-149 (2001)

First Observation of a Rotational Band in Neutron-Rich ^{180}Lu

C. Wheldon, P. M. Walker, P. Chowdhury, I. Shestakova, R. D'Alarcao, I. Ahmad, M. P. Carpenter, D. M. Cullen, R. V. F. Janssens, T. L. Khoo, F. G. Kondev, C. J. Listen C. J. Pearson, Zs. Podolyák, D. Seweryniak, and I. Wiedenhöver
J. Phys. G **27**, L13-L17 (2001)

Study of ^{169}Hf at High Rotational Frequency

K. A. Schmidt, M. Bergström, G. B. Hagemann, B. Herskind, G. Sletten, P. G. Varmette, J. Domscheit, H. Hübel, S. W. Ødegård, S. Frattini, A. Bracco, B. Million, M. P. Carpenter, R. V. F. Janssens, T. L. Khoo, T. Lauritsen, C. J. Lister, S. Siem, I. Wiedenhöver, D. J. Hartley, L. L. Riedinger, A. Maj, W. C. Ma, and R. Terry
Eur. Phys. J. A **12**, 15-28 (2001)

First Measurements of Yrast Excitations in ^{137}I and the Missing 12^+ Isomer in ^{136}Te

A. Korgul, W. Urban, T. Rzaca-Urban, M. Gorska, J. L. Durell, M. J. Leddy, M. A. Jones, W. R. Phillips, A. G. Smith, B. J. Varley, M. Bentaleb, E. Lubkiewicz, N. Schulz, I. Ahmad, and L. R. Morss
Eur. Phys. J. A. **12**, 129-133 (2001)

Experimental Limit to Interstellar ^{244}Pu Abundance

M. Paul, A. Valenta, I. Ahmad, D. Berkovits, C. Bordeanu, S. Ghelberg, Y. Hashimoto, A. Hershkowitz, S. Jiang, T. Nakanishi, and K. Sakamoto
Astrophys. J. **558**, L133-L135 (2001)

Collective Rotational Motion in the $N = Z$ Nucleus ^{36}Ar

C. E. Svensson, A. O. Macchiavelli, A. Juodagalvis, A. Poves, I. Ragnarsson, S. Åberg, D. E. Appelbe, R. A. E. Austin, C. Baktash, G. C. Ball, M. P. Carpenter, E. Caurier, R. M. Clark, M. Cromaz, M. A. Deleplanque, R. M. Diamond, P. Fallon, M. Furlotti, A. Galindo-Uribarri, R. V. F. Janssens, G. J. Lane, I. Y. Lee, M. Lipoglavsek, F. Nowacki, S. D. Paul, D. C. Radford, D. G. Sarantites, D. Seweryniak, F. S. Stephens, V. Tomov, K. Vetter, D. Ward, and C. H. Yu
Proceedings of the Conference on Nuclear Structure 2000, East Lansing, MI, August 15-19, 2000; Nucl. Phys. **A682**, 1c-11c (2001)

Measurement and Analysis of Quadruple ($\alpha\gamma\gamma$) Angular Correlations for High Spin States of ^{24}Mg

I. Wiedenhöver, A. H. Wuosmaa, C. J. Lister, M. P. Carpenter, R. V. F. Janssens, H. Amro, J. Caggiano, A. Heinz, F. G. Kondev, T. Lauritsen, S. Siem, A. Sonzogni, P. Bhattacharyya, M. Devlin, D. G. Sarantites, and L. G. Sobotka
Proceedings of the Conference on Nuclear Structure 2000, East Lansing, MI, August 15-19, 2000; Nucl. Phys. **A682**, 22c-27c (2001)

Rotational Bands Near ^{56}Ni

W. Reviol, D. G. Sarantites, R. J. Charity, V. Tomov, D. Rudolph, R. M. Clark, M. Cromaz, P. Fallon, A. O. Macchiavelli, M. P. Carpenter, D. Seweryniak, and J. Dobaczewski
Proceedings of the Conference on Nuclear Structure 2000, East Lansing, MI, August 15-19, 2000; Nucl. Phys. **A682**, 28c-34c (2001)

Observation of Delayed Alignment in $N = Z$ Nuclei ^{72}Kr , ^{76}Sr , and ^{80}Zr

S. M. Fischer, D. P. Balamuth, C. J. Lister, P. A. Hausladen, M. P. Carpenter, D. Seweryniak, D. Jenkins, D. Svelnys, J. Schwartz, S. J. Freeman, M. Leddy, B. J. Varley, J. Durrell, L. Bernstein, P. Garrett, R. Bauer, J. Becker, D. G. Sarantites, J. Ressler, and N. Fotiades
Proceedings of the Conference on Nuclear Structure 2000, East Lansing, MI, August 15-19, 2000; Nucl. Phys. **A682**, 35c-40c (2001)

In-Beam Study of the $N = Z$ Nucleus $^{66}_{33}\text{As}_{33}$ Using the Decay Tagging Technique

R. Grzywacz, C. H. Yu, Z. Janas, S. D. Paul, J. C. Batchelder, C. R. Bingham, T. N. Ginter, C. J. Gross, J. McConnell, M. Lipoglavsek, A. Piechaczek, D. C. Radford, J. J. Ressler, K. Rykaczewski, J. Shergur, W. B. Walters, E. F. Zganjar, C. Baktash, M. P. Carpenter, R. V. F. Janssens, C. E. Svensson, J. C. Waddington, D. Ward, and E. Dragulescu
Proceedings of the Conference on Nuclear Structure 2000, East Lansing, MI, August 15-19, 2000; Nucl. Phys. **A682**, 41c-47c (2001)

The Structure of High- Z Nuclei from Studies with Gammasphere at ATLAS

R. V. F. Janssens
Proceedings of the Conference on Nuclear Structure 2000, East Lansing, MI, August 15-19, 2000; Nucl. Phys. **A682**, 54c-64c (2001)

Harvesting New Isomers in Neutron-Rich Hafnium Nuclei

P. Chowdhury, I. Shestakova, R. D'Alarcao, C. J. Pearson, Z. Podolyak, P. M. Walker, C. Wheldon, D. M. Cullen, I. Ahmad, M. P. Carpenter, R. V. F. Janssens, T. L. Khoo, F. G. Kondev, C. J. Lister, D. Seweryniak, and I. Wiedenhöver
Proceedings of the Conference on Nuclear Structure 2000, East Lansing, MI, August 15-19, 2000; Nucl. Phys. **A682**, 65c-70c (2001)

Structure of Exotic Nuclei Near and Above ^{208}Pb Populated via Deep-Inelastic Collisions

G. J. Lane, R. Broda, B. Fornal, A. P. Byrne, G. D. Dracoulis, J. Blomqvist, R. M. Clark, M. Cromaz, M. A. Deleplanque, R. M. Diamond, P. Fallon, R. V. F. Janssens, I. Y. Lee, A. O. Macchiavelli, K. H. Maier, M. Rejmund, F. S. Stephens, C. E. Svensson, K. Vetter, D. Ward, I. Wiedenhöver, and J. Wrzesinski
Proceedings of the Conference on Nuclear Structure 2000, East Lansing, MI, August 15-19, 2000; Nucl. Phys. **A682**, 71c-78c (2001)

GAMMASPHERE+FMA: A Journey Beyond the Proton Drip-Line

D. Seweryniak, P. J. Woods, J. J. Ressler, C. N. Davids, A. Heinz, A. A. Sonzogni, J. Uusitalo, W. B. Walters, J. A. Caggiano, M. P. Carpenter, J. A. Cizewski, T. Davinson, K. Y. Ding, N. Fotiades, U. Garg, R. V. F. Janssens, T. L. Khoo, F. G. Kondev, T. Lauritsen, C. J. Lister, P. Reiter, J. Shergur, and I. Wiedenhöver
Proceedings of the Conference on Nuclear Structure 2000, East Lansing, MI, August 15-19, 2000; Nucl. Phys. **A682**, 247c-255c (2001)

First Observation of Excitation Across the ^{100}Sn Core

M. Lipoglavček, C. Baktash, M. P. Carpenter, D. J. Dean, C. Fahlander, M. Hjorth-Jensen, R. V. F. Janssens, A. Likar, J. Nyberg, S. D. Paul, A. Piechaczek, D. C. Radford, D. Rudolph, D. Seweryniak, D. G. Sarantites, M. Vencelj, and C. H. Yu
Proceedings of the Conference on Nuclear Structure 2000, East Lansing, MI, August 15-19, 2000; Nucl. Phys. **A682**, 399c-403c (2001)

Systematic Study of Energy-Spin Entry Distributions at the Proton Dripline in the $A \sim 170$ Region

M. B. Smith, J. A. Cizewski, M. P. Carpenter, F. G. Kondev, R. V. F. Janssens, K. Abu Saleem, I. Ahmad, H. Amro, M. Danchev, C. N. Davids, D. J. Hartley, A. Heinz, T. L. Khoo, T. Lauritsen, C. J. Lister, W. C. Ma, G. L. Poli, J. J. Ressler, W. Reviol, L. L. Riedinger, D. Seweryniak, and I. Wiedenhöver
Proceedings of the Conference on Nuclear Structure 2000, East Lansing, MI, August 15-19, 2000; Nucl. Phys. **A682**, 433c-438c (2001)

Entry Distribution of ^{220}Th : A Method to Determine the Fission Barrier of an Unstable Nucleus

A. Heinz, T. L. Khoo, P. Reiter, I. Ahmad, P. Bhattacharyya, J. Caggiano, M. P. Carpenter, J. A. Cizewski, C. N. Davids, W. F. Henning, R. V. F. Janssens, G. D. Jones, R. Julin, F. G. Kondev, T. Lauritsen, C. J. Lister, D. Seweryniak, S. Siem, A. A. Sonzogni, J. Uusitalo, and I. Wiedenhöver
Proceedings of the Conference on Nuclear Structure 2000, East Lansing, MI, August 15-19, 2000; Nucl. Phys. **A682**, 458c-463c (2001)

First Observation of Excited Structures in Neutron Deficient, Odd-Mass Pt, Au and Hg Nuclei

F. G. Kondev, M. P. Carpenter, R. V. F. Janssens, K. Abu Saleem, I. Ahmad, M. Alcorta, H. Amro, J. Caggiano, J. A. Cizewski, M. Danchev, C. N. Davids, D. J. Hartley, A. Heinz, B. Herskind, R. A. Kaye, T. L. Khoo, T. Lauritsen, C. J. Lister, W. C. Ma, G. L. Poli, J. Ressler, W. Reviol, L. L. Riedinger, D. Seweryniak, S. Siem, M. B. Smith, A. A. Sonzogni, P. G. Varmette, and I. Wiedenhöver
Proceedings of the Conference on Nuclear Structure 2000, East Lansing, MI, August 15-19, 2000; Nucl. Phys. **A682**, 487c-492c (2001)

Decay of $^{135,136}\text{Sn}$ Isolated by Use of a Laser Ion Source and Evidence for a More Harmonic-Oscillator-Like Nuclear Potential

Jason Shergur, Michael Hannawald, Darek Seweryniak, Hans Fynbo, Ulli Koester, Andreas Woehr, Dimitri Fedorov, Valentin Fedoseyev, Viatcheslave Mishin, Per Hoff, Jo Ressler, Abigail Bickley, Bernd Pfeiffer, Haik Simon, Thomas Nilsson, Henryk Mach, Katarina Wilhelmsen Rolander, Helge Raven, Karl-Ludwig Kratz, William Walters, and the ISOLDE Collaboration
Proceedings of the Conference on Nuclear Structure 2000, East Lansing, MI, August 15-19, 2000; Nucl. Phys. **A682**, 493c-497c (2001)

New Results on Structure Effects in Nuclear Fission

K.-H. Schmidt, J. Benlliure, C. Böckstiegel, H.-G. Clerc, A. Grewe, A. Heinz, A. V. Ignatyuk, A. R. Junghans, M. de Jong, J. Müller, M. Pfützner, F. Rejmund, S. Steinhäuser, and B. Voss
Proceedings of the 7th International Conference on Nucleus-Nucleus Collisions, Strasbourg, France, July 3-7, 2000; Nucl. Phys. **A685**, 60c-71c (2001)

Gammasphere at ATLAS: Physics at the Limits

R. V. F. Janssens

Proceedings of the 7th International Conference on Nucleus-Nucleus Collisions, Strasbourg, France, July 3-7, 2000; Nucl. Phys. **A685**, 209c-220c (2001)

Structure of the Halo Nucleus ${}^6\text{He}$ Studied via the ${}^6\text{Li}(t, {}^3\text{He}){}^6\text{He}$ Reaction

T. Nakamura, T. Aumann, D. Bazin, Y. Blumenfeld, B. A. Brown, J. Caggiano, R. Clement, T. Glasmacher, P. A. Lofy, A. Navin, B. V. Pritychenko, B. M. Sherrill, and J. Yurkon
Proceedings of the 7th International Topical Conference on Giant Resonances (GR2000), Osaka, Japan, June 12-15, 2000; Nucl. Phys. **A687**, 97c-102c (2001)

Strangeness Production in Au + Au Collisions at AGS Energies

B. B. Back, R. R. Betts, J. Chang, W. C. Chang, C. Y. Chi, Y. Y. Chu, J. B. Gunning, J. C. Dunlop, W. Eldredge, S. Y. Fung, R. Ganz, E. Garcia-Solis, A. Gillitzer, G. Heintzelman, W. Henning, D. J. Hofman, B. Holzman, J. H. Kang, E. J. Kim, S. Y. Kim, Y. Kwon, D. McLeod, A. Mignerey, M. Moulson, V. Nanal, C. A. Ogilvie, R. Pak, A. Ruangma, D. Russ, R. Seto, J. Stankas, G. S. F. Stephans, H. Wang, F. Wolfs, A. H. Wuosmaa, H. Xiang, G. Xu, H. Yao, and C. Zou (for the E917 Collaboration)
Proceedings of the 5th International Conference on Strangeness in (Quark Matter, Berkeley, CA, July 20-25, 2000; J. Phys. G **27**, 301-309 (2001)

How Strange is PHOBOS? First RHIC Physics Results and Future Prospects

George Stephans (for the PHOBOS Collaboration)

Proceedings of the 5th International Conference on Strangeness in Quark Matter, Berkeley, CA, July 20-25, 2000; J. Phys. G **27**, 659-669 (2001)

Masses and Proton Separation Energies Obtained from Q_α and Q_p Measurements

C. N. Davids, P. J. Woods, J. C. Batchelder, C. R. Bingham, D. J. Blumenthal, L. T. Brown, B. C. Busse, M. P. Carpenter, L. F. Conticchio, T. Davinson, J. DeBoer, S. J. Freeman, S. Hamada, D. J. Henderson, R. J. Irvine, R. V. F. Janssens, H. J. Maier, L. Müller, R. D. Page, H. T. Penttilä, G. L. Poli, D. Seweryniak, F. Soramel, K. S. Toth, W. B. Walters, and B. E. Zimmerman

Proceedings of the 2nd Euroconference on Atomic Physics at Accelerators: Mass Spectrometry (APAC2000), Corsica, France, September 19-23, 2000; Hyperfine Interactions **132**, 133-139 (2001)

Nuclear Structure Far from Stability

C. J. Lister

Proceedings of the Conference on Structure of the Nucleus at the Dawn of the Century (Bologna 2000), Bologna, Italy, May 29-June 3, 2000, eds. G. C. Bonsignori, M. Bruno, A. Ventura, D. Vretenar, and A. Zichichi (World Scientific Publishing Co. 2001) pp. 16-22 (2001)

Octupole Vibration in the Superdeformed Well: First Experimental Evidence

A. Korichi, A. N. Wilson, F. Hannachi, A. Lopez-Martens, M. Rejmund, C. Schück, Ch. Vieu, G. Chmel, A. Georgen, H. Hübel, D. Rossbach, G. Schönwasser, M. Bergström, B. M. Nyakó, J. Timár, D. Bazzacco, S. Lunardi, C. Rossi-Alvarez, P. Bednarczyk, N. Kintz, S. Naguleswaran, A. Astier, D. M. Cullen, J. F. Sharpey-Schafer, T. Lauritsen, and R. Wadsworth

Proceedings of the Conference on Structure of the Nucleus at the Dawn of the Century (Bologna 2000), Bologna, Italy, May 29-June 3, 2000, eds. G. C. Bonsignori, M. Bruno, A. Ventura, and D. Vretenar (World Scientific Publishing Co. 2001) pp. 312-315 (2001)

Experimental and Theoretical Aspects of Proton Radioactivity: Proton Decay of Spherical and Deformed Nuclei

C. N. Davids

Proceedings of the NATO Advanced Study Institute: "Nuclei Far from Stability and Astrophysics", Predeal, Romania, August 28-September 3, 2000, NATO Science Series, eds. D. N. Poenaru, H. Rebel, and J. Wentz (IOS Press, Amsterdam and Kluwer Academic Publishers) Vol. 17, pp. 79-89 (2001)

Binary and Ternary Fission Yields of ^{252}Cf

J. K. Hwang, C. J. Beyer, A. V. Ramayya, J. H. Hamilton, G. M. Ter Akopian, A. V. Daniel, J. O. Rasmussen, S.-C. Wu, R. Donangelo, J. Kormicki, X. Q. Zhang, A. Rodin, A. Formichev, J. Kliman, L. Krupa, Yu. Ts. Oganessian, G. Chubaryan, D. Seweryniak, R. V. F. Janssens, W. C. Ma, R. B. Piercey, and J. D. Cole

Proceedings of the NATO Advanced Study Institute: "Nuclei Far From Stability and Astrophysics", Predeal, Romania, August 28-September 3, 2000, NATO Science Series, eds. D. N. Poenaru, H. Rebel, and J. Wentz (IOS Press, Amsterdam and Kluwer Academic Publishers 2001) Vol. 17, pp. 173-184

Results from the PHOBOS Experiment on Au + Au Collisions at RHIC

Krzysztof Wozniak (for the PHOBOS Collaboration)

From e^+e^- to Heavy Ion Collisions, Proceedings of the 30th International Symposium on Multiparticle Dynamics (ISMD2000), Tihany, Hungary, October 9-15, 2000, eds. Tamás Csörgö, Sándor Hegyi, and Wolfram Kittel (World Scientific Publishing Co., Singapore 2001), pp. 458-46

Coulomb Excitation of $^{124,126}\text{Xe}$ Studied with Segmented Germanium Detectors

W. F. Mueller, I. Wiedenhöver, J. A. Church, D. C. Dinca, T. Glasmacher, Z. Hu, P. A. Lofy, K. L. Miller, H. Olliver, B. C. Perry, B. T. Roeder, M. P. Carpenter, D. Henderson, R. V. F. Janssens, D. G. Jenkins, F. G. Kondev, C. J. Lister, T. Pennington, and A. Gade
April Meeting of the American Physical Society, Washington, DC, April 28-May 1, 2001;
Bull. Am. Phys. Soc. **46**, 36 (2001)

High-Spin States in ^{174}Pt

T. M. Goon, L. L. Riedinger, D. J. Hartley, M. Danchev, F. G. Kondev, M. P. Carpenter, R. V. F. Janssens, K. Abu Saleem, I. Ahmad, M. Alcorta, P. Bhattacharyya, L. T. Brown, J. Caggiano, C. N. Davids, S. M. Fischer, A. Heinz, R. A. Kaye, T. L. Khoo, T. Lauritsen, C. J. Lister, G. L. Poli, J. Ressler, D. Seweryniak, S. Siem, A. A. Sonzogni, J. Uusitalo, I. Wiedenhöver, H. Amro, W. C. Ma, P. G. Varmette, J. A. Cizewski, M. B. Smith, B. Herskind, and R. Nouicer
April Meeting of the American Physical Society, Washington, DC, April 28-May 1, 2001;
Bull. Am. Phys. Soc. **46**, 37 (2001)

Competition Between Terminating and Collective Structures Above Spin $40 \hbar$ in ^{154}Dy

W. C. Ma, J. R. Terry, R. K. Vadapalli, P. G. Varmette, J. W. Watson, J. P. Zhang, S. J. Zhu, T. L. Khoo, R. V. F. Janssens, T. Lauritsen, D. Nisius, I. Ragnarsson, C. T. Zhang, P. Bhattacharyya, P. J. Daly, Z. W. Gradowski, J. H. Hamilton, and A. V. Ramayya
April Meeting of the American Physical Society, Washington, DC, April 28-May 1, 2001;
Bull. Am. Phys. Soc. **46**, 38 (2001)

Anomalous Reduced Hindrance in ^{176}Hf

G. Mukherjee, P. Chowdhury, I. Shestakova, R. D'Alarcao, H. El-Masri, P. M. Walker, C. Wheldon, D. M. Cullen, D. L. Balabanski, M. Danchev, T. M. Goon, D. J. Hartley, L. L. Riedinger, O. Zeidan, M. A. Riley, R. Kaye, G. D. Dracoulis, G. Sletten, K. Abu Saleem, I. Ahmad, M. P. Carpenter, A. Heinz, R. V. F. Janssens, T. L. Khoo, F. G. Kondev, T. Lauritsen, C. J. Lister, D. Seweryniak, and I. Wiedenhöver
April Meeting of the American Physical Society, Washington, DC, April 28-May 1, 2001;
Bull. Am. Phys. Soc. **46**, 52 (2001)

New Four-Quasiparticle Excitations in ^{182}Hf

I. Shestakova, P. Chowdhury, R. D'Alarcao, G. Mukherjee, C. J. Pearson, Z. Podolyak, P. M. Walker, C. Wheldon, D. M. Cullen, I. Ahmad, M. P. Carpenter, R. V. F. Janssens, T. L. Khoo, F. G. Kondev, C. J. Lister, D. Seweryniak, and I. Wiedenhöver
April Meeting of the American Physical Society, Washington, DC, April 28-May 1, 2001;
Bull. Am. Phys. Soc. **46**, 53 (2001)

Nuclear Temperature of 8 GeV/c Negative Pion and Antiproton on Gold Reactions

A. Ruangma, R. Laforest, E. Martin, E. Ramakrishnan, D. J. Rowland, E. M. Winchester, S. J. Yennello, L. Beaulieu, W.-C. Hsi, K. Kwiatkowski, T. Lafort, V. E. Viola, L. Pienkowski, R. G. Korteling, H. Breuer, S. Gushue, L. P. Remsberg, and B. Back
April Meeting of the American Physical Society, Washington, DC, April 28-May 1, 2001;
Bull. Am. Phys. Soc. **46**, 161 (2001)

Study of the $^{29}\text{Si}(^3\text{He}, ^6\text{He})^{26}\text{Si}$ Reaction

Joseph Caggiano, William Bradfield-Smith, John Greene, Rachel Lewis, Peter Parker, Ernst Rehm, and Dale Visser

First Joint Meeting of the Nuclear Physics Divisions of APS and JPS, Wailea, Maui, HI, October 17-20, 2001; Bull. Am. Phys. Soc. **46**, 44 (2001)

Caloric Curve for 8 GeV/c Negative Pion and Antiproton on Gold Reactions

A. Ruangma, R. LaForest, E. Martin, E. Ramakrishnan, D. J. Rowland, E. M. Winchester, S. J. Yennello, L. Beaulieu, W. C. Hsi, K. Kwiatkowski, T. LaFort, V. E. Viola, L. Pienkowski, R. G. Korteling, H. Breuer, S. Gushue, L. P. Remsberg, B. Back, and A. Botvina

First Joint Meeting of the Nuclear Physics Divisions of APS and JPS, Wailea, Maui, HI, October 17-20, 2001; Bull. Am. Phys. Soc. **46**, 48 (2001)

Limits of the Energy-Spin Phase Space Beyond the Proton Drip Line

J. A. Cizewski, M. B. Smith, M. P. Carpenter, F. G. Kondev, T. L. Khoo, T. Lauritsen, R. V. F. Janssens, K. Abu Saleem, I. Ahmad, C. N. Davids, A. Heinz, C. J. Lister, G. L. Poli, J. J. Ressler, D. Seweryniak, I. Wiedenhöver, H. Amro, W. C. Ma, M. Danchev, D. J. Hartley, L. L. Riedinger, and W. Reviol

First Joint Meeting of the Nuclear Physics Divisions of APS and JPS, Wailea, Maui, HI, October 17-20, 2001; Bull. Am. Phys. Soc. **46**, 71 (2001)

New Proton Radioactivities and Spectroscopy Using Proton Decay Tagging

D. Seweryniak

First Joint Meeting of the Nuclear Physics Divisions of APS and JPS, Wailea, Maui, HI, October 17-20, 2001; Bull. Am. Phys. Soc. **46**, 72 (2001)

Physics Along the $N = Z$ Line: Spectroscopy of Odd-Odd and Even-Even Nuclei from ^{56}Ni to ^{100}Sn

C. J. Lister

First Joint Meeting of the Nuclear Physics Divisions of APS and JPS, Wailea, Maui, HI, October 17-20, 2001; Bull. Am. Phys. Soc. **46**, 72 (2001)

Superdeformation in the Doubly Magic Nucleus $^{40}_{20}\text{Ca}_{20}$

E. Ideguchi, D. G. Sarantites, W. Reviol, M. Devlin, F. Lerma, J. N. Wilson, C. Baktash, A. Galindo-Uribarri, A. V. Afanasjev, D. Rudolph, D. R. LaFosse, M. P. Carpenter, R. V. F. Janssens, T. Lauritsen, C. J. Lister, P. Reiter, D. Seweryniak, A. Axelsson, and M. Weiszflog

First Joint Meeting of the Nuclear Physics Divisions of APS and JPS, Wailea, Maui, HI, October 17-20, 2001; Bull. Am. Phys. Soc. **46**, 90 (2001)

A Recoil-Gated Plunger Lifetime Measurement of ^{188}Pb with Gammasphere and the FMA

A. M. Oros-Peusquens, A. Dewald, R. Peusquens, P. Petkov, B. Saha, P. Von Brentano, I. Wiedenhöver, M. Carpenter, A. Heinz, R. V. F. Janssens, F. Kondev, D. Seweryniak, Kh. Abu Salem, J. R. Cooper, C. J. Barton, R. Krucken, U. Garg, S. Zhu, and P. F. Mantica

First Joint Meeting of the Nuclear Physics Divisions of APS and JPS, Wailea, Maui, HI, October 17-20, 2001; Bull. Am. Phys. Soc. **46**, 94 (2001)

Development of a High Resolution, Position-Sensitive Germanium Detector

J. Amann, S. M. Fischer, C. J. Lister, D. Jenkins, T. Sienko, and P. Sangsingkeow
First Joint Meeting of the Nuclear Physics Divisions of APS and JPS, Wailea, Maui, HI,
October 17-20, 2001; Bull. Am. Phys. Soc. **46**, 96 (2001)

Calculations of Target Wheel Damage Under Intense Beams for Super-Heavy Element Production

R. Gabor, J. P. Greene, and A. Heinz
First Joint Meeting of the Nuclear Physics Divisions of APS and JPS, Wailea, Maui, HI,
October 17-20, 2001; Bull. Am. Phys. Soc. **46**, 100 (2001)

Canadian Penning Trap Mass Spectrometer

M. Froese, K. S. Sharma, J. A. Clark, R. C. Barber, J. Vaz, J. C. Wang, F. Buchinger, J. E. Crawford, S. Gulick, R. B. Moore, J. K. P. Lee, A. Heinz, J. Schwartz, D. Seweryniak, and G. Sprouse
First Joint Meeting of the Nuclear Physics Divisions of APS and JPS, Wailea, Maui, HI,
October 17-20, 2001; Bull. Am. Phys. Soc. **46**, 100 (2001)

Reaction Rates for the $^{22}\text{Na}(p,\gamma)$ and $^{22}\text{Ne}(p,\gamma)$ Breakout Reactions

B. Truett, R. Kaye, K. Lister, and D. Jenkins
First Joint Meeting of the Nuclear Physics Divisions of APS and JPS, Wailea, Maui, HI,
October 17-20, 2001; Bull. Am. Phys. Soc. **46**, 107 (2001)

Beta-Decay of ^{109}Te

J. J. Ressler, W. B. Walters, J. Shergur, C. N. Davids, A. Heinz, and D. Seweryniak
First Joint Meeting of the Nuclear Physics Divisions of APS and JPS, Wailea, Maui, HI,
October 17-20, 2001; Bull. Am. Phys. Soc. **46**, 141 (2001)

Spectroscopy of the $T = 1$ Band in the $N = Z$ Nucleus ^{46}V

P. E. Garrett, R. W. Bauer, J. A. Becker, L. A. Bernstein, W. Younes, D. Appelbe, J. A. Cameron, M. Carpenter, R. V. F. Janssens, C. J. Lister, D. Seweryniak, D. D. Warner, and E. Tavukcu
First Joint Meeting of the Nuclear Physics Divisions of APS and JPS, Wailea, Maui, HI,
October 17-20, 2001; Bull. Am. Phys. Soc. **46**, 141 (2001)

Energy Dissipation in Heavy-Ion Reactions

Birger B. Back
221st ACS National Meeting, San Diego, CA, April 1-5, 2001, Book of Abstracts, 82 (2001)

Explosive Nucleosynthesis Studied with Radioactive Beams - Present Status and Future Plans

K. E. Rehm
221st ACS National Meeting, San Diego, CA, April 1-5, 2001, Book of Abstracts, 98 (2001)

The Structure of High-Z Nuclei from Studies with Gammasphere at ATLAS

R. V. F. Janssens

221st ACS National Meeting, San Diego, CA, April 1-5, 2001, Book of Abstracts, 187 (2001)

Levels in the N = 153 Nucleus $^{151}_{98}\text{Cf}$

I. Ahmad

221st ACS National Meeting, San Diego, CA, April 1-5, 2001, Book of Abstracts, 189 (2001)

Two- and Three-Valence-Particle Nuclei ^{134}Sb and ^{135}Sb

P. J. Daly, C. T. Zhang, Z. W. Grabowski, B. Fornal, R. Broda, D. Seweryniak, I. Ahmad, I. Wiedenhöver, M. P. Carpenter, R. V. F. Janssens, T. L. Khoo, T. Lauritsen, C. J. Lister, P. Reiter, and J. Blomqvist

221st ACS National Meeting, San Diego, CA, April 1-5, 2001, Book of Abstracts, 190 (2001)

Single-Particle Structure of Light Sn Nuclei

J. J. Ressler, W. B. Walters, D. Seweryniak, J. Shergur, and A. Heinz

221st ACS National Meeting, San Diego, CA, April 1-5, 2001, Book of Abstracts, 192 (2001)

Status of the ANL Ion Guide and Gas Cooler System

C. Boudreau, F. Buchinger, J. Caggiano, J. Clark, J. E. Crawford, S. Gulick, A. Heinz, J. K. P. Lee, R. B. Moore, D. Seweryniak, K. S. Sharma, J. Vaz, J. Wang, and G. D. Sprouse

222nd ACS National Meeting, Chicago, IL, August 26-30, 2001, Book of Abstracts, 31 (2001)

Gas Cell-Ion Guide System for Laser Spectroscopy at McGill

F. Buchinger, J. Crawford, S. Gulick, J. Lee, A. Hamilton, R. Moir, A. Cassidy, S. Gliga, C. F. Liang, G. Savard, and S. Rastikerdar

222nd ACS National Meeting, Chicago, IL, August 26-30, 2001, Book of Abstracts, 48 (2001)

Limits on the X-Ray Induced Decay of the 31-yr Isomer of ^{178}Hf

Robert S. Rundberg, Irshad Ahmad, John A. Becker, Joseph C. Banar, Donald S. Gemmell, Andreas Kraemer, Ali Mashayekhi, Dennis P. McNabb, Geoffrey G. Miller, Eugene F. Moore, Laurence N. Pangualt, John P. Schiffer, Sarvjit D. Shastri, Tzu F. Wang, and Jeremy B. Wilhelmy

222nd ACS National Meeting, Chicago, IL, August 26-30, 2001, Book of Abstracts, 178 (2001)

Mass Measurements of Proton-Rich Nuclides Using the Canadian Penning Trap Mass Spectrometer

J. A. Clark, R. C. Barber, C. Boudreau, F. Buchinger, J. A. Caggiano, J. E. Crawford, H. Fukutani, S. Gulick, J. C. Hardy, A. Heinz, J. K. P. Lee, M. Maier, R. B. Moore, G. Savard, J. Schwartz, D. Seweryniak, K. S. Sharma, G. Sprouse, J. Vaz, and J. C. Wang
3rd International Conference on Exotic Nuclei and Atomic Masses (ENAM2001),
Hämeenlinna, Finland, July 2-7, 2001, Book of Abstracts, p. A2-5 (2001)

New Results in Proton Radioactivity at Argonne National Laboratory

C. N. Davids, P. J. Woods, H. Mahmud, T. Davinson, H. Esbensen, A. Heinz, G. L. Poli, J. J. Ressler, K. Schmidt, D. Seweryniak, M. B. Smith, A. A. Sonzogni, J. Uusitalo, and W. B. Walters
3rd International Conference on Exotic Nuclei and Atomic Masses (ENAM2001),
Hämeenlinna, Finland, July 2-7, 2001, Book of Abstracts, p. D-3 (2001)

New Insights Into Neutron Rich Nuclei at High Spin

J. H. Hamilton, A. V. Ramayya, X. Q. Zhang, S. J. Zhu, E. F. Jones, J. K. Hwang, X. Y. Luo, J. O. Rasmussen, P. M. Gore, T. N. Ginter, I. Y. Lee, R. V. F. Janssens, I. Ahmad, J. D. Cole, G. M. Ter-Akopian, and Yu. Ts. Oganessian
3rd International Conference on Exotic Nuclei and Atomic Masses (ENAM2001),
Hämeenlinna, Finland, July 2-7, 2001, Book of Abstracts, p. H2-5 (2001)

The Neutron and Proton Two-Particle Nucleus ^{134}Sb : Low Spin States Observed in the Decay of ^{134}Sn

A. Korgul, H. Mach, B. Fogelberg, W. Urban, W. Kurcewics, T. Rzaca-Urban, P. Hoff, H. Gausemel, J. Galy, J. L. Durell, W. R. Phillips, A. G. Smith, B. J. Varley, N. Schulz, I. Ahmad, L. R. Morss, M. Gorska, V. I. Isakov, K. I. Erokhina, J. Blomqvist, F. Andreozzi, L. Coraggio, A. Covello, and A. Gargano
3rd International Conference on Exotic Nuclei and Atomic Masses (ENAM2001),
Hämeenlinna, Finland, July 2-7, 2001, Book of Abstracts, p. H2-6 (2001)

Nuclear Structure in the Nobelium Region

R.-D. Herzberg, N. Amzal, P. A. Butler, A. J. C. Chewter, N. Hammond, R. D. Humphreys, G. D. Jones, R. D. Page, T. Page, J. E. Bastin, C. Scholey, O. Stezowski, T. Enqvist, P. T. Greenlees, P. M. Jones, R. Julin, S. Juutinen, H. Kankaanpää, A. Keenan, H. Kettunen, P. Kuusiniemi, M. Leino, A. P. Leppänen, M. Muikku, P. Nieminen, P. Rahkila, J. Uusitalo, J. Gerl, F. Heßberger, I. Kozhoukharov, Ch. Schlegel, H. J. Wollersheim, K. Helariutta, W. Korten, F. Becker, E. Bouchez, Y. Le Coz, K. Hauschild, A. Hürstel, R. Lucas, M. Rejmund, Ch. Theisen, P. Reiter, T. L. Khoo, C. J. Lister, and K. Eskola
3rd International Conference on Exotic Nuclei and Atomic Masses (ENAM2001),
Hämeenlinna, Finland, July 2-7, 2001, Book of Abstracts, p. I-5 (2001)

Isospin Mixing and Non-Analog β -Decay of ^{74}Rb

E. F. Zhanjar, A. Piechaczek, G. C. Ball, P. Bricault, J. A. Macdonald, J. D'Auria, H.-B. Mak, J. R. Leslie, I. S. Towner, M. Lipoglavsek, G. Savard, V. Iacob, J. C. Hardy, J. L. Wood, D. Kulp, and D. M. Moltz

3rd International Conference on Exotic Nuclei and Atomic Masses (ENAM2001), Hämeenlinna, Finland, July 2-7, 2001, Book of Abstracts, p. J-3 (2001)

Shape Co-Existence, T = 0, 1 Bands and n-p Correlations in the Mass 70 Region

N. S. Kelsall, D. G. Jenkins, A. Afanasjev, D. P. Balamuth, M. Carpenter, R. M. Clark, P. Fallon, S. Fischer, S. Frauendorf, R. V. F. Janssens, C. J. Lister, A. O. Macchiavelli, I. Ragnarsson, I. Rikovska-Stone, D. G. Sarantites, D. Seweryniak, T. A. Sienko, C. E. Svensson, R. Wadsworth, A. N. Wilson, and R. Wyss

3rd International Conference on Exotic Nuclei and Atomic Masses (ENAM2001), Hämeenlinna, Finland, July 2-7, 2001, Book of Abstracts, p. PH-28 (2001)

Rotational Bands in the Proton Emitters ^{131}Eu and ^{141}Ho

D. Seweryniak, P. J. Woods, J. J. Ressler, C. N. Davids, A. Heinz, A. A. Sonzogni, J. Uusitalo, W. B. Walters, J. A. Caggiano, M. P. Carpenter, J. A. Cizewski, T. Davinson, K. Y. Ding, N. Fotiades, U. Garg, R. V. F. Janssens, T. L. Khoo, F. G. Kondev, T. Lauritsen, C. J. Lister, P. Reiter, J. Shergur, and I. Wiedenhöver

3rd International Conference on Exotic Nuclei and Atomic Masses (ENAM2001), Hämeenlinna, Finland, July 2-7, 2001, Book of Abstracts, p. PH-33 (2001)

A Recoil-Gated Plunger Lifetime Measurement of ^{188}Pb with Gammasphere and the FMA

A. M. Oros-Peusquens, A. Dewald, R. Peusquens, P. Petkov, B. Saha, P. von Brentano, I. Wiedenhöver, M. Carpenter, A. Heinz, R. V. F. Janssens, F. Kondev, C. J. Lister, D. Seweryniak, Kh. Abu Saleem, J. R. Cooper, C. J. Barton, R. Krücken, K. Zyromski, C. W. Beausang, Z. Wang, U. Garg, S. Zhu, and P. F. Mantica

3rd International Conference on Exotic Nuclei and Atomic Masses (ENAM2001), Hämeenlinna, Finland, July 2-7, 2001, Book of Abstracts, p. PH-24 (2001)

β -Decay Studies of Light Odd-Mass Sb and Te Nuclides

J. J. Ressler, W. B. Walters, J. Shergur, D. Seweryniak, A. Heinz, and C. Davids

3rd International Conference on Exotic Nuclei and Atomic Masses (ENAM2001), Hämeenlinna, Finland, July 2-7, 2001, Book of Abstracts, p. PH-36 (2001)

Selective Ionization of $^{135-137}\text{Sn}$ Using a Laser-Ion Source

J. Shergur, W. B. Walters, K. L. Kratz, B. Pfeiffer, A. Woehr, D. Seweryniak, M. Hannawald, V. Fedoseyev, V. Mishin, H. Fynbo, P. Hoff, U. Koester, H. Mach, T. Nilsson, J. J. Ressler, K. Rolander, H. Simon, B. A. Brown, A. Bickley, and the ISOLDE Collaboration

3rd International Conference on Exotic Nuclei and Atomic Masses (ENAM2001), Hämeenlinna, Finland, July 2-7, 2001, Book of Abstracts, p. PL-16 (2001)

Recoil-Isomer Tagging Techniques at RITU

C. Scholey, E. S. Paul, P. A. Butler, C. Fox, A. J. C. Chewter, R.-D. Herzberg, R. D. Humphreys, G. D. Jones, R. D. Page, T. Page, J. E. Bastin, A. J. Boston, H. L. Scraggs, D. M. Cullen, A. M. Bruce, P. M. Walker, M. Caamaño, J. Garcés-Narro, M. A. Bentley, D. T. Joss, T. Enqvist, P. T. Greenlees, P. M. Jones, R. Julin, S. Juutinen, H. Kankaanpää, H. Kettunen, P. Kuusiniemi, M. Leino, A. P. Leppänen, M. Muikku, P. Nieminen, J. Pakarinen, P. Rahkila, J. Uusitalo, J. Gerl, I. Kozhoukharov, Ch. Schlegel, Y. Le Coz, Ch. Theism, T. L. Khoo, K. Eskola, and K. Helariutta
3rd International Conference on Exotic Nuclei and Atomic Masses (ENAM2001),
Hämeenlinna, Finland, July 2-7, 2001, Book of Abstracts, p. PL-23 (2001)

Latent Heat and Shell Structure in Simulations of Ion Clusters

John Schiffer

2001 Workshop on Non-Neutral Plasmas, San Diego, CA, July 30-August 2, 2001,
Conference Program p. TUE-011 (2001)

Structure and Formation Mechanism of Heavy Shell-Stabilized Nobelium Nuclei

P. Reiter, T. L. Khoo, T. Lauritsen, C. J. Lister, D. Seweryniak, A. A. Sonzogni, I. Ahmad, N. Amzal, P. Bhattacharyya, P. A. Butler, M. P. Carpenter, A. J. Chewter, J. A. Cizewski, C. N. Davids, K. Y. Ding, N. Fotiades, J. P. Greene, P. T. Greenlees, A. Heinz, R.-D. Herzberg, R. V. F. Janssens, G. D. Jones, F. G. Kondev, W. Korten, M. Leino, S. Siem, J. Uusitalo, K. Vetter, and I. Wiedenhöver
International Nuclear Physics Conference on Nuclear Physics in the 21st Century
(INPC2001), Berkeley, CA, July 30-August 3, 2001, Book of Abstracts, p. 111 (2001)

Breakup Time Scale Studied in the 8 GeV/c Pion Induced Reaction with Au

L. Pienkowski, K. Kwiatkowski, T. Lefort, W.-C. Hsi, L. Beaulieu, V. E. Viola, A. Botvina, B. Back, H. Breuer, S. Gushue, L. P. Remsberg, R. G. Korteling, R. Laforest, E. Martin, E. Ramakrishnan, D. Rowland, A. Ruangma, E. Winchester, and S. J. Yennello
International Nuclear Physics Conference on Nuclear Physics in the 21st Century
(INPC2001), Berkeley, CA, July 30-August 3, 2001, Book of Abstracts, p. 209 (2001)

Test of the Predictive Power of Additivity of Quadrupole Moments in $A \sim 150$ Superdeformed Bands

S. T. Clark, G. Hackman, S. N. Floor, J. Norris, S. J. Sanders, R. M. Clark, P. Fallon, G. J. Lane, A. O. Macchiavelli, C. E. Svensson, and R. V. F. Janssens
International Nuclear Physics Conference on Nuclear Physics in the 21st Century
(INPC2001), Berkeley, CA, July 30-August 3, 2001, Book of Abstracts, p. 232 (2001)

Entry Distributions of ^{220}Th – A Method to Determine the Fission Barrier of an Unstable Nucleus

A. Heinz, T. L. Khoo, P. Reiter, I. Ahmad, P. Bhattacharyya, J. Caggiano, M. P. Carpenter, J. A. Cizewski, C. N. Davids, W. F. Henning, R. V. F. Janssens, G. D. Jones, R. Julin, F. G. Kondev, T. Lauritsen, C. J. Lister, D. Seweryniak, S. Siem, A. A. Sonzogni, J. Uusitalo, and I. Wiedenhöver

International Nuclear Physics Conference on Nuclear Physics in the 21st Century (INPC2001), Berkeley, CA, July 30-August 3, 2001, Book of Abstracts, p. 270 (2001)

Search for Anomalous Backward Angle Scattering $\alpha + ^{44}\text{Ti}$

K. E. Rehm, I. Ahmad, J. Caggiano, P. Collon, J. P. Greene, A. Heinz, R. V. F. Janssens, C. L. Jiang, R. C. Pardo, M. Paul, J. P. Schiffer, R. H. Siemssen, A. H. Wuosmaa, and G. P. Zinkann

International Nuclear Physics Conference on Nuclear Physics in the 21st Century (INPC2001), Berkeley, CA, July 30-August 3, 2001, Book of Abstracts, p. 339 (2001)

A New Determination of the Efficiency Curve for Gammasphere Using ^{252}Cf Source

J. K. Hwang, A. V. Ramayya, J. H. Hamilton, C. J. Beyer, J. O. Rasmussen, Y. X. Luo, S. C. Wu, T. N. Ginter, C. Folden III, P. Fallon, P. Zielinski, K. E. Gregorich, A. O. Macchiavelli, M. Stoyer, S. J. Asztalos, R. V. F. Janssens, I. Ahmad, and J. P. Greene

International Nuclear Physics Conference on Nuclear Physics in the 21st Century (INPC2001), Berkeley, CA, July 30-August 3, 2001, Book of Abstracts, p. 441 (2001)

High-Spin States in ^{38}Ar

R. A. E. Austin, D. E. Appelbe, G. C. Ball, M. P. Carpenter, R. M. Clark, M. Cromaz, R. V. F. Janssens, A. O. Macchiavelli, D. G. Sarantites, C. E. Svensson, and J. C. Waddington

International Nuclear Physics Conference on Nuclear Physics in the 21st Century (INPC2001), Berkeley, CA, July 30-August 3, 2001, Book of Abstracts, p. 546 (2001)

Particle States in ^{131}Sb and $\pi 7/2[413]$ Rotational Band in ^{115}Ag

J. K. Hwang, A. V. Ramayya, J. H. Hamilton, C. J. Beyer, J. O. Rasmussen, Y. X. Luo, S. C. Wu, T. N. Ginter, C. Folden III, P. Fallon, P. Zielinski, K. E. Gregorich, A. O. Macchiavelli, M. Stoyer, S. J. Asztalos, R. V. F. Janssens, I. Ahmad, and J. P. Greene

International Nuclear Physics Conference on Nuclear Physics in the 21st Century (INPC2001), Berkeley, CA, July 30-August 3, 2001, Book of Abstracts, p. 591 (2001)

Low-Energy Coulomb Excitation of the Stable and Unstable Nuclear Beams

W. F. Mueller, I. Wiedenhöver, J. A. Church, D. C. Dinca, J. Enders, T. Glasmacher, Z. Hu, K. L. Miller, H. Olliver, B. C. Perry, B. T. Roeder, M. P. Carpenter, C. N. Davids, D. Henderson, R. V. F. Janssens, C. J. Lister, T. Pennington, D. Seweryniak, L. A. Bernstein, and A. Gade

International Nuclear Physics Conference on Nuclear Physics in the 21st Century (INPC2001), Berkeley, CA, July 30-August 3, 2001, Book of Abstracts, p. 626 (2001)

New Evidence for K-Hindered Decay of a 6-qp Isomer in ^{176}Hf

G. Mukherjee, P. Chowdhury, I. Shestakova, R. D'Alarcao, K. Abu Saleem, I. Ahmad, M. P. Carpenter, A. Heinz, R. V. F. Janssens, T. L. Khoo, F. G. Kondev, T. Lauritsen, C. J. Lister, D. Seweryniak, I. Wiedenhöver, H. El-Masri, P. M. Walker, D. M. Cullen, C. Wheldon, D. L. Balabanski, M. Danchev, T. M. Goon, D. J. Hartley, L. L. Riedinger, O. Zeidan, M. A. Riley, R. Kaye, G. Sletten, and G. D. Dracoulis

International Nuclear Physics Conference on Nuclear Physics in the 21st Century (INPC2001), Berkeley, CA, July 30-August 3, 2001, Book of Abstracts, p. 627 (2001)

Yrast Excitations in Doubly-Magic ^{132}Sn and Its One-Neutron-Hole Neighbor ^{131}Sn

S. K. Saha, P. Bhattacharyya, P. J. Daly, C. T. Zhang, Z. W. Grabowski, R. Broda, B. Fornal, I. Ahmad, D. Seweryniak, I. Wiedenhöver, M. P. Carpenter, R. V. F. Janssens, T. L. Khoo, T. Lauritsen, C. J. Lister, P. Reiter, and J. Blomqvist

International Nuclear Physics Conference on Nuclear Physics in the 21st Century (INPC2001), Berkeley, CA, July 30-August 3, 2001, Book of Abstracts, p. 648 (2001)

New Four-Quasiparticle K-Isomers in Neutron-Rich ^{182}Hf

I. Shestakova, P. Chowdhury, R. D'Alarcao, G. Mukherjee, C. J. Pearson, Zs. Podolyak, P. M. Walker, C. Wheldon, D. M. Cullen, I. Ahmad, M. P. Carpenter, R. V. F. Janssens, T. L. Khoo, F. G. Kondev, C. J. Lister, D. Seweryniak, and I. Wiedenhöver

International Nuclear Physics Conference on Nuclear Physics in the 21st Century (INPC2001), Berkeley, CA, July 30-August 3, 2001, Book of Abstracts, p. 655 (2001)

Experimental Test of the Isospin Mixing Correction in the Superallowed 0^+ to 0^+ Beta Decay of ^{74}Rb via Conversion Electron Spectroscopy

A. Piechaczek, E. F. Zganjar, G. C. Ball, P. Bricault, J. A. Macdonald, J. D'Auria, H. B. Mak, J. R. Leslie, M. Lipoglavsek, G. Savard, V. Iacob, J. C. Hardy, J. L. Wood, D. Kulp, D. M. Moltz, and J. Cerny

International Nuclear Physics Conference on Nuclear Physics in the 21st Century (INPC2001), Berkeley, CA, July 30-August 3, 2001, Book of Abstracts, p. 702 (2001)

Testing the Isobaric Multiplet Mass Equation at High Spin

P. E. Garrett, W. E. Ormand, R. W. Bauer, J. A. Becker, L. A. Bernstein, M. Carpenter, R. V. F. Janssens, C. J. Lister, D. Seweryniak, D. Appelbe, J. A. Cameron, D. D. Warner, and E. Tavukcu

International Nuclear Physics Conference on Nuclear Physics in the 21st Century (INPC2001), Berkeley, CA, July 30-August 3, 2001, Book of Abstracts, p. 730 (2001)

Limits of the Energy-Spin Phase Space at the Proton Drip Line

M. B. Smith, J. A. Cizewski, M. P. Carpenter, F. G. Kondev, R. V. F. Janssens, T. L. Khoo, K. Abu Saleem, I. Ahmad, H. Amro, M. Danchev, C. N. Davids, D. J. Hartley, A. Heinz, T. Lauritsen, C. J. Lister, W. C. Ma, G. L. Poli, J. J. Ressler, W. Reviol, L. L. Riedinger, D. Seweryniak, and I. Wiedenhöver

International Nuclear Physics Conference on Nuclear Physics in the 21st Century (INPC2001), Berkeley, CA, July 30-August 3, 2001, Book of Abstracts, p. 774 (2001)

Recent Experimental and Theoretical Results on Proton Radioactivity

C. N. Davids

Yukawa International Seminar on “Physics of Unstable Nuclei” (YKIS01), Kyoto, Japan,
November 5-10, 2001, Book of Abstracts, p. 51 (2001)

Studies of Excited States in Proton Emitters

Dariusz Seweryniak

221st ACS National Meeting, San Diego, CA, April 1-5, 2001, Book of Abstracts, 140
(2001)

Proton Radioactivity – New Theoretical Results

C. N. Davids and H. Esbensen

221st ACS National Meeting, San Diego, CA, April 1-5, 2001, Book of Abstracts, 138
(2001)

Hot States in Exotic Minima

T. L. Khoo

3rd International Conference on Exotic Nuclei and Atomic Masses (ENAM2001),
Hämeenlinna, Finland, July 2-7, 2001, Book of Abstracts, p. H3-2 (2001)

**OPERATION AND DEVELOPMENT OF ATLAS
and
R & D RELATED TO A FUTURE ADVANCED EXOTIC BEAM FACILITY**

Simultaneous Acceleration of Multiply-Charged Ions Through a Superconducting Linac

P. N. Ostroumov, R. C. Pardo, G. P. Zinkann, K. W. Shepard, and J. A. Nolen

Phys. Rev. Lett. **86**, 2798-2801 (2001)

Heavy-Ion Beam Acceleration of Two-Charge States from an ECR Ion Source

P. N. Ostroumov, K. W. Shepard, V. N. Aseev, and A. A. Kolomiets

Proceedings of the XX International Linac Conference, Monterey, CA, August 21-25, 2000,
eds. A. W. Chao, S. S. L. Yu, and R. D. Ruth, pp. 202-204 (2001)

Multiple Charge State Beam Acceleration at ATLAS

P. N. Ostroumov, R. C. Pardo, G. P. Zinkann, K. W. Shepard, and J. A. Nolen

Proceedings of the XX International Linac Conference, Monterey, CA, August 21-25, 2000,
eds. A. W. Chao, S. S. L. Yu, and R. D. Ruth, pp. 205-207 (2001)

Superconducting Accelerating Structures for a Multi-Beam Driver Linac for RIA

K. W. Shepard and T. E. Tretyakova

Proceedings of the XX International Linac Conference, Monterey, CA, August 21-25, 2000,
eds. A. W. Chao, S. S. L. Yu, and R. D. Ruth, pp. 920-922 (2001)

Multiple-Charge Beam Dynamics in an Ion Linac

P. N. Ostroumov, J. A. Nolen, and K. W. Shepard

Proceedings of the XX International Linac Conference, Monterey, CA, August 21-25, 2000
eds. A. W. Chao, S. S. L. Yu, and R. D. Ruth, pp. 1018-1022 (2001)

Argonne National Laboratory ATLAS Accelerator Tune Archiving System

F. Munson and D. Quock

Proceedings of the 3rd International Workshop on Personal Computers and Particle
Accelerator Controls (PCaPAC 2000), Hamburg, Germany, October 9-12, 2000 (2001)

Optimization of Isotope-Separator-On-Line Targets Based on Monte-Carlo Simulations of Ion
Release Curves

Brahim Mustapha and Jerry Nolen

April Meeting of the American Physical Society, Washington, DC, April 28-May 1, 2001;
Bull. Am. Phys. Soc. **46**, 162 (2001)

Liquid Lithium for High Power Density Fragmentation Targets

J. A. Nolen, C. B. Reed, A. Hassanein, D. J. Morrissey, J. H. Ottarson, and B. M. Sherrill

First Joint Meeting of the Nuclear Physics Divisions of APS and JPS, Wailea, Maui, HI,
October 17-20, 2001; Bull. Am. Phys. Soc. **46**, 17 (2001)

Stopping of Fast Radioactive Ions in a Gas Catcher System

Guy Savard

First Joint Meeting of the Nuclear Physics Divisions of APS and JPS, Wailea, Maui, HI, October 17-20, 2001; Bull. Am. Phys. Soc. **46**, 18 (2001)

Calculations of Range Straggling of High Energy Heavy Ions in Helium Gas Following Lead Absorbers

J. Neubauer, J. Greene, J. A. Nolen, and G. Savard

First Joint Meeting of the Nuclear Physics Divisions of APS and JPS, Wailea, Maui, HI, October 17-20, 2001; Bull. Am. Phys. Soc. **46**, 109 (2001)

Development of a Gas-Catcher System to Stop Relativistic Ions at GSI

Guy Savard, Christoph Scheidenberger, Peter Dendooven, Piet Van Duppen, S. Elisseev, T. Faestermann, H. Geissel, M. Hausmann, M. Hellstroem, C. L. Jiang, E. Kaza, B. Kindler, Yu Litvinov, B. Lommel, M. Maier, D. Morrissey, C. Muenzenberg, B. Mustapha, J. A. Nolen, T. Ohtsubo, B. Sherrill, V. Shishkin, G. D. Sprouse, K. Suemmerer, I. Tanihata, M. Wada, H. Weick, M. Weidenmueller, and B. Zabransky

222nd ACS National Meeting, Chicago, IL, August 26-30, 2001, Book of Abstracts, 67 (2001)

Argonne National Laboratory ATLAS Accelerator Tune Archiving System

Floyd H. Munson and Deborah E. R. Quock

3rd International Workshop on Personal Computers and Particle Accelerator Controls (PCaPAC 2000), Hamburg, Germany, October 9-12, 2000, Abstract ID No. 65 (2001)

Evaluation and Testing of a Low- β Spoke Resonator

Frank Krawczyk, Dominic Chan, Robert Gentzlinger, Richard LaFave, Mike Madrid, Debbie Montoya, Dale Schrage, Alan Shapiro, Tsuyoshi Tajima, and Ken Shepard

2001 Particle Accelerator Conference (PAC2001), Chicago, IL, June 18-22, 2001, Book of Abstracts, MPPH057, p. 21 (2001)

Cold Tests of a Spoke Cavity Prototype for RIA

Michael Kelly, Mark Kedzie, and Kenneth Shepard

2001 Particle Accelerator Conference (PAC2001), Chicago, IL, June 18-22, 2001, Book of Abstracts, MPPH117, p. 31 (2001)

Superconducting Intermediate-Velocity Drift-Tube Cavities for the RIA Drive Linac

Kenneth Shepard, Mark Kedzie, and Michael Kelly

2001 Particle Accelerator Conference (PAC2001), Chicago, IL, June 18-22, 2001, Book of Abstracts, MPPH119, p. 31 (2001)

Coupling RF Power into the Low-Beta Superconducting Cavities of the RIA Driver Linac

Brian Rusnak and Kenneth Shepard

2001 Particle Accelerator Conference (PAC2001), Chicago, IL, June 18-22, 2001, Book of Abstracts, MPPH146, p. 35 (2001)

Singly-Charged Heavy-Ion Beam Studies on 12 MHz RFQ

Michael Kelly, Benny Clifft, Mark Kedzie, Peter Ostroumov, and Kenneth Shepard

2001 Particle Accelerator Conference (PAC2001), Chicago, IL, June 18-22, 2001, Book of Abstracts, ROAAO11, p. 177 (2001)

Design of a Magnetic Optical System for Transport and Matching of Multiple-Charge-State Heavy-Ion Beams

Mauricio Portillo, Vladislav N. Aseev, Jerry A. Nolen, Jr., and Peter N. Ostroumov

2001 Particle Accelerator Conference (PAC2001), Chicago, IL, June 18-22, 2001, Book of Abstracts, RPAH072, p. 192

Design Layout of an Isobar Separator Based on 5th Order Calculations

Mauricio Portillo, Teresa A. Barlow, and Jerry A. Nolen, Jr.

2001 Particle Accelerator Conference (PAC2001), Chicago, IL, June 18-22, 2001, Book of Abstracts, RPAH073, p. 192 (2001)

New Concept for Acceleration of Slow, Low-Charge-State Heavy Ion Beams

Peter Ostroumov and Andrei Kolomiets

2001 Particle Accelerator Conference (PAC2001), Chicago, IL, June 18-22, 2001, Book of Abstracts, FPAH313, p. 276 (2001)

The US RIA Project

Guy Savard

2001 Particle Accelerator Conference (PAC2001), Chicago, IL, June 18-22, 2001, Book of Abstracts, ROPA002, p. 206 (2001)

Design of a Post Accelerator for Rare Isotope Accelerator Facility

Peter Ostroumov, Jerry Nolen, Richard Pardo, Kenneth Shepard, and Andrei Kolomiets

2001 Particle Accelerator Conference (PAC2001), Chicago, IL, June 18-22, 2001, Book of Abstracts, FPAH314, p. 276 (2001)

MEDIUM-ENERGY NUCLEAR PHYSICS RESEARCH

- Evidence for a Three-Nucleon-Force Effect in Proton-Deuteron Elastic Scattering
R. V. Cadman, J. Brack, W. J. Cummings, J. A. Fedchak, B. D. Fox, H. Gao, W. Glöckle, J. Golak, C. Grosshauser, R. J. Holt, C. E. Jones, H. Kamada, E. R. Kinney, M. A. Miller, W. Nagengast, A. Nogga, B. R. Owen, K. Rith, F. Schmidt, E. C. Schulte, J. Sowinski, F. Sperisen, E. L. Thorsland, R. Tobey, J. Wilbert, and H. Witala
Phys. Rev. Lett. **86**, 967-970 (2001)
- Measurement of the Charged Pion Electromagnetic Form Factor
J. Volmer *et al.* and the Jefferson Lab F_π Collaboration
Phys. Rev. Lett. **86**, 1713-1716 (2001)
- Observation of Polarization in Bottomonium Production at $\sqrt{s} = 38.8$ GeV
C. N. Brown *et al.* (FNAL E866/NuSea Collaboration)
Phys. Rev. Lett. **86**, 2529-2532 (2001)
- Polarization Measurements in High-Energy Deuteron Photodisintegration
K. Wijesooriya *et al.* (Jefferson Lab Hall A Collaboration)
Phys. Rev. Lett. **86**, 2975-2979 (2001)
- Measurement of the High Energy Two-Body Deuteron Photodisintegration Differential Cross Section
E. C. Schulte *et al.*
Phys. Rev. Lett. **87**, 102302/1-4 (2001)
- Measurement of the Beam-Spin Azimuthal Asymmetry Associated with Deeply-Virtual Compton Scattering
A. Airapetian *et al.* (for the HERMES Collaboration)
Phys. Rev. Lett. **87**, 182001/1-5 (2001)
- Longitudinal Electroproduction of Charged Pions from ^1H , ^2H , and ^3He
D. Gaskell *et al.*
Phys. Rev. Lett. **87**, 202301/1-5 (2001)
- Double-Spin Asymmetry in the Cross Section for Exclusive ρ^0 Production in Lepton-Proton Scattering
A. Airapetian *et al.*
Phys. Lett. **B513**, 301-310 (2001)
- Systematics of Midrapidity Transverse Energy Distributions in Limited Apertures from $p + \text{Be}$ to $\text{Au} + \text{Au}$ Collisions at Relativistic Energies
T. Abbott *et al.* (E-802 Collaboration)
Phys. Rev. C **63**, 064602/1-25 (2001)

x - and ξ -Scaling of the Nuclear Structure Function at Large x

J. Arrington, C. S. Armstrong, T. Averett, O. K. Baker, L. de Bever, C. W. Bochna, W. Boeglin, B. Bray, R. D. Carlini, G. Collins, C. Cothran, D. Crabb, D. Day, J. A. Dunne, D. Dutta, R. ent, B. W. Filippone, A. Honegger, E. W. Hughes, J. Jensen, J. Jourdan, C. E. Keppel, D. M. Koltenuk, R. Lindgren, A. Lung, D. J. Mack, J. McCarthy, R. D. McKeown, D. Meekins, J. H. Mitchell, H. G. Mkrtchyan, G. Niculescu, I. Niculescu, T. Petitjean, O. Rondon, I. Sick, C. Smith, B. Terburg, W. F. Vulcan, S. A. Wood, C. Yan, J. Zhao, and B. Zihlmann

Phys. Rev. C **64**, 014602/1-5 (2001)

Measurements of the Elastic Electromagnetic Form Factor Ratio $\Phi_p G_{Ep}/G_{Mp}$ via Polarization Transfer

O. Gayou *et al.* (the Jefferson Lab Hall A Collaboration)

Phys. Rev. C **64**, 038202-1/1-4 (2001)

Dynamical Study of the ${}^2\text{He}(e, e'\pi^+)$ Reaction

K. Hafidi and T.-S. H. Lee

Phy. Rev. C **64**, 064607/1-5 (2001)

Improved Measurement of the \bar{d}/\bar{u} Asymmetry in the Nucleon Sea

R. S. Towell *et al.* and the FNAL E866/NuSea Collaboration

Phys. Rev. D **64**, 052002/1-16 (2001)

Hadron Formation in Deep-Inelastic Positron Scattering in a Nuclear Environment

A. Airapetian *et al.* (HERMES Collaboration)

Eur. Phys. J. C **20**, 479-486 (2001)

Multiplicity of Charged and Neutral Pions in Deep-Inelastic Scattering of 27.5 GeV Positrons on Hydrogen

A. Airapetian *et al.* and the HERMES Collaboration

Eur. Phys. J. C **21**, 599-606 (2001)

Beam of Metastable Krypton Atoms Extracted from a rf-Driven Discharge

C. Y. Chen, K. Bailey, X. Du, Y. M. Li, Z.-T. Lu, T. P. O'Connor, L. Young, and G. Winkler

Rev. Sci. Instrum. **72**, 271-272 (2001)

Charged Pion Electroproduction on H , 2H , and 3He

H. E. Jackson (on behalf of the NucPi Collaboration)

Proceedings of the 16th International IUPAP Conference on Few Body Problems in Physics, Taipei, Taiwan, March 6-10, 2000; Nucl. Phys. **A684**, 449c-453c (2001)

Electroproduction of Kaons and Light Hypernuclei

J. Reinhold *et al.*

Proceedings of the 16th International IUPAP Conference on Few Body Problems in Physics, Taipei, Taiwan, March 6-10, 2000; Nucl. Phys. **A684**, 470c-474c (2001)

Measurement of Polarization Observables in Elastic and Inelastic Electron-Deuteron Scattering at the VEPP-3 Storage Ring

D. M. Nikolenko, H. Arenhövel, L. M. Barkov, S. L. Belostotsky, V. F. Dmitriev, M. V. Dyug, R. Gilman, R. J. Holt, Isaeva, C. W. de Jager, E. R. Kinney, R. S. Kowalczyk, B. A. Lazarenko, A. Yu. Loginov, S. I. Mishnev, V. V. Nelyubin, A. V. Osipov, D. H. Potterveld, I. A. Rachek, Yu. V. Shestakov, A. A. Sidorov, V. N. Stibunov, D. K. Toporkov, D. K. Vesnovsky, V. V. Vikhrov, H. de Vries, and S. A. Zevakov
Proceedings of the 16th International IUPAP Conference on Few Body Problems in Physics, Taipei, Taiwan, March 6-10, 2000; Nucl. Phys. **A684**, 525c-527c (2001)

Three-Nucleon Interactions: Evidence from Polarized *pd* Elastic Scattering

E. R. Kinney, R. V. Cadman, J. Brack, W. J. Cummings, J. A. Fedchak, B. D. Fox, H. Gao, W. Glöckle, C. Grosshauser, R. J. Holt, C. E. Jones, M. A. Miller, W. Nagengast, B. R. Owen, K. Rith, F. Schmidt, E. C. Schulte, J. Sowinski, F. Sperisen, E. L. Thorsland, R. Tobey, J. Wilbert, and H. Witala
Proceedings of the XVIIth European Conference on Few-Body Problems in Physics, Évora, Portugal, September 11-16, 2000; Nucl. Phys. **A689**, 33c-40c (2001)

Electroproduction of Kaons on Light Nuclei

B. Zeidman, D. Abbott, A. Ahmidouch, P. Ambrozewicz, C. S. Armstrong, J. Arrington, R. Asaturyan, K. Assamagan, S. Avery, K. Bailey, O. K. Baker, S. Beedoe, H. Bitao, H. Breuer, D. S. Brown, R. Carlini, J. Cha, N. Chant, E. Christy, A. Cochran, L. Cole, G. Collins, C. Cothran, J. Crowder, W. J. Cummings, S. Danagoulian, F. Dohrmann, F. Duncan, J. Dunne, D. Dutta, T. Eden, M. Elaasar, R. Ent, L. Ewell, H. Fenker, H. T. Fortune, Y. Fujii, L. Gan, H. Gao, K. Garrow, D. F. Geesaman, P. Gueye, K. Gustafsson, K. Hafidi, J. O. Hansen, W. Hinton, H. E. Jackson, H. Juengst, C. Keppel, A. Klein, D. Koltenuk, Y. Liang, J. H. Liu, A. Lung, D. Mack, R. Madey, P. Markowitz, C. J. Martoff, D. Meekins, J. Mitchell, T. Miyoshi, H. Mkrtchyan, R. Mohring, S. K. Mtingwa, B. Mueller, T. G. O'Neill, G. Niculescu, I. Niculescu, D. Potterveld, J. W. Price, B. A. Raue, P. E. Reimer, J. Reinhold, J. Roche, P. Roos, M. Sarsour, Y. Sato, G. Savage, R. Sawafta, J. P. Schiffer, R. E. Segel, A. Semenov, S. Stepanyan, V. Tadevosian, S. Tajima, L. Tang, B. Terburg, A. Uzzle, S. Wood, H. Yamaguchi, C. Yan, C. Yan, L. Yuan, M. Zeier, and B. Zihlmann
Proceedings of the VII International Conference on Hypernuclei and Strange Particle Physics (HYP2000), Torino, Italy, October 23-27, 2000; Nucl. Phys. **A691**, 37c-42c (2001)

Electroproduction of Kaons and Light Hypernuclei

Jörg Reinhold (for the Jefferson Lab E91-016 Collaboration)
Proceedings of the Workshop on Hypernuclear Physics with Electromagnetic Probes (HYPJLAB 99), Hampton, VA, December 2-4, 1999, eds. L. Tang and O. Hashimoto, pp. 134-139 (2001)

Atom Trap Trace Analysis

Zheng-Tian Lu, Kevin Bailey, Chun-Yen Chen, Xu Du, Yi-Min Li, Thomas P. O'Connor, and Linda Young

Proceedings of the 17th International Conference on Atomic Physics (CP551), Florence, Italy, June 4-11, 2000, eds. E. Arimondo, P. DeNatale, and M. Inguscio (AIP 2001) pp. 367-381

Structure of the Goldstone Bosons

Roy J. Holt and Paul E. Reimer

Proceedings of the 2nd Workshop on Physics with an Electron Polarized Light-Ion Collider (EPIC 2000), Cambridge, MA, September 14-15, 2000, ed. Richard G. Milner, AIP Conference Proceedings **588**, 234-239 (2001)

Two-Body Photodisintegration of the Deuteron at High Energy

Roy Holt (for the HallC99 Collaboration)

April Meeting of the American Physical Society, Washington, DC, April 28-May 1, 2001; Bull. Am. Phys. Soc. **46**, 41 (2001)

Angular Distribution Measurements of the $d(\gamma,p)n$ Differential Cross Section at High Energies

Elaine Schulte (for the Hall A Collaboration)

April Meeting of the American Physical Society, Washington, DC, April 28-May 1, 2001; Bull. Am. Phys. Soc. **46**, 83 (2001)

Measurement of Proton Polarization in Neutral Pion Photo-Production

Krishni Wijesooriya (for the Jefferson Lab Hall-A Collaboration)

April Meeting of the American Physical Society, Washington, DC, April 28-May 1, 2001; Bull. Am. Phys. Soc. **46**, 83 (2001)

Ratio of (π^-/π^+) from Pion Photo-Production in Deuterium at 1.2 to 5.6 GeV

Hong Xiang (For Hall A Experiment E94-104 at Jefferson Lab)

First Joint Meeting of the Nuclear Physics Divisions of APS and JPS, Wailea, Maui, HI, October 17-20, 2001; Bull. Am. Phys. Soc. **46**, 15 (2001)

The Deuterium to Hydrogen Cross Section Ratio in Inclusive Deep-Inelastic Scattering at HERMES

Kawtar Hafidi (for the HERMES collaboration)

First Joint Meeting of the Nuclear Physics Divisions of APS and JPS, Wailea, Maui, HI, October 17-20, 2001; Bull. Am. Phys. Soc. **46**, 34 (2001)

Electroproduction of Strangeness on Light Nuclei

F. Dohrmann (for the E91-016 Collaboration)

First Joint Meeting of the Nuclear Physics Divisions of APS and JPS, Wailea, Maui, HI, October 17-20, 2001; Bull. Am. Phys. Soc. **46**, 57 (2001)

An Experiment to Measure the Charge Radius of ${}^6\text{He}$

W. Grimes, Z. T. Lu, K. Bailey, and T. O'Connor

First Joint Meeting of the Nuclear Physics Divisions of APS and JPS, Wailea, Maui, HI,
October 17-20, 2001; Bull. Am. Phys. Soc. **46**, 100 (2001)

Atom Trap Trace Analysis, and Search for the 3.5 eV Nuclear Excited States in Th-229

C. Law, Z.-T. Lu, I. Ahmad, L. Young, T. P. O'Connor, K. Bailey, Y. Li, and X. Du

First Joint Meeting of the Nuclear Physics Divisions of APS and JPS, Wailea, Maui, HI,
October 17-20, 2001; Bull. Am. Phys. Soc. **46**, 103 (2001)

Monte Carlo Modeling of a Jefferson Laboratory Spectrometer

O. Okafor, J. Arrington, and E. Schulte

First Joint Meeting of the Nuclear Physics Divisions of APS and JPS, Wailea, Maui, HI,
October 17-20, 2001; Bull. Am. Phys. Soc. **46**, 104 (2001)

Measurement of Polarization Observables in Upsilon and Psi Production with 800 GeV p-Cu Collisions

P. E. Reimer (for FNAL E866/Nusea)

International Nuclear Physics Conference on Nuclear Physics in the 21st Century
(INPC2001), Berkeley, CA, July 30-August 3, 2001, Book of Abstracts, p. 191 (2001)

THEORETICAL PHYSICS

Pair Creation and an X-Ray Free Electron Laser

R. Alkofer, M. B. Hecht, C. D. Roberts, S. M. Schmidt, and D. V. Vinnik
Phys. Rev. Lett. **87**, 193902/1-4 (2001)

Persistence of Deformed Shapes in the Neutron-Deficient Pb Region

R. R. Chasman, J. L. Egido, and L. M. Robledo
Phys. Lett. **B513**, 325-329 (2001)

Coupled-Channel Study of $\gamma p \rightarrow K^+ \Lambda$

Wen-Tai Chiang, F. Tabakin, T.-S. H. Lee, and B. Saghai
Phys. Lett. **B517**, 101-108 (2001)

Quantum Monte Carlo Calculations of Pion Scattering from Li

T.-S. H. Lee and R. B. Wiringa
Phys. Rev. C **63**, 014006/1-5 (2001)

Coupled-Channels Treatment of Deformed Proton Emitters

Henning Esbensen and Cary N. Davids
Phys. Rev. C **63**, 014315/1-13 (2001)

 N - N Bound State

H. Gao, T.-S. H. Lee, and V. Marinov
Phys. Rev. C **63**, 022201(R)/1-3 (2001)

Six-Body Calculation of the α -Deuteron Radiative Capture Cross Section

K. M. Nollett, R. B. Wiringa, and R. Schiavilla
Phys. Rev. C **63**, 024003/1-13 (2001)

Nucleon Resonances in ω Photoproduction

Yongseok Oh, Alexander I. Titov, and T.-S. H. Lee
Phys. Rev. C **63**, 025201/1-9 (2001)

T Dependence of Pseudoscalar and Scalar Correlations

P. Maris, C. D. Roberts, S. M. Schmidt, and P. C. Tandy
Phys. Rev. C **63**, 025202/1-12 (2001)

Valence-Quark Distributions in the Pion

M. B. Hecht, C. D. Roberts, and S. M. Schmidt
Phys. Rev. C **63**, 025213/1-8 (2001)

Radiative α -Capture Cross Sections from Realistic Nucleon-Nucleon Interactions and Variational Monte Carlo Wave Functions

Kenneth M. Nollett

Phys. Rev. C **63**, 054002/1-13 (2001)

Dynamical Study of the Δ Excitation in $N(e, e'\pi)$ Reactions

T. Sato and T.-S. H. Lee

Phys. Rev. C **63**, 055201/1-13 (2001)

Electromagnetic Dissociation of ^8B and the Rate of the $^7\text{Be}(p, \gamma)^8\text{B}$ Reaction in the Sun

B. Davids, Sam M. Austin, D. Bazin, H. Esbensen, B. M. Sherrill, I. J. Thompson, and J. A.

Tostevin

Phys. Rev. C **63**, 065806/1-14 (2001)

Realistic Models of Pion-Exchange Three-Nucleon Interactions

Steven C. Pieper, V. R. Pandharipande, R. B. Wiringa, and J. Carlson

Phys. Rev. C **64**, 014001/1-21 (2001)

Eikonal Approximation in Heavy-Ion Fragmentation Reactions

H. Esbensen and G. F. Bertsch

Phys. Rev. C **64**, 014608/1-6 (2001)

Medium-Mass Nuclei with Δ Excitations Under Compression

Mahmoud A. Hasan, James P. Vary, and T.-S. H. Lee

Phys. Rev. C **64**, 024306/1-8 (2001)

Very Extended Nuclear Shapes Near $A = 100$

R. R. Chasman

Phys. Rev. C **64**, 024311/1-6 (2001)

Neutron Electric Dipole Moment: Constituent-Dressing and Compositeness

M. B. Hecht, C. D. Roberts, and S. M. Schmidt

Phys. Rev. C **64**, 025204/1-9 (2001)

Meson-Exchange πN Models in Three-Dimensional Bethe-Salpeter Formulation

Cheng-Tsung Hung, Shin Nan Yang, and T.-S. H. Lee

Phys. Rev. C **64**, 034309/1-10 (2001)

Benchmark Test Calculation of a Four-Nucleon Bound State

H. Kamada, A. Nogga, W. Glöckle, E. Hiyama, M. Kamimura, K. Varga, Y. Suzuki,

M. Viviani, A. Kievsky, S. Rosati, J. Carlson, Steven C. Pieper, R. B. Wiringa, P. Navrátil,

B. R. Barrett, N. Barnea, W. Leidemann, and G. Orlandini

Phys. Rev. C **64**, 044001/1-8 (2001)

Schwinger-Dyson Approach to Non-Equilibrium Classical Field Theory
Krastan B. Blagoev, Fred Cooper, John Dawson, and Bogdan Mihaila
Phys. Rev. D **64**, 125003/1-15 (2001)

Giant Resonances in Exotic Nuclei
H. Sagawa and H. Esbensen
Nucl. Phys. **A693**, 448-462 (2001)

A Generalized Cauchy Dispersion Formula and the Refractivity of Elemental Semiconductors
D. Y. Smith and Mitio Inokuti
J. Phys.: Condens. Matter **13**, 3883-3893 (2001)

Response to the Commentary by J. F. Ziegler (Radiat. Res. 152, 219-222, 1999)
Stephen M. Seltzer, Mitio Inokuti, Helmut Paul, and Hans Bichsel
Radiation Research **155**, 378-381 (2001)

In Memoriam – Ugo Fano (1912-2001)
Mitio Inokuti
Radiation Research **155**, 753-754 (2001)

Ugo Fano
R. Stephen Berry and Mitio Inokuti
Physics Today **54**, 73-74 (2001)

Quantum Monte Carlo Calculations of Light Nuclei
Steven C. Pieper and R. B. Wiringa
Annu. Rev. Nucl. Part. Sci. **51**, 53-90 (2001)

Ion-Size Effects and the Spatial Extent of Defects
D. Y. Smith and Mitio Inokuti
Radiation Effects and Defects in Solids **155**, 43-49 (2001)

Review of the Recent Applications of the Stochastic Variational Method
Kálmán Varga
Proceedings of the 16th International IUPAP Conference on Few Body Problems in Physics;
Taipei, Taiwan, March 6-10, 2000; Nucl. Phys. **A684**, 209c-217c (2001)

Dynamical Study of Δ Excitation with $N(e, e'\pi)$ Reaction
T.-S. H. Lee and T. Sato
Proceedings of the 16th International IUPAP Conference on Few Body Problems in Physics,
Taipei, Taiwan, March 6-10, 2000; Nucl. Phys. **A684**, 327c-329c (2001)

Scientific Legacy of Robert L. Platzman. Preliminary Report
Mitio Inokuti
Proceedings of the International Symposium on Prospects for Application of Radiation
Toward the 21st Century, Tokyo, Japan, March 13-17, 2000; Radiation Phys. and Chem. **60**,
283-290 (2001)

Ion-Size Effects and the Spatial Extent of Defects

D. Y. Smith and Mitio Inokuti

Proceedings of the 14th International Conference on Defects in Insulating Materials, Johannesburg-Midrand, South Africa, April 3-7, 2000, eds. J. D. Comins, P. E. Ngoepe, and A. T. Davidson (Gordon and Breach Science Publishers 2001) Radiation Effects and Defects in Solids, Vol. 155, Nos. 1-4, part II, pp. 43-49 (2001)

The Representation of Numbers by States in Quantum Mechanics

Paul Benioff

Proceedings of the 5th International Conference on Quantum Communication, Measurement, and Computing, Capri, Italy, July 3-8, 2000 (Kluwer Academic/Plenum Publishers, NY 2001) pp. 171-178

Relativistic Quantum Dynamics of Many-Body Systems

F. Coester and W. N. Polyzou

Proceedings of the International Conference on 150 Years of Quantum Many-Body Theory, UMIST, Manchester, UK, July 10-14, 2000, eds. Raymond F. Bishop, Klaus A. Gernoth, and Niels R. Walet (World Scientific, Singapore 2001) pp. 79-87

The Scientific Legacy of Ugo Fano

Mitio Inokuti

April Meeting of the American Physical Society, Washington, DC, April 28-May 1, 2001; Bull. Am. Phys. Soc. **46**, 61 (2001)

Dynamical Calculations for $d(e, e' \pi^+)$ Reactions

Kawtar Hafidi and Harry Lee

April Meeting of the American Physical Society, Washington, DC, April 28-May 1, 2001; Bull. Am. Phys. Soc. **46**, 84 (2001)

Quark-Gluon Mechanisms of Vector Meson Photoproductions

T.-S. Harry Lee and Yongseok Oh

First Joint Meeting of the Nuclear Physics Divisions of APS and JPS, Wailea, Maui, HI, October 17-20, 2001; Bull. Am. Phys. Soc. **46**, 15 (2001)

Breakup of 170 MeV ^{17}F by ^{208}Pb

J. F. Liang, J. R. Beene, A. Galindo-Uribarri, J. Gomez del Campo, C. J. Gross, M. L. Halbert, P. E. Mueller, D. Shapira, D. W. Stracener, R. L. Varner, H. Esbensen, and I. J. Thompson
First Joint Meeting of the Nuclear Physics Divisions of APS and JPS, Wailea, Maui, HI, October 17-20, 2001; Bull. Am. Phys. Soc. **46**, 118 (2001)

Electromagnetic Dissociation of ^8B and the Rate of the $^7\text{Be}(p, \gamma)^8\text{B}$ Reaction in the Sun

B. Davids, Sam M. Austin, D. Bazin, H. Esbensen, B. M. Sherrill, I. J. Thompson, and J. A. Tostevin

3rd International Conference on Exotic Nuclei and Atomic Masses (ENAM2001), Hämeenlinna, Finland, July 2-7, 2001, Book of Abstracts, p. C-5 (2001)